Abstracts Volume

Archaeoseismology and Palaeoseismology in the Alpine-Himalayan Collisional Zone

Editors

R. Pérez-López, C. Grützner, J. Lario, K. Reicherter and P.G. Silva

1st INQUA-IGCP 567 International Workshop on Earthquake Archaeology and Palaeoseismology

7-13 September 2009
Baelo Claudia (Cádiz, Spain)

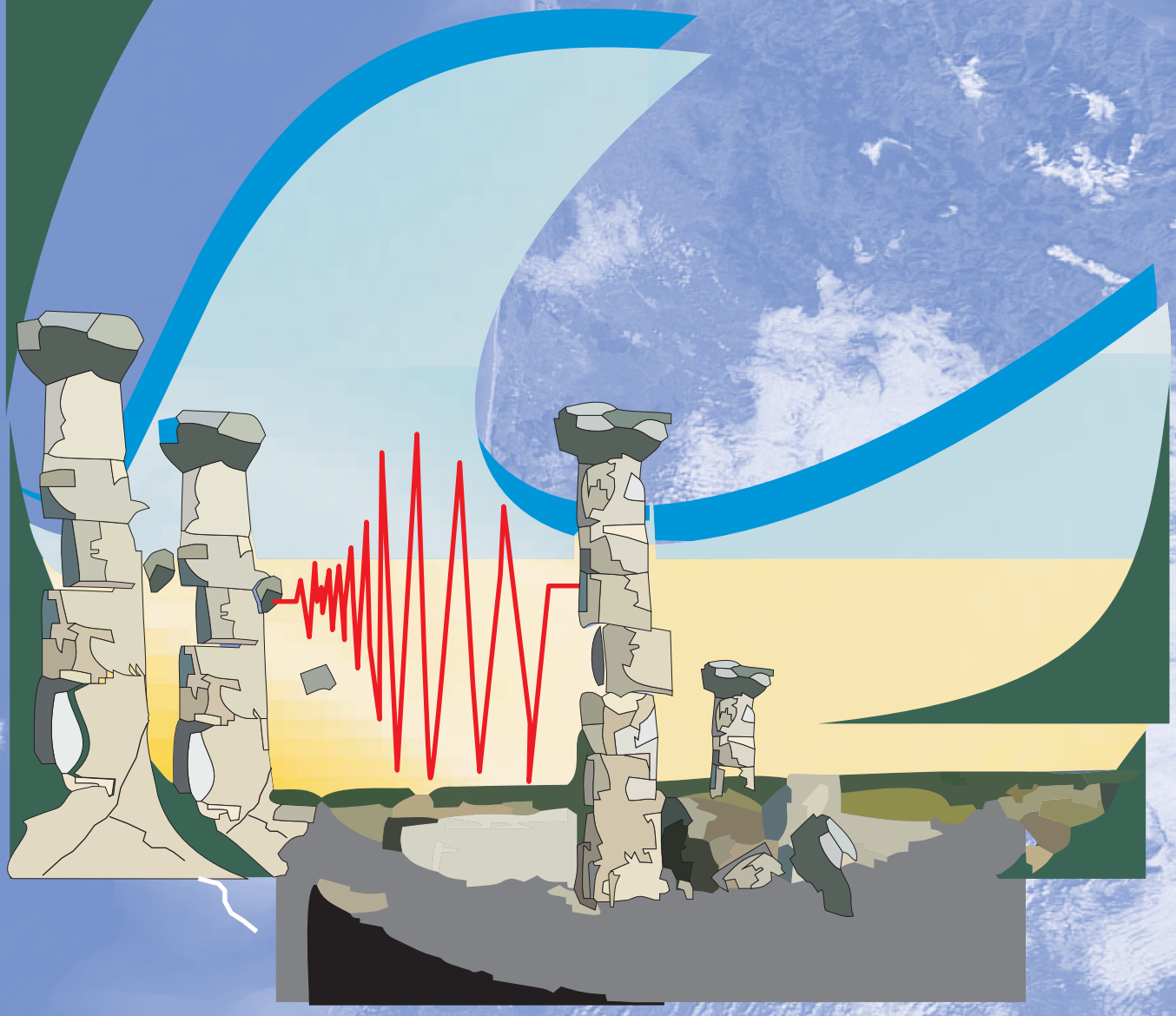

Abstracts Volume

Archaeoseismology and Palaeoseismology in the Alpine-Himalayan Collisional Zone

Editors
R. Pérez-López, C. Grützner, J. Lario, K. Reicherter and P.G. Silva

Focus Area on Paleoseismology and Active Tectonics
INQUA

IUGS UNESCO 567
Earthquake Archaeology
Archaeoseismology along the Alpine-Himalayan seismic zone

This **Abstracts Volume** has been produced for the **1st INQUA-IGCP 567 International Workshop on Earthquake Archaeology and Palaeoseismology** held in Baelo Claudia Roman ruins (Cádiz, Southern Spain). The event has been organized together by the INQUA Focus Area on Paleoseismology and Active Tectonics and the IGCP-567: Earthquake Archaeology.

This scientific meeting has been supported by the Spanish Research Projects ACI2008-0726, CGL08-03998BTE, CGL08-04000BTE and ACTISIS CGL2006-05001/BTE and UNED grant.

RWTH AACHEN UNIVERSITY
VNiVERSiDAD D SALAMANCA
UNED
Instituto Geológico y Minero de España
INQUA
IUGS UNESCO
AEQUA
JUNTA DE ANDALUCIA CONSEJERIA DE CULTURA
CSIC
GOBIERNO DE ESPAÑA
MINISTERIO DE CIENCIA E INNOVACIÓN

Edita e imprime: Sección de Publicaciones de la
Escuela Técnica Superior de Ingenieros
Industriales. Universidad Politécnica
de Madrid.

I.S.B.N.**: 978-84-7484-217-3**
Depósito Legal**: M-31907-2009**

La impresión del presente volumen se ha realizado con una Ayuda del Plan de Promoción de la Investigación de la **UNED**

Preface

During the 15th INQUA Congress (1999), the former Subcommission on Paleoseismicity of the INQUA promoted the compilation of a new scale of macroseismic intensity based on environmental effects only (ESI). A work group including geologists, seismologists and engineers compiled a first version of the scale that was presented at the 16th INQUA Congress, and modified one year later at the 32nd International Geological Congress in Florence. To this end, the INQUA TERPRO (Commission on Terrestrial Processes) approved a specific project (INQUA Scale Project, 2004 - 2007). As an outcome, the revised version of the ESI was ratified during the 17th INQUA Congress in 2007. Here, a Workshop on Earthquake Archaeology and Palaeoseimology in the ancient Roman city of *Baelo Claudia* (Spain) was proposed.

The initiative of the IGCP-567 Project on Earthquake Archaeology was successfully launched in 2008. The *Baelo Claudia* workshop was officially included in the program of scientific activities of this project. Nowadays in 2009, this joint meeting between the INQUA Focus Area on Paleoseismology and the IGCP-567 on Earthquake Archaeology wants to share objectives for a better knowledge of the seismic history of tectonically active settings. Besides the classical catalogues on historical seismicity, these two innovative lines of research try to unmask the ancient seismic behaviour of active zones and faults from the available geological, geomorphological and archaeological records. This effort implies the combination of very different kind of evidence coming from quite diverse scientific approaches, some times in very singular ways. Example of this is the variety of original research presented in this volume of abstracts composed of more than 40 contributions from people of more than 20 different countries, mainly focused on the European, Middle East and Asiatic, Alpine-Himalayan Collision zone.

Finally, we want to draw your attention to a recently published Special Volume of the Geological Society of London, No. 316 (2009), **Palaeoseismology: historical and prehistorical records of earthquake ground effects for seismic hazard assessment**, edited by Klaus Reicherter, Alessandro M. Michetti and Pablo G. Silva Barroso, in which results of of two meetings held in 2006 (European Geosciences Union General Assembly 2006, Session TS4.4, '3000 years of earthquake ground effects in Europe: geological analysis of active faults and benefits for hazard assessment', Vienna, Austria, April 2006; and the ICTP/IAEA workshop on 'The conduct of seismic hazard analyses for critical facilities', Trieste, Italy, May 2006) are summarized.

Lastly, we wish all participants a successful and fruitful conference and workshop in the Roman Baelo Claudia, and we hope that everybody can enjoy southern Spain, the Costa de la Luz, and the marvelous landscape in the Straits of Gibraltar.

The Organizers of the 1st INQUA-IGCP567 Workshop

Pablo G. Silva
Universidad de Salamanca, SPAIN

Klaus Reicherter
RWTH Aachen University, GERMANY

The Organizers of the workshop are grateful to the responsible persons of ***Conjunto Arqueológico Romano de Baelo Claudia*** *(Junta de Andalucía)* for assisting our initiative by giving us access to different facilities of the Museum of Baelo Claudia, as well as all the institutions involved in the organization, and all the people of the Bolonia Bay (Cádiz) around the conference.

PALAEOSEISMOLOGICAL FEATURES OF THE GRANADA FAULT

J.M. Azañón (1, 2), J. García-Mayordomo (3), J.M. Insua-Arévalo (4) and M.J. Rodríguez-Peces (2)

(1) Dpto. de Geodinámica, Facultad de Ciencias, Universidad de Granada. C/Fuentenueva, s/n. 18002-Granada. SPAIN. jazanon@ugr.es, marpeces@ugr.es
(2) Instituto Andaluz de Ciencias de la Tierra, CSIC-Universidad de Granada.
(3) Instituto Geológico y Minero de España (IGME). C/La Calera, 1. 28760-Tres Cantos (Madrid). SPAIN. julian.garcia@igme.es
(4) Dpto. Geodinámica, Facultad de Ciencias Geológicas, Universidad Complutense de Madrid. 28040-Madrid. SPAIN. insuarev@geo.ucm.es

Abstract: *This paper presents preliminary results of a palaeoseismic study of the Granada Fault, a NW-SE active normal fault that produces a Plio-Quaternary throw of 300 m. According to these data, slip rate has been estimated in 0.38 mm/y (Sanz de Galdeano et al., 2003). Several palaeosols, Pleistocene in age, have been affected by this fault. Three different events can be recognized from the accumulative throw. The vertical slip per event ranges from 5 to 7 cm. Following the empirical relationship between moment magnitude and average displacement proposed by Wells and Coppersmith (1994), a magnitude between 5.9 and 6.0 can be preliminary assessed for these events. The palaeosols were sampled and dated using the thermoluminiscence method to constrain these estimates.*

Key words*: Palaeoseismicity, slip ranges, seismic hazard, Central Betics*

ACTIVE FAULTS IN THE GRANADA TOWN

The present-day relief of the margins of the Granada depression is strongly conditioned by the activity of some faults, together with the incision produced by several rivers that drain the area. The faults produce large steps in the relief (Fig. 1). The most important topographic step corresponds to the faults bounding the basement of the basin; these faults are characterised by metre- to hectometre-scale scarps with associated slicken-surfaces and striations; the footwalls of these faults are uplifted blocks with strong relief and deeply incised by rivers. Several steps are found between the flat area of the Granada basin and the ranges where the basement outcrops, which could represent fault scarps variably degraded by erosion of the soft sediments. These steps show NW-SE orientations, in accordance with the orientation of the majority of the normal faults mapped in the margin of the basin (Fig. 2).

Fig. 1: Topographic steps produced by the NW-SE normal faults.

The seismic activity in the Granada depression is high, with a large number of earthquakes, all of them with a moderate to low magnitude ($m_b \leq 5.5$) (De Miguel et al., 1989). The seismicity has its origin mostly at depths between 5 and 17 km (Morales et al., 1997; Serrano et al., 2002) and the focal mechanisms indicate a present-day stress state dominated by a NE-SW extensional axis. This extensional stress field coincides with palaeo-stress determinations from Tortonian and younger sediments, and is perfectly compatible with NW-SE striking normal faults and NE-SW directed extensional transport (Galindo-Zaldívar et al., 1999; Martínez-Martínez et al., 2002).

Fig. 2: NW-SE normal faults outcropping in the northeastern border of the Granada basin near the Granada city. The red square shows the location of the fault shown in Fig. 3.

Taking into account the length of the seismic faults in the area (approximately 17 km) the "realistic" maximum

magnitude of an earthquake would be 5.1 (De Miguel et al., 1989; Peláez Montilla et al., 2002). An earthquake of this magnitude at depths of 5 km would produce maximum vertical displacements of 3 mm in the vertical of its focus (Peláez Montilla et al., 2002).

A detailed study about the longitude and segmentation of the NW-SE active faults outcropping in the surrounding areas of the Granada Town is critical to evaluate the seismic hazard in this place. In a previous analysis, Sanz de Galdeano et al., 2003 attributed a maximum longitude to the Granada fault of 17 km. However, deformation induced by the Granada fault is distributed in a wide area of several kilometres. In this area, it can be appreciated that the fault is segmented in multiple discontinuous planes. By instance, in the Alhambra hill and surrounding areas, the outcropping rocks are affected by several faults with centimetre throws. The lateral continuity of these faults is less than 10 km.

PALAEOSEISMOLOGICAL ASSESSMENT

The seismic capability of the NW-SE faults of the Granada City is assessed studying one of these faults affecting several paleosoils. The studied fault has been located in a vertical urban talus at the suburb of Granada (UTM30N: X-445083; Y-4117927).

The fault, with strike N125ºE and dipping 86º southwards, affects some horizontal levels of silty sand that present pedogenic development (Fig. 2). The dark horizons have been taking as markers to estimate the accumulative displacement of the fault. We took into account the top and the bottom of these dark horizons because their diffuse limits. In addition, we took three samples (Table 1) for thermoluminescence dating (TL) in order to estimate some recurrence of the seismic events and the slip rate of the fault. The result of the accumulative slip, coseismic slip and mean coseismic slip of the fault is presented in the Table 2.

Table 1: TL dating

Sample	Age (ka BP)	X (UTM30N)	Y (UTM30N)
TL-4	> 150	445083	4117927
TL-5	> 150	445083	4117927
TL-6	> 80	445083	4117927

With such a mean coseismic slip of 5.86 cm within a range of 4.8 to 7.0 cm, this fault would be capable to generate events with magnitude 5.9-6.0 following the relationships between moment magnitude and average displacement of Wells and Coppersmith (1994). The accumulative displacement remaining of 50.0 cm of the level D might be generated by 8-9 events considering the mean coseismic slip. Unfortunately, the ages of the samples TL-4, TL-5 and TL-6 are all beyond the age range of the dating technique that is 150 ka. In any case we can estimate some extreme values of recurrence period and slip rate of the fault. In this way, considering the youngest material affected by the fault (Level D) like older than 150 ka, we estimate a seismic recurrence period longer than 16.7 ka. On the other hand, the slip rate of the fault should be considered as a maximum value of 0.003 mm/y, which is remarkable lower than that given by Sanz de Galdeano et al. (2003) as 0.38 mm/y in these faults since the mid-Pleistocene (800 ka). The difference of these two values should be understood as a distribution of the deformation in a complex set of faults that limit the Granada Basin at this edge. Nevertheless, we can not discard a deceleration of the rate during the Upper Pleistocene.

Table 2: Coseismic slip and mean coseismic slip of the fault

Level	Accumulative slip (cm)	Coseismic slip (cm)
D	50.0	
		5.8
C	55.8	
		7.0
B	62.8	
		4.8
A	67.6	
	Mean coseismic slip (cm)	**5.86**

IMPLICATIONS IN SEISMIC HAZARD

Sanz de Galdeano et al. (2003) assessed the seismic potential of the Granada Fault. They estimated a 6.3-6.6 maximum moment magnitude (M_w), and a recurrence time of less than 510 years for a M_w=6.0 earthquake. Recurrence time was obtained using a 0.38 mm/yr slip rate, which results from considering 300 m accumulated vertical offset since the mid-Pleistocene (800 ka). According to these data, the authors classified the Granada Fault as the most active one in the whole Granada Basin. Even though their observations could be regarded as very interesting at the time they were produced, the absence of absolute dating and precise measurements of coseismic deformation, makes their conclusions very arguable.

According to the results obtained in our palaeoseismological analysis, the interest in modelling the Granada Fault as a particular seismogenic source is very limited. A M_w=6.0 maximum magnitude does not represent a particular large value in the tectonic and/or historical seismicity context in the Granada Basin. Furthermore, a minimum mean recurrence time of 16.7 ka means a very low frequency when compared to the extrapolation of the Gutenberg-Richter law of the area (~100 years in Morales et al., 1996).

Nevertheless, these results agree with a model of distributed deformation at this border of the Granada Basin. In this model, the Granada Fault represents a shear band composed of multiple small faults, in contrast to a single large fault which accumulates most of the deformation. In this context, elastic energy is released preferentially by small earthquakes and, exceptionally, by moderate size ones ($M_{w\ máx}$≈6.0).

DISCUSSION AND CONCLUSION

According to the palaeoseismological results obtained from TL dating and direct measurement of coseismic deformation, we regard the seismic hazard of the Granada Fault preliminary as low. However, these results shall be confirmed in following studies. Our study remarks

the importance of performing absolute dating and direct measurement of coseismic deformation in recent sediments (Upper Pleistocene, at least) in order to evaluate properly the current activity and, subsequently, the seismic hazard of particular faults. In this context, the actual activity of many faults in the Granada Basin –which have been assessed based on Plio-Quaternary markers (ca. 5 Ma), could be much lower than it is currently believed.

Finally, the Granada Fault is capable of producing earthquakes as large as 6.0 (±0.3). Whether these earthquakes will be catastrophic or not depends much more on the observance of seismic code provisions by builders and on Civil Protection Plans, rather than on the seismic potential of the Granada Fault. If we consider the rupture of the total length of this fault (<10 km), the maximum magnitude estimated with the relationships between moment magnitude and surface rupture length of Wells and Coppersmith (1994) would be between 6.1-6.2. This magnitude is quite similar to that obtained in our paleoseismological assessment attending to the average displacement (M_w=5.9-6.0). This value is much higher than that given by De Miguel et al. (1989) or Peláez Montilla et al. (2002) as the "realistic" maximum magnitude of 5.1.

Acknowledgements: This study was supported by the research project TOPOIBERIA CONSOLIDER-INGENIO2010 CSD2006-00041 of the Spanish Ministry of Science and Innovation, the research project MMA083/2007 of the Spanish Ministry of Environment and the research project CGL2008-03249/BTE of the Spanish Ministry of Science and Innovation.

References

De Miguel, F., Vidal, F., Alguacil, G., and Guirao, J.M. (1989). Spatial and energic trends of the microearthquakes activity in the Central Betics. Geodinamica Acta, 3, 87-94.

Galindo-Zaldívar, J., Jabaloy, A., Serrano, I., Morales, J., González Lodeiro, F., and Torcal, F. (1999). Recent and present-day stresses in the Granada Basin (Betic Cordilleras): example of a late Miocene - present-day extensional basin in a convergent plate boundary. Tectonics, 18, 686-702.

Martínez-Martínez, J.M., Soto, J.I., Balanyá, J.C. (2002). Orthogonal folding of extensional detachments: structure and origin of the Sierra Nevada elongated dome (Betics, SE Spain). Tectonics, 21, 1-20.

Morales, J., Serrano, I., Vidal, F., and Torcal, F. (1997). The depth of the earthquake activity in the Central Betics (Southern Spain). Geophysical Research Letters, 24, 3289-3292.

Peláez Montilla, J.A., Gil, A.J., Sanz de Galdeano, C., and Rodríguez Caderot, G. (2002). Condicionantes en el diseño de una red geodésica para el control de una falla normal: aplicación a la falla de Granada. Proceedings of the 3ª Asamblea Hispano Portuguesa de Geodesia y Geofísica. Valencia (Spain), 51-55.

Sanz de Galdeano, C., Peláez Montilla, J.A., and López Casado, C. (2003). Seismic potential of the Main Active Faults in the Granada Basin (Southern Spain). Pure and Applied Geophysics, 160, 1537-1556.

Serrano, I., Zhao, D., and Morales, J. (2002). 3-D crustal structure of the extensional Granada Basin in the convergent boundary between the Eurasian and African plates. Tectonophysics, 344, 61-79.

Wells, D. L. and K.J. Coppersmith (1994). New empirical relationships among magnitude, rupture length, rupture area, and surface displacement. Bulletin of the Seismological Society of America, 84(4), 974-1002.

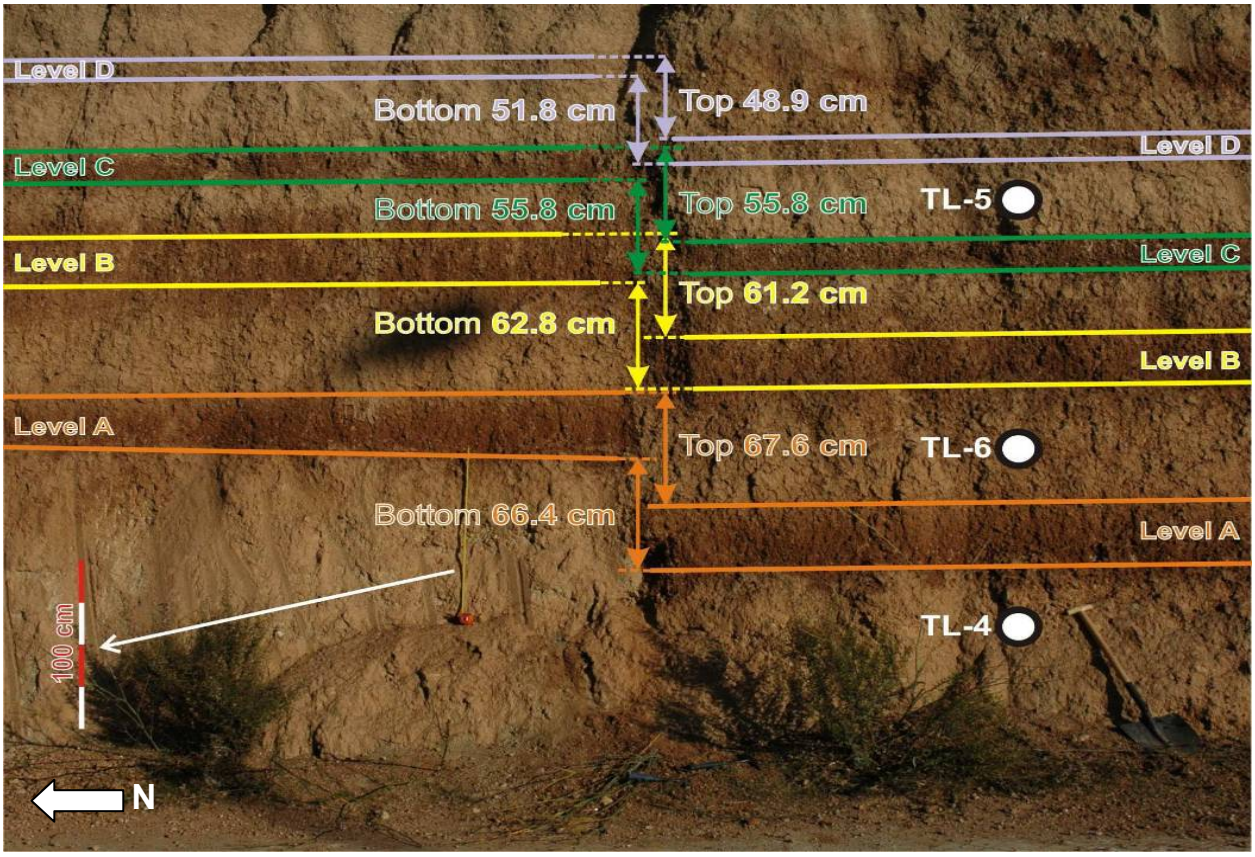

Fig. 3: Palaeoseismological analysis of the Granada Fault. TL-4 and TL-6 are the selected points for thermoluminescence dating

GROUND RUPTURE INDUCED BY 2003 MASBATE EARTHQUAKE, PHILIPPINES

G.M. Besana-Ostman (1), M. Ando (2) and J.F. Fonseca (3)

(1) Physics Department, IST, Av Rovisco Pais, 1,1049-001 Lisboa, PORTUGAL. glenda.besana@gmail.com
(2) Institute of Earth Sciences, Academia Sinica,128 Academia Road Sec. 2, Nankang, Taipei, TAIWAN. ando@earth.sinica.edu.tw
(3) Physics Department, IST, Av Rovisco Pais, 1,1049-001 Lisboa, PORTUGAL. jfonseca@ist.utl.pt

Abstract: *An earthquake (Ms 6.2) occurred along the Masbate section of the Philippine Fault Zone in Masbate, Philippines in 2003 and was associated with at least 23 km of ground rupture with horizontal offsets reach a maximum of 163 cm, and vertical offsets are as high as 23 cm. Evidence were predominantly left-lateral slip includes consistent left-lateral displacement of cultural features along the fault, right-stepping en-echelon fault strands, and local extensional and contractional structures formed at left- and right-steps, respectively. The surface rupture essentially follows the pre-existing fault trace. The 2003 Masbate earthquake aftershock distribution implies a symmetrical ground rupture relative to the epicenter. Based on surface rupture displacements and aftershock distribution, total rupture length and size of 23km and Ms6.2 are suggesting that the mapped surface trace is significantly shorter than expected fault rupture.*

Key words*: slow earthquake, Masbate, Philippine Fault Zone, ground rupture*

INTRODUCTION

On 15 February 2003 at 7:01 p.m. (local time), a moderate earthquake (Ms 6.2) struck the island province of Masbate in east central Philippines. The epicenter was determined by the Philippine Institute of Volcanology and Seismology (PHIVOLCS) to be offshore of Magcaraguit Island at about 22 km deep. Based on epicentral location and focal mechanism solutions, the event was generated along the trace of the Philippine Fault Zone (PFZ) in central Philippines (Fig. 1). Minor damage from the earthquake was expected due to its shallow depth and magnitude.

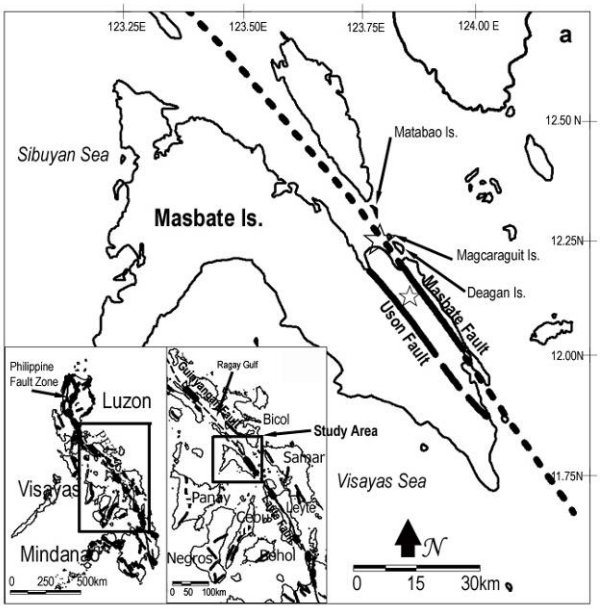

Fig.1: Map showing the study area, location of Masbate fault, the epicenter of the February 15, 2003 earthquake (big open star) and its foreshock (smaller star). Inset maps show the Philippine archipelago, the extent of the PFZ and the study area relative to the PFZ

In this study, special attention was given to the known location of the PFZ (Arante et al., 2003; Besana et al., 2003) during field documentation due to its importance in hazards mitigation particularly for future development and urbanization in the province. This could establish the minimum "setback" necessary for houses, vital utilities and other structures relative to the active fault.

Geologic Setting

The Philippine archipelago is tectonically bounded by several active trenches, the Philippine Trench on the east and the Manila Trench on the west that subduct in opposite direction (Fitch, 1972). Barrier et al. (1991) showed that in this region the northwestward motion of the Philippine Sea plate and Sundaland margin is accommodated obliquely along the Philippine Trench and the PFZ. PFZ is a major left-lateral strike-slip fault that transects the whole archipelago (Willis, 1937) from northwestern Luzon to southern Mindanao (Fig. 1) and is comparable to the San Andreas Fault (Allen, 1962; Besana and Ando, 2005). PFZ has a general strike of N30^{o}-40^{o}W and generated at least ten major seismic events with associated ground rupture since 1860 in central Philippines (Rowlett and Kelleher, 1976). In Masbate Island the trace is located at the southeastern part of the island. In this region, the active faults map of PHIVOLCS (2000) shows at least two parallel structures, the Masbate Fault and Uson Fault as shown in Fig. 1. Masbate has high background seismicity with at least five >M6 earthquakes have occurred during this century with predominantly left-lateral strike-slip focal mechanisms (PHIVOLCS, 1999). Earthquakes recorded during the last 20 years indicate that seismicity generally occurs from 0-35km deep (USGS data).

The mainshock Ms 6.2 of February 15, 2003 was preceded by an Ms 5.2 foreshock five hours earlier. It was located about 10 km south of the mainshock with depths of 30 km and a moment tensor solution

indicative of strike-slip faulting with Mo=5.3x 10^{17} Nm equivalent to a seismic moment magnitude Mw 5.8 (PHIVOLCS, 2003).

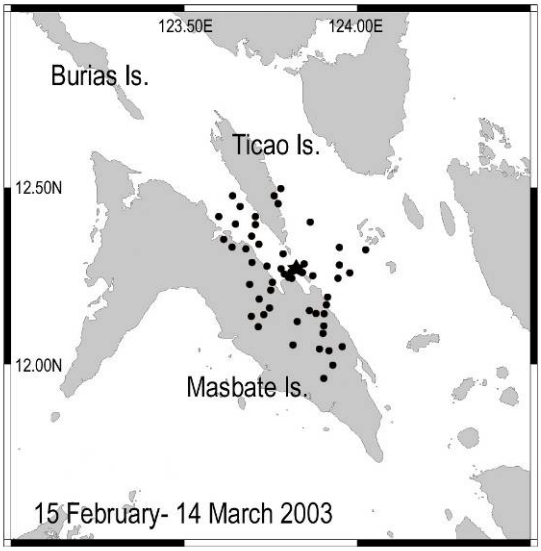

Fig. 2: The plot of 1-month aftershock distribution of the 2003 Masbate earthquake

The Ms 6.2 mainshock struck early in the evening of 15 February 2003 with extensive effect including the nearby provinces. The focal mechanism solution released by PHIVOLCS (2003) suggests a dominantly left-lateral slip along a vertical NW-SE fault that correlated with PFZ in the area. Several days following the mainshock, numerous aftershocks were recorded by the Masbate Seismic Station of PHIVOLCS. Aftershock plots in Fig. 2 were drawn using GMT by Wessel and Smith (1998). The aftershock area indicated at least a 60 km long rupture and distributed about 20 km wide along the Masbate Fault of PFZ.

GROUND RUPTURE

Field mapping in the municipalities of Dimasalang, Palanas and Cataingan showed varying surface effects on the ground and manmade structures caused by the horizontal displacements of the Masbate Fault of the PFZ. Surface manifestations varied from hairline cracks, soil mounds and en echelon fractures along a left-lateral fault. Fig. 3 shows the extent of the ground rupture mapped along the Masbate Fault in Masbate Island which extends to about 23 km. Following are some examples of the mapped ground rupture.

Ground rupture related to the 1:47pm foreshock

Field investigation found that the 1:47pm foreshock caused damages in the epicentral areas. Residents of the affected structures straddling the fault in the municipality of Palanas reported that their houses were damaged by this foreshock with visible cracks on walls and floors as well as on rice fields and gardens. Most of the observed damages caused by fissuring along the fault were mainly on concrete floors and asphalt roads with hairline or ~2-4 mm-wide cracks. In Sta. Cruz, Palanas, the road was fissured during this foreshock and booming sound was heard preceding the quake. Within the epicentral area such as in Nabangig and Matugnaw site, sulfur-like and/or gun powder-like smell was reported that possibly indicate ground fissuring during the foreshock event.

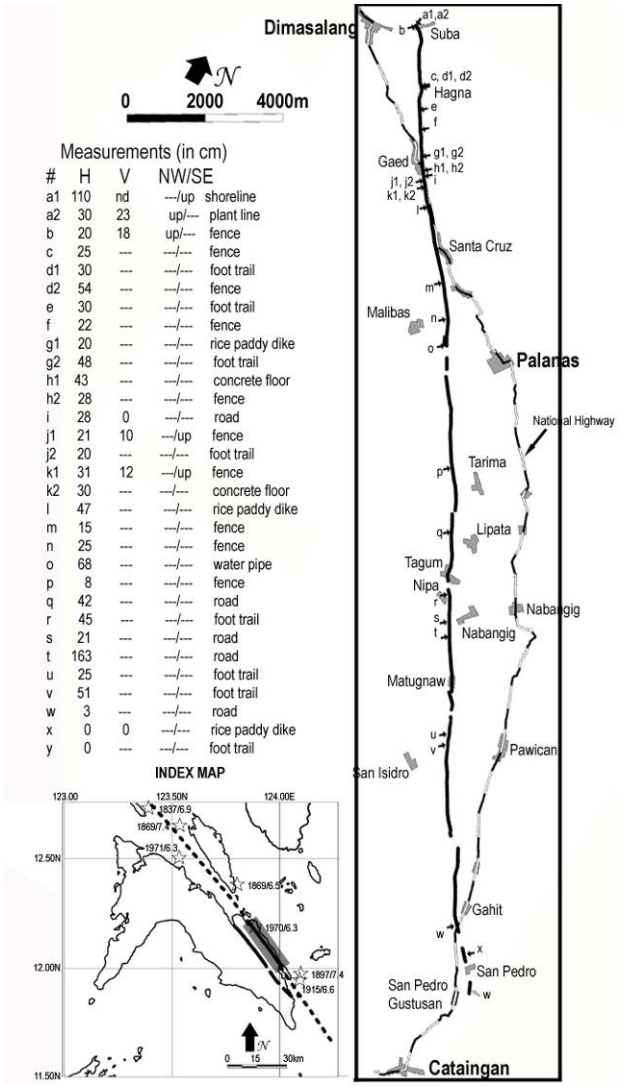

Fig. 3: Map of the ground rupture produced during the 2003 earthquake along the Masbate Fault. Shaded area and stars in the index map are the location of the ground rupture map and the epicenters of historical events in the area, respectively. Small letters in the left table indicate the location of the measured horizontal and vertical displacements along the surface rupture as indicated in the map

Ground rupture related to the 7:0lpm Mainshock - Dimasalang area

In the northernmost portion of Dimasalang, the ground rupture produced during the main shock transected the coastline with apparent left-lateral displacement (Fig. 4). The fault trace is manifested by alternating smooth sand mounds and depressions that eventually were obliterated by waves during high tides and human activities. During low tide, the ground rupture in the shallow portion of Naro Bay was discerned as en echelon faults cutting through the thinly mud-covered dead corals. The en echelon faults are at least a meter in length trending N76^{o}W with a general trend of N62^{o}W. Horizontal displacement measured at this

point was about 80 cm along the shoreline edge with discernable vertical displacement. Some en echelon faults in the deeper portion of the bay about 200 m from the shore were likewise reported by local fishermen.

Fig. 4: Photograph (looking WSW) showing the ground rupture produced along the coastline in Suba, Dimasalang. Note the shoreline that was displaced approximately by 0.8m and the subtle uplift/mound in the foreground of the photo

About 25 m from the shore, the trace can be followed along the N48°W trending fault transecting the sandy beach berm. In the beach terrace, the fault also transected two semi-concrete houses and numerous wooden fences. The wooden fence was displaced horizontally and vertically (northwest block up) by 20cm and 18cm, respectively

- Palanas area

In Sta. Cruz, Palanas, the ground rupture also displaced several man-made structures including semi-concrete to concrete houses, wooden fences, rice paddy dikes and roads and foot trails. Inside one of the gardens, a displaced foot trail (20 cm horizontal displacement) was observed with well-formed mole track. Moreover, a semi-concrete house and a wooden house in the same village were transected by the fault.

Southwards and into Nabangig, Palanas in Sitio Matugnaw, a foot trail was transected by the ground rupture. The trail was horizontally displaced by 45 cm with negligible vertical displacement (site r in Fig. 3). In this area, the en echelon faults have a N60°W trend while the ground rupture is trending N40°W and about 10 cm wide. Across the creek, a small hill is transected by the ground rupture wherein the fault trace is well manifested by right-stepping en echelon fractures and mole tracks with an average length of 150 cm (Fig. 5) located between sites r and s in Fig. 3. Fig. 5 also shows a coconut tree that was transected by one of the en echelon. It was noted that the surrounding geomorphology in Matugnaw area is indicative of a fault saddle. However, since there was no manmade or cultural structure transected, there was no horizontal measurement obtained.

- Cataingan area

Throughout the valley and up to the ridge between Sitio Bogtong and Sito Salag, Pawican of Cataingan municipality, the trace was also observed right-stepping tensional gashes. In Sitio Salag, the trace approaches the upstream area of Nabangig River. The Nabangig River has a very deep gulley and thick vegetation preventing the team to investigate the river vicinities. After crossing the Nabangig River, the trace was found along a pre-existing scarp approximately 150cm high. A fault outcrop was likewise found along the riverbank of Nabangig River.

The fault trace was found again across the asphalt national highway in Gahit, Cataingan about 1km south of Gahit Bridge. Interestingly, this trace widened and became more evident after several weeks. During initial investigation on February 19th, 2003, the surface rupture in this area was just a hairline crack. However, after two weeks the fissure in this road have widened to about 0.8cm along an EW direction with differential horizontal displacement of about 3cm. Moreover, the en echelons became more and apparent along the asphalt road.

Fig. 5: The ground rupture in Matugnaw, Palanas manifested as mole tracks and tensional gashes on grass-covered hill also cutting through the coconut tree.

- Bogtong Island

Based on the projection of the trace from San Pedro, Cataingan municipality, the Island of Bogtong (Fig. 1) was likewise investigated to check the effects of the February 2003 earthquake and the possibility that the ground rupture transects the island.

There was no clear indication of any presence of a fresh ground rupture based on the investigation and accounts by the residents. However, in the eastern side of the island, the limestone hill has a linear flat area. This feature is most probably a fault scarp considering the trend and location of the trace of PFZ in Masbate Island.

DISCUSSION

Based on detailed field mapping, the February 15, 2003 ground rupture has a classic manifestation of left-lateral right-stepping en echelon faults. From Suba in Dimasalang down to San Pedro in Cataingan, ground rupture features are dominantly right-stepping en echelon faults along 34°NNW orientation with well-formed mole tracks in some areas. It has a general trend of N30°W to N60°W that followed the pre-existing active fault trace (with deviation in some places) associated with shear stress and reflective of the type of local materials. Maximum horizontal displacement is 163cm with an average of 40cm. The fissures and ground rupture were obviously wider northwards approaching the epicentral area offshore to the west of Magcaraguit Island. Except for the observed maximum horizontal displacement in Nabangig, the horizontal displacement southeastwards and, the size of each en echelon fractures as well as the width of fault zone from Dimasalang to Cataingan has an apparent decreasing trend. The total length of the mapped onshore ground rupture is approximately 23 km (Fig. 3).

If the distribution of aftershocks would suggest to define the extent of faulting for large earthquakes (Wilson, 1936; Benioff, 1955) as well small events (Buwalda and St. Amand, 1955; Richter, 1955; Brown and Vedder; 1967; McEvilly et al., 1967; Liebermann and Pomeroy, 1970), then the aftershock distribution of the February 2003 event would roughly delineate a rupture length of approximately 54km. More than half of the rupture is apparently offshore.

In terms of the relationship between the length of ground rupture and earthquake magnitude (Bonilla et al., 1984; Wells and Coppersmith, 1994), assuming the February 2003 ground rupture is symmetrical relative to its epicenter, the total ground rupture length would likewise be around 54 km. If such number is considered, the total magnitude for the 2003 event is M7.1 using the empirical relations established by Wells and Coppersmith (1994). This magnitude is much greater than the calculated magnitude both by PHIVOLCS (2003) and USGS (2003) of M6.2. Mapping the ground rupture and correlating it to seismicity evidently show that the Masbate Fault could produce major earthquakes.

Furthermore, through the detailed mapping of the 2003 event, the future ground rupture hazards can be minimized along the Masbate fault, if not be avoided totally. Considering the width of the fault zone, structures to be built in the future is recommended to be constructed at least 2m away from the trace. For high risk and extremely costly structures like nuclear reactors or dams, however, at least 20m should be considered as the setback distance taking into account the observed deviations of the ground rupture from the pre-existing active fault trace.

Acknowledgements: We are indebted to the following institutions and individuals for the coordination, help and support during the mapping activities: The provincial and municipal government of Masbate Island and their constituents. This work was partly supported by the Philippine National Disaster Coordinating Council Calamity Fund 2003 and the Seafloor Geodesy Project of Nagoya University

References

Allen, C.R., (1962). Circum Pacific faulting in the Philippines-Taiwan region, J. Geophys. Res. 85, 3239-3250.

Arante, R.A., Besana, G.M., Dela Cruz, R., Lumbang, R., Maximo, R.P.R., Papiona, K.L., Peñarubia, H., Punongbayan, B.J.T., and Torrevillas, L. (2003). Preliminary Report: 15 February 2003 Masbate Earthquake Investigation. PHIVOLCS Internal Report, 1-9.

Barrier, E., Huchon, P., Aurelio M. (1991). Philippine Fault: A key for Philippine kinematics. Geology, 19, 32-35.

Benioff, H. (1955). Mechanism and strain characteristics of the White Wolf fault as indicated by the aftershock sequence. Bull. 171. Calif. Div. Mines, 199-202.

Besana, G.M. and M. Ando (2005) The central Philippine Fault Zone: location of great earthquakes, slow events, and creep activity. EPS, 57, pp.1-8.

Besana, G.M., Punongbayan, B.J.T., Peñarubia, H., Maximo, R.P.R., Arante, R.A., Papiona, K.L., Torrevillas, L., Dela Cruz, R. and Lumbang, R. (2003). The 15 February 2003 Masbate Earthquake, PHIVOLCS Quick Response Team (QRT) Special Report No.5, 1-28.

Bonilla, M.G., Mark, R.K., and Lienkaemper, J.J. (1984). Statistical relations among earthquake magnitude, surface rupture length, and surface fault displacement. Bull. Seis. Soc. Am., 74, 2379-2411.

Brown, R.D., Jr. and Vedder, J.G. (1967). The Parkfield-Cholame, California earthquakes of June-August 1966; surface tectonic fractures along the San Andreas fault, U.S. Geol. Survey Prof. Paper 579 pages.

Buwalda, J.P. and St. Amand, P. (1955). Geological effects of the Arvin-Tehachapi earthquake, Bull. 171, Calif. State Div. Mines, 41-56.

Fitch, T.J. (1972). Plate convergence, transcurrent faults and internal deformation adjacent to Southeast Asia and the Western Pacific. Jour. Geophys. Res. 77, 23, 4432-4460.

Liebermann, R.B. and Pomeroy, P.W. (1970). Source dimensions of small earthquakes as determined from the size of the aftershock zone.

McEvilly, T.V., Bakun, W.H. and Casaday, K.B. (1967). The Parkfield, California earthquake of 1966. Bull. Seis. Soc. Am., 57. 1221-1244.

PHIVOLCS (1999). Historical Earthquakes in the Philippines, PHIVOLCS, Quezon City, 1:5,000,000 map.

PHIVOLCS (2000). Distribution of active faults and trenches in the Philippines, Active Faults Mapping Group, PHIVOLCS, Quezon City, 1:2,000,000 map.

PHIVOLCS (2003). Preliminary earthquake bulletin no. 2, PHIVOLCS, Quezon City, 1.

Rowlett, H. and Kelleher, J.A. (1976). Evolving seismic and tectonic patterns along the Western margin of the Philippine Sea Plate, Jour. Geophys. Res., 81, 3518-3524.

Wells, D.L. and Coppersmith, K.J. (1994). New empirical relations among magnitude, rupture length, rupture area, and surface displacement. Bull. Seis. Soc. Am., 84, 974-1002.

Wessel, P., and W.H.F. Smith (1998). New, improved version of generic mapping tools released, EOS Trans. AGU 79(47), 579, 1998.

Willis, B. (1937). Geologic observation in the Philippine archipelago, Nat. Resources Council Bull. Manila, Philippines, 13.

Wilson, J.T. (1936). Foreshocks and aftershocks of the Nevada earthquake of December 20, 1932, and the Parkfield earthquake of June, 1934. Bull. Seis. Soc. Am., 26, 189-194.

SIMULATED GROUND MOTIONS OF THE MAY 12 2008, WENCHUAN (CHINA) EARTHQUAKE – COMPARISON WITH DAMAGE DISTRIBUTION

L. W. Bjerrum (1), M.B. Sørensen (2) and K. Atakan (1)

(1) Department of Earth Science, University of Bergen, Allegaten 41A, NO-5007 Bergen, NORWAY. louise.bjerrum@geo.uib.no, kuvvet.atakan@geo.uib.no

(2) Helmholtz Centre Potsdam GFZ German Research Centre for Geosciences, Public Law Foundation State of Brandenburg, Telegrafenberg, D-14473 Potsdam, GERMANY. sorensen@gfz-potsdam.de

Abstract: *The May 12, 2008 Wenchuan earthquake had its epicenter along the Longmenshan Fold and Thrust Belt (LFTB) and ruptured along an approximately 300 km long thrust fault. There is applied a broadband frequency (0.1-10 Hz) hybrid strong ground motion simulation technique, combining deterministic low-frequency and semi-stochastic high-frequency simulation, in order to assess the contributions of the strong ground shaking in the resulting destruction. The simulated ground motion distributions have been calibrated by the actual strong motion records from the Wenchuan earthquake at short distances. Comparisons with the damage distribution from reconnaissance field observations confirms the fault rupture complexity in the resulting ground motion distributions which also control to a large extent the damage distribution. The applied simulation methodology provides a promising platform for predictive studies.*

Key words*: Ground motion simulation, Wenchuan, earthquake damage.*

INTRODUCTION

The large Wenchuan earthquake of 12 May 2008 (M=8.0) in central China had disastrous consequences and caused at least 69,195 casualties, injured 374,177 and 18,392 are still missing (presumed dead) as of May 2009 (USGS). The earthquake occurred along the Longmenshan Fold and Thrust Belt (LFTB). Earthquake of this size has previously not been associated with the LFTB, and the area was in the seismic zonation map of China classified as intensity VII zone (Zhao et al., 2009). The LFTB results from the deformation of the Tibetan Plateau, which is situated between the northward moving Indian plate (4 cm/yr) and the stable Eurasian plate. The collision of the Indian plate results in eastward escape of the Tibetan Plateau. This motion is accommodated along large east-west oriented strike-slip systems as the Kunlun fault in the north and the Xianshuihe fault in the south. The LFTB marks the eastern termination of the actively deforming Tibetan Plateau and represents the boundary from the 65 km thick weak crust in the Tibetan Plateau to the thinner, 35 km, strong crust under the Sichuan Basin. Across the LFTB the eastward motion of the Tibetan Plateau decreases from 14 mm/yr on the western side of the fault to 10 mm/yr on the eastern side in the Sichuan Basin. This differential motion results in compressional stresses of a rate of 4 mm/yr across the fault belt, and it is this motion which reactivates the faults, as observed during the May 12, 2008 earthquake.

In this study we have simulated the ground motion during the Wenchuan earthquake, following the approach of Pulido and Kubo, (2004), Pulido et al., (2004), Sørensen et al., (2007). The low frequency ground motion simulations are based on deterministic wave propagation from an asperity model in a flat layered velocity structure (Bouchon, 1981), while the high frequency ground motions are calculated from a semi-stochastic simulations, also based on an asperity model. For the high-frequencies the stochastic methodology of Boore (1983) is combined with the empirical Green's function method of Irikura (1986). In order to get a smooth transition from the low to the high frequency domain, a frequency-dependent radiation pattern is applied (Pulido and Kubo, 2004). Finally, the different contributions are summed. All calculations are done for bedrock conditions, and site effects are therefore not considered in this study.

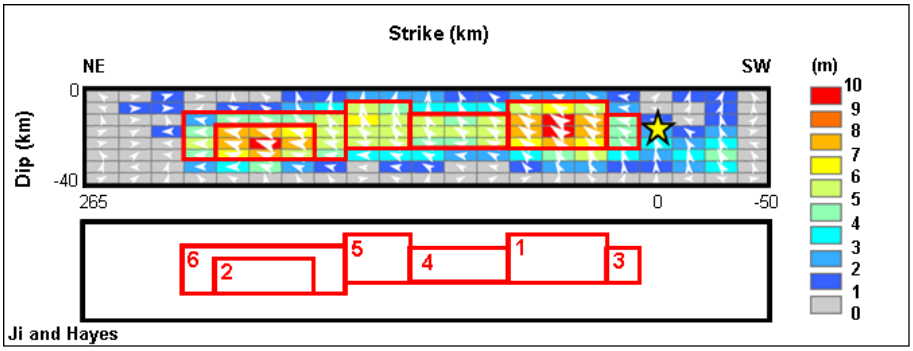

Fig. 1: Input source model, modified from Ji and Hayes (2008). The black box outlines the rupturing fault for which the ground motion simulations are computed and the red boxes outline the asperities. Asperity 1 and 2 are high-slip asperities, while the asperities 3-6 are intermediate-slip asperities.

Table 1: Source parameters used in the ground motion simulations. Stress drop is divided to the asperities following Pulido et al. (2004), rise time and rupture velocity is taken from Koketsu et al (2009) and Nishimura and Yagi (2008), respectively.

Seismic moment		$1.15 \cdot 10^{21}$ N/m
Epicenter		103.30°E/31.1°N
Foc. Mech.	Southern segment	229°/33°/115°
	Northern segment	229°/65°/180°
Average stress drop		3 MPa
Asperity stress drop (high slip)		14.5 MPa
Asperity stress-drop (interm. slip)		8 MPa
Rise time		2.0 ± 0.5 sec
Rupture velocity		2.8 ± 0.4 sec
f_{max}		10 Hz
High frequency attenuation, Q		$100\ f^{0.8}$

In order to model an earthquake scenario the source needs to be defined in terms of geometry and geographical location, rise time, rupture velocity, stress drop and seismic moment. Furthermore, the velocity structure model and the crustal attenuation need to be defined. Asperity location on the fault plane is defined from a finite fault slip model, in the present study the model by Ji and Hayes (2008) has been adopted. This model yields thrust mechanism along the southern segment, whereas a modelled strike-slip movement is in the northern part of the fault. We have included this as different focal mechanisms for each segment. The asperity model is shown in Fig. 1 and the input parameters for the simulation are summarized in Table 1.

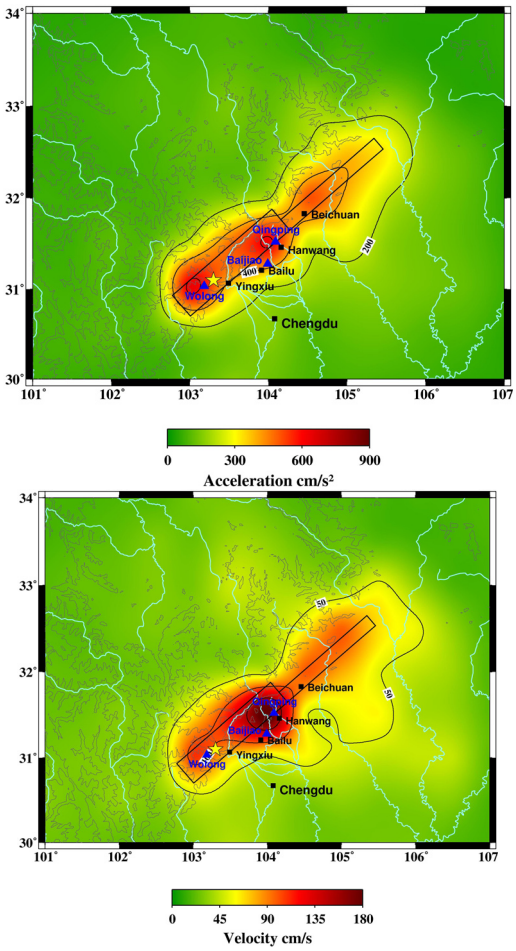

Fig.2: Simulated PGA (top) and PGV (bottom) distributions in the study area. Black boxes indicate the extent of the surface projection of the fault area. The star shows the epicenter, blue triangles indicate three stations; Wolong, Baijiao and Qingping. The black squares mark cities along the fault.

SIMULATION RESULTS AND DISCUSSION

In the ground motion simulation, waveforms are calculated for simulation points across the study area. From these the peak ground motions (PGA and PGV) are retrieved to get an insight of the distribution and extent of the strong ground shaking. PGA and PGV distributions are shown in Fig. 2. It is clear that the strongest ground shaking occurs across the rupturing fault plane, with the largest ground motions associated with the southernmost segment of the fault plane. PGA values reach up to 850 cm/s2 near the epicenter area, similarly for PGV for which values of almost 200 cm/s is predicted. In Fig. 2b, it is seen that the PGV distribution is stretching further north and east of the fault plane than towards south and west. This is probably due to the rupture directivity effect, having an unilateral rupture towards north, and the rupture being of thrust motion in the southern segment, and strike-slip motion along on the northern part of the fault.

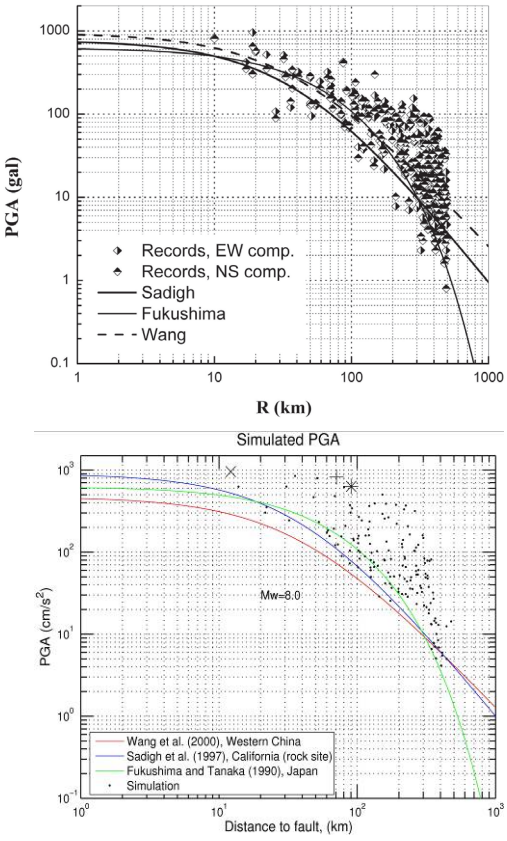

*Fig. 3: Top: Recorded seismic data compared to empirical attenuation relationships (see legend in figure), from Li et al., 2008a. Bottom: Comparison of simulated PGA (black dots) to ground motions predicted by empicical attenuation relations (see legend in figure). The X, + and * show the recorded peak values for Wolong, Baijiao and Qingping, respectively is shown.*

The attenuation of the recorded seismic data is shown in Fig. 3. It is clear that the recorded ground motions gives much higher peak ground acceleration values, than what is predicted by the empirical attenuation relationships. The largest ground motions were recorded by the three near fault stations Wolong, Qingping and Baijiao, which recorded maximum values of 957.7, 824.1 and 633.1 cm/s^2, respectively (Li et al., 2008b). The attenuation of the simulated ground motions found in the present study is shown as the lower graph in Fig. 3. From this it can be seen, that the simulated peak acceleration values are comparable to those recorded during the earthquake.

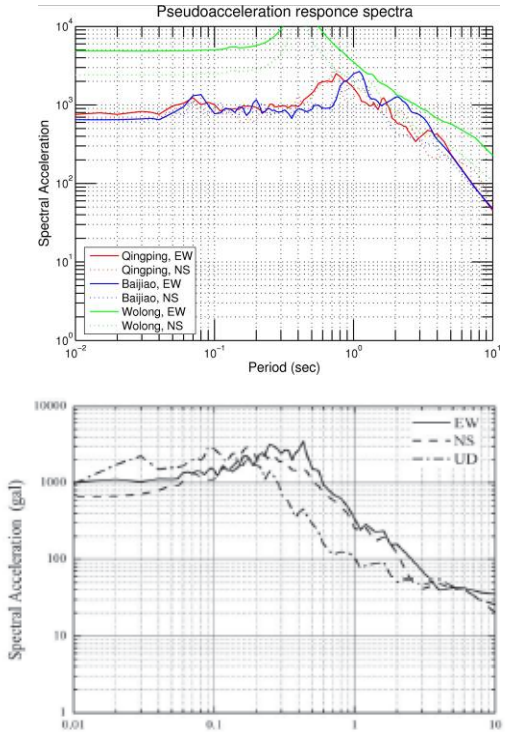

Fig.4: Top: Simulated Pseudoacceleration response spectra for the three stations Qingping, Baijiao and Wolong. The two horizontal components are shown (see legend for specifications). Bottom: Acceleration response spectra obtained from Wolong station in Wenchuan during the mainshock of 12 May 2008, form Li et al., (2008a).

Fig. 4 shows the pseudoacceleration response spectra, from the ground motion simulation, for the stations in Wolong, Qingping and Baijiao (see Fig. 2 for locations). Tthe predominant periods of the simulated ground motions are between 0.1s and 1s. The simulation results are well in agreement with Li et al. (2008a), which estimate the predominant spectral acceleration to be distributed between periods of 0.1s to 0.6s (see the lower graph in Fig. 4) and the ground motion simulation therefore reproduces the frequency content of the seismic waves to a very large extent.

STRONG GROUND SHAKING AND DAMAGE ON BUILDINGS

The affected area suffered severe destruction during the earthquake. The economic losses due to the event are estimated to be 86 billion USD (USGS). The city of Hanwang is located along the fault, approximately 90km NE of the epicentre and had 70,000 inhabitants before the earthquake. During the earthquake 4,500 have lost their lives. In an area of approximately 3km^2 in the central part of Hanwang, 90-95% of the buildings were totally or partially collapsed, resulting in a large uninhabitable area. The picture in Fig. 5 is taken in the area of almost total collapse. The typical buildings in this area are residential buildings of 4-5 stories. In the foreground, rubble from totally collapsed buildings is visible, whereas the buildings in the background are still standing. In this area the adobe structures have almost completely collapsed, whereas the more recent reinforced concrete structures seem to have been able to withstand the strong ground shaking.

Fig.5: Picture taken in Hanwang, inside the 3km^2 area of almost total collapse.

Using a simple empirical relation for fundamental periods of structures (Kramer, 1996), for the typical structures dominating the area in Hanwang, the predominant periods are estimated to be 0.16-0.21s for two story buildings. The first floor is usually used as a shop and the second floor as living area. For five-story apartment buildings on the other hand, the fundamental frequency is estimated to be 0.47-0.56s. Comparing the fundamental periods of the structures in the area to the predominant periods of the seismic signals coincide to a large extent, which is the reason why these buildings have not been able to withstand the ground motion experienced in the area. Furthermore, the older buildings suffered from an insufficient design code, since there have been many revisions of the seismic design code for buildings in China during time, latest in 2001 (Zhao et al., in press). The buildings which are still standing in the area (e.g. like the buildings to the left in the picture) were under construction at the time of the earthquake, and they are assumed to be designed after the latest adequate seismic design code.

CONCLUSIONS

In the present study we have used a hybrid broadband technique for modeling ground motions caused by the May 12, 2008 Wenchuan earthquake. The following conclusions can be drawn from the simulation results:

- The ground motions experienced during the May 12 Wenchuan earthquake were reproduced, and values similar to those recorded on the near field stations in the area, with maximum bedrock ground motions in the order of 850 cm/s2 (PGA) and 200 cm/s (PGV), were obtained.
- The values of the simulated PGA are higher than predicted commonly by empirical attenuation

relations. However, the attenuation of our simulated ground motions agrees very well with the recorded seismic data from the area.
- The predominant periods of the pseudoacceleration response spectra corresponds to predominant periods estimated from the seismic data.
- The predominant periods of the seismic signal corresponded to the fundamental periods of the structures in the area, causing total or partial collapse.

In general the hybrid broadband simulation technique has proven to be a powerful tool for simulating realistic and reasonable ground motions in this retrospect study. The method is therefore useful for predictive studies as long as realistic input models constructed with geological and paleoseismic data are applied.

Acknowledgements: We would like to thank the Earthquake Administration of Sichuan Province, Sichuan Provincial Department of Construction and Sichuan Association for Science & Technology who co-sponsored the post-conference field trip of the 14th World Conference on Earthquake Engineering to the Wenchuan Earthquake Area. We are grateful to the staff from China Earthquake Administration, Earthquake Administration of Sichuan Province, China Southwest Architectural Design and Institute Corp. Ltd., Sichuan Provincial Institute of Architectural Design, Sichuan Association for Science and Technology, Sichuan Provincial People's Hospital and the translators which made this trip possible.

References

Boore, D.M., 1983, Stocastic simulation of high-frequency ground motions based on seismological models of the radiated spectra: Bulletin of the Seismological Society of America, v. 73, p. 1865-1894.

Bouchon, M., 1981, A simple method to calculate Green's functions for elastic layered media: Bulletin of the Seismological Society of America, v. 71, p. 959-971.

Fukushima, Y., and Tanaka, T., 1990, A new attenuation relation for peak horizontal acceleration of strong earthquake ground motions in Japan: Bulletin of Seismological Society of America, v. 80, p. 27.

Irikura, K., 1986, Prediction of strong acceleration motion using empirical Green's functions, Proc. 7th Japan Earthquake Symp.: Japan, p. 151-156.

Ji, C., and Hayes, G., 2008, Source model of the May 12th 2008 Wenchuan earthquake. Available at: http://earthquake.usgs.gov/eqcenter/eqarchives/poster/2008/20080512.php, Volume 2008, USGS.

Koketsu, K., Yokota, Y., Ghasemi, H., Hikima, K., Miyake, H., and Wang, Z., 2009, Source Process and Ground Motions of the 2008 Wenchuan Earthquake: Investigation report of the 2008 Wenchuan Earthquake, China, Grant-in-Aid for Special Purposes of 2008, MEXT, .

Kramer, S.L., 1996, Geotechnical Earthquake Engineering: Upper Sadle River, New Jersey, Prentice Hall.

Li, X., Zhou, Z., Huang, M., Wen, R., Yu, H., Lu, D., Zhou, Y., and Cui, J., 2008a, Preliminary Analysis of Strong-Motion Recordings from the Magnitude 8.0 Wenchuan, China, Earthquake of 12 May 2008: Seismological Research Letters, v. 79, p. 11.

Li, X., Zhou, Z., Yu, H., Wen, R., Lu, D., Huang, M., Zhou, Y., and Cu, J., 2008b, Strong motion observations and recordings from the great Wenchuan Earthquake: Earthquake Engineering and Engineering Vibration, v. 7, p. 12.

Nishimura, N., and Yagi, Y., 2008, Rupture Process for May 12, 2008 Sichuan Earthquake (Ver. 2), http://www.geol.tsukuba.ac.jp/~nisimura/20080512/, Volume 2008: Ibaraki, Japan University of Tsukuba.

Pulido, N., and Kubo, T., 2004, Near-fault strong motion complexity of the 2000 Tottori earthquake (Japan) from a broadband source asperity model: Tectonophysics, v. 390, p. 177-192.

Pulido, N., Ojeda, A., Atakan, A., and Kubo, T., 2004, Strong ground motion estimation in the Sea of Marmara region (Turkey) based on a scenario earthquake: Tectonophysics, v. 391, p. 357-374.

Sadigh, K., Chang, C.-Y., Egan, J.A., Makdisi, F., and Youngs, R.R., 1997, Attenuation Relationships for Shallow Crustal Earthquakes Based on California Strong Motion Data: Seismological Research Letters, v. 68, p. 10.

Sørensen, M.B., Atakan, K., and Pulido, N., 2007, Simulated Strong Ground Motions for the Great M 9.3 Sumatra-Andaman Earthquake of 26 December 2004: Bulletin of the Seismological Society of America, v. 97, p. S139-151.

USGS, Magnitude 7.9 – Eastern Sichuan, China. Webpage, last accessed July 1, 2009. http://earthquake.usgs.gov/eqcenter/eqinthenews/2008/us2008ryan/#summary.

Wang, S.Y., Yu, Y.X., Gao, A.J., and Yan, X.J., 2000, Development of attenuation relations for ground motion in China: Earthquake Research in China, v. 16, p. 8.

Zhao, B., Taucer, F., and Rossetto, T., 2009, Field investigation on the performance of building structures during the 12 May 2008 Wenchuan earthquake in China: Engineering Structures, v. In press.

DATING PALEO-SEISMIC ACTIVITY ON THE CARMEL FAULT DURING THE QUATERNARY, MT. CARMEL, ISRAEL

Braun, Y. (1, 2), Bar-Matthews, M. (2), Ayalon, A. (2), Kagan, E.(1,2) and Agnon, A. (1)

(1) Institute of Earth Sciences, The Hebrew University of Jerusalem, 91904, ISRAEL. yael.braun@mail.huji.ac.il
(2) Geological Survey of Israel, 30 Malkhe Israel St., Jerusalem 95501, ISRAEL.

***Abstract**: Mt. Carmel in northern Israel, a continental uplift ca. 500 m above sea level, is defined by a NW-NNW fault, a branch of the Dead Sea Transform System (DST). The Carmel fault (CF) is observed as a wide zone of deformation about which very little is known concerning the extent of seismic activity during the Quaternary. During the past 3 decades some 47 earthquakes (M>2) occurred along this fault zone with the strongest recorded in 1984 (M = 5.3). Using accurate 230Th/234U ages of collapsed speleothems, we reconstructed seismic activity in Denya Cave, Haifa. During the last 80 ka, 5 age clusters are recognized, separated by periods of quiescence (of an order of 10 millennia). The last cluster appears ca. 11 ka, whilst indications for some younger activity remain to be confirmed.*

***Key words**: earthquakes, paleoseismology, speleothem, seismite*

INTRODUCTION

Mt. Carmel in the north of Israel, a manifestation of tectonic movements, is a continental uplift of more than 500m above sea level. This uplift is defined by the NW to NNW Carmel Fault (CF), a branch of the left-lateral Dead Sea Transform (DST). The DST lies between Arabia and the Sinai-Levant Block (Fig. 1) and exhibits a slip rate of 5.0±1.5 mm/yr (LeBeon et al., 2008). The CF, which continues into the Mediterranean continental shelf (Hofstetter et al., 1989), is observed as a wide zone of deformation rather than a single fault trace (Rotstein et al., 1993).

The CF along with the Gilboa Fault (GF), combine to create a seismically active zone stretching for approximately 130km (Hofstetter et al., 1996; Fig. 2). On August 24, 1984 an earthquake along the CF (of a magnitude {ML} of 5.3) caused slight damage in Haifa and nearby towns (all seismic data derived from the Geophysical Institute of Israel: http://www.seis.mni.gov.il/html/seis/seis_search.html).
This earthquake aroused much interest since very little was known concerning the extent of seismic activity around Mt. Carmel. This seismic event further emphasized the need to understand the tectonic regime of a densely populated and industrialized area. Scholars (Hofstetter et al.1996) also presented data on a series of ca. 550 earthquakes (1.0 ≤ M L≤ 5.3) monitored along the CF during the decade between 1984 and 1994.

Attempts to understand the tectonic regime of a seismically active area necessitate paleoseismic research. Karstic caves can preserve paleoseismic evidence, which can provide fundamental elements for seismotectonic knowledge, seismogenic descriptions and consequently, the evaluation of seismic hazards in an area.

Broken or deformed cave deposits (speleo-seismites) can be used for paleoseismic research since they can be dated with radiometric techniques (e.g. Davenport, 1998; Lacave et al., 2004; Kagan et al., 2005). Thus, they contribute to an earthquake data base as an independent source of information on major earthquake recurrences (Kagan et al., 2005).
The U-Th method, which has a 350 to 500 ka limit, can vastly increase the length of the seismic record during the Quaternary by enabling us to date the time between a break on a speleothem and its regrowth.

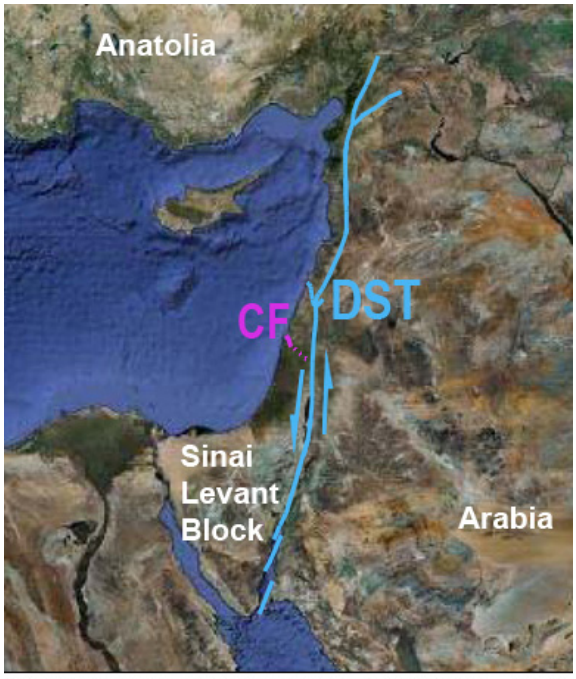

Fig. 1: A regional map showing the setting of DST separating ARABIA from Sinai-Levant Block.

Scholars (e.g. Becker et al., 2005; 2006; Kagan et al., 2005) have proposed that a fundamental aspect of a concise earthquake catalogue is based on a multi-archival approach, which not only enables confirmation of each of the separate findings, but allows for better understanding of the spatial influence of earthquakes on different geological environments and their connections to tectonic settings of a region. Paleoseismic research in Israel,

mostly concentrated on the DST in Israel, is based on many independent sources such as historical and archaeological evidence and geomorphological and geological findings (e.g. Amiran et al., 1994; Marco et al., 1996; Ellenblum et al., 1998; Enzel et al., 2000; Begin et al., 2005; Agnon et al. 2006).

The Carmel region, only cursorily studied, has some karstic caves that offer opportunities for a paleoseismological study of the fault system that defines it, enabling a further enlargement of the limited paleoseismic data base currently available, and perhaps a better understanding of it. The present study offers the possibility of extending the earthquake catalogue for the CF, although it might be limited only to major earthquakes.

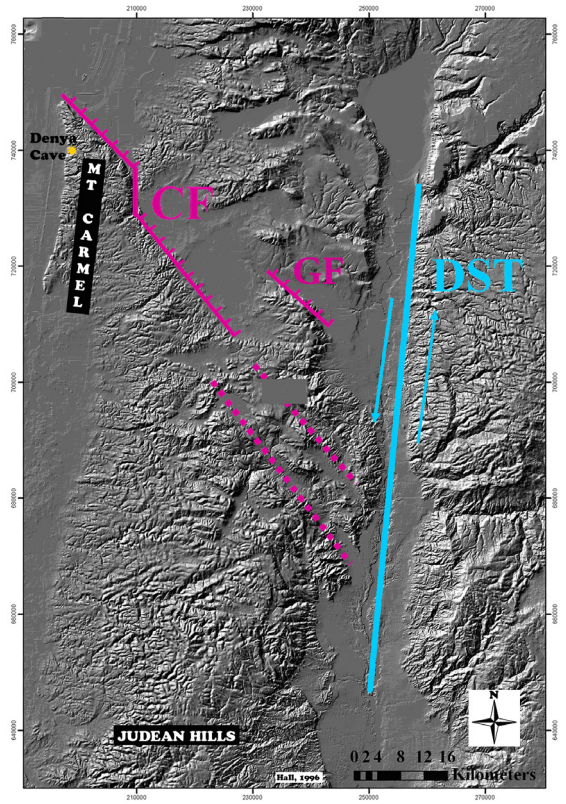

Fig. 2: A DEM map of Northern Israel (Hall, 1996) showing the connection between the CF and the DST, modified from Salamon et al. (2003).

DENYA CAVE AS A KEY PALEOSEISMIC SITE

Denya Cave, located on Mt. Carmel within the Haifa City limits (Fig. 2), is an accessible karstic cave with ideal conditions for studying paleoseismic activity. Located only a few kilometres from the CF, the cave's geological features may have recorded major earthquakes from the DST and perhaps even minor earthquakes from the CF.

METHODS

Following the work of Kagan et al. (2005) in the Judean Hills, which provided ages consistent with independent evidence for strong DST earthquakes, similar kinds of research techniques are applied toDenya Cave in order to examine paleoseismic activity on the CF. The wealth of evidence on the DST contributes to credibility of the findings of Kagan et al (2005). By contrast, paleoseismic evidence on the CF for the Quaternary is virtually non existent. In the case of the CF it is assumed the success of the study by Kagan et al. (2005) would enable us to reconstruct earthquake data for the Carmel region using the same methods.

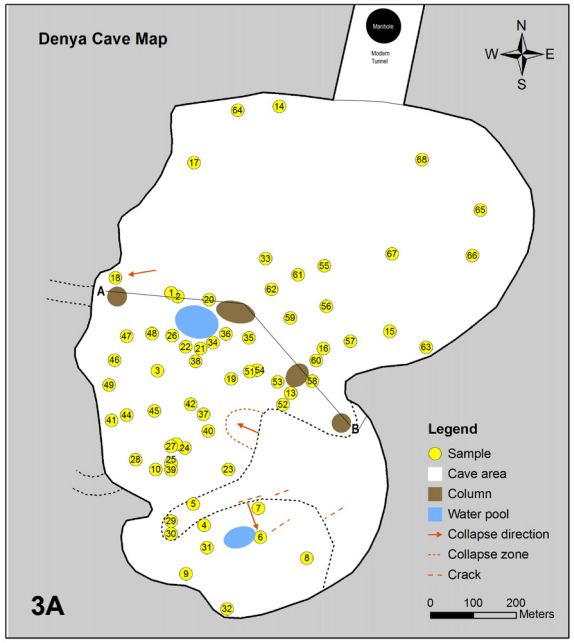

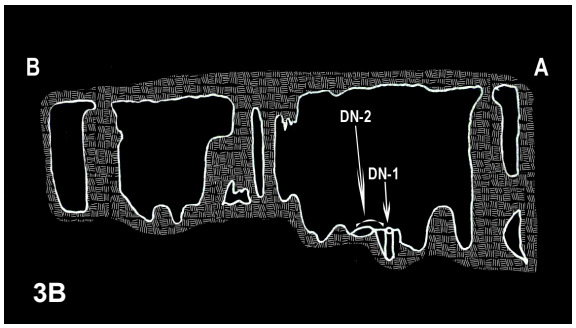

Fig. 3: Denya Cave: A) Plan of Denya Cave upper chamber at approximately floor level. B) Ilustration of section A-B (seen in Fig. 3A). Drawn lines mark broken speleothem formations. C) Picture of cracks in the lower chamber of Denya Cave. Note the speleothems forming below the crack.

Prior to the present study all evidence of non-seismic activity, which could affect results, had to be discounted. Intensive study of the paleoclimate, the geology of the cave and its hyrdrogeological setting, allowed us to exclude evidence for damage from numerous sources. They include anthropogenic activity, ice creep, underground glaciers, frost action, erosion, soil creep, effects of water circulation, flooding, debris flow, incations caused by non-earthquake related activity and slope movements (Becker et al., 2006).

The cave is ca. 50m2 in area and divided into two chambers. In an upper chamber speleothems are abundant. For this chamber a plan was made in order to document sample location (Fig. 3A). Throughout this chamber evidence of collapses is visible in broken speleothems (Fig. 3B), fallen stones and a fallen segment of its wall. In the lower chamber chalk and cherts are exposed, while only few speleothems are found, and those are predominantly below cracks (Fig. 3C).

DATING OF BROKEN SPELEOTHEMS

Broken speleothem samples were collected from all parts of the upper chamber of the cave (yellow markers in Fig. 3). The samples consist of broken stalagmites and stalactites and flowstone cores drilled from the cave floor exposing fallen and embedded speleothems. For each seismite sample a seismic contact (i.e. the precise location at which the laminae of the speleothems are broken. See Fig. 4) was established and the closest laminae to each contact were sampled with a small drill. The last lamina which grew before the break event was termed a pre-seismic sample, while the first one to grow after the break event was termed a post-seismic sample (Fig. 4).

In this study, dating with the U-Th method was conducted on the Multiple Collector Inductively Coupled Plasma Mass Spectrometer (MC-ICP-MS) at the Geological Survey of Israel. The MC-ICP-MS produces high analytical precision results and enables work on small samples (ca. 0.3g) that, due to an ability to sample individual laminae, give ages at high resolutions. The ages found for Denya Cave were calculated as single samples using the age equation according to Broecker and Kaufman (1965).

Ages determined for seismite samples were seen to form clusters at very specific time intervals. Since some samples had high detrital content, their ages had to be corrected (Kaufman et al., 1998). In order to correct for detrital Th, the samples were divided according to the age groupings and plotted on a three dimensional isochron where x=230Th/238U, y=234U/238U and z=232Th/238U (Ludwig and Titterington, 1994), using the Isoplot3.7 program. Ongoing research indicates that those clusters, when falling on a reasonably accurate three dimensional isochron plot, are considered to be groupings of a single age indicating one seismic event.

RESULTS

A total of 68 speleothem samples was taken and inspected from Denya Cave, 32 of which were broken and thus, identified as likely to indicate seismic activity. Some of those samples had more than one seismite (i.e. a record of a single seismic event). The ages obtained from those seismites vary greatly. They indicate seismic activity during the last 350 ka; older samples are in secular equilibrium and cannot be further dated.

A seismic event is associated with the age clusters, but only when seismites appear to be sound indicators of a physical break in the speleothems examined and when there are pre- and post-seismic event samples in the same cluster. Results further show that during the last 80 ka at least five seismic events occurred, causing damage to speleothems in Denya cave (~11, 22, 28, 37 and 55 ka). Indicators for an event at ~5 ka were also found, but they are not strongly substantiated by the types of seismites representing them. Indicators for older events that affected the cave were found, but due to the relatively large error on these ages, we could not identify clusters.

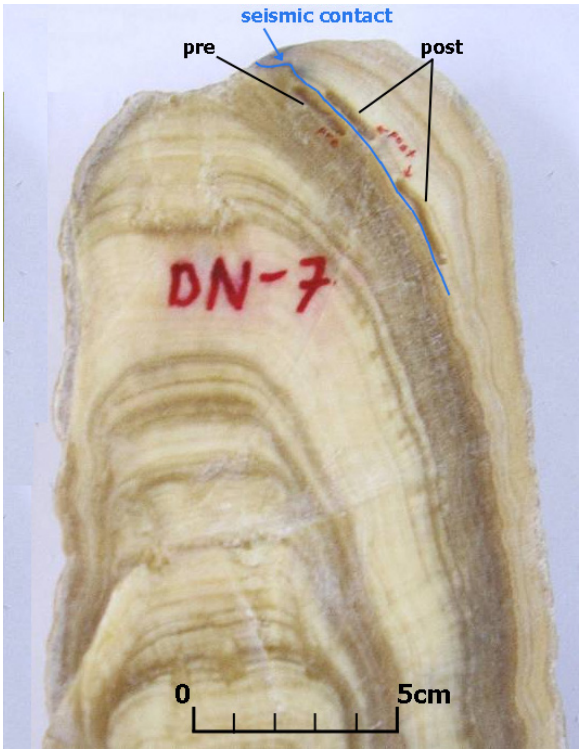

Fig. 4: A seismite from Denya Cave, sample DN-7

CONCLUSIONS

The dating of speleothems using the U-Th method, combined with their subsequent correction for detrital Th, employing the three dimensional isochron plots, represents a new approach to identifying seismic events in the Quaternary. This research in Denya Cave, Mt Carmel, Haifa, indicates that speleothems there recorded five seismic events that caused damage to the cave during the last 80 ka. The latest such event occurred between 11 and 10 ka. Yet another, younger event, at ~5 ka may also have taken place, but additional evidence is necessary to validate that observation.

Acknowledgements: This research was funded by the Israel Science Foundation, Grant no. 1006/2004 to A. Agnon. The authors wish to thank M. Stein, G. Hartman, A. Vaks, and T. Zilberman for useful discussions. All the staff of the Geological Survey of Israel who helped with all technical matters: S. Ashkenazi, Y. Mizrachi, C. Hemo, N. Tapliakov, I. Segal and O. Yoffe. L. Magagritz, M. Laskow, E. Braun, M. Kanari, U. Ryb for

continuous support. N. Shalev, G. Gerber, Y. Burstein, N. Shcheny, Y. Noymaer, E. Merder have contributed labour and effort to the success of this research.

References

Agnon, A., Migowski, C., Marco, S., (2006), Intraclast breccias in laminated sequences reviewed: Recorders of paleo-earthquakes. Special Paper- Geo. S. of A., 401, 195-214. New frontiers in Dead Sea paleoenvironmental research.

Amiran, D.H.K., Arieh, E. and Turcotte, T. (1994), Earthquakes in Israel and Adjacent Areas: Macroseismic Observations since 100 B.C.E. Israel Explor. Jour. 44, 260-305.

Becker, A., Davenport, C.A., Eichenberger, U., Gilli, E., Jeannin, P.Y. and Lacave, C. (2006), Speleosismology: A critical perspective. J. Seismol. 10, 371-388.

Becker, A., Ferry, M., Moneck, K., Schnellmann, M. and Giardini, D. (2005), Multiarchive paleoseismic record of late Pleistocene and Holocene strong earthquakes in Switzerland. Tectonophys. 400, 153-177.

Begin, Z.B., Steinberg, D.M., Ichinose, G.A. and Marco, S. (2005), A 40,000yr unchanging seismic regime in the Dead Sea rift. Geology, 33, 257-260.

Broecker, W.S. and Kaufman, A., (1965) Radiocarbon chronology of Lake Lahontan and Lake Bonneville II, Great Basin, Geol. Soc. Amer. Bull. 76, 537–566.

Davenport, C.A., (1998), Karst as a record of Paleoseismicity. Y. Quinif (Ed), Karst and Tectonics. Contributions to the international symposium on Karst and Tectonics. Relations between Tectonics, Karst and Earthquakes, Speleochrons hors-serie, pp. 41-44.

Ellenblum, R., Marco, S., Agnon, A., Rockwell, T. and Boas, A., (1998), A crusader castle torn apart by the earthquake of dawn, 20 May 1202. Geology, 26, 303-306.

Enzel, Y., Kadan, G. and Eyal, Y., (2000), Holocene earthquakes inferred from a fan delta sequence in the Dead Sea graben. Quat. Res. 53, 1, 34-48.

Hofstetter, A., Ron, H., and van Eck, T., (1989), Mt. Carmel Earthquake Sequence. Seismol. Div. Inst. Petrol. Res. Geophys, Holon, Israel 303/1829/88 (1).

Hofstetter, A., van Eck, T. and Shapira, A., (1996), Seismic activity along fault branches of the Dead Sea-Jordan transform system: The Carmel-Tirza Fault system. Tectonophys. 267, 317-330.

Kaufman, A., Wasserburg, G.J., Porcelli, D., Bar-Matthews, M., Ayalon, A. and Halitcz, L. (1998), U-Th isotope systematics from the Soreq Cave, Israel and climatic correlations. Earth and Planetary Sci. Let., 156, 141-155.

Kagan, E.J., Agnon, A., Bar-Matthews, M. and Ayalon, A., (2005), Dating large infrequent earthquakes by damaged cave deposits. Geology, 33, (4), 261-264.

Lacave, C. Koller, M.G. and Eozcue, J.J. (2004), What can be concluded about seismic history from broken speleothems? J. Earthquake Engineering, 8(3), 431-455.

Maryline Le Beon, Yann Klinger, Abdel Qader Amrat, Amotz Agnon, Louis Dorbath, Gidon Baer, Jean-Claude Ruegg, Olivier Charade and Omar Mayyas, (2008), Slip rate and locking depth from GPS profiles across the southern Dead Sea Transform. J. Geophys. Res., 113, B11403, doi:10.1029/2007JB005280

Ludwig, K.R. and Titterington, D.M. (1994), Calculation of 230Th/U isochrones, ages and errors. Geochimica et Cosmochimica Acta. 58 (22), 5031-5042.

Marco, S., Stein, M., Agnon, A. and Ron, H. (1996), Long-term earthquake clustering: A 50,000 year paleoseismic record in the Dead Sea Graben. J. Geophys. Res., 101, 6179-6191.

Rotstein, Y., Bruner, I. and Kafri, U., (1993), High-resolution seismic imaging of the CF and its implications for the structure of Mt. Carmel. Isr. J. Earth Sci., 42, 55-69.

Salamon, A., Hofstetter, A., Garfunkel, Z. and Ron, H. (2003) Seismotectonics of the Sinai subplate-The eastern Mediterranean region. Geoph. J. Int., 155, 149-173.

A RARE CASE OF PRESERVED EARTHQUAKE RUPTURES IN AN ARCHAEOLOGICAL SITE: MIKRI DOXIPARA – ZONI, NE GREECE

A. Chatzipetros (1) and S. Pavlides (1)

(1) Department of Geology, Aristotle University, 54124, Thessaloniki, GREECE. ac@auth.gr

Abstract: *This abstract describes the results of an archaeoseismological / palaeoseismological research at the site of Mikri Doxipara – Zoni (NE Greece). Faulted layers, surface ruptures, displaced structures, fissures etc. indicate that this site has undergone severe deformation during at least two large, ground rupturing earthquakes. Radiocarbon dating and detailed log analysis suggest that these two earthquakes probably happened in 1752 (Edirne earthquake) and after 960 ± 50 BC. Both earthquakes produced vertical displacement in the order of 0.9-1 m, therefore their magnitude is estimated at ca. 6.5. This site is unique in the sense that faulting is directly correlated to archaeological deformation.*

Key words*: archaeoseismology, palaeoseismology, surface ruptures, Greece*

INTRODUCTION – SETTING

Mikri Doxipara – Zoni excavation site (MDZ) is a Roman burial site located in the low seismicity Evros region (NW Greece), very close to the Greek-Bulgarian-Turkish borders (Fig. 1).

Fig. 1: Location map of Mikri Doxipara – Zoni site in NE Greece. It is in close proximity to the well known Roman cities of Hadrianoupolis, Plotinopolis and Trajanoupolis.

The MDZ site is located on a vantage elevated point, as it is built on a hill overlooking the Vardas river valley. The site was also near the commercial roads linking Hadrianoupolis, Plotinopolis and Hadrianopolis.

The area around MDZ site is modified by both the erosion of Ardas river system in the closer area and Evros river in the broader, as well as by a set of normal faults ranging in strike from WNW-ESE to WSW-ENE (Fig. 2). This fault system has caused the Neogene sediments (locally consisted of marl and fine to medium grained sand) to form a set of hills roughly oriented E-W, smoothed out due to erosion. Relief is not strikingly modified by faults, therefore they would normally considered to be inactive or of low activity (Pavlides et al., 2006a and b, 2007).

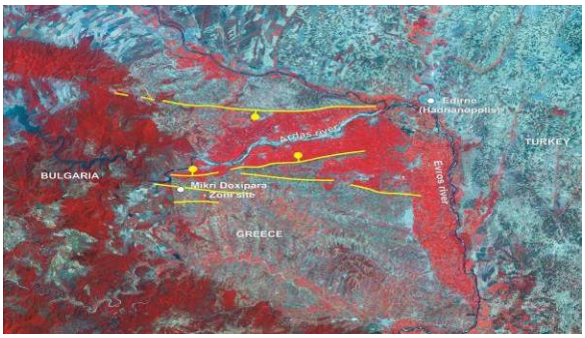

Fig. 2: Landsat image showing the main fault systems that modify the area around Mikri Doxipara – Zoni site.

DISCUSSION

The site consists of a tumulus in which four members of a rich family have been cremated and buried in the beginning of 2nd century AD. The tumulus is very close to the road connecting Hadrianopolis (Edirne) and Philippoupolis (Plovdid). Four excavation pits since 2002, revealed the cremated remains of three males and one female, along with numerous offerings to accompany them into the afterlife (Whitley, 2002-2003).

Fig. 3: Initial topography of the tumulus before the excavation. It is evident that the tumulus is deformed in an E-W direction (photo courtesy: D. Triantafyllos).

The tumulus initial morphology showed signs of grave robbing, as well as of irregular topographical anomalies aligned in an E-W direction. Photographs of the tumulus before the excavation site, as well as large scale topographic maps of the site prepared by the Archaeological Survey, confirm that these small depressions are indeed aligned in an E-W direction (Fig. 3).

Apart from the human remains and the offerings, which include horses, carriages and their equipment, two brick-built altars serving as platforms for offerings to the dead were found. One of them (site DOX 2-1) has been found to be heavily deformed by a system of normal faults, which clearly affect the ground surface of 2nd Century AD (Figs. 4 and 5).

Fig. 4: One of the brick altars that has been faulted and displaced

This system is comprised by several roughly E-W trending normal faults, which form a fairly large depression at the altar site. The maximum observable throw of the main S-dipping surface is 1.9 m, but taking into account the secondary features and the total displacement of the N-dipping antithetic faults, the total net displacement is estimated at *ca.* 0.9 m. This displacement, which is attributed to an earthquake post-dating the date of altar, is well visible in site DOX 2-2 (Fig. 6). The fault system affects the Neogene substratum (marls and fine-grained sands) as well as the artificial deposits that formed the tumulus.

Fig. 5: The actual cracks that were preserved due to the artificial cover of the tumulus

These deposits were removed during the archaeological excavation; hence no direct association to the faulting is possible at this stage.

Secondary faulting and jointing, also affecting the Roman ground surface, has been detected in several other sites in various parts of the excavation.

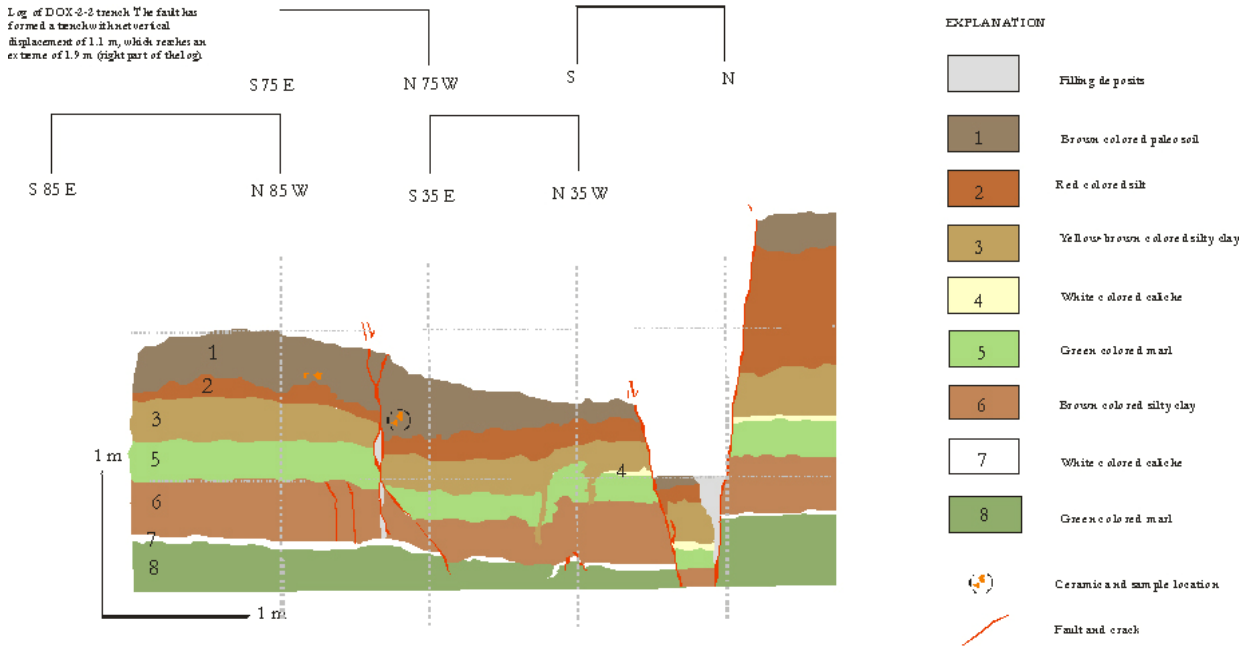

Fig. 6: Log of DOX 2-2 trench, where the maximum net displacement of 90 cm is observed. The fault zone has a width of ca. 2 m and it is attributed to a large, ground rupturing earthquake that postdates 2nd Century AD.

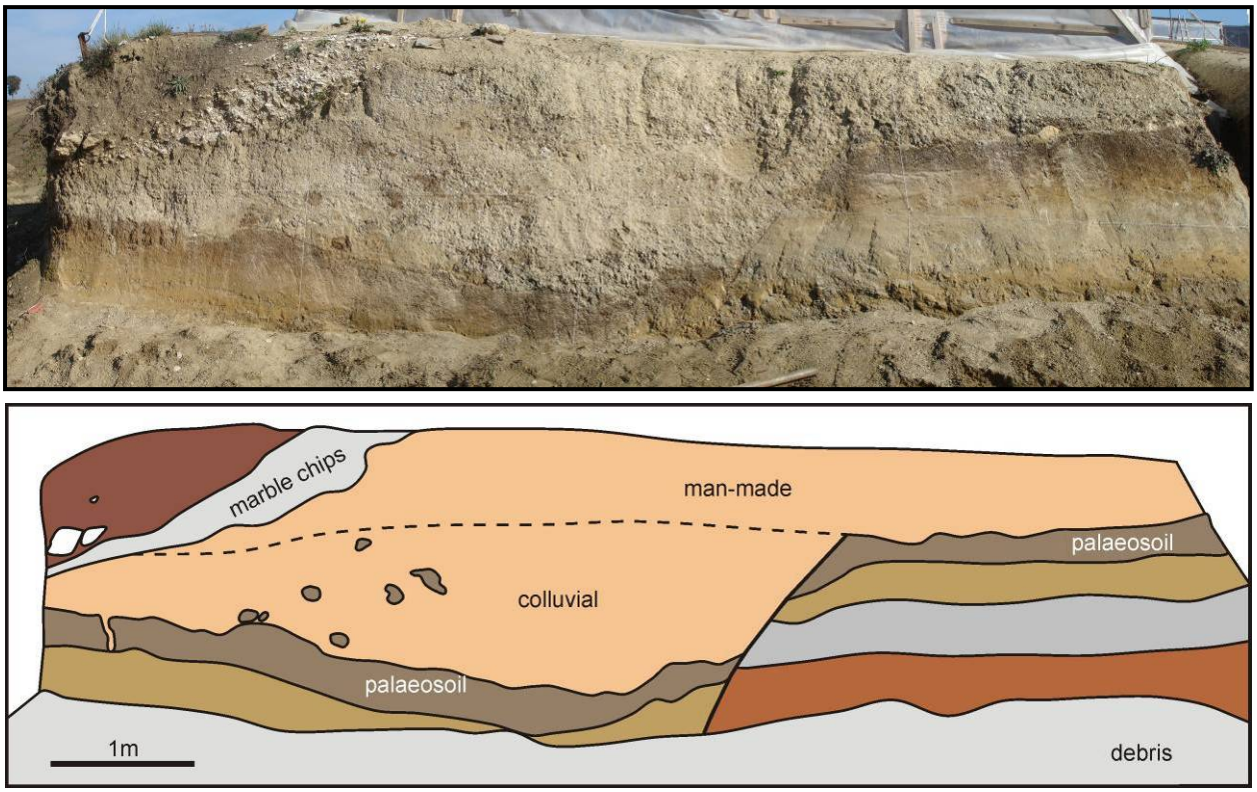

Fig. 7. Photo and interpretation of DOX-1 site, located under a burial. Radiocarbon dating of the palaeoseiol yielded a date at 960 ± 50 BC. Faulting has displaced this palaeosoil, hence it postdates it and predates the Roman artificial cover.

On another excavation site at the tumulus (DOX-1 site, there are indications of another earthquake that predates the one detected in DOX-2 site. This earthquake produced ground rupturing with significant displacement, visible at a cross-section (Fig. 7). A palaeosoil, dated at 960 ± 50 BC, is displaced by a normal fault of roughly E-W strike by about 1 m. This palaeosoil and the associated colluvial deposits of the hangingwall are covered by historical layers of Roman time.

It seems therefore that Mikri Doxipara – Zoni tumulus has been faulted twice during historical times:

1. The last event postdates 2nd century AD and is probably associated with the large Edirne Earthquake of 1752, the only known large event in the area.

2. The penultimate event happened between 960 BC and 2nd Century AD, but most probably occurred closer to the lower limit of this time window, as suggested by microstratigraphy.

It seems therefore that the recurrence interval for large, ground rupturing earthquakes in the area is quite long, which comes in agreement with the current seismotectonic status of the area. Despite the fact that there are no clear geomorphological or geological indications for a large fault zone in the area, the order of displacement per event is large (*ca.* 1 m) and should be taken into account for local seismic hazard assessment.

Taking into account the behavior of normal faults in Greece during historical earthquakes, as well as in paleoseismological research, it is estimated that the earthquakes that formed this fault system were strong ones, possibly at the order of Ms 6.5.

Acknowledgements: Authors are in debt to D. Triantafyllos & D. Terzopoulou, lead archaeologists of the site, as well as A. Kürçer (MTA, Turkey) & A. Zervopoulou (AUTh, Greece) for substantial fieldwork contribution.

References

Pavlides S., Chatzipetros A., Zervopoulou A., Kürçer A. and Triantafyllos D. (2006a). Post-Roman seismic activity in Mikri Doxipara – Zoni archaeological excavation (NE Greece), European Geosciences Union General Assembly, Vienna, Austria, 2-7 April 2006, Geophysical Research Abstracts, 8, 06483

Pavlides S., Chatzipetros A., Zervopoulou A., Kürçer A., Triantafyllos D. and Terzopoulou D. (2006b). Archaeology and seismic hazard: Post-Roman co-seismic fault ruptures in northern Evros (Mikri Doxipara – Zoni, NE Greece) case study, Hazards 2006, Patras, 22-25 June 2006, Abstract volume, 91-92.

Pavlides S., Valkaniotis S. and Chatzipetros A. (2007). Seismically capable faults of Greece and their use in seismic hazard assessment, Proceedings of the 4th International Conference on Earthquake Geotechnical Engineering, Thessaloniki, 25-28 June 2007, Abstract CD, Paper 1609.

Whitley, J. (2002-2003). Archaeology in Greece 2002-2003, Archaeological Reports, 49, 1-88

DISCOVERY OF NATURAL DEFORMATION RELICS IN ANHUI ARCHAEOLOGICAL AREA AND ITS SIGNIFICANCE

Da-Guan, Y. (1), Zhi, S. (2), Xiao-Gi, S. (1), Jie-Ping, T. (3) and An-Guo, C.(1)

(1) Seismological Administration of Anhui Province,Hefei,Anhui, 230031, P.R.CHINA. yaodaquan@hotmail.com
(2) Cultural Relic Archeology Research Institute of Anhui Province,Hefei,Anhui, 230001, P.R.CHINA.
(3) Cultural Relic Manage Department of Tongling City,Tongling,,Anhui, 244001, P.R.CHINA.

Abstract: *In the process of excavating the ancient relics and tombs, recognition of natural deformation is a very important job which leads to the inversion and enrichment of historic and prehistoric deformation records. Recently, cooperating with people in archaeological field, the author investigated some archeological sites in Anhui Province. Some natural deformation traces were found, such as sand veins, faults, deformation of tomb chamber, subsidence of the relics (tomb), and so on. The time when the natural deformation formed is from Longshan Cultural Period to Tang-Song Dynasty. It is the first time the natural deformation has been discovered in Jianghuai area, which locates in the transition belt between South and North China. Apparently, a deep study on these deformation relics would contribute to the review of the crust activity history and the prediction of the activity trend in the future. At the same time it may also develop and enrich the methods and means of research on tectonic activities since Holocene in East China.*

Key words*: Archaeology, natural deformation, recognition, significance.*

INTRODUCTION

East China is densely populated and climate in the area is very humid today. Intense physical and chemical reactions and frequent human activities make it very difficult to protect the relics of tectonic activities. Therefore, for a long time, there are many difficulties in evaluating the tectonic activities in this area in the Quaternary Period, especially in the late Quaternary Period. However, on the other hand, the rapid social and economic developments in East China ask for solving the basic problems about the seismic and geological background and crust stability of this region immediately.

Fortunately, along with the large scale development of the East China, a large amount of ancient sites and tombs have been discovered in the building process of big projects such as high-speed highways and railways, which provides the possibility to understand the natural deformation history in Jianghuai area in the past thousands of years. Seismologists and archaeologists work together to take this valuable opportunity. Bringing the refined chronological stratification into full play, they adapt advanced methodology and technology to record the deformation phenomena in the Quaternary Period, especially in the Prehistoric Cultural Period. An objective tectonic activity evaluation of the transition belt between North China and South China is expected to be acquired by analyzing the great amounts of observation data.

Sponsored by the Anhui Provincial Natural Science Foundation Project Summary and Comprehensive Research on the Neotectonic Activity in Jianghuai Area (070415222), cooperating with archaeologists, the author made an extensive investigation into the ancient sites in Jianghuai area which is located between North China plates and South China plate. Many valuable transient spot data has been protected and collected, through which some natural deformation trace has been carefully recognized and recorded. This article focuses on the most recent findings about the natural deformation trace in the archaeological sites in Anhui Province. Meanwhile, the significance of this work has been predicted as well.

SAND VEINS, FAULTS, CRACKS, JOINTS

Sand veins in the cultural stratum in an ancient site in West Anhui Province

This ancient site locates in the northeast of Dabie Mountain. It's a part of Qinling – Dabie Mountain fold

Fig. 1: (Up) Sand vein discovered in the ancient site in West Anhui Province. (Down) Northern wall in detail.

belt. The degrading metamorphic basement shows strong new activity, which makes this area one of the main earthquake activity zones in East China. According to the historic record, earthquakes of 5.0 magnitude or greater have hit this area for nine times, among which there are two earthquakes of more than 6.0 magnitude. The epicentre presents belt distribution from north to east. The digging site is in the eastnorth of the earthquake zone. Sand veins were discovered in the cultural stratum (Fig. 1).

Fig. 2: The tensile fault in Longshan Cultural Stratum in the ancient site in North Anhui Province (The up photo is the north wall; the down photo is the south wall)

In the above figure (Fig. 1), the grey stratum which, the sand penetrated in is the cultural stratum of Western Zhou Dynasty (about 2,000 years ago). The sand vein originated from a sand stratum 6 meter below the ground. Earthquake liquefaction can account for the origin of the sand vein.

Fault and crack in Longshan cultural stratum of the ancient site in North Anhui Province

This ancient site formed in the Longshan Period. There are tensile faults in the city wall. The strike is 10°, SEE. The dip is nearly vertical. Tensile dislocation is discovered in ash layers and construction heaps. Fault displacement in different layers is about the same, ranging from 3.8 centimeter to 4.5 centimeter. The fracture section is flat, except for the dragging with same direction in the upper surface of the cultural stratum and the fault is displayed in the north wall, south wall and the bottom of the trench (Fig. 2). In the corresponding cultural stratum on the east side, an about 20-centimeter-broad crack is discovered, the direction of which is EN 20°. The crack is filled with black soil. We can see this clearly from the two sides and the bottom of the trench. The fault and crack developed in the same cultural stratum. Both of them seem to be the results of tensile deformation. The fact that they occur in the cultural stratum made of comparatively plastic clay soil and end in the bottom of the upper stratum revealed that they are the relics of quick fracture. Their occurrence can be attributed to earthquake deformation (Yao Daquan, 2004). According to the assembly of fragments of cultural relics, the cultural stratum is Longshan cultural stratum, which has about 4,300 years' history.

Joints discovered in the ancient site in central Anhui Province

Joints are mainly discovered in the prehistoric sites, which have history of about 5,500 years. During the excavation process, generally the joint surfaces are gently inclined and clearly cut through the layers. The cutting crack can be observed in some part of the joints.

DEFORMATION OF BURIAL CHAMBERS

The Fig. 3 is the digging scene of Warring States Period tomb in central Anhui Province: There the bulge deformation is obviously on the bottom of the chamber, which is the characteristic of deformation under compressive stress.

SUBSIDENCE OF THE RELICS

The ancient pathway excavated in a site in North Anhui province is one meter underneath the ground, which is the indicator of a continuous subsiding process. Furrows can be discerned in the silt underneath the north river channel. The furrows are buried by a 1.5-meter-high layer made of rubbles and new deposits. A complex subside-rise-subside process can be perceived from the Fig. 3.

CONCLUSIONS

Based on the above presentation and preliminary analysis, it can be concluded that the archaeological work in ancient sites in Anhui Province has disclosed the natural deformation traces in this area. Cases of natural deformation have happened in Jianghuai area, which locates in the transition belt between North China and South China since Neolithic Age. Among these cases there must be earthquakes. However, we only have the record of earthquakes with more than 5.0 magnitude in this area in the last 500 years. (Huang Weiqiong et al., 1994). Evidently, the above materials play an important role in

our understanding and prediction of earthquakes in this area.

Fig. 3: The bulge deformation on the bottom of the Warring State Period tomb in central Anhui Province

OUTLOOK

The above discovery is groundbreaking and directional. It provides the information for us to understand the deformation history and characteristics, to evaluate the crust stability in this area, and then to explore the tectonic activity property of Central and East China. This article is only a summary of the discovered phenomena. More specific and further research is continuing, which will be described in more elaborate papers in the future.

Recently, in the international academic circle, the trend of trans-disciplinary cooperation in studying the history of tectonic deformation in prehistoric age is gathering momentum. For example, the seismologists, geophysicists, and archaeologists cooperated to study the earthquake liquefaction in New Madrid seismic zone. During the research process, the seismologists worked over the ancient earthquake; the geophysicists help them find the accurate position of liquefaction and trial trench; and the archaeologists determined the exact time of liquefaction by assembling the cultural relics in the trial trench (Tuttle et al. 1999). The research topic of International Geoscience Programme 567(IGCP567) is seismic archaeology. Undoubtedly, the academic cooperation between researchers from seismic and archaeological field is very promising.

Acknowledge:

Acknowledgements: In the end, the authors would like to take this opportunity to express their cordial thanks to their counterparts in Anhui Provincial Institute of Cultural Relics and Archaeology.

References

HUANG Wei-Qiong, LI Wen-Xiang, CAI Xue-Feng.(1994).Research on the completeness of earthquake data in the Chinese mainland. *Acta Seismologica Sinica*,16(4), 423-432(in Chinese).

YAO Da-Quan. (2004).Macroscopic and microscopic evidence of periodical stick-slip deformation in an active fault. *Recent Developments in World Seismology*,(4), 6-10(in Chinese).

Tuttle, M. P., J. Collier, L. W. Wolf, and R. H. Lafferty., 1999, New evidence for a large earthquake in the New Madrid seismic zone between A.D. 1400 and 1670. *Geology*, 27, 7771-7774.

EARTHQUAKE CLUSTERING ALONG THE DEAD SEA FAULT (JORDAN) FROM GEOMORPHOLOGY, PALAEOSEISMOLOGY AND ARCHAEOSEISMOLOGY

M. Ferry (1,2), M. Meghraoui (2), N. Abou Karaki (3) and M. Al-Taj (4).

(1) Centro de Geofísica de Évora, Universidade de Évora, Rua R. Ramalho, 59, 7002-554 Évora, PORTUGAL. matthieu@uevora.pt
(2) Institut de Physique du Globe, Strasbourg, FRANCE.
(3) University of Jordan, Amman, JORDAN.
(4) The Hachemite University, Zarqa, JORDAN.

Abstract: *The recurrence of large and destructive earthquakes along major fault systems is key to understanding their driving mechanism and to infer future behaviour. For the Jordan Valley segment (JVF) of the ~1000-km-long Dead Sea Fault, we provide evidence of episodic behaviour. We combine published historical data, re-appraised archaeological data and original geomorphic analyses and paleoseismic excavations to reveal the behaviour of the fault over the past 50 kyr, with an unprecedented high resolution of the rupture history for the past 14 kyr. Our results indicate a long term average slip-rate of 5 mm/yr, with short-term rate varying between 3.5 and 11 mm/yr. We also document the occurrence of up to 14 M_w > 7 earthquakes along the Jordan Valley segment of the DST during the Holocene. In that the JVF has accumulated 3.5m to 5 m of slip since the most recent major surface rupture in AD 1033 earthquake, we propose that the JV segment may be mature for a large event.*

Key words*: Dead Sea Fault, earthquake clustering, paleoseismology, archeoseismology*

INTRODUCTION

The ~1000 km-long Dead Sea Fault zone (DST) is the primary plate boundary fault between the Arabian and African lithospheric plates (Fig. 1), and has accommodated about 105 km of sinistral slip since early Miocene time (Quennell, 1959).

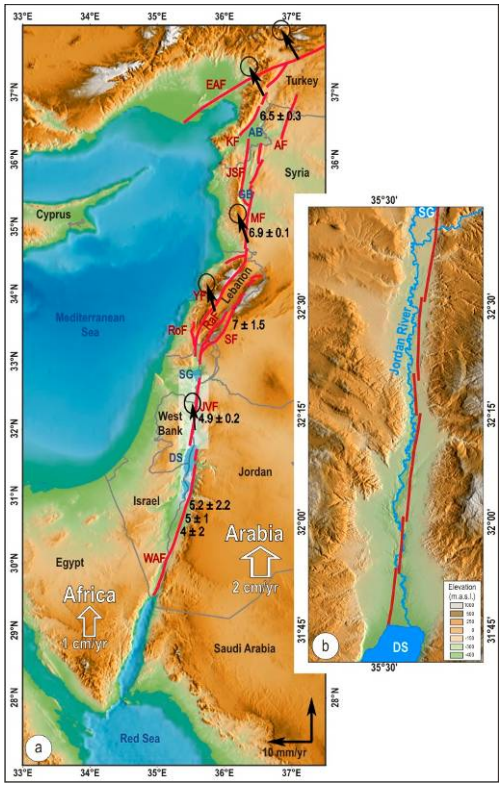

Fig. 1. General setting of the Dead Sea Fault (a) and the Jordan Valley segment (b).

Our study focuses along the 110-km-long Jordan Valley section of the fault zone, which exhibits abundant evidence of significant late Quaternary activity in the form of scarps, offset and deflected drainages and sags. We combine accounts of historical earthquakes and reinterpreted archeological results with new studies on tectonic geomorphology and paleoseismology to develop a 50,000-year record of activity of this important plate boundary fault. This is particularly timely, as a large earthquake in an area of dense population and political strife could potentially affect the entire region.

GEOMORPHOLOGY AND SLIP RATE

We document systematically offset drainages over three regions along the active fault trace. The mostly dendritic drainage pattern is inferred to form as a consequence of gully and streams incising into the soft Lisan lacustrine sediments. The drainages may be grouped into six distinct generations as a function of their incision depth. Assuming that each incision underwent a similar erosion/deposition process, the depth of each of the drainages is inferred to reflect its age. Consequently, the incisions may be sorted chronologically. Based on the history of past lake-level fluctuations and intense rainfall episodes, we identify six climatic events that are likely to have triggered the onset of gully incision episodes.

We measured lateral offsets of individual drainages from analysis of aerial photographs combined with field control points and field measurements. Combining the inferred ages of the various channels along with their estimated offsets yields a slip rate of 4.9 mm/yr averaged over the last 48 kyr (Fig. 2), which agrees with GPS and other geological studies (Reilinger et al., 2006). However, our model also indicates strong variations over short time

spans, with a threefold increase from 3.5 mm/yr to 11 mm/yr during a 2000-yr-long period.

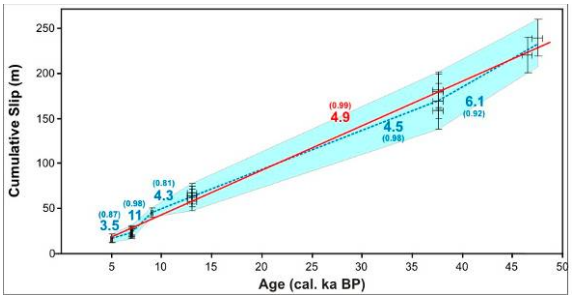

Fig. 2. Slip rate history for the Jordan Valley fault. Solid line shows an average value of 4.9 mm/yr. Dashed line suggests short-term variations from 3.5 to 11 mm/yr (from Ferry et al., 2007).

PALAEOSEISMOLOGY AND ARCHAEOSEISMOLOGY

Paleoseismic trenches excavated across a pull-apart basin show at least two fault movements that can be associated with the major earthquakes (M>7) of A.D. 749 and A.D. 1033. At the archeological site of Tell Es-Saidiyeh, trenches show evidence for up to eight surface ruptures over the past 14 ka, of which the most recent may be correlated to the historical earthquake of A.D. 1033. A critical analysis of archeological observations from ten sites provides for a reinterpretation that 9 to 12 destruction events occurred after about 2900 B.C. Our analysis suggests that for the past 14 ka, the recurrence interval for large earthquakes has been about 600 to 1000 years, and that there have been clusters of seismicity followed by periods of quiescence (Fig. 3).

DISCUSSION

The observed behavior of the Jordan Valley segment of the DST is interpreted to result from alternating periods of quiescence and increased seismic activity. Considering that the last large earthquake in the Jordan Valley occurred in A.D. 1033, the fault may have accumulated 3.5 m to 5 m of potential slip. This argues that the Jordan Valley fault segment may be ripe for a M_w7.4+ earthquake, the occurrence of which in the near future could have far-reaching social and political ramifications.

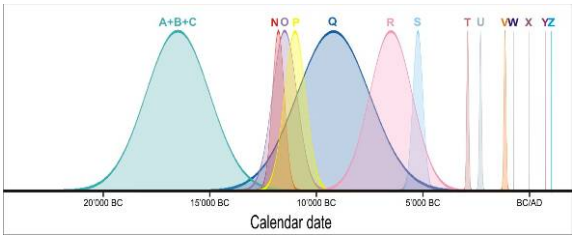

Fig. 3. Probability density functions for the last 13 surface-rupturing earthquakes along the JVF.

Acknowledgements: Authors are indebted to the Deanship of scientific research (University of Jordan), the Jordan Valley Authority, the Natural Resources Authority and Military Commandment and Salman Al-Dhaisat (Royal Jordanian Geographic Center) for their assistance and help during our field investigations.

References

Ferry, M., Meghraoui, M., Abou Karaki, N., Al-Taj, M., Amoush, H., Al-Dhaisat, S., Barjous, M. (2007). A 48-kyr-long slip rate history for the Jordan Valley segment of the Dead Sea Fault. Earth Planet. Sci. Lett., 260, 394-406.

Quennell, A. M. (1959), Tectonics of the Dead Sea Rift, in 20th Int. Geol. Congr., edited, 385-405, Assoc. Serv. Geol. Afr., Mexico.

Reilinger, R., McClusky, S., Vernant, P., Lawrence, S. (2006). GPS constraints on continental deformation in the Africa-Arabia-Eurasia continental collision zone and implications for the dynamics of plate interactions. J. Geophys. Res., 111, doi:10.1029/2005JB004051.

ADVANCES AND TRENDS ON EARTHQUAKE-TRIGGERED LANDSLIDE RESEARCH IN SPAIN

J. García-Mayordomo (1), M.J. Rodríguez Peces (2), J.M. Azañón (2, 3) and J.M. Insua Arévalo (4).

(1) Instituto Geológico y Minero. Investigación en Peligrosidad y Riesgos Geológicos. c/ La Calera, 1 (Tres Cantos) 28760-Madrid. SPAIN. julian.garcia@igme.es
(2) Departamento de Geodinámica. Facultad de Ciencias. Universidad de Granada, c/ Fuentenueva, s/n. 18002-Granada. SPAIN. marpeces@ugr.es
(3) Instituto Andaluz de Ciencias de la Tierra (UGR-CSIC), Granada, SPAIN. jazanon@ugr.es
(4) Departamento de Geodinámica. Universidad Complutense de Madrid. Ciudad Universitaria, s/n 28040-Madrid, SPAIN. insuarev@geo.ucm.es

Abstract: *This work reviews the current situation of earthquake-triggered landslide studies in Spain both from the point of view of regional assessment and site-specific cases. Regional assessments have been undertaken in areas of the Betic Cordillera (South and Southeast Spain): Alcoy Basin, Lorca Basin, Granada Basin and Sierra Nevada Range; and Central Pyrenees (North Spain and Andorra). Specific studies are very scarce, outstanding those related to the Güevéjar landslide (Granada) –triggered by 1755 Lisbon and 1884 Arenas del Rey earthquakes, and to a remarkable rock-slide triggered by 2005 La Paca earthquake (Murcia). Future research lines are appointed, as well as potential applications on Civil Protection and Seismic Hazard Assessment.*

Key words*: Induced landslides, earthquake environmental effects, La Paca, Güevéjar.*

INTRODUCTION

Landslides are one of the most common secondary effects of earthquake vibration. In fact, this phenomenon sometimes produces more victims than damage in buildings itself. Landslides can produce dramatic changes in the landscape and, hence, control the practicality of life-lines in the aftermath of a seismic event (a very recent example is M_w 7.8, 2008 Wenchuan earthquake in China).

The phenomenology of landslides triggered by earthquakes has been thoroughly studied by Keefer (1984, 2002) and Rodríguez et al. (1999). These works concluded that the most common type of earthquake-triggered slope instabilities (landslides s.l.) are rock falls, disrupted soil slides, and rock slides. These types of landslides can be triggered by earthquakes as small as M~4. Additionally, they found a positive correlation between the abundance of landslides and the area affected by them, with earthquake magnitude; although variations due to either specific geological and terrain conditions or seismic parameters are noted.

Earthquake-triggered landslides have also been studied from the point of view of spatial prediction and regional assessment (e.g., Jibson et al., 2000; Luzi and Pergalani, 2000; Romeo, 2000; among others). In these works GIS technologies are intensively used for combining digital geological information with terrain models and seismic input by means of the well known Newmark sliding rigid-block model (Newmark, 1965). Resulting maps have been compared to actual field cases (1994 Northrigde, 1997 Umbria-Marche) drawing satisfactory results and even the proposition of relations between Newmark displacement and probability of failure. Finally, earthquake triggered landslides have also been the subject of site-specific studies. Few works have been devoted to verifying the goodness of the Newmark method in the field in the aftermath of an event (e.g., Wilson and Keefer, 1983). These authors concluded that this method draws reasonable good predictions of coseismic downward slope displacement –provided certain geotechnical conditions are fulfilled. Another set of works are focused on analysing the hypothetical seismic origin of particular landslides associated either to a known historical earthquake (e.g., Jibson and Keefer, 1993) or to paleoseismic events (cf. Jibson, 1996). Actually, when written records are not available, reliable cause-and-effect relationships between specific earthquakes and landslides are difficult to demonstrate. In these cases it is necessary to dismiss the influence of other triggering factors (e.g., intense rainfall, erosion) by means of slope stability back-analysis.

Slope instabilities are reported recurrently in the chronicles of pre-instrumental earthquakes in Spain. It is common to come across short phrases as (Fig. 1): "*…una hendidura de siete leguas se abrió a través de las montañas de Bas…*" (Vielha, 1428), "*…en el sacudimiento de los montes se han juntado dos peñascos, y hay que buscar el camino por otro sitio...*" (Almería, 1522), "*…el monte Cantagallet se abrió en distancia de legua y media…*" (Alcoy, 1620); "*…la sierra de los moros se abrió en dos partes…*" (Alboloduy, 1713), "*…se hundieron unas tierras entre Lorca y Totana…*" (Lorca, 1818); etc. In some cases these descriptions could be related to surface faulting. In fact, Spanish earthquake chronicles are still poor researched from the point of view of environmental earthquake effects (EEE). Most of the research has been devoted to assigning macroseismic intensities based on building damage and social impact. Fortunately, INQUA is currently promoting efforts on that direction, being good examples the EEE international database and the Environmental Seismic Scale (ESI) (Michetti et al., 2007).

Nevertheless the lack of research, Spain has a few significant cases of earthquake triggered landslides. From the historical period the most interesting one is the Güevéjar landslide in Granada (Sanz, 1997; Jimenez Pintor and Azor, 2006), which is discussed later. Respecting to the instrumental period, the most dramatic case may be the river Beiro landslide (Granada). This landslide was triggered by the 1956 Albolote-Atarfe earthquake (M_L=5.0, I_{MSK}=VIII) killing 5 people (IAG, 2009). The earthquake also produced rock-falls around Sierra Elvira. More recently, three seismic series all located in the Murcia Region: 1999 Mula (m_{bLg}=4.8, I_{EMS}=VI), 2002 Bullas (m_{bLg}=5.0, I_{EMS}=V) and 2005 La Paca (m_{bLg}=4.7, I_{EMS}=VI–VII), have produced interesting case-study examples of rock-falls and rock-slides. The 2005 La Paca case is discussed later.

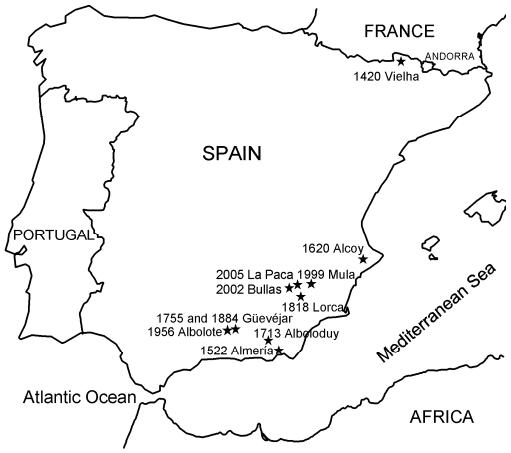

Fig. 1: Location of the earthquakes and towns cited in the text.

REGIONAL ASSESSMENT OF EARTHQUAKE-TRIGGERED LANDSLIDE HAZARD IN SPAIN

Even though in Spain a great number of studies dealing with regional landslide assessment exist, those especifically focussed on analysing the seismic factor are very few: García-Mayordomo (1998, 1999), Mulas et al. (2001 y 2003), Coral Moncayo (2002), Figueras et al. (2005), Delgado et al. (2006), Rodríguez-Peces (2008) and Rodríguez-Peces et al. (2008, 2009a,b). All these works are based on the Newmark method and most of them make use of geospatial information by means of a geographical information system (Idrissi, ArcGIS).

García-Mayordomo (1998, 1999) analysed the stability of two particular slope models widely distributed accross the Alcoy Basin (Alicante, Eastern External Betics), finding that critical accelerations as low as 0.03 g to 0.04 g could potentially trigger landslides. In the same area, Delgado et al. (2006), after modelling the natural variability of geothecnical parameters by means of Montecarlo analysis, obtained a set of maps in terms of the probability associated to a critical acceleration lower than 0.1 g for dry and saturated conditions. He found out a very good correlation between high probability areas and the distribution of actual known cases triggered by the 1620 Alcoy (I_{MSK}=VIII) and 1945 Onteniente (m_{bLg}=4.0, I_{MSK}=VII) earthquakes. From both García-Mayordomo (1999) and Delgado et al. (2006) studies is drawn that earthquake-triggered landslides in the Alcoy Basin appear to be a frequent and repeated phenomena.

Coral Moncayo (2002) and Figueras et al. (2005) works, performed in Andorra (Pyrenees), are particularly outstanding for assessing earthquake-triggered landslide hazard in terms of probability of failure as a function of Newmark displacement –although this is eventually done using Jibson (2000) equation derived from Northridge earthquake data. Newmark displacement is calculated from empirical relationships with Arias Intensity as well as from real accelerograms consistent with the 475-year return period in the area (PGA~0.1 g), and assuming a critical acceleration of 0.01 g. They finally concluded that probability of failure is only significant for slopes greater than 40º.

Mulas et al. (2001 y 2003) works in the valleys of Gállego and Caldarés rivers (central Pyrenees) deal with designing a specific methodology for the quantitative assessment of slope instability levels against the seismic phenomena. Instability levels are derived from a matrix that combines discrete values of a variable dependant on aseismic factors (slope, lithology,…) with another variable dependant on seismic soil response; which is also a function of macroseismic intensity. For intensity levels between VI y VIII (presumably related to the 500-year return period), the authors found out that the areas with the highest levels of instability coincided with the higher parts of the valleys, in contrast with the actually known aseismic instabilities location.

Finally, Rodríguez-Peces, 2008 and Rodríguez-Peces et al. (2008, 2009a,b) studies in the Lorca Basin (Murcia, Eastern Betics) and Granada Basin and Sierra Nevada (Central Betics), are focussed on obtaining Newmark displacement maps for seismic scenarios of engineering significance –e.g., related to certain return periods or to the occurrence of specific earthquakes. First, maps in terms of peak ground acceleration on rock (PGA) related to each scenario are obtained. Then, PGA is modified to account for soil and topographic amplification. Next, critical accelerations are calculated and combined with modified PGA to obtain Newmark displacements for each specific scenario by means of using Jibson's (2007) equation. Finally, the obtained maps are compared with the distribution of slope instabilities and particularly with those few known cases of triggering (Fig. 2). The authors found a good correlation between known instabilities and areas showing Newmark displacement values, particularly for the deterministic scenarios. They conclude suggesting that future instabilities in the Lorca and Granada basin would be fundamentally rock-falls, rock-slides and rock-avalanches, and that only the occurrence of large magnitude earthquake (M_w≥6.0) could possibly produce larger and deeper instabilities or affect extensive areas.

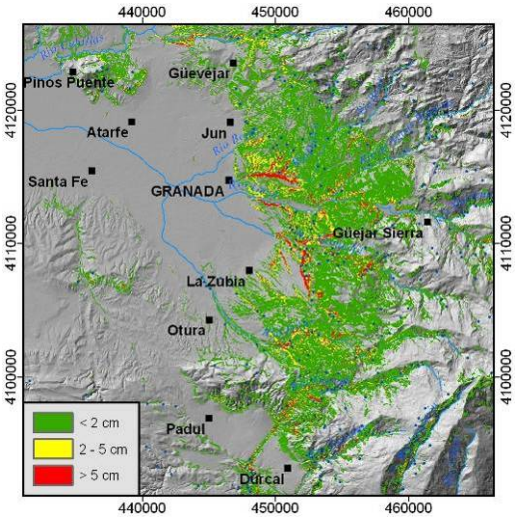

Fig. 2: Newmark displacement map of eastern Granada Basin for a seismic scenario considering the complete rupture of the Granada Fault. Blue dots locate known slope instabilities (modified from Rodríguez-Peces, 2008).

ANALYSIS OF SPECIFIC EARTHQUAKE-TRIGGERED LANDSLIDE CASES

Site-specific studies focused on analysing the dynamic stability of particular slopes known to have failed during an earthquake are very scarce in Spain. At this respect, it is important to clarify that a different kind of studies are those included in civil engineering projects aimed at guaranteeing the stability against earthquakes of modified slopes or man-made earth structures, which are not discussed in this abstract.

From the Spanish seismic historical period (prior to 1920) the most interesting case is the Güevéjar landslide in Granada (Sanz, 1997; Jiménez Pintor and Azor, 2006). This is a large-size paleolandslide (approx. 200 ha, $60 \bullet 10^6$ m3) that was reactivated both in the 1755 Lisbon and 1884 Arenas del Rey earthquakes. It is interesting to note that the epicentre of the Lisbon earthquake is located more than 500 km away from Güevéjar (Martínez Solares and López Arroyo, 2004), and that it was felt with I_{MSK} VI at the village –even though it was badly damaged by the landslide. Similarly, the 1884 Arenas del Rey earthquake (M~6.5) –which was located 50 km far and was felt at the site with I_{MSK} VII, reactivated the landslide provoking the ruin of the village and its definitive move to a safer location. Güevéjar landslide arises many interesting questions: how old is the landslide? Can any other seismic events be inferred and dated from landslide history? What are the factors controlling landslide reactivation from strong ground motion from far sources? How important are site effects? Could be the landslide be reactivated today? etc. The answer to any of these questions will be necessarily based on a geomechanical model of the slope built from geotechnical data and geophysical observations –information so far not available. Rodríguez-Peces et al. (this volume) are starting research on this landslide.

Respecting to instrumental earthquakes, Rodríguez-Peces et al. (2009a and c) have studied in detail 2005 La Paca rock-slide (Fig. 3). A field survey using a terrestrial laser scan was carried out to obtain a high resolution digital elevation model (DEM). In addition, the *Joint Roughness Coefficient* (JRC) and the *Joint Compressive Strength* (JCS) parameters were measured on the failure plane. Subsequently, a stability back-analysis was performed considering a slide failure mechanism. A static safety factor of 1.09, a critical acceleration of 0.09 g and a Newmark displacement of 0.18 cm were calculated. Furthermore, the authors compared these parameters with the ones that could be obtained by GIS considering regional (25 x 25 m) and local scale (2.5 x 2.5 m) DEMs, as well as geotechnical data from bibliography. They concluded that results from regional DEMs can provide not reliable results, while the use of local MDT appears to provide results very similar to site-specific analysis.

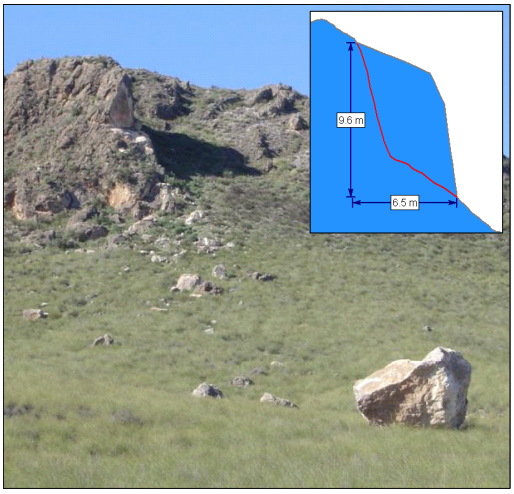

Fig. 3: Rock-slide and subsequent rock-fall associated to 2005 La Paca earthquake (modified from Rodríguez-Peces et al. 2009a and c)

RESEARCH LINES AND TRENDS

A first research line would consist in carrying on detailed studies of slope instabilities univocally known to be associated to recent instrumental earthquakes (e.g., Bullas 2002, La Paca 2005) or events to come. In this cases safety static factors and critical acceleration can be calculated based on field data. In addition, provided that the magnitude and distance-to-the-site of the earthquake are precisely known, Newmark displacements could be calculated from real time-histories. Results from this type of studies can be used to devise relationships between Newmark displacement, type of instability, probability of failure, etc. and be used to calibrate regional scale maps obtained for specific seismic scenarios. Ideally, a probability of failure distribution could eventually be drawn for the particular geological conditions of different Spanish regions.

A second research line would first accomplish a detailed study of historical earthquake chronicles with the aim of identify and locate in the field slope instabilities (or environmental earthquake effects in general) related to the event. Once the most evident cases are identified, a particular study for each one it would proceed. An approach similar to the one described above can be followed, but in this case the main achievement would be to constraint the size and distance-to-the-site of the old

earthquake. In uncertain cases, as well as in very old earthquakes, absolute dating must be necessarily applied.

APPLICATIONS OF THE INVESTIGATIONS

The results of earthquake-triggered landslides research are potentially very interesting for a variety of issues in seismic hazard: evaluation of site and topographic effects, complementation of strong ground motion observations, assessment of the size and level of ground shaking related to particular historical earthquakes or old instrumental ones, etc.

In relation to Civil Protection, maps in terms of critical acceleration –or in terms of Newmark displacement properly calibrated with site specific studies, could be used to simulate the distribution and severity of slope instabilities in relation to a particular seismic scenario in a particular county. These simulations would permit to assess the interruption of lifelines (roads, electric lines, gas pipes, water channels,…) in case of earthquake and, hence, to improve emergency plans in the aftermath of an event.

Acknowledgements: The authors thank Spanish ministries of Science and Environment and IGME for funding most of the research activities that have eventually led to this article. We also thank an anonymous reviewer for thoughtful comments and suggestions which have improved the text.

References

Coral Mocayo, H (2002). Utilización de métodos experimentales y de simulación numérica para la microzonificación sísmica de áreas urbanizadas en Andorra. PhD Thesis, Universidad Politécnica de Cataluña, Cataluña (España), 207pp.

Delgado, J., Peláez, J.A., Tomás R., Estévez, A., López Casado, C., Doménech C. and Cuenca A. (2006). Evaluación de la susceptibilidad de las laderas a sufrir inestabilidades inducidas por terremotos. Aplicación a la cuenca de drenaje del río Serpis (provincia de Alicante). Revista de la Sociedad Geológica de España, 19 (3-4), 197-218.

Figueras, S., Macau, A., Goula, X. and González, M. (2005). Aplicación del método de Newmark para el estudio de los movimientos de ladera activados por terremotos en Andorra. VI Simposio Nacional sobre taludes y laderas inestables, Vol. 3, 12 p., Valencia.

García-Mayordomo, J. (1998). Riesgo Sísmico en la Cuenca de Alcoy (Alicante). Aproximación a una Zonificación Sísmica. Tesis del Máster de Ingeniería Geológica, Universidad Complutense de Madrid (España), 100 pp.

García-Mayordomo, J. (1999). Zonificación Sísmica de la Cuenca de Alcoy mediante un Sistema de Información Geográfico. 1er Congreso Nacional de Ingeniería Sísmica, Murcia, 12-16 de Abril de 1999, Memorias, Tomo Ib, 443-450.

IAG (2009). Instituto Andaluz de Geofísica. www.ugr.es/~iag/ last access: June 2009.

Jibson, R.W. (1996). Use of landslides for paleoseismic analysis. Engineering Geology, 43, 291-323.

Jibson, R.W. (2007). Regression models for estimating coseismic landslide displacement. Engineering Geology, 91, 209-218.

Jibson, R.W. and Keefer, D.K. (1993). Analysis of the seismic origin of landslides: Examples from the New Madrid seismic zone. Geological Society of America Bulletin, 105, 521-536.

Jibson, R.W., Harp, E.L. y Michael, J.A. (2000). A method for producing digital probabilistic seismic landslide hazard maps. Engineering Geology, 58, 271-289.

Jiménez Pintor, J. and Azor, A. (2006). El Deslizamiento de Güevéjar (provincia de Granada): un caso de inestabilidad de laderas inducida por sismos. Geogaceta, 40, 287-290.

Keefer, D.K. (1984). Landslides caused by earthquakes. Geological Society of America Bulletin, 95, 406-421.

Keefer, D.K. (2002). Investigating landslides caused by earthquakes - A historical review. Surveys in Geophysics, 23, 473-510.

Luzi, L. and Pergalani, F. (2000). A correlation between slope failures and accelerometric parameters: the 26 September 1997 earthquake (Umbria-Marche, Italy). Soil Dynamics and Earthquake Engineering, 20, 301-313.

Martínez Solares, J.M. and López Arroyo, A. (2004). The great historical 1755 earthquake. Effects and damage in Spain. Journal of Seismology, 8, 275-294.

Michetti, A.M. et al. (2007). Intensity Scale ESI 2007. In: Guerrieru, L. and Vittori, E. (eds.), Mem. Descr. Carta Geol. d'Italia., vol. 74, Servizio Geologico d'Italia – Dipartimento Difesa del Suolo, APAT, Rome, Italy.

Mulas, J., Ponce de León, D., Martínez, M., and Pardo, J.M. (2001). Diseño de una metodología para la zonificación de la inestabilidad de laderas naturales producidas por terremotos. Aplicación a una zona del Pirineo Central (Huesca). V Simposio Nacional sobre Taludes y Laderas Inestables, Vol. III, 1241-1252.

Mulas, J., Ponce de León, D. and Reoyo, E. (2003). Microzonación sísmica de movimientos de ladera en una zona del Pirineo Central. 2º Congreso Nacional de Ingeniería Sísmica, 13-26.

Newmark, N.M. (1965). Effects of earthquakes on dams and embankments. Geotechnique, 15 (2), 139-160.

Rodríguez, C.E., Bommer, J.J. and Chandler, R.J. (1999). Earthquake-induced landslides: 1980-1997. Soil Dynamics and Earthquake Engineering, 18(5), 325-346.

Rodríguez-Peces, M.J. (2008). Evaluación regional de inestabilidades de ladera por efecto sísmico: Mapas de desplazamiento de Newmark para la Cuenca de Lorca, Cuenca de Granada y Sierra Nevada. Master Thesis in Geology, University of Granada (Spain), 96 pp.

Rodríguez-Peces, M.J., García-Mayordomo, J., Azañón-Hernández, J.M. and Jabaloy Sánchez, A. (2008). Evaluación de inestabilidades de ladera por efecto sísmico en la Cuenca de Lorca (Murcia): Implementación del método de Newmark en un SIG. Boletín Geológico Minero, 119(4), 459-472.

Rodríguez-Peces, M.J., García-Mayordomo, J. and Azañón-Hernández, J.M. (2009a). Comparing Newmark's method at regional, sub-regional and site scales: seismically-induced La Paca rock-fall case (Murcia, SE Spain). 8IWSMRR Workshop Abstract and Short Paper CD, 8th International Workshop on Seismic Microzoning and Risk Reduction, Aguadulce (Almería), 15-18th March 2009.

Rodríguez-Peces, M.J., García-Mayordomo, J., Azañón, J.M. and Jabaloy, A. (2009b). Regional assessment of earthquake-triggered slope instabilities for selected seismic scenarios in the Lorca Basin (Murcia, SE Spain). Engineering Geology (submitted).

Rodríguez-Peces, M.J., García-Mayordomo, J. and Azañón J.M. (2009c). Comparación del método de Newmark a escala regional, local y de emplazamiento: el caso del desprendimiento de la Paca (Murcia, SE España). Geogaceta, in press.

Romeo, R. (2000). Seismically induced landslide displacements: a predictive model. Engineering Geology, 58, 337-351.

Sanz, E., (1997). Le mouvement de versant de Güevejar (Grenade) au cours des tremblements de terre de Lisbonne (1755) et d´Andalousie (1884). Bulletin of the International Association of Engineering Geology, 56, 83-87.

Wilson, R.C. and Keefer, D.K. (1983). Dynamic analysis of a slope failure from the 6 August 1979 Coyote Lake, California, earthquake. Bulletin of the Seismological Society of America, 73, 863-877.

COSEISMIC OFFSET OF THE CAMINO DE CRUCES CONFIRMS THE PEDRO MIGUEL FAULT AS THE CAUSE OF THE AD 1621 PANAMÁ VIEJO EARTHQUAKE

E.M. Gath (1) and T.K. Rockwell (1)

(1) Earth Consultants International, 1642 E. Fourth Street, Santa Ana, CA 92701 USA. gath@earthconsultants.com

Abstract: *We completed a study of the Pedro Miguel fault where it crosses the ca 1520 Camino de Cruces in Central Panama. Using tectonic geomorphic mapping, stream bank exposures, and hand-excavated trenches, we have demonstrated that the fault has generated a 2.8-3.0 meter displacement of the Trail, as well as of all fault-crossing geomorphic features in the local area. A unique cobblestone pavement used for the Trail, combined with the geomorphology, makes pre- and post-event reconstruction of fault slip highly accurate. Fault exposures demonstrate that the youngest alluvial deposits are offset, and the fault projects into the surface topsoil. We conclude that the Pedro Miguel fault last ruptured May 2, 1621 and caused the devastating Panamá Viejo earthquake.*

Key words*: Panamá, paleoseismic, archeoseismic, Cruces*

As part of the seismic hazard investigation for the Panamá Canal Expansion Project's design studies, we completed detailed paleoseismic investigations of the Pedro Miguel, and several other faults (Fig. 1). Our studies of the presumed inactive, but unexplored, Pedro Miguel fault involved logging of over 55 trenches, including three locations where we excavated the fault in 3-D to determine slip and timing in past earthquakes, and fault slip kinematics. These studies revealed the fault as having experienced at least three, 2-3 meter displacement events within the last 1500 years. As such, the fault not only poses a shaking hazard to the Panamá Canal structures, but it also crosses through the proposed footprint of Borinquen Dam. This new earthen embankment dam is 7 km long and 10.6 meters high, is segmented into four parts, and will contain the new approach channel from Gatún Lake to the new Pacific set of locks.

One key piece of data needed for the seismic hazard model was the age of the last displacement event. Based on the apparent youthfulness of offset soils and surface features, we proposed that the latest rupture of the Pedro Miguel fault might have been the earthquake that severely damaged many of the stone and adobe buildings in Panamá Viejo on May 2, 1621. The Panamá region has had other earthquakes between 1535 and 1850 (including in 1541, 1750, 1799 or 1800, 1849? and 1855), but only the historically recorded earthquake in 1621 seems strong enough to correlate with the measured surface fault displacement. However, extensive reworking of charcoal in the fluvial sediments prevented us from definitively proving a historical rupture within the principal trenching area.

Fortunately, the Camino de Cruces, a 1.5 meter wide, cobblestone paved trail (Fig. 2), was built from Panamá Viejo to the town of Cruces on the Chagres River, near the present town of Gamboa, in the early 1500s to transport goods via mule pack trains. From Cruces, the goods and passengers would be loaded onto boats that navigated the Chagres River to its mouth by Fort San Lorenzo. These pack trains consisted of hundreds and even thousands of

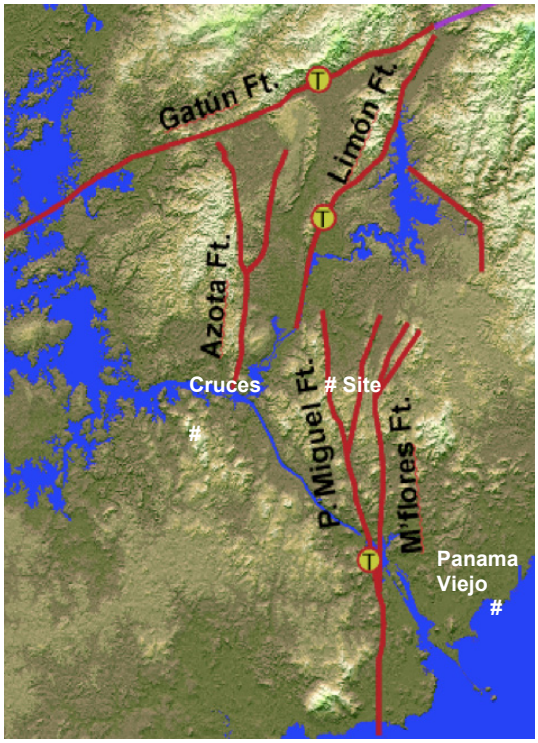

Fig. 1: Active fault map of Central Panamá showing the study site (modified from ECI, 2009).

mules. During the California Gold Rush, thousands of "49'ers" used the Trail to traverse the Isthmus. It was in nearly continuous use until the mid- 1800s when the Panamá Railroad was completed. The Trail crosses the northern extent of the Pedro Miguel fault and provides an excellent archeoseismic piercing line to determine whether the Pedro Miguel fault ruptured in 1621. We conducted a detailed geologic and geomorphic field study of this area to prove whether or not the Trail is offset at the fault, which would be a key factor in general acceptance of the Pedro Miguel fault as active, and its role in generating the 1621 earthquake.

Fig. 2: A photograph of the Las Cruces Trail as it appears today. Although erosion has removed some portions of the trail the cobblestone pavement and larger trail-margin cobbles are still visible in many locations. The rounded, basaltic cobbles that form the trail pavement are typically exotic to the trail location where they were placed.

The site reconnaissance successfully located the Pedro Miguel fault where it crosses the Trail (Fig. 3). At this location, the Trail is abruptly terminated into a projecting sidewall of the stream terrace riser along the toe of which the Trail had been constructed. During the site investigation, we made several other observations that support the theory of a youthful fault offset of the Trail. These observations are listed below from south to north, and illustrated on Fig. 4:

- The rebuilt Trail immediately adjacent to the offset had been relocated to the east and north to smooth out the abrupt 3-meter, 90-degree jog in the Trail.
- The Trail followed along on the first elevated terrace of the stream, and the terrace tread/canyon wall riser is offset 3-4 meters.
- Detailed surveying of the Trail cobbles reveals a segment of the old Trail abruptly severed at the fault, with remnant Trail cobbles preserved under fault-scarp-derived colluvium.
- Right at the fault, the stream is diverted right-laterally over 30 m, forming an incised horseshoe meander.
- The south-facing stream cut exposes several soil-filled fault fissures that flare to the surface.
- The terrace formed between the river meanders has a low (<0.5-m high) scarp across its surface that is on trend with the fault trace.
- Trenches across this scarp reveal upwardly expanded, fissured, and fractured rock, several faults and fault-fissures filled with soil, all at the location of the low scarp.
- The southern wall of the northern river meander is offset at least 2.5 m right-laterally, exposing a fault contact between agglomerate and basalt.
- The north-facing stream cut exposure shows the fault cutting the terrace alluvium, juxtaposing a terrace strath cobble line against fine-grained alluvial deposits.
- The northern wall of the northern river meander is abruptly offset ~3 m right-laterally.
- Two small gullies north of the main river are abruptly offset ~3+ m right-laterally, directly on trend with the fault.
- The gullies expose faulted alluvium and surface soils.

Fig. 3: Photograph of the straight reach of the cobblestone trail as it approaches the fault. The trail is abruptly severed where the left ridgeline has been moved right-laterally in front of the trail, resulting in a 90-degree bend on the trail that would be difficult and inefficient to negotiate with the mule train convoys used on the trail. Photo by P. Williams.

Unfortunately, no charcoal samples or other datable materials were recovered from the offset alluvial deposits. However, based on the relative lack of soil development on the meander terrace surface and their comparison to dated Holocene deposits in Panama, the sediments and subsequent fault rupture are interpreted to be late Holocene in age. Individually, none of these observations is conclusive evidence for a recent fault rupture. But, collectively they make a persuasive case for a 2.8-3.0 meter surface rupture on this fault some time after the Trail was completed around AD 1535 and before it was abandoned in the mid 1800s.

Fig. 5 shows the site currently and as we envision it before the earthquake by back-slipping 2.8 meters along the fault. All of the principal geomorphic features reconstruct across the fault, and the repair of the Trail to eliminate the 90° jog becomes clear, strongly indicating that the displacement occurred post-Trail. The Trail follows the edge of the terrace riser on the east side of the fault, but deviates from a lower riser on the west side of the fault. It is likely that the trail was constructed around a prior displacement of the terrace riser. Particularly compelling is that some of the Trail cobbles are still preserved under the fault scarp-derived colluvium, even though most were recycled to repair the Trail. Because of the historical sensitivity of the site, we were not able to excavate into the scarp to better expose the fault directly offsetting the Trail. However, the presence of the Trail cobbles under the scarp colluvium is persuasive, especially with the consistency of the geomorphic offsets along the fault.

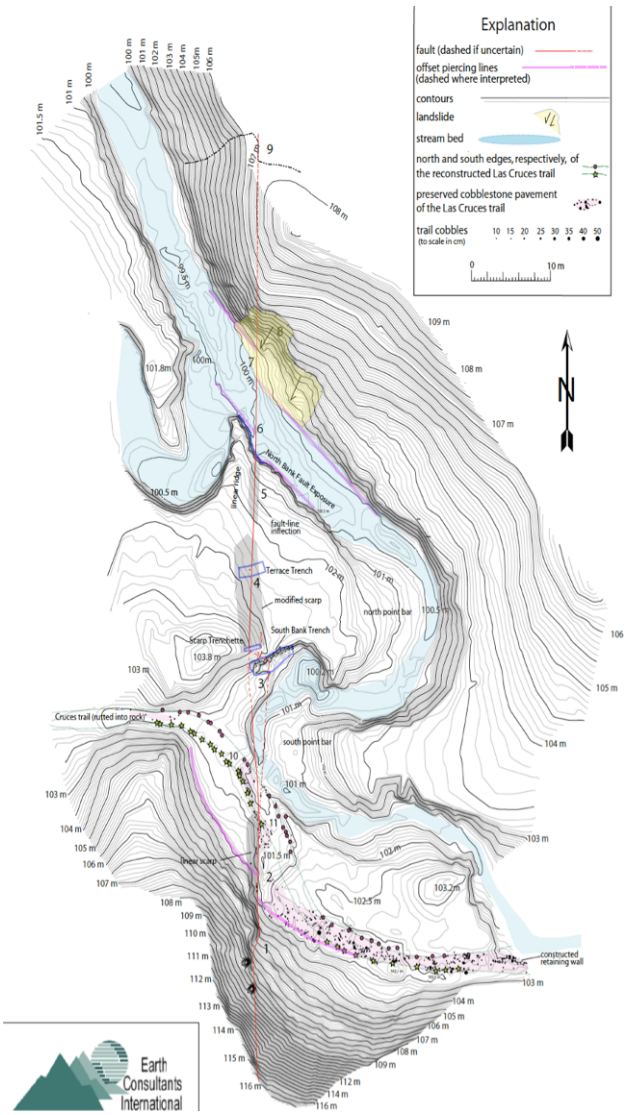

Fig. 4: Detailed map of the study location at the intersection of the Pedro Miguel fault with the Camino de Cruces showing the locations and relationships described in the text. 1: Sidehill scarp; 2: Offset terrace riser and Trail; 3: Fault exposure in stream bank; 4: Linear 0.5 m scarp; 5: Scarp; 6: Offset channel wall and fault exposure in bank; 7: Offset stream bank; 8: Landslide: 9: 3 m offset of gulley and fault exposure.

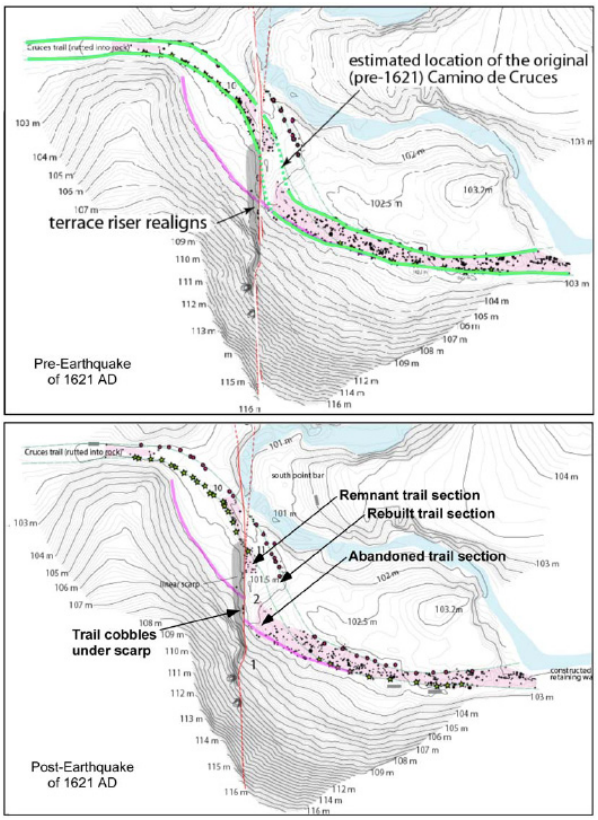

Fig. 5: Reconstruction of the Trail offset by back-slipping 2.8 meters along the fault results in a good fit for the pre-earthquake Trail location. The Trail cobbles and sizes are shown in their surveyed locations. The back-slipping results in a restoration of the terrace riser, and explains the pattern of pre- and post-displacement Trail cobbles adjacent to the fault.

CONCLUSIONS

Using numerous and independent lines of evidence, we conclude that the Pedro Miguel fault has historically ruptured through this area, producing a right-lateral surface offset of the Camino de Cruces of about 3 m, consistent with the findings from paleoseismic studies 20 km south. The displacements of all small-scale geomorphic features are consistent with the amount of displacement of the Camino de Cruces. The observation of Trail cobles under the fault scarp-derived colluvium strongly supports that the Trail had been completed before the offset.

The only reported earthquake, since the 1530s, large enough to generate a 3-meter displacement, is the May 2, 1621 Panamá Viejo earthquake. From this we conclude that the last rupture on the Pedro Miguel fault was the AD 1621 event, an earthquake that significantly damaged Panamá Viejo, and if repeated, would strongly shake the modern Panamá City and all of the Panamá Canal structures on the Pacific side. Because the Pedro Miguel fault has long been assumed to be inactive, these findings have been a surprise to the engineering community. Although the exposures of the fault offsetting late Holocene alluvium are geologically convincing, the archeoseismic evidence of the Camino de Cruces being offset by the fault has proven to be invaluable in gaining general acceptance of the seismic hazard posed by the Pedro Miguel fault.

Acknowledgments: We thank the Autoridad del Canal de Panamá for their support of this project, especially Luis Alfaro, Pastora Franceschi, Rodrigo Lam, and the Survey Division. We also thank all of the ECI staff that assisted, particularly Danielle Verdugo and Patrick Williams.

References

ECI (2009). Appendix D: Documenting the Pedro Miguel Fault's AD 1621 Offset of the Camino de Cruces; in Quantitative Characterization of the Pedro Miguel and Miraflores Faults; unpublished Earth Consultants International consulting report prepared for the Autoridad del Canal de Panamá, February, 2009.

THE *BAELO CLAUDIA* EARTHQUAKE PROBLEM APPROACHED WITH SEMI-QUANTITATIVE LOGIC TREES

C. Grützner (1) and K. Reicherter (1)

(1) Institute for Neotectonics and Natural Hazards, RWTH Aachen University, Lochnerstr. 4-20, 52056 Aachen, GERMANY. c.gruetzner@nug.rwth-aachen.de

Abstract: *The Roman ruins of* Baelo Claudia *at the Strait of Gibraltar (Province Cádiz, Southern Spain) show numerous damages on buildings and infrastructure that bear witness of two earthquakes in the 1st and 4th Century A.D. Comprehensive fieldwork has been taken out during the last years in order to find the seismic source for the events and to determine earthquake parameters. We briefly categorize the results using the semiquantitative logic tree approaches presented by Atakan et al. (2000) and Sintubin and Stewart (2008). The comparison of the logic trees, which take into account palaeoseismological and archaeoseismological observations, respectively, shows that a complementary application of both analyses can provide a far more reliable evaluation of a study site.*

Key words*: palaeoseismology, archaeoseismology, spain, logic tree*

ROMAN RUINS OF *BAELO CLAUDIA*

The westernmost part of the Gibraltar arc hosts the Bolonia Bay, close to the city of Tarifa (Fig. 1). Here, the former Roman town of *Baelo Claudia* dates back to the 2nd Century BC and was, due to its strategic position, an important trade centre. Main income was earned from tuna-fishing and *garum* export (a kind of tuna sauce). The city had approximately 2,000 inhabitants and was surrounded by a massive representative city wall. Main elements of the actual archaeological site are the theatre, the *decumanus* (main street), the forum area, an eastern and a western gate, the temples area, the basilica, and the *macellum* (market hall) (Silliéres, 1997; Alonso-Villalobos et al., 2003). Almost all parts of the ruins show damages that cannot be explained by ground settling effects, erosion, or vandalism. While some of those features could be identified as related to shallow landslides, many of them are caused by earthquakes (Silva et al., 2006, 2009; Goy et al., 1994).

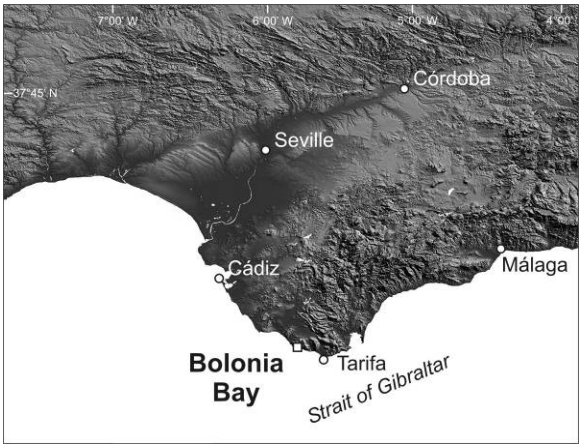

Fig. 1: The Bolonia Bay, location of the Roman remains of the Baelo Claudia village close to the Gibraltar Strait in southern Spain (SRTM data).

Among others, those typical damages include penetrative fractures in masonry blocks, pop up-like deformation of the pavement, corner breakouts of paving stones, dropped keystones of arches, tilted and folded walls, columns that fell in the same directions, and wall offsets. All earthquake damages have been mapped carefully during the last field campaigns and show a clear orientation. Inside the ruins, geophysical prospection methods were used to identify the landslide areas and to map unexcavated remains.

Archaeoseismological investigations mainly concentrated on:
- Identification of earthquake damages
- Classification of earthquake damages
- Mapping of cracks and deformation orientations
- Geophysical investigation of landslide areas inside the ruins
- Dating of event horizons

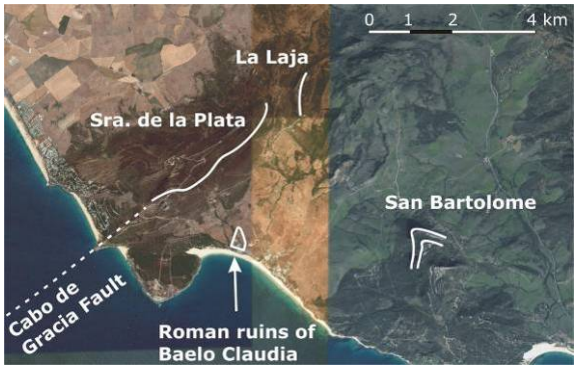

Fig. 2: The Bolonia Bay is surrounded by three steep mounain ranges of Aquitanian calcarenites. Palaeoseismological investigations concentrated on the Sierra de la Plata area.

Recent ^{14}C dating results from the Isis temple and archaeo-stratigraphic classification indicate two earthquake events in the 1st and the 3rd Century AD.

PALAEOSEISMOLOGY IN THE BOLONIA BAY

Extensive fieldwork has been carried out in the surroundings of *Baelo Claudia*. The Bolonia Bay is enclosed by three mountain ranges consisting of Aquitanian calcarenites (Fig. 2). In the east, the San Bartolome reaches an elevation of 448 m a.s.l. and is subject to intense rockfalls that show extraordinary long run-out distances. Soil analysis of the hyperplastic clays at the mountain base and rockfall modelling could proof a piggyback transport mechanism for boulders with volumes of up to 100 m³. In the western and north-western parts of the bay, La Laja and Sierra de la Plata mountain ranges form almost vertical, 80 m high walls, also reaching an altitude of more than 400 m a.s.l. Both units form prominent lineaments with lengths of several kilometers, the Sierra de la Plata, furthermore, connects to the Cabo de Gracia fault that forms the small cape north-west of *Baelo Claudia*. A variety of indications for neotectonic activity can be found along those structures. Intense mass movements can be observed at the mountain ranges as well, supported by the highly plastic clays of the Facinas and Almarchal formations.

The palaeoseismological investigations in the area concentrated on five main aspects:

- Geomorphological analysis of the large-scaled lineaments
- Geological mapping of striae, lineaments, fault planes, and deformation
- Geophysical investigation of probable fault zones
- Trenching of the Cabo de Gracia fault zone
- Landslide and rockfall analyses with regard to seismic triggered mass movements

THE SINTUBIN AND STEWART LOGIC TREE ON ARCHAEOSEISMOLOGY

The logic tree on archaeoseismology compiled by Sintubin and Stewart (2008) is adapted from the classification scheme for palaeoseismological investigations that was presented by Atakan et al. (2000, see Table 1) and which will be discussed in the next chapter.

Table 2: Comparison of the criteria postulated by Atakan et al. (2000) and Sintubin and Stewart (2008)

Atakan et al. (2000)	Sintubin and Stewart (2008)
1. Tectonic setting and strain-rate	1. Tectonic setting
2. Site selection for detailed analysis (site selection criteria)	2. Site environment
3. Extrapolation of the conclusions drawn from the detailed site analysis to the entire fault	3. Site potential
4. Identification of individual palaeo-earthquakes (diagnostic criteria)	4. Identification of damage
5. Dating of palaeo-earthquakes (type of technique)	5. Dating of damage
6. Palaeo-earthquake size estimates (slip on individual events, correlation between trenches)	6. Regional correlation

Basically, the logic tree approach is used to provide quantitatively comparable uncertainty estimations in (not only) archaeoseismological research. Therefore, Sintubin and Stewart (2008) compiled six criteria that have to be evaluated with respect to the certain investigation site properties. Each criterion delivers a quality weight factor QWF inside 0 and 1. The result is a joint probability value P_{es} between 0 and 1. A site confidence level (SCL) ranging from 1 to 10 and corresponding to 7 different stages is introduced in order to enclose information on the excavation quality and the excavation report's completeness. Finally, the archaeoseismological quality factor AQF is P_{es} times SCL.

In this study we applied the scheme of the logic tree to the investigation results from the Roman ruins of *Baelo Claudia* (Goy et al., 1994; Silva et al., 2006, 2009).

1. Tectonic setting
The Bolonia Bay is situated at the active plate boundary between Africa and Europe. Due to this setting and the good background knowledge we assume a QWF of 0.95.

2. Site environment
The Bolonia Bay area has a high seismic potential and the landscape shows several evidence for seismic activity. Implications from landscape signature after Michetti et al. (2005) lead us to choose a QWF of 0.7

3. Site potential
The Roman city was populated with about 2,000 inhabitants and encompassed hundreds of buildings that can be investigated. A long excavation history also adds to the highly reliable documentation. Despite several non-seismic damage mechanisms had to be taken into account, we could clearly distinguish those features from earthquake effects. The result is a QWF of 0.7.

4. Identification of damage
Damages have been identified at dozens of different buildings and at most parts of the paved grounds. Several hundreds of measurements were taken in the ruins, showing a clear spatial orientation and hints for an abrupt shock. As mentioned above, non-seismic damages could be ruled out. The result is a QWF of 0.8.

5. Dating of damage
Written sources on the earthquake events are not available in our case. ^{14}C dating points to two events in the 1st and the 3rd Century A.D., respectively, and seems to be reliable. Archaeo-stratigraphical dating of the event horizons supports these dates. Therefore, we assume a QWF of 0.7.

6. Regional correlation
Although all observations indicate two destructive events at the *Baelo Claudia* study site, there is no evidence from adjacent areas. The known nearby Roman settlements are either unexcavated or do not allow an archaeoseismological analysis. Following Sintubin and Stewart's suggestions, we decided to choose a QWF of 0.4.

The criteria briefly discussed above sum to a P_{es} of 0.12 for *Baelo Claudia*. In our case, the SCL is 8 (stage 6) and the overall AQF computes to 0.95 (Fig. 3).

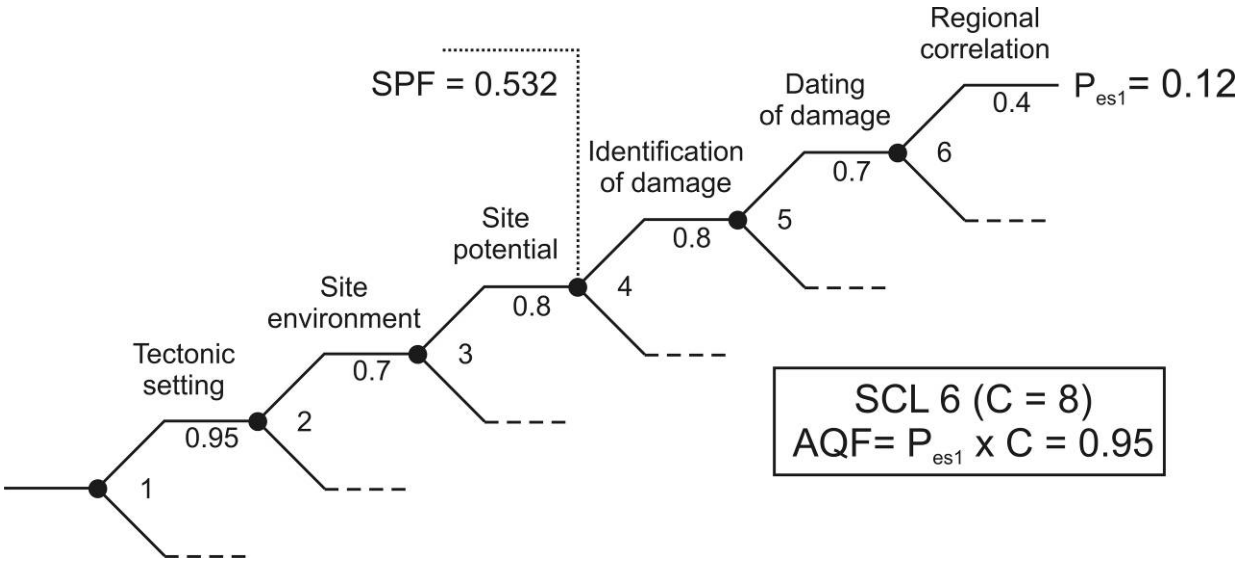

Fig. 3: The logic tree of Sintubin & Stewart (2008), as applied to the Roman ruins of Baelo Claudia*. The resulting overall probability of our preferred end solution is 0.12, the archaeoseismlogical quality factor (AQF) computes to 0.95. SPF means site potential factor and represents an interim result, taking into account the site conditions only.*

THE ATAKAN LOGIC TREE ON PALAEOSEISMOLOGY

In contrast to Sintubin and Stewart (2008), Atakan et al. (2000) created a logic tree that addresses palaeoseismological investigations (Table 1). Nevertheless, especially the first three criteria are comparable and its structure in total was the model for the archaeoseismological approach. Instead of the SCL, another criterion C_{ri} was proposed in 2000, here corresponding to the relative level of importance of a certain study. The palaeoseismic quality factor PQF can finally be calculated by PQF = P_{es} x C_{ri}.
The UNIPAS V3.0 program is designed to automate the calculations and to help with QWF adaption. It can be downloaded from the webpage of Bergen University (http://www.geo.uib.no/seismo/software/unipas/unipas1.html). For the following evaluation we only considered palaeoseismological information available.

1. Tectonic setting and strain-rate
As this criterion is similar to the one of the Sintubin logic tree, we also choose a QWF of 0.95.

2. Site selection for detailed analysis
Prior to detailed palaeoseismological investigation, GPR and geoelectrical measurements have been carried out to find a suitable trenching site. In addition, geomorphological analyses and geological mapping were applied. Due to the complicated topography, the range of available sites was very narrow. This leads to a relatively low QWF of 0.78.

3. Extrapolation of the conclusions drawn from the detailed site analysis to the entire fault
Our trenches all were close to each other and therefore do not cover an area large enough to be representative for the entire fault. We assume a QWF of 0.2.

4. Identification of individual palaeo-earthquakes
From a mere palaeoseismological point of view without the archaeoseismological data from the ruins, the identification of certain events was not possible. Nevertheless, phenomena like slickensides, lineaments, offset soils, ruptured pebbles, rockfalls, and landslides patterns strongly point to local neotectonic activity in the area. The appropriate QWF is 0.5.

5. Dating of palaeo-earthquakes
No direct dating has been taking out at the trenching sites, only the geomorphological analyses and correlations give a rough time frame. This results in a poor QWF of 0.25.

6. Palaeo-earthquake size estimates
From primary and secondary evidences like seismic-triggered landslides and rockfalls, fault length analysis, liquefaction phenomena etc. we estimated a minimum magnitude of M_W>5.5 for any event whose traces have been found. The QWF here is 0.5.

From the single QWF values the PQF results to 0.0093. As the date will be used to complete the local earthquake catalogue, we assumed a C_{ri} of 3. The overall PQF is 0.056 (Fig. 4).

COMPARISON, DISCUSSION AND CONCLUSIONS

For archaeoseismology we can compare our results to the Sagalassos case study of Sintubin and Stewart (2008) only. Given that their AQF is lightly lower than in our case, *Baelo Claudia* mainly benefits from its geological setting, not from the structural data.

Regarding the logic tree for palaeoseismology, our value is twenty times lower than the one computed on the Bree Fault example of Atakan et al. (2000) in Belgium, mainly due to the low possibility of extrapolating the trench observation to the entire fault, to the ambiguous

earthquake patterns in our trenches, and to the lack of dating.

The results of both logic trees applied on the Roman ruins of *Baelo Claudia*, although they may not be comparable that easily, differ significantly and indicate that the archaeoseismological observations are more reliable than the palaeoseismological ones in that special case. As a stand-alone technique, palaeoseismology would have to deal with many uncertainties especially caused by the limits of site selection and earthquake identification. Archaeoseismology provides information that is more detailed and achieves a higher certainty on distinct events, but finds its weak points in regional correlation of data. The combination of both methods and their evaluation by the means of a logic tree lead to a higher level of confidence and give a more particularized quality estimation of the potential of an investigation site. Due to the lack of similar studies and the absence of sufficient numbers of PQFs and AQFs, the classification of our results is finally not possible.

Acknowledgements: This study was financially supported by the German Research Foundation (DFG-project Re 1361/9). We thank the Leibniz Institute at Kiel for radiocarbon dating and the Junta de Andalucía for the permission to work inside the ruins of *Baelo Claudia* and in the Gibraltar Strait National Park.

References

Alonso-Villalobos, F.J., Gracia-Prieto, F.J., Ménanteau, L., Ojeda, R. Benavente, J. & Martínez, J.A. (2003). Paléogeographie de l'anse de Bolonia (Tarifa, Espagne) à l'époque romaine. In: The Mediterranean World Environment and History. Elsevier S.A.S. Amsterdam, 407 -417.

Atakan, K., Midzi, V., Moreno Toiran, B., Vanneste, K., Camelbeeck, T. & Meghraoui, M. (2000). Seismic hazard in regions of present day low seismic activity: uncertainties in the palaeoseismic investigations along the Bree fault scarp (Roer Graben, Belgium). Soil. Dyn. Earthquake, Eng., 20: 415-427.

Goy, J.L., Zazo, C., Mörner, N.A., Hoyos, M., Somoza, L., Lario, J., Bardají, T., Silva, P.G. & Dabrio, J.C. (1994). Pop up-like deformation of a Roman floor and liquefaction structures in SW Spain as possible palaeoseismic indicators. Bulletin of the INQUA Neotectonics Commission, 17, 42-44.

Michetti, A.M., Audemard, F.A. & Marco, S. (2005). Future trends in Palaeoseismology: Integrated study of the seismic landscape as a vital tool in seismic hazard analyses. Tectonophysics 408 (2005) 3–21, doi:10.1016/j.tecto.2005.05.035.

Sillières, P. 1997. Baelo Claudia: Una ciudad Romana de la Bética. Junta de Andalucía - Casa de Velázquez, Madrid.

Silva, P.G., Borja, F., Zazo, C., Goy, J.L., T. Bardají, T., De Luque, L., Lario, J. & Dabrio, C.J. (2005). Archaeoseismic record at the ancient Roman city of Baelo Claudia (Cádiz, South Spain). Tectonophysics, 408, 129-146.

Silva P.G., Reicherter K., Grützner C., Bardají T., Lario J., Goy J.L., Zazo C., & Becker-Heidmann P. (2009). Surface and subsurface palaeoseismic records at the ancient Roman city of Baelo Claudia and the Bolonia Bay area, Cádiz (South Spain). Geological Society, London, Special Publications 2009; v. 316: Palaeoseismology: Historical and prehistorical records of earthquake ground effects for seismic hazard assessment.

Sintubin, M. & Stewart, I.S. (2008). A logical methodology for archaeoseismology: a proof of concept at the archaeological site of Sagalassos, southwest Turkey. Bull. Seism. Soc. Am, 98: 2209-2230.

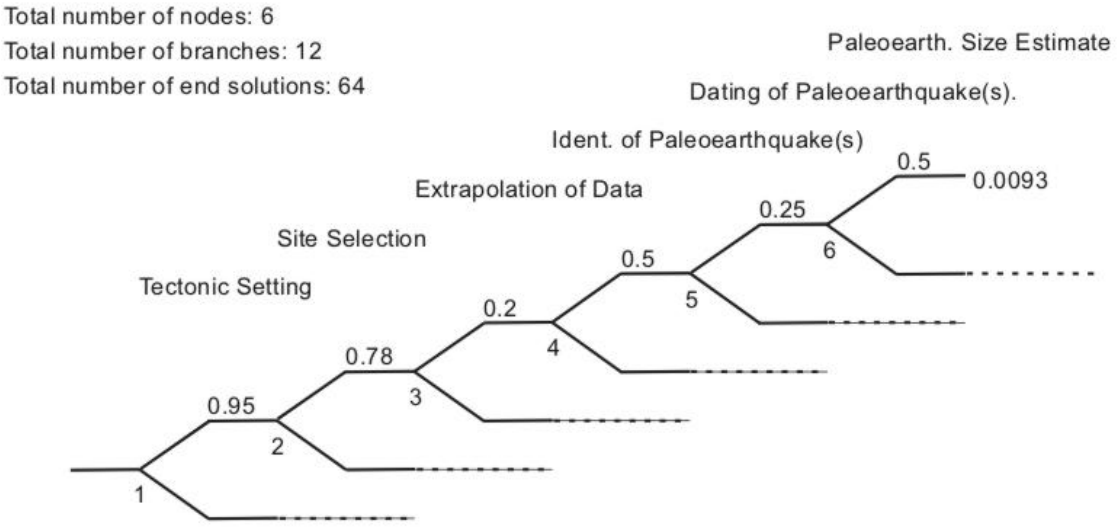

Fig. 4: The Atakan et al. (2000) logic tree for Palaeoseismology consists of 12 branches and 6 nodes at which certain probabilities must be defined. The result is the probability of the preferred end solution, Pes. In the study discussed here, Pes is 0.0093, 20 times lower than the one achieved by Atakan et al. (2000) at the Bree Fault example. UNIPAS V3.0 automatically computes the Pes based on the values entered and creates the graph.

CATALOGUING EARTHQUAKE ENVIRONMENTAL EFFECTS: A TOOL FOR THE COMPARISON OF RECENT, HISTORICAL AND PALEO EARTHQUAKES

L. Guerrieri (1), S. Porfido (2), E. Esposito (2), A.M. Blumetti (1), A.M. Michetti (3), M. Giulianelli (1) and E. Vittori (1)

(1) Geological Survey of Italy, ISPRA, Via Brancati 48, 00144 Roma, ITALY. luca.guerrieri@isprambiente.it; annamaria.blumetti@isprambiente.it; eutizio.vittori@isprambiente.it
(2) Institute for coastal marine environment, IAMC, National Research Council of Italy, Calata Porta di Massa - 80133 Napoli, ITALY. sabina.porfido@iamc.cnr.it; eliana.esposito@iamc.cnr.it
(3) Department of Chemical and Environmental Sciences, University of Insubria, Via Valleggio, 11, 22100, Como, ITALY. alessandro.Michetti@uninsubria.it

Abstract: *A global catalogue of earthquake environmental effects is under construction in the frame of the activities within the 0811 INQUA project. Data collection and implementation is based on volunteer contribution by participants to the project. Based on the applications of the ESI 2007 intensity scale, the catalogue will allow an objective comparison among earthquakes over a geological time-window: in fact, the list of earthquakes will comprehend recent, historical and also paleoearthquakes. Environmental effects induced by five strong earthquakes occurred in the last four centuries in Southern Apennines (Italy) and recorded in historical sources have been reviewed and catalogued in a standard way in order to illustrate the added value provided by this approach for seismic hazard assessment and the relevant role played by the historical sources for the characterization of earthquake environmental effects in Italy.*

Key words*: Earthquake Environmental Effects, ESI 2007 intensity scale, historical seismic catalogues, paleoseismicity, Italy*

INTRODUCTION

Earthquake Environmental Effects (EEEs) are any phenomena generated by a seismic event in the natural environment (Michetti et al., 2007). They can be categorized in two main types:

- Primary effects: the surface expression of the seismogenic tectonic source, including surface faulting, surface uplift and subsidence and any other surface evidence of coseismic tectonic deformation;
- Secondary effects: phenomena generally induced by the ground shaking. They are conveniently classified into eight main categories: slope movements, ground settlements, ground cracks, hydrological anomalies, anomalous waves (including tsunamis), other effects (tree shaking, dust clouds, jumping stones).

The use of EEEs for intensity assessment has been recently promoted by the ESI 2007 (Environmental Seismic Intensity) scale since it will unquestionably provide an added value to traditional intensity evaluations being applicable also in not inhabited areas and not afflicted by saturation of all diagnostic effects even for the greatest earthquakes. In addition, some environmental morphogenetic effects (either primary and secondary) can be stored in the palaeoseismological record, allowing to expand the time window for seismic hazard assessment up to tens of thousands of years (e.g. Guerrieri et al., 2007; Porfido et al., 2007).

The aim of this note is i) to point out the added value provided by cataloguing EEEs in a standardized way in order to allow an objective comparison of historical earthquakes, with recent and paleo events in terms of intensity assessment; ii) to illustrate some examples of Italian historical earthquakes whit particular focus on the retrieval of environmental effects from the original descriptions.

THE EEE CATALOGUE

In the frame of the INQUA (International Union for Quaternary Research) activities, a network of geologists, seismologists and engineers experts in the characterization of environmental effects from modern, historical and paleoseismic earthquakes is working on designing and compiling a new catalogue of Earthquake Environmental Effects (EEE Catalogue) of seismic events worldwide.

The main objective of the EEE Catalogue will be to bridge a gap between recent, historical and also paleoearthquakes (e.g. data deriving from paleoseismic investigations).

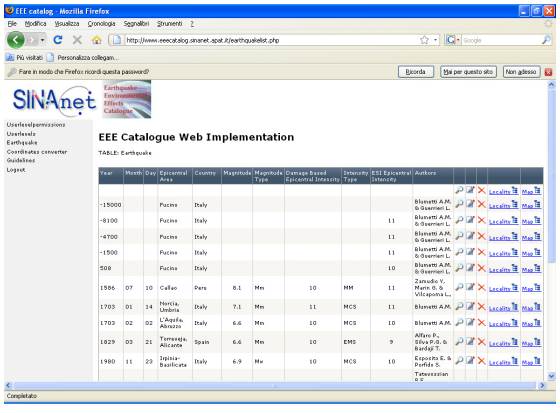

Fig. 1.The web interface for the remote implementation of the EEE Catalogue http://www.eeecatalog.sinanet.apat.it/login.php

The general structure is based on two available "pioneer inventories" (the EEE database http://www.apat.gov.it/INQUA/ and the catalogue of earthquake ground effects in Spain (Silva et al., 2008) and comprehends three different levels of detail: earthquake, locality and site. A spatial component of the EEE catalogue has been developed using the Google Maps platform. in order to depict the spatial distribution of the recorded effects. The remote implementation of the catalogue will be based on a volunteer collaboration of the participants (Fig. 1). Data will be published in the catalogue after a validation of their compliance in order to ensure scientific and technical standards.

One of the added values of the EEE catalogue will be the information on EEEs induced by paleoearthquakes (mainly coseismic surface displacements) thanks to the strong development of paleoseismological investigations. This information, although very far to be complete, can be used as a diagnostic tool for intensity assessment based on a tens of thousands years long time window. For example, in the Fucino area (Central Apennines, Italy) it is possible to compare in terms of surface displacements, the effects induced by at least 4 paleoearthquakes in the last 15,000 years with those induced the 1915 event.

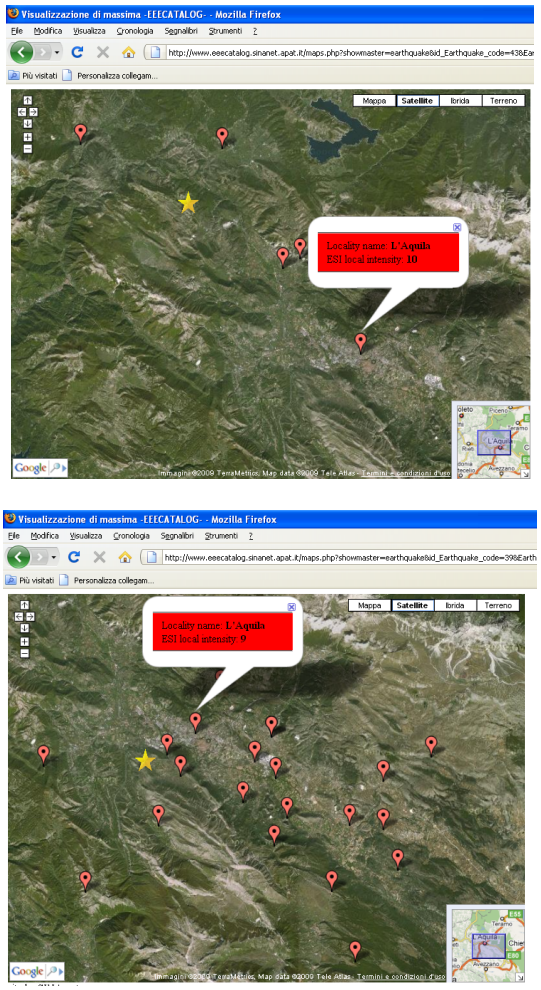

Fig. 2: Distribution of localities with EEEs triggered by the 1703 (up) and 2009 (down) earthquakes in the L'Aquila region (Central Apennines, Italy). The EEE characteristics and spatial distribution have provides ESI intensity degrees equal to X (1703 event) and IX (2009 event)

The catalogue will allow also an objective comparison between historical and recent earthquakes occurred in the same area. For example (Fig. 2), surface effects induced by the 2009 April 6th event at L'Aquila and surroundings compared with those induced by an historical but well documented event occurred in the same area on 1703 February 2nd, clearly evidences that the more recent event was at least one degree less intense than the previous one. This was pointed out by the extent of surface faulting as well as the total area of secondary effects.

Of course, the most complete collection of EEEs regards recent earthquakes. In fact, these events take advantage from "ad hoc" field surveys frequently integrated with data from remote sensing for a more systematic and extensive dataset. In this direction goes the contribution of the EEE Catalogue to the GEO (Group on Earth Observations, www.earthobservations.org) initiative, with particular regard to the SBA "Disasters" (Task DI-09-01: Systematic Monitoring for Geohazards Risk Assessment).

CATALOGUING EARTHQUAKE ENVIRONMENTAL EFFECTS IN ITALY: ANALYSES OF SOME STRONG EARTHQUAKES

A catalogue of earthquake environmental effects in Italy is an essential tool for i) research studies, since it is helpful for the identification of active/capable faults; ii) Civil Protection purposes, especially for the emergency management; iii) territorial planning, since it allow to contour the most vulnerable areas in terms of geological effects (e.g. landslides).

Thanks to the extraordinary wealth of information retrievable from historical documents (chronicles, letters, newspapers, scientific reports) and iconographic (pictures, draws, photographs, etc.), the historical record of Italian earthquakes spans in more than two millennia long time-window. Thus, even for the compilation of an inventory of seismically-induced effects for the Italian region, the use of historical sources is crucial.

The compilation of the Italian catalogue is still in progress in the frame of the aforementioned INQUA 0811 project: in the following we have reported some synthetic information about EEEs triggered by 5 strong historical events (MCS / ESI > X and inferred magnitude 6.6<M<6.9)) in a relatively homogeneous setting within the Southern Apennines. These earthquakes occurred in the last four centuries.(Fig.3) (epicentres in Fig. 3).

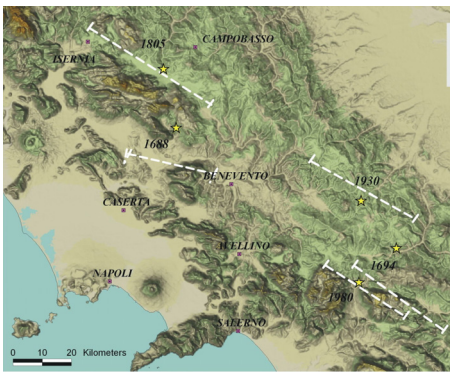

Fig. 3: Epicenters (yellow stars) and end-to-end length of rutprue zones (white lines) regarding five strong historical earthquakes in Southern Apennines (see text)

Table 1: Surface faulting extent resulting from the revision of historical sources and, only for starred (*), events with field observations

Date	Epicentral area	Victims	MCS intensity	Surface faulting
1688.06.05 (*)	Sannio	10,000	> X	**SRL: 32 km Max D = 90 cm**
1694.09.08	Irpinia-Basilicata	6,000	> X	**SRL: 38 km**
1805.07.26 (*)	Molise	6,000	> X	**SRL: 40 km Max D = 150 cm**
1930.07.23 (*)	Irpinia	1,404	X	**SRL:38 km; Max D: 40 cm**
1980.11.23 (*)	Irpinia-Basilicata	3,000	X	**SRL: 40 km Max D = 100 cm**

The analyses were conducted in details on the 5 June 1688 earthquake in the Sannio area, the 5 September 1694 and the 23 November 1980 events in the Campania-Basilicata regions, the 26 July 1805 earthquakes in the Molise region and the 23 July 1930 events in the Irpinia area (Table 1).

Historical sources have provided enough information to estimate the extent of surface faulting, expressed in terms of rupture length (SRL), maximum displacements (Max D) and the area of secondary effects (Oddone 1932; Serva, 1985a, b; Esposito et al., 1987; Esposito et al.,1998; Porfido et al., 2002; Blumetti et al., 2002).

Rupture length values, ranging from 30 to 40 km, are comparable and also consistent with damage based MCS intensities and have been sufficient to estimate the epicentral intensity according to the ESI 2007 scale (Serva et al.,2007).

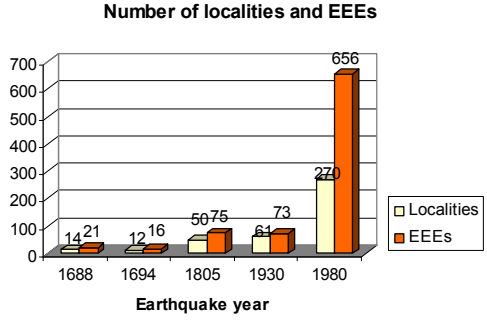

Fig. 4: Number of localities and EEEs (secondary) for each of the analysed earthquakes (see text)

Regarding secondary effects, the wealth of information for each event can be roughly measured by the number of localities with EEEs and by the total number of EEEs (Fig. 4). Of course, the age of the earthquake strongly influences these numbers that, although cannot be used as an independent measure of the earthquake size, highlight anyway the most important effects on natural environment. This scenario, integrated with effects on damages, depict the most reliable image of the earthquake effects.

Among secondary effects, slope movements are typically the most common effect, generally followed by ground cracks and hydrological anomalies. It is also noteworthy that the maximum distance from the fault of the main types of landslides for the five earthquake fall within the envelope curves for magnitude proposed by Keefer (1984).

Most hydrological changes occurred within 30–110 km from the fault rupture segment, the maximum distance of such variations from the fault was 190 km (Porfido et al., 2002; Esposito et al. 2009).

In conclusion , even if the type and the relevance of surface effects strongly depend on local geologic, geomorphic and tectonic setting, their characterization allows for a realistic estimation of source parameters, and for a proper evaluation of the environmental vulnerability in the presence of significant releases of seismic energy.

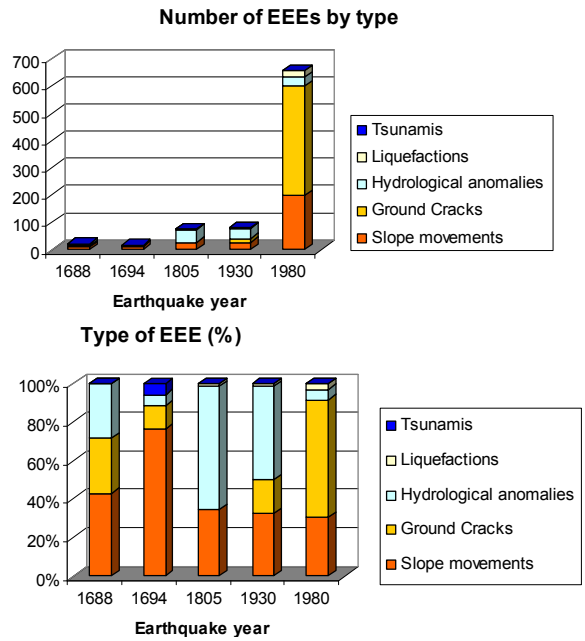

Fig. 5: Type of EEEs for each earthquake (above) and in % (below)

CONCLUSIONS

The compilation of the Earthquake Environmental Effects catalogue, in progress in the frame of the 0811 INQUA Project, will allow for the first time an objective comparison of recent, historical and paleoearthquakes. Preliminary results of the EEE catalogue implementation are showing that it is possible to compare the earthquake size in terms of ESI intensity, even if data sources are very different.

The analyses of five strong earthquakes in Southern Apennines has clearly shown the importance of historical documents for the collection of EEEs in the Italian area and pointed out the typical scenario of environmental effects induced by a intensity $\geq$X (i.e. M ~ 7) earthquake.

For these reasons, the added value provided by the EEE catalogue is evident. Therefore it will be very helpful, not only for scientific purposes but also for a correct definition of most vulnerable areas and consequent measures to be adopted for the mitigation of seismic risk.

Acknowledgments: Sincere thanks are due to the Organizing Committee of the International Workshop on Earthquake Archaeology and Palaeoseismology for their technical support.

References

Blumetti, A.M., Esposito, E., Ferreli, L., Michetti, A.M., Porfido, S., Serva, L., Vittori, E., 2002. New data and reinterpretation of the November 23, 1980, M 6.9, Irpinia-Lucania earthquake (Southern Apennine) coseismic surface effects. International Workshop ''Largescale vertical movements and related gravitational processes''. Studi Geologici Camerti 2002, 19–27.

Esposito, E., Luongo, G., Marturano, A., Porfido, S., 1987. Il terremoto di S.Anna del 26 Luglio1805. Memorie della Societa` Geologica Italiana,vol. 37, 171-191, Roma.

Esposito, E., Gargiulo, A., Iaccarino, G., Porfido, S., 1998. Distribuzione dei fenomeni franosi riattivati dai terremoti dell'Appennino meridionale.Censimento delle frane del terremoto del 1980. Proceedings of the International Convention on Prevention of Hydrogeological Hazards. C.N.R-IRPI , vol. I, 409-429,Torino.

Esposito, E., Pece, R., Porfido, S., and Tranfaglia, G.: Ground effects and hydrological changes in the Southern Apennines (Italy) in response to the 23 July 1930 earthquake (MS=6.7), Nat. Hazards Earth Syst. Sci., 9, 539-550.

Guerrieri L., Tatevossian R., Vittori E., Comerci V., Esposito E., Michetti A.M., Porfido S. and Serva L. (2007). Earthquake environmental effects (EEE) and intensity assessment: the INQUA scale project. Boll. Soc. Geol. It. (Ital. J. Geosci.), Vol. 126, No. 2, 375-386, Roma.

Keefer, D. K.,(1984). Landslides caused by earthquakes. Bull. Geol. Soc. of America, 95,406-421.

Michetti A.M., Esposito E., Guerrieri L., Porfido S., Serva L., Tatevossian R., Vittori E., Audemard F., Azuma T., Clague J., Comerci V., Gurpinar A., Mc Calpin J., Mohammadioun B., Morner N.A., Ota Y. & Roghozin E. (2007). Intensity Scale ESI 2007. In. Guerrieri L. & Vittori E. (Eds.): Memorie Descrittive Carta Geologica. d'Italia., vol. 74, Servizio Geologico d'Italia – Dipartimento Difesa del Suolo, APAT, Roma, 53 pp.

Oddone, E. (1932). Studio sul terremoto avvenuto il 23 luglio 1930 nell'Irpinia. Relazione a S. E. il Ministro dell'Agricoltura e Foresta. La meteorologia pratica 13, 16–26, (77–84, 116–125, 171–176).

Porfido S., Esposito E., Vittori E., Tranfaglia G., Guerrieri L., Pece R. (2007). Seismically induced ground effects of the 1805, 1930 and 1980 earthquakes in the Southern Apennines (Italy). Boll.Soc.Geol.It. (Ital .J. Geosci.), Vol. 126, No. 2, 333-346, Roma.

Porfido, S., Esposito, E., Michetti, A.M.,Blumetti,A.M.,Vittori, E.,Tranfaglia, G., Guerrieri, L., Ferreli, L., Serva, L.(2000).. The geological evidence for earthquakes induced effects in the Southern pennines (Italy). Surveys in Geophysics 23, 529–562.

Porfido S., Esposito E., Vittori E., Tranfaglia G., Guerrieri L., Pece R. (2007). Seismically induced ground effects of the 1805, 1930 and 1980 earthquakes in the Southern Apennines (Italy). Boll.Soc.Geol.It. (Ital .J. Geosci.), Vol. 126, No. 2, 333-346, Roma.

Reicherter, K., Michetti. A., P.G. Silva (eds.). (2009). Palaeoseismology: Historical and Prehistorical Records of Earthquake Ground Effects for Seismic Hazard Assessment. Geological Society of London, Special Publications, 316. London, U.K.

Serva, L., (1985a) The earthquake of June 5, 1688 in Campania. In:Postpischl, D. (Ed.), Atlas of Isoseismal Maps of Italian Earthquakes,vol. 114(2A). CNR-PFGRoma, pp. 44–45.

Serva, L., (1985b). The earthquake of September 8, 1694 in Campania-Lucania. In: Postpischl, D. (Ed.), Atlas of Isoseismal Maps of Italian Earthquakes, vol. 114(2A). CNR-PFG, Roma, pp. 50–51.

Serva L., Esposito E., Guerrieri L., Porfido S., Vittori E. & Comerci V. (2007). Environmental Effects from some historical earthquakes in Southern Apennines (Italy) and macroseismic intensity asseessment. Contribution to INQUA EEE scale project. Quaternary International, Volumes 173-174, pp. 30-44

Silva, P. G., Rodríguez Pascua, M. A., Pérez-López, R., Bardaji, T., Lario, J., Alfaro, P., Martínez-Díaz, J.J., Reicherter, K., Giménez García, J., Giner, J., Azañón, J.M., Goy, J.L., Zazo C. (2008). Catalogacion de los efectos geologicos y ambientales de los terremotos en Espana en la Escala ESI 2007 y su aplicacion a los estudions paleosismologicos. Geotemas, 6, 1063-1066.

THE RÍO GRÍO DEPRESSION (IBERIAN RANGE, NE SPAIN). NEOTECTONIC GRABEN VS. FLUVIAL VALLEY

F. Gutiérrez (1), P. Lucha (1) and L. Jordá (2)

(1) Dpto. Ciencias de la Tierra, Univ. de Zaragoza, C/. Pedro Cerbuna 12, 50009 Zaragoza, SPAIN. fgutier@unizar.es
(2) Calle de La Cañada 5, Portal A, 2º Izq, 28720 Bustarviejo, Madrid, SPAIN.

Abstract: *This contribution presents a geomorphological map of the Río Grío depression, located in the central sector of the Iberian Range, NE Spain. In previous geological maps this depression, ca. 30 km long, has been interpreted as an erosional fluvial valley. Geomorphological mapping reveals that it corresponds to a neotectonic graben filled by alluvial fan deposits and subsequently dissected by the axial Grío River and its tributaries. The length of the normal faults indicates that some of the mapped neotectonic structures have the potential to generate earthquakes with moment magnitudes as high as 6.8. This work suggests that there may be a limited knowledge on the distribution recent faults in some sectors of Spain and that a higher input on the geomorphology and Quaternary geology in the geological maps would help to overcome this weakness.*

Key words*: neotectonic graben, fluvial incision, geomorphological mapping, seismic hazard.*

INTRODUCTION

The Iberian Range, with a prevalent NW-SE structural trend, is located in the NE of the Iberian Peninsula. This intraplate orogene results from the tectonic inversion of Mesozoic basins occurred from late Cretaceous to Early-Middle Miocene times (orogenic stage). During the postorogenic stage extensional tectonics generated grabens superimposed on the previous contractional structures. Although an extensional stress field has prevailed in the central sector of the Iberian Range from the Middle Miocene up to the present-day, two main phases of graben development can be differentiated (Capote et al., 2002; Gutiérrez et al., 2008). The first extensional phase produced the Calatayud and Teruel Grabens, both around 100 km long and filled with Mio-Pliocene terrestrial sediments. The second extensional phase started in the Late Pliocene and generated new tectonic depressions like the Daroca Half-graben and the Jiloca Polje-graben (Fig. 1). Recently, new Plio-Quaternary grabens have been discovered through the elaboration of geomorphological maps, like the Munébrega Half-graben, which is superimposed on the SW margin of the Calatayud Neogene Graben (Gutiérrez, 1996). Three faulting events younger than 72 ka have been inferred from a trench dug across the master fault of this fault-angle depression (Gutiérrez et al., 2009). In this work we interpret for the first time the Río Grío valley, located to the NE of the Calatayud Neogene Graben, as a dissected neotectonic graben (Fig. 1).

GEOLOGICAL SETTING

The NW-SE-trending Río Grío morphostructural depression is located within the so-called Calatayud-Montalbán Massif, one of the main Paleozoic outcrops of the Iberian Range. The massif is primarily composed of strongly indurated sandstones and argillites of Precambrian and Paleozoic age. These formations are divided into two main structural units bounded by a major Variscan thrust known as the Datos Thrust (Álvaro, 1991). This structure runs along the Río Grío depression (Gozalo and Liñán, 1988) and is largely concealed by the graben fill alluvium (Fig. 1). In the studied area the SW-dipping Datos Thrust shows a linear trace indicating a high angle (Álvaro, 1991), probably caused by subsequent Variscan and/or Alpine folding. The hanging wall of the Datos Thrust, designated as the Badules Unit, is composed of Precambrian, Cambrian and Ordovician formations. The footwall is named the Herrera Unit and in the mapped sector the outcropping rocks include Ordovician and Silurian formations. The structure of the Precambrian and Paleozoic rocks is dominated by NW-SE-trending and NE-verging folds and reverse faults. The Badules Unit is affected by the NW-SE trending and SW dipping Jarque Thrust. North of La Aldehuela, this thrust, called Inogés Fault by Aragonés et al. (1980), is situated along the foot of the Vicort Range front at the southwestern edge of the Río Grío structural depression (Fig. 1). In the northern sector of the Río Grío structural depression the Paleozoic rocks of the Herrera Unit are overlain unconformably by two outcrops of Mesozoic and Paleogene formations affected by Alpine compressional structures (Fig. 1). The Paleogene sediments correspond to folded alluvial fan conglomerates. Locally, subjacent dissolution of the gypsum-bearing Keuper facies, Late Triassic in age, has produced recent deformational structures of gravitational origin with a restricted spatial distribution (Fig. 1).

DESCRIPTION OF THE RÍO GRÍO GRABEN

The 27 km long and NW-SE trending Río Grío Graben is flanked by prominent ranges made up of resistant Paleozoic rocks, the Vicort-Modorra Range to the SW and the Algairén Range to the NE. The Vicort-Modorra Range constitutes an uplifted horst that separates the Calatayud Graben and the Río Grío Graben. The Río Grío morphostrutural depression is filled with alluvial fan deposits that have been deeply dissected by the longitudinal Grío River and its tributaries.

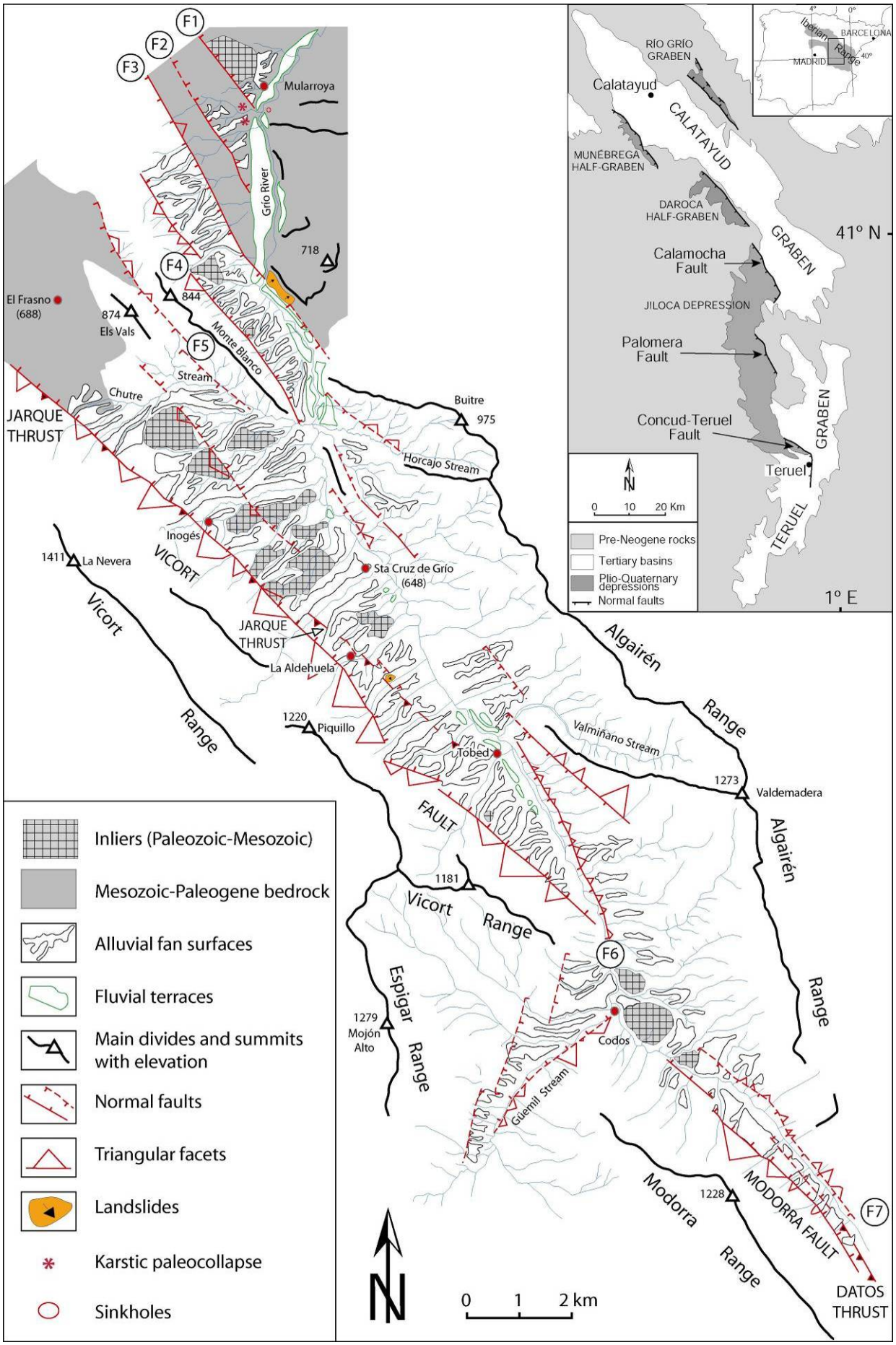

Fig. 1: Geomorphological map of the Río Grío Graben.

The graben has a markedly asymmetric geometry. The southwestern margin is controlled by two linear and well-defined normal faults; the 15.5 km long Vicort Fault and the 5.9 km long Modorra Fault. North of La Aldehuela the trace of NE-dipping Vicort Fault coincides with that of the SW-dipping Jarque or Inogés Thrust mapped by Aragonés et al. (1980). Both the Vicort and Modorra faults have a conspicuous geomorphic expression, showing linear mountain fronts with triangular facets up to 230 m. The trace of the fault coincides with the sharp rectilinear apical boundary in the alluvial fans deposited on the hanging wall. Unfortunately, no exposures showing the expectable normal fault contact between the alluvial fan sediments and the Paleozoic rocks of the uplifted blocks have been found along these range fronts. Some of the morphometric parameters of the mapped faults are presented in table 1. The Vicort and Modorra fault are separated in Codos area by a gap with a traverse tectonic depression controlled by NNE-SSW- and NE-SE-trending cross-faults and drained by the Güemil River.

Table 1. Strike (St) and length (L) of the main mapped faults, dominant lithology (Lith) in the range front, height (H) and slope (S) of the largest triangular facet and expected moment magnitudes based on the fault length and the regressions proposed by Wells and Coppersmith (1994) for normal faults (Mw W-C) and by Stirling et al. (2002) for preinstrumental earthquakes (Mw S). Lithology: Q: Quartzite; L: Limestone; C: Conglomerate; A: Argillite.

Fault	St	L	Lith	H	S	Mw W-C	Mw S
Vicort	135	15.5	Q	230	27	6.2	6.8
Modorra	136	5.9	Q	140	23	5.9	6.5
F1	148	1.7	L				
F2	147	2.8	L			5.4	6.2
F3	147	6.5	C, L	60	21	5.9	6.5
F4	146	5.8	Q	60	19	5.9	6.5
F5	148	5	Q	50	26	5.8	6.4
F6	155	4.5	A, Q	60	13	5.7	6.4
F7	137	4.1	Q	90	30	5.7	6.4

The northeastern margin of the depression is controlled by a series of shorter faults with a less obvious geomorphic expression. The trace of some of these faults coincides with the scarped northeastern margin of the Grío River fluvial valley (faults F7, F6 and southern portion of F3). Consequently, the triangular facets mapped along the northeastern margin of the Río Grío valley, generally steeper, may have a mixed tectonic and fluvial origin. The fault situated SE of Codos (F7) runs next and parallel to the Datos Thrust, suggesting that it may correspond to the postorogenic negative reactivation of the latter. In its NW portion this fault (F7) has offset alluvial fan deposits (Fig. 2) creating a downhill-facing scarp around 37 m high. The anomalous oblique orientation of some tributary drainages in the NE margin of the depression seems to be controlled by uplifted (Horcajo Stream) or backtilted fault blocks (Valmiñano Stream) in combination with stepovers.

The northern sector of the graben shows a more complex structure composed of a sequence of horsten and grabens around 1 km wide controlled by NW-SE-trending normal faults with an en échelon right-stepping arrangement. Here, the Grío River constitutes an oblique drainage with respect to the graben faults rather than a longitudinal one. These faults are defined by linear scarps with triangular facets and an abrupt termination of the alluvial fan units. The graben bounded by fault F5 and the Vicort Fault corresponds to the southernmost sector of the so-called Morés Graben, in which Triassic formations are downfaulted between fault blocks of Paleozoic rocks. The termination of these faults in our map is based on the disappearance of triangular facets and alluvial fan sediments in the downdropped block. A normal fault contact between the alluvial fan sediments and the footwall bedrock has been inferred from an outcrop of fault F1 southwest of Mularroya. To the NE of Fault F2 and at the left margin of the Grío Valley, a small drainage has exposed alluvial fan deposits affected by several vertical failure planes. A N145E strike has been measured in one of these fault planes. Between faults F1 and F2, in cuttings of the A-2302 and the old N-II roads, the alluvial fan deposits are affected by failure planes attributable to paleocollapse structures caused by the karstification of the underlying Triassic evaporites. In a cutting of the abandoned N-II road, tilted alluvial fan sediments are downdropped within highly brecciated early Jurassic carbonate rocks. We attribute this structure that does not appear in the opposite cut to evaporite interstratal dissolution and collapse.

Fig. 2: Normal fault F7 juxtaposing alluvial fan deposits against strongly deformed Paleozoic rocks.

The Río Grío graben depression is largely occupied by dissected alluvial fans. The majority of these fans are situated to the west of the Grío River. In the northern sector the NE inclination of the fan surfaces is controlled by the NW-SE trending horst and graben structure, rather than being directed towards the Grío River. The alluvial fan deposits overlie a very irregular paleorelief and show a highly variable thickness, typically higher than 30 m. Locally the alluvial fill is interrupted by rounded inliers of Paleozoic or Mesozoic rocks that protrude over the top of the fan surfaces. In Tobed area, where the base of the basin fill is probably below the current base level, we have measured a minimum thickness of 90 m of alluvium. The alluvial sequence is dominated by tabular bodies of massive angular gravels and boulders with a sandy matrix and of massive sands with scattered clasts (sheetflood deposits). Some gravel beds with a matrix-supported texture correspond to debris flow facies. Several terrace levels have been mapped north of Codos inset with respect to the alluvial fan units. This morpho-stratigraphic sequence records two main evolutionary phases: (1) A first period of alluvial filling controlled by tectonic subsidence. (2) A second period in which tectonic subsidence was not high enough to counterbalance the

incision trend of the drainage network. Probably, the transformation from an aggradational to an incisional tectonic basin was determined by alterations in the drainage network (i.e. base level drops, captures) that induced a change from a poorly drained basin to a basin effectively drained by a high gradient axial river. In the absence of chronological information on the alluvial fan sediments, based on their geomorphic setting and regional paleogeographic evolution we estimate that may have a Plio-Quaternary age.

The alluvial fan deposits and surfaces are locally offset by intrabasinal faults. The Paleozoic rocks associated with these faults are commonly strongly crushed and their low resistance to erosion favours an anomalous development of badlands. The faults dipping towards the valley produce downhill-facing scarps (fault between Modorra Fault and F7), whereas antithetic faults dipping towards the basin margins are expressed as uphill-facing scarps (Fig. 3). A GPR survey carried out across the antislope scarp situated SE of La Aldehuela has allowed us to infer tilted beds truncated by a steep SW dipping failure plane (Fig. 3).

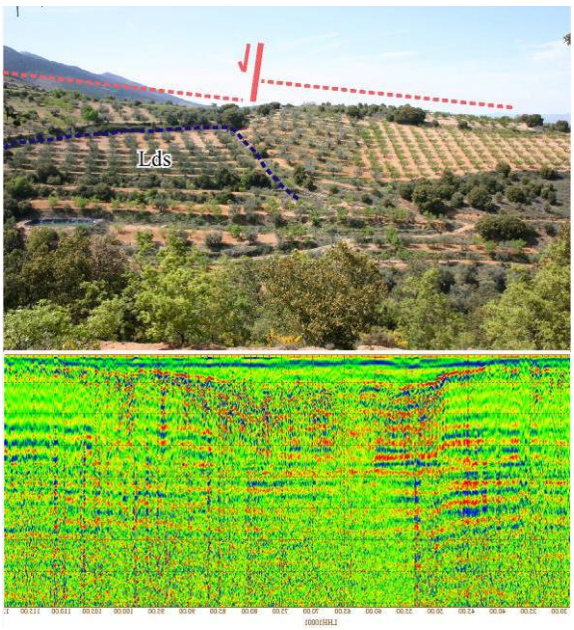

Fig. 3: Uphill facing scarp produced by an antithetic fault SE of La Aldehuela. Lds: landslide. GPR survey performed across the antislope scarp.

FINAL CONSIDERATIONS

One of the main tasks of geologists in seismic hazard assessment is the identification and mapping of recent faults that might have the potential to generate earthquakes. Based on the geomorphological map presented, some of the neotectonic faults that control the Río Grío graben are long enough to produce earthquakes with damaging magnitude (Table 1). However, the Río Grío valley has been interpreted as an erosional fluvial valley in all the geological maps published by the Spanish Geological Survey, including the geological cross sections (Aragonés et al., 1980; Olivé et al., 1983). Additionally, a detailed geological map recently elaborated for the Mularroya Reservoir Project does not represent any of the Plio-Quaternary faults depicted in our geomorphological map. Consequently, those cartographic works lead to an underestimation of the seismic hazard in the area. Conversely, the 1:1.000.000 Neotectonic Map of Spain, largely derived from geomorphological maps, depicts schematically the Río Grío valley as a linear depression bounded by two long neotectonic faults (Baena et al., 1998). Probably, some of the reasons why the neotectonic faults were overlooked in the geological maps include: (1) Most of the faults are not exposed. (2) Their identification need to be based on geomorphic criteria and careful mapping of Quaternary sediments, traditionally two secondary aspects in the elaboration of classical geological maps in Spain. This work suggests that the current knowledge on the distribution of neotectonic faults in some sectors of Spain may be quite limited and that geomorphology and Quaternary geology should receive more attention when producing geological maps in areas were young faulting may occur (McCalpin, 2008). This preliminary work will serve as the basis to conduct geophysical surveys and trenches aimed at checking inferred faults and unravelling the paleoseismic record of the tectonic structures.

References

Álvaro, M. (1991). Tectónica. In: Memoria y Mapa Geológico de España, E. 1:200.000. Daroca (40). (Gabaldón, V., coord.). IGME, Madrid, 177-204.

Aragonés, E., Hernández, A,; Ramírez del Pozo, J., Aguilar, M.J. (1980). Memoria y Mapa Geológico de España, E. 1:50.000. La Almunia de Doña Gomina (410). IGME, Madrid, 40 pp.

Baena, J., Moreno, F., Nozal, F., Alfaro, J.A., Barranco, L. (1998). Mapa Neotectónico de España, E. 1:1.000.000. IGME-ENRESA, Madrid.

Capote, R., Muñoz, J.A., Simón, J.L., Liesa, C.L., Arlegui, L.E. (2002). Alpine tectonics I: the Alpine system north of the Betic Cordillera. In: The Geology of Spain (W. Gibbons and T. Moreno, eds.). The Geological Society, London, 367-400.

Gozalo, R., Liñán, E. (1988). Los materiales hercínicos de la Cordillera Ibérica en el contexto del Macizo Ibérico. Estudios Geológicos, 44, 399-404.

Gutiérrez, F. (1996). Gypsum karstification induced subsidence (Calatatud Graben, Iberian Range, Spain). Geomorphology, 16, 277-293.

Gutiérrez, F., Gutiérrez, M., Gracia, F.J., McCalpin, J.P., Lucha, P., Guerrero, J. (2008). Plio-Quaternary extensional seismotectonics and drainage network development in the central sector of the Iberian Range (NE Spain). Geomorphology, 102, 1, 21-42.

Gutiérrez, F., Masana, E., González, A., Guerrero, J., Lucha, P., McCalpin, J.P. (2009). Late Quaternary paleoseismic evidence on the Munébrega Half-graben fault (Iberian Range, Spain). International Journal of Earth Sciences, in press.

Olivé, A., del Olmo, P., Portero, J.M. (1983). Memoria y Mapa Geológico de España, E. 1:50.000. Paniza (438). IGME, Madrid, 43 pp.

McCalpin, J. (2008). Reevaluation of Geologic Hazards in a Mountain Setting; The Case of the Climax 7.5' Quadrangle, Central Colorado, USA. 33rd International Geological Congress. Oslo. Abstract.

Stirling, M., Rhoades, D., Berryman, K. (2002). Comparison of earthquake scaling relations derived from data of the instrumental and preinstrumental era. Bulletin of the Seismological Society of America, 92 (2), 812-830

Wells DL, Coppersmith KJ (1994) New empirical relationships among magnitude, rupture length, rupture width, rupture area, and surface displacement. Bulletin of the Seismological Society of America, 84 (4), 974-1002.

DYNAMIC RESPONSE OF SIMPLE STRUCTURES

K.G. Hinzen (1)

(1) Earthquake Geology Group, Cologne University, Vinzenz-Pallotti-Str. 26, 51429 Bergisch Gladbach. GERMANY.
hinzen@uni-koeln.de

Abstract: *Two discrete element models, a three-part structured column and a 52-block wall, with the size of archaeological remains found in Susita, Israel, and Selinute, Italy, are used to study principal aspects of the dynamic behaviour during earthquake related ground motions. Systematic variation of frequency and maximum amplitude of ground motion shows that the impact pattern of a simply structured, uncemented wall reveals limited information about the nature of the ground motion. When activated by modified measured earthquake ground motion, the column model exhibits chaotic behaviour similar to coupled pendulums. Very small changes in initial conditions and/or time-dependent input forces produce unpredictable behaviour. The longer the input motion lasts, the more complex-structured the resultant ground motion becomes. Knowledge of the mechanics and dynamics of building elements typical for classical archaeological structures is an essential tool to test the seismogenic hypothesis of documented damages.*

Key words*: Column, Block Wall, Discrete Element Model, Archaeoseismology.*

INTRODUCTION

One of the main challenges for carrying out archaeo-seismic field studies is the deduction of damage scenarios. Even for cases that seem obvious concerning the nature of the damaging process, all other possible scenarios have to be taken into account. In order to further understand the reaction of archaeologically excavated structures to external forces such as earthquakes and other natural dynamic or anthropogenic sources, we studied simple structural elements.

Here we present some results from the investigation of simple columns and block walls motivated by the toppled columns of the so-called 'cathedral' in Susita (Fig. 1a) above the banks of the Sea of Galilee and the toppled block wall of the Triolo temple in Selinute (Fig. 1b), Sicily. We used similar-sized structural elements for the basic model.

MODELING PROCEDURE

Several previous studies have shown that much can be learned from numeric experiments with block structures using finite and discrete element techniques (i.e. Augusti and Sinopoli,1992; Konstantinidis and Makris, 2005; Psycharis, 2007; Hinzen, 2009). While finite element (FE) models, a standard in civil engineering, are able to predict dynamic stability and failure limits, discrete element (DE) models are suitable for modelling post failure movements of building parts. In archaeoseismology we are forced to deal with the 'final result' of the damage process, therefore the consideration of post failure movements of building parts is of special interest and speaks for the use of DE models. However, this limits the analysis to situations where the elastic properties and material strength are not crucial as for free standing columns and block structures without mortar or complex clamping devices. These are ideal candidates for DE modelling.

The aim of this study is the evaluation of the principal behaviour of simple structures, not the development of appropriate scenarios for the two archaeological sites. Therefore, only rough measures were taken from photographs and published plans of the church columns and the temple wall and non site-specific ground motions are used.

Column Model

Fig. 2a shows the column model in two versions, (1) completely rotational symmetric with round pedestal and capital and (2) with square base of the pedestal and capital top like those in Figure 1a. Total height is in both cases 5.8 m with contributions of 0.3, 4.7 and 0.8 m from the pedestal, the shaft and the capital, respectively. With a density of 2.7 Mg/m^3, the weight of the three parts is 490, 3570, and 760 kg. Joints between the column parts and between the pedestal and the base block have six degrees of freedom. Contact forces are of stick slip type with static and dynamic coefficients of 0.7 and 0.6, respectively and a contact frequency of 200 Hz.

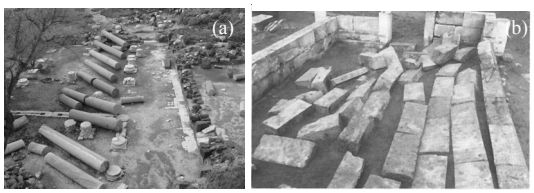

Fig. 1: (a) Row of toppled columns of the 'cathedral' in Susita, Israel (Photo: Hinzen); (b) fallen block wall of the Triolo temple at Selinute, Sicily (from Bottari, 2008)

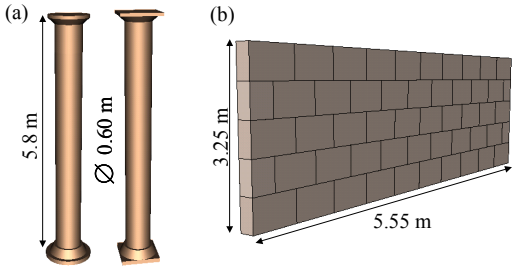

Fig. 2: Discrete element model of (a) rotational symmetric three part column (left) and a column with square pedestal and capital (right); (b) a 52-block wall.

Wall Model
The wall (Figure 2 b) consist of 52 blocks in 5 rows with 48 blocks of 0.65 x 0.55 x 0.3 m and 635 kg and four blocks at the edges of half that size. Material and contact forces were similar to those from the column model.

Input ground motion
In case of the column model ground motions were based on the measured strong motion record of the 2004 Parkfield earthquake (www.cosmos-eq.org). During the test calculations presented in this study, varying amounts of noise were added to the measured data. Amplitudes of the Gaussian-distributed noise were between 1% and 0.00001% of the measured peak ground displacement (PGD) in each of the three components of the lateral movement to test the sensitivity of the resulting trajectories on small changes of the input motion. Rotational movements were not regarded in this study.

In case of the wall, input time functions were simple single harmonic cycles with frequencies between 0.2 and 2.0 Hz and peak accelerations (PGA) of 0.25 to 6.0 m/s^2.

RESULTS

Column model
While all action and reaction forces as well as linear and angular parameters of all column parts are calculated in order to summarize the column motion during the tests with one parameter, the modulus of the trajectory vector (MTV) of the center of gravity of the column shaft was chosen. This parameter is zero, when the shaft center is in the initial equilibrium position. Local maxima in the modulus occur each time the shaft is at a turning point of the column's rocking motion.

Fig. 3 shows the time variation of the MTV during 20 numerical tests, in which the noise amplitude added to the original ground motion was 0.001% of PGD. Up to more than 6 s of the total 20 s duration, the MTV is equal for all experiments. However, at the local maximum at 7.0 s the traces start to deviate progressively with time. At this maximum the column shaft comes close to an indifferent equilibrium. Here very minor differences in the input function (due to the stochastic character of the added noise) determine the further trajectory. While in 9 cases the column finally falls after two times passing close to the initial position (local minima in the MTV), in the other cases the toppling occurs after one or two additional rocking cycles. In one case the column even survives the test and does not topple. Additional tests with other noise amplitudes showed that the point where the MTV start to deviate systematically shifts to later times with decreasing noise amplitude.

A second set of calculations was made with the square pedestal base and capital top, a model closer to the archetype (Fig. 2a) using exactly the same input motions as in the previous test. The comparison of MTVs in Figure 3 with those for the perfect rotational symmetric model shows that these rather small changes in the model shapes with only minor changes in mass, are essential for the dynamic behaviour. This is mainly due to the square pedestal, which links the column to the base. Monitoring all forces between the pedestal and the ground shows relatively large differences for square and round shapes (this will be shown in detail by animations during the presentation).

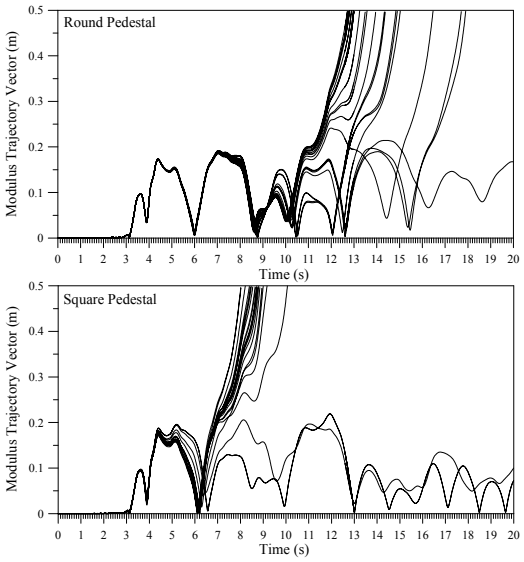

Fig.3: Modulus of the trajectory vector of the centre of mass of the column shafts (Fig. 2a) during dynamic loading. The heavier line parameterizes the columns movement when no noise is added to the measured ground motion; thin lines show results for 20 tests including noise with an amplitude of 0.001% of the PGD. Upper and lower diagrams give the results for a round and square shaped pedestal, respectively

The different shape leads to a starting separation of the MTV already at the local maximum at 4.4 s. In 18 cases the column falls after one more pass through the equilibrium position. However as shown in Fig.3, in two cases the column survives the earthquake.

Wall model
The sinusoidal ground motions used to move the base of the block wall model were applied in x-direction (orthogonal to the wall trend) alone, in the x- and vertical z-direction, simultaneously without phase shift, in both horizontal directions and in a fourth set of calculations in all three spatial directions. The impact patterns of the toppled wall are shown in Figure 4. Increasing frequencies of the ground motion require increasing values of PGA to topple the wall. When the wall topples three basic cases can be distinguished: (1) wall turns over as a whole and comes to a rest on the ground almost intact; (2) wall turns over as a whole; however the rows of blocks separate with an increasing trend from bottom to top; (3) blocks move separately and build an unstructured pile parallel to the foundation.

While the transition from (1) to (2) is mainly determined by the peak ground acceleration, case (3) occurs for ground motion frequencies significantly higher than the basic eigenfrequency of the wall as a whole in the direction perpendicular to the wall trend.

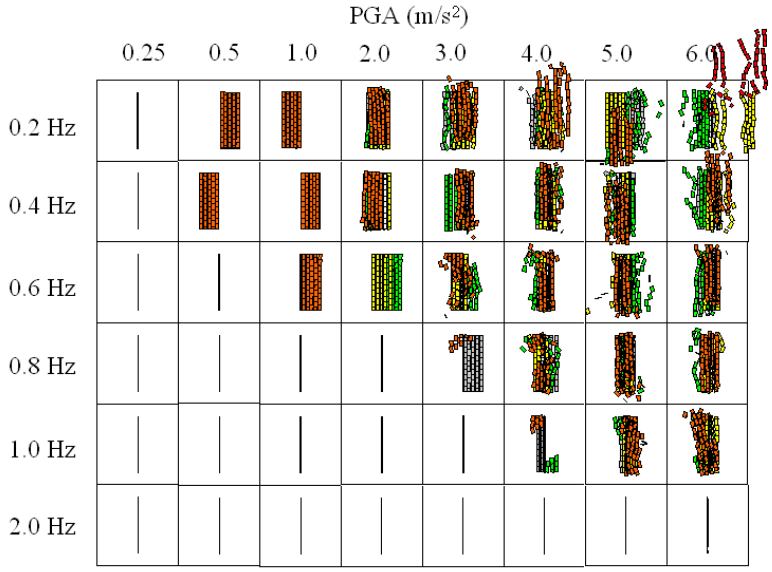

Fig. 4: Impact patterns of toppled block walls (see Fig. 2 for dimensions). Rows and columns contain the patterns for constant frequency and peak ground acceleration, respectively. Coordinates of the corner points of the vertical middle plane of the blocks are used to plot the final block position. Blocks upright at the end of the experiment appear as straight lines. Colors indicate the differences in ground motion components: x-comp, xz-comp, xy-comp, xyz-comp. As only the contact forces to the neighboring blocks and the ground were regarded in this model, the rubble piles categorized as case (3) do not show the real situation, as blocks do not interact with distant neighbors. However in case of toppling types (1) and (2) the impact pattern is completely covered by the model.

CONCLUSIONS

Two discrete element models, one of a simple 3-part column and one of a 52-block wall were used to study principal aspects of their dynamic behaviour, failure mechanisms, and final resting positions of the displaced blocks. Even though rigid block models with visco-elastic contact forces do not include elastic deformations within the individual blocks, they give insight in the general dynamic behaviour of simple structures.

Sensitivity studies of the behaviour of a totally rotational symmetric column were based on a measured earthquake ground motion. This motion from the Parkfield earthquake in 2005 shows a clear horizontally polarized motion at the time of the largest displacement. Even such highly impulsive movement produces progressively diverging dynamic behaviour of the column when small stochastic changes in the range of 1/10,000 of the PGD are applied. The chaotic character of the dynamic response indicates how problematic a detailed prediction of failure mechanisms is. The experiments in which 5% to 10% of the tests the columns survived the dynamic load, even though the change in the input ground motion was in the range of any measuring accuracy of seismic motions show that statistical approaches are necessary to predict ground motion parameters, which lead to failure of structures similar to those used in these tests.

Tests of a block wall with (unrealistic) simple sinusoidal ground motions indicate a relation between the impact patterns of the blocks on the ground after toppling. However to interpret field cases like the one shown in Fig.1, a more complicated situation that includes the influence of corners must be taken into account. Small changes of shape of the base and top in the column model lead to significant change in the toppling behaviour and indicate the importance of precise measurements and careful reconstruction during the construction of archaeoseismic models for dynamic tests.

The discrete element method is an appropriate tool for basic studies of dynamically loaded structures, with realistic earthquake-related ground motions. Combined with 3D laser scans and stochastic approaches it will help to advance quantitative archaeoseismology.

Acknowledgements: Parts of this study were financed by Deutsche Forschungsgemeinschaft (DFG HI660/2.-1). H. Kehmeier assisted with model calculations. I thank R. Kovalev for his help and support in the model set up and S.K. Reamer for discussions and improving the manuscript.

References

Augusti, G., and A. Sinopoli (1992). Modeling the dynamics of large block structures, Meccanica 27, 195-211.

Hinzen, K.-G. (2009). Topeling columns in arcaeoseismology, Bull. Seismol. Soc. Am., in press.

Konstantinidis, D., and N. Makris (2005). Seismic response of multidrum classical columns, Earthquake Engineering and Structural Dynamics 34, 1243-1270.

Psycharis, I.N. (2007). A probe into the seismic history of Athens, Greece from the current state of a classical monument. Earthquake Spectra 23, 393-415.

QUANTITATIVE METHODS IN ARCHAEOSEISMOLOGY

K.G. Hinzen (1), C. Fleischer (1), S. K. Reamer (1), S. Schreiber (1), S. Schütte (2) and B. Yerli (3)

(1) Earthquake Geology Group, Cologne University, Vinzenz-Pallotti-Str. 26, 51429 Bergisch Gladbach. GERMANY. hinzen@uni-koeln.de
(2) Archaeological Zone Cologne, City of Cologne, Heumarkt 64-66, 50667 Köln, GERMANY
(3) Institute Geology, Mineralogy and Geophysics, Ruhr-Universität Bochum, Universitätsstraße 150, 44801 Bochum, GERMANY.

Abstract: *Within the multidisciplinary field of archaeoseismology, quantitative methods have begun to be utilized more prevalently. We propose a scheme of applying quantitative models to test the seismogenic hypothesis of observed damages. The combination of 3D structural models of buildings or their remains based on phase shift laser scanner measurements with high resolution digital images allow the construction of damage and/or deformation inventory and assists the archaeological work during an excavation. 3D surface meshes derived from the same scan data are the basis for Finite or Discrete Element models of the structures. The effect of site-specific earthquake-related ground motions, other natural causes, and anthropogenic influences, are simulated and compared with the damage inventory. However, due to the high level of complexity of the problems no definite answers should be expected from quantitative models in all cases.*

Key words*: Quantitative Methods, archaeoseismology.*

INTRODUCTION

The early approaches in the relatively young field of archaeoseismology were qualitative, consisting mainly of descriptions of observed damages in archaeological excavations and were often highly speculative with regards to the damage processes. Increasingly, quantitative models have recently begun to be employed. Galladini et al. (2006) summarized complete archaeoseismic studies in a flow chart, emphasizing quantitative models as crucial tools to validate or eliminate a seismogenic hypothesis, which usually forms the basis for an archaeoseismic investigation. In Fig. 1, we propose a scheme that concentrates on archaeoseismic problems in which off-fault ground motions are the suspected cause of damages to manmade structures. We apply this scheme in two projects: the Archaeological Zone Cologne, Germany and the ancient Lycian City of Pinara, SW Turkey.

LASER SCANNING

Advanced 3D laser scans combined with high-resolution digital photographs allow detailed damage analysis even for cases where the stability of the excavated objects, safety or the lack of time prevents a thorough classical archaeological documentation. (An example will be given in the accompanying paper of Schreiber et al., 2009). Using the phase shift instead of travel time of the laser beam allows very rapid data acquisition with several million points per minute and results in a resolution of 1-2 mm in the 0.5 to 75 m distance range.

While we combine individual scans, perform signal-enhancing filtering and combination with color photos with the Reconstructor software tool, standard CAD and GIS tools are used to set up the damage inventory. Parallel to this inventory and based on the same raw data, orthophotos, crosscuts and 3D mesh surfaces are constructed. In excavation-parallel studies, as in the above-mentioned Cologne field case, the scanned images

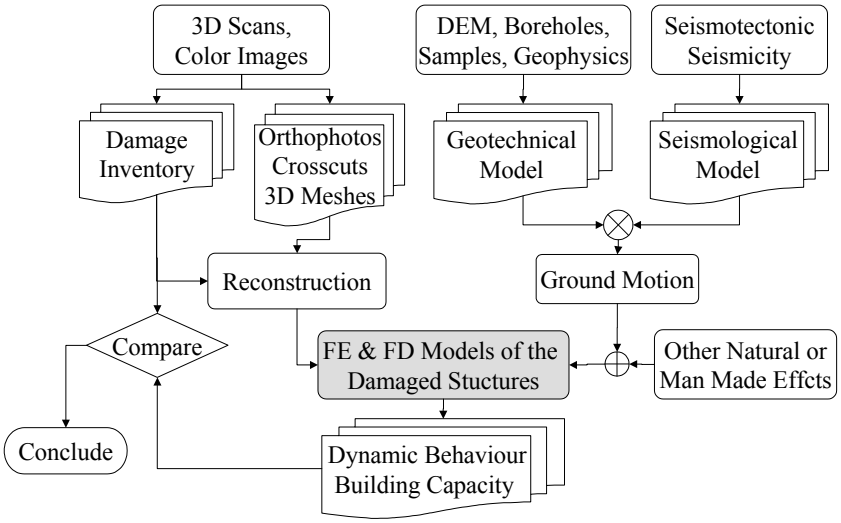

Fig. 1: Schematic flow chart of quantitative archaeoseismic modelling.

are a valuable addition to the routine archaeological work and essential for the reconstruction of heavily damaged structures. The 3D mesh surfaces are processed and transformed into Finite Element or Discrete Element models of the structures under consideration.

GEOTECHNICAL MODEL

Subsoil behaviour during earthquake-like ground motion loading can have a profound influence on damages. Even buildings with a high structural resistance to vibration loading can be heavily damaged if ground failure occurs, as is suspected for the Cologne field case. Based on contemporary DEM reconstructed from 370 boreholes, explorations, penetration tests, and geotechnical in situ and laboratory measurements 2D models are evaluated with the GeoSlope program in terms of static and dynamic slope stability and liquefaction potential. The detailed geotechnical models of the Tertiary and Quaternary *softrock* layers also help to determine site-specific seismic ground motions.

GROUND MOTION MODEL

The seismotectonic regime of the region under consideration and active fault maps provide the framework to deduce potential seismic sources. Standard seismological procedures such as the calculation of Greens functions and subsource models can be used to calculate synthetic seismograms for extended earthquake sources including appropriate rupture simulation (Fig. 1). In regions where strong motion records of recent earthquakes are available, these can be used to calibrate the models.

In addition to the computation of synthetic earthquake-related ground motions, the realization of input time functions for testing non-seismogenic causes is necessary. In the accompanying paper by Yerli et al. (2009), the possible effects of looters using explosive charges and levers is discussed. The effects of these possible causes should be compared to earthquake loading for the case of Arttumpara's sarcophagus in the ancient Lycien city of Pinara, SW Turkey.

STRUCTURE MODEL

In the central part of the flowchart in Fig. 1 is the model of the damaged structure. Classical Finite and Discrete Element models (FE and DE models) provide insight into the static and dynamic behaviour of buildings in whole or in part. FE models allow the formulation of elastic and non-elastic deformations of dynamically loaded structures and the determination of building capacities. DE models are based on the assumption of rigid bodies, coupled by visco-elastic forces, and allow calculation of block trajectories even if the structure disintegrates due to the strength of the loading. The third accompanying paper by Hinzen (2009) shows possibilities and limits in the application of DE models applied to columns and a simple block wall.

CONCLUSION

The nature of the damage-causing effects as a result of numerical test series is compared with the damage inventory. Under favourable conditions, the damage pattern of archaeologically-excavated structures can reveal enough information to conclusively test a seismogenic hypothesis or narrow down the parameter range of the ground motions. However, a detailed damage inventory and precise measurements of the structure(s) are necessary. Often the site conditions are crucial and have to be included in the determination of site-specific strong motion seismograms. Due to the high level of complexity of the problems, no unambiguous results can be expected from all quantitative models. Large efforts are necessary to narrow down the manifold model parameters enough that clear conclusions can be postulated. In some cases, changes and alterations during the period since the damage occurred might even make this impossible.

Acknowledgements: Parts of this study were financed by Deutsche Forschungsgemeinschaft (DFG HI660/2-1).

References

Galadini, F., Hinzen, K.G. and Stiros, S. (2006). Archaeo-seismology: methodological issues and procedure. Journal of Seismology, 10, 395-414.

Hinzen, K.G. (2009). Dynamic Response of Simple Structures. 1st INQUA-IGCP-567 International Workshop on Earthquake Archaeology and Palaeoseismology, Baelo Claudia, Spain, this volume.

Schreiber, S., Hinzen, K.G. and Fleischer, C. (2009). An application of 3D laserscanning in archaeology and archaeoseismology - the Medieval cesspit in the Archaeological Zone Cologne, Germany. 1st INQUA-IGCP-567 International Workshop on Earthquake Archaeology and Palaeoseismology, Baelo Claudia, Spain, this volume.

Yerli, B., Schreiber, S., Hinzen, K.G. and Ten Veen. J. (2009). Testing the hypothesis of earthquake-related damage in structures in the Lycian ancient city of Pınara, SW Turkey. 1st INQUA-IGCP-567 International Workshop on Earthquake Archaeology and Palaeoseismology, Baelo Claudia, Spain, this volume.

ROCK FALL HAZARD MAPPING AND RUN OUT SIMULATION - A CASE STUDY FROM BOLONIA BAY, SOUTHERN SPAIN

N. Höbig (1), A. Braun (2), C. Grützner (1), T. Fernández-Steeger (2) and K. Reicherter (1)

(1) Institute of Neotectonics and Natural Hazards, RWTH Aachen University, Lochnerstr. 4-20, 52056 Aachen. GERMANY.
(2) Department of Engineering Geology and Hydrogeology, RWTH Aachen University, Lochnerstr. 4-20, 52056 Aachen, GERMANY.
nicole.hoebig@rwth-aachen.de

***Abstract**: For a case study on rock fall simulation and hazard mapping the rock fall site around the San Bartolomé mountain ridge in Southern Spain was investigated. The major aim was to analyse the potential of rock falls and the risk of the inhabitants of the villages Betis and El Chaparral. Thus rock fall debris were mapped in detail to analyse them with regard to possible trigger mechanisms. Different empirical and numerical runout simulations were computed and resulted in three possibilities for rock movement. According to trigger mechanisms and predicted runout distances rock fall hazard maps were created and risk analysis was undertaken.*

***Key words**: rock falls, runout analysis, trigger mechanism, risk assessment*

INTRODUCTION

A rock fall analysis for hazard mapping in the Bolonia Bay Region close to Tarifa (Spain) was undertaken (Fig. 1). The NE and SW-side of the San Bartolomé mountain ridge were investigated and mapped in detail to identify the hazardous areas. The deposits of large-scaled rock fall blocks and debris were mapped and runout distances were determined based on GIS analysis. Since housing areas are located beneath the source zone and large blocks may be found close to houses and settlements, there is a risk for inhabitants to be victim of rock falls and damage of houses or infrastructure.

Fig. 1: Overview of the San Bartolomé with the two main investigation areas.

GEOLOGICAL SETTING

The Bolonia Bay is part of the Flysch zone of the Betic Cordillera. Steep rock walls, which consist of quartzitic Aljibe sandstone shape the NE- and SW-flank of the San Bartolomé mountain ridge. This turbiditic Miocene rock is intensively weathered and shows a distinct, perpendicular shaped joint pattern. The joint system causes large boulders, which are tilted or rotated out of the rock wall as a consequence of gravitational mass movements or possible earthquakes (Silva et al., 2009) (Fig. 2).

The deposits are widespread beneath the source zone and reach runout distances of up to 2 kilometers and sizes from 2 m^3 up to 350 m^3. For more than 300 blocks data on size, shape, type of rock and location were collected.

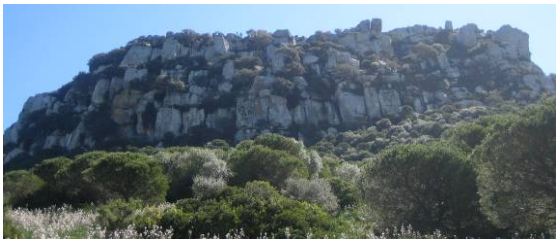

Fig. 2: Intensely joined and weathered source zone with rotating boulders on the N-side of the San Bartolomé.

RUNOUT ANALYSIS

As a first step runout analysis was performed using empirical models. Most empirical models for rock fall analysis are based on relationships between topographical factors and runout distances. Two important models are the "Fahrböschung" or "angle of reach", introduced 1932 by Heim and the "shadow angle" by Evans and Hungr (1993). The principle of both models is shown in figure 3. The identification of minimum angles can serve as an approximate runout distance prediction. In different case studies minimum values for the angle of reach and the shadow angle were postulated. Evans and Hungr (1993) observed a lower limit for the angle of reach of 28,43° and a minimum shadow angle of 27,5°. Dorren (2003) proposed a range of 22-30° for the minimum shadow angle.

The angle of reach and the shadow angle were calculated for the rock fall deposits on the west flank of the San Bartolomé mountain ridge using the geographical information system ArcGIS (ESRI).

Compared to the proposed minimum angles from the case studies, the models fit quiet well for some areas close to the rock fall source zone (green background in Fig. 4). In areas with large travel distances (more than 300

to 400 m) the calculated values for angle of reach and shadow angle did not fit the usual ranges, especially on the SW-flank of the San Bartolomé mountain ridge, see white background in Fig. 4.

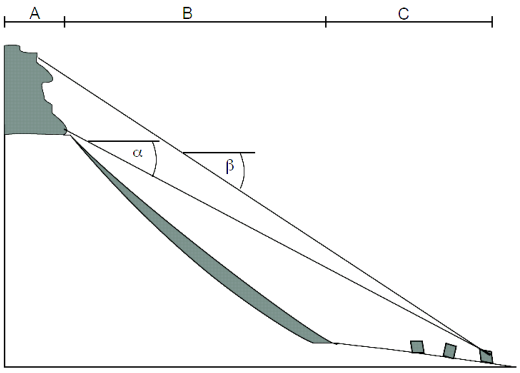

Fig. 3: Angle of reach (β) and shadow angle (α) according to Evans and Hungr (1993) with source zone A, talus slope B and shadow C.

Furthermore, a numerical trajectory based model, the computer programme Rockfall 6.1 was used for runout analysis. Rockfall 6.1 enables the simulation of the fall of rocks down a two-dimensional slope with certain surface conditions (Spang 1995; Spang 2001). The programme computes the rock fall path, total kinetic energy, bounce heights and runout distances.

The simulation was performed for several slope profiles on both sides of the mountain under recent surface conditions (covered soil) and under extreme conditions

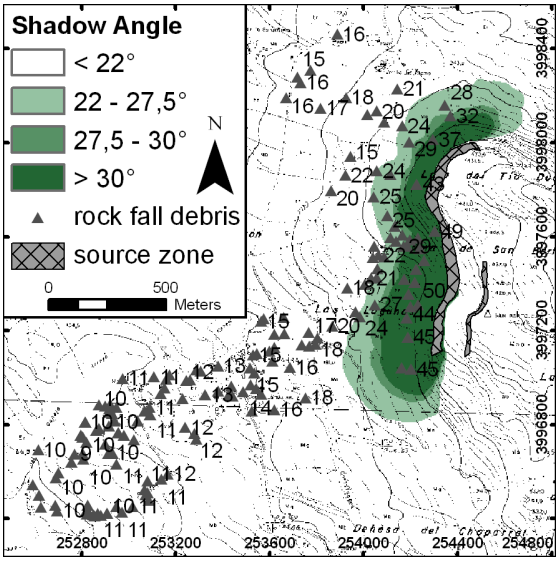

Fig. 4: Calculated shadow angles with minimum shadow angles

(bare rock). The slope profiles were identified with GIS by extracting steepest paths from a digital elevation model.

The results of the simulation under recent conditions are shown in Fig. 5. The simulation fits very well the depositions on the east flank and on the NW-flank of the San Bartolomé mountain ridge. Again, the areas with large travel distances on the SW-flank mark an exception. Even under extreme conditions the simulation does not achieve the runout distances of the depositions.

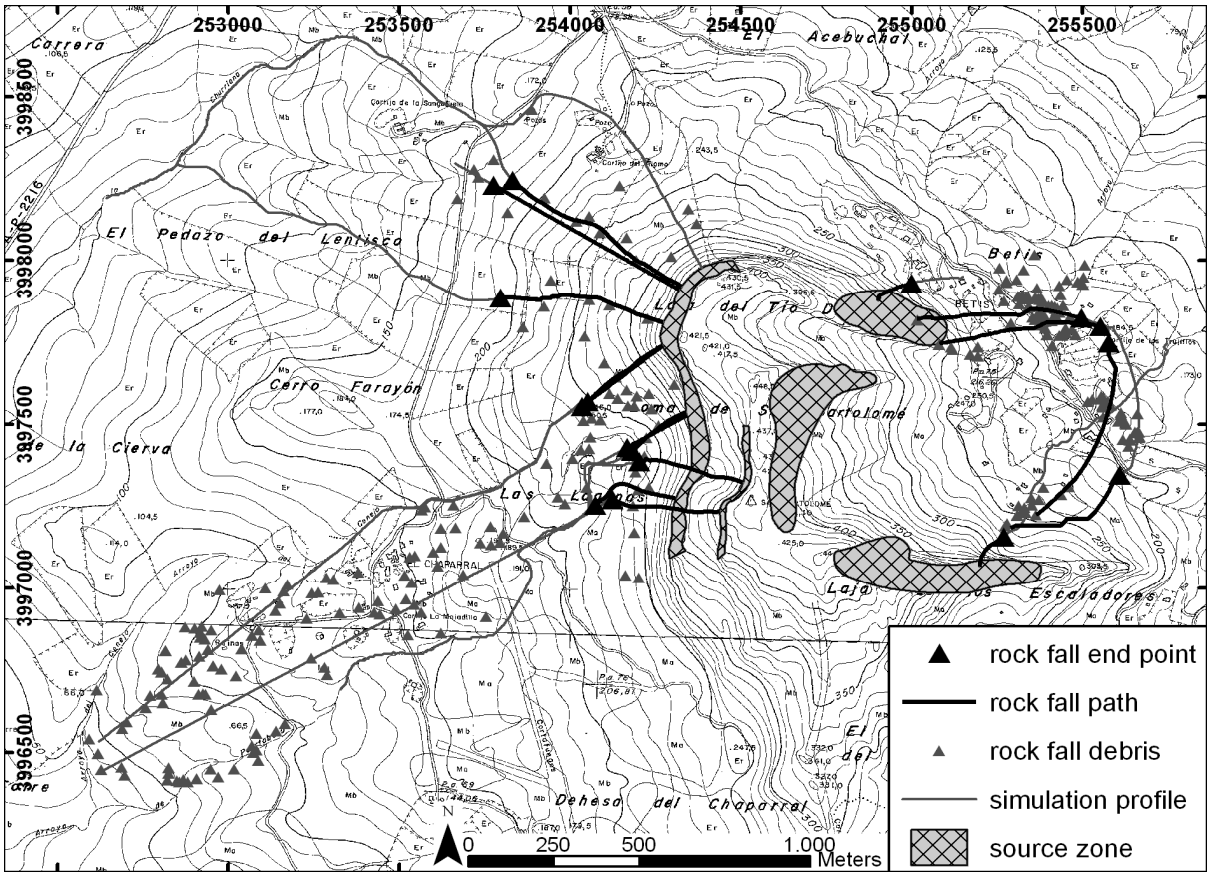

Fig. 5: The results of the numerical rockfall simulation with Rockfall 6.1 under recent conditions.

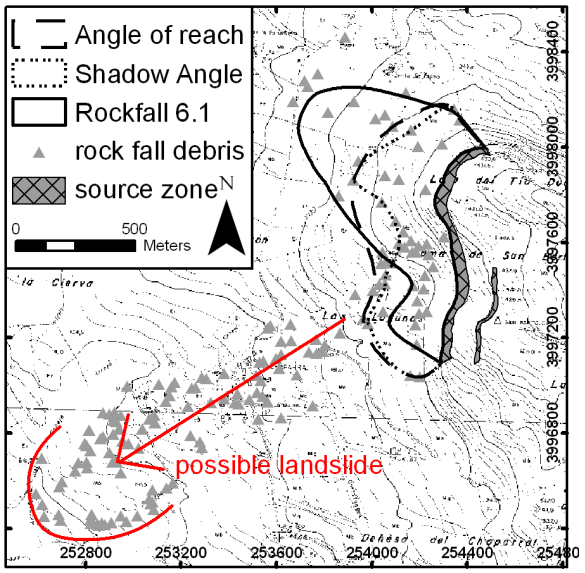

Fig. 6: Comparison of the results of three different models for runout prediction and possible landslide.

A comparison of the different model predictions for runout distances is shown in Fig. 6. Results of all models (empirical and numerical) agree with observed runout distances in some areas. Here rock fall deposits might be characterised as younger events. In other areas, especially on the SW-flank, observed runout distances vary strongly from model predictions. A secondary post-depositional transport of older rockfall deposits, by a landslide or by creep might provide an explanation. A possible landslide that can be derived from the topography is shown in figure 6. Another explanation is a debris avalanche that was triggered by an earthquake.

HAZARD MAPPING

As a preliminary step for risk analysis a hazard map, which includes rockfall susceptable zones, is required. The evaluation of the modelled data demands a choice of one classification including adequate methods.

The classification after Aleotti and Chowdhury (1998) was picked for hazard mapping, which distinguishes between qualitative and quantitative approaches. Qualitative methods contain e.g. geomorphologic analysis or index- or parameter maps and the quantitative methods consist of statistical or geotechnical operations. In this study, the geomorphologic analsis and the deterministic simulation with Rockfall 6.1 (Spang and Sonser, 1995) was combined to generate the hazard map.

By using ArcGIS, the source zones, deposit areas, and rockfall traces were created and combined. These computation resulted in three rockfall susceptible zones, which belong to different source areas, as shown in Fig. 7.

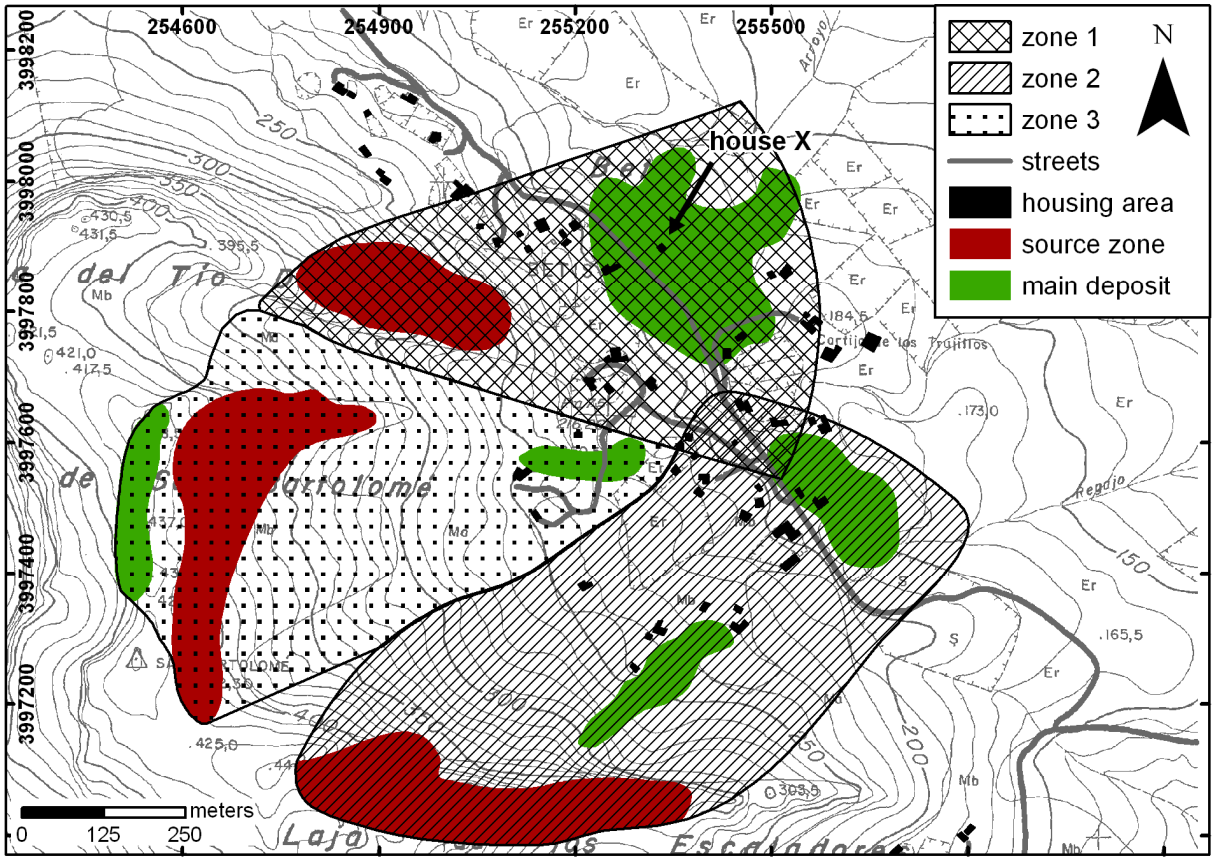

Fig. 7: Hazard map, as a result of combining data of field survey and simulations, with endangered zones and infrastructure on the NE-side of the San Bartolomé.

RISK ANALYSIS

The created hazard map contains regions which are in general endangered by possible rockfall events. In contrast to that the risk analysis includes the probability that somebody or something is influenced by a negative event, e.g. rock falls.

Our study comprises probability calculation, which regards different recurrence intervals of possible trigger mechanisms. Intense weathering and earthquakes are assumed to be triggers. For weathering induced rock fall the recurrence interval is supposed to be 20 years. Moreover for seismic triggered mass movement palaeoseismological and archeoseismological investigations already showed that destructive, local earthquakes with at least magnitude 6 occurred in the region (Silva et al. 2006; Silva et al. 2009). Resulting from a frequency-magnitude analysis a recurrence interval of 100 years for a magnitude 6 earthquake and 1000 years for a magnitude 7 earthquake were extrapolated. For these trigger mechanisms a probability calculation was made.

This calculation considers three different possibilities:

(0) to be at the wrong place (w.p.)
(1) to be there at the wrong time (w.t.)
(2) the possibility that an event happens (recurrence intervals)

This describes the following equations after Lee and Jones (2004), which were used (with P = probability) for calculation:

P(wrong place) = size abode / size danger zone
P(wrong time) = duration of stay / hours per day
P(affected) = P(w. p.) * P(w. t.) * P(event)

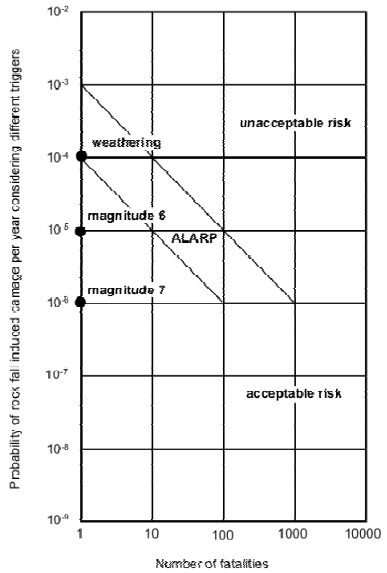

Fig. 8: Evaluation of the probability calculation by the ALARP principle (changed after Fell & Hartford, 1997).

These equations were estimated for one chosen house in the investigation area (see „house X“ in Fig. 7). It results in a probability of $5{,}2*10^{-4}$ for weathering and for the earthquakes with magnitude 6 and 7 the probability calculation resulted in one to two magnitudes less.

For assessing the calculated probabilities we followed an approach after Fell and Hartford (1997), which was in origin developed for dam construction. It is the so-called ALARP-principle, where ALARP means "as low as reasonibly practible". The diagramm (Fig. 8) shows that weathering-induced rock fall events close to the ALARP zone. Although there is a permanent risk for the inhabitants the evaluation indicates that no protection structures are required.

The result of risk assessment, which was based on the application of empirical and numerical runout analysis, indicates that there is an acceptable risk for the inhabitants. According to that and the low population density, no protection structures are required. Since the area is located in a nature protection area and settling into the region is not longer allowed, an indirect protection measure is provided. The long runout distances of the rock fall depostits on the SW-side of the San Bartolomé are assumed to be caused by an unusual event like a piggyback transport on a landslide or seismic induced mass movement. In this part of the deposition area in the near future no further rock falls are expected.

References

Aleotti, P., Chowdhury, R. (1998). Landslide hazard assessment: summary review and new perspectives. Bull. Eng. Geol. Environ 58, 21-44.

Dorren, L. K. (2003). A review of rockfall mechanics and modelling approaches. Progress in Physical Geography, 27,1, 69–87.

Evans, S., Hungr, O. (1993). The assessment of rockfall hazard at the base of talus slopes. Canadian Geotechnical Journal, 30, 620–636.

Fell, R., Hartford, D. (1997). Landslide risk assessment. In Cruden, D. & Fell, R. (Hrsg.) Landslide risk assessment. Proceedings of the international workshop on landslide risk assessment, 51-110.

Heim, A. (1932). Bergsturz und Menschenleben. Vjschr. d. Naturforsch Ges. Zürich, 216 pp. (in German)

Lee, E.M. & Jones, D.K.C. (2004). Landslide risk assessment. p. 404.

Silva, P.G., Goy, J.L., Zazo, C., Bardaji, T., Lario, J., Somoza, L., Luque, L., & Gonzales-Hernandez, F.M. (2006). Neotectonic fault mapping at the Gibraltar Strait Tunel area, Bolonia Bay (South Spain). Engineering Geology, 84, 31-47.

Silva, P.G., Reicherter, K., Grützner, C., Bardaji, T., Lario, J., Goy, J.L., Zazo, C. & Becker-Heidmann, P. (2009). Surface and subsurface paleoseismic records at the ancient Roman city of Baelo Claudia and the Bolonia Bay area, Cadiz (South Spain). In: Historical and prehistorical records of earthquake ground effects for seismic hazard assessment. (edited by Reicherter, K., Michetti, A.M. & Silva, P.G.). Geol Soc. London, Spec. Publ., 316, 93-121.

Spang R. M., Krauter, E. (2001). Rockfall simulation – a state of the art tool for risk assessement and dimensioning of rockfall barriers. In: Kühne, M. et al.: UEF International Conference on Landslides -Causes, Impacts and Countermeasures, Davos, Switzerland, 607–613

Spang, R.M., Sonser, Th. (1995). Optimized rockfall protection by "Rockfall". Proc 8th Int Congress Rock Mechanics, 3, 1233-1242.

TECTONIC MORPHOLOGY OF THE LAKE OHRID BASIN (FYROM, ALBANIA)

N. Hoffmann (1), K. Reicherter (1); C. Grützner (1), T. Wiatr (1) and T. Fernández-Steeger (2)

(1) Neotectonics and Natural Hazards, RWTH Aachen University. Lochnerstr. 4-20. 52056 Aachen, GERMANY
n.hoffmann@nug.rwth-aachen.de
(2) Chair of Engineering Geology and Hydrogeology, RWTH Aachen University. Lochnerstr. 4-20. 52056 Aachen, GERMANY

***Abstract**: The Ohrid Basin is a major N-S trending graben structure located on the border of Macedonia (FYROM) and Albania, associated with other basins in the Dinaride mountain belt. Within the basin an "ancient lake" developed since the Late Miocene/Pliocene. Since the beginning of basin formation around 700 m of sediment accumulated in the lake, the initial stage of basin formation is a strike-slip movement followed by extension. The general geodynamic setting of the Lake Ohrid area can be described with a "basin and range" situation. The multidisciplinary ICDP-SCOPSCO initiative is currently investigating Lake Ohrid and its environs in order to launch a deep drilling project.*

***Key words**: Palaeostress, Palaeoseismology, Macedonia, Albania*

INTRODUCTION

The evolution of the Lake Ohrid Basin is not only discussed by geoscientist but is also a big issue to the biology community because of the high number of endemsim. In order to understand the mechanisms that affected the Western Macedonian area the multidisciplinary ICDP-SCOPSCO project will be carried out at Lake Ohrid. Within this a structural and tectonomorphological study is accomplished at the vicinity of the lake.

Lake Ohrid considered as an "ancient lake" was tectonically formed during the late Tertiary in the extensional periods of the Palaeogene and Neogene (Dmurzdanov et al. 2004). The main objective of the observation is to delineate the (neo)tectonic history of the lake. We combined the data of the palaeostress analysis with those of the joint and fracture analysis to track the assumed lineations which we derived from satellite images and old geological maps. In addition features such as fold axes of older deformation phases were measured to accomplish the picture of different deformation phases.

The area which was investigated stretches from the east of the Lake including the Mountains of the Galicica National Park to the west where up to now only the areas close to the shore lines were taken into account. Because of rapidly rising relief on both sides of the lake, data taken on top of the mountains are not representative for the given research topic. The northern tip of the investigated area is the outlet of the river Crni Drim and the south is limited by the end of the aggradations plain. Therefore the investigation focused on fault planes with striae close to the western and eastern shorelines of the lake. The lithologies are mainly Triassic limestones and Mesozoic ophiolites.

The origin of the lake formation is unclear, possibly an older tectonic transtensional phase or reactivation led to a pull-apart like opening of the basin, followed by E-W directed extension. A certain influence of basement structures on the present-day fault patterns has been assumed, but not proven. Present-day slip rates of faults estimated by GPS are smaller than 1 to 2 mm/a (Burchfiel et al., 2006), but the uncertainties are larger than the observed movement. GPS data are still not precise enough to discriminate active faulting.

GEOGRAPHY AND GEOLOGY OF THE LAKE OHRID BASIN

The Lake Ohrid Basin (40°54' - 41°10' N, 20°38' - 20°48' E) is located at the border of the Former Yugoslavian Republic of Macedonia (FYROM) and Albania stretching over a length of c. 30 km and a width of c. 15 km. Within the basin an "ancient lake" developed. The time frame of the lake evolution ranges between 2-10 Ma depending on different authors. Clear is that the lake formed in an early stage of the basin development and probably as an initial small river crossing the graben. (Albrecht and Wilke 2008). The lake at an altitude of 693 m a.s.l. is surrounded by the horst of the Galicica Mountain Range with a height of 1750 m - 2200 m to the east and the Mokra Mountain Chain with a height of c. 1500 m to the west. With almost

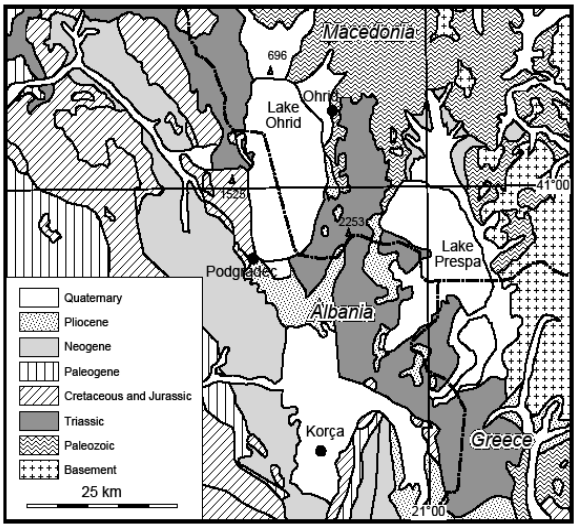

Fig.1: Geological Map of the Lake Ohrid region (Wagner et al 2008)

290 m water depth the basin accumulated about 700 m of sediments since the Late Miocene/Pliocene. The basin morphology is relativeley simple with a general N-S orientation and straight shorelines.

The region of the Ohrid Basin is part of the Alpine orogeny that formed during late Jurassic to Miocene and belongs to the N-S trending system of the Dinarides and Hellenides. The orientation of the basin matches the general orientation basins of the Balkan region. All graben structures like the Korce Basin are bent to N-S trending faults. In Fig. 1 it is clear that the strike of the basins (N-S) does not correspond to the strike of the major tectonic units (NW-SE). This already gives evidence that the basins are formed due to a younger deformation stage. Through the Pliocene the Ohrid and the Korce Basin belonged to the same lake-river-system and have been disconnected lateron.

NEOTECTONICS AND SEISMICITY

FYROM and Albania are seismic active regions. Especially, the intramontane basins of Late Neogene age form highly active seismic zones in the region with a high risk of moderate earthquakes. Several moderate earthquakes have been reported during the last few centuries (Muco 1998; NEIC database, USGS). Major earthquakes occurred during historical times. Lychnidos (the ancient city of Ohrid) was destroyed completely by an earthquake in 526 AD. It was rebuilt by Emperor Justinian (527-565), who

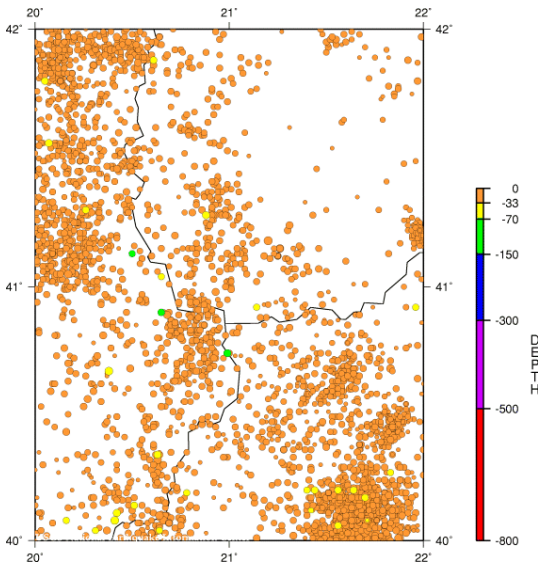

Fig.2: Seismicity Map NEIC database

was born in the vicinity, and was called by him Justiniana Prima, i.e. the most important of the several new cities that bore his name. The last prominent earthquake took place in on 18th February 1911 at 21.35 close to Lake Ohrid Basin, (M 6.7, corresponding to EMS X; 15 km depth, N 40.9°, E 20,8°). The last earthquake occurred on Jan 8th 2009 with a magnitude of M_W=4.9 close to the lake. Hypocenter depths scatter between 10 and 25 km but some deeper earthquakes occur between 25 kmand 50 km depth. Very rarely intermediate earthquakes around 100 km depth are observed. Small and moderate earthquakes (< M 5.5) take place predominantly along major fault zones, and are concentrated along the margins of the Ohrid Basin. The Ohrid-Korça Zone is considered to be the region of the highest seismic hazard in the Albanian-Macedonian Corridor based on present-day seismicity (see Fig. 2) (Aliaj et al., 2004). The present day tectonic regime can be divided in a coastal domain of compression at the Adriatic coast followed by an interior domain of extension dominated by north striking normal faults to the west (see Aliaj et al. 2004).

TECTONIC GEOMORPHOLOGY

The Ohrid Basin meets all criteria of an active, seismogenic landscape: linear step-like fault scarps occur in the landscape and under water in the lake. Wineglass shaped valleys, wind gaps, triangular facets and well preserved scarps are exposed (see Fig. 3). Also rotated blocks can be inferred by the geomorphology. Postglacial (or Late Pleistocene) bedrock fault scarps at Lake Ohrid are long-lived expressions of repeated surface faulting in tectonically active regions, where erosion cannot outpace the fault slip. Generally, the faults and fault scarps are getting younger towards the basin center, as depicted on seismic and hydroacoustic profiles. Additionally, mass

Fig.3: Topography at Lake Ohrids east coast. View from N.

movement bodies within the lake and also onshore (rockfalls, landslides, sub-aqueous slides, homogenites, turbidites) are likely to be seismically triggered, eventually damming the outflow of Lake Ohrid temporarily.

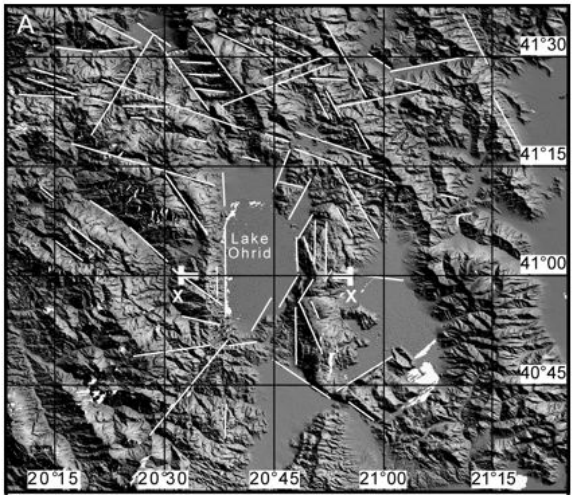

Fig.4: Shaded relief of the Lake Ohrid area (based on Shuttle Radar Topographic Mission data, light from east). Morphological lineations (white lines) frame the lake (Wagner et al 2008)

Lake Ohrid is situated in a zone controlled largely by extension in the Peshkopia-Korça belt, trending N-S in the eastern part of Albania. It is framed in the W by N-S trending lineations and in the E by sets of N-S and NNE-SSW trending lineations (see Fig. 4). Active faults displace

and warp palaeosols (Fig. 5) in the area south of Ohrid city.

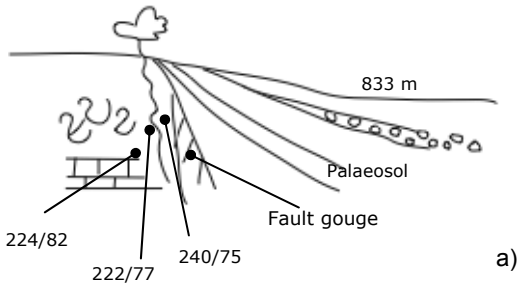

Fig.5: Fault with tilted Palaeosol south of Ohrid city. a) values of dip direction and dip angle are displayed. b) photograph of the fault with person as scale.

FAULT-SLIP ANALYSIS

We studied 24 sites with suitable fault-slip data for stress inversion. These sites are spread on the east and west coast of the lake. On each location we measured a representative number of fault planes concerning the spatial orientation of fault plane (dip direction, dip) and striae (azimuth, plunge) and additional the sense of slip (reverse, normal, dextral or sinistral). The data base was heterogeneous (Fig. 6) so special separation techniques needed to be applied to get good results.

The first step in processing the collected data was to correct the datasets due to minimal measurement failures. Therefore, the lineations are rotated along a great circle which is defined by the lineation and the pole of the fault plane to align on the fault plane (Tectonics FP by Reiter & Acs 1996-2003). Next we calculated the PT-axes from the fault plane datasets. The best results were achieved with a theta angle of 30°. These heterogeneous data were separated by hand. The separation on the PT-axes projection was performed with Tectonics FP. The results already gave a tendency of three sigma1 directions: NW-SE, NE-SW and vertical. These first results met our expectations drawn from the DEM observation. After Sippel et al. 2008 good results have been achieved by combining the multiple inverse method after Yamaji (2000) with the sorting of the data by PT-projection.

With this hypothesis we applied the multiple inverese method after Yamaji (Yamaji et al. 2000). This method is useful especially on datasets where a polyphase stress history can be inferred. Thus we chose this method to investigate the spatial and temporal variations of palaeostress in the Ohrid Basin. The multiple inverse method is based on the Wallace-Bott hypothesis. Wallace (1951) and Bott (1959) stated that fault movements are expected to occur in the direction parallel to the maximum shear stress on fault planes. Finally, we used different sets of striae, which could be relative dated and data from foldaxes to develop a relative dating of the stress states.

Fig. 6: Angelier plot of fault plane and slickenside lineation of three representative outcrops at the east coast

JOINT MAPPING

The cliffs along the east coast of Lake Ohrid were mapped structurally by identifying and measuring joints, bedding and faults in mainly Triassic limestones. The data were sorted, corrected and plotted as rose digrams for each outcrop (see Fig. 7). In total four dominant strike directions of joints were identified, these are N-S, W-E, NW-SE, and NE-SW oriented. All sets are pervasive. The N-S set is related to the youngest deformation, according the faults and geomorphology around the lakes, substantiated by earthquake focal mechanisms (Wagner et al., 2008). The older joint sets are related to the Tertiary deformation phase. Remarkably, N-S joints are confined to N-S faults, which we interpret as a very localized deformation. Blocks in between those N-S faults remain unaffected by the recent deformation.

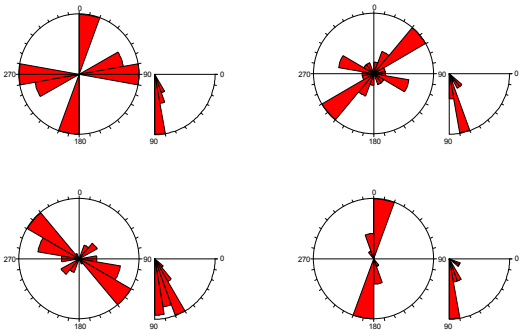

Fig.7: Examples for the joint sets at the east coast of Lake Ohrid

E-W trending joint sets occur in the southeastern part of the lake, very close to the large E-W trending Galicica wind gap. Faulting there is not obvious; however, the Galicica ridge is displaced right-laterally and also vertically. The rigde crest heights vary from 1970 m in the north and 2255 m in the south, resulting in 285 m of vertical offset. Also, strike changes from NNE in the north towards NNW in the south. The E-W structures are also cut by N-S trending faults.

CONCLUSIONS

From the palaeostress analysis three subsequent main phases of deformation can be assumed: NW-SE shortening, NE-SW shortening and a present-day E-W extension.

The shortening is related to Alpine nappe emplacement and folding, the change of the stress field in Late Miocene/Quaternary times leads to overall extension and predominant normal faulting and basin formation. Most probably after the compressional phase, sinistral strike-slip faults developed parallel to the orogenic front, initiating basin formation. Those are partly reactivated during E-W directed extension, and normal faulting on N-S trending faults.

OUTLOOK

The further investigation includes reseistivity geoelectrics and Ground Penetrating Radar surveys, to trace the lineations in the field, LiDAR measurements to investigate the faut planes and the associated striae, which are not accessible and coring in the aggradation plains of the lake to gain further data on the lake evolution.

Acknowledgements: We would like to thank the Hydrobiological Institute of Ohrid especially Goce Kostoski and Zoran Spirkovski for the great support. We also thank our students Nina Engels, Sandra Fuhrmann, Eva Hölzer, Jochen Hürtgen, Tim Krüger, Christopher Lederer, Ariane Liermann, Max Oberröhrmann, Rebecca Peters, Andi Rudersdorf, Dorothee Uerschels, Melanie Walter and Katharina Wohlfart for their dedication and great discussions in the field.

References

Albrecht, C., Wilke, T. (2008). Lake Ohrid: biodiversity and evolution. Hydrobiologia, 615, 103-140.

Aliaj, S. et al (2004). Probabilistic seismic hazard maps for Albania. 13th World Conf. Earthquake Engineering, Vancouver, B.C., Canada, paper no. 2469, 14 pp.

Bott, M.H.P. (1959). The mechanics of oblique slip faulting. Geological Magazine 96 (2), 109–117.

Burchfiel et al. (2006). GPS results for Macedonia and its importance for the tectonics of the Southern Balkan extensional regime. Tectonophysics 413, 239–248.

Dumurdzanov, N., Serafimovski, T., Burchfiel, B.C. (2005). Cenozoic tectonics of Macedonia and its relation to South Balkan extensional regime. Geosphere, 1, 1-22.

Muço, B. (1998). Catalogue of ML 3,0 earthquakes in Albania from 1976 to 1995 and distribution of seismic energy released. Tectonophysics, 292, 311–319.

Sippel, J. (2008). Palaeostress states at the south-western margin of the Central European Basin System — Application of fault-slip analysis to unravel a polyphase deformation pattern. Tectonophysics 470, 129-146.

Wagner et al (2008). The potential of Lake Ohrid for long-term palaeoenvironmental reconstructions. Palaeogeography, Palaeoclimatology, Palaeoecology 259, 341–356.

Wallace, R.E., (1951). Geometry of shearing stress and relation to faulting. Journal of Geology 59 (2), 118–130.

Yamaji, A., (2000). The multiple inverse method: a new technique to separate stresses from heterogeneous fault-slip data. J. Struct. Geol. 22, 441-452.

UPPER PLEISTOCENE TECTONIC ACTIVITY IN THE CENTRAL PYRENEES RANGE (NAVARRA, N SPAIN)

J.M. Insua Arévalo (1) and J. García-Mayordomo (2)

(1) Departamento de Geodinámica. Universidad Complutense de Madrid. c/ José Antonio Novais, 2. 28040-Madrid, SPAIN. insuarev@geo.ucm.es
(2) Instituto Geológico y Minero de España. Área de Investigación en Peligrosidad y Riesgos Geológicos. C/La Calera, 1 (Tres Cantos). 28760-Madrid. SPAIN. julian.garcia@igme.es

Abstract: *This work analyses some geomorphologic aspects of fluvial terraces relating to a fault-related folding which is rising up the Sierra of Leyre in the central part of the Pyrenees. The terraces have been dated by thermoluminiscence (TL) method as Upper Pleistocene (<125 ka). The maximum magnitude and recurrence period of the fault are estimated by empirical relationships, as 6.4 M_w and 6000 years, respectively.*

Key words*: earthquake, morphotectonic, Pyrenees, terrace, thermoluminiscesce.*

INTRODUCTION

During last decades, the study of growing of active geological structures (post-miocene) presents a special interest in the understanding of the velocity of development of the morphology of the terrain, even more, in the landscape evolution. The formation and growing of structures like folds, or lifted-up or tilted blocks associated to the neotectonic activity (since Upper Miocene) have been related to the recurrent coseismic activity linked to the occurrence of mayor paleoearthquakes during millions of years (King *et al.*, 1988).

The seismicity of the Central Pyrenees is considered as *moderate*, although historical earthquakes reached a maximum MSK intensity of VIII (Martes, Huesca, in 1923) have been recorded. This seismicity reveals the current tectonic activity of the region that has leaved some geological marks in the zone during the Quaternary Period. It has been described some tectonic deformations in the alluvial terraces of the rivers Segre and Noguera Ribagorzana in the southern part of the central Pyrenees (Escuer & Goula,1992), even active faulting in the western French Pyrenees affecting Holocene deposits (Alasset & Meghraoui, 2005).

In this work, we show preliminary results from some geomorphological aspects related mainly to fluvial terraces, which point out an Upper Pleistocene tectonic activity at the Central Pyrenees Range.

GEOLOGICAL FRAME

The study area (Fig. 1) is located in the western sector of the central Pyrenees Range, within the South Pyrenean Zone (Cámara and Klimowitz, 1985). The South Pyrenean Zone constitutes the external part of the Pyrenean belt and is a Tertiary unit overriding to the south the Ebro foreland basin.

The Tertiary sediments are folded and affected by thrusts with general E-W direction developed under the alpine compression generated by the convergence of the African and Eurasian plates.

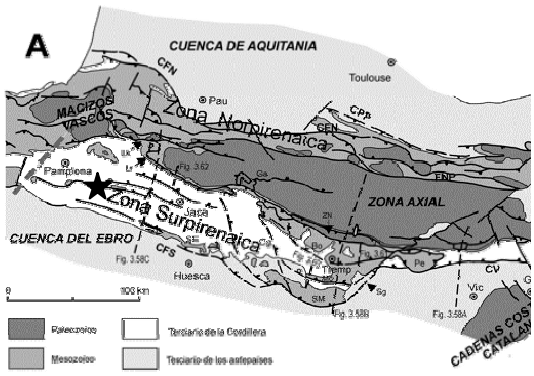

Fig. 1: Location of the study area (black star) in the geological sketch of the Pyrenees Range (Varnolas & Pujalte, 2004).

The study area focuses at one of these E-W structures (Sierra de Leyre) made up of tertiary and cretaceous calcareous rocks reaching up to 1356 m of heihgt. The western lateral end of the sierra is controlled by an anticline cut by the Irati River along a sharp gorge (Foz de Lumibier) (Fig. 2). The quaternary fluvial deposits of the Irati River have recorded some deformations related to the recent tectonic activity of the structure.

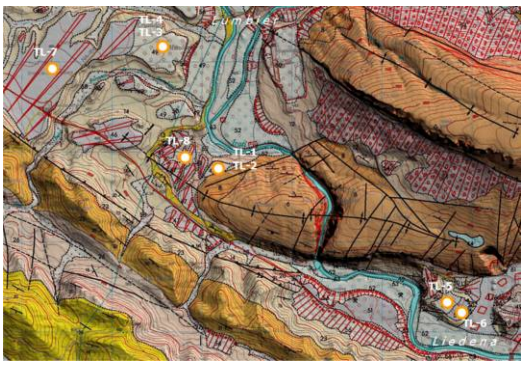

Fig. 2: Geological map of the study area (Gobierno de Navarra, 1997a). The white and orange dots show the location of the TL samples.

OBSERVED DEFORMATIONS

We have analyzed the geological and geomorphological maps (Gobierno de Navarra, 1997a, b), as well as the digital terrain model, and stereoscopic pairs of aerial photos, identifying six terraces at the Irati River: T1 (+40m), T2 (+36m), T3 (+30m), T4 (+24m), T5 (+10m) and T6 (+5m). Several topographic profiles have been made in order to examine possible deformation relating with the tectonic activity.

The profile shown in Fig. 3 runs along the highest terraces T1 (+40m) at the right side of the Irati River to the north of the anticline of the sierra. The slope of the terrace surface has 0.2º. We have identified a deposit of fluvial terrace located just over the folded sierra, at the place of *Biezcas*, which is lifted with respect to the trend of the slight slope of the others.

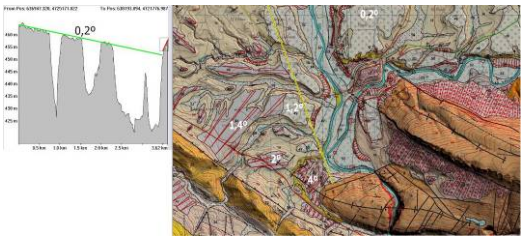

Fig. 3: Topographic profile along the terraces T1 (+40m) at the right side of the Irati River to the north of the sierra. The terrace located just over the folded sierra is lifted with respect to the trend of the slight slope (0.2º) of the others.

This fact could be related to the grow of the anticline that built up the sierra. The northern flank of the fold lifts the terrace deposit up to 43m over the thalweg of the river, 3m higher than the highest terrace identifying at the area. Unfortunately, the farming works has modified remarkably the original deposit loosing the initial slope of the terrace surface, and no tilting could be measurement. Nevertheless, attending to the trend of the slope of the surface of the highest terrace T1 (+40m) to the North, the terrace of Biezcas is lifted 4 m as a minimum.

At the other side of the sierra, a second topographic profile runs along different terraces (Fig. 4). The profile has a stepped shape for comparing purposes. The first segment of the profile runs along the terrace T1 (+40m) showing an angle of slope of 2º to the ESE. This slope value is remarkably higher than that of the terrace at the other side of the sierra. The segment running through the following terraces seems to be quite flat again. In this case it is difficult to fit the deformation to the grow of the anticline of the sierra because of the oblique orientation of the slope. In any case, such a slope in a terrace have to be related with a tectonic origin, like a minor fault which accommodate the local deformation, in absence of other possible mechanisms like halocinetic processes.

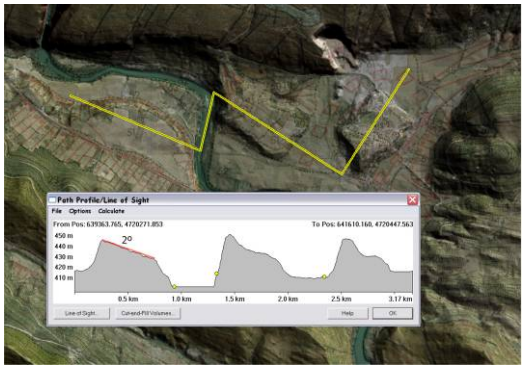

Fig. 4: Topographic profile along the terraces (+40m) of the Irati River to the south of the sierra. The terrace located at the right side is tilted up to 2º. Compare the slope with that of the terraces located to the north of the sierra (See Fig.3).

THERMOLUMINISCENDE DATING

In order to determine the age of the deformation found at the study area, eight samples were collected at different units for dating by Thermoluminiscence procedure (TL) (see Fig. 1 for location). Not only the terraces involved in the deformation where considered, but also other levels and coluvial material were taking into account to acquire a better understanding of the evolution of the structure and the landscape.

The TL dating procedure considers the light exposure occurring during transport of the sediment grains in a dispersed state, prior to their deposition (Forman, 1989). The ages obtained by this method are presented in the Fig. 5.

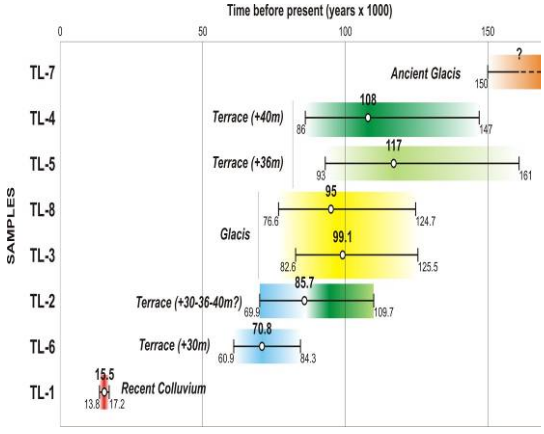

Fig. 5: TL age of the samples (white dot) with interval of error. The samples are grouped by geological unit and put into order from older to younger

The age of the terraces could be considered, in general, include into the Upper Pleistocene (<125 ka). The highest (T1(+40m)) should be the oldest, although the T2 (+36m) presents an older age. Therefore, we should take the age of T1 (+40m) as older than 108 ka, and T2 (+36m) as younger than 117 ka. The terrace T3 (+30m) is the youngest terrace dated.

The terrace of Biezcas, where the sample TL-2 was taken, it is difficult to assign to one of the levels of the identified terraces because the age could fit any of them. In this way, the vertical displacement because of the deformation of the fold could be estimated between 4 and 13 m, with uplift rates for the northern flank from 0.03 to 0.18 m/ka, depending on the terrace level and its age.

Unfortunately, the terrace tilted 2º located to the south of the sierra could not be dated because of administrative reasons. However, the development of the soil profile of the terrace, its extension and its height with respect to the riverbed, make us to consider it belonged to the level of terrace T1 (+40m).

CONCLUSIONS

The deformation of the terraces seems to be associated with the activity of a fault-related folding, which is rising up the Sierra of Leyre at least during the upper Pleistocene. Therefore, the fault of Leyre is a reverse blind fault, which gives us valuable information of the state of stress within the crust in this area of the Pyrenees Range. Besides, the maximum magnitude (6.4 Mw) and recurrence period (6,000 years) of the fault are estimated by empirical relationships (Wells & Coppersmith, 1994).

Acknowledgements: This work is supported by the Research Project (004/SGTB/2007/8.1): Analisis y Seguimiento del Embalse de Itoiz: Estabilidad de Laderas, Sismicidad y Condiciones Geotecnicas (Analisys and Monitoring of the Itoiz Reservoir: Slope Stability, Seismicity and Geotechnical Conditions) founding by the Environmental Ministry of Spain and the Geological Institute of Spain (IGME).

References

Alasset, P.J. and Meghraoui, M. (2005). Active faulting in the western Pyréneés (France): Paleoseismic evidence for late Holocene ruptures. Tectonophysics, 409, 39–54.

Cámara, P. and, Klimowitz, J., (1985). Interpretación geodinámica de la vertiente centro-occidental surpirenaica (cuencas de Jaca-Tremp). Estudios Geológicos, 41, 391–404.

Escuer, J. and Goula, X. (1992). Deformaciones cuaternarias asociadas al anticlinal de Barbastro-Balaguer. Implicaciones simotectónicas. Actas del III Congreso Geológico de España y VIII Congreso Latinoamericano de Geología. Salamanca. Tomo 2, 41-45.

Forman, S.L. (1989). Applications and limitations of thermoluminiscence to date Quaternary sediments. Quaternary International, 1, 47-59.

Gobierno de Navarra (1997a). Cartografía Geológica escala 1:25.000 Hoja nº 174-II Lumbier.

Gobierno de Navarra (1997b). Cartografía Geomorfológica escala 1:25.000 Hoja nº 174-II Lumbier.

King, G.C.P., R.S. Stein y J.B. Rundle, (1988). The growth of geological structures by repeated Earthquakes. 1. Conceptual framework. Journal of Geophysical Research, 93(B11): 13.307-13.318.

Varnolas, A. and Pujalte, V. (2004). La Cordillera Pirenaica. Definición, límites y división. In: Geología de España. Ed: J.A. Vera. 233-241.

Wells, D. L. y K.J. Coppersmith, (1994). New empirical relationships among magnitude, rupture length, rupture area, and surface displacement. Bulletin of the Seismological Society of America, 84(4): 974-1002.

ARCHAEOSEISMOLOGICAL APPROACH ON STONE HERITAGES IN GYEONGJU AREA, SE KOREA

K. Jin (1), M. Lee (1) and Y.S. Kim (1,)*

(1) Dept. of Environmental Geosciences, Pukyong National University, Busan 608-737, KOREA. * ysk7909@pknu.ac.kr

Abstract: *According to historical records, the Gyeongju area has significantly been affected by earthquakes. Recently, a fallen carved Buddha statue was found in Gyeongju. Based on the artistic style of the Buddha, the carving age of the Buddha statue is accidentally coincided with the time of the earthquake in 779 A.D. Therefore, the possibility of interrelationship between the fallen Buddha statue and the 779 earthquake was examined, and its original location and direction were restored. For these purposes, the fracture patterns within the fallen Buddha statue and the surrounding outcrop were compared. Consequently, they are well matched if the fallen Buddha statue is rotated back 20° clockwise supposing its upright position. Although we can not sure about the consistency of the timing between the falling of the statue and the 779 earthquake, the Buddha statue must be fallen down by any episodic forces. Other possible earthquake damages are shown on some other historical heritages in this area and also reported in historical records. According to the recent geological and archaeoseismological studies, the Gyeongju area might not be free from future earthquakes hazards.*

Key words*: historical heritage, archaeoseismology, Gyeongju, earthquake*

INTRODUCTION

The Korean peninsula has been considered to be relatively tectonically safe compared with neighboring countries such as Japan and Taiwan, because it locates within the Eurasian intracontinental region. However, many Quaternary faults have recently been reported along the Yangsan and Ulsan faults, major tectonic features in SE Korea (Fig. 1). In particular, historical records for the Gyeongju area, one of the oldest capital cities in Korea, demonstrate that seismic events have significantly affected lives and properties of this city. The study area is a useful place for paleoseismological studies, because it contains many historical heritages. For example, the 779 earthquake reported in a famous historic book, Samguksagi, had an inferred magnitude of M=6.7 and resulted in over one hundred causalities and many destructions of buildings (Lee and Na, 1983; Lee and Jin, 1991; Lee, 1998). Other earthquake damages were also reported in historical records. Therefore, the aim of this study is examining the affects of paleoseismological events recorded on cultural heritages in Gyeongju area.

GENERAL GEOLOGY

The basement of the study area consists of Cretaceous sedimentary rocks forming part of the Gyeongsang Basin, which is intruded by Cretaceous and Tertiary igneous rocks (Fig. 1). The study area, Gyeongju city, is located around the junction between the Yangsan and Ulsan faults. The geometry of the intersection between the Yangsan and Ulsan faults is quite similar to the simulated model of λ-fault (Du and Aydin, 1995) and reported small scale λ-fault (Kim et al., 2000). Recently, more than 20 Quaternary faults have been reported around the Yangsan and Ulsan fault system, which are the major fault system around the Gyeongsang Basin (Lee and Jin, 1991; Kyung and Okada, 1995; Jang, 2001; Kim and Jin, 2006). These indicate that the study area is a potential area to be affected by high earthquake activities.

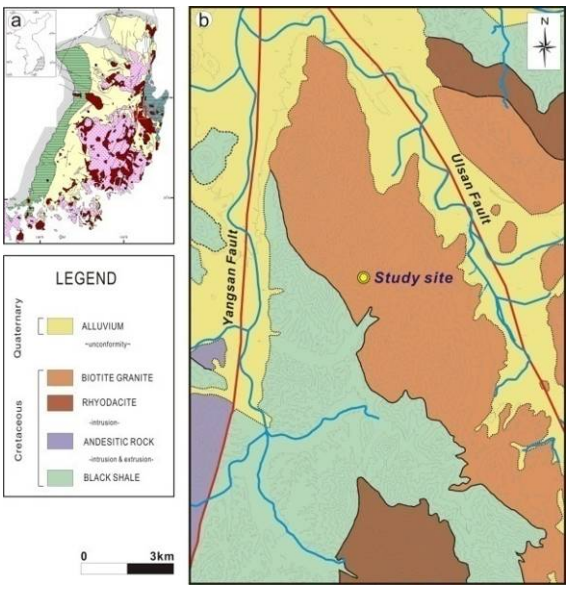

Fig. 1: Location and geological maps of the study area (from Jin et al., in press).

RESTORATION OF THE ORIGINAL POSITION OF THE FALLEN BUDDHA STATUE

In May of 2007, a fallen rock with carved Buddha statue was discovered, which was resting on the 45° slope of the Yeolam valley, Gyeongju (Fig. 2). The Buddha statue was carved on Cretaceous granite. Based on the artistic style of the Buddha statue, the construction age of the Buddha

statue was estimated around late 8th century. Its weight is about 70 tons and its dimension is about 250×190×620 cm. Accidentally, the timing of the earthquake in 779 AD is coincide with the carving age of the Buddha statue. Therefore, the possibility of the interrelationship between the falling of the Buddha statue and the 779 AD earthquake was examined, and its original location and direction were restored.

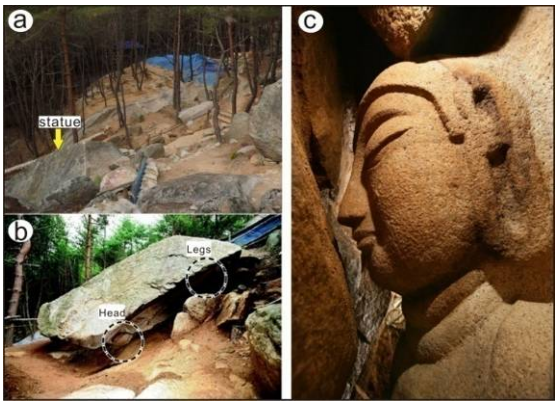

Fig. 2: a) & b) Overview of the study site showing unstable slope and the fallen Yeolam Buddha statue. c) close-up photograph of the face of the Yeolam Buddha statue (from Jin et al., in press).

To trace the original position of the fallen Buddha statue, we performed the fracture analysis on the fallen Buddha statue and in situ granite. A well exposed outcrop was selected to analyze the structural elements such as faults, joints, and veins. A 1m × 1m grids were made for this fracture mapping (Fig. 3). We also measured other fractures in situ granites and enveloping planes of the Buddha statue.

Four main fracture sets were identified in the *in situ* granite. The attitudes of the fracture sets are recognized as follows: EW/65°N (*set* A), N12°E/79°SE (*set* B), N63°W/55NE (*set* C), NS/82°W (*set* D), and N13°W/8°SW (*set* E; sheeting joints) (Fig. 3, 4). The fracture sets were named from *set* A to *set* E, arbitrarily. The fallen Buddha statue is enveloped by six planes. The attitudes of the five planes are as follows: N36°W/60°NE (bottom plane), N24°E/36°NW (back side), N77°W/58°SW (south side) EW/68°N (north side) (Fig. 4). We could not measure the carving plane, because of the protection plan of the cultural properties.

The fractures measured around the fallen Buddha statue are compared with the fracture sets determined from the in situ granite. The fractures measured off the fallen Buddha statue well matched with the fracture sets from in situ granite if the fallen statue were rotated 20° clockwise back to its original position. Therefore, it is interpreted that the Buddha statue fell down with 20° anticlockwise rotation (Fig. 4).

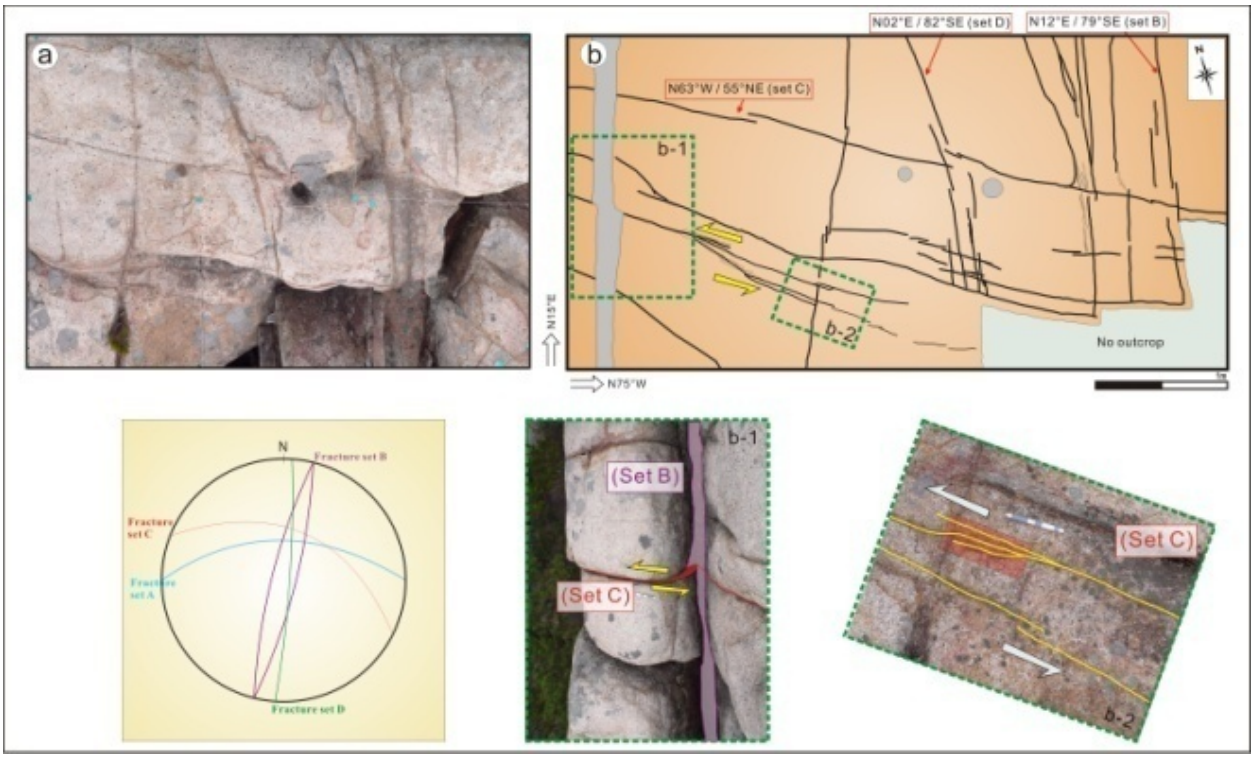

Fig. 3: Detailed grid map on the horizontal plane around the fallen Yeolam Buddha statue. a) Photo mosaic of the horizontal plane. b) Sketch map of the structural elements and locations of sense indicators of the horizontal section. Note that the equal-area stereographic projection shows fracture sets developed in horizontal plane. b-1 & b-2: Slip sense indicators on the horizontal plane show left-lateral slip set C cross-cutting set B (from Jin et al., in press).

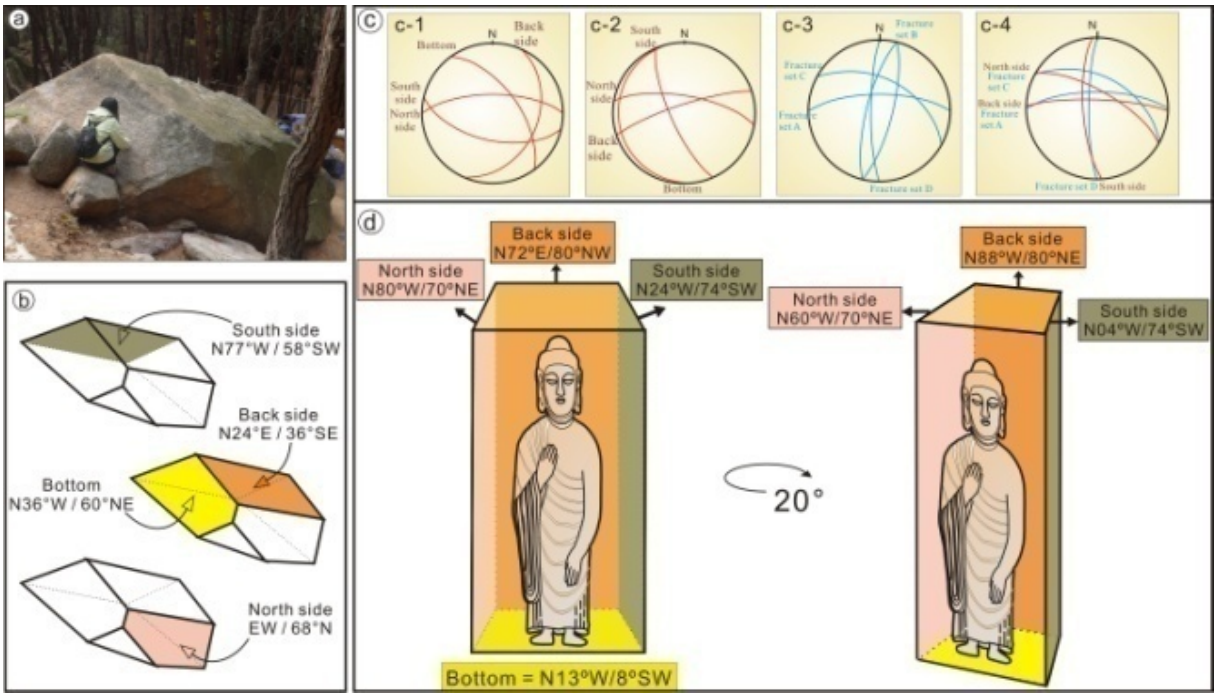

Fig. 4: a) Photograph shows the resting position of the fallen Yeolam Buddha statue. A geologist is measuring the fractures on the rock block of the statue. b) Measured fracture surfaces surrounding the fallen Yeolam Buddha statue. c-1) Equal-area stereographic projection for the present-state surrounding surfaces of the fallen statue. c-2) Restored stereographic projection of the surrounding surfaces by matching the sheeting joint with the bottom surface of the statue. c-3) Equal-area stereographic projection shows major fracture sets within in situ granite. c-4) The major fracture sets in the statue are 20° rotation of the fracture sets to the clockwise direction, major fracture sets within in situ granite, and the matching of the these fracture systems. d) Block diagrams show upright position in present state (left) and restored position with 20° clockwise.

OTHER EXAMPLES

The Gyeongju city is the capital city of the Silla Dynasty for 1000 years from 57 BC to 935 AD. It contains many historical heritages and records. According to historical records, the city has experienced many big earthquakes, which have resulted in extensive damages to the heritages of the Silla Dynasty.

Hwangryongsa nine-story wooden pagoda

The Hwangryongsa nine-story wooden pagoda was built in 645 AD. It has been repaired six times. Especially, according to the Chaljubongi, one of the historical records of Silla Dynasty, the pagoda has been destroyed by an earthquake occurring in the 8th and 9th centuries. It was fragile because of its big height (approximately 80 m).

Cheomseongdae observatory

Gravity is always a common factor in any construction. However, horizontal force is not common, its action is episodic, and its magnitudes are uncertain (Marco, 2008). Therefore, large heavy block is only shifted by earthquakes, unless the construction was ever buried (Marco, 2008). The Cheomseongdae observatory (Fig. 5) was built during the Queen Seondeok period (632-647 AD) of the Silla Dynasty. It is the oldest astronomical observatory in East Asia. It is 5.17 m in diameter and 9.4 m in height, with 362 stone blocks. The Cheomseongdae leans to the north about 4° and it shows a horizontal shift in its large ashlars (Fig. 5), which may be caused by episodic forces. In other words, only earthquakes could have shifted the large blocks by horizontal sliding. Historical records also support that the Cheomseongdae was damaged by big earthquakes.

The Seokgatap

The Bulguksa Temple was built in 751 AD. It contains two pagodas, the Seokgatap and the Dabotap. In 1966, the Mukseojipyeon, the historical records, was discovered during repairing the Seokgatap. It reports that the Seokgatap has been destroyed twice in 1024 and 1038 by big earthquakes (National Museum of Korea, 1997). It also records that stairs and bridges of the Bulguksa Temple were destroyed by big earthquake (National Museum of Korea, 1997).

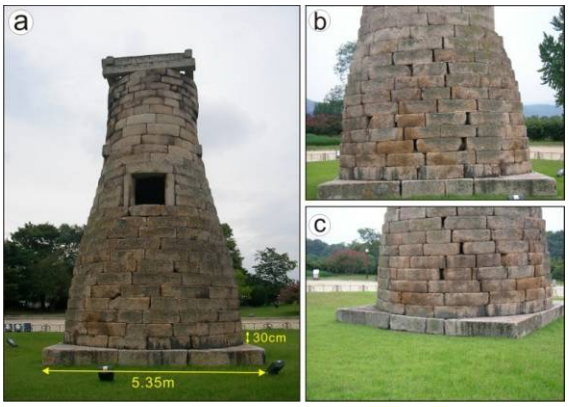

Fig. 5: a) Overview of the damaged Cheomseongdae obsevatory in Gyeongju. b) & c) Horizontal shift of ashlars of the Cheomseongdae. The cause is attributed to earthquakes.

DISCUSSION

The falling time of the Buddha statue is important to analyse earthquake hazards for a specific earthquake. From the artistic style and weathering condition of the Buddha statue, the falling time could be estimated roughly. However, we can not determine the exact falling time from these methods. Recently, optically stimulated luminescence (OSL) dating method has emerged as a powerful dating method for these cases, because quartz and feldspar to be dated are abundant in this situation (Choi et al, 2009). The fallen Buddha statue is lying on the weathering soil of Cretaceous granite. If we can collect suitable materials for OSL dating, the falling time could be determined. It could indicate the interrelationship between the falling Buddha statue and 779 AD earthquake. Therefore, further studies are required to solve this problem.

Many Quaternary faults were reported around the study area. The aerial photograph of the area shows obviously NE-SW, NNE-SSW, and E-W trending lineaments. Data obtained from trenches excavated across active faults are of great value in studies of earthquake hazards. Therefore, if we find Quaternary faults around the Buddha statue, they could provide useful information for paleo-earthquakes in this area.

CONCLUSIONS

The study area is located around the junction between the Yangsan and Ulsan faults. Recently many Quaternary faults have been reported along the Yangsan and Ulsan faults encouraging researches on the fault activities and associated paleoseismicities. According to historical records, the study area was significantly affected by earthquakes. The earthquakes produced heavy casualties and damages in historical properties. Although we need additional absolute dating data, the falling time of the Buddha looks coincident with the 779 AD earthquake, which killed over one hundred people. Fracture sets measured from the fallen Buddha statue well match with those fractures measured from nearby in situ granite if the fallen statue were rotated 20° clockwise back into their original positions. It indicates that the Buddha statue might be fallen down with 20° counterclockwise rotation. Although we can not sure about the consistency of the timing between the falling time of the Buddha statue and the 779 AD earthquake, it must be fallen down by any episodic force such as landslides or earthquakes. This idea is supported by the weathering condition of the Buddha statue, the distribution of surrounding blocks, and the geomorphological pattern of the slope around the statue. Other earthquake damages were also reported in historical records. Based on recent geological and archaeoseismological studies, the Gyeongju area might not be free from future earthquake hazards.

Acknowledgements: This work was funded by the Korea Meteorological Administration Research and Development Program under Grant CATER 2008-5502.

References

Chang, T.W. (2001). Quaternary tectonic activity at the Eastern Block of the Ulsan Fault. Journal of the Geological Society of Korea, 37, 431-444 (in Korean with English abstract).

Choi, J.H., Kim, J.W., Murray, A.S., Hong, D.G., Chang, H.W., Cheong, C.-S. (2009). OSL dating of marine terrace sediments on the southeastern coast of Korea with implications for Quaternary tectonics. Quanternary International, 1999, 3-14.

Du, Y., Aydin, A. (1995). Shear fracture patterns and connectivity at geometric complexities along strike-slip faults. Journal of Geophysical Research, 100, 18093-18102.

Jin, K., Lee, M., Kim, Y-S. (in press). Geological study on the collapse of a carved stone Buddha statue in Yeolam valley of Namsan, Gyeongju, Korea. Journal of the Geological Society of Korea (in Korean with English abstract).

Kim, B. S. (1143). Samguksagi.

Kim, Y.-S., Andrews, J.R., Sanderson, D.J. (2000). Damage zones around strike-slip fault systems and strike-slip fault evolution, Cracking Haven, southwest England. Geoscience Journal, 4, 53-72.

Kim, Y.-S., Jin, K. (2006). Estimated earthquake magnitude from the Yugye Fault displacement on a trench section in Pohang, SE Korea. Journal of the Geological Society of Korea, 42, 79-94 (in Korean with English abstract).

Kyung, J.G., Okada, A. (1995). Liquefaction phenomena due to the occurrences of great earthquakes; some cases in central Japan and Korea. Journal of the Geological Society of Korea, 31, 237-250.

Lee, K. and Na, S. H. (1983). A study of microearthquake activity of the Yangsan fault. Journal of the Geological Society of Korea, 19, 127-135.

Lee, K., Jin, Y.G. (1991). Segmentation of the Yangsan fault system: geophysical studies on major faults in the Kyeongsang basin. Journal of the Geological Society of Korea, 27, 434-449.

Lee, K. (1998). Historical earthquake data of Korean, Journal of the Korea Geophysical Society, 1, 3-22.

Marco, S. (2008). Recognition of earthquake-related damage in archaeological sites: Examples from the Dead Sea fault zone. Tectonophysics, 453, 148-156.

National Museum of Korea (1997). News.

LANDSLIDES ON ANCIENT FILL STRUCTURES INDUCED BY THE 16th CENTURY EARTHQUAKE IN THE KINKI DISTRICT, JAPAN

T. Kamai (1) and A. Sangawa(2)

(1) Disaster Prevention Research Institute, Kyoto University. Gokasho, Uji, Kyoto, JAPAN. kamai@landslide.dpri.kyoto-u.ac.jp
(2) Geological Survey of Japan, Higashi, Tsukuba, JAPAN. sangawa.a@aist.go.jp

Abstract: *Landslides on ancient burial mounds, Imashiro-zuka and Nishimotome-zuka, induced by historical earthquake related to the tectonic movement of an active fault systems located between northern Osaka and Kobe are discussed. Obvious interior structures of landslides revealed the deformation process of the landslides, and provided significant information for discussing landslide mechanisms. that rapid increasing pore water pressure was necessary to allow sufficient slide along the almost horizontal slip surfaces developed in the main part of the landslide bodies. Liquefaction analysis using both the results of dynamic triaxial compression tests and earthquake response analysis showed liquefaction in the foundation of the mound possibly was the mechanism of the landsliding on the Nishimotome-zuka mound. Today, these ancient burial mounds in the Kinki district are located in both rural and urban regions across Japan and landslides on these mounds provide unique information about issues related to the long-term stability of modern large-scale constructions.*

Key words: landslide*, burial mound, earthquake, Japan*

INTRODUCTION

Kofun, ancient burial tomb with double mounds, are not only famous 3 to 7th century AD historical monuments of East Asia, but also impressive large-scale fill structures that were constructed across Japan and overlapping urban regions in modern times. Landslides are often found on Kofun mounds providing important information on both landslide mechanisms and risk mitigation of earthquake disaster (Sangawa, 1992).

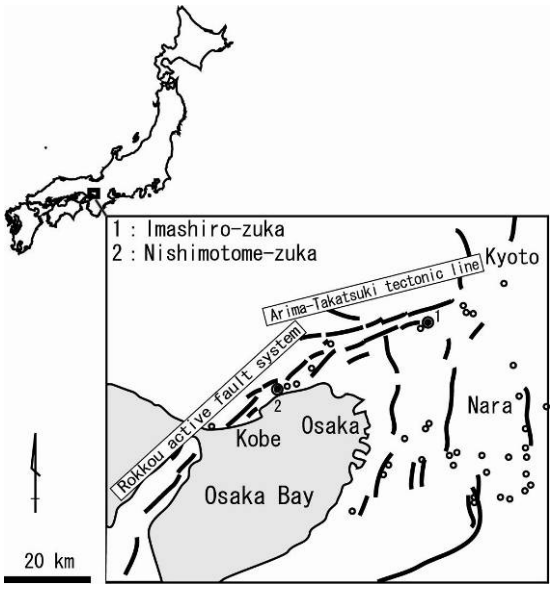

Fig.1 Distributions of large-scale ancient tomb mounds and active fault systems in the Kinki district

The two mounds, the Imashiro-zuka and the Nishimotome-zuka in the northern Osaka to Kobe urban district. are located along active fault systems at the border of the northern Osaka sedimentary basin, and likely collapsed due to the same historical earthquake in the 16th century (Fig.1). Obvious interior structures of the landslides and deformations of the mounds were revealed in the trenches constructed during archaeological surveys from 2000 to 2004. The chance to observe the total cross section of a landslide where the triggering mechanism is clearly known is unique. Our investigations provide not only the first detailed description of landslides on the ancient mounds, but also valuable case studies of the collapse of modern large-scale embankments induced by strong earthquake motion in urban regions.

LANDSLIDES OF THE IMASHIRO-ZUKA

Based on archaeological research, The Imashiro-zuka is considered to be the tomb of the Great Emperor Keitai who died in 531 AD. Archaeological research on Imashiro-zuka started in 1996, the first detailed research on an Emperor's tomb mound in Japan, and remarkable archaeological achievements, mainly numerous ceramics, have been found. It was also discovered that a landslide drastically deformed the tomb mound.

The Imashiro-zuka mound was built on the alluvial sediments, clay and fan deposits, filling the Minou lowland graben structure bordered by the Arima-Takatsuki tectonic line. The Ai fault which constitutes the southern flank of the graben structure, is invisible on the surface up to 1 km west of the Imashiro-zuka, however, the mound is located directly on the strike of the fault runs right below the mound. Trench investigations 2 km west of the Imashiro-zuka conducted by the Geological Survey of Japan revealed that the Ai fault during the 1596 Keicho-Fushimi earthquake moved at least 3 meters in right lateral direction and several centimeters in south bound vertical direction. This means that the Imashiro-zuka is one of the largest fill structures located in the region of the highest seismic activity in the world.

Structure of Landslides

The head scarps of the landslides are easily distinguished on the mound. Seven landslides developed on the slope of the tomb mound (Fig.2). Horizontally layered small, hand-made soil blocks comprised the fill (embankment) of the mound. The remains of'scaly mosaic' (fish skin) structures corresponding to each soil block are oriented almost horizontally in the original non-disturbed part of the mound. Thus, deformation of these horizontal units of the scaly mosaic structure is a valid indicator of the deformation caused by landslides and other artificial disturbances of the mound.

Both landslide 1 and 2 are deep-seated landslides along with almost horizontal slip surface while landslide #3 is a shallow slope failure on steep slope. Both types of landslides involved mass transfer in a highly fluid state after collapse, resulting in long travel length relative to the height of the mound. The deep-seated landslides are distributed mainly on the northern side of the mound which coincide with the downward side of the Ai fault indicating that the landslides were affected by differences in the geological conditions of the foundation.

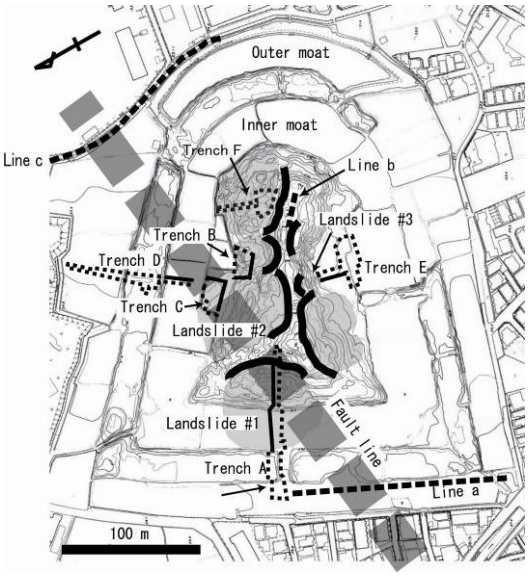

Fig.2 Plan view of the Imashiro-zuka. Shadowed areas show location of landslides. Line a,b,c are the course of the surface wave exploration.

Process of landslide

Observations in the trenches of landslide 1 and 2 (Fig.3) indicate the occurrence of both co-seismic stages of landslide movement; an initial stage with a small cyclic displacement corresponding to the basal shear and an advanced stage of one-way sliding corresponding to development of the slip surface in the clay of the basement. These two co-seismic stages of movement indicate that the changing boundary conditions such as increasing of pore water pressure are significant factors in the landslide movement. The shear resistance should significantly decrease with increasing pore water pressure along the slip surface as shown by the liquefied clay-injection structure (flame structure) in the middle part of landslide 2. The fully landslide structure including flow slide in the toe part might be completed in the post-seismic stage (Fig.4).

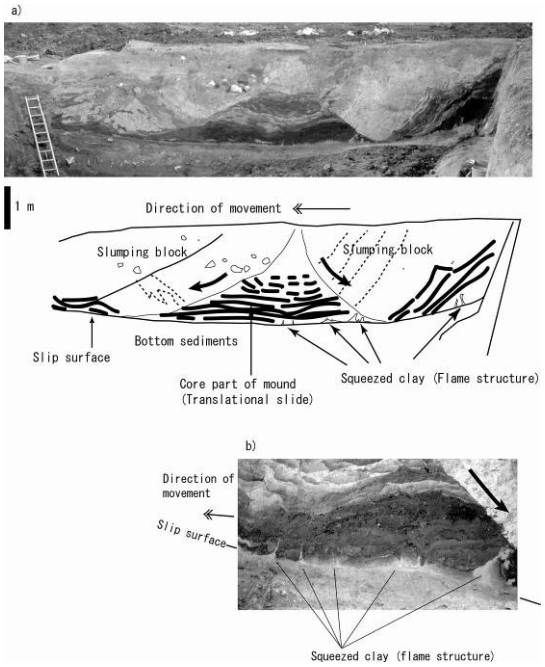

Fig.3 Photos and sketches of the inner structure of landslide #2 (trench C)

a) Longitudinal section: Slump blocks were observed on both sides of the central block of almost horizontal movement.

b) Squeezed (liquefied) clay structure (flame structure). Clay was injected into the basal part of the mound along the slip surface.

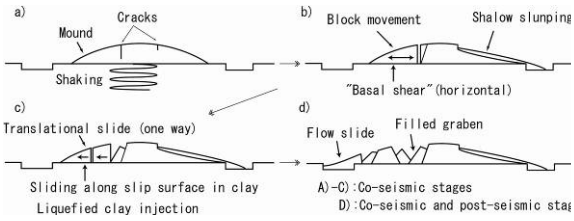

Fig 4 Schematic model of landsliding in Imashiro-zuka

LANDSLIDES OF THE NISHIMOTOME-ZUKA

The Nishimotome-zuka is located in Kobe City, Hyougo Prefecture, approximately 60 km southwest of Imashiro-zuka. The current coastline located 200 m from Nishimotome-zuka is the result of reclamation after the 19th century. When Nishimotome-zuka was constructed it was located at 6 m elevation, and 100 m inshore of the ancient coast.

The mound is located on the fan of the Tsuga River. The main foundation bed of the mound is a gravel layer containing boulders, however, the southern half of the rear square of the mound is situated on shore sand. The intensive disaster zone of the 1995 Hyougoken-nanbu earthquake included the location of the mound. Liquefaction of natural ground induced by the 1995 Hyougoken-nanbu earthquake are scattered around the ancient shore sand region that surrounds the mound,

however, the massive 1995 earthquake did not damage the mound itself.

Structure of Landslides

The two landslides developed on the mound as shown in Fig.5. A landslide in the southwestern corner of the rear square mound (landslide #1) is relatively large, 40 m long, 70 wide, and 2-5 m deep. The destroyed chamber shows that the landslide at the head was displaceed 2 m vertically and 1.2 m horizontally.

The displacement of the toe from its original position was not directly observed, however, it was estimated to be less than 5 m based on the topography of the surroundings. The short travel distance of the landslide is significantly different from the case of the Imashiro-zuka mound.

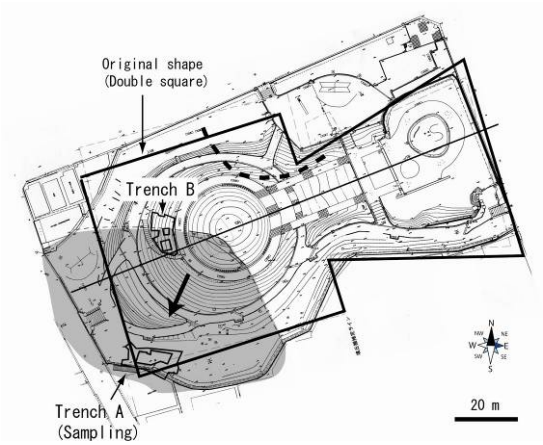

Fig.5 Plan view of Nishimotome-zuka

Process of landslide

The foundation bed of the landslide at the southwestern corner of the Nishimotome-zuka mound consisted of shore sand of the ancient cost, and sand dykes revealing evidence of liquefaction were discovered at the base of the landslide.

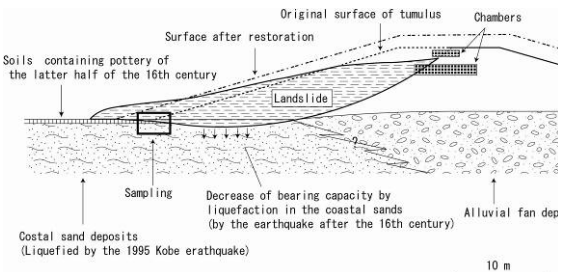

Fig. 6 Schematic cross section showing landslide mechanism of the Nishimotome-zuka

Fig. 6 is a schematic cross section of Nishimotome-zuka showing the landslide mechanism. The main part of the landslide fell down along the steep sloping slip surface (minor normal faults) through rapid decreasing of the bearing capacity of the foundation bed of the mound initiated by the fully liquefaction of the ground.

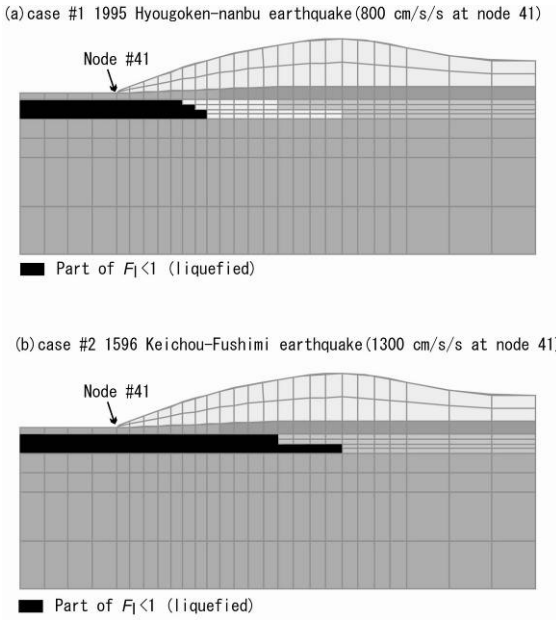

Fig. 7 Distributions of the elements with Fl<1 (liquefacted).

Deformation of the chamber indicates that the vertical displacement was larger than the horizontal displacement because of the unique mechanism of the landslide.

The distributions of liquefaction elements were estimated by calcuration of F_l. The liquefaction resistance ratio (R_{max}) was estimated by cyclic triaxial test of undisturbed samples, and the maximum cyclic shear stress ratio (L_{max}) was estimated using by the results of earthquake response analysis (FLUSH). The resulted F_l in reaching a value less than 1.0 agrees with the state of liquefaction of the ground in the both earthquake , the 1995 Kobe earthquake and the 1596 Keicho-Fushimi earthquake (Fig.7)

CONCLUSIONS

Recent urban developments, mainly housing, roads and lifeline constructions, thoroughly invaded the surroundings of the two mounds. The landslides on both mounds are symbolicly representing the risk associated with unstable ground conditions in the urban region of the Kinki district. Thus, the landslides on these ancient mounds provide important information on issues of our modern society.

Acknowledgements: The authors are deeply indebted to Dr. Karin Laursen Sidle for her helpful comments and language revision of the draft

References

Sangawa, A. (1992). Jishin Koukogaku. The Archaeological Seismology. Chuko Bokks, (Japanese), 251 pp.

EVALUATION OF ROCKFALL HAZARD TO THE TOWN OF QIRYAT SHEMONA, N. ISRAEL – POSSIBLE CORRELATION TO EARTHQUAKES

M. Kanari (1), O. Katz (2), N. Porat (2), R. Weinberger (2) and S. Marco(1)

(1) Department of Geophysics and Planetary Sciences, Tel-Aviv University, Tel-Aviv 69978, ISRAEL. kanarimo@tau.ac.il
(2) Geological Survey of Israel, 30 Malkhe Israel St., Jerusalem 95501, Israel

Abstract: *We estimate rockfall hazard for the town of Qiryat-Shemona, situated at the bottom of a fault controlled escarpment bounding the Dead Sea Transform at N. Israel. Aerial photos predating the town founding show boulders of 1 m^3-150 m^3 within the town premises. The study determines: a. the area subject to rockfall hazard and predicted kinetic properties of falling blocks (using CRSP v4); b. ages of rockfall events and estimated recurrence interval, and possible triggering by earthquakes (using OSL dating of block-soil interface); It is concluded that particular parts at SW of town are subject to rockfall hazard. OSL age analysis of rockfall events coincides with selected M>6.5 earthquakes and yields 850 years recurrence time and last rockfall probably triggered by the 1202 AD earthquake. Block velocities of 10–15 m/s and kinetic energy of 18,000–45,000 kJ are predicted for block volumes of ca. 125 m^3.*

Key words*: rockfall, hazard, rockfall simulation*

INTRODUCTION

The study evaluates rockfall hazard for the town of Qiryat-Shemona, which lies in the northern Hula Valley (N. Israel), part of a series of extensional basins that formed along the Dead Sea Transform (DST) active fault system (Freund et al., 1970; Garfunkel, 1981). The town is located at the foot of the fault-controlled Naftali Mountain ridge, which rises to its west (Fig. 1). New quarters of the town are being planned and built below the ridge crawling up the slopes. These slopes are spotted with large, scattered, cliff-derived limestone boulders, which have apparently traveled there by rockfall mechanism. The 40-m-thick Ein-El-Assad Formation limestone outcrops provide a source material for rock blocks. Aerial photos from 1946–1951 show boulders of volumes of 1–150 m^3 situated within the now built town premises (Fig. 2). The study examines: (a) which are the feasible downhill trajectories of falling blocks, where do blocks stop, and what is the urban-area subject to rockfall hazard? (b) when did rockfalls occur and what is the estimated recurrence interval?

To answer these questions hundreds of rock-blocks were

Fig. 1: Location map of Qiryat-Shemona (study area). Dead Sea Transform marked in pink

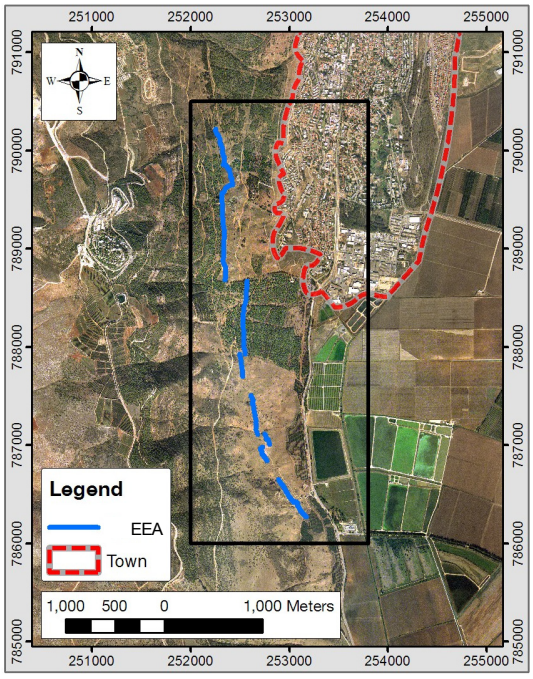

Fig. 2: Map of the study area (in black rectangle). Ein-El-Assad Formation escarpment (EEA) is marked by blue line; town area in red dashed line

mapped on the slopes above Qiryat-Shemona using both field surveys and aerial photos and their volume and spatial distributions are analyzed; burial ages of soil samples from beneath large fallen blocks were determined by OSL; rockfall trajectories were simulated using the commercial program CRSP v4 (Jones et al., 2000). Hazard evaluation maps for Qiryat-Shemona were compiled from the results of rockfall simulations. Simulated analyses of block velocity and kinetic energy may be used as parameters for the design of mitigation of rockfall damage for Qiryat-Shemona. Rockfall hazard estimation is derived from rockfall recurrence time based on OSL age determinations.

DISCUSSION

Results show that the block volume distribution follows an exponential function of the form ax^b where a=0.4 and X is block volume (m^3), with b value –1.17, in agreement with worldwide rockfall inventories (Dussauge-Peisser et al., 2002; Dussauge et al., 2003; Guzzetti et al., 2003; Malamud et al., 2004). Mapped maximal downhill block travel distances combined with slope morphological analysis were used to calibrate the simulation program variables, which were later used to simulate possible downhill rockfall block trajectories towards the town premises.

Simulation results were used to compile the rockfall hazard map (Fig. 3), derived from maximal travel distance of the largest simulated blocks (D=6.2 m, V=125 m^3) from 25 rockfall simulation profiles performed using CRSP. Another map was compiled for location-specific mitigation design considerations, introducing detailed locations where future rockfalls are predicted to impact town premises, at which kinetic analysis was performed. Block velocity and kinetic energy analyses at town border impact locations, provided by CRSP were used in order to obtain worst-case hazard evaluation. At these analysis points, predicted block impact velocity varies between 10–15 m/s (mean 12.2 m/s with SD 1.7 m/s) and kinetic energy between 18,000–45,000 kJ (mean 31,000 kJ with SD=9000 kJ). These values may be used as general guidelines for rockfall damage mitigation for the entire study area. It is concluded that at the south-westernmost part of town, life and property are at rockfall hazard in particular areas.

Sensitivity analysis for block initial horizontal velocity (V_x), which represents horizontal acceleration induced during an earthquake, was performed in CRSP using velocities of up to 3 m/s. No significance was observed on simulated block travel distances compared to V_x=0 m/s (no initial horizontal velocity). It is concluded that the main affect of earthquake induced acceleration on the studied rockfalls is in triggering them rather than affecting block travel distance, once detached from the cliff mass.

The nine OSL age results from the current study, combined with ages of large earthquakes determined suggested by two other studies (Kagan et al., 2005; Yagoda-Biran, 2008) demonstrate clustering around dates that coincide with selected known M>6.5 earthquakes, historic and prehistoric (Table 1; Fig. 4). The known earthquakes were selected from historical earthquake

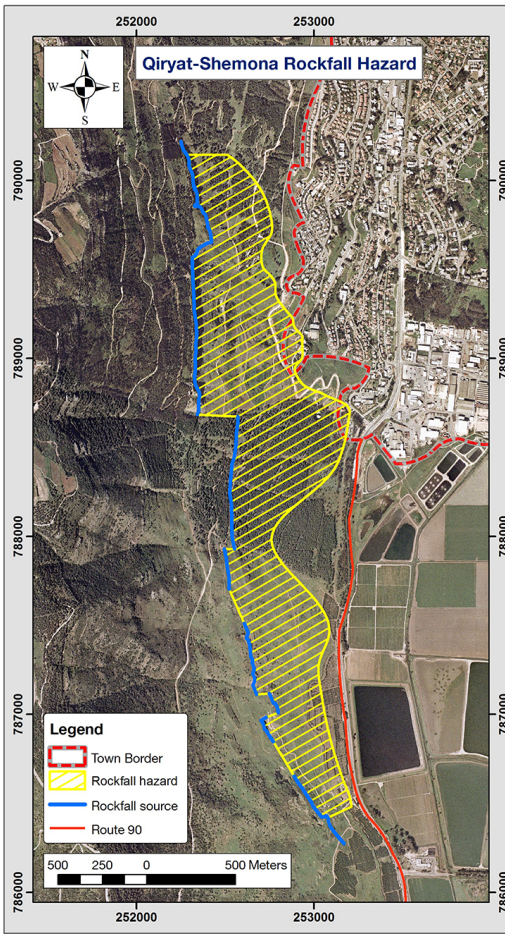

Fig. 3: Rockfall hazard map of Qiryat-Shemona. Source of rockfall (Ein-El-Assad formation) marked in blue line; area subject to rockfall hazard (from source escarpment to 100% of blocks stop line) dashed in yellow; town border line in red dashed line; Route 90 in orange solid line. Map compiled from maximal travel distance (100% of blocks stop line) of 25 simulation profiles performed using CRSP.

catalogs (Amiran et al., 1994; Guidoboni and Comastri, 2005; Guidoboni et al., 1994) based on two considerations: (a) their estimated maximum intensity is 'IX' or higher (EMS local intensity scale); (b) the distance between the study area and affected localities reported in the catalogs does not exceed 100 km following Keefer's (1984) upper limit for disrupted slides or falls triggered by earthquakes. It is concluded that earthquakes of large intensities (depending on local ground acceleration) are the triggering mechanism of the studied rockfalls, yet apparently not all large earthquakes trigger rockfall.

Analysis of currently available OSL ages of rockfall events yields an 850 years recurrence time and suggests that the last rockfall was triggered by the 1202 AD earthquake. The recurrence time of 850 years corresponds to recurrence time of M=6.5 earthquakes in the DST (Begin, 2005). However, since hundreds of blocks are scattered on the studied slope, nine OSL ages cannot provide a robust statistical basis of rockfall recurrence pattern. The determination of additional several dozens of OSL ages is required to obtain a reliable analysis of rockfall recurrence pattern.

*Table 1: Rockfall triggering candidate events and evidence type**

Age Cluster	Candidate Triggering Event
0.9 ±0.05 ka	1202 AD earthquake (his)
1.5 ±0.05 ka	551 AD earthquake (his)
2.2 ±0.05 ka	199 BC earthquake (his)
2.7 ±0.05 ka**	759 BC earthquake (ps; his: book of Amos)
4.0 ±0.7 ka	~2050 BC (ps); no historic data; †
6.0 ±1.0 ka	No ps data; †

* Evidence types are: known historic earthquakes (his), paleoseismic evidence (ps)
** Dashed line separates known historic earthquakes from unreported in history and prehistoric earthquakes
† Other evidence correlated to large (Mw 7 or more) earthquakes (Kagan et al., 2005; Yagoda-Biran, 2008)
Candidate earthquakes were selected from historical earthquake catalogs (Amiran et al., 1994; Guidoboni and Comastri, 2005; Guidoboni et al., 1994).

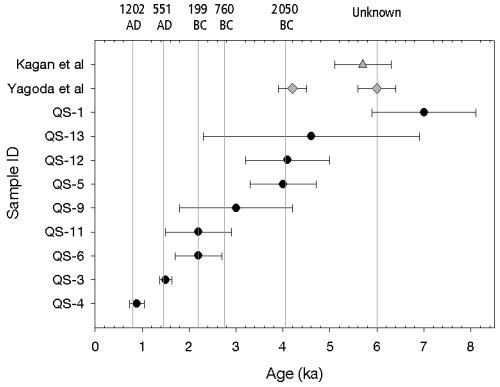

Fig. 4: OSL ages and suggested rockfall triggers. OSL age results for the past 8000 years in black circles with error bars; ages of earthquakes determined by Yagoda (2008) in gray diamonds and by Kagan et al. (2005) in gray triangle; corresponding dates of earthquakes suggested as rockfall triggers in gray lines and labeled at top axis. Earthquakes selected from historical earthquake catalogs (Amiran et al., 1994; Guidoboni and Comastri, 2005; Guidoboni et al., 1994).

SUMMARY

We estimate rockfall hazard for the town of Qiryat-Shemona, Dead Sea Transform, N. Israel. It is concluded that particular parts at SW of town are subject to rockfall hazard. Predicted block velocities and kinetic energy are 10–15 m/s and 18,000–45,000 kJ, respectively (for block volumes of ca. 125 m^3). According to preliminary OSL age determination it is apparent that the rockfall events coincide with selected M>6.5 earthquakes. Recurrence interval for the events is 850 years, while the last rockfall probably triggered by the 1202 AD earthquake. For further reading about the rockfall hazard estimation and OSL age determination discussed above, see Kanari (2008).

References

Amiran, D.H.K., Arieh, E. and Turcotte, T. (1994). Earthquakes in Israel and Adjacent Areas - Macroseismic Observations since 100 Bce. Israel Exploration Journal, 44(3-4): 260-305.

Begin, Z.B. (2005). Destructive earthquakes in the Jordan Valley and the Dead Sea — their reoccurrence interval and the probability of their occurrence, Geol. Surv. Israel, Report GSI/12/2005.

Dussauge-Peisser, C. et al. (2002). Probabilistic approach to rock fall hazard assessment: potential of historical data analysis. Nat. Hazards Earth Syst. Sci., 2: 15-26.

Dussauge, C., Grasso, J.R. and Helmstetter, A.S. (2003). Statistical analysis of rockfall volume distributions: Implications for rockfall dynamics. Journal of Geophysical Research-Solid Earth, 108(B6).

Freund, R. et al. (1970). Shear Along Dead-Sea Rift. Philosophical Transactions of the Royal Society of London Series a-Mathematical and Physical Sciences, 267(1181): 107-130.

Garfunkel, Z. (1981). Internal structure of the dead-sea leaky transform (rift) in relation to plate kinematics. Tectonophysics, 80(1-4): 81-108.

Guidoboni, E. and Comastri, A. (2005). Catalogue of earthquakes and tsunamis in the Mediterranean area from the 11th to the 15th century. Istituto Nazionale di Geofisica e Vulcanologia, Rome, 1037 pp.

Guidoboni, E., Comastri, A. and Traina, G. (1994). Catalogues of Ancient Earthquakes in the Mediterranean Area up to the 10th Century. Instituto Nazionale di Geofisica, Roma, 504 pp.

Guzzetti, F., Reichenbach, P. and Wieczorek, G.F. (2003). Rockfall hazard and risk assessment in the Yosemite Valley, California, USA. Nat. Hazards Earth Syst. Sci., 3: 491-503.

Jones, C.L., Higgins, J.D. and Andrew, R.D. (2000). Colorado Rockfall Simulation Program Version 4.0 Manual. CDOT-SYMB-CGS-99-1, Colorado Department of Transportation, Denver, CO 80222.

Kagan, E.J., Agnon, A., Bar-Matthews, M. and Ayalon, A. (2005). Dating large infrequent earthquakes by damaged cave deposits. Geology, 33(4): 261-264.

Kanari, M. (2008). Evaluation of rockfall hazard to Qiryat-Shemona - possible correlation to earthquakes. GSI/24/2008, Geol. Surv. Isr., Jerusalem.

Keefer, D.K. (1984). Landslides caused by earthquakes. Geol Soc Am Bull, 95(4): 406-421.

Malamud, B.D., Turcotte, D.L., Guzzetti, F. and Reichenbach, P. (2004). Landslide inventories and their statistical properties. Earth Surface Processes and Landforms, 29(6): 687-711.

Yagoda-Biran, G. (20080. Seismic hazard estimation along eastern margins of Sea of Galilee by back analysis of seismically induced natural and structural failures. (In Hebrew). GSI/02/08, Geol. Surv. Isr., Jerusalem.

TSUNAMIGENIC DEPOSITS ALONG THE SOUTHERN GULF OF CÁDIZ (SOUTHWESTERN SPAIN) CAUSED BY TSUNAMI IN 1755?

B. Koster (1), D. Vonberg (1) and K. Reicherter (1)

(1) RWTH Aachen University, Neotectonics and Natural Hazards, Lochnerstr. 4-20, D-52056 Aachen, GERMANY.
Benjamin.Koster@rwth-aachen.de, David.Vonberg@rwth-aachen.de

Abstract: *Shallow drilling in coastal areas proved sedimentary evidence for palaeo-tsunamis along a 50 km long segment of the Atlantic coast of southern Spain. The study area was the coast between Barbate and Zahara de los Atunes, both on top of rocky cliffs as well as in lagunas and along sedimentary beaches. In our studies we focused on drill cores, on which we did sedimentary analysis (sieve curves), as well as magnetic susceptibility and foraminifera identification. They give us clues to one or more tsunami events in this region. Different characteristics have been detected and evaluated, such as "fining-up" sequences with coarse shell debris and rising magnetic susceptibility as well as outcropped "backwash" sediments at Barbate beach. Geomorphologic clues by former publications can be validated like the bridge at Los Lances Bay which acted like a huge flute mark.*

Key words*: 1755 Lisbon tsunami, tsunamites, back flow sediments, Gulf of Cádiz*

TSUNAMIGENIC DEPOSITS ALONG THE COAST BETWEEN BARBATE AND TARIFA

Outcrop evidence and shallow percussion drilling in coastal areas proved sedimentary evidence for palaeotsunamis along a 50 km long segment of the Atlantic coast of southern Spain. We studied the coast between Barbate and Tarifa (Fig. 1 and Fig. 2), situated on top of rocky cliffs as well as in lagunas and along sedimentary beaches (Marismas de Barbate and Zahara de los Atunes, Los Lances N of Tarifa). Also, we focused on bays (Bolonia, Valdevaqueros), which are most probably sheltered from direct tsunami wave action. However, reflections of the waves may occur and may hit these bays. In these bays, the Roman villages of Baelo Claudia and Mellaria, respectively, have been situated (e.g. Silva et al., 2006, 2009).

Fig. 1: Map of the study area between Barbate and Tarifa; every dot indicate a location of shallow drilling to detect tsunamite layers.

Following, we will describe the different situations at several locations in the study area.

Marismas de Barbate

The marshlands of Barbate have only little elevation of about 0 to 1.0 m above mean sea level and are flooded permanently by the tide. This ideal tsunamite reservoir was probed with percussion coring with an open window sampler. We reached depths of about 5.0 meters. After core description the same site was drilled with a sampler with PVC liners for lab analyses. Cores provided evidence for tsunamigenic layers. Laboratory analyses validated the clues of the field-work.

We found "fining-up" sequences, typical for tsunamites (Bryant, 2007), with coarse grain size at the bottom up to fine clays at the top of these layers, as well as shell debris. The sequences include foraminifera, such as sponge spiculae sp., elphidium crispum and globigerina sp. They are indicator for tsunamigenic deposits, in fact their habitat lies in deep water regions. Deep water foraminifera can only deposit at landside by an event, which affects the whole water head (e.g. Nott, 2006; Bryant, 2007).

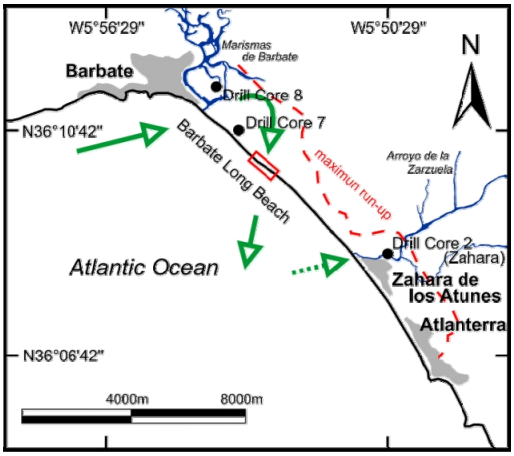

Fig. 2: Map of theBarbate and Zahara de los Atunes area with possible tsunami action (green arrows); box at the beach shows place of outcrop evidence near to Barbate.

Rising magnetic susceptibility within the "fining-up" sequences validated the tsunamigenic grain size distribution.

Beach section between Barbate and Zahara de los Atunes
The 5 km long rock cliff has been mapped, leveled, sampled (including sediment lacquer films; Fig. 3). We have surprisingly found only one layer on top of the basement at the cliff, in varying altitudes between 1.0 and 4.5 m above mean sea level. The basement is Cretaceous to Eocene flysch deposits or OIS 5 terraces (Tyrrhenian) of approximately 125 ky. The dark sandy layer of about 1.0 meter thickness constitutes a "fining-up" sequence with a coarse-grained base with conglomerates, shell debris and charcoal. These deposits are channeled and clasts are imbricated, palaeo-flow direction is towards the Atlantic. As the beach sands are white to yellowish and the layer is dark, organic- and clay mineral-rich, but sandy, we interpret this layer as a back flow. Palaeo-current directions endorse these observations and the evidence that only one layer is preserved. Presumably, former tsunamites were eroded due to multiple wave action and the cliff was “cleaned” to the basement by the waves.

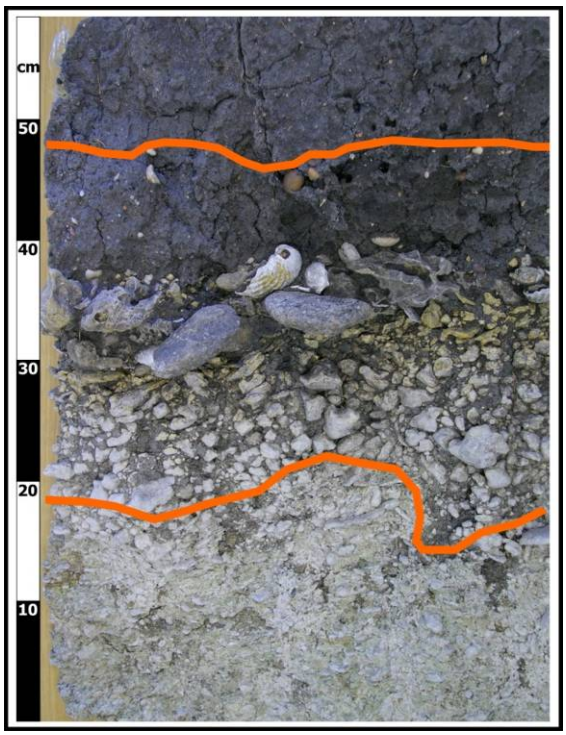

Fig. 3: Sediment lacquer film of the "back-wash" sediment, outcropped at the beach of Barbate; Bottom line is the boundary of flysch deposits and “back-wash” sediment (erosive base); Top line is the boundary of “back-wash” sediment and topsoil.

The dark clayey marshlands of Barbate have been reworked and the tsunamite was deposited as a mixture of beach sands, boulders and shell and the clayey marsh deposits during the back flow of the last major wave. The Flandrian transgression had a maximum at about 7.000 to 6000 years BP and reached altitudes of 3.0 to 4.0 m above the present sea level and cannot account for these deposits. Our interpretation of the principal sediment-depositing mechanisms effective in tsunami surges is based on field observations of deposit geometry and internal sedimentary characteristics, which are clearly not related to a beach.

Shallow drilling at location B 7 give us further clues for a tsunami event. Three “fining-up” sequences on top of each other show us that accordingly more than one wave of the so-called tsunami wave train is documented by these deposits. Also “rip-up” clasts - mostly angular clasts which are imbricated by clayey sediments - are detected in the sedimentary drilling core at this location.

Bolonia Bay
Here, we investigated the Roman ruins of Baelo Claudia. As mentioned above, several indicators of tsunami deposits have been published. We are currently investigating deposits in the ruins, which may also contain tsunami-reworked “post-Roman” colluvium (Silva et al., 2009). Also, the deposits described by Becker-Heidmann et al. (2007) are under examination. The “block fields” of Garcia et al. (2006) are related to small creek mouths into the Atlantic, we regard these as storm deposits reworking fluvial pebbles. They are only found near the creeks and in heights of 2.0 meters to 3.0 meters above the mean sea level along the beach.

Valdevaqueros Bay (Mellaria)
In this bay the rests of the Roman village of Mellaria are partly exposed, they are not excavated and covered by 2.0 meters of sandy, clayey sediments. The laguna of Valdevaqueros yields dark organic-rich marshy sediments, which may possibly be reworked during wave action. We have drilled a profile perpendicular to the coast up to 4.0 m depth. Surprisingly, laboratory analysis gave no clues to tsunami event in this area. The sedimentary cores of Valdevaqueros do not contain any tsunamigenic features. Either tsunami deposits are reworked and/or eroded by the river nearby or the tsunami waves did not hit Valdevaqueros frontally due to wave directions of the 1755 Lisbon event and bay protection. As well the locality of Mellaria is not the one indicated by Gracia et al. (2006), who put the village in the Los Lances bay. Mellaria was a Roman fishery village directly at the coast.

Los Lances area (Tarifa)
The marshlands of the Río Jara north of Tarifa are called Los Lances (Fig. 4). Here, wash-over fans of the Lisbon tsunami (without age constraints) (Gracia et al., 2006).

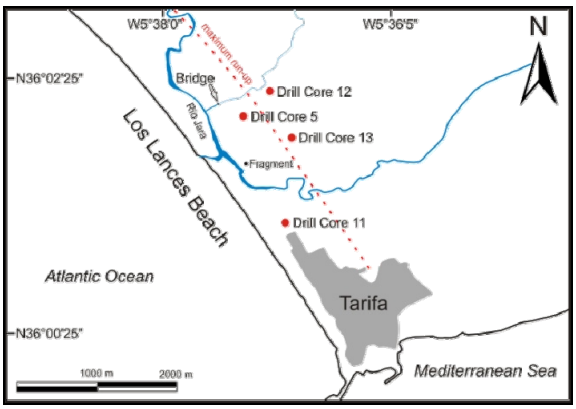

Fig. 4: Map of Los Lances Bay near Tarifa; washover fans caused by the 1755 tsunami are also illustrated.

We have drilled a profile perpendicular and parallel to the coast up to 4.0 m depth. We have found similar intercalations of tsunamites downhole, which are

interpreted as either an expression of repeated earthquake activity or tsunami-like waves induced by submarine slides. This sedimentary drilling core B 5 shows three significant "fining-up" sequences. The upper one reaches from clayey sediments at the top to coarser grained, unsorted pebbly layers containing shell debris and a certain composition of microfossils. Both of the two lower fining-up sequences are clearly cut at their base where the changeover to the next core meter is located, indicating sedimentary fall while drilling. Every fining-up sequence contains a similar composition of microfossils as well as shell debris in the lower parts near the base. Mainly foraminifera such as Elphidium Crispum and Quinqueloculina sp., both of which are found in 20 meters to 30 meters dephts of water, were also found in tsunamites at the south Portuguese coast assigned to the 1755 event (Bryant et al., 2007), once more confirming the tsunamigenic origin of these units. Storm events as potential cause of these deposits can be excluded because at present they would not even reach further inland than 250 meters to 280 meters (Gracia et al., 2006). Considering the great depth of about 4.0 m, the lower "fining-up" sequences can be related to former tsunami events, what has to be proved by dating of certain sections in the near future.

Also the damage to the old bridge at Los Lances Bay (Fig. 5) is described by Gracia et al. (2006) as reason to the tsunami in 1755.

Fig. 5: The old bridge at Los Lances Bay.

It was constructed by the beginning of the 18th century and partly destroyed by the 1755 tsunami. The distribution of erosion and accumulation zones around this structure suggests that the bridge acted as an obstacle to the tsunami waves, and all the system could be considered as a huge flute mark.

CONCLUSIONS

Combined, we describe new findings of tsunami deposits along the coast between *Barbate* and *Tarifa*.

In conclusion, we have found several different distinctive features of tsunamigenic deposits along the Spanish Atlantic coast, which are characterized by:

- Clast-supported, polymodal, boulder-bearing basal deposits composed mostly of well rounded clasts and fewer angular clasts, which are partly imbricated.
- Normal grading or crude normal grading. The lateral changes in characteristics of depositional facies are common and abrupt (channels)
- Clay to sand-sized, bioclastic (and Roman ceramic)-rich matrix is poorly sorted, implying that soft sediments eroded at the lower erosional surface contributed to the tsunami deposit.
- Mixed source of sediments (beach and marshes).
- Deep water foraminifera deposited by high energy event, such as a tsunami.

These features are interpreted as non-cohesive and sediment-loaded subaquatic density flows and deposits of successive waves in the tsunami wave train. The incorporation of sediments derived from mixed sources within the tsunami deposits, such as angular clasts from nearby subaerial settings, rounded clasts reworked from beach gravels, and shell debris and yellowish beach sands eroded from older, and unconsolidated, shoreface deposits are interpreted as back flow or back wash deposits.

OUTLOOK

Further fieldwork in the study area near to Barbate beach will concentrate on palaeo-relief, which can be detected by GPR, to evaluate the display of tsunamigenic deposits along the beach and the inland.

Also ^{14}C dating of some samples within the PVC liners is in progress, to ensure, that the event took place at 1755, which is the final question of this project.

Acknowledgements: We would like to thank Spanish-German Acciones Integradas Program HA2004-0098, by the Spanish Research Projects CGL2005-04655/BTE (USAL), CGL2005-01336/BTE (CSIC) and by Deutsche Forschungsgemeinschaft Project Re 1361/9 for the contingency to realize our fieldwork and studies.

References

Becker-Heidmann, P. Reicherter, K., Silva, P.G. (2007). ^{14}C dated charcoal and sediment drilling cores as first evidence of Holocene tsunamis at the Southern Spanish coast. in: Radiocarbon; 49, 2, 827-835. (Proceedings of the 19th International Radiocarbon Conference; edited by Bronk Ramsey, C. & Higham, T.F.G.)

Bryant, E. (2007). Tsunami - The Underrated Hazard; by Edward Bryant, Springer-Verlag GmbH.

Gracia, F.J., Alonso, C., Benavente, J., Anfuso, G., Del-Río, L. (2006). The different coastal records of the 1755 Tsunami waves along the Atlantic Spanish Coast. Z. Geomorph. N.F., Suppl.Vol. 146, 195-220. (A. Scheffers. & D. Kelletat, ed.)

Nott, J. (2006). Extreme Events: A Physical Reconstruction and Risk Assessment; (chapter: „Tsunamis"). by Jonathan Nott, Cambridge University Press, 109-140

Silva, P.G., Goy, J.L., Zazo, C., T. Bardají, T., Lario, J., Somoza, L., Luque, L., Gonzales-Hernández, F.M. (2006). Neotectonic fault mapping at the Gibraltar Strait Tunel area, Bolonia Bay (South Spain). Engineering Geology, 84, 31-47.

Silva P.G., Reicherter K., Grützner C., Bardají T., Lario J., Goy J.L., Zazo C., & Becker-Heidmann P., (2009). Surface and subsurface palaeoseismic records at the ancient Roman city of Baelo Claudia and the Bolonia Bay area, Cádiz (South Spain). Geological Society, London, Special Publications 2009; v. 316: Palaeoseismology: Historical and prehistorical records of earthquake ground effects for seismic hazard assessment.

PALAEOSEISMOLOGICAL INVESTIGATIONS USING SPELEOTHEMS: CASE STUDY OF TWO CAVES IN RHODOPES MOUNTAINS, SOUTHERN BULGARIA

K. Kostov (1), S. Shanov (1) and G. Surányi (2)

(1) Geological Institute of Bulgarian Academy of Sciences, Acad. G. Bonchev Str., 24, 1113 Sofia, BULGARIA. kskostov@geology.bas.bg
(2) MTA-ELTE Geological, Geophysical and Space Science Research Group, Pázmány Péter sétány 1/C, 1117 Budapest, HUNGARY

Abstract: *The aim of this paper is to report the results of the accomplished seismotectonic investigations in two caves in Rhodopes Mountains, Southern Bulgaria. The Yamata Cave and Shepran Dupka Cave are located in the Dobrostan karst massif, south-east of the city of Plovdiv. Both caves are located in the hanging wall of the clearly morphologically expressed Dobrostan fault. In the caves are measured the directions of the fallen and perturbed speleothems, recovered with new generations of stalagmites. The rose-diagrams of the preferred directions are similar for the two caves. The performed U-series dating of the deformed speleothems suppose an activation of the Dobrostan fault during the Pleistocene.*

Key words*: palaeoseismology, speleothems, Rhodopes Mts, Bulgaria*

INTRODUCTION

The seismicity of Bulgaria is characterized by instrumental records and fragmentary historical archives that covered a period up to 2000 years ago. The first historical data about the effect of catastrophic earthquake on the contemporary Bulgarian lands is the destruction of the ancient town of Bizone, near Kavarna, NE Bulgaria in the 2^{-nd} half of the I^{-st} century B.C. (Grigorova, Grigorov, 1964). The seismic hazard assessment is primarily based on the estimation of the return period of the large earthquakes. For this purpose it is necessary to search additional data about catastrophic paleoseismic events during prehistoric time.

The caves are well protected from most of the exogenic geomorphologic processes: erosion, denudation, deflation, etc. In this context, the cave deposits are a medium favorable to the conservation of damaging evidences caused by tectonic events. The broken and deformed speleothems in the caves are accepted by many researchers as a good tool for palaeoseismic reconstructions. The "seismothems" (speleothems potentially broken by a seismic event - *sensu* Quinif, 1999) can be dated (U/Th, C^{14}, etc.) and offer possibilities to obtain the age of the palaeoevent that caused the collapsing (Forti, 1998, Forti & Postpischl, 1984, Gilli, 1995, Quinif, 1996, Camelbeeck. 1998, Delaby, 2000, etc.). At the other hand, recently performed seismologic investigations on speleothems (Lacave *et al.*, 2004), modelling of speleothem ruptures (Cadorin *et al.*, 2000) and field observations after strong earthquakes (Gilli *et al.,* 1999, Gilli, 2005) shows that the most of the speleothems are stable to the impact of seismic waves.

The aim of this paper is to report the results from study of the deformed speleothems in two caves in Rhodopes Mts, Southern Bulgaria.

DESCRIPTION OF THE CAVES

The studied caves are situated in the northern parts of Rhodopes Mts, about 45 km south-east of Plovdiv.

The Shepran Cave and Yamata Cave are developed in the highly karstified Proterosoic marbles of the Dobrostan marble formation. From structural point of view, the caves are situated in different tectonic blocks, separated by series of parallel normal faults with WE strike, dipping to South (Fig. 1).

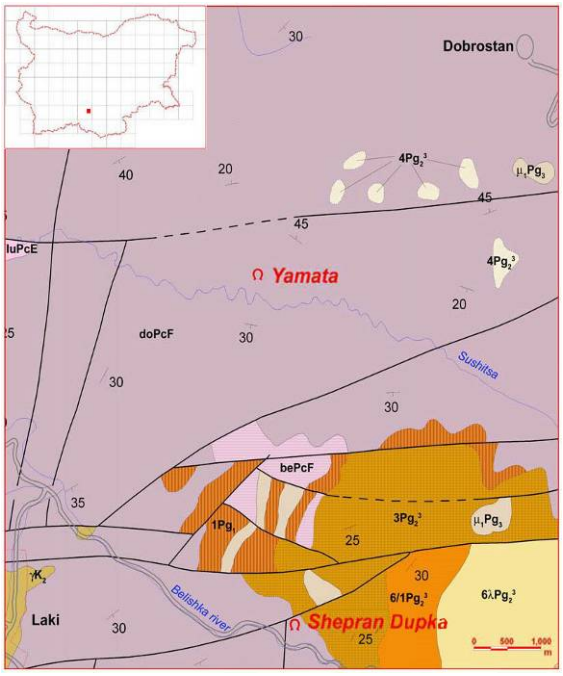

Fig. 1: Location of the caves and geological map of the studied area (after Kozhuharov et al., 1994)

The Shepran Cave is located on the southern slope of the Dobrostan massif (Central Rhodopes Mts., South Bulgaria) with elevation of 840 m. a.s.l. This dry fossil cave consists of gallery with length of 260 m and 18 m pit at the end parts. The total denivelation of the cave is 39 m and the volume – 3010 m^3. The cave is rich of different speleothems, mostly of them perturbed (fallen stalagmites, recovered with new speleothems.

The Yamata Cave is situated in the middle parts of the Dobrostan plateau, in the deep valley of Sushitsa River. The cave entrance is 860 m.a.s.l. The length of the cave is 183 m.

METHOD

In this investigation is used the technique of measurement of the preferred directions of the deformed speleothems, described in the works of Gilli (1995), Delaby (2000), Dublyansky (1995), *etc*. The method is based on the idea that the availability of clearly expressed maxima in the spatial orientation of the broken and deformed speleothems (stalagmites, stalactones) is an indicator about the seismotectonic origin of the deformations.

For this purpose, the studied caves must be well protected against anthropogenic impact (recent vandalism or availability of prehistoric artefacts). There are no traces of glaciation during the Pleistocene in the Rhodopes Mts – some researchers accept the movement of ice as a reason for destruction of speleothems (Gilli, 2005).

The caves are dry, without underground streams and dynamic fluvial deposits that is necessary precondition for such type of seismotectonic study.

RESULTS

From the comparatively wide range of seismotectonic speleoindicators described in previous works (Bini *et al*., 1992, Dublyansky, 1995, Quinif, 1996, 2000, Delaby, 2000, Gilli, 1995, 2005) the following elements are established in the studied caves:

A) *Fallen stalagmites*. The fallen stalagmites are the most expressive seismothems. The "stalagmite's cemeteries" (sensu Quinif 2000) in some caves represents the best evidence for seismotectonic or neotectonic activity. In the Shepran Cave are measured the directions of 46 broken stalagmites and 50 stalagmites in Yamata Cave. The maximal size of the studied speleothems is up to 140 cm in height and 40 cm in diameter. All of the samples are recovered with new speleothems. The stastistical analysis of the deformations gives well individualised directions in the both caves with three almost identical maxima in the rose-diagrams of their orientation (Fig. 2).
B) *Displaced and inclined stalactones*. One of the attractive features of the Shepran Cave and Yamata Cave are the anomalies established on massive columns with height up to 4 m and 1 m in diameter.
C) *Broken soda-straws*. Being in the initial stage of the stalactites development, the soda-straws are the speleothems that are the most amenable to the seismic effects. In some places of the two caves are established broken thin stalactites soldered with calcite deposits onto the floor.

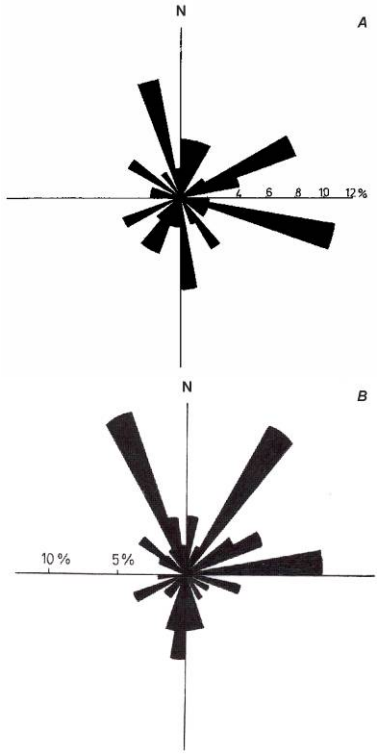

Fig. 2: Rose-diagrams of the preferred directions of broken and recovered with new sinter generation stalagmites in the caves Shepran Cave (A, 46 measurements) and Yamata Cave (B, 50 measurements)

Four U-series age determinations, using mass spectrometry, were performed on speleothems samples from Yamata Cave. The dating is accomplished by Dr. Surányi with usage of plasma ICP-MC spectrometer (Thermo Corp., Germany). The samples Yamata 1 and Yamata 2 are taken from the top of 140 cm fallen stalagmite and from the base of a small active stalagmite that is cover the fallen one. The obtained ages are ~300 kyr BP (the non-precise age is because of an availability of clay materials in the sample) for Yamata 1 and 48.2 (± 0.9) kyr BP for Yamata 2.

The ages 229 kyr (± 17) kyr BP (Yamata 3) and 317 (± 26) kyr BP (Yamata 4) are for samples, taken from the base of a 26 cm high stalagmite formed on an inclined massive 170 cm stalagmite (Fig. 3) and from calcite deposits, that covered the top of a fallen stalagmite.

DISCUSSION AND CONCLUSION

The results of the investigations in the Rhodopes Mountains give a reason to postulate that the deformations or the destruction of the speleothems are not due to the deformation of their basements. The only possible explanation of the sudden loosing of equilibrium and broke down of the stalagmites is the impact of some horizontal acceleration, creating in them shear stress exceeding the strength of the material. This type of

effects can be expected if the tectonic block, with the concerned cave is suddenly displaced along tectonic fault seismically activated. In this part of the Rhodopes Mts. significant quantities of broken speleothems have been discovered in caves situated inside subsided and horizontally displaced blocks near clearly expressed active faults.

Fig. 3: Coring of a stalagmite with 26 cm height formed on an inclined massive stalagmite in Yamata Cave

The rose-diagrams of the fallen stalagmites can indicate the horizontal component of the predominant direction of displacements (the opposite direction of the maximums) of the hanging wall of the fault. The deformations of speleothems in 11 caves in different karst areas in Bulgaria, located in the hanging walls of active or capable faults are investigated in detail by Kostov (2008).

The similar orientations of the deformed speleothems in Yamata Cave and Shepran Cave suppose the effect of common seismotectonic event during the Pleistocene, connected with possible activation of the Dobrostan fault.

The study denotes the important role of the movement itself of the tectonic block during the process of rupturing and displacement along an active or capable fault.

Aknowledgments: This study is supported by the project "Traces of paleoseismicity in karstic caves" of the National Science Fund to the Ministry of Education and Science of Bulgaria.

References

Bini, A., Quinif, Y., Sules, O, Uggeri, A. (1992). Les mouvements tectoniques recents dans les grottes du Monte Campo dei Fiori (Lombardie, Italie). Karstologia, 19, 23-30.

Cadorin, J.-F., Jongmans, D., Plumier, A., Quinif, Y., Camelbeeck, T. (2000). Modelling of speleothems rupture. Proc. "Han 2000" workshop, 13-17. 03. 2000, Han-sur-Lesse, Belgium, 27-30.

Camelbeeck, T. (1998). Speleothems as palaeoseismic indicators: the point of view of a seismologist. Contr. Int. Symp. Karst & Tectonics, 9-12. 03. 1998, Han-sur-Lesse, Belgium, 23-24.

Delaby, S. (2000). Palaeoseismic investigations in Belgium caves. Proc. "Han 2000" workshop, 13-17. 03. 2000, Han-sur-Lesse, Belgium, 45-48.

Dublyansky, V. (1995). Sights of intense earthquakes in karst regions (with special reference to the Mountain Crimea). Geomorphologia, 1, 38-46 (In Russian with English abstract).

Forti, P., Postpischl, D. (1984). Seismotectonics and paleoseismic analyses using karst sediments. Marine Geology, 55, 145-161.

Forti, P. (1998). Seismotectonic and paleoseismic studies from speleothems: the state of the art. Spelochronos hors-serie - 1998, 79-81.

Gilli, E. (1995). Recording of earth movements in karst. 5-th Int. Conf. Seizm. Zonation, 17-19. 10. 1995, Nice, Ouest Edit., Nantes, 1305-1314.

Gilli, E. (2005). Review on the use of natural cave speleothems as palaeoseismic or neotectonics indicators. C. R. Geoscience, 337, 1208-1215.

Gilli, E., Levret, A., Sollogoub, P., Delange, P. (1999). Research on February 18, 1996 earthquake in the caves of St-Paul-de-Fenouillet area (Pyrenees-Orientales, France). Geodinamica Acta, 12 (3-4), 143-158.

Grigorova, E., Grigorov, B. (1964). The epicenters and the seismic lines in Bulgaria. Sofia, BAS edition, 84 pp.(In Bulgarian with English abstract).

Kostov, K. (2008). Paleoseismological indications in karst terrains. Ph.D. thesis, Sofia, Geological Institute of BAS, 191 pp.

Kozhuharov, D., Kozhuharova, E., Marinova, R., Katzkov, N. (1994). Explanatory note to the Geological map of Bulgaria, M 1:100000, sheet "Chepelare", Sofia, 74 pp.

Lacave, C., Koller, M. G., Ezogue, J. J. (2004). What can be concluded about seismic history from broken and unbroken speleothems? Journal of Earthquake Engineering, 8, 3, 431-455.

Quinif, Y. (1996). Enregistrement et datation des effets sismo-tectoniques par l'etude des speleothemes. Ann. Soc. Geol. Belgique, 119, 1, p. 1-13.

Quinif, Y. (1999). Etude d'un sismotheme dans le Reseau Sud de la Grotte de Han-sur-Lesse. Speleochronos, 10, p. 33-46.

Quinif, Y. (2000). Karst and sismotectonics: speleothems as paleoseismic indicators. Proc. "Han 2000" workshop, 13-17. 03. 2000, Han-sur-Lesse, Belgium, 121-124.

CHARACTERISTICS AND PALEOSEISMIC STUDY OF THE QUATERNARY EUPCHEON FAULT IN SOUTHEAST KOREA

*M. Lee (1), S.R. Han (1), T. Shim (2) and Y.S., Kim (1, *)*

(1) Dept. of Environmental Geosciences, Pukyong National University, Busan 608-737, KOREA.
(2) Safety Technology Division, Korea Institute of Nuclear Safety, Daejeon 305-338, KOREA. * ysk7909@pknu.ac.kr

Abstract: *The Eupcheon Fault is one of the Quaternary faults developed in southeastern part of Korean peninsula. The fault is located 1.8 km away from the Weolsung nuclear power plant to the south. Based on the fault analysis developed in marine terrace deposits, the Eupcheon Fault was developed as a syn-depositional fault. At least four faulting events are recognized based on colluvial wedges and displacement-distance (d-x) analysis. The Eupcheon Fault cuts the third level Quaternary marine terraces (40-50 m), which is relatively higher compared with other regions (25-33m). An N-S trending fault is discovered in the northern extent of the Eupcheon Fault, which composed of several fault gouges indicating multiple deformations. The hanging wall block of the fault shows highly damaged fracture patterns indicating that the hanging wall is weaker than footwall. Therefore, detailed analysis of fault characteristics and fault zones must be a very useful way to assure the seismic hazard assessment of the site for nuclear power plants.*

Key words: *Eupcheon Fault, fault analysis, displacement-distance, seismic* hazard assessment

INTRODUCTION

Generally, the Korean peninsula has been considered as tectonically safe region from earthquakes, because it is located in stable margin of the Eurasian plate. However, more than 36 Quaternary faults have recently been reported from the southeastern part of Korea (Fig. 1; Kee et al., 2007). These Quaternary faults are almost distributed around the Yangsan and Ulsan faults, SE Korea. Recently the Eupcheon Fault is reported (Kyung et al., 1999; Chang, 2001; Park et al., 2006) close to the Weolsung Nuclear Power Plant (WNPP), which is located 1.8 km away from the WNPP to the south. Seismic hazard assessment associated with the Eupcheon Fault is very important in terms of the safety concerns in nuclear power plant industry. Therefore, we described the basic geometry and characteristics and interpreted movement seismic history of the fault. For this purpose, geometric analysis and d-x analysis are carried out from a trench excavated across the Eupcheon Fault to understand its movement history and kinematics (Kim et al., in review). Furthermore, detailed fault zone analyses are carried out in the northern extent of the fault to understand the condition of site foundation.

LOCAL GEOLOGIC SETTING

The basement of the study area consists of Cretaceous sediment rocks, which have been intruded by Cretaceous and Tertiary igneous rocks, mainly granites and dykes of various compositions. The intraplate deformation of microplates initiated back-arc rifting and the spreading of the East Sea in the Oligocene to early Miocene (e.g. Kimura & Tamaki, 1986; Yoon & Chough, 1995). Tertiary basins along the eastern margin of the Gyeongsang Basin are associated with the extension of the East Sea. Collision of the Bonin Arc with central Honshu caused back-arc closing and crustal shortening in the Middle Miocene (e.g. Kim and Park, 2006).

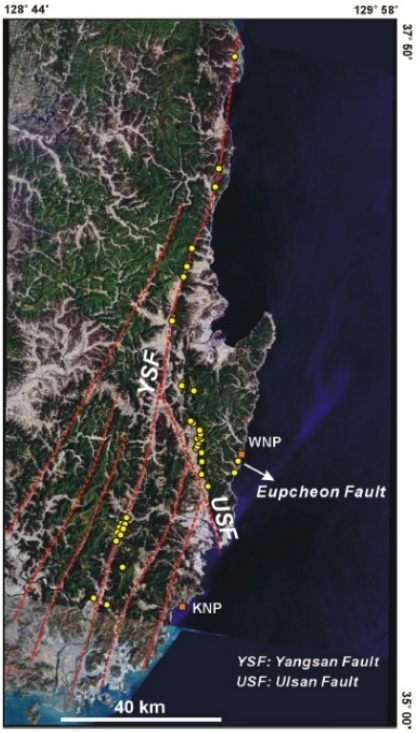

Fig. 1: Distribution of Quaternary faults (yellow circle) in southeast Korean Peninsula (WNP: Weolsung Nuclear Power Plant, KNP: Kori Nuclear Power Plant; from Kee et al., 2007).

Thirty-six, Quaternary fault close to study area have been mapped in detail. Most of them show a right lateral strike-slip or reverse movement (Kyung et al., 1999; Chang, 2001; Park et al., 2006) coincident with focal mechanism solution from recent earthquakes (Kim et al., 2006; Park et al., 2007). According to the focal mechanism solution (Kim et al., 2006), both the subducting Pacific plate and the collision of the Indian Plate with the Eurasian continent result in a maximum principal stress

trending ENE/WSW in the Korean peninsula and ESE/WNW in the east on the East Sea (Choi et al., 2008).

The Quaternary terrace deposits in the southeastern part of the Korean Peninsula were developed parallel to the coastline at five different elevations. The Eupcheon Fault is developed in the third marine terrace about 30–50 m above sea level. The marine terrace of the study area is relatively higher than other regions indicating local tectonic uplift. The average long-term uplift rates are 0.31 (~0.3)m/ka in the study area, but other regions uplift rates are 0.18 (~0.2) m/ka (Choi et al., 2008).

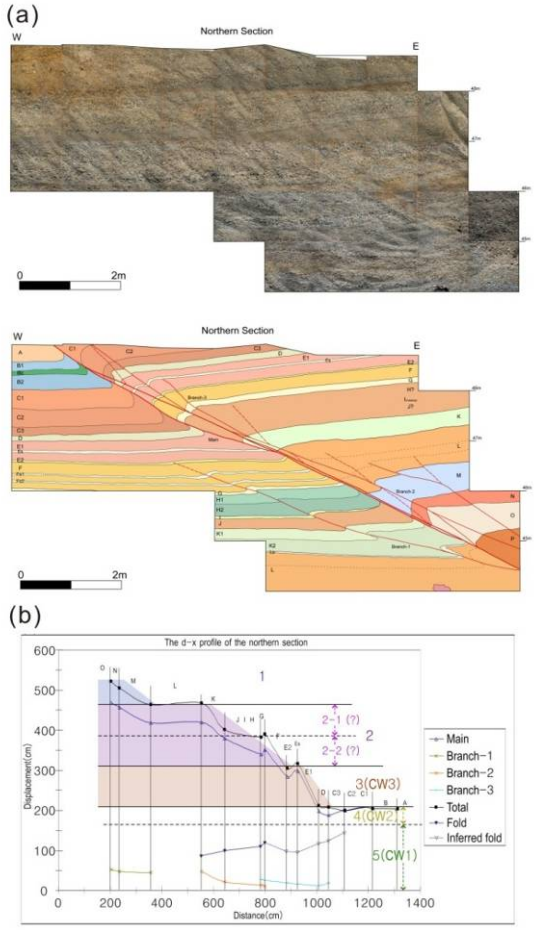

Fig. 2: Photomosaic and sketch logs of the northern lower trench walls(a), displacement–distance (d–x) data for the northern (b). Note that the trends show several step-like features that indicate cumulated displacement. The displacements accommodated by drag folding are generally constant along the fault. However, the displacements slightly increase in inverse proportion to the total displacement, which may indicate that some of the displacement associated with faulting is accommodated by folding at fault tips. The displacement accommodated by drag folding is not included to the amount of the total displacement (from Kim et al., in rev.)

GENERAL CHARACTERISTICS OF THE EUPCHEON FAULT

The Eupcheon Fault, one of the identified Quaternary faults, was discovered during the construction of a primary school in an area close to a nuclear power plant. The Eupcheon Fault consists of one main reverse fault (N20°E/40°SE) with approximately 6-7m displacement, and synthetic and antithetic faults. It also includes mesoscale structures such as hangingwall anticlines, drag folds, back thrusts, pop-up structures, flat-ramp geometries, fault-related folds, and duplexes in unconsolidated sediments (Kim et al., 2004). The orientation of the new trench (Fig. 2) was about 140°, almost perpendicular to the strike of the fault, and the trench was about 25 m in length, 3-5 m in width, and 8-11 m in depth depending on the location within the trench (Kim et al., in review; Fig. 2a).

The trench shows an upper section in the northern wall that included three sedimentary wedges that correspond to periods of surface faulting, and two lower sections that recorded thrust events cutting the marine terraces. Kim et al.(in review) measured the displacements across the fault based on the established sedimentary sequences. Some layers in the footwall are thinner than hanging wall, which probably indicates the development of topographic relief between hanging wall and footwall since sedimentation and syn-depositional faulting. Moreover, d-x profiles reveal consistent step-like patterns indicative of repeated faulting (Fig. 2b). Therefore, the total cumulative displacement along the fault is about 6 m, and four or five faulting events are recognized based on the existence of colluvial wedges and the d-x profiles. Furthermore, these indicate that the amount of slip in each event might be in the range of 0.7 to 1.8 m (Kim et al., in review). Kim et al.(in review) suggests that this maximum slip corresponds to earthquake magnitudes in the range of Mw 6.3 to 7.0 based on the relationship between maximum slip and moment magnitude suggested by Wells and Coppersmith (1994).

AGE CONSTRAIN OF THE FAULT ACTIVITY AND THE MARINE TERRACE DEPOSITS

Marine terraces are developed extensively along the southeastern coast of the Korean peninsula. Marine terraces are valuable materials for discerning late Quaternary vertical displacement and deformation based on optically stimulated luminescence (OSL) dating method. The Eupcheon Fault cuts the unconsolidated third level Quaternary marine terrace. Many studies suggest the age of fault activity of the Eupcheon Fault, using ESR and OSR age dating methods (e.g. Lee et al., 2007, Choi et al., 2008, Choi et al., 2009). The reported OSL age from this trench site in the third marine terrace is in the range of 110-120ka (Choi et al., 2003).

Based on the ESR dating result, the fault has been reactivated at least five times such as 2000, 1300, 900-1100, 700-800, and 500-600ka ago. However, ESR dating ages are older than the terrace ages, suggesting that they do not represent the youngest faulting event. These data suggest that the Eupcheon Fault can be classified as a potentially active fault.

GEOMETRIC FAULT PATTERNS IN THE NORTHERN EXTENT OF THE EUPCHEON FAULT

Recently, a east dipping, N-S trending fault was discovered during developed in the construction of new Weolsung nuclear power plant construction site in the northern extent of the Eupchon Fault.

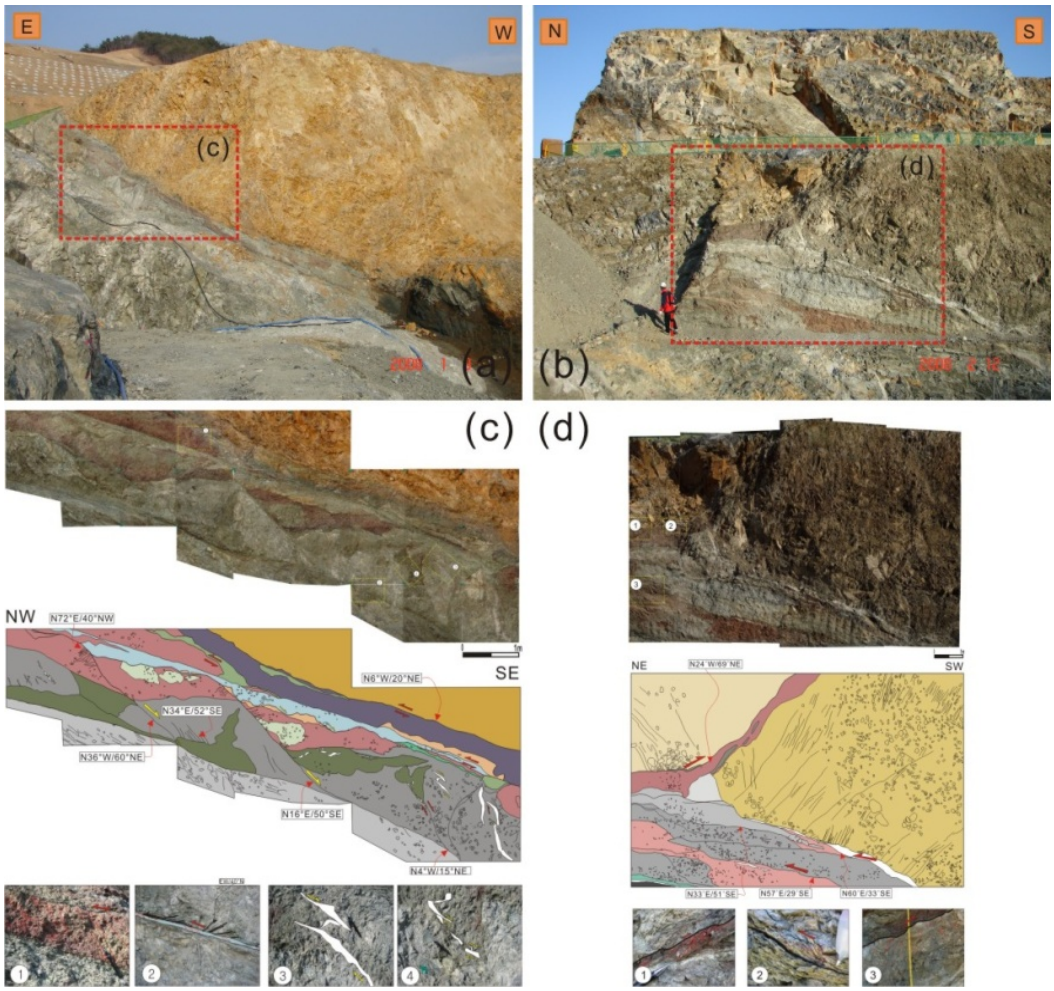

Fig. 3: The photographs of outcrops along the northern extent of the Eupcheon Fault in new Weolsung nuclear power plant(a, b). photo mosaic and sketch map, and detailed photographs and sketches showing movement senses(c, d).

This location is the northern extent of the Euchon Fault. The fault deformed the Cretaceous sedimentary rocks developed in the construction site. of the Gyeongsang supergroup. Well-exposed vertical and horizontal sections are analyzed so as to understand 3-dimensional fault geometry and fault evolution. A well exposed 1 km long and up to 2m thick reactivated fault zone is studied developed (Fig. 3). The main N-S striking fault zone shows various fault gouge bands and S-C fabrics, which that indicate discrete stages of normal and reverse fault movements during several stages of deformation. The fault gouges within the fault zone occur as splits or merge into another fault zone rather than crosscut each other. These may indicators suggest indicate that the major fault has been evolved into in this study area ia mature fault system.

FAULT SLIP ANALYSIS AND REACTIVATION

To understand the transport direction of the fault, we analyzed the relative timing of kinematic indicators, such as cleavages, lineations, and slickensides (Fig. 4a, b). The results show consistent slip pattern (Fig. 4c). The slip data indicates that the fault zone experienced repeated movements including normal movement under SE extension and reverse movement under NNW compression (Fig. 4d)

HAZARD ASSESSMENT AROUND THE EUPCHEON FAULT

Generally, earthquakes occur along preexisting active faults (e.g. Ota, 1999; Chen et al., 2002; Ota et al., 2004; Ota et al., 2005). This suggests that detailed mapping of active faults is a key for understanding future surface faulting. One of the important characteristics of earthquake hazard is that no serious damage occurs on the footwall although buildings are located very close to a fault (Ota et al., 2005).

Hanging wall block in the study area also represents a wide range of damages such as wide fracture zone, large volume of distributed deformation, and alteration by groundwater (Fig. 3a). Therefore, the fault geometries and kinematics are important factors to evaluate conditions of important sites. Furthermore, fault damage zones (Kim et al., 2004) around faults are very important indications for the seismic hazard assessment due to secondary fractures and aftershocks (Kim and Sanderson, 2008).

CONCLUSION

The Eupcheon Fault is one of the identified Quaternary faults in SE Korea. This is of particular importance because it is located only 1.8 km away from the Weolsung Nuclear Power Plant. According to fault and d-x profile analyses, this fault was a syn-depositional fault. Four or five faulting events are recognized based on the existence of colluvial wedges and the d-x profiles. The Eupcheon Fault developed in the third marine terrace in a age range of 110-120ka (OSL), which is slightly higher than other regions. The N-S trending fault in the northern extent of the Eupcheon Fault shows several fault gouge bands indicating multiple faulting events. According to the fracture and fault zone analysis, the hanging wall part is much weaker than footwall part. It indicates that important sites such as nuclear power plant must be locate on the footwall part of a fault for safety. Furthermore, the understanding of fault damage zones must be very helpful for site investigation.

Acknowledgement: This work was funded by the Korea Institute of Nuclear Safety under Grant KOSEF 2009-062378.

References

Chang, T.W. (2001). Quaternary tectonic activity at the eastern block of the Ulsan fault. *Journal of the Geological Society of Korea* 37, 431-444 (in Korean with English abstract).

Chen, Y.-G., Chen, W.S., Wang, Y., Lo, P.W., Lee, J.C., Liu, T.K.b(2002). Geomorphic evidence for prior earthquakes: lessons from the 1999 Chichi earthquake in central Taiwan. *Geology* 30 (2), 171– 174.

Choi, J.H., Kim, J.W., Murry, A.S., Hong, D.G., Chang, H.W., Cheong, C.-S. (2009). OSL dating of marine terrace sediments on the southeastern coast of Korea with implications for Quaternary tectonics. *Quaternary International* 199, 3-14.

Choi, J.H., Murry, A.S., Jain, M., Cheong, C.-S., Chang, H.W. (2003). Luminescene dating of well-sorted marine terrace sediments on the southeastern coast of Korea. Quaternary Science Reviews 22, 407-421.

Choi, S.-J., Merritts, D.J., Ota, Y. (2008). Elevations and ages of marine terraces and late Quaternary rock uplift in southeastern Korea. *Journal of Geophysical Research* 113, B10403.

Kee, W.-S., Hwang, J.H., Song, K.-Y., Kihm, Y.-H. (2007). Structural characteristics of Quaternary reverse faulting on the Eupcheon fault, SE Korea. *Journal of the Geological Society of Korea* 43, 311-333 (in Korean with English abstract).

Kim, Y.-S., Kim, J.H., Jin, K. (In review). interpretation of faulting events and accumulated displacement history upon the Quaternary Eupcheon Fault, Korea. *Tectonophysics*.

Kim, Y.-S., Sanderson, D.J. (2008). *Earthquake and fault propagation, displacement and damage zone.* 2008 Nova Science Publishers, Inc. ISBN: 978-1-60456-827-1.

Kim, Y.-S., Park, J.-Y. (2006). Cenozoic deformation history of the area around Yangnam-Yangbuk, SE Korea and its tectonic significance. *Journal of Asian Earth Sciences* 26, 1-20.

Kim, Y.-S., Park, J.Y., Kim, J.H., Shin, H.C., Sanderson, D.J. (2004). Thrust geometries in unconsolidated Quaternary sediments and evolution of the Eupcheon Fault, southeast Korea. *The Island Arc* 12, 403-435.

Kimura, G., Tamaki, K., (1986). Collision, rotation, and back-arc spreading in the region of the Okhotsk and Japan Seas. *Tectonics* 5, 389-401.

Kyung, J.B., Lee, K., Okada, A., Watanabe, M., Suzuki, Y., Takemura, K. (1999). Study of fault characteristics by trench survey in the Sangcheon-ri area in the southeastern paet of Yangsan Fault, southeastern Korea. *Journal of Korean Earth Science Society* 20, 101-110.

Lee, H,-K., Yang, J.-S. (2007). ESR dating of the Eupcheon fault, South Korea. Quaternary geochronology 2, 392-397.

Ota, Y., Chen, Y.-G., Chen, W.-S., (2005). Review of paleoseismological and active fault studies in Taiwan in the light of the Chichi earthquake of September 21, 1999. *Tectonophysics* 508, 63-77.

Ota, Y., Watanabe, M., Suzuki, Y., Sawa, H. (2004). Geomorphological identification of pre-exiting active Chelungpu Fault in central Taiwan, especially its relation to the location of the surface rupture by the 1999 Chichi earthquake. *Quaternary International* 115–166, 155– 166.

Ota, Y., Yamaguchi, M. (1999). Surface deformation by the 1999 Chichi earthquake in central Taiwan. *Chiri (Geograpahy)* 44-12, 8 –15 (in Japanese).

Park, J.-C., Kim, W., Chung, T.W., Baag, C.-E., Ree, J.-H. (2007). Focal mechanisms of recent earthquakes in the southern Korean Peninsula. *Geophysics Journal of International* 169, 1104-1104.

Park, Y., Ree, J.-H., Yoo, S.-H. (2006). Fault slip analysis of Quaternary faults in southeastern Korea, *Gondwana Res*. 9, 118-125.

Yoon, S.H., Chough, S.K. (1995) Regional strike slip in the eastern continental margin of Korea and its tectonic implications for the evolution of Ulleung Basin, East Sea (Sea of Japan). *Geological Society of America Bulletin* 107, 83-97.

Wells, D.L., Coppersmith, K.J. (1994). New empirical relationships among magnitude, rupture length, rupture width, rupture area, and surface displacement. *Bulletin of Seismological Society of America* 84, 974-1002.

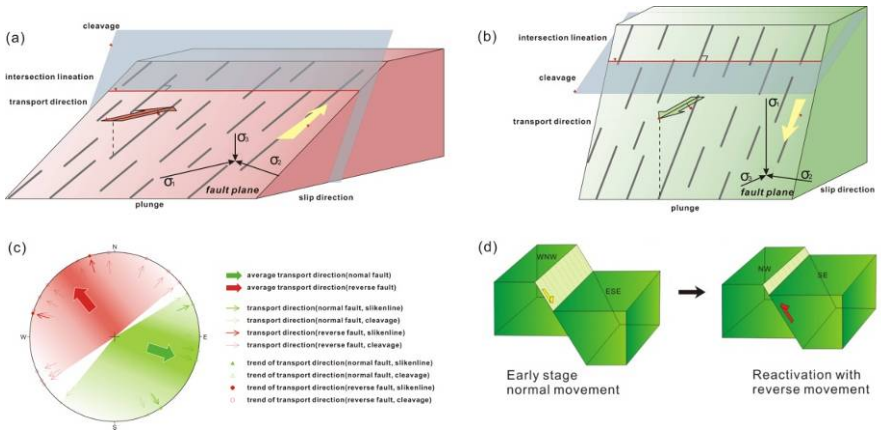

Fig. 4: Block diagram of a reverse fault (a) and a normal fault (b) and associated slip factors, transport direction along the main fault (c), schematic diagram of the movement (d).

PALEOSEISMIC EVIDENCE FROM BROKEN SUBMARINE CARBONATE CHIMNEYS IN THE GULF OF CADIZ (SOUTHERN SPAIN)

A. Maestro (1), G. Jané (1), J. García-Mayordomo (1), B. Fernández-Revuelta (2), M.A. Rodríguez-Pascua (1) and J..J. Martínez-Díaz (3)

(1) Departamento de Investigación y Prospectiva Geocientífica, Instituto Geológico y Minero de España. C/ Ríos Rosas, 23. 28003-Madrid. SPAIN. a.maestro@igme.es, g.jane@igme.es, julian.garcia@igme.es, ma.rodriguez@igme.es.
(2) Subdirección General de Centros Tecnológicos y Plataformas Científico-Tecnológicas, Ministerio de Ciencia e Innovación. C/Albacete, 5. 28027-Madrid. SPAIN. barbara.frevuelta@micinn.es
(3) Dep. Geodinámica, Facultad de Geología, Universidad Complutense de Madrid. C/ José Antonio Novais 2. 28040-Madrid. SPAIN. jmdiaz@geo.ucm.es

Abstract: *During the 2000 and 2001 R/V Cornide de Saavedra cruises, vast fields of hydrocarbon-derived carbonate chimneys were discovered and sampled along of the Cadiz Contourite Channel and Guadalquivir Diapiric Ridge. Observations from an underwater camera revealed a spectacular high density of pipe-like chimneys, some of them longer than 1 m, lying over the sea floor, and some protruding from muddy sediment. The major axes of the fallen chimneys present a regular spatial distribution in a NW-SE direction. The basal morphology of them shows common characteristics of an angular breakage associated with flexo-traction process. The homogeneous distribution and the basal morphology of the chimneys imply that the cause of its rupture is related to oscillatory ground motion due to a seismic event. Considering the mechanical properties of the chimney and the geological and topographical conditions of the area to ground motion amplification we have estimated that the magnitude of the earthquake necessary to break the chimneys was about 7 and that the responsible fault is probably located right under the chimneys field or very close to them.*

Key words: *Broken carbonate chimneys, paleoseismic activity, Cadiz Contourite Channel, Guadalquivir Diapiric Ridge*

INTRODUCTION

In the last years, numerous studies have discovered and sampled vast fields of lying hydrocarbon-derived carbonate chimneys along the Gulf of Cadiz continental slope at depths between 500 and 1200 m (Fig. 1A). They are located in the Guadalquivir Diapiric Ridge (GDR) and the Cadiz Contourite Channel (CCC) (Díaz-del-Río et al., 2003) (Fig. 1B). The GDR is a prominent structural high with steep slopes up to 25º and irregular crest at water depths between 800 and 950 m. This ridge is likewise a linear lower-middle Miocene plastic marls diapiric ridge which trends NE-SW. In the southern edge of the GDR is located the CCC. The CCC is known to siphon off the southern branch of the Mediterranean Outflow Water (MOW) Lower Water Mass as it makes its way generally westwards along the south Iberian margin. Bottom current velocity estimates for the CCC, are typically in the range 0.2 to 0.8 m s^{-1} (Hernández-Molina et al., 2006).

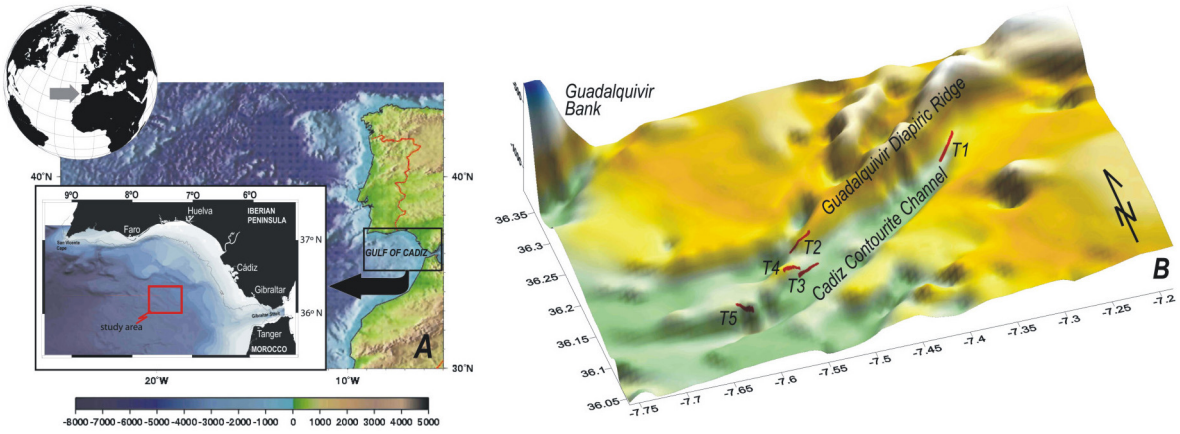

Fig. 1: A) Shaded bathymetry map of Iberia, northwest Africa and Central Atlantic (Smith and Sandwell, 1997) with the location of the study area. B) Multibeam compilation of the study area by Zitellini et al. (2009) with location of the main morphological features and the photographic tracklines analysed in this work.

Analysis of the 1798 photographs taken during the 2000 R/V Cornide de Saavedra cruise involved systematically recording data on seafloor length and orientation of major axis of the carbonate chimneys (Fig. 2). In five transects studied (Fig. 1B) 5861 chimneys have been identified lying scattered in dense concentrations over the seabed with 13 cm average length and, about 1 m maximum length and the diameter varies between 2.3

and 18 cm. Although most of these chimneys lie horizontally on the sea floor, about 220 chimneys have been found protruding from muddy sediments in vertical position. The higher chimneys concentrations are located in the Cornide High. The fallen chimneys present a regular spatial distribution in a NW-SE direction. The basal morphology of them shows common characteristics of an angular breakage associated with flexo-traction processes, typical of slender structures. This character is very significant because it prove that the chimneys were broken at their base. This interpretation is contrasts with the idea of some authors that propose the drop of the chimneys due to topple by remobilization the sediments inside of the chimneys with subsequent collapse (Díaz-del-Río et al., 2003; Fernandez-Puga, 2004). Moreover, the preferential orientation of the fallen pieces points to coseismic shake as the mechanisms driving the chimneys rupture. During an earthquake chimneys may break, more specifically by the vertical and horizontal acceleration of the ground during the passage of seismic waves. The horizontal component of the acceleration may be responsible for part of the horizontal displacement. The direction of the oscillation is parallel to the direction of propagation of the seismic wave and produces strong extensional stress at the bases of the chimneys. As a result, the chimneys bend and fracture it along a horizontal plane near its base and finally topple it.

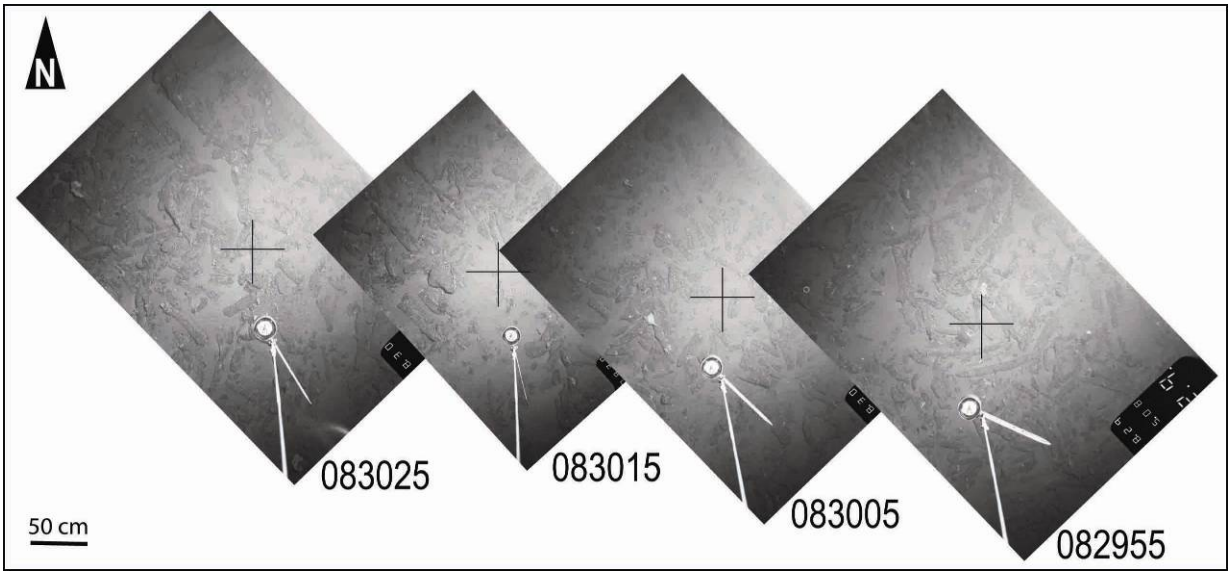

Fig. 2: Bottom photographs of the carbonate chimneys taken a BENTHOS underwater camera along the crest of the Cornide High (T5), at depths between 950 and 970 m. See Fig. 1B for location.

This work proposes the magnitude and location of the fault that generated the earthquake that caused the rupture of the carbonate chimneys located on the Guadalquivir Diapiric Ridge and the Cadiz Contourite Channel after they had been exhumed at the seafloor.

GEOLOGICAL SETTING

The Gulf of Cadiz is located in the southwestern part of the Iberian Plate. This region straddles the E-W trending segment of the Eurasian-Africa plate boundary that extends from Azores to the Mediterranean Sea, between the Gloria Fault and the western end of the Alpine Mediterranean belt, the Gibraltar Arc. The diffuse nature of this segment of the plate boundary is widely accepted on the basis of the related seismicity that is characterized by scattered shallow- and intermediate-type earthquakes (Buforn et al., 1995). Earthquake fault plane solutions support the existence of a wide transpression zone ascribed to the slow (2-4 mm/year) oblique NW-SE convergence that initiated in the late Miocene. The plate convergence is responsible for the reactivation of the older rift faults, and a number of large, active, tectonic structures have been detected along the continental margin and within the oceanic domain (Zitellini et al., 2001). The main faults that accommodate the NW-SE shortening in the Gulf of Cadiz are the Horseshoe Fault, the Marquês de Pombal Fault, the Tagus Abyssal Plain Fault and the Pereira de Sousa Fault on the western margin (Zitellini et al., 1999; Terrinha et al., 2003; Gràcia et al., 2003b; Zitellini et al., 2004; Cunha, 2006), and the Guadalquivir Bank Fault on the southern margin (Gràcia et al., 2003a). Since historical times a number of destructive earthquakes/tsunamis has been reported to have occurred in SW Iberia like the tsunami of 60-63 B.C. (Campos, 1991), which devastated the city of Cadiz, and 1531 and 1722 events that struck the coast of SW Portugal. This area was also the source of the famous 1755 Lisbon Earthquake, the most terrifying cataclysm to have occurred since historical times in Western Europe with an estimated earthquake magnitude of 8.5-8.7 (Martins and Mendes, 1990). The largest recent earthquakes were in the Gorringe Bank (28 February 1969, Ms 7.9) and in the northern Gulf of Cadiz (15 March 1964, Ms 6.2).

MECHANICAL PROPERTIES OF CHIMNEYS

Several dredge hauls were also taken during the 2000 and 2001 Coornide de Saavedra cruises, mainly across the Guadalquivir Diapiric Ridge and the Cadiz Contourite Channel. Chimneys obtained from these sources have been used to determinate mechanical properties of the carbonate chimneys. Various laboratory tests have been performed on the carbonate chimneys taken in the Gulf of Cadiz in order to determine their mechanical

properties. The mean value of specific mass (□□ of the chimneys is 2309.66 Kg/m^3. The Young's modulus (E) average is about 23.5 GPa obtained on basis of S and P waves velocities. The variation around these values is 4.6 GPa. The resistance in simple compression is between 29 and 88 MPa, while the tensile resistance evaluated by static bending tests on three samples is ranging between 3 and 6.1 MPa. The mean value and the standard deviation of these failure stresses are 4.6 and 1.55 MPa, respectively, with a minimum value of 3 MPa.

HOW BIG WAS THIS EARTHQUAKE?

The chimneys are located preferentially on top of topographic relieves and are founded on a thick layer of very soft mud. Both conditions are particularly prone to ground motion amplification. Topographic amplification effects are well known to happen on top of ridges and on steep slopes, which are the conditions for most of the chimneys' fields. Many building seismic codes account for the topographic effect; for instance, Eurocode-8 evaluates this effect as a factor of 1.2 to 1.4. In addition, amplification due to soft soil conditions is also a very well known effect. Clay or silt thick deposits with high water content are particularly significant for this effect and, in fact, these are the soil conditions of the chimneys' fields. Mean shear velocity for the first 30 m (Vs_{30}) is used in seismic codes to evaluate the soil amplification factor. In our case, we estimate a Vs_{30} of 140 m/s from mean P-wave velocity (Vp) measured in a 25 m depth well drilled in the vicinity of the chimneys' fields and using the correlation of Castagna et al. (1985). For this kind of soils with such a low Vs_{30}, seismic code provisions account for the highest amplification factors, which are of the order of 2.0 to 2.5 (e.g. Eurocode-8, NEHRP). Furthermore, considering that the maximum thickness of the soft layer varies between 70 and 110 m, its natural resonance period can be estimated in between 2 and 3 seconds, approximately (cf. Kramer, 1996).

The chimneys can be regarded as very rigid objects. They are in general much shorter than 2 meters and narrower than 20 cm. The most frequent Height/Diameter ratio (H/D) is 4 and the modal chimney can be regarded as 30 cm tall and 8 cm wide. Assuming them as cantilever beams their natural period of vibration can be estimated as low as 0.003 to 0.050 seconds (Cadorin et al., 2000). Such a low vibration period means that the chimneys were particularly sensitive to the higher frequencies of the seismic ground motion. For this range of frequencies a very convenient parameter to evaluate the amplitude of strong ground motion is the horizontal peak ground acceleration (PGA) (i.e, the largest horizontal acceleration value recorded by an accelerometer). Hence, comparing the minimum acceleration needed to break down the chimneys to PGA drawn from ground motion prediction equations (GMPEs) can be used as a first order approximation to the most likely seismic scenario (i.e. an earthquake defined by a certain magnitude and distance).

The minimum acceleration needed to break the chimneys has been calculated simplifying the seismic ground motion as a harmonic wave. Although this is a simplification, it is very convenient to represent the moment when PGA was reached during the shaking. The acceleration values obtained exhibit a wide dispersion (0.21-0.69 g), depending strongly on H/D parameter. Considering H/D ratios of 4, which represent the modal chimney, minimum breaking acceleration values range from 0.43 to 0.51 g. We shall focus on the upper limit of this range to compare with PGA drawn from GMPEs.

WHERE WAS THE EARTHQUAKE GENERATED?: LOCATION THE CAUSATIVE FAULT

Even though there are many ground motion prediction equations (GMPE) derived from the most important seismic regions of the world (cf. Douglas, 2003), there is no one specifically performed for the south Iberian Atlantic margin. We have then selected a few from the specialized literature (Boore et al.,1997; Ambraseys and Douglas, 2003; and Ambraseys et al., 2005), which share the following characteristics: they are derive from extensive databases that comprise large regions of the world; measure the same horizontal component of acceleration; account for shallow crustal earthquakes (h<30 km); they are statistically significant for large magnitude earthquakes (M=7.6-7.8) and for short distances (R<15 km); use the Mw or Ms scale; and, use the same distance metric, the so-called Joyner and Boore distance (R_{jb}) (i.e. the shortest distance to the surface projection of the rupture plane).

The GMPEs have been used iteratively to find out the best correspondence of their average PGA prediction with the upper limit of the minimum acceleration for breaking the chimneys. We have particularly looked at two different scenarios: (A) an earthquake produced by a fault located right under the chimneys field (R_{jb}=0 km); and, (B) an earthquake located as far as possible from the chimneys field. For Scenario (A) we deduce a minimum Mw 7.2, while for Scenario (B) we deduced a R_{jb} distance of 6 km for a Mw=7.8 earthquake, that is the maximum magnitude that the GMPEs can account for –nevertheless, extrapolation to Mw=8.0 provides a similar value of 7 km. Taking into account the dimensions of the rupture area that such large earthquakes produce, Scenario (B) implies that the surface trace of the causative fault could be located at a horizontal distance varying from 35 to 60 km, considering a 60º or 30º fault dip, respectively. It is important to notice the huge uncertainties associated to these estimations. For instance, if we considered the median PGA+1 s.d., magnitudes could be as low as 5.4 and 6.4, respectively for scenarios A and B. However, neither a Mw 5.2 R_{jb}=0 km or a Mw=6.4 R_{jb}=6 km earthquakes could explain the widespread distribution of broken chimneys along tenths of kilometres-provided all the chimneys were tumbled during the same event).

Finally, another possible scenario could be devised if invoking the occurrence of a very large magnitude earthquake (Mw>8.0) at a very long distance (D>300 km). As in the 1985 Mexico City earthquake, the predominant vibration period of such an earthquake would be closer to the natural period of the soft layer where the chimneys are founded, so facilitating the occurrence of a resonance effect.

CONCLUSIONS

Analysis of the 1798 photographs recollected on the Guadalquivir Diapiric Ridge and the Cadiz Contornite Channel in the Gulf of Cadiz has allowed to identify 5861 chimneys lying scattered in dense concentrations over the seabed. The fallen chimneys present a regular spatial distribution in a NW-SE direction. The basal morphology of them shows common characteristics of an angular breakage associated with flexo-traction processes. These characters are very significant because they are a strong indication for the seismic origin of chimneys rupture.

On the basis of the geological characteristics of the area and the mechanical properties of the carbonate chimneys it has been determined from ground motion prediction equations a first order approximation to the most likely seismic scenario. We have particularly looked at two different scenarios: (A) an earthquake produced by a fault located right under the chimneys field (R_{jb}=0 km) with a minimum Mw 7.2; and, (B) an earthquake located about 6 km far from the chimneys field with a Mw=7.8 earthquake. Probably this fault was the Guadalquivir Bank Fault, that present a NE-SW trend and it is very close of the study area.

Acknowledgements: We thank all those who participated in the research cruises of the TASYO project, especially the Main Researches of TASYO project, Luis Somoza (Instituto Geológico y Minero de España, IGME) and Victor Díaz-del-Río (Instituto Español de Oceanografía, IEO) and the captains and crews of the research vessel R/V Cornide de Saavedra. This research was funded by the Spanish Marine Science and Technology Program, under the CONTOURIBER Project CTM2008-06399-C04-01/MAR. It is also a contribution to the project CONSOLIDER-INGENIO 2010 CSD2006-0041-TOPOIBERIA.

References

Ambraseys, N.N., Douglas, J. (2003). Near-field horizontal and vertical earthquake ground motions. Soil Dynamics and Earthquake Engineering, 23, 1-18.

Ambraseys, N.N., Douglas, J., Sarma, S.K., Smith, P.M. (2005). Equations for the estimation of ground motion from shallow crustal earthquakes using data from Europe and the Middle East: Horizontal peak ground acceleration and spectral acceleration. Bulletin of Earthquake Engineering, 37, 1-53.

Boore, D.M., Joyner, W.B., Fumal, T.E. (1997). Equation for estimating horizontal response spectra and peak acceleration from Western North American Earthquakes: a summary of recent work. Seismological Research Letters, 68, 128-153.

Buforn, E., Sanz de Galdeano, C., Udías, A. (1995). Seismotectonics of the Ibero-Maghrebian region. Tectonophysics, 248, 247-261.

Cadorin, J.F., Jongmans, D., Plumier, A., Camelbeeck, T., Quinif, Y. (2000). Modelling of speleothem rupture. Proceedings of the Conference HAN 2000-Potential for large earthquakes in low seismic activity regions of Europe. Han-sur-Lesse, Belgium, 27-30.

Campos, M.L. (1991). Tsunami hazard on the Spanish coasts of the Iberian Peninsula. Science of Tsunami Hazards, 9 (1), 83-90.

Castagna, J. P., Batzle, M. L. y Eastwood, R. L. (1985). Relationship between compressional wave and shear wave velocities in clastic silicate rocks. Geophysics, (50), 571-581.

Cunha, T. (2006). Gravity anomalies over the SW Protuguese Margin and their tectonic implications. 5º Simposio sobre a Margem Ibérica Atlântica, Aveiro.

Díaz-del-Río, V., Somoza, L., Martínez-Frias, J., Mata, M.P., Delgado, A., Hernández-Molina, F.J., Lunar, R., Martín-Rubí, J.A., Maestro, A., Fernández-Puga, M.C., León, R., Llave, E., Medialdea, T., Vázquez, J.T. (2003). Vast fields of hydrocarbon-derived carbonate chimneys related to the accretionary wedge/olistostrome of the Gulf of Cádiz. Sedimentary Processes and Seafloor Hydrocarbon Emission on Deep European Continental Margins. Marine Geology, 195 (1-4), 177-200.

Douglas, J. (2003). Earthquake ground motion estimation using strong-motion records: A review of equations for the estimation of peak ground acceleration and response spectral ordinates. Earth-Science Reviews, 61(1–2), 43–104.

Fernández-Puga, M.C. (2004). Diapirismo y estructuras de expulsión de gases hidrocarburos en el talud continental del Golfo de Cádiz. Tesis de Licenciatura, Facultad de Ciencias del Mar, Universidad de Cádiz.

Gràcia, E., Dañobeitia, J., Vergés, J., Bartolomé, R. (2003a). Crustal architecture and tectonic evolution of the Gulf of Cadiz (SW Iberian margin) at the convergence of the Eurasian and African plates. Tectonics, 22(4).

Gràcia, E., Dañobeitia, J., Vergés, J., Córdoba, D., PARSIFAL Team (2003b). Mapping active faults offshore Portugal (36ºN-38ºN): implications seismic hazard assessment along the southwest Iberian margin. Geology, 31(1), 83-86.

Hernández-Molina, F.J., Llave, E., Stow, D.A.V., García, M., Somoza, L., Vázquez, J.T., Lobo, F.J., Maestro, A., Díaz del Río, V., León, R., Medialdea, T., Gardner, J. (2006). The contourite depositional system of the Gulf of Cádiz: A sedimentary model related to the bottom current activity of the Mediterranean outflow water and its interaction with the continental margin. Deep-Sea Research II, 53, 1420-1463.

Kramer, S.L. (1996). Geotechnical Earthquake Engineering. Prentice-Hall, 653 p.

Martins, I., Mendes, V.L.A. (1990). Contribuçao para o estudo da sismicidade de Portugal comtinental. Universidade de Lisboa, Instituto Geofísico do Infante D. Luís, publicaçao nº 18, 70 p.

Smith, W.H.F., Sandwell, D.T. (1997). Global sea floor topography from satellite altimetry and ship depth soundings. Science, 277 (5334), 1956-1962.

Terrinha, P., Pinheiro, L.M., Henriet, J.P., Matias, L., Ivanov, M.K., Monteiro, J.H., Akhmetzhanov, A., Volkonskaya, A., Cunha, T., Shaskin, P., Rovere, M. (2003). Tsunamigenic-seismogenic structures, neotectonics, sedimentary processes and slope instability on the southwest Portuguese Margin. Marine Geology, 195(1-4), 55-73.

Zitellini, N., Chierici, F., Sartori, R., Torelli, L. (1999). The tectonic source of the 1755 Lisbon earthquake and tsunami. Annali di Geofisica, 42,(1).

Zitellini, N., Mendes, L.A., Córdoba, D., Dañobeitia, J., Nicolich, R., Pellis, G., Ribeiro, A., Sartori, R., Torelli, L., Bartolomé, R., Bortoluzzi, G., Calafato, A., Carrilho, F., Casoni, L., Chierici, F., Corela, C., Correggiari, A., Della Vedova, B., Gràcia, E., Jornet, P., Landuzzi, M., Ligi, M., Magagnoli, A., Marozzi, G., Matias, L., Penitenti, D., Rodríguez, P., Rovere, M., Terrinha, L., Vigliotti, L., Zahinos-Ruiz, A. (2001). Source of the 1755 Lisbon earthquake and tsunami investigated. Eos Trans. AGU, 82 (26), 285-291.

Zitellini, N., Rovere, M., Terrinha, P., Chierici, F., Matias, L., BIGSETS Team (2004). Neogene Through Quaternary Tectonic Reactivation of SW Iberian Passive Margin. Pure and Applied Geophysics, 161, 565-587.

Zitellini, N., Gràcia, E., Matias, L., Terrinha, P., Abreu, M.A., DeAlteriis, G., Henriet, J.P., Dañobeitia, J.J., Masson, D.G., Mulder, T., Ramella, R., Somoza, L., Díez, S. (2009). The quest for the Africa–Eurasia plate boundary west of the Strait of Gibraltar. Earth and Planetary Science Letters, 280, 13-50.

EARTHQUAKE GROUND EFFECTS DURING MODERATE EVENTS: THE L'AQUILA 2009 EVENT CASE HISTORY

A.M. Michetti (1), E. Vittori (2), A. Berlusconi (1), A.M. Blumetti (2), V. Comerci (2), P. Di Manna (2), E. Esposito (3), L. Guerrieri (2), F. Livio (1), S. Porfido (3) and G. Sileo (1)

(1) Department of Chemical and Environmental Sciences, University of Insubria, Via Valleggio, 11, 22100, Como, ITALY. alessandro.Michetti@uninsubria.it; giancanio.sileo@uninsubria.it; franz.livio@uninsubria.it
(2) Geological Survey of Italy, ISPRA, Via Brancati 48, 00144 Roma, ITALY. eutizio.vittori@isprambiente.it ; luca.guerrieri@isprambiente.it; annamaria.blumetti@isprambiente.it; valerio.comerci@isprambiente.it ; pio.dimanna@isprambiente.it
(3) Institute for coastal marine environment, National Research Council of Italy, Calata Porta di Massa - 80133 Napoli, ITALY. sabina.porfido@iamc.cnr.it

Abstract: *On April 6th, 2009, a M_w 6.3 earthquake rocked the town of L'Aquila (Central Italy) and surroundings, inducing a noteworthy number of effects on the environment. Earthquakes with M_w between 6 and 6.5 are of relevant interest in the Mediterranean Region because of their frequency and their consequences in this densely populated area. The L'Aquila event is representative of the geological effects to be expected: ca. 200 effects on the environment have been recognized, allowing us to estimate an epicentral Intensity IX, by applying the ESI 2007 scale. The post seismic evolution of some ground fractures is under monitoring, in particular along the reactivated Paganica fault.*

Key words*: Earthquake Environmental Effects, moderate earthquakes, seismic hazard*

INTRODUCTION

The growing threat posed by geological effects of earthquakes to ever-expanding human settlements and infrastructures has been made more and more evident by the large events that have rocked various regions of the earth in the last years (Turkey 1999, Taiwan 1999, Indonesia 2004, Kashmir 2005, Sichuan 2008). Concern is therefore eventually growing for those urban areas where a rapid economic growth has often lead to neglect even in the recent past the historical and paleoseismic evidence. However, far from negligible hazard can be also posed by environmental effects following moderate earthquakes, as proven by several examples, among which the April 6, 2009, Mw 6.3 L'Aquila event is the most recent one. Moderate events in the range of Mw 6.0 to 6.5 are of special importance in the Mediterranean Region, since A) they are relatively frequent in most of the Mediterranean countries and B) the damage expected from similar events is relatively large, due to the local historical and cultural setting, and increasing vulnerability of the anthropic environment. The relevant geological effects and strong societal impact from moderate seismic events has been also recently illustrated by the July 16, 2007, Mw 6.6, Kashiwazaki – Kariwa earthquake in Japan, that damaged the largest Nuclear Power Plant site in the world. The 2009 L'Aquila earthquake is used here to illustrate the type and size of geological effects to be expected, strongly dependent on local geology and morphology, and their impact on human structures.

SEISMICITY DATA ON THE APRIL 6 2009 L'AQUILA EARTHQUAKE

After several months of anomalous seismic activity in the Abruzzo region of Central Italy, on April 6th, 2009, at 01:32 GMT the Central Apennines were rocked by a moderate-size earthquake (Ml 5.9, Mw 6.2, depth around 9 km). The epicentre was located near the historical town of L'Aquila (Fig. 1), which was severely damaged together with many villages in the surroundings. The death toll was of 307 casualties. Two M > 5 shocks followed on April 7th (Ml=5.3; epicentre about 10 km SE of L'Aquila) and on April 9th (Ml = 5.1; epicentre near Campotosto, about 15 km NW of L'Aquila). The seismic sequence, still far from its end in July 2009, being M > 4 events still present (Fig. 1), has affected to date an about 40 km long zone, elongated in the NW-SE direction. The focal mechanisms clearly define a NW-SE trending normal faulting mechanism, in good agreement with the tectonic setting of the region (Fig. 2), characterized by a "Basin and Range" landscape due to a segmented belt of capable normal faults (e.g., Blumetti and Guerrieri, 2007).

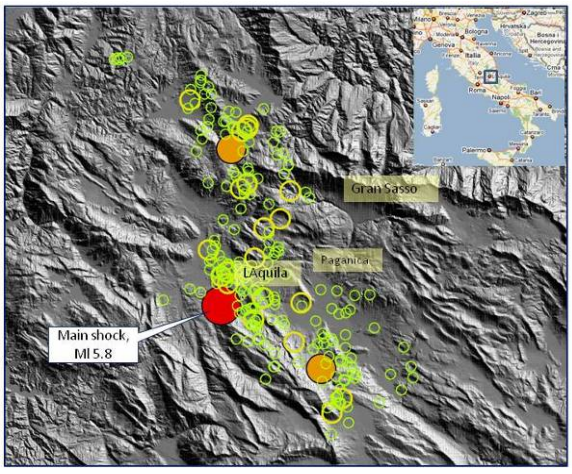

Fig. 1: The Basin and Range morphology of the epicentarl region and the 2009 seismic sequence: orange circles: main aftershocks = Ml>5, yellow circles = Ml>4, green circles = Ml>3. The Quaternary intermountain basins, among which that of L'Aquila (Middle Aterno Valley), and fault-generated mountain fronts, including the highest peak of the Apennines (Gran Sasso, 2912 m), are quite evident

The scenario of damages to buildings compiled by the QUick Earthquake Survey Team (QUEST, Galli and Camassi, 2009) shows a maximum intensity of X MCS occurred in single localities within areas characterized by a lower level of damages (Is ≤ VIII MCS). These peaks of intensity appear to have been caused by a peculiar seismic vulnerability, associated in some cases to evident site effects (e.g., Onna and other villages in the Middle Aterno Valley located on soft alluvial and lake sediments).
The same region experienced several strong earthquakes in historical times (1349, 1461, 1703, 1762, with intensities ranging from IX to X MCS and estimated magnitudes in the order of 7). For the 1703 seismic sequence, contemporary written accounts (e.g., Uria de Llanos, 1703) describe important geological effects, evidence of a much larger magnitude (M7) compared to the April 6, 2009 event.

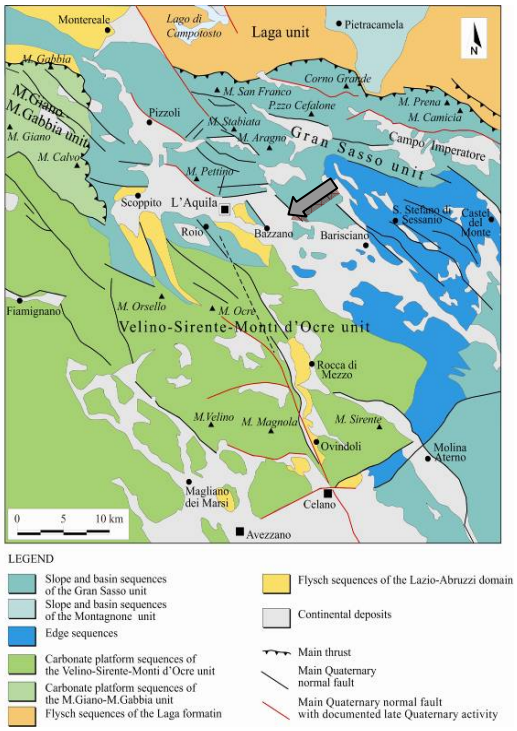

Fig. 2: Structural sketch of the L'Aquila region (from Blumetti et al., 2002). The yellow arrow shows the Paganica fault)

THE GEOLOGICAL EFFECTS

In the period April 6– May 7, 2009, a total amount of 184 effects were mapped over an area of at least 1000 km^2. Their location is reported in Fig. 3.

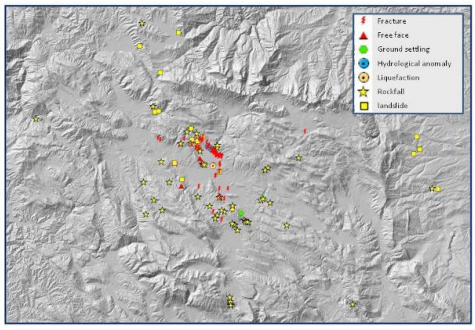

Fig. 3: Map of the geological effects accompanying the April 6, 2009, shock

Primary effects
Evidence of surface faulting was only seen along the Paganica fault, while subdued tectonic effects were seen along other known faults in the epicentral area (Fig. 4).

Ground ruptures along the Paganica fault
A set of discontinuous but well aligned ground ruptures was found in correspondence of the Paganica fault (yellow arrow in Fig. 2). These ruptures, trending between N120 and N140, could be traced for a length of at least 2.6 km, reaching in some sites vertical offsets of 7-8 cm (Fig. 5). They could be easily observed on paved/concrete and often dirt roads and on other artificial surfaces, as well as on buildings and hard fences. Particularly evident was the pipeline rupture of the Gran Sasso aqueduct (Fig. 6). The same set of fractures was locally well evident also on natural/farmed soil.

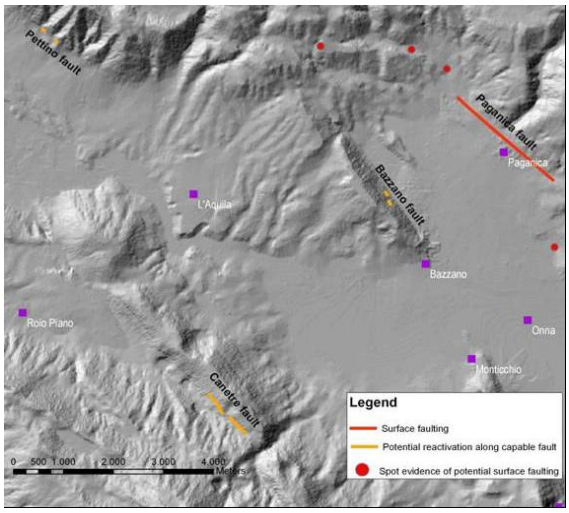

Fig. 4: Fault reactivation at Paganica and evidence of potential reactivation along other faults

These ruptures are a clear evidence of coseismic surface faulting. This interpretation is in good agreement with the seismological data (distribution of aftershocks, focal mechanisms) and with the coseismic field of deformations resulting by the comparison of pre- and post- event SAR images.

Fig. 5: The Paganica ruptures were traced in the ground, across buildings and concrete roads, more or less continuously, for at least 2.6 km with offsets up to 7-8 cm, which locally continued to increase in the following weeks

The coseismic reactivation of the Paganica fault caused the rupture of the Gran Sasso aqueduct. The very high pressure of the water flowing from the damaged pipeline

excavated a deep trench, thus providing extraordinary exposures of faulted sediments and unquivocal evidence of previous, larger, coseismic surface faulting events.

Fig. 6: The site where the aqueduct was broken by coseismic faulting

It is important to underline a remarkable post-seismic evolution of these ruptures, in terms of progressive increasing of offsets, lengths and widths. Eye-witnesses have reported the occurrence of new fractures also some days after the main shock. Several research teams have started to monitor these fractures, documenting post-seismic creep of at least several millimetres.

Some other evidence (discontinuous but aligned ground cracks) could be interpreted as the possible NW extension of the Paganica ruptures. Furthermore, coseismic fractures opened in cultivated fields N of Onna and, with a length of some hundred metres and direction N140-N160. If we include these evidence in the rupture zone of the seismogenic fault, the length of the surface rupture may reach about 6 km.

Surface effects along other active faults
Specific surveys were conducted along all the active faults known in the area (Fig. 4). Along the Pettino fault only local ground ruptures, some tens of meters in length with offsets up to 10 cm were found, without evidence of actual surface faulting.

Along the Bazzano fault, which is a N310 trending normal fault antithetic to the Paganica fault, we observed a discontinuous free face with offsets locally up to 5-6 cm, marked also by the distribution of moss. This evidence might be interpreted as a centimetric coseismic surface reactivation of the Bazzano fault together with a significant debris compaction, as shown by the irregular distribution of offsets.

Another free face was found along the N125 trending Canetre fault not far from Roio. A constant offset of about 1 cm was seen for at least 1 km. This effect was evident not only along debris-rock contacts but also along rock to rock contacts.

Secondary effects
Secondary effects (basically gravitational movements and fractures) induced by the ground shaking had a widespread distribution.

Gravity movements
Numerous rock falls (78% of gravitational movements, Fig. 7) occurred especially from calcareous slopes. Among them, one of the most impressive falls took place above the village of Fossa, which was directly damaged by huge boulders (Fig. 8). Residual risk of rock falls caused the temporary closure of some important roads.

Other important rock falls were seen within the Gran Sasso mountain range (rock avalanches), along the NE slope of Mt. Bazzano and on the north-facing cliffs of Stiffe (several cubic meters in size).

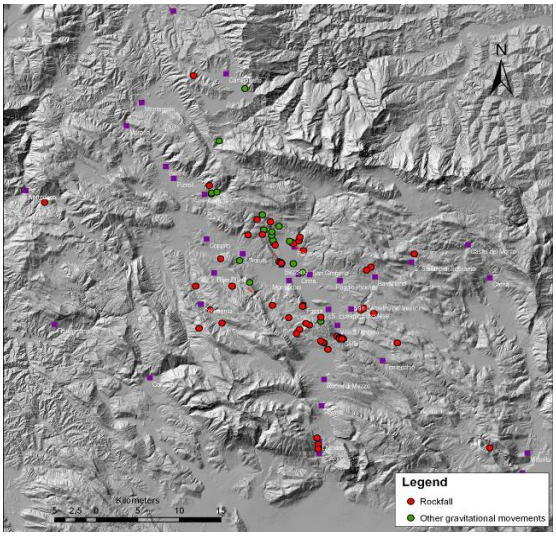

Fig. 7: Distribution of slope movements by type

Other types of slope movements, generally affecting artificial fills, occurred along several roads, including the highway A24. Around the Lake Sinizzo, near San Demetrio ne' Vestini, impressive ground failures along the whole shoreline were observed (Fig. 9). In the other sinkholes of the area (generally empty of water) no remarkable effects were found.

Fig. 8: Fossa rockfall: huge boulders on a paved road

Fractures
Besides the fractures previously described as primary effects, many fractures were induced by shaking in the bare ground as well as in paved roads and in artificial works. Two bridges on the Aterno River (near Onna, and near Fossa) were severely damaged by the failures of the supporting embankments. Also some of these fractures showed a significant temporal evolution (widening).

Liquefaction
The only remarkable liquefaction feature was found by the geologists of the Abruzzo River Basin Authority at Vittorito (near Sulmona), hence relatively far from the epicenter (Fig. 10).

Fig. 9: Ground failures along the shore of Lake Sinizzo

Hydrological anomalies

At Tempera (W of Paganica) the springs of Capo Vera experienced temporary effects of turbidity, and significant changes of water discharge. Some springs disappeared or shifted for some hundreds of meters. A shallow well ran dry.

Fig. 10: Mud/sand volcano near Vittorito (courtesy by G. Pipponzi, AdB Abruzzo)

CONCLUSIONS

The L'Aquila earthquake generated a widespread set of geological effects on the natural environment.
Clear evidence of surface faulting was found along the Paganica fault, which is regarded as the causative structure of this earthquake. The maximum surface displacement was ca. 7-8 cm.

It is noteworthy that the Paganica fault was already mapped in the Sheet L'Aquila of the CARG project, the official geological map of the Italian territory (scale 1:50,000) printed by the ISPRA Italian Geological Survey; and also recorded in the ITHACA database, the inventory of Italian capable faults, implemented by the ISPRA Italian Geological Survey on the basis of available paleoseismological and seismotectonic studies. Nevertheless, it was considered a secondary element when compared to several nearby more prominent capable faults. The same fault also exhibits evidence of larger surface faulting events in the past. This pinpoints the need to pay the due attention also to "minor" structures and also leaves open the question about the real seismic potential of the area.

Other potential reactivations along mapped capable faults (Pettino, Campo Imperatore, Bazzano and Roio faults) were observed, but they can hardly represent the surface expression of seismogenic faulting. Anyway, they could still represent tectonic ruptures along sympathetic and/or antithetic faults.

Secondary effects were mapped over an area of ca. 1000 km^2, mostly gravity movements and ground fissures. Regarding slope movements, rock falls in calcareous slopes and artificial cuts were the most common type of effect. Sliding phenomena also occurred, threatening in some cases the road infrastructures. Numerous ground cracks, especially in loose unconsolidated sediments, and fractures in paved roads were surveyed, mostly induced by shaking.

The scenario of environmental effects includes also some minor liquefactions, hydrological anomalies and some local peculiar effects (e.g., the ground failures along the shores of the Lake Sinizzo). The general picture of geological environmental effects is typical for earthquakes of magnitude around 6. Preliminary assessments with the ESI 2007 scale indicate that the epicentral intensity was equal to IX. This provides an objective calibration, in terms of scenario of geological effects, for a better intensity assessment of historical earthquakes occurred in the same area (e.g., the 1703 earthquake sequence). The post seismic evolution of these effects, especially the ruptures along the Paganica fault, is still going on. A significant increase in offsets and width of some fractures was noted in the weeks after the mainshock. A monitoring is being carried out with high precision instruments (e.g. LIDAR) in order to understand the phenomenon in the frame of a collaboration among several academic and research institutes, which includes the ISPRA Italian Geological Survey, the University of Insubria, the National Research Council of Italy, the Geological Survey of Trento Province, the Birkbeck/UCL – University College of London, the University of Durham and the Geological Survey of Israel.

Acknowledgements: AMM, AB, FL and GS have been funded by the L'Aquila eq. Special Grant from University of Insubria.

References

Blumetti A.M**.,** GuerrieriI L. (2007) - Fault-generated mountain fronts and the identification of fault segments: implications for seismic hazard assessment. Boll. Soc. Geol. It. (Ital.J.Geosci.), Vol. 126, No. 2 ,. 307-322.

Blumetti A.M., Di Filippo M. Zaffiro P., Marsan P. & Toro B. (2002) - Seismic hazard characterization of the city of L'Aquila (Abruzzo, Central Italy): new data from geological, morphotectonic and gravity prospecting analyses. Studi Geologici Camerti, Volume Speciale, Int. Workshop Camerino-Rome, 21-26 Giugno 1999, 7-18.

Galli P., Camassi R. (2009) - Rapporto sugli effetti del terremoto aquilano del 6 aprile 2009. RPT03 – 20.04.2009. QUEST - INGV

Michetti A.M., Esposito E., Guerrieri L., Porfido S., Serva L., Tatevossian R., Vittori E., Audemard F., Azuma T., Clague J., Comerci V., Gurpinar A., Mc Calpin J., Mohammadioun B., Morner N.A., Ota Y. & Roghozin E. (2007) - Intensity Scale ESI 2007. In. Guerrieri L. & Vittori E. (Eds.): *Memorie Descrittive Carta Geologica. d'Italia.,* vol. 74, Servizio Geologico d'Italia – Dipartimento Difesa del Suolo, APAT, Roma, 53 pp.

Servizio Geologico d'Italia (2006) - Cartografia geologica ufficiale Foglio CARG 1:50,000 N. 359, L'Aquila.

Uria de Llanos A. (1703) - Relazione o vero itinerario fatto dall'auditore Alfonso Uria de Llanos per riconoscere li danni causati dalli passati terremoti seguiti li 14 Gennaro e 2 Febbraro MDCCIII. Stamperia Gaetano Zenobi, Roma.

PALEOSEISMOLOGY ALONG THE CARBONERAS FAULT: INTEGRATED ONSHORE-OFFSHORE EVIDENCE OF SEISMOGENIC ACTIVITY

X. Moreno (1,2), E. Gràcia (1), E. Masana (2), Á. Rodés (2), R. Bartolomé (1) and R. Pallàs (2)

(1) Unitat de Tecnologia Marina-CSIC, Centre Mediterrani d'Investigacions Marines i Ambientals. 08003-Barcelona, SPAIN.
(2) Dept. de Geodinàmica i Geofísica, Facultat de Geologia, Universitat de Barcelona. 08028-Barcelona, SPAIN. Email: xmoreno@cmima.csic.es

Abstract: *The aim of this integrated onshore-offshore study is to establish the seismic potential of the Carboneras Fault (CF) (Eastern Betics). Onshore, the paleoseismological study was performed along La Serrata segment through geomorphological, microtopographic, trenching and dating analysis. Offshore, the study was carried out based on high-resolution geophysical data, coring and dating analysis. Seismic profiles show a large variability of transpressive structures along the fault zone coinciding with onshore structures. Both, onshore and offshore studies show faulted Quaternary layers and mass movement deposits related to paleoearthquakes suggesting that CF is seismogenic. Analysis of trench walls show evidence of a minimum of six events since the Mid Pleistocene, a mean recurrence period of 20 ka and constrain the time of the last earthquake between 772 AD and 889 AD.*

Key words*: Eastern Betics, Alboran Sea, active tectonics, slow faults*

INTRODUCTION

Major cities from southeastern Iberian Peninsula were historically damaged and destroyed by catastrophic earthquakes, i.e. Almería 1487 (VIII), 1522 (IX), 1659 (VIII), 1804 (VIII) (Bousquet, 1979; Benito et al., 2006). But the accuracy of historical epicenters location is too low to establish a precise relationship between individual faults and earthquakes.

Despite historical events, the seismogenic behaviour of southern Iberian Peninsula faults, with shallow (2 to 4 km) (Stich et al., 2006) low-to-moderate magnitude instrumental seismicity, is poorly understood (e.g. Masana et al., 2005), leading to an underestimation of the seismic hazard. Furthermore, the continuation of faults offshore and the marine seismogenic sources are poorly known. The Carboneras Fault, a large fault zone with neat morphologic expression, is a good opportunity to study the response of Quaternary marine and terrestrial deposits to the recent tectonic activity in south Spain.

SEISMOTECTONIC AND GEOMORPHOLOGIC SETTING OF THE REGION

SE Spain hosts the slow convergent plate boundary between Africa and Iberia (4-5 mm/yr) which is characterized by a 400 km wide zone of diffuse seismicity (Argus et al., 1989; DeMets et al., 1990). In the Eastern Betics, shortening is accommodated by a left-lateral strike-slip fault system referred to as the Eastern Betics Shear Zone (EBSZ) (Bousquet, 1979; Sanz-De-Galdeano, 1990). The EBSZ fault system extends southwards in the Alboran Sea, changing its name to Trans-Alboran Shear Zone and connecting with the north-African NE-SW faults (De Larouzière et al., 1988)

The Carboneras Fault with a length of almost 50 km onshore and more than 100 km offshore is one of the longest structures of the EBSZ (Gràcia et al., 2006). Despite scarce seismicity associated to this fault, its geomorphology reveals recent activity, suggesting long recurrence (10^4 years) behavior as found in other faults along the EBSZ (Masana et al., 2004).

OBJECTIVE AND METHODS

We present results of an integrated onshore-offshore paleoseismic study which aims to establish the seismic potential of the Carboneras Fault.

Onshore, after identifying La Serrata as the segment of the Carboneras Fault with stronger evidence of Quaternary tectonic activity by geomorphological and microtopographic analyses, a detailed paleoseismological study was carried out in 5 sites (17 trenches) along the NW boudanry of the range. Materials involved in the deformation have been dated with different methods (U/Th, TL, ^{14}C and ^{10}Be) depending on the nature and age estimation of the sediments.

The IMPULS marine geophysical survey (RV Hespérides) was carried out with the aim to characterize the geometry and deep structure of the fault offshore based on swath-bathymetry, high-resolution multichannel seismics and very-high-resolution sub-bottom profiler TOPAS. In addition, marine sediment cores were acquired during IMPULS and CARBMED cruises (M69/1, RV Meteor) to sample and date (^{14}C) characteristic reflectors observed in the TOPAS profiles.

This study attempts to assign the first paleoseismological parameters (geometry of the fault, slip-rates, recurrence periods, elapsed time since the last earthquake and maximum magnitude) of the Carboneras Fault and

approach the long term (Quaternary) behavior of this active structure.

RESULTS AND DISCUSSION

Onshore Carboneras Fault

La Serrata is a linear range bounded by faults, which front shows geomorphological evidence of Quaternary tectonic activity: deflected drainage, beheaded alluvial fans, alluvial fans without a source area and faulted and folded Quaternary deposits. Slip rate estimates were obtained by dating the sediments involved in deformation. At El Puntal site, a remarkable outcrop shows a pierced segment of well stratified Early Pleistocene sediments uplifted a minimum of 50 metres with respect to the same sediments outcroping in nearby channel bottoms (Fig. 1). Assuming a minimum age for the Early Pleistocene alluvial unit of 870 ka BP (upper limit of the Early Pleistocene) and a maximum age of 2358 ka BP according to ERS results for related travertine, (Wenzens 1992), we estimate a minimum dip-slip rate between 0.02 and 0.06 mm/a. Further ^{10}Be results will better constrain the age of the Early Pleistocene alluvial fan.

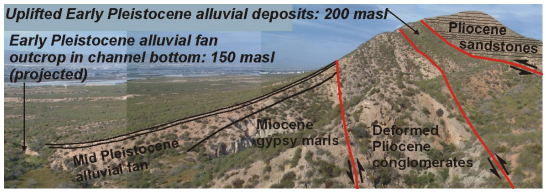

Fig. 1: Panoramic view of the pierced and uplifted Early Pleistocene alluvial fan sediments at La Serrata segment.

Offset channels (Fig. 2) observed all along La Serrata have accumulated about 100 metres of displacement along strike. We estimate that the channels are younger than the interfluvial Late Pleistocene alluvial units but older than the calcrete crust formed on Mid Pleistocene alluvial fans (between 210.2 – 130.8 ka BP according to U/Th results) where channels are incised, which suggests a minimum strike-slip rate of 0.54 mm/a. Thus, from geomorphological observations, strike-slip displacement seems to be around 10 times larger than dip-slip rate.

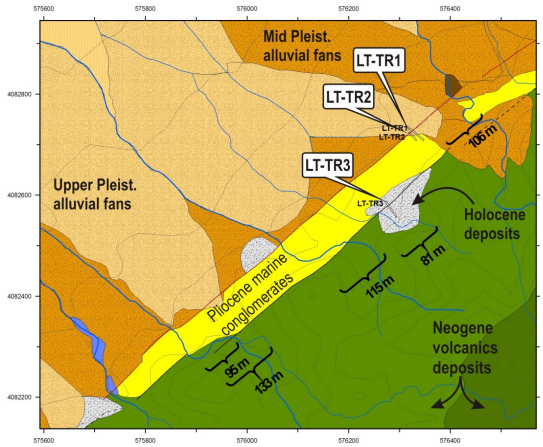

Fig. 2: Example of offset drainage along La Serrata range, at Los Trances site.

At El Hacho site trenches perpendicular to the fault were open across an evidenced fault scarp to detect paleoearthquake evidence (Moreno et al., 2007). The trenches exposed two fault zones, one of them reaching up to the surface faulting all Pleistocene units. Chaotic and wedged deposits were interpreted as colluvial wedges related to sharp fault movements proving the seismic behaviour of the fault. A minimum of 4 events were identified in the trenches, two at the base of the colluvial wedges: E_h1 and E_h2 constrained by TL between Mid Pleistocene age and 49.9 ka BP; and two younger events between faulted and unaltered units: E_h3 constrained by TL between 41.5 ka BP and 26.6 ka BP, and E_h4 constrained between 30.8 and present time in this tench.

Also, at El Hacho site, a 3D trenching survey with trenches parallel to the fault showed a faulted and buried paleochannel (Moreno et al., 2008). Radiocarbon analyses date this paleochannel as 772-937 AD. Two events are infered from this faulted paleochannel, the first one would have displaced the drainage course and the second one would have faulted the channel infill. The first event is interpreted to be event E_h4 deduced in trenches across to the fault, adjusting the its upper age in 1061 BP. The second event afecting the paleochannel (E_h5) has an age constrained between the age of the infilling material (1313 ka BP) and present time. The horizontal maximum offset of the paleochannel is 3 m, and although part of this offset could have not a tectonic origin, a minimum strike-slip rate of 0.1 mm/a for the last 30 ka can be estimated taking into account the age of the incised alluvial fan.

Trenches digged in fluvial sediments (El Hacho gully, Cerro Blanco and Pecho de los Cristos sites) show fluvial deposits overlaying the fault zone. Near El Hacho site, the fluvial sediment was dated by ^{14}C (Moreno et al., 2007) suggesting seismic silence since 688-889 AD.

Thus, the faulted paleochannel and unfaulted fluvial sediments seem to precisely constrain the age of the last earthquake (E_h5) in this segment of the fault between 1313 BP and 1061 BP, and suggest an elapsed time since the last earthquake of 1061 to 1178 yrs. A fault relay to a parallel fault trace could also explain the similar ages between faulted and indisturbed sediments.

At Los Trances site, an artificial wall shows older faulted Quaternary sediments depicting at least 2 events: E_t1 and E_t2 delimiting faulted and non faulted Mid Pleistocene sediments and constrained between Mid Pleistocene and 180,1 ka BP (Fig. 3 below) according to U/Th results. A trench was open parallel to the wall to observe the upper faulted sediments and a different fault zone structure was shown. Here two younger events were defined and ages were constrained by TL: E_t3 (83 – 69.1 ka BP) and E_t4 (38 – Present) (Fig. 3 above). From these four events; three of them correlate well with events observed at El Hacho.

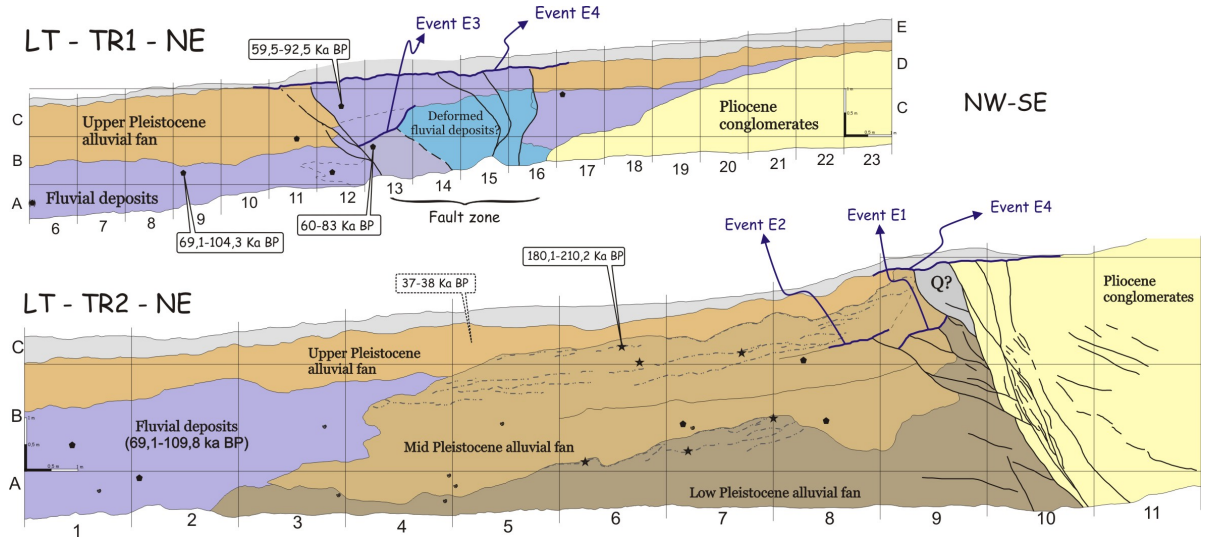

Fig. 3: Trench walls from Los Trances site where Quaternary sediments can be observed faulted up to the surface. A total of 4 events are identified. Location of trenches in Fig. 2.

Offshore Carboneras Fault

The high-resolution IMPULS multichannel seismic profiles allows to identify up to 7 seismostratigraphic units above the Messinian uncomformity (Fig. 4a,e,f).

The profiles show a great variability of structures along the fault zone, in part due to the interaction between "en echelon" traces: positive flower structures can be observed at the shelf, southwards simple reverse faults block the gullies draining from the shelf (Gràcia et al., 2006) (Fig. 4e), and complex compresive structures appear at the southern segment like pressure ridges (Fig. 4f) slowly dimed towards the south and finally buried by hemipelagic sediments.

TOPAS profiles show the shallowest geometries of the fault and evidence recent activity by fault scarps and displaced reflectors (Fig. 4b,c,d). Also towards the south, sediments overlay the fault zone suggesting a decrease of the fault activity. From existing sediment core analyses from the Almería channel (Bozzano et al., accepted) sedimentation rates are calculated and slip rates can be

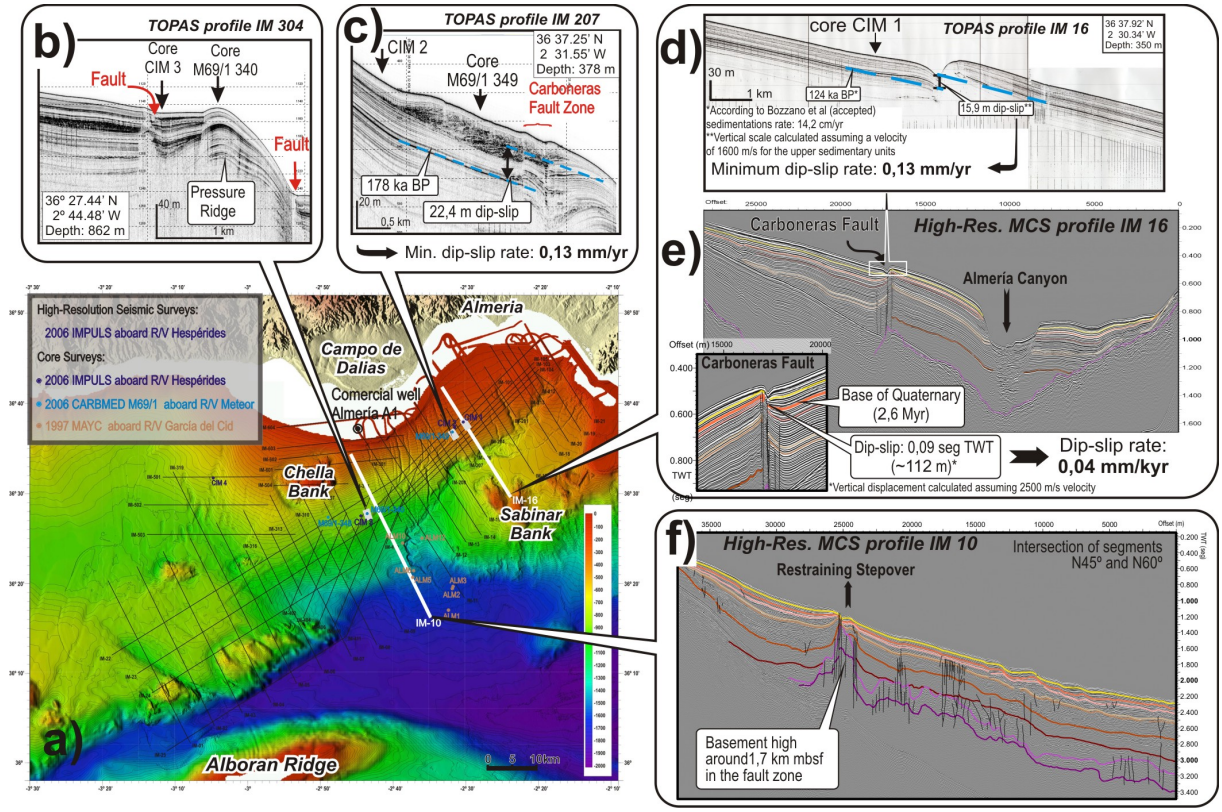

Fig. 4: a) Bathymetric map of the study area south of the Almería margin and location of MCS profiles, TOPAS profiles and sediment cores acquired during the marine surveys. b,c,d) TOPAS profiles showing the Carboneras Fault Zone and Late Quaternary sediments faulted up to the surface. Sediment cores are located in each profile. e,f) High-resolution multichannel seismic profiles with reflectors defining the seismostratigraphic units at the Carboneras Fault Zone, units appear faulted up to the surface.

obtained from TOPAS displaced reflectors. Profile IM-16 (Fig. 4d) shows a highly reflected horizon displaced 21 metres vertically suggesting a dip-slip rate of 0.14 mm/a for the Late Quaternary time. The same dip-slip rate is obtained in TOPAS profile IM 207 (Fig. 4c) where a faulted landslide deposit is observed.

Applying the same exercise to multichannel seismic profiles, a vertical slip of around 112 m is observed for the reflector delimiting Early Quaternary and Late Pleistocene sequences. A mean dip-slip rate of 0,04 mm/a is obtained since the base of the Quaternary, a similar value to the one obtained onshore since Early Pleistocene time. This is a smaller slip-rate than the one obtained with TOPAS profiles since the Late Pleistocene (0.13 mm/a) suggesting either an increase of the slip rate through the Quaternary or a change in the kinematics of the fault with an increase in dip-slip component.

CONCLUSIONS

Both onshore and offshore studies show faulted Quaternary layers and mass movement deposits related to deformation events (paleoearthquakes). Trench walls evidence a minimum of six events since the Mid Pleistocene. The four younger events occurred during the last 80 ka, suggesting a mean recurrence period of 20 ka, or 13.5 ka if we take into account the last 5 earthquakes. A faulted and buried paleochannel records a minimum of two events during the last 30 ka and constrain the last earthquake to AD 772-889. The horizontal maximum displacement observed for the paleochannel is 3 m, suggesting a minimum strike-slip rate of 0.1 mm/a for the last 30 ka. This is much smaller than the 0.6 mm/a lateral strike-slip calculated for the last 200 ka by displaced valleys across the faulted NW boundary of La Serrata. Further analyses will clarified if the 0.1 mm/a lateral strike-slip rate is underestimated or if it is the result of a decreasing slip rate through the Quaternary. On the other hand, offshore, very high resolution seismic profiles together with sedimentary analysis of marine sediments suggest a mean vertical slip of 0.13 mm/a for the last 178 ka. The study provides evidence for the seismogenic behaviour for the Carboneras fault and provides its first paleoseismological parameters, contributing to a more realistic seismic hazard value for the seismic catalogue.

Acknowledgements: This work has been funded by Spanish national projects IMPULS (REN 2003-05996/MAR), EVENT (CGL2006-12861-C02-01, and -02), and MCYT acciones complementarias "Caracterización del potencial sísmico de la falla de Carboneras mediante trincheras" (CGL2004-20214-E) and "Streamer" (CTM2004-21203-E). It is also supported by the Consolider-Ingenio 2010 programme, CSD 2006-0004 "Topo-Iberia". We specially thank the captain, crew, technical staff and scientist involved on the marine cruises IMPULS and M69/1. We are also grateful to the scientist and dating technicians involved in the trenching surveys for their collaboration throughout data acquisition and further discussions.

References

Argus, D.F., Gordon, R.G., DeMets, C., Stein, S. (1989). Closure of the Africa-Eurasia-North America Plate Motion Circuit and Tectonics of the Gloria Fault. Journal of Geophysical Research, 94 (B5), 5585-5602.

Benito, M.B., Gaspar-Escribano, J.M., García-Mayordomo, J., Jiménez, M.E., García Rodríguez, M.J. (2006). Proyecto RISMUR: Evaluación de la peligrosidad sísmica. Instituto Geográfico Nacional y Protección Civil de Murcia, Madrid. 121 pp.

Bousquet, J.C. (1979). Quaternary strike-slip faults in southeastern Spain. Tectonophysics, 52 (1-4), 277-286.

Bozzano, G., Alonso, B., Ercilla, G., Estrada, F., García, M. (2009). Late Pleistocene and Holocene depositional facies of the Almeria Channel (Western Mediterranean). Special Publication of the Geological Society of London, In press.

De Larouzière, F.D., Bolze, J., Bordet, P., Hernandez, J., Montenat, C., Ott d'Estevou, P. (1988). The Betic segment of the lithospheric Trans-Alboran shear zone during the Late Miocene. Tectonophysics, 152 (1-2), 41-52.

DeMets, C., Gordon, R.G., Argus, D.F., Stein, S. (1990). Current plate motions. Geophysical Journal International, 101(2), 425-478.

Gràcia, E., Pallàs, R., Soto, J. I., Comas, M., Moreno, X., Masana, E., Santanach, P., Diez, S., García, M., Dañobeitia, J. (2006). Active faulting offshore SE Spain (Alboran Sea): Implications for earthquake hazard assessment in the Southern Iberian Margin. Earth and Planetary Science Letters, 241, 734-749.

Martínez Díaz, J.J., Hernández Enrile, J.L. (2004). Neotectonics and morphotectonics of the southern Almería region (Betic Cordillera-Spain) kinematic implications. International Journal of Earth Sciences, 93, 189-206.

Masana, E., Martínez-Díaz, J.J., Hernández-Enrile, J.L., Santanach, S. (2004) The Alhama de Murcia fault (SE Spain), a seismogenic fault in a diffuse plate boundary: Seismotectonic implications for the Ibero-Magrebian region. Journal of Geophysical Research, 109, doi:10.1029/2002JB002359.

Masana, E., Pallàs, R., Perea, H., Ortuño, M., Martínez-Díaz, J.J., García-Meléndez, E., Santanach, P. (2005). Large Holocene morphogenic earthquakes along the Albox fault, Betic Cordillera, Spain. Journal of Geodynamics, 40 (2-3), 119-133.

Moreno, X., Masana, E., Gràcia, E., Pallás, R., Ruano, P., Coll, M., Stepancikova, P., Santanach, P. (2007). Primeras evidencias de paleoterremotos en la falla de Carboneras: estudio paleosismológico en el segmento de La Serrata. Geogaceta, 41, 135-138.

Moreno, X., Masana, E., Gràcia, E., Bartolomé, R., Piqué-Serra, O. (2008). Estudio paleosismológico de la Falla de Carboneras: Evidencias tierra-mar de actividad tectónica reciente. GeoTemas, 10, 1035-1038.

Sanz de Galdeano, C. (1990). Geologic evolution of the Betic Cordilleras in the Western Mediterranean, Miocene to the present. Tectonophysics, 172 (1-2), 107-119.

Stich, D., Serpelloni, E., Mancilla, F., Morales, J. (2006). Kinematics of the Iberia-Maghreb plate contact from seismic moment tensors and GPS obsrvations. Tectonophysics, 426, 295-317.

Wenzens, G. (1992). The influence of tectonics and climate on the Villafranchian morphogenesis in semiarid Southeastern Spain. Zeitschrift für Geomorphologie, 84, 173-184.

LIQUEFACTION AS EVIDENCE OF PALEOSEISMICS

N.A. Mörner (1)

(1) Paleogeophysics & Geodynamics, Rösundavägen 17, 13336 Saltsjöbaden, SWEDEN. morner@pog.nu

Abstract: *The process of liquefaction is an important factor in the study of paleoseismics. It starts to form at earthquake magnitudes in the order of 5–5.5. The spatial distribution of a single liquefaction event is related to the magnitude of the event. Therefore, a key issue in paleoseismology is to identify and date liquefaction structures to separate events. The type of structure, the size of structures and the material in liquefaction and venting are other key issues in the registration of past liquefaction events. Recently, we have been able to identify multiple phases of liquefaction events. They are interpreted in terms of shocks and after-shocks. Liquefaction structures are identified globally and all throughout geological time. The present paper, however, is strongly focused on liquefaction events in glacial to postglacial sediments in Sweden, where they are also linked to faults, fractures, slides and tsunami events. Often they were dated to a single varve year.*

Key words*: Liquefaction, dating, spatial distribution, multiple phases.*

LIQUEFACTION

The phenomenon of ”liquefaction” refers to the process where a sediment layer or a part of a sediment layer is transformed into a fluid or fluidized stage (from Latin: *lique facere*). This occurs post-depositionally (sometimes also “synsedimentary”). There are different ways of generating liquefaction. The most common process is earthquake shaking.

The shaking motions at an earthquake may lead to a reorganisation of the internal distribution of grains and water so that the sediment becomes fluid. This makes deposits of sand and course silt most susceptible for liquefaction. Also, fine gravel may fairly easily become liquefied. Courser and finer sediments (course gravel to pebbles and clay to fine silt) liquefaction only occurs rarely and under special conditions. The postdepositional liquefaction of a stratified sandy bed implies that the original stratification becomes totally or partly erased into a structureless bed (Fig. 1). By magnetic methods, we have shown that also clay and fine silt beds may be subjected to an internal liquefaction (Mörner and Sun, 2008).

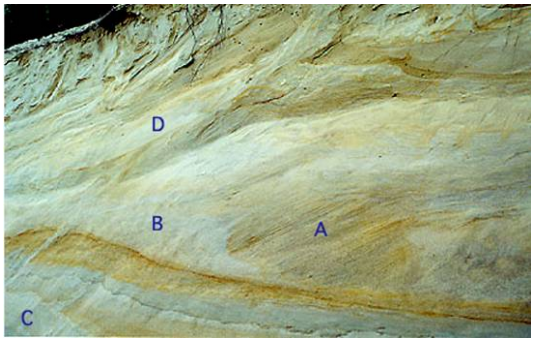

Fig. 1: The primary bedding (A) has become erased by liquefaction into a structureless bed (B). Beds C and D of structureless sand refer to a 2nd and 3rd phase of liquefaction with venting (from Mörner, 2003; site Olivelund). This event is dated at the autumn of varve 10,430 BP.

A liquefied bed will behave like a “heavy fluid” – allowing big blocks and eroded fragments to “swim” in the liquefied bed (Fig. 2). This also opens for density redistribution – heavy beds sinking down and lighter beds flaming upwards (Fig. 3). This also leads to venting of liquefied material and formation of mud-volcanoes. The size of venting structures and the material to become vented are strongly linked to the magnitude of earthquake.

Fig. 2: Liquefied sand behaving like a “heavy fluid, in which blocks may “swim” (from Mörner, 2003; site: Olivelund).

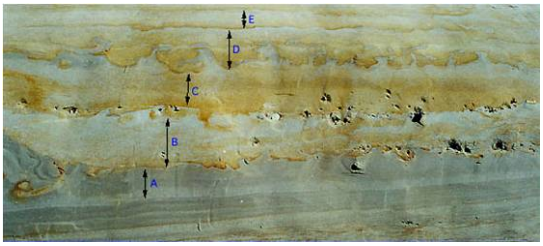

Fig. 3: Five sedimentary cycles (A-E) affected by post-depositional liquefaction in varve year 9428 BP causing the fine sediments to flame upwards and the course sediments to sink downwards (from Mörner, 2003; site Rödbäck).

Liquefaction may strike a stratified sedimentary bed quite differently; strongly deforming some beds and leaving others virtually unaffected (Fig. 4).

Fig. 4: Differential liquefaction of a stratified bed at a paleoseismic event at 12,400 BP (Mörner, 2003, 2008; site Hunnestad).

The material vented behaves quite differently with respect to grain sizes. In a large mushroom structure a laminar flow is recorded by the stratification of sand and course silt grains, a turbulent flow by the totally random distribution of fine grains measured by the anisotropy of magnetic susceptibility (AMS), and a free flow of the very small particles controlling the magnetic polarity (ChRM) allowing a firm orientation with respect to the geomagnetic pole.

The spatial distribution of liquefaction as to a single event is more or less linearly related to the magnitude of the earthquake.

Liquefaction structures are usually formed at earthquakes of a minimum magnitude in the order of M 5–5.5. This implies that the recording of past liquefactions tells us that the magnitude ought to be, at least, above ~5.5 (with respect to the Richter-scale).

Because earthquakes usually are not single events, but rather a cluster of shocks and after-shocks, one would expect to see not just one phase of liquefaction, but multiple phases (Mörner, 2003).

Fig. 5: Five successive phases (1–5) of liquefaction of the 9663 vBP paleoseismic event, interpreted to represent shocks and after-shocks of the same earthquake event (from Mörner, 2003, 2008; site: Myra West). Five successive phases were also recorded at a site (Hög) located 35 km away.

Liquefaction and venting of liquefied material are recorded at numerous sites in Sweden (Mörner, 2003, 2005, 2008). The spatial distribution of one and the same liquefaction event – 320x100 km for the 10,430 vBP event and 80x40 km for the 9663 vBP event – gives evidence of high-magnitude events.

At several events, we were able to record multiple phases of liquefaction. At the 9663 vBP paleoseismic event, we recorded 5 successive phases (Fig. 5), interpreted in terms of shock and after-shocks.

The size and type of liquefaction structures have a bearing on the magnitude. In some cases we have recorded the venting of gravel, even course gravel and pebbles (Figs. 6–7). This calls for magnitudes in the order of M>8. One such event is dated at 10,388 vBP and another at 6100 BP (Mörner, 2003, 2008).

Fig. 6: Venting not only of sand but also gravel and pebbles at the 10,388 vBP event (Mörner, 2003, 2008; site Turinge grusgrop). This calls for a high-magnitude paleoseismic event (M>8).

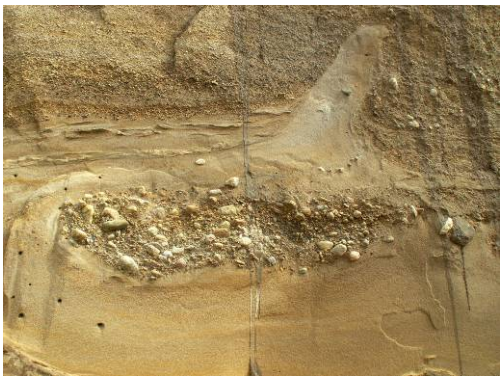

Fig. 7: Structureless liquefied sand as a part of the venting of sand-gravel-pebbles in the Fig. 6 site.

Seismic shaking may also generate wavy patterns of previously horizontal sand and clay beds (Fig. 8; cf. Mörner, 2003; Mörner and Sun, 2008).

Extensive turbidites are often formed by the sediment masses set in motion by slides, liquefaction and tsunami waves. Their spatial distribution is 300x200 km for the 10,430 vBP event and 320x90 km for the 9663 vBP event. They stick out as distinct “marker-varves” (Fig. 9). This allows a very precise dating as to the Swedish Varve Chronology.

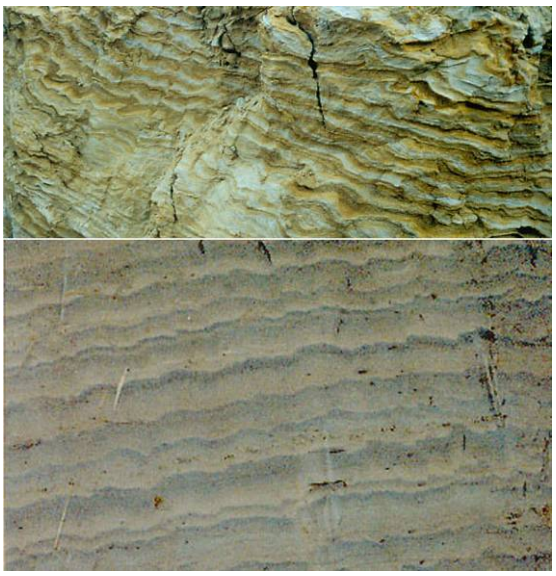

Fig. 8: Seismic ground shaking may sometimes generate wavy patterns in sand (above) and clay (below) (from Mörner, 2003). The wavy clay layers have increased paleomagnetic intensity suggesting internal fluidization (Mörner and Sun, 2008).

Fig. 9: The 9663 vBP turbidite (seismite) of graded bedding, here seen as a distinct marker-bed witin the annually varved clay (from Mörner, 2003).

In Sweden, we have been able to tie the liquefaction events into singular varve years by that providing an annual resolution allowing us to determine spatial and temporal factors.

At present, we have identified, dated and described 59 separate paleoseismic events in Sweden (Fig. 10). Most of those generated liquefaction structures (and 16 of them generated tsunami events). All events are recorded by multiple criteria; e.g. primary faults, bedrock fracturing, sediment deformation, liquefaction, slides, tsunami events and turbidites (see the eight papers listed in References).

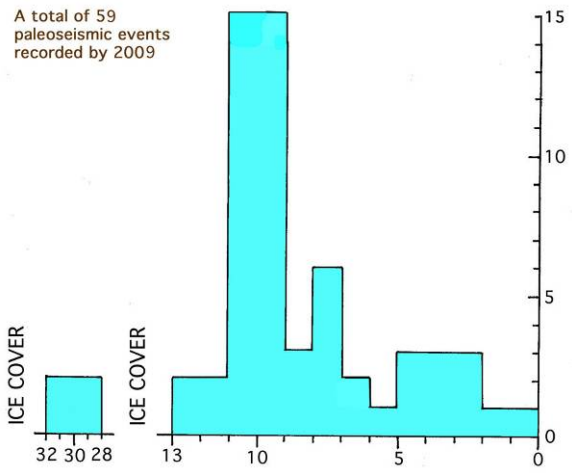

Fig. 10: Time distribution in thousands of years BP of the 59 paleoseismic events recorded in Sweden (Mörner, 2003, 2005, 2008, 2009).

CONCLUSIONS

Liquefaction provides very essential information for the understanding and interpretation of paleoseismic (and archaeoseismic) events.

References

Mörner, N.-A., 1996. Liquefaction and varve disturbace as evidence of paleoseismic events and tsunamis: the autumn 10,430 BP event in Sweden. Quat. Sci. Rev., 15, 939-948.

Mörner, N.-A., 2003. Paleoseismicity of Sweden – a novel paradigm. A contribution to INQUA from its Sub-commission of Paleoseismology, Reno 2003, ISBN-91-631-4072-1, 320 pp.

Mörner, N.-A., 2004. Active faults and paleoseismicity in Fennoscandia, especially Sweden: Primary structures and secondary effects. Tectonophysics, 380, 139-157.

Mörner, N.-A., 2005. An investigation and catalogue of paleoseismology in Sweden. Tectonophysics, 408, 265-307.

Mörner, N.-A., 2008. Paleoseismicity and Uplift of Sweden. Guidebook, Excursion 11 at 33rd IGC, Oslo 2008, 107 pp, www.33IGC.org.

Mörner, N.-A., 2009. Late Holocene earthquake geology in Sweden. Geol. Soc. London, Spec. Publ., 316, 197-188.

Mörner, N.-A. & Sun, G., 2008. Paleoearthquake deformations recorded by magnetic variables. Earth Planet Sci. Letters, 267, 495-502.

Mörner, N.-A., Tröften, P.E., Sjöberg, R., Grant, D., Dawson, S., Bronge, C., Kvamsdal, O. & Sidén, 2000. Deglacial paleoseismicity in Sweden: the 9663 BP Iggesund event. Quat. Sci. Rev., 19, 1461-1468.

CRITERIA TO DISTINGUISH NEOTECTONIC FROM OTHER ACTIVE FAULTS: EXAMPLES FROM THE CENTRAL PYRENEES

M. Ortuño (1)

(1) RISKNAT group. Dept. Geodinàmica i Geofísica. Universitat de Barcelona (Spain) C/Martí i Franquès s/n. 08028-Barcelona, SPAIN. maria.ortuno@ub.edu

Abstract: *In several settings, such us the high mountain environment or the karstic terrains, active faults might be the result of non-tectonic processes, all of which can be grouped under the term "active deformation". To characterize the seismogenic potential of a fault and, thus, its associated seismic hazard, it is necessary to determine the causes of its activity. However, the nature of the deformation along a faults is, often, not obvious. To deal with this problem, a number of criteria have been reviewed and proposed in order to constitute a working-guide to determine the origin of faulting. Two examples of the Maladeta massif (Spanish Central Pyrenees) illustrate how very different processes are capable to generate similar scarp-forms and how one single fault scarp might be the result of their simultaneous interaction.*

Key words*: neotectonics, non-tectonic faults, composite fault, active deformation*

INTRODUCCION

Active faults can be defined as planes of fracture along which displacement takes place or has taken place in recent times. Besides the plate tectonics, other sources of forces in the upper crust must be taken into account as causes of deformation. The term "active deformation" might serve as an *umbrella* to refer to all processes causing deformation along faults (Ortuño, 2008).

In certain settings, the magnitude of the non tectonic stresses might equal or overpass the tectonic ones. Straightforward examples are deglaciated regions where the isostatic forces are controlling the activity of pre-existing faults (i.e. Stewart et al. 2000) or areas where the intrusion of magmatic or salty domes are responsible for fault generation or fault reactivation.

In contrast with these phenomena, that can take place up to tens of kilometres under the earth surface, surface processes might also be the cause of new generation or reactivation of faults. Such is the case of the instability phenomena (slope mass movements and subsidence) (i.e. Chighira, 1992) and the crust unloading effects produced by drainage of a lake or melting of ice masses (Hampel and Hetzel, 2006; Ustaszewsky et al., 2008). Accordingly, these forces must be interacting simultaneously in a particular area of the crust, and thus, the movement along a fault could be due to more than one process. To deal with this situation, Ustaszewsky et al. (2008) have proposed the term "composite faults" to refer active faults in the Swiss Alps in which deformation is controlled by tectonic, gravitational, and elastic rebound forces.

Paleosismological studies are always preceded by the identification of active faults in the landscape through geomorphological and geophysical methods. However, in these studies, the causes of deformation are frequently obviated or not enough discussed. Even when the seismogenic nature of the faulting can be showed, the possibility of deformation being owed to non-tectonic forces must be discussed since the misinterpretation of a fault origin could invalidate the results derived from paleosismological analysis (i.e. recurrence time, maximum magnitude earthquake, etc.). To better constrain the nature of faulting, we need to perform or consider more regional studies. In order to contribute to this task, a number of criteria are revised below.

Ortuño (2008) recognize the composite nature of several cases of faulting in the Spanish Pyrenees. Two of these active structures are analyzed in this work, to illustrate how the use the discussed criteria can help to better characterize the nature of faulting, and thus, its seismogenic potential.

USEFUL CRITERIA

The difficulties in differentiating tectonics from non-tectonics faults have constantly worried geologists. McCalpin (1999) collected and discussed criteria to distinguish tectonic from gravitational faults. This work has been reviewed and extended by Ortuño (2008), who proposed a guideline for the use of different criteria to determine the origin of faulting. Criteria can be grouped into morphologic, kinetic-structural and others (such as chronology of deformation or processes spatial distribution). Most of them have to do with the feasibility of the different processes causing deformation. By this reason, the origin of the fault is often suspected by the rejection of all other possible origins. Best results are achieved by combining the greater number of criteria.

Morphologic criteria

Morphologic features that should be considered to understand the nature of the faulting can be grouped in quantitative and qualitative.

The most useful quantitative criteria are slope and relief, rupture length, cumulative displacement, changes in offset along the fault trace, maximum offset to trace length ratio (D/L), and depth of deformation. Some

relevant qualitative criteria are position and orientation of the fault with respect to the relief and the slope, curvature and continuity of the fault trace. Landform assemblage and landscape evolution might be definitive criteria.

Kinetic and structural criteria
Deformation observed both at trench and outcrop might provide important information regarding the nature of faulting. Quantitative criteria refer to cumulative displacement and slip rate as well as orientation of the fault, dip and slip with respect to the pre-existing tectonics and the present and recent stress orientation obtained from other sources (i.e. focal mechanisms, recent local and regional tectonics, drillings, etc.). Qualitative criteria refer to textural and structural features of deformation, as well as style of faulting (strike slip, normal or reverse).

Other criteria
The temporal constrain of deformation might be a helpful criteria to explore a particular origin of faulting. For example, the occurrence of coseismic deformation would reinforce a seismogenic origin inferred by the use of other criteria. Faulting constrained to a deglaciation episode would suggest isostasy or elastic rebound as causes of deformation.

The spatial distribution of seismicity, maximum uplift rates or enhanced depositional/erosive processes with respect to the location of the fault might as well be clue aspects to determine the fault origin.

EXAMPLES FROM THE MALADETA MASSIF (CENTRAL PYRENEES)

The Maladeta massif (Fig. 1) is located at the core of the Pyrenean range, in the paleo-margin between the Iberian and the Eurasian plates. Owing to the small convergence rate between these plates (< 0,5 mm/a; Nocquet and Calais, 2004), neotectonic faults in the Pyrenees are expected to behave as slow faults (with slip rates <0,2 mm/yr).

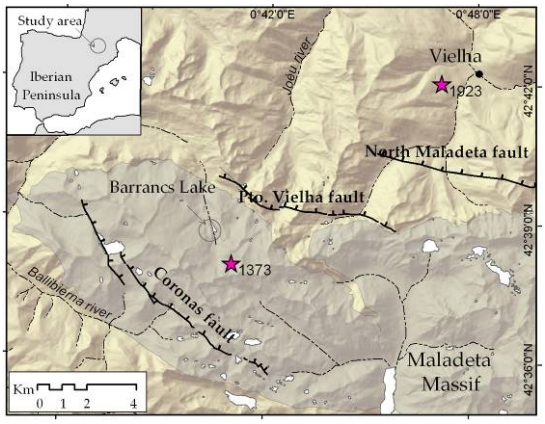

Fig. 1: Digital elevation model showing the location of the Maladeta Massif, in the core of the Pyrenean range, and the epicentres of the two damaging historical earthquakes (star-symbol). Main active faults in the area are indicated. The shaded area corresponds to the granitic batholith.

The study area has been scenario of two damaging historic earthquakes, one in 1373 AD (M_w~6.2) and the most recent one in 1923 AD (M_w= 5.8) (Ortuño et al. 2008). The North Maladeta fault in the study area has been identified as the most probable seimogenic source of the latter earthquake and as a possible source of the former one. The Coronas fault is among other close seismogenic structures that could account as a probable candidate source for the 1373 AD event (Ortuño, 2008).

Active faults in the area are mainly identified by the associated offset of glacial surfaces, such as polished surfaces and valley walls. In all cases, faults are reactivated preexisting structures, inherited from the Variscan and Alpine orogenies. These faults affect mainly late Variscan granitic rocks of the Maladeta massif, and occasionally, the metasedimentary paleozoic country rocks.
The landscape is characterized by deeply incised alpine valleys and a recent deglaciation history (Pallas et al. 2006). Besides the neotectonic origin of the identified active faults, other possible causes of movement are: a) slope instability by slow gravitational deformation; and b) elastic rebound of the upper cortical level due to the postglacial rebound (see Ustaszwesky et al. 2008 for details regarding this phenomenon).

The Coronas fault
The Coronas fault (Fig. 2 and 3) is an 11.5 km length rectilinear scarp formed along a preexisting fault breccia outcropping along the northern Ballibierna valley. The systematic increase of the slope offset towards the centre of the fault trace (up to 155 m) does not seem to be the product of enhanced erosion and suggests that the structure is an active fault. This fault has been interpreted as a composite fault in which movement is controlled by neotectonics, but also by slow gravitational deformation.

The main evidences to suspect a neotectonic origin are the length and continuity of the geomorphological trace, the step-like location with respect to the seismogenic North Maladeta fault, and the macroseismal location of the 1373 AD earthquake epicentre, about 3 km north of its trace. This epicentre location (Fig. 3) is in accordance with the surface projection of the Coronas fault plane, and agrees with the 12 km depth estimated for the hypocentre location of the event. This estimation is based on the analysis of the macroseismic data of this earthquake and the maximum depth of the seismogenic crust of the area obtained from the instrumental seismicity (see Ortuño, 2008). According to the relations proposed by Wells and Coppersmith (1994) and assuming the total rupture of the fault length (11.5 km), this fault would be capable to produce a 6.2 M_w event. However, the earthquake location uncertainty (25 km radius) leads to consider other faults in the area, such as the North Maladeta fault or the Port de Vielha fault, as possible seismogenic sources (Fig. 1).

Fig. 2: The Coronas fault scarp. The polishing of the fault plane is owed to the last glacial advance, indicating the scarp formed prior to the last maximum glacial advance in the area (~23-25 ka ago).

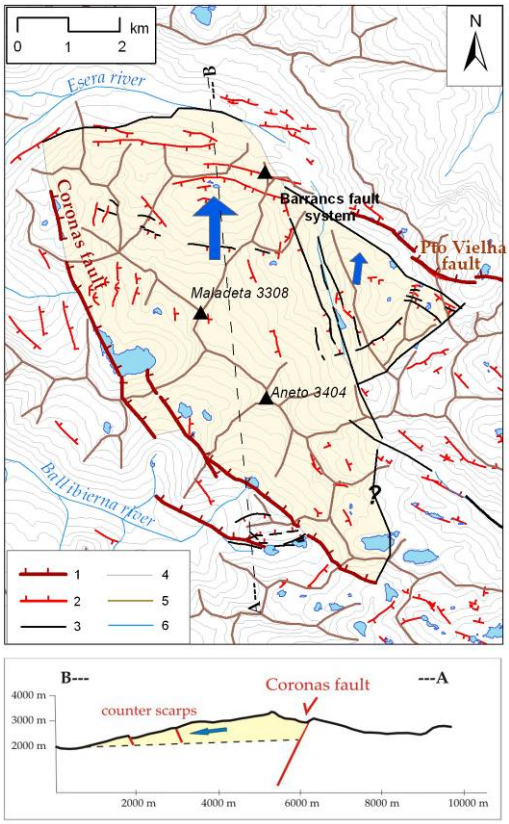

Fig. 3: Above: Geomorphologic sketch showing the location of the Coronas fault and the Barrancs fault system and other scarps with respect to topography. 1.Main faults 2. Minor scarps. 3. Inferred limits of gravitational deformation. 4. 100 m countour lines. 5 watersheds. 6 rivers. Below: Topographic cross section and interpretation of the Aneto gravitational collapse.

The slow gravitational component of the movement is attributed to the fault on the basis of its position in the Aneto massif. The great altitude difference between the ridge (up to 3404 m) and the Esera river (~1900 m), shown in *Fig. 3*, supports the hypothesis of the northwards gravitational collapse of the ridge. The observed offset can be linked to a deep seated slope gravitational deformation (DGSD) of huge dimensions. Physical models performed in analogous conditions (Bachmann et al. 2006) support the feasibility of the gravitational failure, which would be linked to the development of a new formed sliding basal plane, branched in depth to the Coronas fault. The northwards movement would be generating a great rear scarp (the Coronas scarp, Fig. 2) as well as smaller antislope scarps in the opposite valley (cross section in Fig. 3). This component of the movement allows explaining the great fault offset with respect to its length, which yields a D/L value of 0.013, one order of magnitude greater than the expected for pure neotectonic faults. The fact of the fault being also neotectonic and seismogenic reinforces the feasibility of the ridge collapse, since the seismic shacking, amplified in the ridges, will facilitate the movement along discontinuities (see Ortuño, 2008 for further discussion).

The Barrancs fault system

Faults in the Barrancs fault system bound the Barrancs lake longitudinally and are oriented NNW-SSE, oblique to the major neotectonic features in the area (Fig. 1). The two main faults are identified by the offset of a polished glacial whaleback hill located at the bottom of the Barrancs valley. The scarps develop on old shear zones, have lengths between 0.2 and 1.2 km and a maximum height of 20 m. Displacement vector can be estimated restoring the shape of the offseted whaleback surface, that dates form the last glacial maximum (~ 23-25 ka, Pallas et al. 2006). Episodic displacement on one of the faults is evidenced by 3 different weathering strips on the fault plane (Fig. 4). Fault planes do not show glacial polishment. However, preservation of glacial striae on the fault scarps at several locations indicates that the fault surface is affected by glacial erosion, probably during the Younger Dryas episode (~ 12-15 ka; Pallas et al., 2006). Although these smaller faults could be secondary tectonic features produced by seismic shaking along the Coronas fault or the Port de Vielha fault, their short lengths do not allow attributing them a seismogenic potential. The D/L ratio of the scarps and the high slip rates inferred from their postglacial age (>0,8 mm/a) do not support the pure neotectonic origin for these faults.

These faults have been interpreted as secondary faults in association with the northwards collapse of the Aneto Massif (Fig.3). Evidences accounting for this origin are the measured displacement vector and the relative position with respect to the Coronas fault. According to the model for the collapse of the massif (Fig. 3), the slip along the Barrancs faults could be the result of differential movement of the Barrancs block and the Aneto block. Fig. *5* shows the proposed chronology for the formation and modification of the scarps.

Fig. 4: Fault scarp in the Barranc fault system. Slip vector is marked by an arrow at the centre and dip of the fault. It indicates main dip slip with minor left lateral displacement. Notice the 3 bands of different alteration degree that can be distinguished in the fault face.

CONCLUDING REMARKS

The exposed examples of composite faults from the Maladeta Massif illustrate the difficulty to determine the origin of faulting in certain settings. The combination of the greater possible number of criteria helps to reject or accept the different causes of movement along faults.

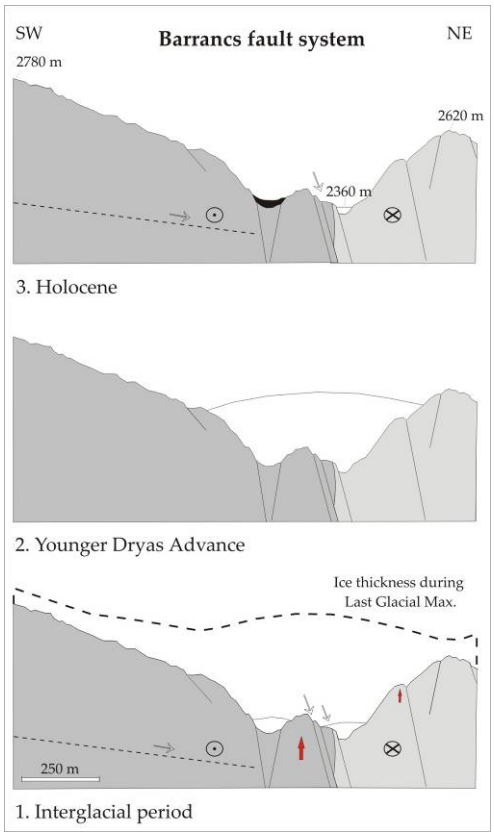

Fig. 5: Proposed evolution for the formation and modification of the scarps in the Barrancs system. 1.After the Last Glacial Maximum, the gravitational collapse of the Aneto massif would have produce extrussion of the valley bottom and left lateral displacement along the faults. 2 The advance of the ice masses during the Younger Dryas accounts for the generation of glacial striae in the faul face. 3. During the Holocene, some minor movement could have been occurred along the faults due to DSGD and seismic triggering.

Analysis of the geomorphological and structural recent evolution, together with the comprehension of the litho-structural heritage and the regional setting are essential to understand the nature of faulting, and therefore, the relevance of future paleosismological and trenching studies in a particular area.

Acknowledgements: This research was sponsored by the Spanish Ministerio de Ciencia y Tecnología and the Catalan goverment, which support RISKNAT group. Thanks are due to Pere Santanach Prat, who supervised and contribute with constructive comments to the author's PhD thesis, from which this extended abstract is derived.

References

Bachmann, D., Bouissou, S., Chemenda, A. (2006). Influence of large scale topography on gravitational rock mass movements: new insights from physical modeling. Geophysical Research Letters, 33 (21) 1-4.

Chighira, M. (1992). Long-term gravitational deformation of rock by mass rock creep. Engineering Geology, 32 (3) 157-184.

Hampel, A. and Hetzel, R. (2006). Response of normal faults to glacial-interglacial fluctuations of ice and water masses on Earth's surface, J. Geophys. Res., 111, B06406, doi:10.1029/2005JB004124.

McCalpin, J.P. (1999). Criteria for determining the seismic significance of sackungen and other scarplike landforms in mountainous regions. Techniques for identifying faults and determining their origins, U.S. Nuclear Regulatory Commision, NUREG/CR-5503, Appendix A, pp A122-A142.

Nocquet, J.M. y Calais, E. (2004). Geodetic measurements of crustal deformation in thewestern Mediterranean and Europe. Pure Appl. Geophys, 161, 661-681.

Ortuño, M. (2008). Deformación activa en el Pirineo Central: la falla Norte de la Maladeta y otras fallas activas. Unpublished PhD. Thesis, Universitat de Barcelona, 346 p.

Ortuño, M., Queralt, P., Martí, A., Ledo, J., Masana, E., Perea, H., Santanach, P. (2008). The North Maladeta Fault (Spanish Central Pyrenees) as the Vielha 1923 earthquake seismic source: recent activity revealed by geomorphological and geophysical research. Tectonophysics, 45, 246-262.

Pallàs, R., Rodés, A., Braucher, R., Carcaillet, J., Ortuño, M., Bordonau, J., Bourlès, D.,Vilaplana, J.M., Masana, E., Santanach, P. (2006). Late Pleistocene and Holocene glaciation in the Pyrenees: a critical review and new evidence from ^{10}Be exposure ages, South-central. Pyrenees. Quat. Sci. Rev., 25, 2937-2963.

Stewart, I. S., Sauber, J. y Rose, J. (2000). Glacio-seismotectonics: ice sheets, crustal deformation and seismicity. Quaternary Science Reviews, 19, 1367-1389.

Ustaszewski, M., Hampel, A. y Pfiffner, A. (2008). Composite faults in the Swiss Alps formed by the interplay of tectonics, gravitation and postglacial rebound: an integrated field and modelling study. Swiss J. Geosci., DOI 10.1007/s00015-007-1249-1.

Wells, D.L. y Coppersmith, K.J. (1994). Empirical relationships among magnitude, rupture length, rupture area, and surface displacement. Bull. Seismol. Soc. Am., 82, 974-1002.

THE ESI 2007, THE INTENSITY ATTENUATION RELATIONSHIPS AND POSSIBLE GAINS FOR SEISMIC HAZARD MAPS

I.D. Papanikolaou (1, 2)

(1) Laboratory of Mineralogy & Geology, Department of Geological Sciences and Atmospheric Environment, Agricultural University of Athens, 75 Iera Odos Str., 118 55 Athens , GREECE.
(2) Aon-Benfield-UCL Hazard Research Centre, Department of Earth Sciences, University College London, Gower Str. WC1E6BT London, UK. i.papanikolaou@ucl.ac.uk

Abstract: *Fault slip-rates are of decisive importance for the seismic hazard assessment. However, sensitivity analysis in geological fault slip-rate seismic hazard maps demonstrates that the uncertainty in the attenuation relationships is much higher than the implied uncertainty in slip-rates, so that even if a more accurate slip-rate estimation is achieved, it would have little impact on the final outcomes. The recent introduction of the Earthquake Environmental Intensity (ESI) 2007 promises to offer higher objectivity in the process of assessing macroseismic intensities particularly in the epicentral area than traditional intensity scales that are influenced by human parameters. The ESI 2007 scale follows the same criteria-environmental effects for all events and can compare not only events from different settings, but also contemporary and future earthquakes with historical events. As a result, a re-appraisal of historical and recent earthquakes so as to constrain the ESI 2007 scale may prove beneficial for the seismic hazard assessment by reducing the uncertainty implied in the attenuation laws and eventually in the seismic hazard maps.*

Key words*: intensity, seismic hazard assessment, active faults, earthquake environmental effects.*

INTRODUCTION

The macroseismic intensity is not solely used for the description of earthquake effects, but predominantly is a major seismic hazard parameter, since it describes the damage pattern. The new Environmental Seismic Intensity Scale (ESI 2007), introduced by INQUA, incorporates the advances and achievements of Palaeoseismology and Earthquake Geology and evaluates earthquake size and epicentre solely from the Earthquake Environmental Effects (EEE) (Michetti et al., 2007). This paper: a) demonstrates quantitatively how significant is the uncertainty in the empirically based attenuation laws of the existing traditional intensities for the seismic hazard maps and b) shows how the ESI 2007 intensity scale could prove beneficial for the seismic hazard assessment by reducing the aforementioned uncertainty.

THE INTENSITY AS A HAZARD PARAMETER

Seismic shaking is usually expressed in terms of macroseismic intensity or peak ground acceleration and both parameters are widely used in seismic hazard maps. However, peak acceleration values can be a poor guide to the shaking and damage expected pattern, partly because the overall damage may be more closely correlated to the total duration of the strong-motion than to any particular peak on the record and it is mainly introduced for civil and construction engineering purposes (e.g. Bolt, 1999, Coburn and Spence, 2002). Therefore, intensity is the direct measure of damage.

INTENSITY ATTENUATION RELATIONSHIPS

Isoseismals are lines that separate different intensity values and represent the macroseismic information obtained by the quantification of the effects and damage produced by an earthquake. The isoseismal maps are used to derive empirical relations for the decrease of intensity with distance, which then are incorporated into the attenuation laws and used to assess the seismic hazard. Therefore, in order to define the seismic hazard at a given site, it is necessary to know the expected attenuation of intensity with epicentral distance. These attenuation curves are compiled based on the statistical elaboration of historical and instrumental data (Fig.1).

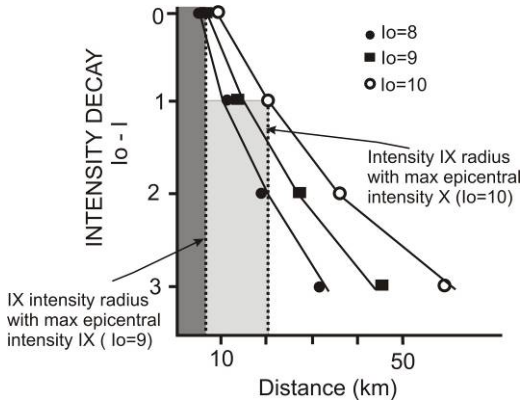

Fig. 1: Attenuation law derived from the statistical elaboration of historical and instrumental data for the Apennines in Italy (Modified from Grandori et al. 1991). Earthquakes with epicentral intensity IX (I_0=9) have a mean radius of 6-7 km for the intensity IX isoseismal (dark grey), whereas events with epicentral intensity X (I_0=10) have a mean radius of 20-21 km for the isoseismal IX (light grey).

However, there is a large variation in the data, which adds uncertainty in the seismic hazard assessment. This variation is nicely portrayed in an empirical magnitude-intensity database compiled by D'Amico et al. (1999), which is presented in Table 1. This database is extracted from instrumental catalogues ranging from 1880 to 1980, covering the whole Mediterranean region. Table 1 for example, shows that epicentral intensity X has been

produced by significantly different magnitude events, ranging from M=6.0 to M=7.0.

Table 1. Distribution of the magnitude values for each intensity class in the Mediterranean region (modified from D'Amico et al., 1999).

Intensity	Number of events	Lower Magnitude	Upper Magnitude	Mean Magnitude
VIII	161	5.0	5.9	5.4
VIII-IX	20	5.7	6.3	6.0
IX	53	5.8	6.7	6.2
IX-X	**5**	**6.3**	**6.9**	**6.5**
X	**18**	**6.0**	**7.0**	**6.6**

Following Table 1, on average, a Ms=6.5 earthquake is expected to produce an epicentral intensity IX or X (or IX+). However, the exact value of the epicentral intensity is crucial for the determination of the area affected around the epicentre and the attenuation relationships. Indeed, historical data of macroseismic intensity versus epicentral distance published by Grandori et al. (1991), covering the whole Apennines in Italy, shows that earthquakes with epicentral intensity IX have a mean radius of 6 km for the intensity IX isoseismal, whereas earthquakes with epicentral intensity X have a mean radius of 10 km for the X isoseismal and a mean radius of 20 km for the isoseismal IX (Fig.1). As a result, for an Ms 6.5 depending on the maximum epicentral intensity value, the radius of isoseismal IX ranges from 6 up to 20 km with a mean value of around 12-13 km. Similar values (ranging from 7 up to 22 km) have also been reported for other regions such as the Sino-Korean craton (Lee and Kim, 2002) indicating that there is some consistency concerning intensity-attenuation relationships worldwide, confirming also this high variability.

FAULT SLIP-RATES AND SEISMIC HAZARD MAPS

Fault specific approaches and geological data are becoming very important for the seismic hazard assessment, by providing quantitative assessments through measurement of geologically recorded slip on active faults (Michetti et al., 2005). Fault slip-rate data sample much greater periods of time, providing a more reliable estimate of hazard than the historical earthquake record (e.g. Yeats and Prentice, 1996). Therefore, it is widely accepted that only geological fault slip-rate data can cover the incompleteness of the historical and instrumental catalogues, providing a more reliable estimate of hazard and higher spatial resolution than the historical record. Based on slip-rate data and the fault geometry, we can construct seismic hazard maps purely from geological data (Papanikolaou 2003, Roberts et al., 2004).

The methodology has been developed in a GIS, which offers great power for manipulation and analysis of data, extending several applications and enabling us to run different hazard scenarios. According to this methodology (see Roberts et al., 2004), fault throw-rates are firstly converted into earthquake frequencies, assuming that each fault ruptures in "floating" earthquakes, which are distributed around a mean magnitude of fixed size. Then, this information is turned into a hazard map after using: i) empirical relationships between coseismic slip values, rupture lengths and earthquake magnitudes, and ii) empirical relationships between earthquake magnitudes and intensity distributions. The final product is a high spatial resolution seismic hazard map showing how many times each location has been shaken at a certain intensity value (e.g. intensity VIII or IX) over a fixed time period, which can be easily transformed into a map of recurrence intervals.

Such a map has been constructed for the region of the Southern Apennines based on the fault geometry and slip-rate data of Papanikolaou and Roberts (2007). Figure 2 shows how many times a locality could receive energy levels capable of producing shaking at intensity IX or higher, assuming homogeneous bedrock geology, a circular pattern of energy release and 12.5 km radius of isoseismal IX, which following the previous chapter, is regarded as the mean value. In this map, each fault ruptures in "floating" earthquakes, which are distributed around a mean magnitude of Ms=6.5.

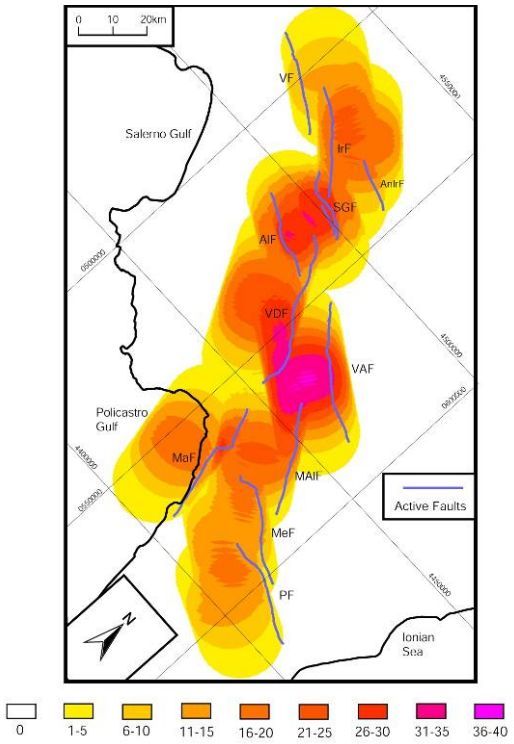

Fig.2: Map showing how many times a locality shakes at intensities ≥IX in 18 kyrs, assuming homogenous bedrock geology, a circular pattern of energy release and a 12.5 km radius of isoseismal IX. VF - Volturara Fault; IrF - Irpinia Fault; AntIrF - Antithetic Irpinia Fault; SGrF - San Gregorio Fault; AlF - Alburni Fault; VDF - Vallo di Diano Fault; VAF - Val' D Agri Fault; MaF - Maratea Fault; MAF - Monte Alpi Fault; MeF - Mercure Fault; PF - Pollino Fault. Fault pattern from Papanikolaou and Roberts (2007).

Areas of high shaking frequency are observed towards the centre of the fault array, where the fastest slipping faults are located (0.8-0.9 mm/yr). In particular, the area of highest shaking frequency is located in the hangingwall centre of the Val' D' Agri fault, which will receive enough energy to shake at intensity IX or higher up to 36 times in 18 kyrs. On the other hand, the hangingwall centres of the Volturara and the Pollino distal faults will shake only about 10-15 times at intensities ≥IX because these faults

are of lower slip-rates (Pollino 0.3 mm/yr; Volturara 0.3 mm/yr).

Sensitivity Analysis

A sensitivity analysis was carried out to determine the way different isoseismal dimensions influence the shaking frequency maps. As a result, a new shaking frequency map has been constructed by increasing the dimensions of isoseismal IX from a 12.5 km radius to a 20 km radius (Fig.3); which is an extreme upper value for a Ms=6.5 earthquake in the southern Apennines.

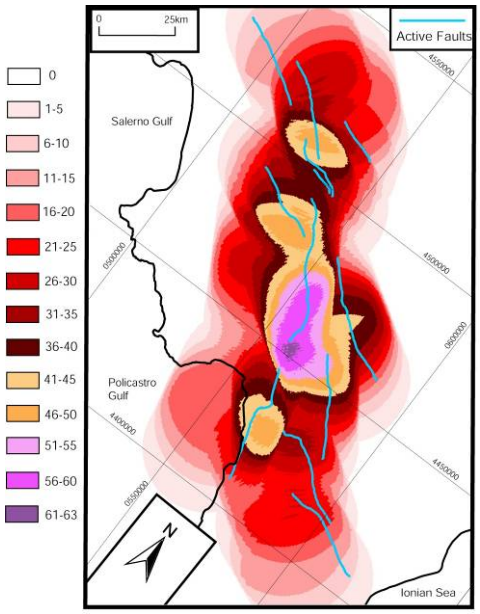

Fig.3 :Map showing how many times a locality receives enough energy to shake at intensities ≥IX in 18 kyrs, assuming homogenous bedrock geology, a circular pattern of energy release and a 20 km radius of isoseismal IX which is an extreme upper value for a Ms=6.5 earthquake in the southern Apennines.

By implementing larger dimensions for the intensity IX isoseismals the affected area, as expected, has been enlarged. In order to: i) quantify the differences in terms of frequency of earthquake shaking between Figures 2 and 3, and ii) delineate how these differences are distributed spatially; a third map has been constructed and presented in Figure 4. In a few words, Figure 4 maps the differences by subtracting the shaking frequency map constructed with a 12.5 km radius of isoseismal IX from the shaking frequency map constructed using a 20 km radius of isoseismal IX. The highest difference is observed in the area of the stepover between the Vallo di Diano and the Maratea faults, where more than 50 additional events (up to 58) are calculated (Fig. 4). This is a substantial ten fold increase between the hazard map constructed using a 12.5 km radius of isoseismal IX and the map constructed with a 20 km radius of isoseismal IX.

When applying a 20 km radius, each isoseismal occupies 156% more area compared to the area covered by a 12.5 km radius isoseismal (1256 km^2 instead of 491 km^2). However, there is only a 75% increase in the maximum frequency value (63 instead of 36). Hence, it should be noted that this increase of frequency values is not distributed uniformly in the study area. For example, in the stepover of the Vallo di Diano and the Val' D' Agri faults, there is almost a ten fold increase (1000%) in frequency values, whereas in other areas such as the hangingwall centres of the Val' D' Agri, the Monte Alpi and the San Gregorio faults there is only a 10-25% increase. Therefore, it is clear that the hazard pattern is modified in a non-spatially uniform way so that the 156% increase of the area affected from a single isoseismal can not be extrapolated uniformly to the entire map.

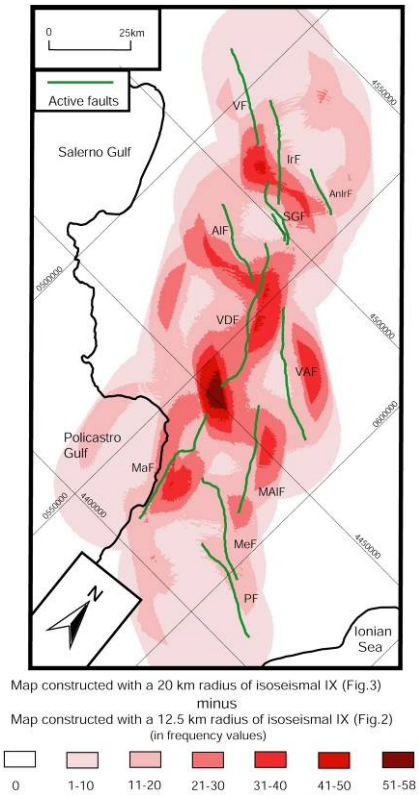

Fig.4: Map showing the frequency differences between Fig. 2 and 3 by subtracting the hazard map constructed with a 12.5 km radius from the hazard map using a 20 km radius of isoseismal IX.

THE ESI 2007

Traditional intensities from which attenuation laws are extracted are based on human parameters. However, when using the effects on man and manmade environment to assess the macroseismic intensity, then intensity will tend to reflect mainly the economic development and the cultural setting of the area that experienced the earthquake, instead of its "strength" (Serva, 1994). The Earthquake Environmental Effects (EEE) are not influenced by human parameters as the traditional intensity scales (MCS, MM, EMS 1992, etc) predominantly imply. The ESI 2007 provides a quantitative analysis and description of the EEE offering a more credible documentation and has already been easily applied in several events worldwide (Lalinde and Sanchez, 2007, Papathanassiou and Pavlides 2007, Serva et al., 2007, Papanikolaou et al., 2009). Among other advantages this scale: i) allows the accurate assessment of intensity in sparsely populated areas, ii) provide a reliable estimation of earthquake size with increasing accuracy towards the highest levels of the scale, where raditional scales saturate and ground effects are the only ones that permit a reliable estimation of earthquake size and iii) allows the comparison among future, recent and historical earthquakes (Michetti et al., 2004).

It is possible that a portion of this variation in the data that introduces the large uncertainty in the attenuation laws stems from the way macroseismic effects have been assessed. Thus, wherever feasible, by reconstructing the macroseismic field of historical earthquakes, through the use of the ESI 2007 scale, uncertainties may be significantly reduced (Papanikolaou et al., 2009).

DISCUSSION

Sensitivity analysis showed that the error introduced by the implied uncertainty in the dimensions of modelled isoseismals is significantly larger than the fault slip-rate error of ± 20 %. This is remarkable because it shows that input parameters such as the isoseismal dimensions which themselves are derived from empirical attenuation relationships, influence the results more significantly than the uncertainty implied from the fault slip-rate data, which govern the earthquake recurrence.

Herein, it should be noted that the complication and uncertainty in earthquake ground motion and consequently in the attenuation/amplification relationships is not only related to the way intensity values have been assigned and isoseismal lines have been drawn, but also emerges from several other factors, which are critical but not accurately known. In particular, uncertainty in the seismic hazard assessment stems from factors such as the fault geometry, slip-rates, the earthquake occurrence model etc. Moreover, there is also an intrinsic variability in seismic shaking caused by basin-edge induced surface waves, focusing and defocusing effects and scattering in general that cannot be reduced in any model (e.g. Field et al., 2000). Therefore, there is little hope that all uncertainties implied by the attenuation/amplification relationship can be fully reduced. However, it is also probable that part of this uncertainty stems out of the intensity evaluation, whereas the application of the ESI 2007 scale could limit the uncertainties.

CONCLUSIONS

Seismic hazard maps are highly sensitive to the attenuation relationship used, forming a major source of uncertainty and in several cases they overshadow all the other factors of uncertainty, even slip-rates which govern the earthquake occurrence.

Earthquake Environmental Effects provide higher objectivity in the process of assigning intensity values, so that the ESI 2007 scale is the best tool to compare recent, historic and pre-historic earthquakes as well as earthquakes from different tectonic settings. A re-appraisal of recent and historical earthquakes so as to constrain the ESI 2007 scale and the extraction of ESI-based attenuation laws, may prove beneficial for the seismic hazard assessment by reducing the present day large uncertainty implied in the attenuation laws.

References

Bolt, B.A., 1999. Earthquakes. W.H. Freeman and Company, New York, 366pp.

Coburn, A. and Spence, R. 2002. Earthquake protection. 420p. John Wiley&Sons, Ltd, West Sussex, England.

D'Amico, V., Albarello, D., & Mantovani, E. (1999). A distribution-Free Analysis of Magnitude-Intensity Relationships: an Application to the Mediterranean Region. Phys. Chem. Earth 24, 517-521.

Grandori, G., Drei, A., Perotti, F. and Tagliani, A. (1991). Macroseismic intensity versus epicentral distance: the case of Central Italy. Tectonophysics 193, 165-171.

Field, E.H., and the SCEC Phase III Working group, (2000). Accounting for site effects in probabilistic seismic hazard analyses of southern California: Overview of the SCEC Phase III report. Bulletin of the Seismological Society of America 90, S1-S31.

Lalinde, C-P. and Sanchez J.J. (2007). Earthquake Environmental Effects in Colombia during the past 35 years: INQUA scale Project. Bulletin of the Seismological Society of America 97, 646-654.

Lee, K., & Kim, J-K. (2002). Intensity Attenuation in the Sino-Korean Craton. Bulletin of the Seismological Society of America 92, 783-793.

Michetti, A.M., Esposito, E., Gurpinar, A., Mohammadioun, B., Mohammadioun, J., Porfido, S., Rogozhin, E., Serva, L., Tatevossian, R., Vittori, E., Audemard, F., Comerci, V., Marco, S., McCaplin, J. and Morner, N.A. (2004). The INQUA scale: An innovative approach for assessing earthquake intensities based on seismically-induced ground effects in natural environment. Sp. paper Mem. Descr. Carta Geologica D' Italia LXVII, pp.118 Roma.

Michetti, A.M., Audemard, F.A. and Marco, S. (2005). Future trends in paleoseismology: Integrated study of the seismic landscape as a vital tool in seismic hazard analyses. Tectonophysics 408, 3-21.

Michetti, A.M. et al. (2007). Intensità scale ESI 2007. In Guerrieri L.and Vittori, E. (Eds): Mem. Descr. Carta Geol. d' Italia 74, Servizio Geologico d' Italia-Dipartimento Difesa del Suolo, APAT, Rome Italy.

Papanikolaou, I. D. (2003). Generation of high-resolution seismic hazard maps in extensional tectonic settings through integration of earthquake geology, fault mechanics theory and GIS techniques. Unpublished PhD thesis, University of London. 437pp.

Papanikolaou, I.D. and Roberts G.P. (2007). Geometry, kinematics and deformation rates along the active normal fault system in the Southern Apennines: implications for fault growth. Journal of Structural Geology 29, 166-188.

Papanikolaou, I.D. Papanikolaou, D.I, and Lekkas, E.L. (2009). Advances and limitations of the environmental seismic intensity scale (ESI 2007) regarding near-field and far-field effects from recent earthquakes in Greece. Implications for the seismic hazard assessment. From Reicherter, K., Michetti, A.M., and Silva, P.G. (eds), Paleoseismology: Historical and Prehistorical Records of Earthquake Ground Effects for Seismic Hazard Assessment. Special Publication of the Geological Society of London 316, 11-30.

Papathanassiou, G. and Pavlides, S. (2007). Using the INQUA scale for the assessment of intensity. Case study on the 2003 Lefkada (Ionian Islands), Greece earthquake. Quaternary International 173-174, 4-14.

Roberts, G.P., Cowie, P., Papanikolaou, I. and Michetti, A.M. (2004). Fault scaling relationships, deformation rates and seismic hazards: An example from the Lazio-Abruzzo Apennines, central Italy. Journal of Structural Geology 26, 377-398.

Serva, L. (1994). Ground effects in the intensity scales. Terra Nova 6, 414-416.

Serva, L., Esposito, E., Guerrieri, L., Porfido, S., Vittori, E. and Commerci, V. (2007). Environmental effects from five historical earthquakes in southern Apennines (Italy) and macroseismic intensity assessment: Contribution to INQUA EEE Scale project. Quaternary International 173-174, 30-44.

Yeats, R.S. and Prentice, C.S. (1996). Introduction to special section: Paleoseismology. Journal of Geophysical Research 101, 5847-5853.

GIS-BASED DATABASE OF EARTHQUAKE-INDUCED LIQUEFACTION MANIFESTATIONS IN BROADER AEGEAN REGION, DALO v1.0

G. Papathanassiou (1) and S. Pavlides (1)

(1) Dpto. Geology, Aristotle University of Thessaloniki, Egnatia str. 54124-Thessaloniki. GREECE. gpapatha@auth.gr

Abstract: *The goal of this study was the development of a database comprised by historical information regarding liquefaction manifestations in Greece and broader Aegean region and the projection of their spatial distribution under a GIS environment. For the achievement of this goal, historical descriptions of earthquake-induced liquefaction were collected and a database was constructed under MsAccess software. Afterwards, specific fields of the dataset, including information of the liquefied sites, were uploaded to internet via Google Earth software, permitting freely interactive navigation through its interface. The GIS-based database can be viewed at the web site http://users.auth.gr/`gpapatha/dalo.html where three maps were uploaded. The outcome of this study can be helpful especially to decision makers and urban planners since it can be used as a screening guide of liquefaction hazard for avoiding in advance liquefaction prone areas.*

Key words*: liquefaction, database, GIS, earthquake*

INTRODUCTION

One of the preliminary studies that should be realized for the assessment of an earthquake-induced ground effects in an area is the investigation of the occurrence of similar phenomena during the past. In order to achieve this goal, scientists search into historical sources for reports describing primary and secondary effects induced by the event. Taking into account these historical documents, the delineation of areas prone to an event is accomplishable, since ground deformations have the tendency to re-occur in the same places. Therefore, landslide inventory maps are compiled in order to define zones prone to sliding while earthquake primary effects such as surface ruptures and secondary effects such as landslides, subsidence and liquefaction can be predicted using information published on seismic catalogues.

In particular, regrading soil liquefaction, Youd (1984) stated that evidence of past liquefaction phenomena indicates a possible high liquefaction hazard because liquefaction tends to recur at the same site, providing site conditions have not changed. Moreover, according to Iwasaki (1986) sites that liquefied during the past earthquakes have high potential to reliquefy by succeeding events. Thus, the identification of past liquefied sites in an area could represent the first step for its classification as liquefaction prone zone.

Following the above statemement and in order to correlate the epicentral distance of the liquefied sites to the earthquake magnitude, several researchers collected data and published preliminary databases of historical liquefaction occurrences. Particularly, Kuribayashi and Tatsuoka (1975) provided data from 32 historic Japanese earthquakes, Papadopoulos and Lefkopoulos (1993) updated the data, collected by Ambraseys (1988), with 30 new cases from Greece while Wakamatsu (1993) supplement the work of Kuribayashi and Tatsuoka (1975) with new data from 67 Japanese earthquakes. The last decade, Galli (2000) and Aydan et al. (2000) re-evaluated seismic parameters of Italian and Turkish earthquakes, respectively, while a dataset consisted of 88 earthquake-induced liquefaction cases from the broader Aegean region was published by Papathanassiou et al. (2005).

The objective of this study is to further develop and extent the dataset of liquefaction-induced ground deformation in Greece (Papathanassiou et al., 2005), and link the provided information to a GIS platform. In order to achieve this goal, the introduced parameters to the dataset were re-evaluated while new data of liquefaction case histories, generated by recent earthquakes were added (ex. June 8th, 2008 event). In addition, all the included information to the previous excel-version (Papathanassiou et al., 2005) was introduced to a new database that was consrtucted under Ms-Access environment, creating the DALOv1.0. Additional info was inserted regarding the quantitative characteristics of the lqiuefied sites. Moreover, the Database of historical Liquefaction Occurrences, DALOv1.0, was linked to a GIS platform, using the free software of Google Earth, for plotting the data. Both the Ms-Access file (.mdb) and the Google earth file (.kmz) of Dalo v1.0 are open- files easily accesable, and can be downloaded from the web site http://users.auth.gr/~gpapatha/dalo.htm.

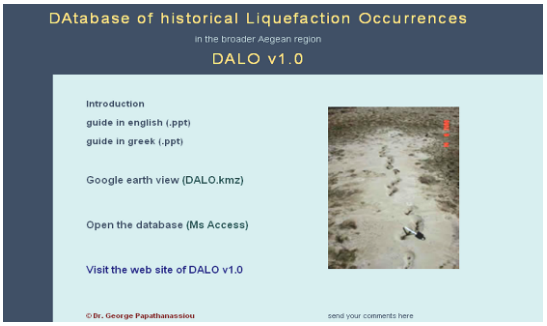

Fig. 1: View of the first page of the CD-ROM, showing the available options

In addition, the Database of historical Liquefaction Occurrences was also released on CD-ROM where via the first page (index.html), several options are offered (Fig. 1). In particular, the files DALO.mdb (Ms-Access), the DALO.kmz (google earth projection) and a guide (Power Point file) regarding the navigation into the database can be downloaded.

DEVELOPMENT OF THE DATABASE

The Database of historical Liquefaction Occurrences DALO v1.0 is an open-access file where information regarding liquefaction-induced ground and/or structural deformations is provided. The first entry in the dataset is in the 16th century AD, particularly the 1509 Instanbul event, while the cut-off data for this project is provided by the earthquake-induced liquefaction of June 8th, 2009 in NW Peloponnesus, Greece. However, it should be mentioned that the oldest events, which were included in the seismic catalogues and correlated to liquefaction-induced failures are the 373 B.C. and 478 A.C events in Eliki and Sistos areas, respectively.

The majority of collected data are correlated to events occurred in the 20th century since almost all the earthquake-induced secondary effects, triggered at that period, were observed and reported. Obviously, the small number of historical descriptions of liquefaction phenomena in the earlier centuries generally is due to the fact that most of the events were not reported. Most of the data (55 cases) in this paper concerning earthquakes that have taken place in Greece while the database contains also 25 cases of earthquake-induced liquefaction from Turkey, 5 cases from Albania and 1 case from Bulgaria and Montenegro, respectively. Moreover, the outcome of this study was that at a total of 321 sites, liquefaction manifestations were reported. In Greece, liquefaction phenomena were triggered more than once mainly at the Gulf of Corinth and at the islands of the Ionian Sea. In the surrounding region, liquefaction phenomena were mainly reported at the coastal zone of the Sea of Marmara (Turkey) and on river deposits in Bulgaria and in Turkey. For a comprehensive description of the dataset, the reader is referred to Papathanassiou et al. (2005).

Tables and forms

The constructed six tables, used for the introduction of data, are cross-linked by key using elements that are common to several tables, such as the earthquake ID, the failure ID, site ID and reference ID. The independent tables include information regarding the earthquake, the liquefied site, the causative fault, the type of failure, the recorded ground motion and the historical source from where the description of liquefaction failures was collected.

In particular, the table Earthquake defines the earthquake characteristics such as magnitude, epicenter's coordinates (latitude, longitude), and the focal depth of the event, date of occurrence, country, and maximum intensity. Information regarding the site, where liquefaction phenomena were reported, is providing by the table Area; including data regarding the epicentral and fault distance, information for the surficial geology of the area, the coordinates of the liquefied site, description and quantitative parameters of the liquefaction-induced failure, map of failures, data provided by borings with in-situ tests (SPT, CPT, Vs) and the recorded values of ground motion. Table Fault provides information regarding the causative fault such as the type of fault (normal, reverse, and strike-slip), length (km), and the average of the horizontal and vertical displacement while in few cases a map of the surface ruptures is included. Table Groundmotion includes the recorded ground motion, providing the values of peak ground acceleration, peak ground velocity and peak ground dispalcement as they were recorded by accelerographs and the relatively time-histories.

Furthermore, the table Reference includes information regarding the source (article) from where the description of liquefaction manifestation was collected such as the author's name, title of paper, journal and year of publication and the table Failures provides the coding of the description of the liquefaction-induced ground and/or structural deformation.

The presentation of the collected data is accomplished using forms that were grouped in two main categories (Fig. 2). The first group contains information of earthquake-induced liquefaction characteristics while the second one includes data regarding the liquefied site. The navigation into the database is accomplished by an introductive form which gives the researcher the opportunity to select one of these two groups for browsing through its contents.

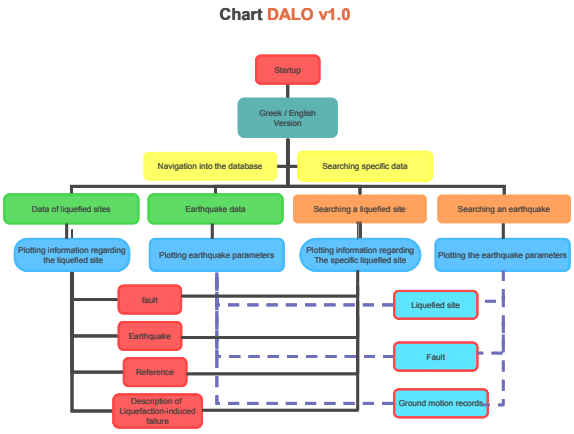

Fig. 2: Chart of the Database of historical Liquefaction Occurrences where the correlations among the introduced elements are shown

Moreover, searching for a specific liquefied site or an earthquake that triggered liquefaction phenomena is now possible and can be achieved by selecting the relatively options, appeared in the menu at the right side of the introductive form (figure 3). This searching is realized using the primary keys of EqID and siteID, respectively and the user can either select an earthquake based on the date of occurrence or a liquefied site based on its location.

The keys located at the left of the form (Fig. 3), lead to the basic forms of DALO v1.0, Area and Earthquake, respectively, where information that were introduced at the tables Earthquake and Area are presented. Moreover, the type of liquefaction-induced failure has been

introduced using a failureID. For viewing the detailed description of the failure, the user should select the key damage presented in the menu located at the bottom of the Area form. Furtermore, the key earthquake leads to a form where the earthquake parameters are presented, the key reference leads to the form Reference and the key fault data leads to the form Fault. In addition, fields presenting the recorded values of ground motion at the liquefied site have been created, despite the fact that in the broader Aegean region such type of data/recordings are few. Moreover, a brief description of the secondary effects that were triggered by the event and a map of the failure's distribution are provided. The keys site, fault and ground motion, located at the bottom of the form, are used for the linking of the earthquake form with the relatively forms where information regarding the liquefied site, the fault and the recorded ground motion were introduced.

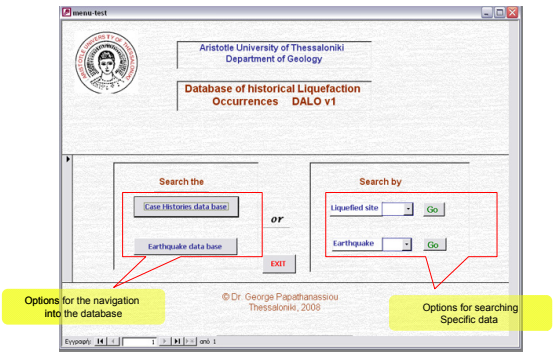

Fig. 3. Introductive form of DALO v1.0

LINKIND DALO v1.0 WITH A GIS PLATFORM

The next step of our study was the development of a user-friendly web interface, where the inserted information to the database DALO v1.0 is presented. In particullar, the goal of this project was to plot the distribution of the liquefied site in conjuction with basic information regarding the liquefaction case histories. In order to achieve this goal, the Google Earth software was selected due to the worldwide availability since it is a free application, it can be easily downloaded from the web site http://earth.google.com/index.html and because it provides the opportunity to compile maps accessible via internet.

The inserted liquefaction case histories to the DALO v1.0 were initially separated into two groups depending on their location; sites in Greece and in surrounding regions, respectively. Afterwards, two maps showing the spatial distribution of liquefaction manifestation in Greece and in surrounding regions were compiled using the employed coordinates to the database (Fig 4). In addition, a map showing the distribution of the epicenters of the earthquake-induced liquefaction was compiled. Thereby, three maps were created using the Google Earth software and grouped as layers into a file of kmz format (Dalo.kmz). This file is included to the CD-ROM while the three compiled maps can be viewed as separate elements at the web site adress of DALO v1.0 (http://users.auth.gr/~gpapatha/dalo.htm).

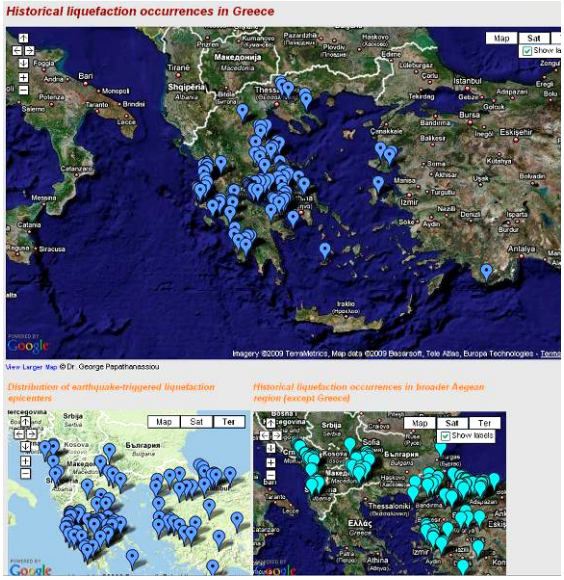

Fig. 4: Home page of DALO v1.0 showing the three compiled maps of liquefied sites in Greece and sourrounding countries

The icons on these maps represent either liquefied sites or epicenters of earthquake-induced liquefaction. In particular, at the map located at the top of Fig. 4, is shown the distribution of liquefied sites in Greece while the map at the right corner includes the liquefied sites in the surrounding countries. At the third map, towards the left corner, the epicenters of the "causative" events are plotted. Information regarding the liquefaction manifestations is accessed by clicking on the icons. In particular, every icon of liquefied sites includes data regarding the date of occurrence, the location and a short description of the liquefaction-induced failures. Moreover, in some case histories, mainly after 1950, photo of the failure is also included. The icons at the map of earthquake epicenters include information regarding the date of occurrence, the historical source and a brief description of the secondary effects that were generated by the shock. In addition, the option See details leads to an html page presenting the whole data that were introduced to the database, for the earthquake.

CONCLUSIONS

The basic aim of this study was the development of a database of historical liquefaction occurrences in the broader Aegean region in a GIS environment. This goal was achieved using the Ms-Access and the Google Earth softwares, respectively. Initially, a digital version of the published by Papathanassiou et al. (2005) database was created where information regarding liquefied sites and parameters of earthquake-induced liquefaction was introduced. Afterwards, basic parameters were linked to a GIS environment using the Google Earth software and three maps regarding the distribution of liquefied sites in Greece, in the broader Aegean region and the distribution of the earthquake-induced liquefaction epicenter's were compiled. These maps that were uploaded to the web address of DALO v1.0, http://users.auth.gr/~gpapatha/dalo.htm included data that were further used for the compilation of the preliminary susceptibility map of Greece (Papathanassiou et al., 2009) in conjuction to the distribution of the quaternary deposits and the seismic hazard map as they

were published by IGME (1983) and EAK (2000), respectively. The next step of our project is to include information relating to earthquake-induced landslides and evaluate the macroseismic intensity based on ESI 2007 scale in every site.

References

Ambraseys, N. N, (1988). Engineering seismology International Journal Earthquake Engineering Structural Dynamics, 17, 1-105

Aydan, O, Ulusay, R, Kumsar, H, Tuncay, E, (2000). Site investigation and Engineering evaluation of the Duzce-Bolu earthquake of November 12, 1999, Turkish Earthquake Foundation, Instanbul. Report No. TDV/DR 09-51, 307pp.

EAK, (2000). Greek Seismic Code, OASP, Athens, 72 pp and 7 Appendixes.

Galli, P. (2000). New empirical relationships between magnitude and distance for Liquefaction, Tectonophysics, 324, 169-187.

IGME, (1983). Geological map of Greece, compiled by Bornovas I, ZRodoyianni-Tsiabaou Th., Athens

Iwasaki, T, (1986). Soil liquefaction studies in Japan: state-of-the-art, Soil dynamics and Earthquake Engineering, 5 (1), 1-71

Kuribayashi, E, Tatsuoka, F, (1975). Brief review of liquefaction during earthquakes in Japan, Soils and foundations 15, 81-92.

Papadopoulos, A.G, Lefkopoulos, G, (1993). Magnitude – distance relation for liquefaction in soil from earthquakes, Bulletin of Seismological. Society America, 83 (3), 925-938.

Papathanassiou, G, Pavlides, S, Christaras, B, Pitilakis, K , (2005). Liquefaction case histories and empirical relations of earthquake magnitude versus distance from the broader Aegean Region, Journal of Geodynamics, 40, 257-278

Papathanasiou, G, Pavlides, S, Valkaniotis, S, Chatzipetros, A, (2009). Towards the compilation of liquefaction susceptibility map of Greece, Seismological Research Letters 80 (2), 316.

Youd, T.L (1984). Recurrence of liquefaction at the same site, Proceedings of the 8th World Conference on Earthquake Engineering, 3, 231-238

Wakamatsu, K, (1993). History of Soil liquefaction in Japan and Assessment of Liquefaction Potential based on Geomorphology, PhD Thesis, Waseda University Tokyo, Japan, 245pp.

ROMAN, VISIGOTHIC AND ISLAMIC EVIDENCE OF EARTHQUAKES RECORDED IN THE ARCHAEOLOGICAL SITE OF "EL TOLMO DE MINATEDA" (PREBETIC ZONE, SOUTHEAST OF SPAIN)

M.A. Rodríguez-Pascua (1), L. Abad Casal (2), R. Pérez-López (1), B. Gamo Parra (3), P.G. Silva (4), V.H. Garduño-Monroy (5), J.L. Giner-Robles (6), I. Israde-Alcántara (5), J. Bischoff (7) and J.P. Calvo (1)

(1) Departamento de Investigación y Prospectiva Geocientífica, Instituto Geológico y Minero de España. C/ Ríos Rosas, 23. 28003-Madrid. SPAIN. ma.rodriguez@igme.es, r.perez@igme.es , jose.calvo@igme.es
(2) Universidad de Alicante. Facultad de Filosofía y Letras. Dpto. de Prehistoria, Arqueología, Filología Griega y Filología Latina. Carretera Sant Vicent del Raspeig s/n. 03690 Sant Vicent del Raspeig – Alicante. SPAIN. E-mail: lorenzo.abad@ua.es
(3) Museo de Albacete. Junta de Comunidades de Castilla-La Mancha. Parque de Abelardo Sánchez, s/n. 02002-Albacete. SPAIN. bgamo@jccm.es
(4) Dpto. Geología Universidad Salamanca, Escuela Politécnica Superior de Ávila, 05003-Ávila. SPAIN. pgsilva@usal.es
(5) Universidad Michoacana. Morelia. Michoacán, 58060 MEXICO. E-mail: vgmonroy@zeus.umich.mx, aisrade@zeus.umich.mx
(6) Dpto. Geología. Facultad de Ciencias. Universidad Autónoma de Madrid. Cantoblanco. Tres Cantos. Madrid. SPAIN. E-mail: jlginer@gmail.es
(7) Laboratory of Geochronology. United States Geological Survey. 345 Middlefield Road, MS 211, Menlo Park, CA 94025. USA. E-mail: jbischoff@usgs.gov

Abstract: *The archaeological site of "El Tolmo de Minateda" is located within the Albacete province (SE of Spain) and shows a continuous time record of ancient civilizations from 3500 yr BP onwards. However, three temporal gaps were identified in this archaeological record, all of them in relationship with a sudden and unclear abandonment of the city (Centuries 1st, 7th and 9th). The archaeological evidence supports the possibility that moderate strong earthquakes were the cause of such abandonments: oriented columns fallen, collapsed walls and arches, abandonment of irrigation systems and fresh-water supplies, crashed pottery, etc. Despite of the scarce of the instrumental seismicity and a few historical chronicles, paleoseismic studies performed in the neighbouring zone (Hellín) suggest the presence of closer seismic sources as faults affecting Quaternary alluvial, lacustrine deposits and colluviums. In this work, we propose the possibility that three moderate (M 6) earthquakes devastated the ancient Roman city of Ilunum (Century 1st AD), the Visigothic city of Elo (Century 7th AD) and the Islamic city of Madinat Iyih (Century 9thAD), all of them the same place: "El Tolmo de Minateda".*

Key words: *Roman, Visigothic, Islamic, earthquake, "Tolmo de Minateda", Southeast of Spain.*

INTRODUCTION

"El Tolmo de Minateda" is one of the best representative archaeological sites within the Albacete province (SE Spain), with a well-preserved record for the last c.a. 3500 years BP. During this epoch, various cultures and ancients civilizations were settled in this site, in parallelism with the historical periods of Spain: Iberians, Romans, Byzantines, Muslims and Christians. The "El Tolmo de Minateda" represents a strategically geographical point between the Iberian Meseta and the Mediterranean zone, and this explains the ongoing and well-preserved archaeological record. During this time of almost 3500 yrs, "El Tolmo" shows three abandonments and destructions in three different ages: Roman (Century 1st-2th AD), Visigoth (Century 7th AD) and Islamic (Century 9th AD). The seismic activity of the active faults in this zone could affect the archaeological site and produce the lack of record in these three historic periods.

GEOGRAPHYCAL AND GEOLOGICAL SEETING

"El Tolmo de Minateda" is located between the villages of Cordovilla and Agramón, at the southernmost area of the Albacete province (SE of Spain) (Fig. 1). This archaeological site appears close to the Betic Cordillera and is related with two major strike-slip faults, Pozohondo and Lietor (Fig. 1B). Both structures are active faults trending NW-SE, affecting Quaternary alluvial and colluviums deposits and with a trace longitude about 90 km approximately (Rodríguez-Pascua et al., 2003).

ARCHAEOSEISMIC EVIDENCE

The archaeological record of this ancient city supports evidence for earthquake damage linked to three periods of city abandonment and destruction, including oriented collapse of walls, watchtowers and columns, oriented cracking of walls and column drums, as well as "in situ" broken pottery, abrupt abandonment of kilns, and anomalous sedimentary infilling of canals and water supply facilities. Additionally, large scale rock landslides containing Visigothic carved tombs are also apparently associated with these episodes, constituting one of the few geo-archaeological earthquake ground effects reported in this zone.

Earthquake evidence during the roman period (Century 1st-2th AD)

In the High Roman Empire this zone was moderately occupied by people, although some evidence supports the idea that the principal city of Ilunum was deserted (Roman name of the "El Tolmo").

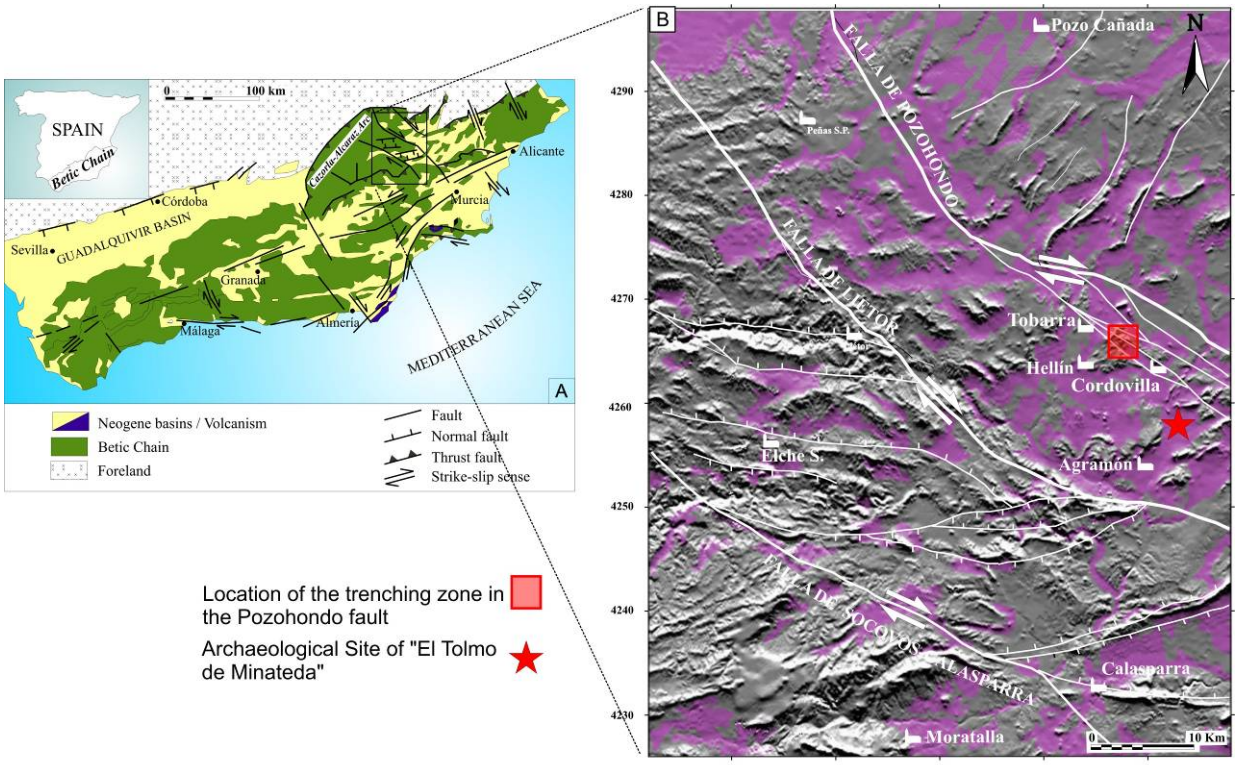

Fig. 1: (A) Geographic location of the studied area. (B) Detailed structural map of the archaeological site of the ancient city "Tolmo de Minateda" (red star) (Albacete province). Socovos-Calasparra, Lietor and Pozohondo faults represent major strike-slip faults with palaeoseismic evidence of recent activity and the location of the trenches in the Pozohondo Fault (dashed square).

Evidence of this abandonment includes the partial detritical infilling of the fresh-water supply and irrigation canals in the Zama town (close to Ilunum), as well as the increasing population dispersion outwards from the site (Abad-Casal, 1998). As potential coseismic effects, both the solid defensive wall and the watchtowers in the entrance of de city collapsed (Fig. 2), and it is possible identify penetrative fractures across the in-situ remained stone blocks.

Fig. 2: Collapsed defensive wall dated in the Visigothic period.

Earthquake evidence during the visigothic period (Century 7th AD)

During the middle Visigothic Period (Century 7th AD), there is a lack of archaeological record associated with an unexplained abandonment of El Tolmo, (named as Elo during this period) (Abad-Casal et al., 1998)). Associated to this abandonment and as potential coseismic effects, the defensive wall at the "El Reguerón", as well as part of the City Wall collapsed. The watchtowers in the entrance of de city collapsed (Fig. 2), and it is possible identify penetrative fractures across the in situ remained stone blocks. Furthermore, this collapse was dipping not towards the main dip slope direction. This wall was founded on the solid Miocene sandstone, being the main way trough the city gate and which displays a continuous deep wheel-tracks, carved on the sandstone substratum.

During the Visigoth period, a Basilica was built at the top of the town (Abad-Casal et al., 2000). The Basilica was also damaged, coeval with the wall collapse, showing fallen columns with an approximate N-S trending, and dipping towards the north. The arches of the main nave of the basilica and the principal vault was also collapsed (Fig. 3). Moreover, the key stone of the arch appeared in a vertical position and there are cracks dipping 45º and affecting the Basilica pillars. These types of cracks have been cited as possible coseismic effects by other works (e.g. Silva et al., 2009).

Fig. 3: Collapsed arch of the Visigothic Basilica.

Earthquake evidence during the islamic period (Century 9th AD)

In this period, a part of the city was reconstructed on the Visigothic ruins and by the Moslem and was called as Madinat Iyih (Gutiérrez-Lloret, 2000). The eventual abandonment of the city was inferred from the lack of any archaeological record between the 9th and 10th centuries AD. Moreover, multiple pottery artifacts were destroyed by walls collapses in the interior of the buildings (Fig.4). In fact, the whole of the ceramic district collapsed during this period.

Fig. 4: Fragmented in situ Islamic pottery.

Historical documents suggest possible seismic geological effects affecting to the ground water level. Carmona González (1998) cited these documents and told that the springs of the "El Tolmo" were dried by the Christians and appeared 50 km southward from this site. This effect is common during an earthquake, amply documented and registered in the ESI-07 scale (Michetti et al., 2007; Silva et al., 2008).

Other geological effects of this possible earthquake are the large landslides affecting anthropomorphic tombs carved by the Visigoths (Fig. 5). This large landslide corresponds to the south part of the butte, and is more recent than those preserved in the northern slope connected with the Visigothic episode of destruction. The wasted sandstone blocks appear weakly weathered and uncovered by colluviums. Scars on the cliff are fresh scarps, with nearly vertical free-faces displaying a very poor lichen evolution. Individual mobilized blocks can reach dimensions of about 4000 m^3, and the total mobilized material at the northern slope comprises 500 m^3.

In order to illustrate the landsliding susceptibility of the butte cliffs, it can be said that some historical reports seem to indicate that landslide scars were presumably reactivated as far-field effects from the well-known Lisbon earthquake (1755 AD). An historic chronicle from the close village of Agramon (Fig. 1B for location) literally reported: "*de una montaña se desprendió mucha parte*" (a large part of a mountain collapsed; Martínez-Solares, 2001), and there are many more historic reports for the 1755 event mentioning similar gravitational processes in this zone.

PALEOSEISMIC EVIDENCE

Several palaeoseismological studies close to the "El Tolmo" (within the 15 km of radius) revealed active seismic sources in the surroundings (Rodríguez-Pascua et al., 2008; Pérez-López et al., 2009; Rodríguez-Pascua et al., 2009). The closest seismic source corresponds to the Pozohondo Fault, a NW-SE trending strike-slip and ca 90 km long (see Fig.1 for location). In detail, this fault exhibits an active segment, the Tobarra-Cordovilla segment (15 km length), which shows a complex graben basin affecting Quaternary lacustrine deposits and displaying well-preserved coseismic fault scarps with large cracks of metric scale affecting recent soils.

Furthermore, the present landscape along this fault segment is controlled by active faulting, with the occurrence of a dammed lake caused by the obstruction of the drainage by Late Pleistocene to Holocene surface ruptures. Rodríguez-Pascua et al. (2008) obtained a relative dating of the youngest fault scarp using the scarp diffusion equation, calibrated for the semi-arid climate of SE Spain (Pérez-López et al., 2007), ranging between the ages 3 BC and 920 AD, and with the highest likelihood about 500-700 AD. Recent trench digging in this fault shows the last important earthquake aged by radiocarbon in between the Century 1st – 5th AD.

Fig. 5: Rock fall whit anthropomorphic tombs

CONCLUSIONS

Fig. 6 resumes the tentative proposal of the historic evolution of "EL Tolmo de Minateda" from archaeoseismic studies. Three possible earthquakes affected this archaeological site. The first earthquake occurred in the High Roman Empire (Centuries 1st-2th AD).

The city collapsed and it was abandoned. Paleoseismological studies in the Pozohondo Fault (10 km northward) show one earthquake of 6<M<7, dated in the Century 1st AD by radiocarbon measurements. We propose this ancient earthquake as a possible cause for the massive desertion of Ilunum. The second one occurred during the Visigothic period (Century 7th AD), the city of Elo was destroyed and showing documented damage: oriented fallen columns, collapsed arches, cracks dipping 45º in the masonry blocks, etc. The last earthquake probably occurred during the Islamic period (Centuries 9th). In this case the archaeoseismological evidences are based on the collapse of the city of Madinat Iyih (pottery destroyed in situ, etc.) and secondary earthquake ground effects as large landslide affecting anthropomorphic tombs of Visigoth era (*post-quem*). The assumed damage of the "El Tolmo" from the last two earthquakes, suggests that the epicentre could be located close to the ancient city but, until now, there is not paleoseismological evidence for the seismic source.

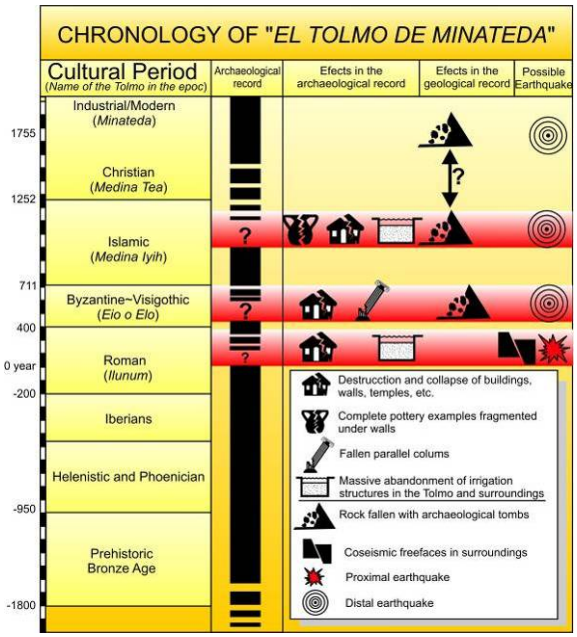

Fig. 6: Chronological archaeoseismic scheme proposed for the ancient city of "Tolmo de Minateda"

Acknowledgements: This work is supported by the Spanish Projects: ACTISIS CGL2006-05001/BTE and ACI2008-0726. It is a contribution to the IGCP 567Project.

References

Abad-Casal, L., Gutiérrez-Lloret, S., Sanz-Gamo, R. (1998). El Tolmo de Minateda, una historia de tres mil quinientos años. Ed. Junta de Comunidades de Castilla – La Mancha. Toledo. 161 p.

Abad-Casal, L., Gutiérrez-Lloret, S. y Gamo-Parras, B. (2000). La basílica y el baptisterio del Tolmo de Minateda (Hellín, Albacete). Archivo Español de Arqueología, 73, 193-221.

Carmona González, A. (1998). El noroeste murciano en época árabe. Miscelanea Medieval Murciana. Vol XXI-XXII. Años 1997-1998, 59-70.

Gutiérrez-Lloret, S. (2000). La identificación de Madinat Iyih y su relación con la sede episcopal Elotana. Nuevas perspectivas sobre viejos problemas. Scripta in Honorem E. A. Llobregat, Alicante, 481-501.

Martínez-Solares, J. M. (2001). Los efectos en España del Terremoto de Lisboa (1 de noviembre de 1755). Ed. Dirección General del Instituto Geográfico Nacional. Madrid. 756 p.

Michetti, A.M. et al. (2007). Intensity Scale ESI-2007. Memorie Descriptive Della Carta Geologica D'Italia, 74. APAT, SystemCart Srl, Roma, Italia.

Pérez-López, R., M.A. Rodríguez-Pascua, J.L Giner-Robles, J.P. Calvo, V.H. Garduño-Monroy, I. Israde-Alcantara and J. Bischoff (2007). Calibration of the diffusion constant (K_0) for dating coseismic fault scarps by using the diffusion equation: application to the Alboraj earthquake, Albacete, SE Spain. In: Contribuciones al Estudio del Periodo Cuaternario. J. Lario y P.G. Silva, eds., 161-162. AEQUA, Avila (España).

Pérez-López R., M. A. Rodríguez-Pascua, J. L. Giner-Robles, J. J. Martínez-Díaz, A. Marcos-Nuez, P. G. Silva, M. Bejar and J. P. Calvo (2009). Speleoseismology and palaeoseismicity of Benis Cave (Murcia, SE Spain): coseismic effects of the 1999 Mula earthquake (mb 4.8). Geological Society, London, Special Publications, 316, 207-216.

Rodríguez-Pascua, M.A., De Vicente, G., Calvo, J.P., Pérez-López, R. (2003). Similarities between recent seismic activity and paleoseismites during the Late Miocene in the External Betic Chain: relationship by "b" value and fractal dimension. Journal of Structural Geology, 25, 749–763.

Rodríguez-Pascua, M. A., Pérez-López, R., Calvo, J. P., y García del Cura, M. A. (2008). Recent seismogenic fault activity in a Late Quaternary closed-lake graben basin (Albacete, SE Spain). Geomorphology, 102, 169–178.

Rodríguez-Pascua, M.A., Bischoff, J. et al. (2009). Estimation of the tectonic slip-rate from Quaternary lacustrine facies within the intraplate Albacete province (SE of Spain). Sedimentology (accepted)

Silva, P.G., M.A. Rodríguez-Pascua, R. Pérez-López, T. Bardají, J. Lario, P. Alfaro, J.J. Martínez-Díaz, K. Reicherter, J. Giménez, J. Giner, J.M. Azañón, J.L. Goy, C. Zazo (2008): Catalogación de los efectos geológicos y ambientales de los terremotos en España en la Escala ESI-2007 y su aplicación a los estudios paleosismológicos. Geotemas, 10, 318.

Silva, P.G., Reicherter, K., Grützner, C., Bardají, T., Lario, J., Goy, J.L., Zazo, C. and Becker-Heidmann, P. (2009): Surface and subsurface palaeoseismic records at the ancient Roman city of Baelo Claudia and the Bolonia Bay area, Cádiz (south Spain). Geological Society, London, Special Publications, 316, 93-121.

A COMPREHENSIVE CLASSIFICATION OF EARTHQUAKE ARCHAEOLOGICAL EFFECTS (EAE) FOR STRUCTURAL STRAIN ANALYSIS IN ARCHAEOSEISMOLOGY

M. A. Rodríguez-Pascua (1), R. Pérez-López (1), J.L. Giner-Robles (2), P. G. Silva (3), V.H. Garduño-Monroy (4) and K. Reicherter (5)

(1) Departamento de Investigación y Prospectiva Geocientífica, Instituto Geológico y Minero de España. C/ Ríos Rosas, 23. 28003-Madrid. SPAIN. ma.rodriguez@igme.es, r.perez@igme.es
(2) Dpto. Geología. Facultad de Ciencias. Universidad Autónoma de Madrid. Cantoblanco. Tres Cantos. Madrid. SPAIN. jlginer@gmail.es
(3) Dpto. Geología Universidad Salamanca, Escuela Politécnica Superior de Ávila, 05003-Ávila. SPAIN. E-mail: pgsilva@usal.es
(4) Universidad Michoacana. Morelia. Michoacán, 58060 MEXICO. vgmonroy@zeus.umich.mx
(5) Lehr-und Forschungsgebiet Neotektonik und Georisiken. RWTH Aachen University. Lochnerstr. 4-20. 52056 Aachen, GERMANY. k.reicherter@nug.rwth-aachen.de

Abstract: *One of the key arguments in Archaeoseismology consists to identify how quantity of the observed damage is related with ancient earthquakes. Abandonments, ruins or wars are general causes assumed by archaeologists and natural disasters are rarely considered. In this work, we propose a comprehensive classification of Earthquakes Archaeological Effects (EAE) with the aim of carry out geological structural analysis. The objective of this classification is to recognize the tectonic strain field responsible of the buildings damage and the relationship with the potential earthquake or related-earthquake natural disaster. Several examples at Baelo Claudia (South of Spain) of such EAEs are shown.*

Key words: *earthquake archaeological effect, strain field, structural geology, archaeoseismology.*

INTRODUCTION

Strain structures detected in archaeological sites affecting to buildings, monuments, defensive constructions etc., could have different origins, for example seismic origin, intervening slope process, unstable soils, differential overburden during the burial process, or simply collapsed remains due to eventual building abandonment or war destruction, etc. For this reason, it is necessary identify the trigger mechanism of the damaged structure to assign a seismic origin. There are various works devoted to this question (e.g. Stiros, 1996, Nur and Cline, 2000, Bottari, 2003, Kovach, 2004, and Nur and Burgess, 2008). These authors developed a compilation of criteria for identifying earthquake occurrence from archaeological data. With this aim, we propose a preliminary classification of earthquake archaeological effects (EAE) based on the type of EAE (coseismic, postseismic), description (impact, wall tilting, floor folding, etc.) and the location of the effects (related to the geologic effects or to the fabric of the building) (Fig.1). The relevance of this classification is for the reason that, once the EAE is recognized, it is possible to analyze the strain field related with the seismic source by applying the classical structural techniques on strain analysis (both ductile and brittle analyses).

The anisotropy inherent in the seismic wave (i.e. the direction of the seismic ray propagation), generates a strain field constrained by the seismic source parameters: distance from the archaeological site to the epicentre, magnitude of the earthquake, hypocentral depth, type of arrival wave, etc. This fact implicates that the ductile and brittle structures affecting monuments, walls and buildings could be analysed using the classic structural techniques developed in geology. The results obtained from this analyses, allow us to reconstruct the coseismic strain ellipse, oriented according to the type of the earthquake (normal, reverse or strike-slip) and defined by the principal strain axes: *ey* (maximum horizontal shortening), *ex* (minimum horizontal shortening) and *ez* (vertical axis).

CLASSIFICATION OF EAE

The interest of in the characterization of EAE is to recognize archaeoseismic damage due earthquake phenomena from other damage assigned to ruins, wars or abandonment, among others. Furthermore, a good establishment of potential EAE in a particular archaeological site supports indirect information of the seismic source for earthquake hazard assessment.

Following the recent classification of earthquake environmental effects (EEE) established in the ESI-07 Intensity Scale (Michetti, et al., 2007) we propose a classification of EAE based on strain structures due to "coseismic effects" (direct or primary effects) and structures generated by "postseismic effects" (indirect or secondary effects) (Fig. 1). This subdivision separates effects related with the seismic source from those effects "as a consequence" of a large earthquake affecting a populated site.

PRIMARY COSEISMIC EFFECTS

We have divided the primary coseismic effects in (1) *geological effects* and (2) *building fabric effects* (Fig. 1).

Geological effects

These effects are well described from the macroseismic scale of environmental earthquake effect (ESI07, Michetti et al., 2007). This scale separates primary effects as fault scarp, surface rupture, and tectonic uplift/subsidence from secondary effects as liquefaction, landslides, tsunamis, etc.

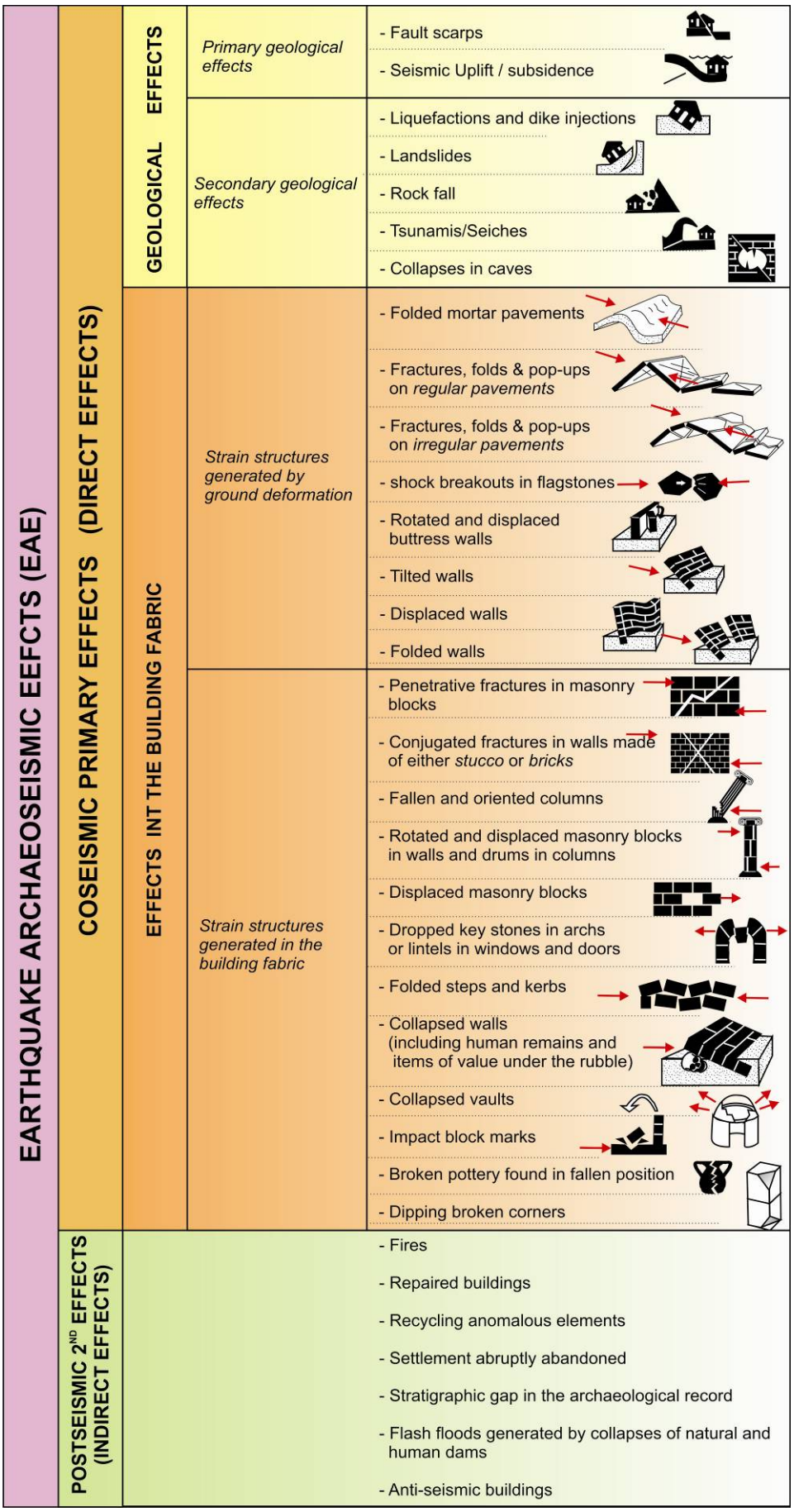

Fig. 1: A comprehensive classification of Earthquake Archaeological Effects (EAE), based on primary and secondary geological effects of earthquakes (After ESI07 macroseismic scale, Michetti et al., 2007) and building damage. Red arrows indicate the possible seismic wave orientation. See text for further explanation.

Geological effects recognized as EAE are referred a fault planes crossing the ancient town, soil displacements due to seismic shaking, city damage for landslides and rockfalls, liquefaction generating tilted monuments, remains buried by seismites and tsunamites within the archaeological stratigraphic sections. This kind of effects is the traditionally cited ones in the still young archaeoseismological literature.

Building fabric coseismic effects

These effects indicate direct damage on buildings associated to ground deformation and/or seismic waves. First of all, a complete understanding of the type of construction (masonry, mortar type, column type, arch construction etc.) used by ancient cultures in each particular archaeological site is needed. This architectural knowledge allows recognizing those potential buildings to find archaeoseismic effects and discards those other ones damaged by secondary effects.

Fig. 2: Kink folds in an irregular pavement. Decumanus Maximum in the Roman City of Baelo Claudia (Cadiz, Spain)

In this case the differentiation of damage produced by (a) natural ground instability or (b) seismic ground shacking is a starting key point. Some good examples of probable ground shacking deformations are folded pavements (Fig. 2), shocks and oriented fracturing in pavement flagstones, folded mortar floors, pop up-like structures on pavements, titled and folded masonry walls, etc. (Fig. 3). Other deformations exclusively affecting to the building fabrics will be: penetrative fractures on masonry blocks, displaced or differentially rotated arches (Fig. 4) or, broken pottery found in fallen position, etc.

SECONDARY POSTSEISMIC EFFECTS

Other common deformations observed in present damaged archaeological remains are typically linked to the abandonment and eventual ruin of the site. Roof and vault collapses of habited houses commonly trigger fires by the burning of the wood fabric of most of the pre-modern roofs. Flash flood events triggered by earthquake severe damage on ancient earth dams is also a source of information but, complicate for decoding and interpretation. Eventually the development of ancient antiseismic either structures or building designs (Fig. 5) are a key feature talking about previous strong seismic shaking events. Destructive horizons within the geoarchaeological record tell about histories of city reconstruction. In this case the identification of demolition horizons linked to city reconstruction after severe earthquake damage is also a common feature in archaeoseismological sites. In the same way the analyses of recycled and reutilized architectural elements also can indicate the nature and age of city reconstruction.

Fig. 3: Tilted wall in the defensive wall of the Roman City of Baelo Claudia (Cadiz, Spain)

Eventually, the burial history of the archaeological site can introduce complementary deformation and/or amplify the existing ones. An analysis of the present geomorphology of the area, operating geomorphic process during burial and the urban geology of the studied site are necessary to understand the existing deformation, if deformation is coeval and finite.

All the aforementioned structures of deformation are listed in the table of Figure 1, which illustrate most of the deformational structures we can see today in archaeological sites formerly affected by at least one earthquake. As in classical palaeoseismic analysis the building fabric coseismic effects has to be ascribed to a particular geoarchaeological horizon, which will be the earthquake horizon. In this sense before the structural analysis of building deformation we have to collect the complete geoarchaeological history of the city.

The simplest analysis of orientation of many of the building fabric effects can help to put constrains on the directivity or not of related ground deformation (e.g. Silva et al., 2009). Consistently oriented building deformation will indicate the sense of ground movement, but also to differentiate it for other non-oriented deformations caused by other phenomena. The determination of the geographical quadrant in which presumably a seismic source (NE, SW, etc.) was located for an historic, non-documented, event is a quality step provided by the archaeoseismology.

CONCLUSIONS: THE GEOLOGICAL STRUCTURAL ANALYSIS OF DAMAGED STRUCTURES

The application of classical techniques on geological structural analysis for ductile and brittle deformations affecting buildings is a second quality step. The analysis of the strain may allow the calculation of the strain ellipsoid associated with the arrival of seismic wave. For the interpretation of the results derived from structural analysis is important the previous classification of the structures following the aforementioned EAE guidelines.

Fig. 4: Slipped lintel in a window (window head) of the Forum of the Roman City of Baelo Claudia (Cadiz, Spain)

The strain solutions obtained from the structural analysis of damaged building and pavement fabrics can be compared to those obtained from instrumental seismicity, Quaternary tectonic structures around the studied zones, etc. The similarity between the strain ellipsoid derived by pure geological analysis and by archaeoseismological analysis will point to the seismic origin of the analysed structures, although strongly depending on the time/date of the deformation. This should be established as a standard to be applied in archaeological sites to determine possible seismic deformation.

Therefore the application of the classification EAE proposed in this paper will help to formalize archaeoseismological investigations, putting some quality steps to undertake a more comprehensive parameterization of ancient earthquakes.

Fig. 5: Arch of the main entrance of the defensive wall in Carmona (Seville, Spain) Islamic Period

Acknowledgements: This work is supported by the Spanish Projects: ACTISIS CGL2006-05001/BTE and ACI2008-0726. It is a contribution to the IGCP 567Project.

References

Bottari, C. (2003). Ancient constructions as markers of tectonic deformation and of strong seismic motions. Proceedings, 11th FIG Symposium on Deformation Measurements, Santorini, Greece, 2003.

Kovach, R. L. (2004). Early earthquakes of the Americas. Cambridge University Press. Cambridge. 268 p.

Michetti, A.M. et al. (2007). Intensity Scale ESI-2007. Memorie Descriptive Della Carta Geologica D'Italia, 74. APAT, SystemCart Srl, Roma, Italia.

Nur, A. and Burgess, D. (2008). Apocalypse: Earthquakes, Archaeology and the Wrath of God. Princeton University Press. Princeton and Oxford. 309 p.

Nur, Amos and Cline, Eric H., (2000). Poseidon's horses: Plate tectonics and earthquakes storms in the Late Bronze Age Aegean and Eastern Mediterranean. Journal of Archaeology Science, 27, 43-63.

Silva, P.G., Reicherter, K., Grützner, C., Bardají, T., Lario, J., Goy, J.L., Zazo, C. and Becker-Heidmann, P. (2009). Surface and subsurface palaeoseismic records at the ancient Roman city of Baelo Claudia and the Bolonia Bay area, Cádiz (south Spain). Geological Society of London, Special Publication, 316: 93-121.

Stiros, S. C. (1996). Identification of Earthquakes from Archaeological Data: Methodology, Criteria and Limitations. In Stiros, S. and Jones, R., eds., Archaeoseismology. Fitch Laboratory Occasional Paper 7. British School at Athens: 129-152.

PRELIMINARY RESULTS OF STATIC AND DYNAMIC RECONSTRUCTION OF GÜEVÉJAR LANDSLIDE (GRANADA, SPAIN) DURING 1755 LISBON AND 1884 ANDALUSIAN EARTHQUAKES

M.J. Rodríguez Peces (1), J. García-Mayordomo (2), J.M. Azañón (1, 3), J.M. Insua Arévalo (4) and J. Jiménez Pintor (5)

(1) Departamento de Geodinámica. Facultad de Ciencias. Universidad de Granada, C/Fuentenueva, s/n. 18002-Granada. SPAIN. marpeces@ugr.es
(2) Instituto Geológico y Minero. Investigación en Peligrosidad y Riesgos Geológicos. C/La Calera, 1 (Tres Cantos). 28760-Madrid. SPAIN. julian.garcia@igme.es
(3) Instituto Andaluz de Ciencias de la Tierra (UGR-CSIC), Granada, SPAIN. jazanon@ugr.es
(4) Departamento de Geodinámica. Universidad Complutense de Madrid. Ciudad Universitaria, s/n. 28040-Madrid, SPAIN. insuarev@geo.ucm.es
(5) Departamento de Ingeniería del Terreno, Ayesa. Avda. Marie Curie, s/n. 41092-Sevilla. SPAIN. jjpintor@ayesa.es

Abstract: *In this work, we present preliminary results of a reconstruction of the Güevéjar landslide (Granada, south Spain) during the 1755 Lisbon and 1884 Andalusian earthquakes. We perform a back-analysis of the landslide to estimate the static safety factor and the critical acceleration previous to both earthquakes and for the present-day situation. We obtain a critical intensity of V which matches the minimum intensity grade required to trigger coherent landslides. We conclude that the Güevéjar landslide is stable at present-day conditions but its reactivation is expected in case of an earthquake with a similar intensity to that during the 1884 Andalusian earthquake (I=VI-VII) or larger.*

Key words*: earthquake, Güevéjar, landslide, newmark*

INTRODUCTION

Earthquake-triggered landslides can be analyzed to estimate some characteristic of paleo-earthquakes which triggered them. Such paleoseismic landslide studies thus can help to reconstruct the seismic shaking history of a site or a region (Jibson, 1996).

The Güevéjar landslide is located near the Güevéjar and Nívar villages about 10 km to the north of Granada in the northern edge of the Granada Basin (south Spain). This great rotational landslide was caused by the 1755 Lisbon earthquake with epicentral intensity of XI-XII and magnitude 8.5 (Martínez Solares and López Arroyo, 2004) and was reactivated later by the 1884 Andalusian (or Arenas del Rey) earthquake with epicentral intensity of X and magnitud 6.5-7.0 (Muñoz and Udías, 1981). In both events, the Güevéjar village was destroyed but it was reconstructed in 1887 at its actual location outside the landslide area.

In this work, we show preliminary results of a reconstruction of the Güevéjar landslide during the 1755 and 1884 earthquakes. We based the analysis on previous works (Sanz, 1992, Jiménez Pintor, 2006; Jiménez Pintor and Azor, 2006) and field data to perform a back-analysis of Güevéjar landslide to estimate the static safety factor and the critical acceleration for both earthquakes and for the present-day situation.

GEOLOGY

The sedimentary materials outcropping in the study area belong to the continental infilling of the Granada Basin, one of the Neogene-Quaternary intramontane depressions located in the central part of the Betic Cordillera. The lithologies identified in the landslide area are from bottom to top: a) lignite-bearing marls (upper Turolian); b) clays, silts and conglomerates (Pliocene); c) marls and oncolitic limestones (Pleistocene); d) travertines (Pleistocene). The materials affected by the rupture surface are the lignite-bearing marls and the clays, silts and conglomerates.

A detailed geological map of the Güevéjar landslide can be found in Jiménez Pintor and Azor (2006). We used this map and field data to perform our slope model fitting the thickness and distribution of the sediments, the location of the water table and the main scarps of the 1755 and 1884 landslides.

METHODOLOGY

The back-analysis of the landslide is made with the 2D slope stability analysis software Slide (Rocscience Inc., 2003). This program calculates safety factors for circular and non-circular slope failure surfaces based on a number of widely used limit equilibrium techniques.

We firstly derived a slope profile from a 10 m x 10 m pixel-size digital elevation model at Güevéjar landslide location. This slope profile represents the maximum path of the landslide and we used previous works data obtained from similar landslide materials to set their strength parameters (Azañón et al., 2006). In our slope model, we have obtained the safety factor after each earthquake setting a non-circular slope failure surface and estimating a equivalent peak ground acceleration (PGA) using different Intensity-PGA relationships for the Mediterranean zone. Then, we removed the seismic acceleration to obtain the static safety factor previous to the each earthquake. The minimum seismic acceleration

to overcome shear resistance and initiate the displacement of the landslide is calculated by:

$$a_c = (SF - 1)g \sin(\alpha) \qquad [1]$$

where a_c is the critical acceleration (in gravity units, 1g = 9.81 m/s^2), g is the gravity acceleration, SF is the static safety factor and α is the thrust angle. For rotational movement, Newmark (1965) showed that the thrust angle is the angle between the vertical and a line segment connecting the center of gravity of the landslide mass and the center of the slip circle.

THE 1755 GÜEVÉJAR LANDSLIDE

Pre-1755 topography (Fig. 1) was reconstructed using a GIS. We subtracted the contour lines of the actual landslide area and interpolated the previous topography. The 1755 Lisbon earthquake was felt in Güevéjar with a intensity of VI. We estimated a equivalent peak ground acceleration (PGA) of 0.06-0.10g. The safety factor obtained based on Morgenstern-Price limit equilibrium method is close to one (SF=0.98). This value is agree with the observation that the 1755 landslide did not have much displacement. Removing the seismic acceleration, we obtained a static safety factor previous to the earthquake of 1.26. The thrust angle obtained is 12º and the critical acceleration is 0.05g which is equivalent to a critical intensity of V which is one intensity grade lower that caused by 1755 Lisbon earthquake. This critical intensity value is in agreement with the minimum intensity (I=V) required to trigger coherent landslides as reported in historical earthquakes (Keefer, 1984; Keefer, 2003).

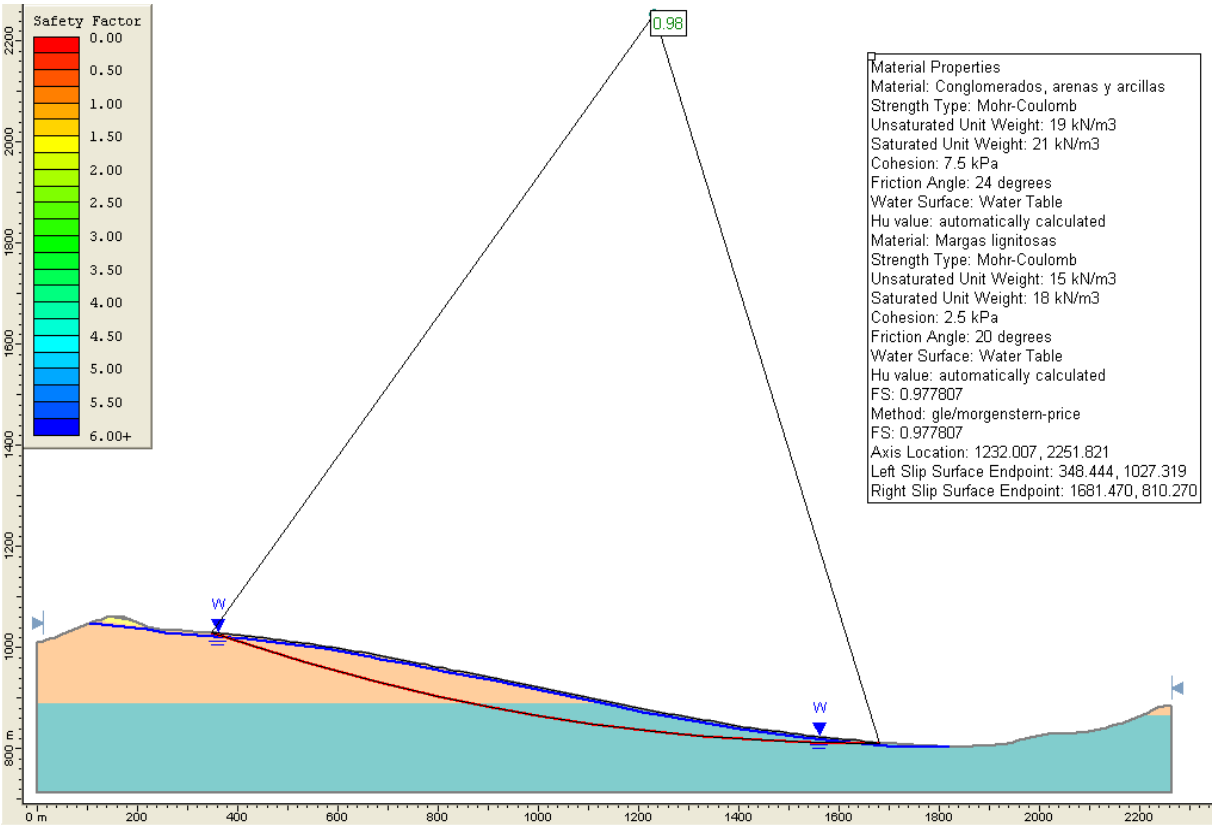

Fig. 1: Idealized cross-section of the 1755 landslide in saturated conditions. Soil properties are shown for each designated layer in the computer model. Obtained safety factor are also shown.

THE 1884 GÜEVÉJAR LANDSLIDE

We have considered that the pre-1884 topography (Fig. 2) is similar to the pre-1755 topography at the scale of the model and the results will not be affected too much. The 1884 Andalusian earthquake was felt in Güevéjar with a intensity of VII (Muñoz and Udías, 1981). In this case, estimated PGA values are 0.11-0.18g. The safety factor obtained using the Morgenstern-Price method is lower than the previous case (SF=0.89). This value is coherent with the fact that the 1884 landslide mass had more displacement. Removing the seismic acceleration, we obtained a static safety factor previous to the earthquake of 1.40. The thrust angle obtained is 14º and the critical acceleration is 0.10g which is equivalent to a critical intensity of VI which is one intensity grade lower than caused by 1884 Andalusian earthquake.

THE PRESENT-DAY GÜEVÉJAR LANDSLIDE

We have used the present-day topography (Fig. 3) and the 1884 slope surface rupture. The static safety factor obtained is stable (SF=1.91). Therefore, the landslide is estable in both dry and saturated conditions. However, ocurrence of small secondary landslides in the toe of the landslide seems possible, however these are not further analyzed in this work.

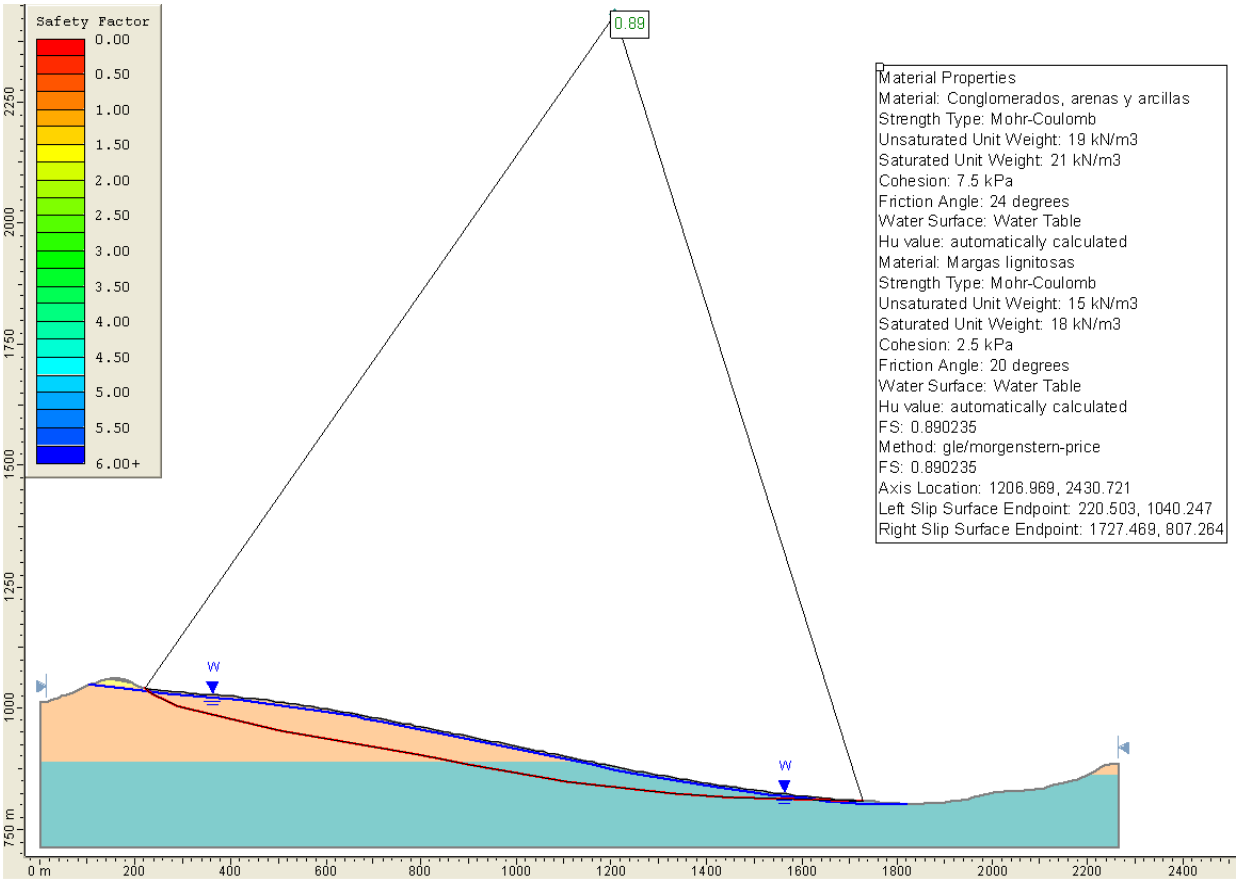

Fig. 2: Idealized cross-section of the 1884 landslide in saturated conditions. Soil properties are shown for each designated layer in the computer model. Obtained safety factor are also shown.

The thrust angle obtained is 8º and the critical acceleration is 0.13g which is equivalent to a critical intensity of VI-VII which is similar to the intensity grade caused by 1884 Andalusian earthquake.

CONCLUSIONS

We have developed a preliminary reconstruction of the Güevéjar landslide during the 1755 Lisbon and 1884 Andalusian earthquakes. Future investigations with a more accurate landslide model based on real geotechnical data and fitting the failure surface with geophysical and borehole data will give further insight into the failure mechanisms.

Taking into account the preliminar nature of the results, we can conclude the Güevéjar landslide is stable at present-day conditions even though we consider a complete saturation of the slope. The reactivation of Güevéjar landslide is only expected in case of an earthquake with a similar intensity to that during the 1884 Andalusian earthquake (I=VI-VII) or larger.

Acknowledgements: This study was supported by research project TOPOIBERIA CONSOLIDER-INGENIO2010 CSD2006-00041 of Spanish Ministry of Science and Innovation, research project MMA083/2007 of Spanish Ministry of Environment and research project CGL2008-03249/BTE of Spanish Ministry of Science and Innovation.

References

Azañón, J.M., Azor, A., Cardenal Escarcena, J.F., Delgado García, J., Delgado Marchal, J., Gómez Molina, A., López Chicano, M., López Sánchez, J.M., Mallorqui Franquet, J.J., Martín Rosales, W., Mata de Castro, E., Mateos Riuz, R., Nieto García, F., Peña Ruano, J.A., Pérez García, J.L., Puerma Castillo, M., Rodríguez Fernández, J., Teixidó Ullod, T., Tomás Jover, R., Tsige Aga, M., Yesares García, J. (2006). Estudio sobre la predicción y mitigación de movimientos de ladera en vías de comunicación estratégicas de la Junta de Andalucía. Informe final. Instituto Andaluz de Ciencias de la Tierra, CSIC-UGR (Ed.), Granada (Spain).

Jibson, R.W. (1996). Use of landslides for paleoseismic analysis. Engineering Geology, 43, 291-323.

Jiménez Pintor, J. El deslizamiento de Güevéjar. M.Sc. Thesis in Engineering Geology. Universidad de Granada, 85 pp.

Jiménez Pintor, J. and Azor, A. (2006). El Deslizamiento de Güevéjar (provincia de Granada): un caso de inestabilidad de laderas inducida por sismos. Geogaceta, 40, 287-290.

Keefer, D.K (1984). Landslides caused by earthquakes. Geological Society of America Bulletin, 95, 406-421.

Keefer, D.K. (2002). Investigating landslides caused by earthquakes - A historical review. Surveys in Geophysics, 23, 473-510.

Martínez Solares, J.M. and López Arroyo, A. (2004). The great historical 1755 earthquake. Effects and damage in Spain. Journal of Seismology, 8, 275-294.

Muñoz, D. and Udías, A. (1981). Estudio de los parámetros y serie de replicas del terremoto de Andalucía del 25 de Diciembre de 1884 y la sismicidad de la región de Granada-Málaga. In: El Terremoto de Andalucía de 25 de Diciembre de 1884. Instituto Geográfico Nacional (Ed.), Madrid (Spain), 95-139.

Newmark, N.M. (1965). Effects of earthquakes on dams and embankments. Géotechnique, 15, 139-160.

Sanz Pérez, E. (1992). El deslizamiento de ladera de Güevéjar (Granada) durante los terremotos de Lisboa (1755) y Andalucía (1884). III Simposio Nacional sobre Taludes y Laderas Inestables. La Coruña (Spain), 195-203.

Rocscience Inc. (2003). Slide 5.0 User's Guide. Part I. 199 pp.

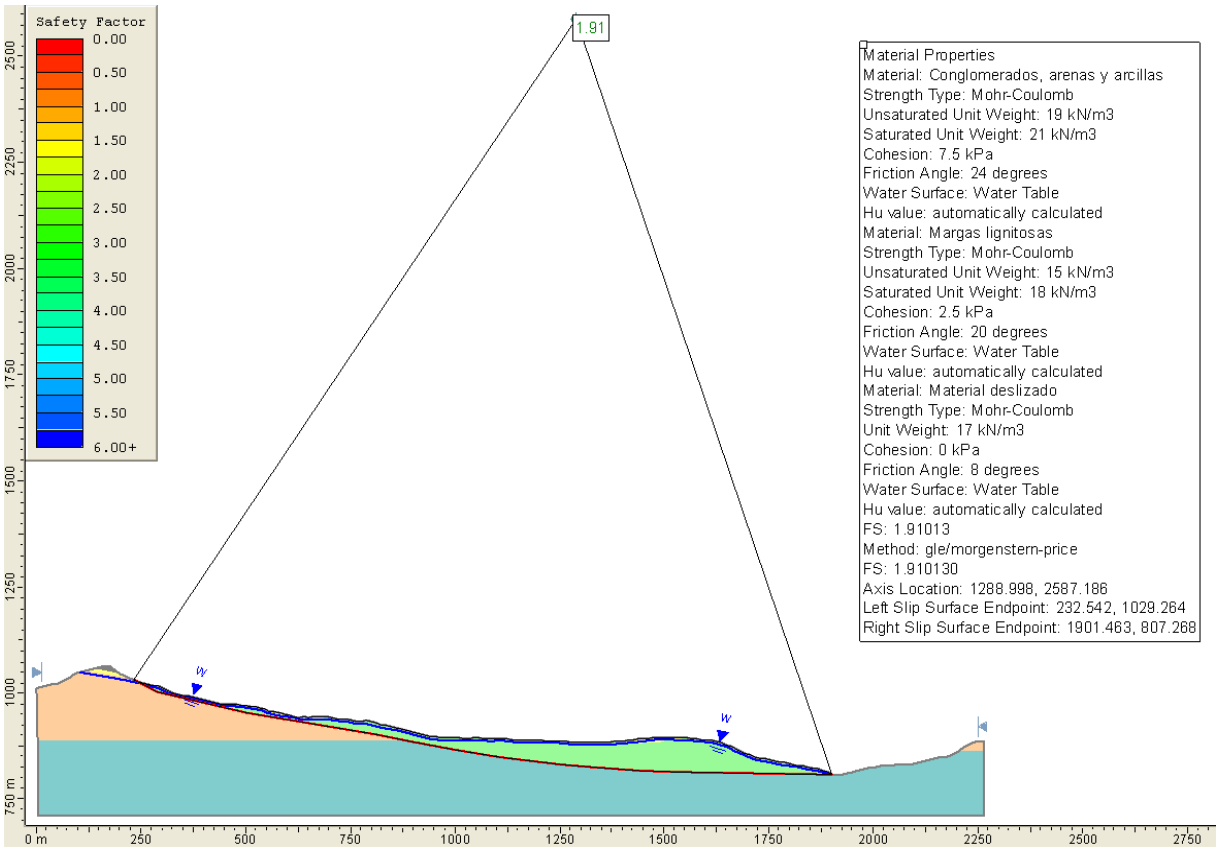

Fig. 3: Idealized cross-section of the present-day landslide in saturated conditions. Soil properties are shown for each designated layer in the computer model. Obtained static safety factor are also shown.

GEOMARKERS OF AD 1755 TSUNAMI ON GIBRALTAR

J. Rodríguez-Vidal (1), L.M. Cáceres (1), F. Ruiz (1), M. Abad (1), D. Fa (2), G. Finlayson (2), J.C. Finlayson (2) and G. Bailey (3)

(1) Dpto. Geodinámica y Paleontología, Facultad de CC. Experimentales, Campus del Carmen, Universidad de Huelva, Avda. Tres de Marzo s/n, 21071 Huelva. SPAIN. jrvidal@uhu.es
(2) The Gibraltar Museum, 18-20 Bomb House Lane, Gibraltar. U.K.
(3) Department of Archaeology, University of York, The King's Manor, York YO1 7EP, UK.

Abstract: *Evidence of the 1755 tsunami along the coast of Gibraltar is registered at three different heights, all being formed by the same type of accretions produced by the re-deposition of earlier sediments. Along a shallow sandy shore, the tsunami wave reached a height of 2m, whereas along steep, cliff-lined shores it surpassed 5m. Submerged platforms were affected by erosional backwash to a depth of 20m. The tsunamigenic sediments exhibit a bimodal granulometry, mainly composed of sands and bioclasts with a coarser fraction composed of marine shells faunal remains, together with stone fragments derived from the rocky substrate.*

Key words*: Lisbon tsunami,* ^{14}*C date, run-up, Gibraltar.*

INTRODUCTION

Although the Atlantic part of European coasts is at considerably less seismic risk than that of the Pacific or Indian Oceans, there is historical and geological evidence of seismogenic tsunamis that affected Western Europe. The most active zone is situated to the SW of Portugal (Cape São Vicente), apparently the source of the last and most destructive tsunami – that known as "1755 Lisbon Earthquake", M_w 8.5-9.0. The historical evidence and sediments that this tsunami has left on the Portuguese and Spanish coasts can serve as an example to test the use of such indicators in the localisation of its epicentral zone. The greater or lesser precision in the search will depend on the quality and reliability of the markers used and on the suitability of the coastal outcrop.

The effects of this tsunami upon the coastline of the Strait of Gibraltar have not been studied, but we do have historical records (James, 1771) of its impact upon the harbour and shipping at Gibraltar.

In this study we aim to provide an initial contribution to the historical and geological evidences of this tsunami and of its effects upon various coastlines (low-lying and sandy, rocky and cliff-lined shores), as well as submerged zones around the Rock of Gibraltar.

DISCUSSION

A historical account of the effects of the Great Tsunami of Lisbon on the coast of Gibraltar is provided by Lieutenant T. James (1771) in his book on the coasts of the Strait and its surrounding regions: "This earthquake, perceived at Gibraltar, was in the forenoon on the first of November one thousand seven hundred and fifty-five, it began with a trembling which lasted half a minute, then a violent shock, and went off gradually as it began; the sea rose every fifteen minutes six feet eight inches, and fell so low that boats and all the small craft near the shore were left aground, as were numbers of small fish; and on the third, fourth and fifth of the said month, small shocks were felt" (G in Fig.1). This means that in the harbour area and possibly within the adjoining Bay, the height of the tsunami wave reaching the coast was only 2 m a.s.l. (solid line in Fig. 1).

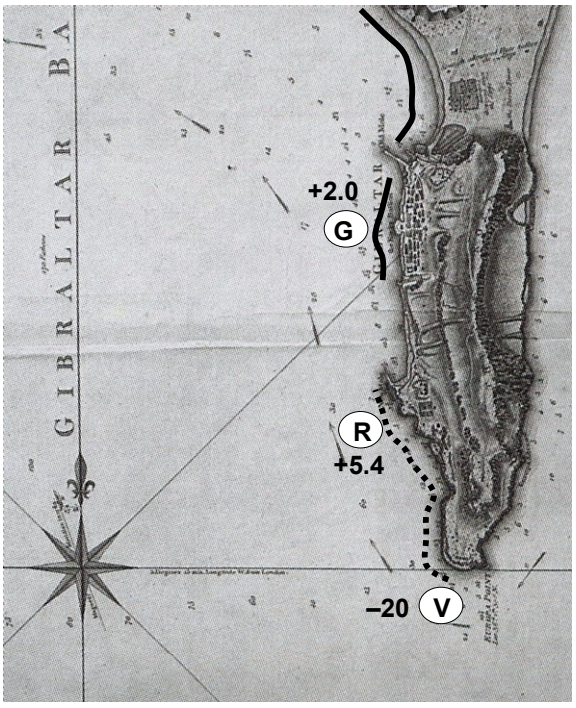

Fig. 1: Original cartography of Gibraltar published in 1738-1750. G and solid line. Gibraltar harbour, R. Rosia Bay, dotted line. Rocky and cliffed coast, V. Vladi's Reef. Number is the topographic location of tsunami record in meters.

On the rocky outcrop which forms the southern flank of Rosia Bay and upon which sits Parsons Lodge Battery, a number of south-oriented open-crevices are visible (Fig. 2), where we have discovered sedimentary accumulations

associated with various tsunamis (< 3000 cal BP, unpublished), one of which is that of AD 1755 (R in Fig. 1).

These deposits exhibit a bimodal granulometry and are composed of siliceous sands and bioclasts with gastropod and bivalve shells and other marine faunal remains, together with angular dolomite fragments derived from the faces of the crevice. Depending on age, deposits are more or less compacted, cemented or covered with a thin speleothem layer.

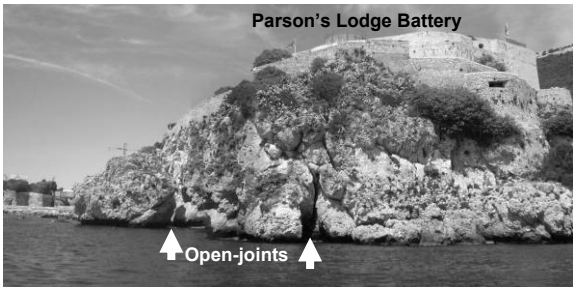

Fig. 2: Rosia Bay site (R in Fig. 1) and its Parson's Lodge southern flank. Extensional open-joints filled by tsunami sediments

Although this coastal zone was artificially scarped by the British Military for defensive reasons, this did not take place until shortly after the tsunami: "… on the SW, side of Rosia Bay, was discovered, in the year 1769, a huge mass of petrifactions of a very singular kind. The workmen who were employed in scarping the face of the rock to render it less accessible, after having wrought, by mining, through about ten feet of solid limestone came to a vast congeries of bones, blended and consolidated together in a confused manner with limestone of various sorts, freestones, spars, selenites, stalactites and calcareous crystallizations and incrustations …" (after White, 1913). It was this engineering activity that led to the discovery of the historic Quaternary fossil "Rosia Bay bone breccia".

The highest a.s.l. evidence of the tsunami sediment can be found at 5.4 m above Gibraltar Chart datum and they consist of disarticulated valves of *Chlamys* sp., which have yielded a ^{14}C date (360-72 cal BP, Table 1), and is indicative of the minimum height reached by the tsunami wave when it impacted the cliff below Parsons Lodge.

A less evident register of the effects of the tsunami, but for that no less significant, can be found 20 m below the surface of the sea, south of Europa Point, on a submerged platform (Vladi's Flat). Along its southern border a small rocky ridge (Vladi's Reef) can be seen with a number of small caves opening to the north. As from 2005, these caves have been the focus of underwater archaeological excavations (GIBRAMAR Project).

The caves and cavities along Vladi's Reef have acted as traps for disturbed sediments stemming from the plain immediately to their north. Their interior is covered with beach-worn cobbles with encrusted marine organisms, which have provided a date range of 667-541 cal BP (Table 1), a period during which the strong marine currents and storms in the area only allowed for the persistence of rolled pebbles and boulders. Covering these stones, and presently forming the sea bed, is a fine sandy deposit, with numerous shell fragments that date to 360-179 cal BP. This last deposit (VLA-047) appears to have formed from the physical translocation of sediments from Vladi's Flats due to the backwash of AD 1755 tsunami.

Table 1: Database of ^{14}C marine samples and calibrated ages. Laboratory: (CNA) Centro Nacional de Aceleradores, Sevilla, Spain, (OxA) Oxford Radiocarbon Accelerator Unit, U.K. (a) AMS analysis, (b) Marine04 calibration curve (Hughen et al., 2004) and the program Calib rev. 5.0.1 (Stuiver and Reimer (1993), ΔR= –135±20 ^{14}C years (Soares and Dias, 2006; Soares, 2008).

Field code	Lab. code	^{14}C age [a]	δ^{13}C‰	2 σ range cal BP age [b]
GB0804	CNA136	460 ± 45	1.4	72 – 360
VLA047	OxA15864	491 ± 22	0.9	179 – 360
VLA044	OxA15824	907± 27	1.4	541 – 667

The VLA-047 sample (Table 1), although dominated by sand, contains a high proportion of gravels which are interpreted as high-energy deposit. The larger, coarser fraction is composed of bioclastic fragments and small subangular dolomite pebbles. Both of these have been affected by bioerosion (*Entobia*) and the development of a localised ferruginous coating. The relatively low proportion of silts and clays in the sample (21%) indicate that the sediment was deposited in a high-energy environment, where finer sediments were transported away from the site but coarser grains steadily accumulated.

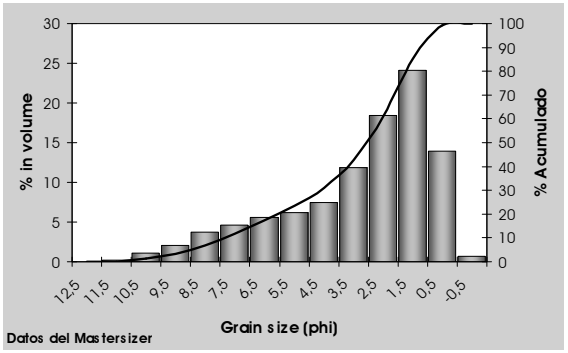

Fig. 3: Sediment granulometry of the sample VLA-047 from Vladi's Reef (V in Fig. 1), 20 m below sea level.

Regarding the faunistic component, macrofauna are very abundant, especially bivalves (fragments of *Acanthocardia tuberculata, Venus pollastra* and *Venerupis romboides*), and gastropods (*Hinia reticulata*, *Bittium reticulatum* and *Natica alderi*); as well as cheilostomatid bryozoans, echinoderm spines (probably cidaroidans), crab claws and fragments of balanid cirripeds. In contrast, the microfauna are not particularly abundant, with an almost total absence of planktonic foraminifera. Amongst those present, fragments of miliolids are common and occasional specimens of *Ammonia beccarii, Elphidium crispum* and *Planorbulina mediterranensis* were found. Some ostracod species present were *Bairdia mediterranea* (frequent), *Loxoconcha rhomboidea* (rare), *Xestoleberis dispar* (rare), *Xestoleberis communis* (rare), *Urocythereis oblonga* (frequent) and *Aurila convexa* (rare). The macrofaunal and microfaunal assemblages found correspond to, and can be broadly associated with,

well-oxygenated coastal or shallow water environments that are adjacent to an open marine platform.
A similar deposit was reported by Abrantes et al. (2005) in the mouth of the River Tagus in Lisbon, being equally ascribed to the AD 1755 tsunami. The energy of this tsunami estimated to have eroded 160–355 years of the sedimentary marine record and instantaneously deposited a 19 cm sediment bed consisting of a lower layer of silt sized heavy mineral particles, followed by a coarser layer composed of reworked shell fragments.

When compared to other Atlantic coastal sectors where wave heights exceeded 15 m, the evidences presented for this tsunami along the Gibraltar coast indicate that, at least in this area, the wave energy was superficially attenuated. Nevertheless, this energy left its most visible mark along the rocky coasts, where the onslaught of the wave reached above 5 m, and the significant erosive power of the currents caused by the submarine backwash reached depths of 20 m.

Acknowledgements: Supported by two Spanish I+D+I projects (CTM2006-06722/MAR and CGL2006-01412/BTE) and AHRC Research Grants (AH/E009409/1).

References

Abrantes, F., Lebreiro, S., Gil, I., Rodrigues, T., Bartels-Jónsdóttir, H., Oliveira, P., Kissel, C., Grimalt, J.O. (2005). Shallow marine sediment cores record climate variability and earthquake activity off Lisbon (Portugal) for the last 2000 years. Quaternary Science Reviews, 24, 2477–2494.

Hughen, K.A., Baillie, M.G., Bard, E., Beck, J.W., Bertrand, C.J.H., Blackwell, P.G., Buck, C.E., Burr, G.S., Cutler, K.B., Damon, P.E., Edwards, R.L., Fairbanks, R.G., Friedrich, M., Guilderson, T.P., Kromer, B., McCormac, G., Manning, S., Bronk Ramsey, C., Reimer, P.J., Reimer, R.W., Remmele, S., Southon, J.R., Stuiver, M., Talamo, S., Taylor, F.W., Van der Plicht, J., Weyhenmeyer, C.E. (2004). Marine04: marine radiocarbon age calibration, 0-26 cal kyr BP. Radiocarbon, 46, 1059-1086.

James, T, (1771). The History of the Herculean Straits, now called The Straits of Gibraltar: including those ports of Spain and Barbary that lies contiguous thereto, London, vol.2, 414 pp.

Soares, A.M.M. (2008). Radiocarbon dating of marine samples from Gulf of Cadiz. Abstracts Annual Conference IGCP 495, Faro (Portugal), 6-7.

Soares, A.M.M., Dias, J.M.A. (2006). Coastal upwelling and radiocarbon-evidence for temporal fluctuations in ocean reservoir effect off Portugal during the Holocene. Radiocarbon, 48, 45-60.

Stuiver, M., Reimer, P.J. (1993). Extended ^{14}C data base and revised CALIB 3.0 ^{14}C age calibration. Radiocarbon, 35, 215-230.

White, J. (1913). Fauna Calpensis (A Natural History of Gibraltar and Southern Spain). Edited by W.H. Mullens, The Selborne Society, London, 24 pp.

THE IMPORTANT KEY FACTOR OF PALEOTECTONIC STUDIES ON SEISMIC HAZARD EVALUATION OF MOSHAMPA DAM AND HYDROPOWER PLANT

H. Samari (1) and A. Mobini (2)

(1) Islamic Azad University- Mahallat Branch, Geology Group, Mahallat, Markazi province, IRAN. Hsamari@yahoo.com
(2) Tamavan Consulting Engineers, No.1, 2nd Alley, Kaj St., Fatemi St., Tehran 1414763442, IRAN. mobini@tamavan.com

Abstract: *Moshampa dam and hydropower plant project site is located within the northwest of Central Iran zone. Paleotectonics studies reveals that NE1 fault in northeast of the site, (38.5km) is the most important seismic source. No seismic data of it's activity has been found, but based on paleotectonic evidence it is considered as an active fault. This fault, after a gap distance through its two terminals in northwest and southeast, is connected to two active faults. Tectonics and paleotectonic studies reveal that, the NE1 fault as a middle fault segment belongs to the large paleobasement fault that marks the borders of Alborz, Azerbaijan and central Iran seismotectonic provinces. Seismotectonic data show both of two segments of both sides of this basement fault have been active for several times in 20th century. In spite of historical and 20th century seismic gap in the middle segment of this basement fault (NE1), its tectonic setting indicates, that probably some earthquakes will occur around NE1 fault in the future.*

Key words*: Paleotectonics, Basement fault, Central Iran, Moshampa*

INTRODUCTION

As it was mentioned earlier, the Moshampa dam and power plant is located at the northwest of the Central Iran structural zone. Based on seismicity, geology and topography conditions, the type of dam is earth rock fill with central clay core. The height of dam is 124m and reservoir normal water volume is about 700MCM.The powerhouse is located in the vicinity of dam in the left abutment which its net head is 88.78m, its total discharge is 142.24m^3/s, total power out put is about 110MW (4*27.5) and total energy is about 170GWH.

The Alborz, Azerbaijan and Zagros structural zones respectively situated at the northwest, north and southwest of the site. The closest active fault to the project site is the NE1 fault segment, 13.7km to the northeast. Due to the importance of the site, the studied area encompasses a radius of 300 kilometers. First, the tectonic unit of the Central Iran is described and in the next section, its seismic characteristics are briefly explained.

TECTONICS OF THE CENTRAL IRAN

Central Iran zone, which has a triangular shape, is one of the main tectonic units in Iran. It is considered as one of the largest and most complex geological zones. This zone comprises of the oldest metamorphic rocks (Precambrian) up to the recent active and semi-active volcanoes. In fact, this region could be regarded as the oldest location of the continent within Iran, which has experienced numerous geological events. The thickness of the Early Precambrian rocks outcrop at Central Iran is more than ten thousand meters, which itself is formed from the erosion of the old igneous rocks. This series is severely metamorphosed by the Katangan orogeny movements and has established the Central Iran platform. In turn, this platform is covered by the continental sediments or shallow marine Late Precambrian to Triassic sediments, which is better known as the platform cover. However, the epirogenic movement that usually causes vertical earth movements along the faults also causes the paraconformity and facies change Moreover, evaporate sediments were sometimes created in Neo-Proterozoic and Paleozoic. The crystalline basement of Central Iran and its platform cover has been cut by large faults since Paleozoic. Based on stratigraphy gaps in some regions, the basement has experienced continuous vertical movements that have had some influence in the formation of Tertiary volcanoes.

SEISMOTECTONICS OF THE CENTRAL IRAN

The Central Iran is situated between two Zagros & Alborz-Kopedagh thrusted and folded mountain belts, which is trapped between the Eurasian plate in the north and the Arabian plate in the south due to the Arabian plate movement to the northeast. Thus, it is under a compressive regime in direction of N20E, where the old Central Iran structures during the various orogenic phases are reactivated and with their subsequent movements are triggering earthquakes. The seismotectonic studies of the Central Iran reveal the following interesting and important facts:

- The distribution of earthquake epicenters are not homogeneous (mostly in northwest, west and northeast)
- The earthquakes of the Central Iran have higher magnitudes in comparison to the other parts of Iran
- Focal depths of earthquakes in Central Iran are shallower than in other parts of Iran
- The return period of the earthquakes in Central Iran is longer
- The activity of the thrust faults as well as the deformation of the earth surface is the influential factor in seismic activities of the Central Iran.

MAIN ACTIVE FAULTS IN THE STUDIED AREA

According to the small-scale seismotectonic maps, the active faults at the periphery of the site are concentrated in two locations. The first group is within a 50 kilometer

radius and the second is within a 50–100 kilometer radius (Fig. 1). The NE1 fault, 13.7 kilometers northeast of the site and Takht-e-Solayman fault, 43.5 kilometers southwest of the site are examples of the first group. The small-scale seismotectonic maps do not indicate another active fault within a 50-kilometer radius of the site. The Soltaniyeh and Zanjan faults in the southeast, Masouleh and Sangavar faults in the northeast, northern and southern Bozqoush faults in the north and the North Tabriz fault in the northwest of the site area are amongst the faults of the second group. It is important to point out that the seismic activities of these faults based on the historical and 20th century earthquakes are confirmed.

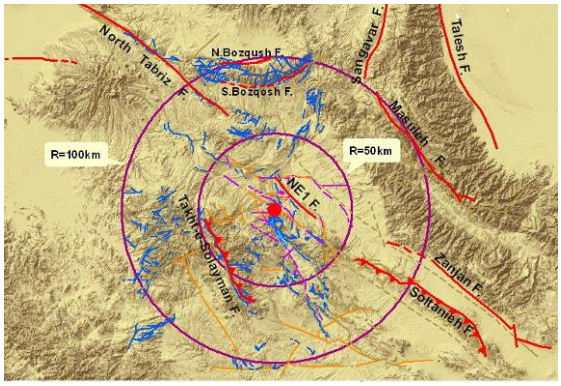

Fig. 1: Faults location at the periphery of the site on the Land Sat satellite image

The first group faults are within a 50-kilometer radius of the site and if they are active, with the considerable length and appropriate distance to the site could impose considerable acceleration to the dam and the power plant structure. Due to the importance of this issue, the field visits are conducted with the aid of large-scale geological maps and satellite images in order to detect other faults within the 50-kilometer radius of the site. These studies resulted in identification of several other faults with the maximum lengths of 2 to 3 kilometers. They could be considered as minor faults. They mostly have general northwest–southeast and northeast-southwest trends complying with the direction of main stress in the region. However, minor faults with other trends were also observed.

Among the mentioned minor faults at the vicinity of the Moshampa dam and power plant, four faults are relevant. They have almost parallel trends extending from northwest to the southeast at the southwest of NE1 fault and at the northeast of the Moshampa project site. These faults are called NE2, NE3 and NE4, respectively based on their distance from the dam site (Fig. 2). As it was mentioned earlier, NE1 fault is located at the northeast of the site. It is along the direction of North Tabriz and Soltaniyeh faults with the length of 38.7km. On the small-scale seismotectonic maps of Iran, this fault has been shown without any specific name. The NE2 fault is located 4 kilometers from the site, which according to these studies, has a length of 25km. The layers displacement along this fault is quite visible on the satellite images. The NE3 fault is 1000 meters northeast of the site with a length of 16.5 km. The NE4 fault is 350 meters downstream of the site with a length of 2km. The field visits indicate that NE3 & NE4 faults have affected the layers of upper red formation.

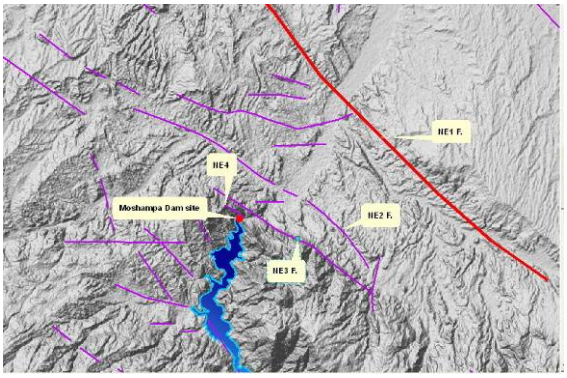

Fig. 2: A view of the faults at the vicinity of the site

SEISMOTECTONIC SPECIFICATION OF THE STUDIED AREA

The conducted seismotectonic studies point out that the region around the Moshampa site (within 40-kilometer radius) had no seismic activity during the 20th century and the earlier centuries. This conclusion is based on the data collected from several seismic centers as ISC, IIEES, and BHRC. Albeit a great number of these earthquakes occurred in the Azerbaijan, Alborz and northwestern part of Zagros seismotectonic zones within the 300-kilometer radius of the site. In light of the seismic characteristics of the Central Iran seismotectonic zone, the return period of earthquakes in this province is higher and its magnitude is greater than the Zagros & Alborz–Kopehdagh zones. The above-mentioned fact is to be taken into account, although the project site and its 40-kilometer radius have never possessed seismic activity during the 20th century and the centuries before that. Due to the seismic nature of Central Iran, it is possible that the region could experience strong earthquakes in near future. Thus, for the estimation of maximum seismic parameters of earth movement, all the parameters related to the site are taken into consideration.

The statistical study of the earthquakes around the Moshampa site indicates the followings:

- 34 historical earthquakes with the magnitude of over Ms5 are recorded at the periphery of the site, which the closest took place (50 kilometers away) in 1880 with the magnitude of Ms5.6.
- During 1900 to 1962, only 12 earthquakes with the magnitude of over Ms5 occurred within a 300-kilometer radius.
- The greatest earthquake took place in 1990 with the magnitude of Ms7.4 at a distance of 158 kilometers from the site.
- The closest earthquake (in the 20th century) happened in 1903 with the magnitude of Ms5.6, about 40 kilometers from the site.

The return period of earthquakes are calculated in this study via three methods of Gutenberg-Richter, Final Value Fitting (Gumble & Hovel function), and Kijko-Selevol within a 300-kilometer radius from the Moshampa dam and power plant site. It seems that the calculation of historical earthquakes makes the results of Kijko-Selevol method more accurate and more reliable. According to

this method, the magnitude of the earthquakes (M_s) for a 100-year return period within the radiuses of 50, 100, 200 and 300 kilometers are 4, 5.1, 6.4 and 6.8, respectively.

ASSESSMENT OF FAULTS ACTIVITY BASED ON THE REGIONAL TECTONICS

It is evident for the estimation of maximum parameters of earth movement with the deterministic method and even the introduction of parameters for various seismic design levels with the probabilistic method based on the seismic line sources, identification of active faults at the periphery of the site are highly important. Although the seismotectonic maps at the periphery of the site within 200 to 300 kilometers are usually prepared, the performance of the active faults within the 30 to 50-kilometer radius is considered as the most important seismic scenario. In other words, the faults beyond the 50-kilometer radius of the dam site impose little acceleration (less than 0.1g) to the dam site, in case they become reactivated. Normally, this range of acceleration inflicts no damage to the dam and power plant structures. The conducted studies point out that with the 60-kilometer radius of the Moshampa dam and power plant site, the prominent faults in terms of seismic potential and location are the Takht-e-Solayman and NE1 faults. The Takht-e-Solayman fault with the thrust mechanism and northwest-southeast strike is related to the two epicenters, therefore it could be considered as an active fault in the seismic analysis. The distribution of the epicenters for earthquakes occurred within the 300 kilometer radius is shown in (Fig. 3).

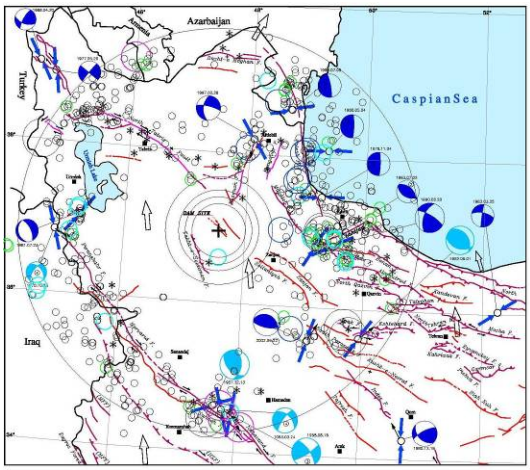

Fig. 3: The seismotectonic map of the Moshampa dam & power plant site within the 300-kilometer radius

It is evident that the site is located in a place where the frequency of events is inconsistent. According to Figure 3, within the 300-kilometer radius, the closest earthquake to the site was 40 kilometers to its southwest and within the 50-kilometer radius only one historical earthquake has taken place. The two mentioned earthquakes are related to the Takht-e-Solayman Fault. At the 60-kilometer distance, only one more historical earthquake has been recorded and within the 90-kilometer radius, no other earthquake is recorded. The other earthquakes are concentrated beyond the radius of 90 kilometer from the site mostly around the North Tabriz fault, western end of Alborz and northwestern part of Zagros seismotectonic provinces. From the distribution pattern of the earthquake epicenters and their lack of presence at the vicinity of the site, it is not possible to comment on the nearby fault activities by the customary method. At least, it could be concluded that they have had no activity during the 20th century. On the other hand, the lack of recent alluvium has prevented the study of shear effects by the faults activities in the recent period. In this regard, only the tectonic and paleotectonic studies are to be conducted.

These studies indicate that the NE1 Fault is the middle segment of a major basement fault comprised on North Tabriz fault in the northwest extended to the Soltaniyeh fault in the southwest with the length of 450km. This is the separating border between the western Alborz and Soltaniyeh-Mishu structural zones. It is mentioning that the geological maps show this basement fault after a distance gap is connected to Qom-Zefreh fault towards the southwest. Thus, its total length from the North Tabriz fault to the Qom-Zefreh fault is over 900km.

The seismotectonic studies of this major fault, which is comprised of several segments, indicate that most of its segments have had seismic activities during the 20th century. In other words, they could be considered as active fault segments. However, there are segments like the NE1 fault segment that did not reactivate in historical or 20th century time. Albeit, due to their tectonic characteristics and structural links with the other fault segments, their inactivity in the 20th century does not rule out the potential for future activities. NE2, NE3 and NE4 faults have a completely parallel trend with the NE1 fault segment. They are located at the southwest of the NE1 fault segment. The field studies and the tectonic and seismotectonic assessments indicate that these faults are inactive and probably will not impose any danger to the dam during its normal life time. Moreover, due to their considerable distance to the NE1 fault, the activity of the NE1 fault will not affect them. During the tectonic evolution of the Moshampa dam and power plant site, at least from the Cenozoic (Miocene) up to now, no significant fault at the upper crust has occurred. From what has been mentioned above, no essential change in the dam during its normal life time will be expected. It could be concluded that the faulting hazard at the dam and power plant foundation from the general tectonics point of view is not relevant.

SITE CHARACTERISTICS

The basement rock of the Moshampa dam and power plant site is generated by the Qom formation (Oligo-Miocene). This formation in the studied region is comprised of limestone, schistose limestone, tuff and schistose tuff. However, the intercalations of marl are present between the above-mentioned units. The geophysical studies for determination of shear wave velocity in these rock bodies at the dam axis are conducted via the seismic (refraction) method. The results indicate that the average velocity of the primary wave at the site is 3500m/s. Since the average density of the site's rocks is 2.5t/m^3, the velocity of the shear wave is 1400m/s. Thus, the rocks contained in the basement of the Moshampa dam and power plant site are classified as stiff rocks.

THE ESTIMATION OF SEISMIC PARAMETERS

The pertinent data and information including the mechanism of the faults, the appearance and the geometry of the faults and the seismotectonic specifications of the studied area are to be considered in this method. In this regard, the North Tabriz, Bozqoush, Masouleh, Soltaniyeh, Takht-e-Solayman, Zanjan and NE1 faults were evaluated. With reference to the magnitude, geometrical specifications and the measured distances of the seismic line sources at the periphery of the site with the aid of reliable attenuation equations, the maximum horizontal and vertical acceleration amounts for the 50% and 84% levels were calculated. Eventually based on the measured parameters calculated by the various attenuation equations with the aid of the logic tree, the NE1 fault was considered as the most important seismic line source at the vicinity of the Moshampa dam and power plant site. Moreover, the acceleration values resulted from its reactivation is recommended to be used as the maximum credible earthquake parameters (MCE) for 50% and 84% levels (Table 1).

Table 1: Maximum credible earthquake accelerations

Fault Name	PGHA(g)		PGVA(g)	
	H50%	H84%	V50%	V84%
NE1	0.28	0.43	0.19	0.33

The analysis of seismic risk via the probabilistic method comprises of the relationship between the strong earth movement parameters and the possibility of their occurrence at the project site within a specific time period with the aid of mathematical and probabilistic methods. The most important criterion in the aforesaid method is to have access to reliable statistical data of the previous earthquakes in the region. In this study, the point and line seismic sources models were utilized and the tectonic specifications of the site, logic tree method and engineering judgment of maximum horizontal and vertical acceleration parameters at the Moshampa project site for design basic and maximum design earthquakes were recommended (Table 2). Finally, it should be pointed out that due to the tectonic specifications of the Moshampa project site and the conducted studies, the values calculated for the 50% and 84% level are recommended for the final values.

Table 2: Seismic design parameters for Moshampa site

Earthquake Design Levels	Return Period (year)	Maximum Value of Acceleration (g)			
		50%		84%	
		V	H	V	H
DBE	1000	0.11	0.16	0.19	0.25
MDE	1500	0.14	0.19	0.23	0.29

CONCLUSIONS

This article aims at explaining the importance of tectonic and paleseismic studies at the vicinity of vital structures, which shows to have no connection with the seismic point and line sources at the first glance. If only the seismotectonic data of the site's periphery has been evaluated for the activities of the faults, in other words, the relationship between the faults, historical and the 20th century epicenters as well as the impact of the faults on the recent sediments have been analyzed, definitely the Takht-e-Solayman fault would have been considered as the most important seismic source. Subsequently, the parameters of the earth's strong movements for the maximum credible earthquake (84% level) for the horizontal and vertical values would have been 0.17g and 0.11g, respectively. These values are much smaller than the results obtained from the point sources, which were calculated for the return period of 10000 years (equivalent to the MCE return period) for the 84% level, horizontal value of 0.45g and vertical value of 0.36g. While the tectonic and paleseismic studies revealed that the NE1 fault segment is the most important seismic scenario at the periphery of Moshampa dam and power plant site. Although no earthquake in relation to the NE1 fault or within the 40-kilometer radius of the site has been recorded in the 20th century, this study concludes that the tectonic conditions and the location of the Moshampa dam and power plant site indicates that in the near future (during the normal life time of the structure) the occurrence of a relatively strong earthquake at the periphery of the Moshampa site is highly probable.

Acknowledgements: We would like to express our appreciation to Mr. Samani for accompanying in field geology and Mr. Karimi-Haghighi for editing the paper.

References

Aghanabati, A. (2006). Geology of Iran. Ministry of Industry and Mine, Geological Survey of Iran, 558 pp.

Ambraseys, N. N. and Melville, C. P. (1982). A History of Persian Earthquakes. Cambridge University Press.219pp.

Ambraseys, N. N. and Douglas, J. (2003). Near Field Horizontal & Vertical Earthquake Ground Motion. Soil Dynamics and Earthquake Engineering, 23(1), 1-18.

Campbell, K. W. and Bozorgnia, Y. (2003). Updated Near-Source Ground Motion (Attenuation) Relation for Horizontal and Vertical Components of Peak Ground Acceleration and Acceleration Response Spectra. Bulletin of the Seismological Society of America, 93(1). 314-331.

Jackson, J.A., & McKenzie, D.P. (1984). Active tectonics of the Alpine-Himalayan belt between western Turkey and Pakistan. Geophys, 77,185-264.

Jackson, J.A., & McKenzie, D.P. (1988). The relationship between plate motions and seismic moment tensors and the rates of active deformation in the Mediterranean and Middle East. Geophys, 93, 45-73.

Samari, H. (2006). Seismotectonics studies on Moshampa dam & HPP site. Tamavan consulting engineers, Tehran-Iran.

ICOLD, (1989). International Commission on Large Dams, "Selecting Seismic Parameters for Large Dams, Guidelines Bulletin 72.

Wells, D. L. and Coppersmith, K. J. (1994). "New Empirical Relationships among Magnitude, Rupture Length, Rupture Width, Rupture Area and Surface Displacement", Bulletin of the Seismological Society of America, 84(4), 974-1002.

EVIDENCE FOR A HOLOCENE EARTHQUAKE RECORDED IN A FLUVIAL-ARCHAEOLOGICAL SEQUENCE OF THE SEGURA RIVER, SE SPAIN

M. Sánchez-Gómez (1), C. Martínez-Sánchez (2), F García-García (1), J.A. Peláez (3), F. Pérez-Valera (1) and M. Martínez-Andreu (5)

(1) Departamento de Geología, Universidad de Jaén, Campus Las Lagunillas, 23071-Jaén, SPAIN. msgomez@ujaen.es
(2) ArqueoTec, C/ González Adalid 13 2º planta, 30002-Murcia, SPAIN. consueloms@telefonica.net
(3) Departamento de Física, Universidad de Jaén, Campus Las Lagunillas, 23071-Jaén, SPAIN. japelaez@ujaen.es
(4) Museo Arqueológico de Cartagena, C/ Ramón y Cajal 45, 30204-Cartagena, SPAIN. miguelmarand@yahoo.es

Abstract: *The archaeological excavation of a rock shelter (Abrigo del Pozo) in one of the slopes of the Segura River (SE Spain) has revealed a exceptionally preserved sedimentary record spanning from the Paleolithic to the present-day. The sedimentary analysis of the excavation indicates that human occupation was controlled by fluvial environmental evolution. However, an anomalous and continuous layer of large stones results in a disturbance of human occupation and normal fluvial sedimentation. We interpreted the anomalous level as related to a palaeoearthquake responsible for the collapse of the roof and walls of the rock shelter between 5820 +/- 50 BP and 3710 +/- 40 BP. A nearby earthquake of M 5.5 – 6.0 is the most plausible cause for the collapse. Several regional faults, included the Socovos-Calasparra fault less than 2 km apart, could be the responsible of the event.*

Key words*: rock shelter, palaeoearthquake. North-eastern Betics. fluvial sedimentation*

INTRODUCTION

The Betic Cordillera is the Spanish region with highest seismic hazard (Peláez and López-Casado, 2002). Nevertheless, at present a limited number of studies have issued the effects of palaeoearthquakes (e.g. Silva et al., 1997; Masana et al., 2004). Trench studies constitute an effective tool to establish the seismic history of a fault, but they need to identify previously the fault as least as potentially active. The Betic Cordillera has a composite tectonic history with a large number of mapped faults, most of them being at present inactive. Therefore, one of the main tasks in the region is to recognize large palaeoearthquakes in the geological and archaeological records as well as to identify the associated faults.

This work analyzes the sedimentary infilling of a cave, adjacent to the Segura River in SE Spain. This cave has recorded almost continuous human presence since the Palaeolithic and evidence of a catastrophic breakdown. We will propose that this collapse was caused by a seismic event, then examining the implications of this earthquake in the neighbourhood, where no other significant Holocene earthquake is known. This study highlights the potential of archaeological shelters for identifying and dating earthquakes, if they are revisited from a palaeoseismologic point of view.

GEOLOGICAL SETTING

The Abrigo del Pozo (Pozo Rock Shelter) is located in Sierra del Molino, a carbonate massif belonging to the Prebetic Zone of the Betic Cordillera. The rock shelter is about 30 m-long, with a maximum depth of 9 m and an average height ≥ 2 m. It is located at the foot of a cliff in a canyon-shaped valley incised by the Segura River. The present-day height of the cave floor above the average stream level is about 4 m. The cave section and position in relation to the fluvial channel provide a comfortable and secure habitat. Rock paints and abundant archaeological remnants reveal a reiterated use as prehistoric residence, refuge or sanctuary. Nevertheless, the access is difficult due to its location amid the canyon, this fact having preserved the rock shelter from later alterations and vandalism.

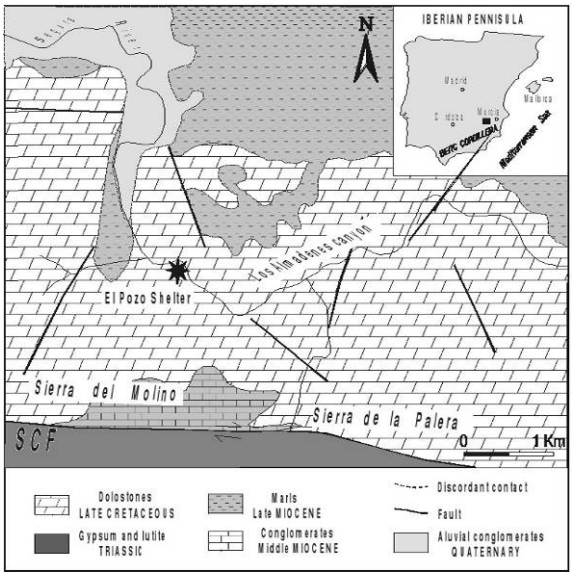

Fig. 1: Geological sketch indicating the location of the studied rock shelter. SCF = Socovos-Calasparra Fault

Abrigo del Pozo is only 1,5 km from Socovos-Calasparra Fault (Fig. 1), a 70 km-long fault that constitute a major regional structure with geomorphologic evidences of Quaternary displacements (Rodríguez-Pascua, 1998). During the last century only one mb 4.5 small earthquake (Cieza, June 13th, 1936) has been located at the eastern end. Nevertheless, other relatively close structures have produced instrumental seismic swarms, including main earthquakes with magnitudes in the range mb 4.0-5.0

(e.g. Mula, 1999 or Bullas 2002), showing a potentially seismic activity in the region.

SEDIMENTARY AND ARCHAEOLOGICAL RECORD

The general stratigraphic succession of the site consists of a fining-upward cycle, basically beginning with gravels and/or sands of a meandering channel and concluding with flood-plain lutites (Figs. 2 and 3). The cycle consists of three intervals, which correspond to fluvial subenvironments determined by sedimentological analysis. From bottom to top the facies association are: 1) channel filling, 2) channel abandonment and 3) flood plain. This vertical succession of lithofacies with upward decreasing energy characterizes sedimentation in a typical meandering-dominated flood plain.

The particular sedimentary conditions occurred here have preserved very well seven anthropogenic layers intercalated with the fluvial deposits (Fig. 3). Each one was covered by a fluvial flow that has preserved the archaeological record, separating one anthropogenic level from other and avoiding the alteration of the remnants by human activity during the next period.

Human habitat appears controlled by fluvial environmental evolution: it was sporadic during the channel work (facies association A and B, fig 3) and more intense when rock shelter floor topography was homogenized at the level of the flood plain of the main channel (facies C).

Fig.2: Main archaeological trench showing the habitat levels (dark) and a bed with outsized clasts (MRC, massive rock collapse). Sedimentological interpretation is showed in Fig. 3.

A bed with outsized clasts (MRC level, Figs. 2 and 3) appears intercalated in fine sands and lutites of the facies association C, overlying the N2 anthropogenic layer (5820 +/- 50 BP). The bed consists of very angular and scattered cobbles and boulders of sandy dolostones lacking internal organization. The grain size and the textural maturity of the clasts are genetically independent of the facies association C, deposited at lower regime flow in a flood-plain where the bed intercalates. Thus, the MRC level is unconnected with purely fluvial processes. This level directly overlays the N2 level, sealing fire and bone-food remnants. Scarce artefacts have been found among the stones of the MRC. The MRC level and the scarce anthropogenic remains are completely covered by the next flood sand level, and the next occupation level (Ch, Fig. 2; 3710 +/- 40 BP).

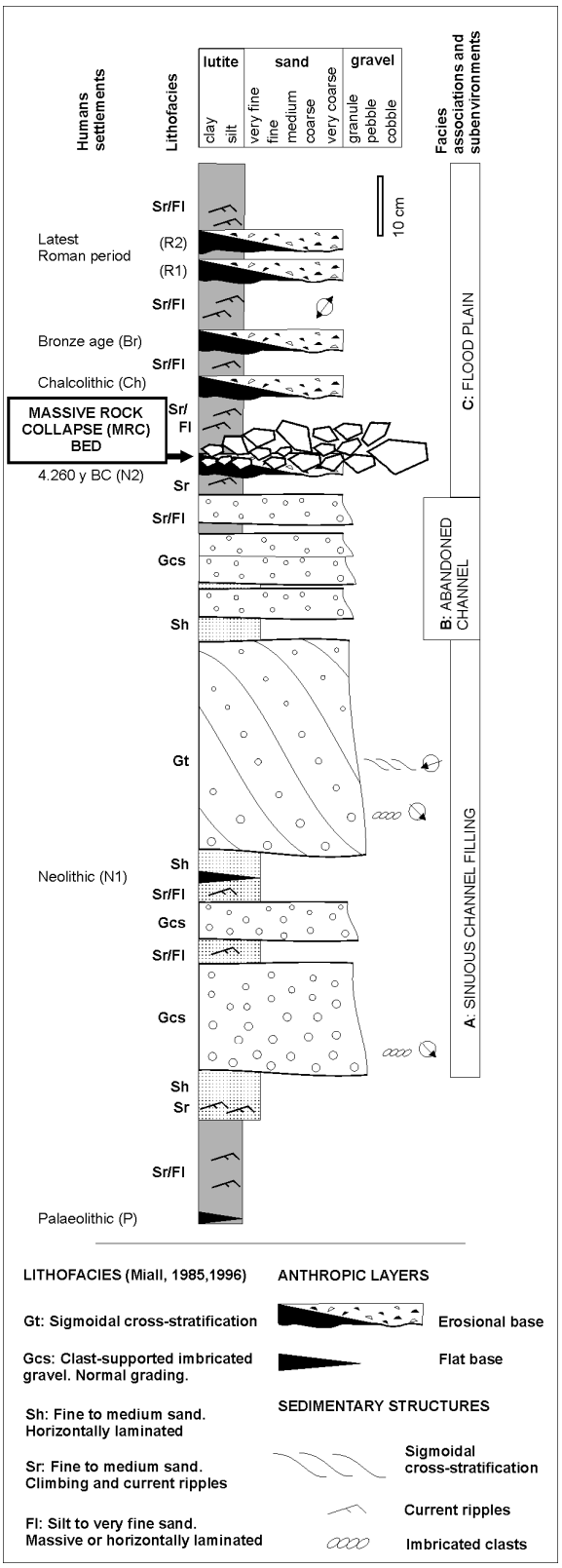

Fig.3: Detailed stratigraphic column from the archaeological site, with indication of the lithofacies and facies associations.

The fluvial sediments studied present rounded particles with an average maximum size of coarse-grained gravel. Thus, the MRC level with pebble- and cobble-sized blocks represents an exceptionally coarse-grained layer. It is made up of fragmented sandy dolomites from the walls and roof of the rock shelter. Larger fragments are fractured, though they preserve most of the original joints

between pieces. Fragments have not faces altered by fire with only minor smoke imprint observed in some of them. The horizontal distribution of the fragments is almost regular, though in some places adjacent but separated stones can be fitted together.

All of the pieces of evidence described above suggest that rock fragments in the MRC level fell from the roof of the shelter. The collapse should have occurred in a short interval of time, interrupting the routine use of the shelter by the Neolithic settlement. Abundant artefacts and bones were trapped under the MRC level, which, in turn, was buried by the next overflow level.

DISCUSSION

In our view, an earthquake might account for such a sudden and general collapse. In this hypothesis, the rock shelter roof, altered to a certain degree by weathering and/or anthropogenic processes, would stay metastable until the seismic shake. Rock falls induced by earthquakes occur only when joints become large and well developed cracks (Matmon et al., 2005).

Other hypothesis as glacial overload cannot be expected at this latitude and altitude in middle Holocene times. Cliff retreat, a normal process in the geomorphic evolution (Ahnert, 1996), would yield block accumulation at the entrance of the rock shelter, but not distributed below the protected area. Moreover, frost-wedging in rock shelters would produce small-sized rock fragments all along the sedimentary record, without concentration in a particular level. A hypothetical human devastating action could not explain the size and distribution of fragments.

At that moment a question remain: which ground motion might cause this breakdown? The answer is the same that for the generic question: which ground motions can cause collapses or falls? Without more related studies, this topic must be attended as a typical landslide problem. Peak ground horizontal accelerations (PGA) values, worldwide used in seismic hazard, clearly are not a reliable parameter for this type of studies (Harp and Wilson, 1995). On the contrary, Arias intensity values, a measure of earthquake intensity based on instrumental records (Arias, 1970) and claimed to be a measure of the total seismic energy absorbed by the ground is the most used intensity in earthquake triggered landslide investigations. Arias intensity considers the full range of frequencies recorded in an accelerogram, as well as the duration of the ground motion.

Using data from Californian earthquakes, Harp and Wilson (1995) proved that with horizontal Arias intensity values above 0.25-0.30 m/sec, on average, seismically induced rock falls and rock slides can be observed. But in several cases, values above 0.1 m/sec were enough. Using the known relationship by Sabetta and Pugliese (1996) between horizontal Arias intensity, moment magnitude and rupture distance, we can estimate that a M 5.5 earthquake can provide expected Arias intensity values of the order of 0.4 m/s at the rupture, and above 0.1 m/sec at distances to the rupture below 10 km, considering stiff rocks. For an M 6.0 earthquake, Arias intensity values of the order of 1.2 m/s at the rupture, and values above 0.1 m/sec at distances below 20 km, are expected.

CONCLUSIONS

Archaeological excavations in the Abrigo del Pozo have shown the presence of a rock collapse level above the main Neolithic occupation level, which interrupts the regular use of the shelter as habitat. This collapse is interpreted as a seismic event, dated between 5820 +/- 50 BP (age of the underlying habitation level, N2) and 3710 +/- 40 BP (age of the overlying anthropic level, Ch, Fig. 2).

The most plausible event causing this collapse is an M 5.5-6.0 earthquake with focus at 10-20 km, generating Arias intensity values above 0.1msec-1. This assumption, together with the regional seismotectonic context, point to a seismic source located to the south in a nearby area. One of the most reliable structures capable to produce such an earthquake is the Socovos-Calasparra fault, which, however, has not significant seismic activity in the instrumental record. Future regional palaeoseismic investigations should take into account the existence of more seismic evidences in the 5800-3700 BP interval, in order to identify the earthquake source and improve the seismic hazard assessment.

Acknowledgements: The present study has been co-sponsored by the Consejería de Educación y Cultura of the Murcia Region and the grant CGL2006-10202/BTE, from the I+D programme of the MICINN, partially financed by FEDER funds of the European Union

References

Ahnert, F. 1996. Introduction to Geomorphology, Arnold, London. 352 pp

Arias, A. (1970). A measure of earthquake intensity. In: Hansen, R.J. (Ed.), Seismic Design for Nuclear Power Plants. MIT Press, Cambridge, MA, pp. 438–483.

Harp, E.L., Wilson, R.C. (1995). Shaking intensity thresholds for rock falls and slides: evidence from 1987 Superstition Hills earthquake strong-motion records. Bull. Seismol. Soc. Am 85, 1739–1757.

Masana, E., Martinez-Diaz, J. J., Hernandez-Enrile, J. L. & Santanach, P. 2004. The Alhama de Murcia fault (SE Spain), a seismogenic fault in a diffuse plate boundary: Seismotectonic implications for the Ibero-Magrebian region. Journal of Geophysical Research-Solid Earth 109 (B1), B01301.

Matmon, A., Shaked, Y., Porat, N., Enzel, Y., Finkel, R., Lifton, N., Boaretto, E. & Agnon, A. 2005. Landscape development in an hyperarid sandstone environment along the margins of the Dead Sea fault: Implications from dated rock falls. Earth and Planetary Science Letters 240 (3-4), 803-817.

Peláez, J.A., and López Casado, C. (2002). Seismic hazard estimate at the Iberian Peninsula. Pure and Applied Geophysics, 159, 2699-2713.

Rodríguez-Pascua, M. A. 1998. Paleosismicidad y sismotectónica de las cuencas lacustres Neógenas del Prebético de Albacete. Ph. D. thesis, Universidad Complutense, Madrid, 358 pp.

Sabetta, F., and Pugliese, A. (1996). Estimation of response spectra and simulation of nonstationary earthquake ground motions. Bull. Seismol. Soc. Am. 86, 337-352.

Silva, P. G., Goy, J. L., Zazo, C., Lario, J. & Bardaji, T. 1997. Paleoseismic indications along 'aseismic' fault segments in the Guadalentin Depression (SE Spain). Journal of Geodynamics 24(1-4), 105-115.

EVIDENCE FOR A MEDIEVAL EARTHQUAKE IN THE AACHEN AREA (GERMANY), REVEALED BY STRUCTURAL DAMAGE IN THE CATHEDRAL

A. Schaub (1), K. Reicherter (2), C. Grützner (2) and T. Fernández-Steeger (3)

(1) Archaeologist of Aachen city; Verwaltungsgebäude Am Marschiertor, Lagerhausstraße 20, 52064 Aachen, GERMANY
(2) Neotectonics and Natural Hazards, RWTH Aachen University. Lochnerstr. 4-20. 52056 Aachen, GERMANY
(3) Chair of Engineering Geology and Hydrogeology, RWTH Aachen University. Lochnerstr. 4-20. 52056 Aachen, GERMANY
Andreas.Schaub@mail.aachen.de, k.reicherter@nug.rwth-aachen.de

Abstract: *Archaeoseismological and palaeoseismological investigations in the Carolingian Chapel of the Aachen Cathedral proved evidence for an earthquake with a minimum magnitude of 5.5 in the beginning of the 9th century AD. Systematic cracks in the stone masonry, ground floor and foundations, as well as in the cupola of the chapel, point to a high-energy event. Repair of the damaged structures suggest that those were carried out during the construction of the chapel in Carolingian times. Furthermore, clay-filled cracks, so-called "injection structures", are filled from below by squeezing high-plasticity clay into sharp-edged broken Pleistocene eolian sediments (Loess), underpinning our findings with geological observations. Historical documents, the construction history of the chapel and coin findings support the idea of a damaging earthquake in the Aachen area in 803 AD.*

Key words*: archaeoseismology, injection structures, structural damage, Lower Rhine Graben*

INTRODUCTION

Geological and seismotectonic background

The neotectonic and landscape evolution of the Lower Rhine Graben (LRG) in western Germany are directly linked to the Alpine Orogeny and mainly characterized by subsidence. However, secondary processes (like earthquakes, extensional tectonics, volcanism, influence of glaciation/deglaciation of northern Central Europe, and anthropogenic modifications, i.e. open cast lignite mining) influence strongly landscape. The geomorphology of the area is typical for a "seismogenic landscape", with pronounced scarps and active faulting, here mainly normal faults (Fig.2).

Aachen is situated along the northernmost edge and on the frontal Variscan thrust fault, trending NE-SW. One of the major fault lies directly below the plaza between the palatine and the Carolingian chapel (Figs. 1 and 3). Younger, NW-SE trending normal faults cut and displaced these older structures (Fig.3). Palaeoseismic and historical earthquake data suggest several major events during prehistoric times (Camelbeeck and Meghraoui, 1998; Vanneste et al., 2001, Hinzen and Reamer, 2007), instrumental data, however, show only minor to moderate seismicity (with a maximum during the Roermond earthquake, April 13th 1992, ML 5.8). Some well-preserved remains of structures of Cologne from the late Roman period (4th century AD) show severe building damage (Hinzen and Schütte, 2002). The Praetorium, seat of the Roman administration and palace, was located on the banks of a former side arm of the Rhine River. Lack of any traces of attempted repairs and written sources which document use of the building for a long time after the end of the Roman Empire favour a sudden onset of damage over a gradual process (Hinzen and Schütte, 2002). These authors dated the earthquake activity observed in Cologne in 800 to 840 AD.

In contrast to the Dutch and Belgium parts of the LRG, the German elements of the Lower Rhine Graben are poorly studied, with the exception of several trench studies by the Geologischer Dienst of NRW (Skupin et al., 2008). Here, we report on probable earthquake-related structural damage and palaeoearthquakes in the Lower Rhine Graben area.

Historical background

Charlemagne (Charles the Great) had placed the centre of his kingdom during Carolingian times in Aachen, Germany (Aquisgrana). This medieval period and his regency are regarded to set a benchmark in the birth of Europe, and are associated with a period of extensive constructions in Aachen.

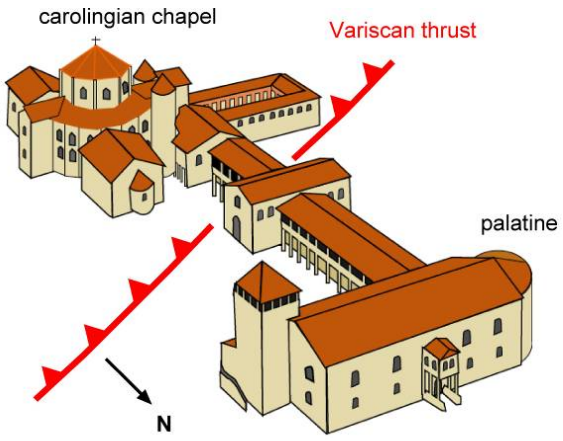

Fig. 1: Model of the Carolingian Palatine and octagon Chapel in Aachen, with Variscan thrust fault

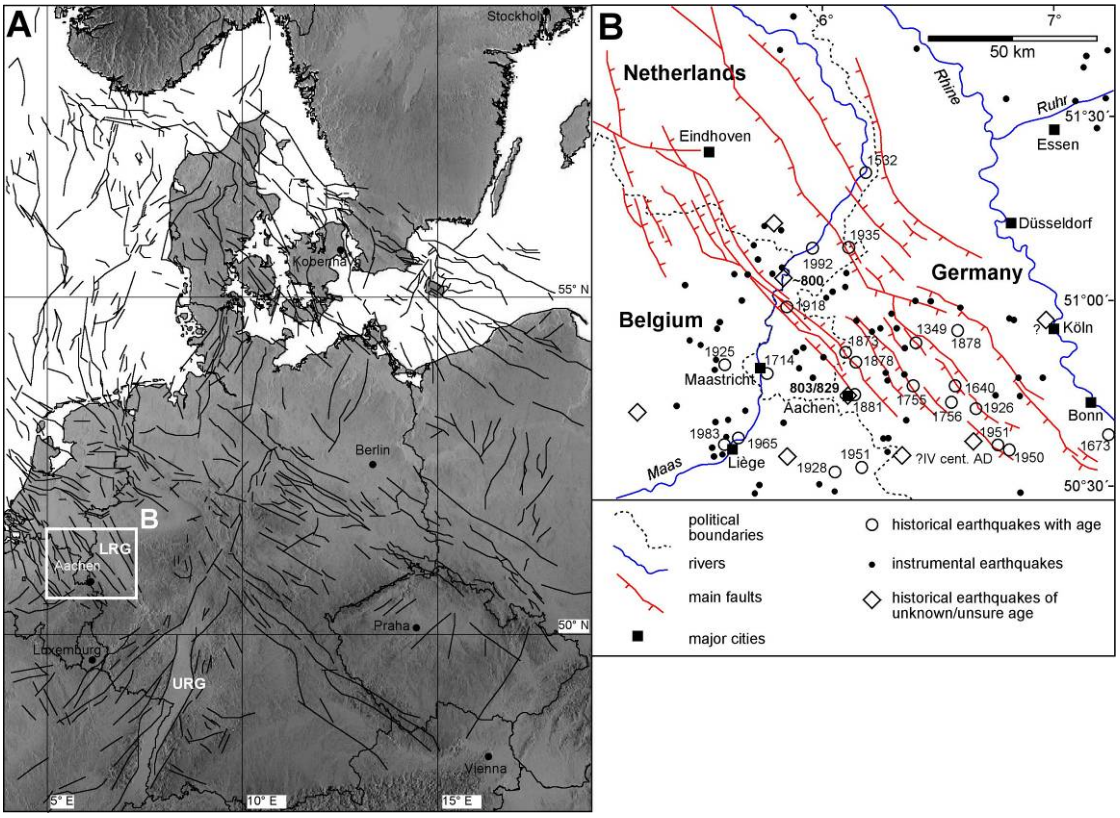

Fig. 2: A Location and tectonic features of Germany; B. location and tectonic structures in the Aachen and Lower Rhine Graben areas with historical earthquakes

During archaeological and geotechnical investigations, the Carolingian part of the Aachen Cathedral is excavated. Below the cathedral Roman thermes have been found. The Carolingian part (Palatine Chapel) of the Cathedral (Fig.1), which was the first building in Germany joint to the UNESCO World Heritage list (1978), forms in the inner part an octagon, which is surrounded by a hexadecagon. The walls are deeply founded (up to 5 m), and are partly up to 2.4 m thick.

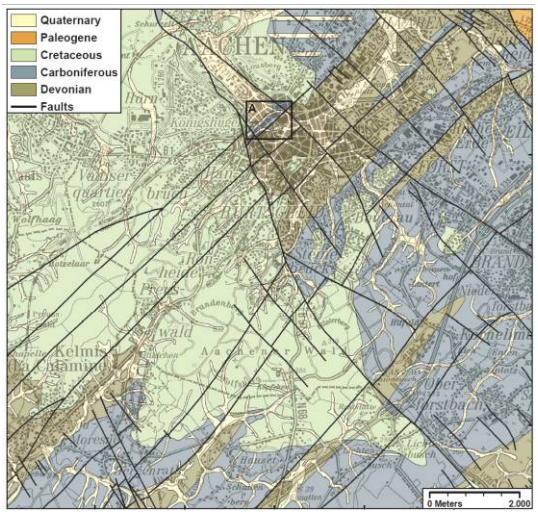

Fig. 3: Geological map of Aachen

Aachen is as well a historic spa city since Roman times due to occurrence of thermal springs. In 1656, a great fire devastated Aachen. The cathedral was rebuilt several times in the 14th and 17th centuries; the lemon-press roof of the octagon chapel is baroque. The main tower was reconstructed in the late 19th century. The vivacious history of the Cathedral left their imprints in architectural styles and modifications.

The Cathedral is founded on Devonian blue limestones and shales, covered by Pleistocene loess. Also, remains of Roman buildings, like a hypocaustum, a small channel and thermes are situated below this part of the Cathedral.

Fig.4: Aachen Cathedral, central part is Carolingian, to the right is the Gothic choir

PALAEOSEISMIC EVIDENCE

Structural damage

In the outer wall of the NW segment of the hexadecagon open cracks are found, which cut the entire wall not following the crude stone masonry. In the same segment,

subsidence of the floor of about 50 cm with lateral dragging can be observed and furthermore a concrete reconstruction of the subsided floor during Carolingian times. Up to now this is the only part of the Cathedral where two ground floors of Carolingian age can be found (Fig. 5). During the still lasting excavation further cracks have been found in the wall of the octagon. Cracks are systematically (Fig. 6) with a maximum oriented NW-SW according to the present-day principal stresses in Central Europe (Reicherter et al., 2008).

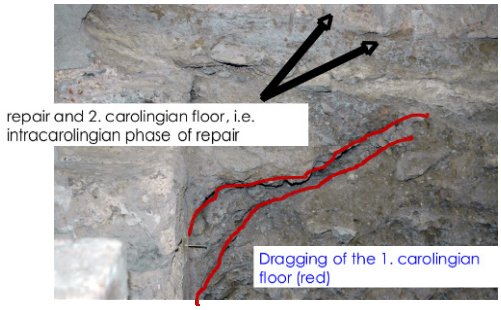

Fig. 5: Ground floor damage and repair

Large cracks have also been found in the roof of the chapel (Fig. 7). These cracks are lead-filled and sealed with Carolingian mortar. This evidence also suggests an intra-Carolingian phase of repair.

Archaeological investigations imply that obviously the chapel was architectonically not finished, when the damage occurred. Most probably the damage happened before the official inauguration.

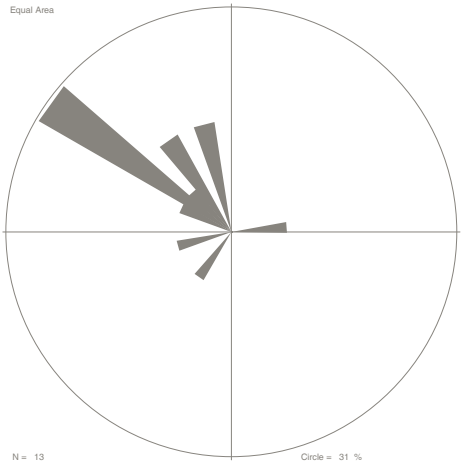

Fig. 6: Orientation of the wall cracks

Geological evidence

In the WNW section, the loessy and loamy sediments show angular cracks and fragments (Fig. 8 and 9), which are not related to permafrost features but are interpreted as liquefaction. Furthermore, some of the cracks are filled with black sterile clay from below as they open downwards. These structures may be interpreted as "injection structures" or features of weathered Devonian claystones into the overlying Pleistocene.

However, some of the upper portions of the cracks yield Roman ceramic fragments and charcoal, quite similar to

Fig. 7: Damage in the roof of the chapel

those sediments found in adjacent Roman waste dumps, pointing to a mixture of underlying and covering materials. Liquefaction and injections structures occur usually during earthquake with a magnitude higher than 5.5, which is corroborated by large cracks in the massive outer walls.

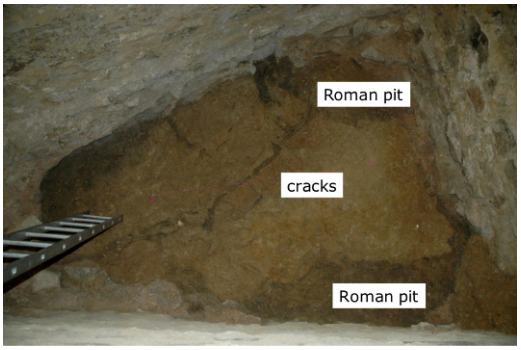

Fig. 8: Clay-filled cracks in the sterile soil of the chapel (Pleistocene Loess)

HISTORICAL EARTHQUAKES AND DATING

The earthquake catalogues (e.g., von Hoff, 1840) and the Annales regni Francorum (Kurze, 1895) provide two important passages for historical earthquakes in the region of Aachen. Both fall into a relatively short time interval. One in winter 803 AD: "*Hoc hieme circa ipsum palatium et finitimas regiones terrae motus factus et mortalitas subsecuta est.*" The later 829 AD (between Ash Wednesday and Easter) description „*Aquisgrani terrae motus noctu factus ventusque tam vehemens coortus ut non solum humiliores domos, verum etiam ipsam sanctae Dei genitricis basilicam, quam capellam vocant, tegulis plumbeis tectam non modica denudaret parte*". Both notes tell of earthquake shaking and significant structural damage (e.g. lead bricks fallen off the roof) and fatalities.

Due to rich findings and dating of charcoal in several levels, the original and the restored floor, successful radiometric dating was carried out to get time constraints

on the exact date of the earthquake event. This was also important to get a time frame of the construction of the chapel. So, construction started earliest in 798 AD, supported by findings of a Carolus denar of a maximum age of 794 AD during the excavations. The construction was terminated latest in 813 AD.

Fig. 9: Detail of the sharp-edged clay-filled cracks in the Pleistocene Loess, suggesting a high-energy event

CONCLUSIONS

Several typical indicators of earthquake deformation (structural and geological) have been found in the Carolingian Chapel of Aachen, which indicate a high-energy event, probably accustomed by differential ground settling. Historical documents reveal evidence for two earthquakes in the considered time interval. Palaeoseismic trenching investigations of Vanneste et al. (2001) found surface rupturing during an earthquake near Bree (Belgium), which happened around 800 AD and assigned a palaeomagnitude of M 6.4 to this earthquake (see also summary in Camelbeeck et al., 2007). Also, the structural damage in Cologne (Hinzen and Schütte, 2002) occurred around 800 to 840 AD. These authors end up with a minimum magnitude of 5.8.

If we take into account that structural damage in the Aachen Cathedral occurred during the construction, as evidenced by the warped ground floor (see Fig. 5), we favour strongly the 803 AD event as the candidate earthquake for the damage in the medieval Aachen city area. The observed damage, including the liquefied "injection structures" suggest a minimum magnitude for this event around 5.5. However, up to date trenching studies to localize the causative fault in the Aachen area is missing. Currently, we are mapping and surveying faults in the area.

Acknowledgements: We thank Helmut Maintz, the Master builder (Dombaumeister, Cathedral Architect) of the Aachen Cathedral, for support and access.

References

Camelbeeck, T., and Meghraoui, M. (1998). Geological and geophysical evidence for large paleoearthquakes with surface faulting in the Roer Graben (northwest Europe), Geophys. J. Int., 132, 347 - 362.

Camelbeeck, T., Vanneste, K., Alexandre, P., Verbeeck, K., Petermans, T., Rosset, P., Everaerts, M., Warnant, R. and Van Camp, M. (2007). Relevance of active faulting and seismicity studies to assessments of long-term earthquake activity and maximum magnitude in intraplate northwest Europe, between the Lower Rhine Embayment and the North Sea. GSA, Spec. Paper, 425, 193-224.

Hinzen, K.-G. and Schütte, S. (2002). Evidence for earthquake damage on Roman buildings in Cologne, Germany. Seismological Research Letters, 74, 121-137.

Hinzen, K.-G. and Reamer, S.K. (2007). Seismicity, seismotectonics, and seismic hazard in the northern Rhine area. GSA, Spec. Paper, 425, 225-242.

Kurze, F., (1895). Annales regni Francorum iude ab a. 741 ad a. 829, qui dicuntur Annales Laurissenses maiores et Einhardi (Hannover).

Skupin, K., Buschhüter, K., Hopp, H., Lehmann, K., Pelzing, R., Prüfert, J., Salamon. M., Schollmayer, G., Techner, A. and Wrede, V., (2008). Paläoseismische Untersuchungen im Bereich der Neiderrheinischen Bucht. Scriptum, 17, 5-72 (in German).

Reicherter, K., Froitzheim, N., Jarosiński, M., Badura, J., Franzke, H.-J., Hansen, M., Hübscher, C., Müller, R., Poprawa, P., Reinecker, J., Stackebrandt, W., Voigt, T., von Eynatten, H. and Zuchiewicz, W., 2008. Alpine Tectonics II – Central Europe north of the Alps (Geology of Central Europe; McCann, T. (ed) book section). Spec. Publ. Geol. Soc. London, 59 pp.

Von Hoff, K.E.A., (1840). Chronik der Erdbeben und Vulcan-Ausbrüche, I. Theil (Justus Perthes, Gotha), pp. 470.

Vanneste, K., Verbeeck, K., Camelbeeck, T., Paulissen. E., Meghraoui, M., Renardy, F., Jongmanns, D. and Frechen.M. (2001). Surface-rupturing history of the Bree fault scarp, Roer Valley Grabe: Evidence for six events since the late Pleistocene. J. of Seismology, 5, 329-359.

AN APPLICATION OF 3D LASER SCANNING IN ARCHAEOLOGY AND ARCHAEOSEISMOLOGY: THE MEDIEVAL CESSPIT IN THE ARCHAEOLOGICAL ZONE COLOGNE, GERMANY

S. Schreiber (1), K.G. Hinzen (1) and C. Fleischer (3)

(1) Earthquake Geology Group, Cologne University, Vinzenz-Pallotti-Str. 26, 51429 Bergisch Gladbach. GERMANY. stephan.schreiber@uni-koeln.de

Abstract: *In 2007 the construction of a large museum area within remains of the Roman and medieval Cologne (Germany) started in the historic city center. A medieval cesspit discovered during the excavations exhibits large deformations and heavy damages. The static conditions of the cesspit demanded restoration work during the excavation. A 3D laser scanner was used to create a virtual model of the unrestored structure. The damages were precisely mapped and a quantitative database for further investigation of the damages was established. The collected data enhance the preservation efforts and present the cultural heritage in an unaltered in situ condition. In addition to providing documentation of the restoration, the data are critical for investigating a possible seismogenic origin for the observed damages.*

Key words*: Archaeoseismology, 3D Laser Scanning, Cologne, Cultural Heritage*

INTRODUCTION

The construction of the Archaeological Zone Cologne (AZC) in the historic city center of Cologne, Germany began in 2007 and entails excavation of large areas of the Roman and medieval Cologne (Fig.1). Several buildings in the AZC exhibit structural damage. 2003 Hinzen & Schütte proposed a possible seismogenic cause for damages observed in those sections that had been excavated in the 1950s and 1970s. The Deutsche Forschungsgemeinschaft (DFG) funded a project to further test this hypothesis. Part of the project is a detailed mapping of the excavated buildings in the AZC using a phase based 3D laser scanner. The resulting database of the structural damages will be a cornerstone for finite or discrete element models of selected building elements. The mapping focuses on the Roman excavactions; however, during the excavation a medieval cesspit was discovered in front of the historic city hall of Cologne. After the excavation of the first few meters of the cesspit, the static situation required restoration of the walls before the excavation could continue. This experience convinced the archaeologists that the cesspit would have to be modified in its entirety to be successfully excavated. Therefore, the only record of the original cesspit was a virtual model provided by the 3D laser scan. We began mapping the cesspit before the first reconstructions and continued successively for each new section (0.5-1.0m) excavated.

LOCATION

The investigated area is located in the old city center of Cologne, Germany (Fig. 1A). Cologne is located in the eastern part of the Lower Rhine Embayment (LRE) a young sedimentary basin with ongoing seismic activity. The LRE belongs to the most active seismic region north of the Alps. The instrumental and historical records for the region document more than 20 damaging earthquakes in the last 300 years.

Additional surface rupturing events are confirmed by paleoseismological investigations in the area (e.g. Camelbeeck & Meghraoui, 1998). Hinzen and Reamer (2007) estimate a maximum magnitude of 7.0 for the area.

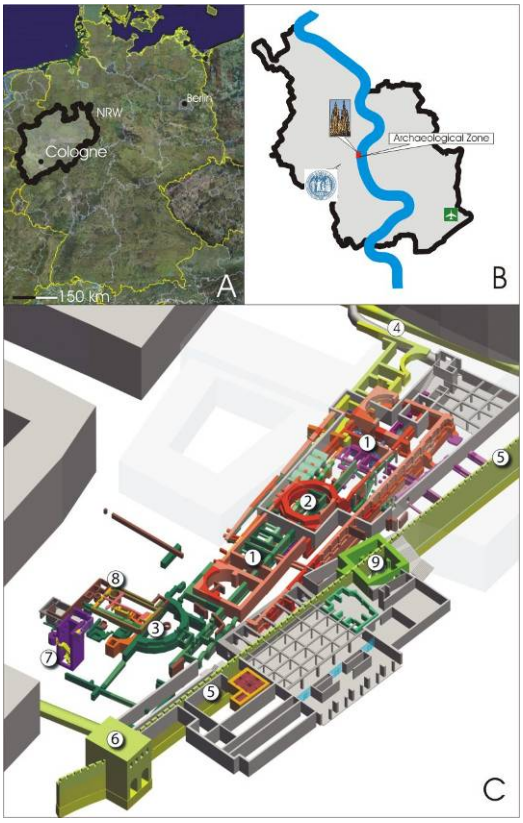

Fig.1: Location of the investigation area in Germany (A) and in the city of Cologne (B). C shows a map of the AZC: 1: Praetorium, 2: Octogon, 3: Eastern atrium of the synagogue with Roman well, 4: Roman sewer, 5: Roman city wall, 6: Porta Martis, 7: Jewish Mikveh, 8: Synagogue with medieval cesspit, 9: Basement of tower of the medieval city hall. (Fig. 1A: Google Earth, 2008; Fig. 1C: AZC, 2008)

THE ARCHAEOLOGICAL ZONE COLOGNE

After its completion estimated in 2011 the AZC will be one of the largest underground museums in Europe. The AZC is part of the structural program of the state North-Rhine-Westphalia, Regionale2010. The final museum area will cover 7000 m² of archaeological records in the historic city center of Cologne (Fig. 1B, C). Two large subject areas dominate the museum district: The Roman Cologne and the medieval Jewish quarter of Cologne.

The Jewish community in Cologne, first mentioned in the city annals in 321 A.D., is the oldest known community north of the Alps. In 1183 the Jewish people moved to the historical city center, the area which is currently being excavated. The Jewish Quarter includes remains of four synagogue buildings, the Mikveh with a bathhouse, a bakery, a wedding house and a hospice (Grübel, 1999).

THE CESSPIT

The cesspit is located within the remains of the medieval Jewish synagogue. The assumed period of use is from 1000 to 1400 A.D.

The cylinder-shaped construction has an overall minimum depth of 6.5 m and a diameter of 2.3–2.5 m. The top of the western wall is a 40-cm wide and 90-cm long sledge formerly used as an inlet into the cesspit. The construction is built up by ca. 50 layers of small to medium tuff blocks (10 x 15 cm). At a depth of 1.7 m the western wall is made of larger tuff blocks of irregular shape (20 x 30 cm) and parts of hexagonal basalt columns. During the excavation, a damaged area was detected at a depth of 3.5 m in the eastern wall. In addition to the goal of creating a model of the unrestored cesspit for further archaeological investigations, the damage zone required detailed mapping in order to link this structural damage to the records from other sections in the AZC.

METHODOLOGY & INSTRUMENTATION

A 3D–phase–laser scanner FARO Photon80 in combination with a Nikon D200 digital SRL camera is used for the mapping (Fig. 2A). The scanning device uses a permanent bundled infrared beam, which is directed, to the measurement area with a rotating mirror. Reflections of the beam from a target are detected and the phase shift to the outgoing signal is used to determine the distance of the reflection point. With additional instrumental parameters including the position of the rotating mirror and the horizontal position of the scanner, the Cartesian coordinates are calculated for every collected point. The intensity of the reflected beam is used to assign a reflectance value to each target point.

The final product is a pointcloud with three coordinates and the intensity value. An advantage of the phase method is the fast acquisition of the measured points in the order of 120,000 points per second. Scanners based on pulsed beams and two-way travel time measurements are usually slower (ca. 4000 points/s).

Three discrete wavelengths of 1.2 m, 9.6 m and 76 m provide increased accuracy. The scanner has a resolution of 0.009° in vertical and 0.00076° in the horizontal direction. The distance accuracy is +/-2 mm at 25 m distance on a plain reference area with 90% reflectivity.

The created pointcloud is adjusted to the horizontal with an internal inclinometer with an accuracy of 0.1°. The inclinometer can be used within a range of 15°, eliminating time-consuming adjustments during the data acquisition in the field.

The cesspit was mapped during seven excavation stages. The scanner equipment was lowered down to the centre of the cesspit with an electrical winch, and one or two scans at different heights above the base level were made (Fig. 2A). These scans were merged during post processing. The scans were collected at 1/4th of the maximum available resolution, and were deemed sufficient for the target distances in the cesspit (1.0-1.3m). A full resolution scan would have required more than 60 minutes of recording time and more than 1 GB of disk space.

In addition to the pointcloud data, digital photos were collected using a digital SRL camera with a 10.5 mm fisheye objective and 10.2 Megapixel. The camera was attached to the scanner as illustrated in figure 2A. With this configuration, the camera records from the same positions as the rotating mirror once the scan is finished. The photos have a directed orientation so they can be overlaid on the point cloud and used to colorize the data. In this step of the post processing every single point of the cloud is assigned an RGB value extracted from the digital photos.

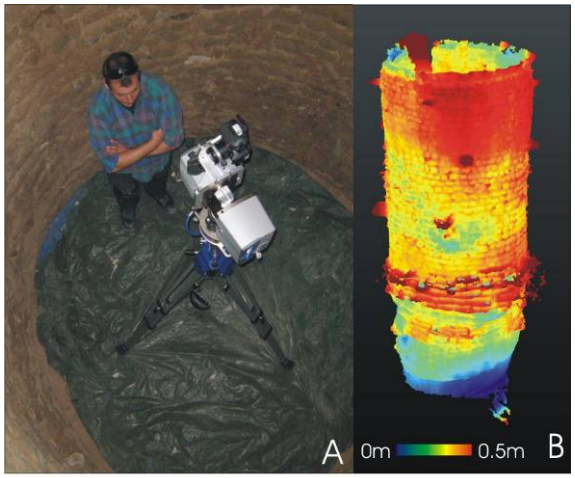

Fig.2: (A) FARO Photon 80 3D laserscanner with installed digital SRL camera in the cesspit. (B) Combined scan of the medieval cesspit, colors show the deviance from a virtual cylinder with a diameter of 1.8 m. (Photo 2(A): S.K.Reamer, 2008)

PROCESSING

Raw scan data were processed with the FARO Scene and JRC Reconstructor programs. The data analysis is dependent on the desired results. For presentation purposes the scans are filtered with FARO Scene, colored using the digital photos and exported to JRC Reconstructor, where superfluous data points are removed. For quantitative measurements and construction of 3D models, the data are imported directly into the Reconstructor software.

Two filters are used for processing the scans in FARO Scene: (1) a stray filter removes scan points that result from hitting two objects e.g. at edges and scan points that result from hitting no object within the working area of the scanner (e.g. laser points to the sky); (2) the second filter removes noisy points. So-called "dark" scan points reflect only a very small amount of the light beam and increase the noise in the scan. After the application of the filters, the photos are attached and the pointcloud is colorized. The last step is to export the colored scan to the Reconstructor software, where points outside the area of interest are removed and additional filters can be applied.

DAMAGES

The damage zone of the cesspit was investigated in detail. It is limited to a 2.5 m x 3.5 m wide area at a depth between 3.5 m and 6.0 m measured from the top (47.5–45.0 m a.s.l.). At a depth of 4.0 m the major damage area includes the entire perimeter of the cesspit resulting in a nearly complete separation of the cesspit walls.

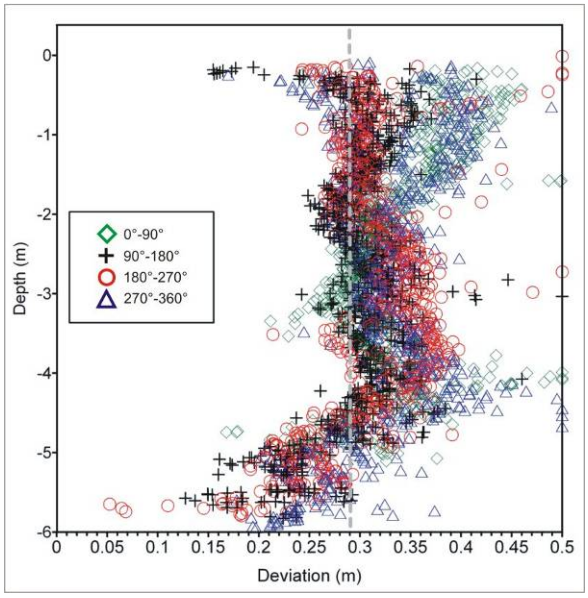

Fig. 3: Deviation of the points of the uppermost 6 m of the cesspit vs. the depth below surface level. For clarity only 1 out of 1000 measured points is shown. The symbols show the azimuth of each point

To further quantify the damage, the measured cesspit surface was compared to an ideal cylinder with a diameter of 2.38 m and a length of 6.46 m. The ideal cylinder was fixed using the points from the cesspit and a best-fit routine. The resulting cylinder was aligned to the local reference system. The deviation was also calculated from a smaller ideal cylinder. The color codes in Fig. 2B illustrate the deviations between the cesspit and the ideal cylinder. In Fig. 3, the directional data are shown compared to the ideal best-fit cylinder (grey line).

The data show a maximum displacement between 8 and 20 cm in the depth range 3.5 to 6.0 m. At a depth of 4.0 m the damage area of the northeastern wall is clearly visible (green diamonds in Fig. 3). These results correspond to similar measurements from a Roman well located 15 m east of the cesspit that also exhibits strong deformations, here at a depth of 38-44 m a.s.l. The area of investigation is located at the slope of a former sidearm of the Rhine River. In both, the cesspit and the Roman well, the damage zones are at the level of the natural ground. A medieval well ca. 20 m to the South, however shows no significant damages, suggesting a *terminus ante quem*. The large deviations in the first meter of the cesspit in figure 3 result from the inlet and the doming of the construction at the top.

DISCUSSION

We present a case study for application of 3D laser scanning in archaeology and archaeoseismology. Due to safety reasons, it was not possible to excavate the entire medieval cesspit in the Archaeological Zone Cologne, without successive restorations. The 3D laser scanning allowed reconstruction of a virtual cesspit model in its unrestored condition. When the excavation is finished and the pit secured, differences between the original and the final excavated structure can be further quantified. In addition, the 3D virtual model allows quantification of damages at a resolution of 1-2 mm. To investigate the cause of these damages (e.g. anthropogenic, seismogenic etc.) the damage database thus created provides a foundation for further numerical analysis of the structures to be combined with additional geodetic data and the archaeological results, in particular estimates for absolute time scales.

Acknowledgements: The project is financed by the Deutsche Forschungsgemeinschaft (DFG Hi660/2-1). We are grateful to the staff of the Archaeological Zone Cologne for the cooperation. Sharon K. Reamer helped shaping the manuscript.

References

Camelbeek, T. & Meghraoui, M. (1998): Geological and geophysical evidence for large palaeo-earthquakes with surface faulting in the Roer Graben (northwest Europe). Geophysical Journal International, Vol. 132, 2, 347-362.

Grübel, M. (1999). Seit 321 – Juden in Köln – Synagogue Community of Koeln

Hinzen, K.-G., and Reamer, S.K. (2007). Seismicity, seismotectonics, and seismic hazard in the northern Rhine area, in Stein, S., and Mazzotti, S., ed., Continental Intraplate Earthquakes: Science, Hazard, and Policy Issues: Geological Society of America Special Paper 425, p. 225–242.

Hinzen, K.-G. and S. Schütte (2003). Evidence for Earthquake Damage on Roman Buildings in Cologne, Germany. Seismological Research Letters, 74, 124-140.

GEOLOGICAL AND ARCHAEOLOGICAL RECORD OF THE 1504 AD CARMONA EARTHQUAKE (GUADALQUIVIR BASIN, SOUTH SPAIN): A REVIEW AFTER BONSOR (1918) BASED ON THE ESI-2007 SCALE

P.G. Silva (1), M.A. Rodríguez Pascua (2), R. Pérez López (2), J.L. Giner-Robles (3), J. Lario (4), T. Bardají (6), J.L. Goy (1) and C. Zazo (6)

(1) Dpto. Geología, Escuela Politécnica Superior de Ávila, Universidad de Salamanca. Hornos Caleros, 50. 05003-Ávila. SPAIN. pgsilva@usal.es
(2) Área de Riesgos Geológicos. Instituto Geológico y Minero de España. Ríos Rosas, 23. 28003-Madrid. SPAIN. ma.rodriguez@igme.es, r.perez@igme.es
(3) Dpto. Geología. Facultad de Ciencias. Universidad Autónoma de Madrid. Tres Cantos. Madrid. SPAIN.
(4) Facultad de Ciencias. Universidad Nacional de Educación a Distancia (UNED), 28040-Madrid. SPAIN
(5) Dpto. Geología, Universidad de Alcalá de Henares, 28871- Alcalá de Henares, Madrid SPAIN
(6) Dpto. Geología, Museo Nacional de Ciencias Naturales (CSIC), 28006-Madrid SPAIN

Abstract: *Data reported by George Bonsor (1918) about damage in the City of Carmona (Sevilla, South Spain) triggered by the 1504 AD Earthquake (X MSK) constitutes the first archaeoseismological report published in the Spanish Scientific literature. This work analyses and updates de Bonsor's data in the basis of the ESI-2007 Intensity Scale. Most of the described damage at the ancient Arab Castle of Carmona can be attributed to large landslide events on the Late Neogene calcarenites of "Los Alcores Scarp". Severely damaged localities within the Guadalquivir river floodplain can be attributed to site effect as probed by the documented far-field effects of the 1755 AD Lisbon with maximum intensities of VIII-IX MSK in this zone. The archaeological record around Carmona reach the Century 8th BC, and there are documented deformations of remains from early excavations in the Late 19th Century. Their analysis will result in a better knowledge of the seismicity within the Guadalquivir Basin.*

Key words*: Earthquake ground effects, Archaeoseismology, Guadalquivir Basin, South Spain.*

INTRODUCTION

George Bonsor (1885-1930), one of the archaeologists promoting the first modern excavations at *Baelo Claudia*, had its initial archaeological training around the Carmona County (Sevilla), documenting Tartesian, Roman, and Visigoth necropolis around Los Alcores Scarp. During the Congress of the Spanish Association for Progress of Science held in Sevilla in the year 1917, Bonsor meet one of the epoch outstanding geologists (Hernández-Pacheco, 1918). Their collaboration gave place to the publication of the earliest archeoseismological paper in Spain, in which ground deformations are related with the earthquake occurred on 5th April 1504 AD (Bonsor, 1918). The Carmona earthquake has been included in different published seismic catalogues (i.e. Galbis, 1932), with assigned maximum intensities of X MSK (Mezcua and Martínez Solares, 1983) and VIII-IX EMS (Martínez Solares y Mezcua, 2002) at their macroseismic epicentre around the locality of Carmona, about 30km northeast of Sevilla. Macroseismic information is available for no more than fifteen localities (Bonsor, 1918; Galbis,1932). This contribution offers a review of the earthquake ground effects and its archeoseis-mological record, on the light of the ESI-2007 Intensity Scale (Michetti et al., 2007), based on the observations of Bonsor and in progress field-research.

EARTHQUAKE DATA

Maximum intensities documented for the 1504 AD Carmona earthquake are clearly related to highly vulnerable sites from the geological point of view. These sites coincide with the floodplain of the Guadalquivir River (VIII to IX MSK) and the cuesta-type scarp of Los Alcores carved in gently dipping Late Neogene calcarenites where most of the damage occurred (X MSK). The earthquake caused 32 deaths, partial destruction of the Roman-Medieval city walls, most of the churches and towers of the city suffered severe damage, and many roofs and walls of houses collapsed. The most relevant documented damage was the Partial collapse of the ancient Arab Castle built on the Los Alcores Scarp in the eastern zone of the city (Bonsor, 1918). The cities of Sevilla, Alcalá del Rio, Cantillana, Tocina, Lora del Río, Villanueva del Rio, and Palma del Rio, located between 23-45 km away from the macroseismic epicentre suffered severe damage in churches, towers, city walls and village houses.

The earthquake was felt in most of the Iberian Peninsula and Northern Africa. At localities as far as Medina del Campo and Murcia (500-400 km away) caused panic (III-IV MSK?), it was strongly felt in North Africa, Málaga and Granada in a radius of about 150-200 km (V MSK) and destructive in El Algarve (SW Portugal) about 200 km away (≥ VI MSK?). However, the area of maximum damage within the Guadlaquivir Depression was of about 1300 km^2 (Fig. 1). Due to the very widely felt area, it could be an intermediate depth event. Different empirical approaches assign to this earthquake an estimated Magnitude of 6.2-6.8 Mw (FAUST PROJECT, Martínez Solares 2003), locating the epicentre at 5º36'W – 37º23ºN about 3 km SE of Carmona City, with a radius of confidence (epicentral error) of 14,2 km. No relevant faults are located in this area, except apparent gravity faults affecting the mainland scarp of the city and the controversial Guadalquivir Fault. This is a suspect fault zone separating the Palaeozoic materials of the Iberian massif from the Neogene materials of the Guadalquivir Basin (foreland basin of the Betic Cordillera) running NE-SW along the northern border of the Guadalquivir river valley (Goy et al., 1994), about 40 km North of Carmona (Fig. 1).

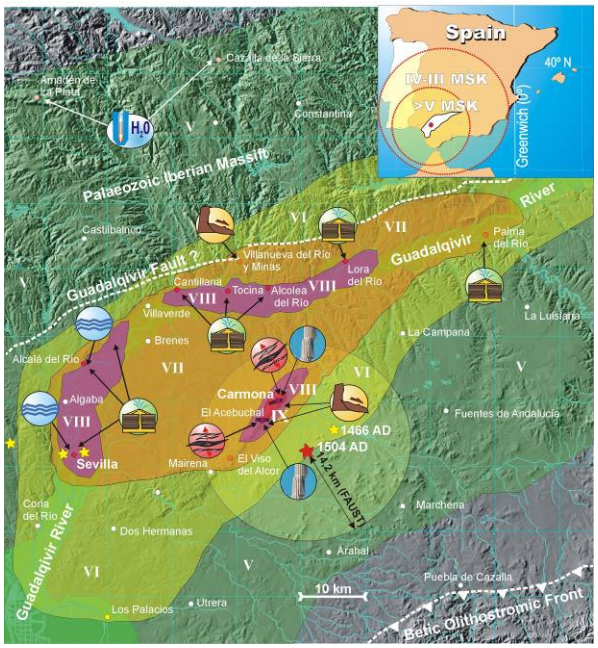

Fig. 1: Isoseismal Map (MSK) of the 1504 AD Carmona Earthquake based on historical descriptions and coseismic secondary effects illustrating categories of the ESI-2007 Scale (ground cracks, slope movements, liquefaction processes, anomalous waves and flooding in rivers and temporary turbidity changes in wells) and sites with archaeoseismic damage (IGCP567 Logo). Epicentral location parameters (red star) and error radius are from FAUST PROJECT: http://faustproject.com. Yellow stars indicate the macroseismic location of other historic moderate events (VI-VII MSK) Colours of localities indicate the recorded MSK intensity. White dots indicate no data. The delineation of isoseismal lines SE of Carmona is tentative (no data available for this zone)

The 1504 AD Carmona Event can be considered a seismic sequence which lasted almost one month and a half, when a main aftershock (V EMS) caused damage in the previously affected macroseismic area. Before, in 1466 AD a previous strong event (VIII EMS) caused significant damage around the same area of the Guadalquivir valley, but especially in the cities of Carmona and Sevilla (Galbis, 1932). The seismicity of the zone records about 30 seismic events for the period 900 – 1900 AD along the Guadalquivir Valley following the suspect Guadalquivir Fault. There are four recorded historical macroseismic areas in Sevilla (VIII EMS), Carmona (VIII-IX EMS), Córdoba (V-VI EMS) and Andújar (VIII-IX EMS).

EFFECTS ON NATURAL ENVIRONMENT

Coseismic ground effects produced by the earthquake can be classified as secondary effects of the ESI-2007 Scale (Michetti et al., 2007) including the categories of Slope Movements and large ground cracks (Los Alcores Scarp and Carmona City, about 3 to 10 km away). Liquefactions were widely reported within the Guadalquivir flood plain between Sevilla and Palma del Rio (45 km away). Anomalous waves in the Guadalquivir River, were only reported in Sevilla, 23 km away from the epicentre. Finally, within the category of Hydrological changes, temporal variation in the turbidity of wells were reported on two distant localities (Amadén de la Plata y Cazalla), located in the palaeozoic basement on the NW margin of the Guadalquivir Depression, about 60 to 70 km away of the epicentral area. The isoseismal map of figure 1 is not a conventional one due to the scarcity of the macroseismic data. It only illustrates theoretical MSK-ESI2007 intensity zones at the macroseismic area in relation to the topography (scarps) and the geology of the area (Guadalquivir flood plain) where main ground coseismic effects were recorded.

Slope Movements and Rockfalls.

These ground failures are mainly related with Los Alcores Scarp where the Carmona City is founded. This scarpment is a NW-SE trending active geomorphic feature within the southern margin of the Guadalquivir river valley, subject to relevant rockfalls, large landslides triggering differential settlement of buildings (Rodríguez Vidal and González Diez, 1987; Serrat and Ruíz; 1988; Baena, 1993). Free face of the scarp develops in a 30 to 70 m thick calcarenitic unit, resting upon a thicker marly messinian sequence and plastic olisthostromic sequences coming from the Betic Cordillera front located to the SE. The Palaeozoic substratum is about 1000 metres depth beneath the City of Carmona, whilst in the opposite margin of the Guadalquivir valley, about 30 km NW, the metamorphic Palaeozoic materials outcrop at the surface (Fig. 1).

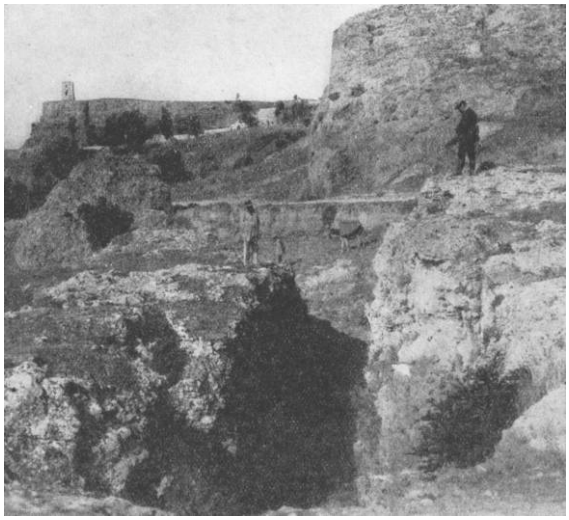

Fig. 2: Blocks of the Landslide triggered by the 1504 AD Carmona Earthquake affecting to the ancient Arab Castle (Original Photo Hernández-Pacheco, 1956)

Los Alcores Scarp is 140 m high in Carmona to about 40m high in Alcalá de Guadaira (25 km SE) where the scarp progressively dies-out. The scarp is a lineal geomorphic feature stepped by orthogonal NW-SE and NNE-SSW faults affecting to the Late Neogene calcarenites (Baena, 1993; Serrat and Ruíz, 1988). Faulting give place to relevant altitudinal changes of about 10-5 m on the scarp elevation. However, most of these intervening faults have been the preferential place for gully development from the Middle-Late Pleistocene, so their trace can only be delineated by means of the geomorphic anomalies recorded at the top of the scarp. Large landslide events were recorded along this scarp. The main one affected to the Alcázar (Arab Castle) of Carmona as documented by Bonsor (1918). Maximum vertical displacement of the slide was of 1.8 m with associated left lateral displacements of a maximum of 1.4 m. The larger fracture

affecting the Alcázar was about 500 m long, 6,6 m wide, seated to a depth of 8 m, where it is about 3.5m wide. The main fracture had a E-W orientation in the Castle walls, but a NE-SW towards the city for at least 1 km (Fig. 3). The total mobilised material for this individual landslide exceed 800,000 m^3, indicating an ESI-2007 intensity ≥ VIII. Additionally, large calcarenite blocks between 10 and 500 m^3 rolled downslope for a maximum distance of about 1 km (Figs. 3 and 4). Similar fractures and scattered rockfalls where also documented along 25 km between the localities of Carmona and Alcalá de Guadaira (Bonsor, 1918). Some of the individual blocks exceed 300 m^3, as is the case of the Tartessic "Peña de los Sacrificios" (Century 8-6th BC) located at the ancient necropolis of "El Acebuchal" 3 km SW of Carmona. In this case this corresponds to more ancient large rockfall events previous to the 1504 event studied here. Finally, 1,5 km SE of Carmona rockfalls affected the ancient Visigoth graves (Century 5th – 7th AD) carved of the calcarenites at the top of the cliff in the Cuesta del Chorrillo Site about 1 km SE of the damaged Castle. Large blocks with inset Visigoth graves were removed from the cliff and rolled downslope. In this case rockfall events are older than the 8th Century AD (Muslim Conquest of Iberia) but may correspond to pre 1504 AD events.

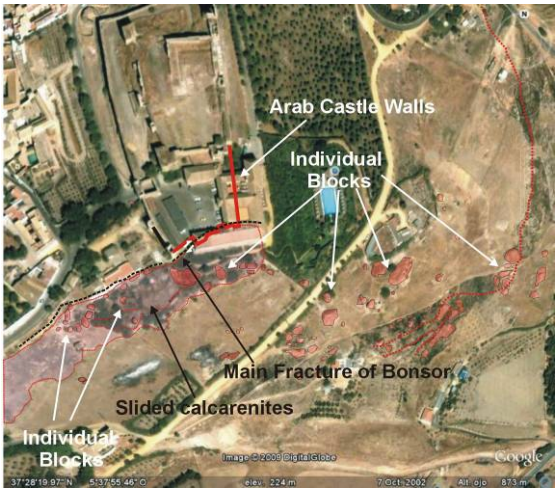

Fig. 3: Aerial plant-view (Goggle Earth) displaying the E-W fracture on the Castle walls mapped by Bonsor (1918) in the framework of mapped landslide area and individual blocks that rolled down during the 1504 AD Carmona Earthquake. The recent building constructed on the ancient damaged ruins of the Castle is the Parador de Turismo of Carmona

Fractures and Ground cracks.

Main fractures and cracks occurred in relation with the aforementioned landslide event affecting the Alcázar (Fig. 3). The main open crack ruptured the hard-rock calcarenitic substratum it was more than 1 km long and had a variable width from 0.85 to 5 m. The maximum width (2-5 m) was recorded within the city close to the ancient Convent of "Los Jerónimos". Two more subparallel large cracks where documented by Bonsor (1918). All these fractures had a broad orientation of E-W at the cliff to NE-SW within the city. Large cracks where also documented at the ancient roman necropolis of Carmona (1st Century BC – 2nd Century AD) affecting the big cave-graves carved on the calcarenites with broad SE-NW orientation about 2 km East of the Alcázar. Cracks had centimetric opening affecting both the floors and the roofs of the graves, in some of them causing partial collapses of the roofs (Bonsor, 1918). Similar fractures occurred from a distance of 3 km SW of Carmona at the ancient Necropolis of "El Acebuchal". Bonsor (1918) documented an open fracture of at least 500 m length affecting both, a post-neolithic settlement and ancient tartessic graves (Century 8-6th BC). At the tartessic graves zone the fracture had about 200 m length, an opening of 0.5-1.5 m and a depth of 3-4 m, with a broad NE-SW orientation. Features and dimensions of the aforementioned open cracks point to maximum IX-X ESI-2007 intensities over Los Alcores Cliff.

Fig. 4: Present view of the Los Alcores Scarp at the ancient Arab Castle affected by landsliding during the 1504 AD event. Big arrows (landslided blocks ≥ 300 m^3). Small arrows (blocks <80 m^3) rolled downslope

Liquefaction processes.

Localized liquefaction about 25 to 43 km away from the epicentre was reported in the Guadlaquivir floodplain affecting the localities of Sevilla, Alcalá del Rio, Cantillana, Tocina y Palma del Rio covering an area of about 450 km^2. General descriptions indicate opening of ground fissures and big craterlets in the soft-sediemntary filling of the floodplain accompanied by ejection of sand and muddy water. Historical descriptions indicate that water ejection ceased immediately after the ground shacking, and fissures and craterlets were sealed. The precise location of these effects is today impossible to envisage due to the short-term preservation in the geomorphic record of this kind of coseismic features. These scarce data indicate a minimum VIII ESI-2007 intensity for the Guadalquivir floodplain, with two main zones of about 180-200 km^2 each (Sevilla-Alcalá and Cantillana-Palma del Río zones; Fig. 1).

Anomalous waves and overflow of river courses.

This secondary effect is only reported for the cities of Alcalá del Río and mainly Sevilla (Fig. 1). Significant waves were observed surpassing the meter scale. The water level was elevated about three-four times its normal level causing shoaling and destruction of boats, fish mortality and many overflow cases in the country side accompanied by land subsidence. Some trees were partially covered by the water between Sevilla and Alcalá del Río.

Increase of the turbidity of water in wells and springs.

The increase of turbidity of water on springs is only expressly cited for the localities of Almadén de la Plata and Cazalla de la Sierra located 67 and 60 km away from the macroseismic epicentre on the Palaeozoic basement at the northern margin of the Guadalquivir Depression (Fig. 1). However historical descriptions indicate that this phenomenon affected many wells and springs of all the destroyed cities around the Guadalquivir Depression

(Bonsor, 1918). These descriptions indicate that minimum intensities of about V-IV ESI-2007 affected all the localities in a radius of about 70 km around the epicentre.

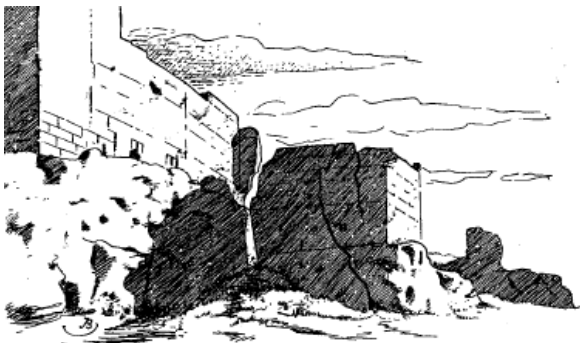

Fig. 5: Original draw of Bonsor (1918) illustrating the large fracture affecting the southern walls of the ancient Alcázar (Arab Castle) of Carmona

DOCUMENTED ARCHAEOSEISMIC DAMAGE

Archeoseismic damage documented in Carmona site has its maximum illustrative case in the damage of the ancient Alcázar carefully mapped by Bonsor in 1918 (Figs. 3 and 5). The damage has been described in previous sections in relation to landslide events and fractures. The rest of the damage cases within the city, mainly affecting to convents, churches and related towers is presently impossible to document at the reported buildings. Most of the church towers were severely damaged by the far-field effects of the well-known 1755 AD Lisbon Earthquake, felt with intensity VIII MSK/VII EMS in Carmona and IX MSK/VIII EMS within the Guadalquivir Valley affecting the same localities as the 1504 AD event (Martínez Solares, 2001). In Carmona most of the Church-towers were severely affected, some of them collapsed and most of them were demolished or rebuilt. On the Contrary, the documentation of Bonsor (1918) and Galbis (1932) will allow the analysis of cited archeoseismological damage of previous historic events probably affecting the ancient tartesian, phoenician, roman and Visigoth remains around Carmona between the Century 8th BC and 7th AD. This will help us assess (or identify) the occurrence of proto-historic seismic events. The only documented historic earthquake before the 1504 AD is the 1466 AD Carmona event (Galbis, 1932) of VIII MSK intensity. Galbis (1932) described severe damages in the Carmona Walls, in the ancient Queen Castle (northern zone of Carmona), eventually demolished in 1501 AD before the studied event and in the so-called "Caños de Carmona" a large roman aqueduct at Sevilla City.

CONCLUSIONS

Paleoseismic and archaeoseismic damage at the Carmona city and county documented by Bonsor (1918) deserves to implement a preliminary macroseismic analysis of the 1504 AD event. All the documented effects can be catalogued as secondary ground effects of the ESI-2007 Scale.

Maximum intensities of IX ESI-2007 can be preliminary assessed for the Carmona City in the basis of documented landslide events, rockfalls and fractures affecting the Alcázar. VII-VIII ESI-2007 intensity can be proposed for the floodplain zone of the Guadalquivir River affected by this event based on a variety of documented secondary coseismic effects. Far field effects of the 1755 AD Lisbon Earthquake in this zone clearly illustrate the high seismic vulnerability of these zones indicating the unfavourable geological site conditions and the topographic effects causing high amplification that was recorded in the intensity distribution of the macroseismic zone of the 1504 AD event. Additionally a wide variety of archeoseismological information is available for this sector of the Guadalquivir valley, ranging from the 8th Century BC to the 7th Century AD. The field-analysis of this information will help to understand the seismic cycles and recurrence intervals of this zone of the Guadalquivir Basin, placed in a relevant crustal boundary between the Palaeozoic massif of the Iberian Peninsula (to the NW) and the Olisthostromic Front of the Betic Cordillera (to the SE).

Acknowledgements: This work has been supported by the Spanish research projects ACI2008-0726, CGL08-03998BTE, CGL08-04000BTE and ACTISIS CGL2006-05001/BTE. This is a contribution of the Spanish Working Group of the INQUA Focus Group on Paleoseismology and Active Tectonics and to the IGCP 567Project.

.

References

Baena, R. (1993): Evolución cuaternaria (3 M.a) de la Depresión del Medio-Bajo Guadalquivir y sus márgenes (Córdoba y Sevilla). Tesis Doctoral Universidad de Sevilla, Sevilla, Spain. 589 pp.

Bonsor, J. (1918): El terremoto de 1504 en Carmona y en los Alcores. Bol. R. Soc. Esp. Hist. Natural, 18, 115-123.

Galbis Rodríguez, J. (1932). Catálogo Sísmico de la zona comprendida entre los meridianos 5º E y 20º W de Greenwich y los paralelos 45º y 25º Norte, Tomo I. Instituto Geográfico Catastral y de Estadística, Madrid.

Goy, J.L., Zazo, C. and Rodríguez-Vidal, J. (1994). Cordilleras Béticas – Islas Baleares. In: Geomorfología de España (M. Gutiérrez Elorza Ed.). Ed. Rueda, Madrid (Spain). 123-157.

Hernández-Pacheco, E. (1918). Nota adicional a la del Sr. Bonsor respecto al terremoto de Carmona. Bol. R. Soc. Esp. Hist. Natural, 18. 123-126.

Hernández-Pacheco, E. (1956). Fisografía del Solar Hispano. Mem. Real Acad. Ciencias Exactas, Físicas y Naturales, 26 (Serie Ciencias Naturales). Madrid.

Martínez Solares, J.M. (2001). Los efectos en España del Terremoto de Lisboad (1 de noviembre de 1755). Monografías IGN, 19. IGN, Madrid (Spain), 253 pp.

Martínez Solares, J.M. (2003). Sismicidad histórica de la Península Ibérica. Física de La Tierra, 15. 13-18.

Martínez Solares, J.M. and Mezcua, J. (2002). Catálogo Sísmico de la Península ibérica (880 AC – 1900 AD). Monografías IGN, 18. IGN, Madrid (Spain), 253 pp.

Michetti, A.M. et al. (2007): Intensity Scale ESI-2007. Memorie Descriptive Della Carta Geologica D'Italia, 74. APAT, SystemCart Srl, Roma, Italia.

Rodríguez Vidal, J. and González Díez, I. (1987): Dinámica de vertientes en los Alcores (Carmona, Sevilla). Actas VII Reunión sobre el Cuaternario, AEQUA, Santander (Spain), pp. 107-114.

Serrat, D. and Ruiz, J.L. (1988): Mapa Geomofológico de Carmona (985). Mapa Geológico de España 1:50.000. 2ª Edición. IGME, Madrid. 39 pp.

ARCHAEOSEISMOLOGY: PAST, PRESENT AND FUTURE

M. Sintubin (1), I.S. Stewart (2), T. Niemi (3) and E. Altunel (4)

(1) Department of Earth & Environmental Sciences, Katholieke Universiteit Leuven, Celestijnenlaan 200E, B-3001 Leuven. BELGIUM. manuel.sintubin@ees.kuleuven.be
(2) School of Earth, Ocean & Environmental Sciences, University of Plymouth, Plymouth PL4 8AA, U.K. iain.stewart@plymouth.ac.uk
(3) Department of Geosciences, University of Missouri-Kansas City, 5110 Rockhill Road, Kansas City, Missouri 64110-2499, U.S.A. niemit@umkc.edu
(4) Department of Geological Engineering, Eskişehir Osmangazi Üniversitesi, 26480, Eskişehir, TURKEY. ealtunel@ogu.edu.tr

Abstract: *Reflecting on the burgeoning scientific discipline of archaeoseismology a clear trend can be discerned. What started as an "extravaganza" in a good story (archaeological perspective) became a multidisciplinary effort to get a maximum amount of information on the parameters of ancient earthquakes out of archaeological evidence (seismological and archaeoseismological perspective). A clear shift can be observed from a more qualitative approach focussing on the extension of earthquake catalogues to a more quantitative approach concerning site effects. But looking into the future, the vocation of archaeoseismology may lie elsewhere. Archaeoseismology could become a holistic interdisciplinary discipline concerned with establishing the essential earthquake culture in a region (sociological perspective).*

Key words*: archaeology, earthquake, seismic culture*

ARCHAEOSEISMOLOGY

Archaeoseismology is the study of ancient earthquakes through traces left into archaeology the archaeological record. In this respect it is commonly considered that this burgeoning scientific discipline aims at bridging the gap between instrumental and historical seismology on one side and palaeoseismology and earthquake geology on the other (e.g. Caputo and Helly, 2008).

To date, the scientific community remains rather sceptical as to whether cultural material data – destruction layers, structural damage to manmade constructions, displaced manmade structures, indications of repair and abandonment, and inscriptions – can reliably be used as earthquake indicators at all. The extent to which this research field can contribute to seismic-hazard analysis still remains to be proven.

PAST: AN ARCHAEOLOGICAL PERSPECTIVE

Archaeologists, like e.g. Arthur Evans (1928) or Claude Schaeffer (1948), introduced earthquakes into archaeology. Earthquakes were used rather indiscriminately – as a '*deus ex machina*' – to explain the otherwise inexplicable, such as the sudden desertion of a site or its destruction at a time when no marauders were known. Earthquakes simply added drama and conjecture to a site's history. In such interpretations the basic physical parameters of earthquakes are often ignored, especially where imprecise age control leads to discrete multiple seismic events being amalgamated, thereby giving rise to seismological monsters (Guidoboni, 2002) that are "beyond the limits of possible" (Ambraseys et al. 2002). While critics portray this approach as neocatastrophism (Ambraseys, 2006), advocates see the earthquake hypothesis as the simplest solution, referring to Occam's razor (Nur, 2008). The question should though be asked if calling upon earthquakes shouldn't rather be seen as an easy trap in earthquake-prone regions.

PRESENT: A SEISMOLOGICAL PERSPECTIVE

An accurate catalogue of historical and prehistorical earthquakes is a necessary tool for assessing the seismic hazard of a region. And yet, the archaeological record would seem ideal to augment the grossly incomplete historical records of past seismicity. Historical catalogues typically document only a few percent (Ambraseys et al., 2002) of the damaging seismic shocks that have struck a region over centuries to millennia. The missing population of earthquakes clearly tempers reliable seismic-hazard assessment, but information on seismic effects at archaeological sites can extend the earthquake record beyond written sources, and consequently, ought not to be neglected (Kovach and Nur, 2006). So it seems perplexing that archaeological data have thus far been largely neglected by seismic-hazard practitioners.

But once again some pitfalls are to be avoided that adds to the scepticism by seismologists with respect to archaeoseismology. On the one hand, the danger exists that the anomalous or "rogue" earthquakes, supposedly proven by archaeologists, will be used by seismologists as real events in a seismic-hazard analysis (Ambraseys et al., 2002). On the other hand, confronting historical earthquake catalogues and archaeological data also carries a risk. The correlation of archaeological evidence – often with a poor temporal resolution – with documented earthquakes in a catalogue produces circular reasoning (Niemi, 2008)

Seismic-hazard practitioners need exact dates and magnitudes of past earthquakes. The question can be asked if archaeological evidence can actually provide the seismologist this information.

Fig. 1: Series of aligned fallen columns (top: Susita, Golan Heights; bottom: Knidos, Turkey), typical earthquake-characteristic damage?

PRESENT: AN ARCHAEOSEISMOLOGICAL PERSPECTIVE

Archaeoseismology is plagued by many of the same ambiguities that geologists encounter when interpreting earthquake indicators in the landscape or in palaeoseismological trenches. All are prone to naturally disruptive processes that can mimic the expression of seismic rupture or shaking. But cultural material data bear the additional vagaries of uncertain human action, from the questionable quality of construction to the potential for manmade destruction. The result is that it is difficult – if not impossible – to irrefutably distinguish between damage caused by man or competing natural agents. Typologies of earthquake-characteristic damage (Fig. 1) have been proposed but when subjected to critical appraisal – in particular through numerical and analogue modelling (e.g. Hinzen et al., 2009) – most of these typologies do not pass the test. Even if they could, it remains uncertain how the seismic traces in destruction layers and dislocated buildings can be meaningfully translated into earthquake parameters such as intensity, peak ground acceleration, etc.

To overcome these uncertainties, conceptual – primarily qualitative – archaeoseismological schemes have been proposed, consisting of a list of points of interest (Karcz and Kafri, 1978, Nikonov, 1988, Rapp, 1986, Stiros, 1996), key research questions (Guidoboni, 1996), or flow charts (Galadini et al., 2006) that ought to be considered during the investigation of an archaeological site by collaborative teams of seismologists, geologists, archaeologists, architects and historians. Most of these schemes have been grafted onto archaeological investigations in the eastern Mediterranean and in the Middle East, with strong dependence on identifying structural damage to buildings and other cultural remains at specific sites.

A more quantitative scheme has been proposed by Hinzen (2005) in the form of a feasibility matrix for archaeoseismological findings that evaluates a probability of occurrence of a proposed ancient earthquake and that can be directly used as a weighting factor in probabilistic-based estimations of the seismic hazard. Sintubin and Stewart (2008) integrated the competing schemes into a standardised, semiquantitative logic-tree formalism for archaeoseismology, assessing the level of certainty to which an archaeological site has recorded an ancient earthquake.

In spite of all these efforts and given the all too obvious limitations and constraints of the archaeological record, perhaps it is timely to reconsider what archaeoseismology is all about. Can we legitimately claim that it is a potential contributor to probabilistic seismic hazard studies? Or does the true value of archaeoseismological research lie elsewhere?

Archaeological sites may have a potentially unique value in earthquake science. Rather than simply augmenting earthquake catalogues with – potentially highly conjectural – ancient earthquakes, ancient archaeological sites can be used strategically to examine specific earthquake scenarios. Key targets could be those major events that appear form historical accounts to be atypically destructive, but whose excessive reach and intensity warrant careful appraisal, e.g., events such as the A.D. 21 July 365 Crete earthquake and tsunami. In this context, archaeological sites become “seismoscopes” – the testing ground for predicted site effects of ancient earthquake models.

FUTURE: A SOCIOLOGICAL PERSPECTIVE?

But maybe the scope and goals of archaeoseismological studies should still be broadened, benefiting from more intimate collaborations between earthquake geologists and archaeologists in deciphering the precise role of earthquakes in the cultural history of a site. A better appreciation of the complex dynamics by which ancient cultures dealt with and responded to damaging earthquakes, might shed light on the resilience of past societies and their relative capacity to withstand seismic shocks.

By highlighting how their ancestors coped with earthquakes, archaeoseismology could play a key role in fostering better earthquake preparedness in modern local communities that are equally threatened. After all, natural disasters are no physical phenomena, but are social phenomena (Shimoyama 2002). Rather than simply deriving crude parameters for ancient earthquakes,

archaeoseismology could instead become a more holistic and interdisciplinary research field concerned with establishing the essential earthquake culture in a region (Sintubin et al., 2008). The International Geoscience Programme IGCP 567 *Earthquake Archaeology: Archaeoseismology along the Alpine-Himalayan Seismic Zone* (ees.kuleuven.be/igcp567/) provides the forum to pursue these goals.

Acknowledgements: This paper is a contribution to the UNESCO-funded International Geoscience Programme IGCP 567 *Earthquake Archaeology: Archaeoseismology along the Alpine-Himalayan Seismic Zone*.

References

Ambraseys, N. N. (2006). Earthquakes and archaeology. Journal of Archaeological Science, 33, 1008-1016.

Ambraseys, N. N., Jackson, J. A., Melville, C. P. (2002). Historical Seismicity and Tectonics: The Case of the Eastern Mediterranean and the Middle East. In: International Handbook of Earthquake and Engineering Seismology (edited by Lee, W. H. K., Kanamori, H., Jennings, P. C. and Kisslinger, C.). International Geophysics Series 81A. Academic Press, Amsterdam, 747-763.

Caputo, R., Helly, B. (2008). The use of distinct disciplines to investigate past earthquakes. Tectonophysics, 453(1-4), 7-19.

Evans, A. 1928. The Palace of Minos, part II., London.

Galadini, F., Hinzen, K.-G., Stiros, S. C. 2006. Archaeoseismology: Methodological issues and procedure. Journal of Seismology, 10, 395-414.

Guidoboni, E. (1996). Archaeology and Historical Seismology: the Need for Collaboration in the Mediterranean Area. In: Archaeoseismology (edited by Stiros, S. C. and Jones, R. E.). Fitch Laboratory Occasional Paper 7. Institute of Geology and Mineral Exploration and The British Scholl at Athens, Athens, 7-13.

Guidoboni, E. (2002). Historical Seismology: the Long Memory of the Inhabited World. In: International Handbook of Earthquake and Engineering Seismology (edited by Lee, W. H. K., Kanamori, H., Jennings, P. C. and Kisslinger, C.). International Geophysics Series 81A. Academic Press, Amsterdam, 775-790.

Hinzen, K.-G. (2005). The use of engineering seismological models to interpret archaeoseismological findings in Tolbiacum, Germany: A case study. Bulletin of the Seismological Society of America 95, 521-539.

Hinzen, K.-G., Fleischer, C., Reamer, S.K., Schreiber, S., Schütte, S. and Yerli, B. (2009). Quantitative Methods in Archaeoseismology. 1st INQUA-IGCP567 International Workshop on Earthquake Archaeology and Palaeoseismology, Baelo Claudia, Spain, this volume.

Karcz, I. and Kafri, U. (1978). Evaluation of supposed archaeoseismic damage in Israel. Journal of Archaeological Science, 5, 237-253.

Kovach, R. L. and Nur, A. (2006). Earthquakes and Archaeology: Neocatastrophism or Science? In: EOS, Transactions, American Geophysical Union, 87, 317-318.

Niemi, T. (2008). Historical Earthquake Catalogues and Archaeological Data: Avoiding Circular Reasoning. Seismological Research Letters, 79(2), 289.

Nikonov, A. A. (1988). On the methodology of archaeoseismic research into historical monuments. In: Engineering Geology of Ancient Works (edited by Marinos, P. G. and Koukis, G. C.). Balkema, Rotterdam, 1315-1320.

Nur, A. (2008). Apocalypse. Earthquakes, Archaeology, and the Wrath of God. Princeton University Press, Princeton.

Rapp, G. J. (1986). Assessing Archaeological Evidence for Seismic Catastrophies. Geoarchaeology: An International Journal, 1(4), 365-379.

Schaeffer, C. F. A. (1948). Stratigraphie Comparée et Chronologie de l'Asie Occidentale. Oxford University Press, London.

Shimoyama, S. (2002). Basic characteristics of disasters. In: Natural Disasters and Cultural Change (edited by Torrence, R. and Grattan, J.). One World Archaeology 45. Routledge, London and New York, 19-27.

Sintubin, M. and Stewart, I. S. (2008). A Logical Methodology for Archaeoseismology: A Proof of Concept at the Archaeological Site of Sagalassos, Southwest Turkey. Bulletin of the Seismological Society of America, 98(5), 2209-2230.

Sintubin, M., Stewart, I. S., Niemi, T. and Altunel, E. (2008). Earthquake Archaeology - Just a Good Story? Seismological Research Letters, 79(6), 767-768.

Stiros, S. C. (1996). Identification of Earthquakes from Archaeological Data: Methodology, Criteria and Limitations. In: Archaeoseismology (edited by Stiros, S. C. and Jones, R. E.). Fitch Laboratory Occasional Paper 7. Institute of Geology and Mineral Exploration and The British Scholl at Athens, Athens, 129-152.

GEOLOGICAL-GEOMORPHOLOGICAL SETTING AND HUMAN INTERFERENCE DURING THE 13TH-15TH CENTURIES AD. AT VILNIUS LOWER CASTLE, EAST LITHUANIA

M. Stančikaitė (1), D. Kisielienė (1), J. Mažeika (1), R. Guobytė (2) and P. Blaževičius (3)

(1) Institute of Geology and Geography, Ševčenkos, 13. 03223-Vilnius. LITHUANIA. stancikaite@geo.lt
(2) Lithuanian Geological Survey, Konarskio, 35. 03223-Vilnius. LITHUANIA. rimante.guobyte@lgt.lt
(3) Institute of History and Archaeology of the Baltic Sea Region, University of Klaipėda. Tilžės, 13. 91251-Klaipėda. LITHUANIA. povilas@lietuvospilys.lt

Abstract: *Together with the archaeological data, results of geological-geomorphological investigations alongside with palaeobotanical data (pollen and plant macrofossils) and isotope (^{14}C) measurements were applied for the reconstruction of environmental situation and pattern of human activity during 13th-15th Century AD. in the surroundings of Vilnius Lower Castle. Studied zone is located on the third sandy terraces of river Neris (54º41"N, 25º17"E) surrounded by the residual relief formed during the retreat of the Late Weichselian ice sheet. A prominent complex of morainic hills (up to 160m a.s.l.) appears eastwards from the Castle zone and transform westwards into flat, sandy terraces (90m a.s.l.) of alluvial origin. Evidence of continuous cultivation of cereals including F. esculentum and S. cereale was coincident with landscape clearing indicated during the later 13th and early 14th Century AD. Temporary decline of human activity was recorded in the middle of 14th Century AD. The expansion of Vilnius Town recorded during the later 14th Century AD. continued during the 15th century AD. which is known as a period of economic and cultural prosperity.*

Key words: *environmental history, Middle Ages, Vilnius Castle, Lithuania*

INTRODUCTION

Multidisciplinary research on cultural landscape history provides scientists and society with a new data describing character and pattern of the human activity during the different stages of the prehistory or historical times. Evaluation of the environmental conditions and influence of different nature processes into the society may have been indicated as one of the main aims of similar survey.

Recent multidisciplinary investigations (geological-geomorphological survey, palaeobotanical (pollen and plant macroremain) and isotope (^{14}C) analysis) alongside with archaeological excavations were applied for the reconstruction of the environmental and human history in the territory of Vilnius Lower Castle, east Lithuania (Fig. 1A).

DISCUSSION

Formation of the surface in the biggest part of the present Lithuania territory has been determined by the Late Weichselian ice sheet (Guobytė, 2002). Marginal formations of this Glaciation cross the south eastern part of the country (Fig. 1B) creating characteristic landscape of Vilnius Town with Vilnius Castles are within these marginal formations, in the confluence of Neris and Vilnelė Rivers that makes landscape even more attractive (Fig. 2A). The prominent hills, of erosive origin, that appear eastwards from the Vilnelė River transform westwards into flat, sandy terraces of alluvial origin. Constructed on this landscape, the Vilnius Castles complex consisted of an Upper Castle that was situated on a top of an erosion hill (~140 m a.s.l.) and a Lower Castle (91.6 m a.s.l.) that stretched at the foot of it (Fig. 2B). Constructions of the buildings were accurately fit to the geomorphological pattern of the territory (Fig. 3) especially during the earliest stages of the population.

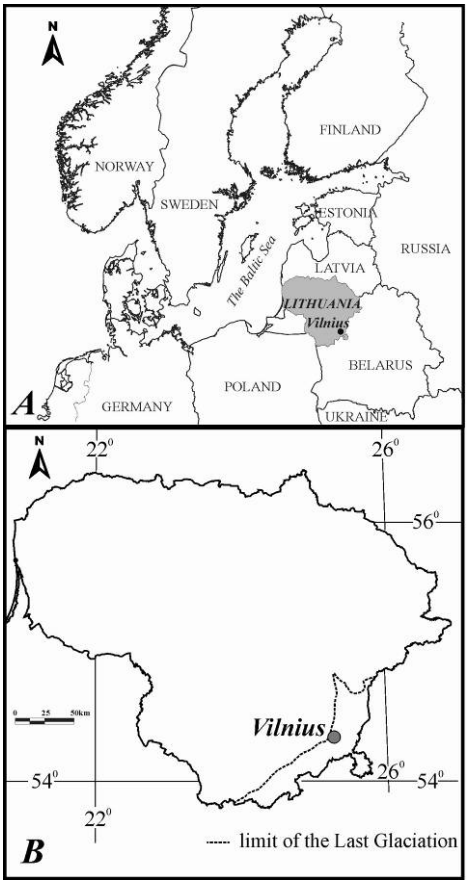

Fig. 1: Location of investigated site

In the area later occupied by Vilnius Lower Castle the oldest permanent settlement was established during the 5th–8th centuries AD. (Tautavičius and Urbanavičius, 1995). During the 9th–12th centuries human activity increased there, and from the onset of the 13th century AD., which generally coincides with the beginning of the Middle Ages in Lithuania (Kuncevičius, 2005), Vilnius became the centre of the Lithuanian state (Kitkauskas, 1989).

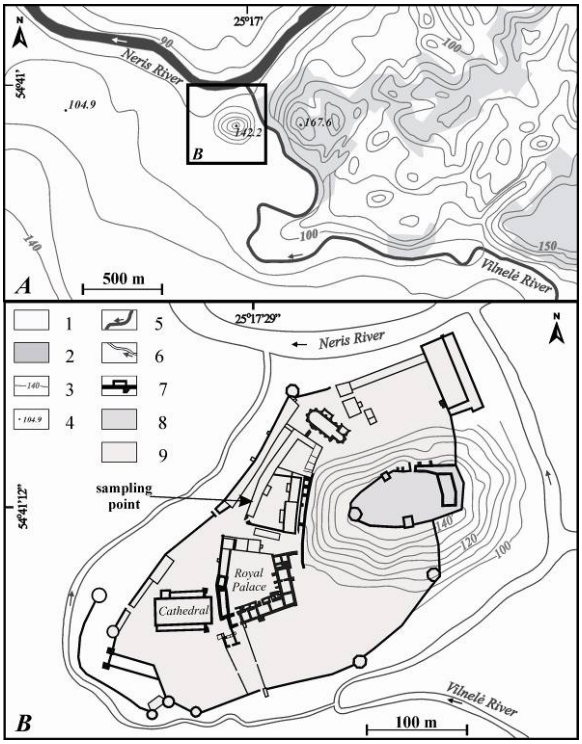

Fig. 2: Topographical situation of the Vilnius Castles
1-town area; 2-forested area; 3-isoline, m a.s.l.;
4-altitude, m a.s.l.; 5-rivers; 6-rivers and artificial streams; 7-buildings and constructions;
8-territory of Upper Castle; 9-territory of Lower Castle.

Vilnius Town was first mentioned in medieval documents in 1323–1325 AD. (Bumblauskas, 2005). Importance of Vilnius Town began to decrease in the 17th AD. century after the town was pillaged and burned by the Russian army in 1655 AD.

As recorded in historical documents, Vilnius began to prosper at the beginning of the 14th Century AD., when the overall importance of the town as a centre in this part of Europe for trade, religion, and politics noticeably increased and it was densely populated by the mid-14th Century AD. Intensive population growth resulted in significant environmental changes, as recorded by the archaeobotanical data. A low proportion of tree pollen suggests that woodland was replaced by open meadows and arable fields. *Panicum miliaceum* and *Secale cereale* macroremains and pollen of Cerealia, *Cannabis sativa*, *Linum usitatissimum* and *Fagopyrum*, point to intensive agricultural activity. As it is rather difficult to imagine intensive cultivation in this small, densely-populated area, we can assume that most of the pollen had been brought in to the Lower Castle together with the crop. The palaeoecological reconstruction indicates that some environmental changes took place at the site in the middle of the 14th Century AD. The abundance of ruderal taxa points to the existence of fallow land or an intensive settlement nearby. It is possible that these changes resulted from a reduction in agricultural activities or relocation of open plots outside the investigated site.

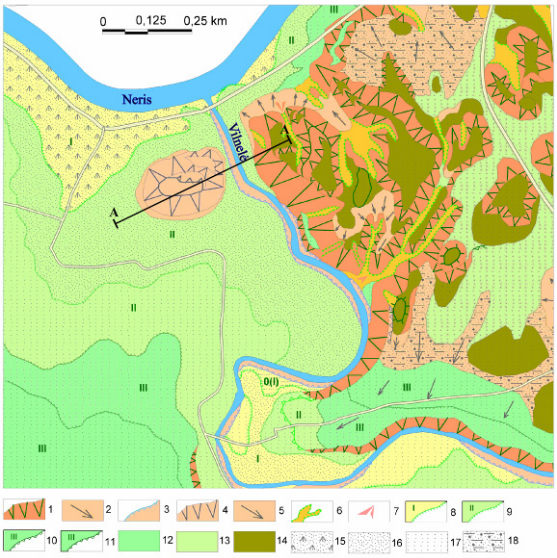

Fig. 3: Geological-geomorphological map of the area (original scale 1:10 000, compiled by R. Guobytė)
1-steep erosion slopes (natural); 2-flat slopes or fragments; 3-low (up to 1-3m) bank of river Vilnelė; 4-artificial slopes and terraces of the Castle hill; 5-gentle fragments of the flat relief; 6- bottom of ravine; 7-deltas of deliuvial origin; 8-the first terrace; 9-the second terrace consisting of two levels; 10-11-the third terrace consisting of two levels; 12-narrow fragments of glaciofluvial terrace on the steep slopes of erosion hills; 13-flat inter-hilly plains on the surface of erosion massive; 14-sandy hills of erosion massive – marginal formations of Saalian Glaciation; Composition of the surface sediments: 15-sand with organic; 16-very fine or fine grained sand; 17-fine grained sand with admixture of various grained sand and gravel; 18-various grained sand with clay; A – A geological cross section.

Archaeological and historical records document considerable increases in the human population of Vilnius during the second half of the 14th Century AD. (Urbanavičius, 2003), a period of significant changes in the history of the Lithuanian state and of Vilnius. In 1387, after the Christianization of Lithuania, Vilnius was granted Magdeburg Rights, and new parishes inhabited by strong Russian and German communities began to grow (Bumblauskas, 2005). Correspondingly rise in human pressure on the local environment increased. An open landscape with little woodland predominated in the region as shown by the archaeobotanical record. The presence of *Ficus carica* points to foreign trade.

Beinning of the 15th Century AD. was a period of progressive economic and cultural development in Lithuania and in Vilnius, which had become an important economic and trading centre for the entire eastern Baltic region (Urbanavičius, 2003). Low values of tree pollen and a predominance of long-distance transported *Pinus* pollen demonstrate the existence of large open areas, which in turn suggests the progressive development of the town. Macroremains of *Panicum miliaceum*, *Fagopyrum esculentum* and etc. together with weeds of cereals, flax

and millet fields, indicates that intensive agriculture took place in the region.

Acknowledgements: This study was funded by the Lithuanian State Science and Studies Foundation, as a part of the "PALEOKLIMATAS" project (C-07008).

References

Bumblauskas, A. (2005). Senosios Lietuvos istorija 1009–1795 (History of the ancient Lithuania 1009–1795). Ed. R. Paknio leidykla, Vilnius, 520 pp.

Guobytė, R. (2002). Lithuanian surface: geology, geomorphology and deglaciation. Abstract of doctoral dissertation. Vilnius University, Vilnius, 31 pp.

Kitkauskas, N. (1989). Vilniaus Pilys. Statyba ir architektūra. (Vilnius Castle. Construction and architecture). Ed. Mokslas, Vilnius, 273 pp.

Kuncevičius, A. (2005). Lietuvos viduramžių archeologija (Lithuanian Medieval Archaeology). Ed. Versus aureus, Vilnius, 200 pp.

Tautavičius, A., Urbanavičius, V. (1995). Archeologiniai tyrimai (Archeological investigations). En: Vilniaus Žemutinės pilies rūmai (1990–1993 metų tyrimai) (A. Tautavičius, ed.). Leidybos centras, Vilnius, 112–132.

Urbanavičius, V. (2003). Vilniaus Žemutinės pilies rūmai, 1996–1998 metų tyrimai (The Lower Castle of the Vilnius Palace, investigations of 1996–1998). Ed. Sapnų sala, Vilnius, 310 ppŽemutinės pilies rūmai (1990–1993 metų tyrimai) (A. Tautavičius, ed.). Leidybos centras, Vilnius, 112–132.

TRENCHING SURVEY ON THE SOUTH-EASTERN SECTION OF THE SUDETIC MARGINAL FAULT (NE BOHEMIAN MASSIF, INTRAPLATE REGION OF CENTRAL EUROPE)

P. Štěpančíková (1), J. Hók (2) and D. Nývlt (3)

(1) Dpt. Engineering Geology and Geofactors, Institute of Rock Structure and Mechanics, Academy of Sciences of the Czech Republic, V Holesovickach 41, 18209-Prague, CZECH REPUBLIC. stepancikova@irsm.cas.cz
(2) Dpt. Geology and Paleontology, Faculty of Science, Comenius University in Bratislava, Bratislava-Mlynská dolina, 842 15, Bratislava 4, SLOVAKIA. hok@fns.uniba.sk
(3) Czech Geological Survey, Brno Branch, Leitnerova 22, 658 69, Brno, CZECH REPUBLIC. daniel.nyvlt@geology.cz

Abstract: *The study area is situated in the north-eastern part of the Bohemian Massif and comprises the Czech portion of the morphologically well-pronounced NW-SE trending Sudetic Marginal Fault zone (SMF). In order to assess its Late Quaternary activity, trenching survey at two main localities were carried out. Due to petrological, sedimentological, and structural analyses, along with utilization of dating techniques, at least four movements since Mid Miocene within the SMF zone were documented. Moreover, the youngest event occurring in early Holocene as a prehistoric earthquake is suggested. It has appeared that trenching technique is the most powerful tool for near-fault investigation as the study localities are situated in intraplate region which has been considered to be of a low displacement rate and moreover in well vegetated area avoiding fault outcrops.*

Key words*: trenching, Sudetic Marginal Fault, Late Quaternary activity, intraplate region*

The study area is situated in the north-eastern part of the Bohemian Massif and comprises the Czech portion of the NW-SE trending Sudetic Marginal Fault zone (SMF). The zone represents one of the morphologically most prominent tectonic feature in central Europe (Badura et al., 2003, 2007). The structure relates to a well-pronounced mountain front of the Sudetic mountains at the length of 130km (Fig. 1). Despite the distinctiveness of the zone and the fact that neotectonic activity of the SMF has been studied intensively for several decades (e.g. Oberc and Dyjor, 1969; Mastalerz and Wojewoda, 1993; Dyjor, 1995; Krzyszkowski and Bowman, 1998; Krzyszkowski and Pijet, 1993; Krzyszkowski et al., 1995, 2000; Migoń, 1993; Ivan, 1997; Badura et al., 2003, 2007; Štěpančíková et al., 2008), its faulting history has not been fully elucidated yet. The SMF has been assumed to be a normal, steeply-dipping, fault (Oberc, 1977), although also a horizontal component has been documented (Mastalerz and Wojewoda, 1993). Within the fault zone, also Neogene vulcanites, mineral springs occur and epicentres of historical earthquakes are located. These earthquakes were estimated to reach epicentral intensity I_0=4-7, which, by Guterch and Lewandowska-Marciniak (2002), corresponds to

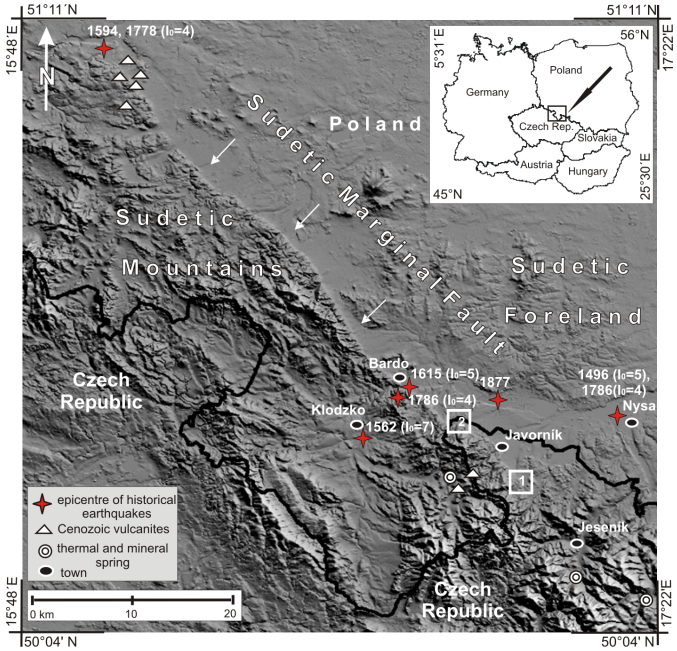

Fig. 1. Topographic situation of the morphologically well-pronounced Sudetic Marginal Fault dividing Sudetic Mountains and Sudetic Foreland. Numbered squares 1 – locality Vlčice, 2 – locality Bílá Voda. Data on historic earthquakes by Guterch and Lewandowska-Marciniak, 2002)

macroseismic magnitude M_M=3-4.9. However, these magnitudes are not considered to be enough for creating a relief (cf. McCalpin 1996). Thus, the presented research using near-fault investigation in artificial trenches in the Czech portion of the SMF was carried out in order to discover probable pre-historic faulting responsible for the mountain front morphology as well as to reveal the kinematics of the fault.

In order to select a suitable site for trenching, geomorphological investigation, analysis of the digital elevation model, and geophysical sounding (multi-electrode method, GPR) were carried out. The results of trenching in two localities (Vlčice and Bílá Voda) are presented here.

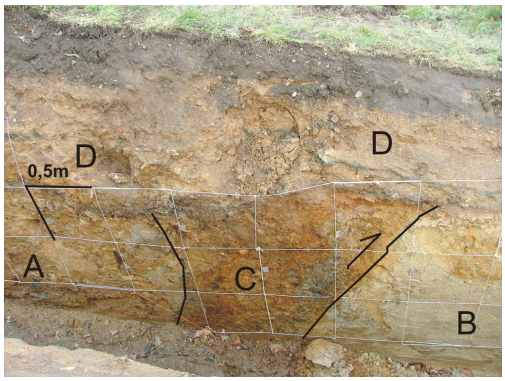

Fig. 2: Strike-slip fault zone with a feature of flower structure documented in the trench in Vlčice site. A – older Miocene unit, B – younger Miocene unit, C - deformation zone, D - early Holocene colluvium. Note the dragged B unit layers.

The trenching across the SMF at the first locality Vlčice on the N-S trending mountain front revealed succession of sedimentary units disturbed by tectonic features. The trench exposed crystalline rocks, three units of early to mid Miocene fluvial to limnic sediments with organic-rich beds (with graphite), Pleistocene alluvial fan deposits, and three sequences of Holocene colluvium. Several faults were documented: reverse faults (strike 160°, dip 40-70° to SW) displacing crystallinics over Miocene deposits, a subvertical deformation structure (probably strike-slip) within the Miocene sediments (strike 35°, dip 75° ESE; Fig. 2), and minor normal faults within the youngest Miocene unit (strike 145°, 45° to NE). Moreover, the three Miocene sedimentary members, positioned vertically next to each other, were probably dragged by the reverse fault. To determine the age of the identified deformations variously dated sediments were used. The dating included: known age of mid Miocene deposits, radiocarbon dating of charcoal and paleosols, and supposed Late Pleistocene age of the last gelifluction. Time constraint of the identified fault movements is given in Table 1. Movements disturbing Neogene deposits and pre-dating last gelifluction involve the reverse faulting that displaced crystalline rocks over the Miocene deposits, and horizontal movements. The younger movements occurred by reverse and normal faults.

One of the younger reverse fault within the crystalline rocks probably created a coseismic relief step, which is concealed by early Holocene colluvial deposits (10,940±140 cal. yrs BP). This step was documented 0.6 m high at the distance of 1.3 m and was covered by a colluvial wedge-like form. As the step must have been seen on the surface before the deposition of the Holocene sediments and at the same time it is not affected by Late Pleistocene gelifluction, the movements occurred probably on the boundary Pleistocene/Holocene. The youngest movements probably occurred in the lowest part of the slope and were related to normal faults. The faults cut the Miocene sediments and divide two area with diverse erosion/depositional regime. Moreover, this zone coincides with spring area and low resistivity zone shown by the geophysical sounding. This normal faulting predates the soil sediment (410±80 cal. yrs BP) buried by the youngest colluvium.

Trenching at the second locality Bílá Voda was carried out across NW-SE trending mountain front. The exposure revealed strike-slip fault zone (striking 135°-150°) dividing Paleozoic crystalline rock and Late Pleistocene colluvial deposits derived from the fault zone (Fig. 3). The deposits overlay Miocene sediments, which are warped. The fault has a flower structure character and shows several repeated movements. Kinematic indicators within the older structures show a sinistral component. However, the sense of the youngest movements will be able to recognize based on further trenching in this locality, since the recent stresses inferred from GPS and micro-displacements measuring are not unequivocal (see Badura et al., 2007, Štěpančíková et al., 2008).

Table 1: Time constraint of faulting history within the SMF identified at the trenching site Vlčice. The ages are based on the age of deformed sediments, radiocarbon dating of charcoals, and paleosols covering the deformed sediments.

type of deformation	time limits of movements	
	maximum	minimum
reverse faulting	15 Ma yrs BP	15-11 ka BP
horizontal movements	15 Ma yrs BP	15-11 ka BP
reverse faulting	15-11ka yrs BP	10,940 ± 140 cal. yrs BP
latest normal faulting	10,940 ± 140 cal BP	410 ± 80 calBP

Dating of movements is based mainly on the relative age of the Late Pleistocene fault-related colluvial deposits. Besides clasts of tectonic breccia, they include pebbles of eratic material coming from glacial deposits, whereas the last continental glacier reached the study area in Elsterian 2 (400-460 ka). Moreover, the Pleistocene deposits, fault zone, and crystalline rocks are covered by geliflucted layers of all the involved rock types and then by the youngest Holocene colluvial deposits (800±50 cal. yrs BP). Younger individual faults of the fault zone penetrate the Late Pleistocene deposits but they are concealed by the geliflucted layers. Since the coarse-grained fault-related deposits are quite homogeneous at the whole thickness (maximum confirmed 3.5m), no individual faulting events could be recognized. The youngest movements (probably horizontal with some vertical component) displaced even the geliflucted layers, while the vertical displacement made up around 35 cm (Fig. 4). These displaced layers are concealed by the recent Holocene colluvium. To estimate the magnitude of this last event, further trenching focused on horizontal offset identification will be necessary.

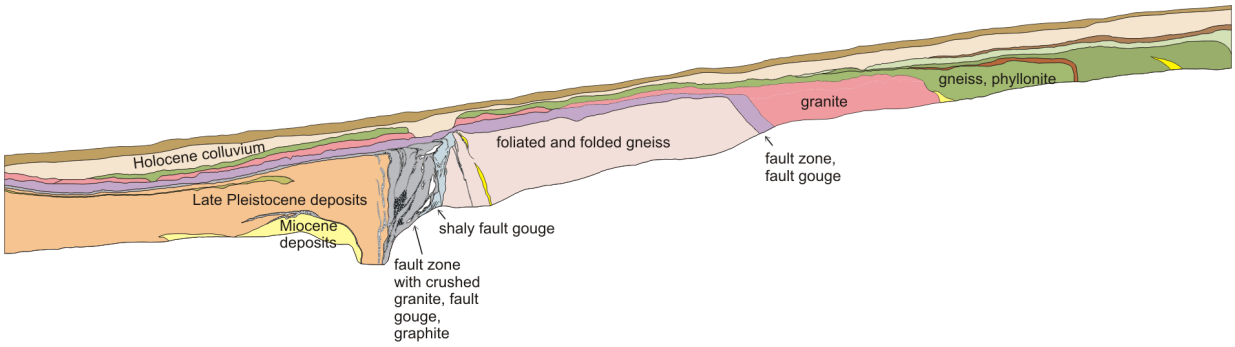

Fig. 3: Simplified log of the trench in Bílá Voda site with geological information. Geliflucted layers of crystalline rocks covering the crystalline bedrock and Pleistocene sediments are depicted in the same colour as their maternal rocks.

To conclude: due to petrological, sedimentological, and structural analyses, along with utilization of dating techniques, at least four movement phases from Mid Miocene to Holocene within the SMF zone were documented in the trenches. As during Pleistocene the area has been repeatedly reached by a continental ice-sheet, a record of Pleistocene tectonic activity is poorly preserved in the studied site and only wide time constraints can be proposed. However, Late Quaternary tectonic activity was revealed and even a prehistoric earthquake suggested.

The trenching technique has appeared to be a powerful tool of near-fault investigation since the study area is situated in a well-vegetated region with moderate climate and therefore devoid of fault outcrops. Moreover, the study area is situated in an intraplate region with a low displacement rate; consequently, higher erosion rate exceeds displacement rate, which does not favor the preservation of fault scarps.

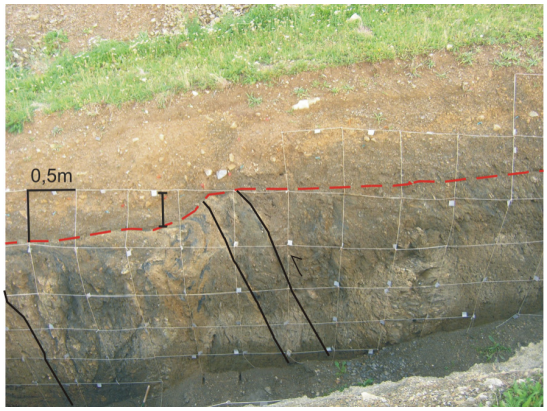

Fig.4: Vertical displacement (around 35cm) of Late Pleistocene geliflucted layers probably by strike-slip faults with a reverse component.

Acknowledgements: The research was supported by the Grant Agency of the Czech Republic No. 205/06/1828, by the Slovak Research and Development Agency under the contract No. APVV-0158-06 and has been elaborated within the Institute Research Plan of the Institute of Rock Structure and Mechanics, Academy of Sciences of the Czech Republic, No. AVOZ30460519.

References

Badura, J., Zuchiewicz, W., Górecki, A., Sroka, W., Przybylski, B., Zyszkowska, M. (2003): Morphotectonic properties of the Sudetic Marginal Fault, SW Poland. Acta Montana, Series A, 24 (131), 21-49.

Badura, J., Zuchiewicz, W., Štěpančíková, P., Przybylski, B., Kontny, B., Cacoń, S. (2007): The Sudetic Marginal Fault: a young morphotectonic feature at the NE margin of the Bohemian Massif, Central Europe. Acta Geodyn. Geomater., 4: 4 (148), 1-23.

Dyjor, S. (1995): Young Quaternary and recent crustal movements in Lower Silesia, SW Poland. Folia Quaternaria, 66, 51-58.

Guterch, B., Lewandowska-Marciniak, H. (2002): Seismicity and seismic hazard in Poland. Folia Quaternaria, 73, 85-99.

Ivan, A. (1997): Topography of the Marginal Sudetic Fault in the Rychlebské hory Mts. and geomorphological aspects of epiplatform orogenesis in the NE part of the Bohemian Massif. Moravian Geographical Reports, Brno, 5 (1), 3-17.

Krzyszkowski, D., Bowman, D. (1998): Neotectonic Deformation of Pleistocene Deposits Along the Sudetic Marginal Fault, Southwestern Poland. Earth Surface Processes and Landforms, 22 (6), 545-562.

Krzyszkowski, D., Pijet, E. (1993): Morphological effects of Pleistocene fault activity in the Sowie Mts., southwestern Poland. Zeitschr. Geomorph., N.F., Suppl.-Bd. 94, 243-259.

Krzyszkowski, D., Migoń, P., Sroka, W. (1995): Neotectonic Quaternary history of the Sudetic Marginal fault, SW Poland, Folia Quaternaria, 66, 73-98.

Krzyszkowski, D., Przybylski, B., Badura, J. (2000): The role of neotectonics and glaciation on terrace formation along the Nysa Kłodzka River in the Sudeten Mountains (southwestern Poland). Geomorphology, 33, 149-166.

Mastalerz, K., Wojewoda, J. (1993): Alluvial-fan sedimentation along an active strike-slip fault: Plio-Pleistocene Pre-Kaczawa fan, SW Poland. Spec. Publs. Int. Assoc. Sedimen. ,17, 293-304.

McCalpin, J. ed. (1996): Paleoseismology. Academic press, 588 pp.

Migoń, P. (1993): Geomorphological characteristics of mature fault-generated range fronts, Sudetes Mts., Southwestern Poland. Zeitschr.Geomorph. N. F., Suppl.-Bd. 94, 223-241.

Oberc, J., Dyjor, S. (1969): Uskok sudecki brzeżny. Biul. Inst. Geol., 236, 41-142.

Oberc, J. (1977): The Late Alpine Epoch in south-west Poland. In: W. Pozaryski (ed.), Geology of Poland, IV, Tectonics, Wydawn. Geol., Warszawa, 451-475.

Štěpančíková, P., Stemberk, J., Vilímek, V., Košťák, B. (2008): Neotectonic development of drainage networks in the East Sudeten Mountains and monitoring of recent fault displacements (Czech Republic). Special Issue on: Impact of Active econics and Uplift on Fluvial Landscapes and River Valley Development. Geomorphology, 102 (1), 68-80.

GEOMORPHOLOGY, PALEOSEISMOLOGY AND GEOLOGICAL ANALYSIS FOR SEISMIC HAZARD ESTIMATIONS

M. Tahir Mian (1)

(1) Hostel Building, Street # 1, Sector H-8/1, Islamabad, PAKISTAN. miantahir45@hotmail.com

Abstract: *Geomorphology is described as a tool for the identification of active tectonics. A discussion on paleoseismology, with a case study of Caporio site in Rieti region, central Italy and other approaches for seismic hazard estimation is presented. Evaluation of landforms and deposits are providing basic data for seismic hazard estimation. Geomorphic indices and landform assemblages are useful in regional evaluation to identify relative tectonics activities. In the recent years, appreciable progress has been made in the area of paleoseismology where documentation of ages and displacement of various young geological features has had great impact on seismic hazard estimation. Paleoseismic techniques include identification of structures related to strong earthquakes and assessment of the magnitude of the causative event. A fundamental element of any geological analysis for seismic hazard is to estimate the size of earthquake that can occur along a fault or within a region. Other than paleoseismology there are many, commonly used, approaches to earthquake size analysis.*

Key words*: Geomorphology, Paleoseismology, Geological Analysis, Seismic Hazard*

INTRODUCTION

Geomorphology (Seismic Landscape)

Presence of well developed tectonics geomorphic features is recognised as the most reliable criteria for identifying active faulting. Reconnaissance work to identify areas where active tectonics is particularly significant generally involves the use of geomorphic indices (sensitive to rock resistance, climatic change, or tectonics process) or assemblages of landforms produced or modified by active tectonics process.

Geomorphic Indices and Active Tectonics

Geomorphic indices are very useful tools because they quickly provide insight concerning specific area or sites in a region that is adjusting to relatively rapid rates of active tectonics deformation.

Stream-Gradient Index (SL): Anomalously high indices in rock of low or uniform resistance are a possible indicator of active tectonics. Areas where stream-gradient indices are low are associated with two general conditions: areas where soft sedimentary rocks are abundant and along major strike-slip faults where horizontal movement has crushed the rocks, producing zones low in resistance to erosion.

Mountain-Front Sinuosity (Smf): Mountain front associated with active uplift are relatively straight, but if the rate of uplift is reduced or ceased, erosional process will begin to form sinuous front that becomes more irregular with time. Low values of Smf (1.1 to 1.14) suggest active tectonics.

Ratio of Valley Floor Width to Valley Height: Comparison of Vf values measured from valleys emerging from different mountain fronts or different parts of the same front provides an indication whether streams are actively downcutting (forming V-shaped valleys with low Vf) in response to active tectonics or are being eroded laterally (forming broad valley with high Vf) in response to relative stability of the front.

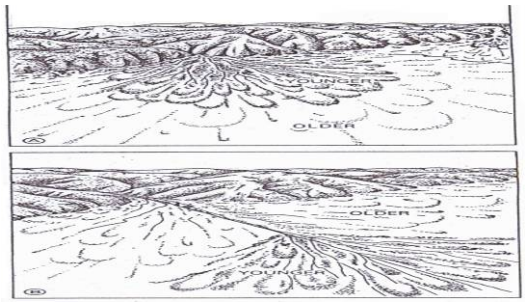

Figure 1: Alluvial fan morphology: (A) deposition adjacent to mountain front and (B) deposition shifted down-fan as a result of fan-head entrenchment

Tectonics Geomorphology and Landform Assemblage

Alluvial Fans: When the rate of the uplift of the mountain front is high relative to rate of stream-channel downcutting in the mountain and to fan deposition, then fan head deposition tends to occur, and the youngest fan segment is near the apex of the fan. If the rate of uplift of the mountain is less than or equal to the rate of downcutting of the stream in the mountain, then fan-head trenching occurs and deposition is shifted down-fan. Younger fan segments will then be found well away from the mountain front (Fig. 1 shows the two conditions).

Strike-Slip Faulting: Active strike slip faulting produces a characteristic assemblage of landforms (Fig. 2).

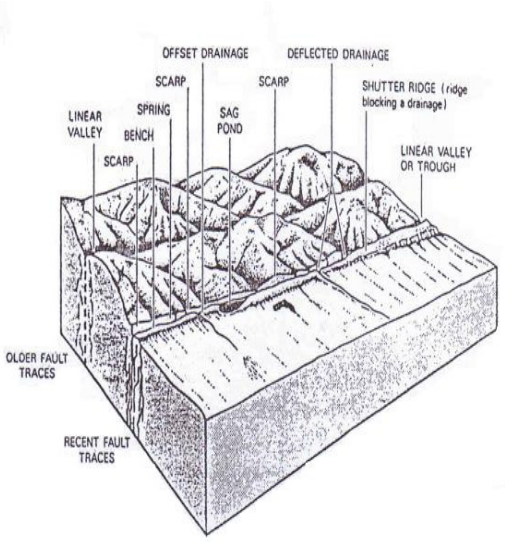

Fig. 2: Assemblage of landforms associated with active strike-slip faulting (modified from Wesson et al., 1975)

PALEOSEISMOLOGY AND SEISMIC HAZARD

It is not uncommon to identify the specific dates of strong earthquakes (the ones that are relevant for their impact on the society) along a fault over the past few thousand of years, permitting a fare better quantitative understanding of the local earthquake hazard than has ever been possible before.

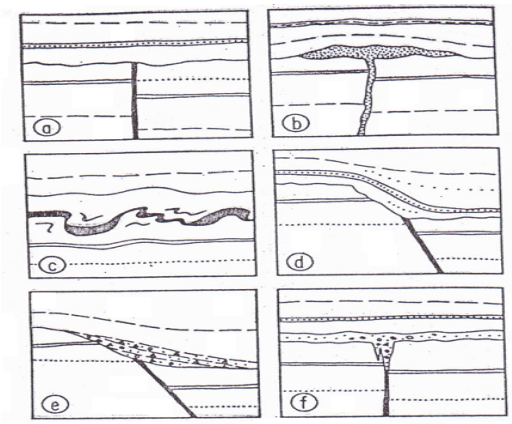

Figure 3: Sketch diagrams of cross sections of geologic relations that might result from individual paleo-earthquakes.

A tremendous advantage of paleoseismic studies is that they offer the opportunity to extend the seismicity record to an appropriate time window (i.e. the Holocene for interplate areas and the whole Quaternary for intraplate areas). Objectives of Paleoseismology are:

- To recognise "Seismites" by comprehensive geological investigations, including trenching (Fig. 3).
- To identify the seismic source producing a specific seismite through tectonics and geophysics.
- To quantify the "energy" (intensity or magnitude) by using displacement vs magnitude relationships (Fig. 4).

A Case Study

The magnitude *vs* displacement relationship has been used for seismic hazard measurement from paleoseismic evidence in the Rieti region, central Italy.

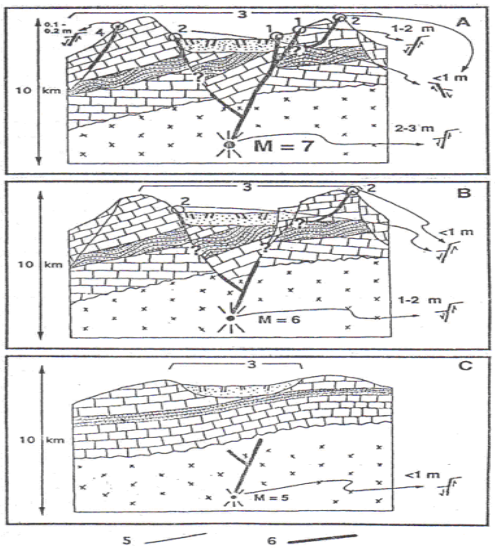

Fig. 4: Diagram showing our model of surface displacement vs. magnitude relationships for a region in crustal extension like the Central Apeninnes in Italy

Rieti region is a part of the central Apeninnes, a mountain belt characterized by active extentional tectonics. This area has three paleoseismic sites along the normal fault system at the eastern boundary of Rieti graben which is the main Quaternary structures of this region. Evidence of late Pleistocene and Holocene earthquake rupture is well preserved.

One of these sites called Caporio site was personally visited by the author (Photo). At Caporio site a recent

Photo: CAPORIO site in Rieti Region of Central Apennines

quarry excavation along the fault provides a cross section of a graben in the limestone bedrock. In excess of 20m of upper Quaternary slope deposits fill this graben. The accumulation of such a thick colluvial sequence is the result of a small valley trending perpendicularly to the graben in the mountain slope. Near the base a volcanic layer provides a marker suitable for evaluating the displacement inside the graben. This layer is offset 5m at one fault and dragged against the second fault. Located down relative to the graben and in the non faulted coluvial sequence the same layer is present near the bedrock at the bottom of the slope deposits, suggesting that the 20m of displacement occurred after its deposition. Several channel fill deposits are preserved in another fault in the upper 10m of the graben, which indicate deflection in the original course of such channels. This suggests that recurrent surface faulting events occurred at this site.

The observed surficial fault breaks show vertical offset of 0.5-1.0m, with normal slip. According to magnitude vs displacement relationships it comes out to be a threshold magnitude of 6.5 for primary faulting like at Caporio site.

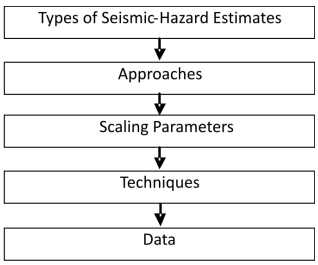

Figure 5: Flow Chart showing the major categories developed for the earthquake size estimation procedure

SEISMIC HAZARD ESTIMATIONS

Estimating earthquake size is not simple and many methods are in use. Understanding the type of earthquake size estimate made (e.g. local magnitude, surface-wave magnitude, or seismic moment), and being consistent throughout the analysis is very important. Different approaches and techniques are in practice, for the estimation of earthquake size for seismic hazard.

Estimating Earthquake Sizes

An estimation procedure has been divided into five parts in order to understand the individual components making up the procedure. These divisions are: the type of seismic hazard estimate approaches, scaling parameters, techniques, and data (Fig. 5).

Types of Seismic Hazard Estimates

The type of seismic hazard estimate needed, guides the development of seismic hazard analysis. The way the uncertainties in data are considered or weighed in the analysis depends on the type of seismic hazard estimate. (A few types of commonly used earthquake estimates are as follows.)

- Characteristic Earthquake
- Maximum Earthquake
- Maximum Credible Earthquake (MCE)
- Floating Earthquakes

Approaches

- Historical earthquake approach
- Paleoseismic Approach
- Source Characterization Approach.
- Regional Approach
- Relative-Comparison Approach

Scaling Parameters

- Historical Seismicity
- Fault Rupture Length
- Fault Rupture Area
- Fault Displacement
- Seismic Moment
- Strain Rate

Techniques

- Historical Seismicity Technique:
- Earthquake Size-Fault Parameter Correlations: These relations can be applied by estimating fault rupture length, area and displacement.

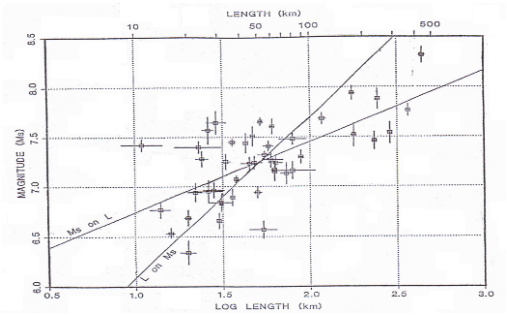

Fig. 6: Data and regression for surface-wave magnitude vs. length of surface rupture (from Bonilla and others, 1984).

- Fault Rupture Length: A relationship developed (Fig. 6) from all historical earthquake events studies. Correlation is used to convert the length parameter into earthquake size parameter by Bonilla and others (1984), is Ms = 6.04 + 0.704 (log L), where L is the surface rupture length in kilometers and the relation is valid over the range of Ms = 5.5 – 8. Wesnousky (1986) has used seismic moment rather than magnitude in length correlations (Fig. 7). Fault-rupture-length relations are widely used in interplate regions to determine an average or expected earthquake size. These values can be used directly for characteristic and maximum earthquake estimates.

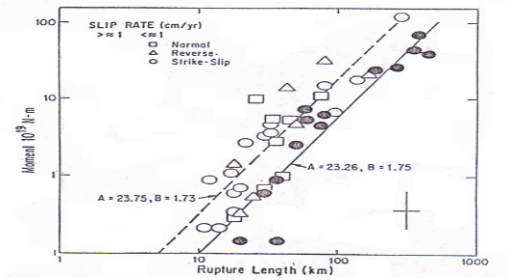

Fig. 7: Seismic moment vs. earthquake rupture length; data from faults with slip rates above and below 1 cm/yr are distinguished as well as the sense of displacement. Equations for lines are log M0 = A + B log L, the right regression line is for slip rates greater than 1cm/yr (solid circles); the left line is for slip rates less than 1 cm/yr (from Wesnousky, 1986)

- Fault-rupture Area: Once the fault rupture area is estimated, empirical relations such as by Wyss (1979) can be used (Fig. 8). This relation is M= log A +4.5 for M>5.6 where M is magnitude and A is fault area in square kilometers. Fault area method is especially useful in areas with an unusually deep seismogenic zone that could accommodate large potential earthquakes. Fault area relations can also be used in cases where a fault is blind or buried, such as blind thrust under an actively deforming anticline.

- Fault Displacement: Empirical earthquake size-fault displacement relationship is developed by Slemmons (1982a) and Bonila and others (1984) by correlating surface wave magnitude with maximum displacement. An example of one of these relationships using all earthquakes is shown in Fig. 9.

- Seismic Moment (Fig. 10)
- Strain Rate Technique

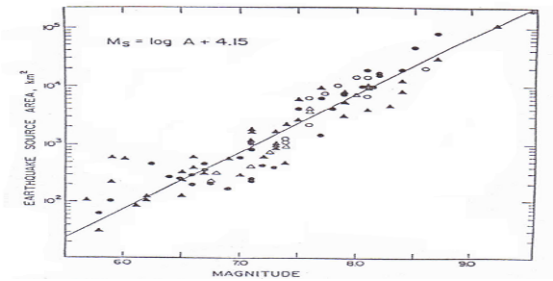

Fig. 8: Data and regression for magnitude vs. fault-rupture area (from Wyss, 1979).

Data

Data include the information collected as various input values used for the size estimation

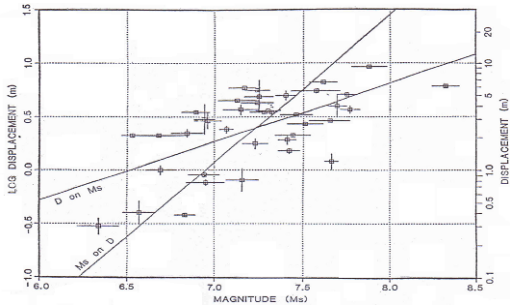

Fig. 9: Data and regression for surface-wave magnitude vs. maximum surface displacement (from Bonilla and others, 1984)

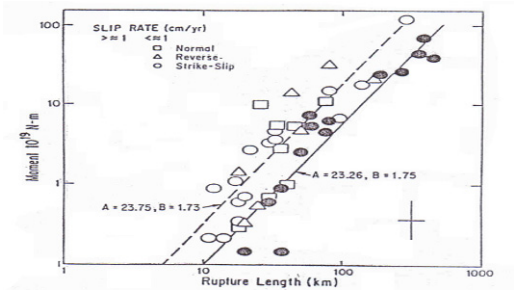

Fig. 10: Log fault length vs. log moment for large interplate and intraplate earthquakes (Scholz et al, 1986)

Acknowledgements: Thanks to Dr. Leonello Serva for his invaluable contribution towards supervision, guidance and all the way help for successful completion of this work at ANPA, Italy. This work was carried out during a 6 month fellowship award by International Atomic Energy Agency (IAEA) to the author.Eutizio Vittori, A. M. Michetti and Luca Ferreli provided all the logistic help alongwith some very stimulating discussions on paleoseismology and capable faults.

.

References

Allen C.R. (1986). Seismological and Paleoseismological Tehniques of Research in Active Tectonics. Active Tectonics, National Academy Press, Washington D.C, PP. 148 – 153.

Brunamonte F., Michetti A. M., Serva L. and Vittori E. (1993). Seismic Hazard Evaluation in Central Italy: Preliminary results of the Rieti Basin Project. Annali Di Geofisica, vol.xxxvi, (1), April, PP. 253-262,

Depolo C.M. and Slemmons DB. (1990). Estimation of Earthquake size for Seismic Hazards. Reviews in Engineering Geology, Vol. viii, Geological Society of America, Inc. 3300 Penrose Place, P.O Box 9140, Boulder, Colorado 80301, 1-28.

Keller E. A. "Investigation of Active Tectonics: Use of Surficial Earth Processes". In: Active Tectonics, National Academy Press, Washington D.C, PP. 136-147, 1986.

Mayer L. (1986). Tectonics Geomorphology of Escarpments and Mountain Fronts., In Active Tectonics, National Academy Press, Washington D.C, 125-135.

Michetti A. M., Brunamonte F., Serva L., Whitney R.A. (1995) Seismic Hazard Assessment From Paleoseismic Evidence in the Rieti Region, Central Italy. Proceedings of International Congress on perspective in Paleoseismology, 63-82.

Michetti A.M. (1993). Coseismic Surface Displacemet Vs Magmitude: Relationship from Paleoseismological Analysis in the central Apeninnes (Italy). Proceedings of the CRCM, 93, Kobe, December 6-11, 375-380.

Ramelli A.R. (1990). Implications of the Meers Fault on Seismic Potential in the Central United States. Reviews in Engineering Geology, Vol. viii, Geological Society of America, Inc. 3300, 59-75.

Reiter L. (1990). Earthquake Hazard Analysis. Columbia University Press, New York, 97p.

Schumm S.A. (1986). Alluvial River Response to Active Tectonics". In: Active Tectonics, National Academy Press, Washington D.C, PP. 80-94.

Schwartz D.P. and Coppersmith K.J. (1986). Seismic Hazard: New Trends in Analysis using Geologic Data. In: Active Tectonics, National Academy Press, Washinton D.C, PP.215-230.

Serva L. (1993). An Analysis of the World Major Regulatory Guides for Nuclear Power Plant Seismic Design. Engianucleare/ANNO. 10/N.2/May-SEPTEMBER, PP. 77-96.

Slemmons D. B. and Depolo C.M. (1986). Evaluation of Active Faulting and Associated Hazards. In: Active Tectonics, National Academy Press, Washington D.C, PP. 45-61.

Vittori E. Sylos Labini S. and Serva L. (1991). Paleoseismology: Review of the state of the art. Investigation of Historical Earthquakes in Europe, Tectonophysics, 193, 9-32.

Yeats R.S. (1986). Active Faults Related to Folding, In: Active Tectonics, National Academy Press, Washington D.C, PP. 63-79

ON THE PROBLEM OF MAGNITUDE CALIBRATION OF PALAEOEARTHQUAKES IN BAIKAL REGION, RUSSIA

R.E. Tatevossian (1)

(1) Institute of Physics of the Earth, Russian Ac. Sci., Ul. B. Gruzinskaya, 10. 123995, Moscow. RUSSIA. ruben@ifz.ru

Abstract: *intensity of the muya earthquake is assessed based on macroseismic and geological data. Macroseismic effect distribution confirms source depth at 20-22 km. Deep source agrees with seismic rupture length 25 km: i.e. Only a part of the source length exposed on the surface. Comparison with length of paleoseismodislocations shows that it is a regional feature. Epicentral intensity based on surface ruptures is assed x degrees in esi2007 scale. Ignoring geological effects will underestimate epicentral intensity up to two degrees. Source mechanism with three sub-sources is in agreement with segmentation of surface ruptures. Sub-sources are of strike-slip type with small normal component; essential normal slip at surface is probably not representative for the source and is due to accommodation of strike-slip movement along with a system of sub-parallel en echelon ruptures under tension.*

Key words*: Baikal, palaeoearthquakes, strong earthquakes*

INTRODUCTION

Baikal is a unique zone of active continental rift (e. g. Doser, 1991). Being such, it attracts research activities of specialists in different fields of Earth sciences. Systematic studies of palaeoearthquakes started in the Baikal seismic region in early 1960s; first regional catalogue of palaeoearthquakes was published in Kondorskaya & Shebalin (1977) (Fig. 1)

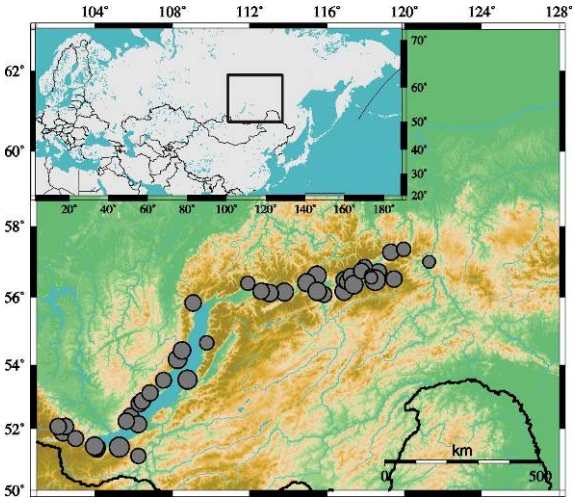

Fig. 1: Palaeoearthquake epicentres in Baikal region according to Kondorskaya & Shebalin (1977). Symbol size is proportional to magnitude

Length and maximum offset amplitude of palaeoseismostructures (PSS) reported in the catalogue are shown in Fig. 2. Even quick look at the parameters arise suspicions: maximum offsets of 5 PSS exceed 30 m. But the exceptionally large values of maximum offsets are not the only suspicious data. Surface rupture length (SRL) and the offset along it are correlated (Wells & Coppersmith, 1994). Data on Fig. 3 is in contradiction with this observation: for PSS length less than 5 km, more than 10 m of vertical offset are reported. Possibly, errors in measurements are responsible for the inconsistency between PSS length and the offset. However, the inconsistency is so much regular that we should look for certain physical background as possible explanation.

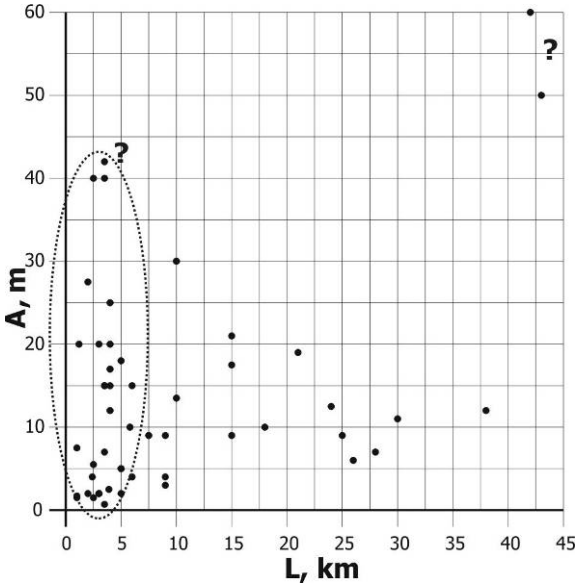

Fig. 2: PSS length (L, km) and vertical offset (A, m) according to Kondorskaya & Shebalin (1977)

Magnitudes are defined based on the PSS parameters and, certainly, discrepancies between PSS parameters affect magnitude calibration. In Fig. 3 are shown magnitudes of different kinds reported in Kondorskaya & Shebalin (1977) catalogue. ML is magnitude based on PSS length, Ma – on maximum offset, Mf – final magnitude value. Magnitudes based on PSS offset are systematically larger than those derived from PSS length. The difference in average reaches 1.25 units. Mf values are somewhere in between the ML and Ma, but there is no any regularity in Mf assessment. Note also that some ML values are ascribed arbitrary (open stars).

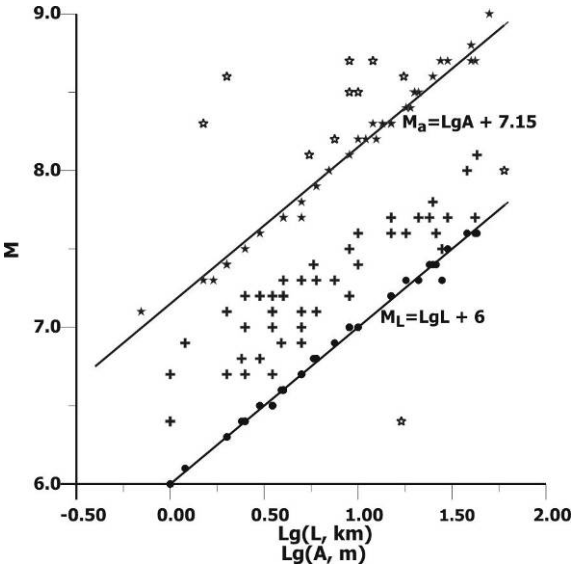

Fig. 3: Relationships among magnitude assessments of different kinds for palaeoerathquakes: ML (dots), Ma (stars) and Mf (crosses). Blank stars are for magnitudes, which do not follow the correlation relationship. See text for details.

THE MUYA, 1957, EARTHQUAKE

The Muya, 1957 (M=7.6) earthquake is the largest instrumentally recorded seismic event in the region. A complex set of surface ruptures was associated with it. They were studied and reported by the special expedition of Solonenko et al. (1966). We can use detailed information on this earthquake to understand if there are some specific regional conditions, which cause the unusual relationships between PSS length and the offset. Finding of this *cause* is the goal of the paper.

Location of the Muya earthquake and seismic source mechanisms in the region according to (Global Centroid Moment Tensor Catalog, 2009) are shown in Fig. 4. There are no focal mechanism solutions reported immediately in the epicentral area of the Muya earthquake but in its vicinities normal faulting were observed; to the east strike-slip faulting dominates.

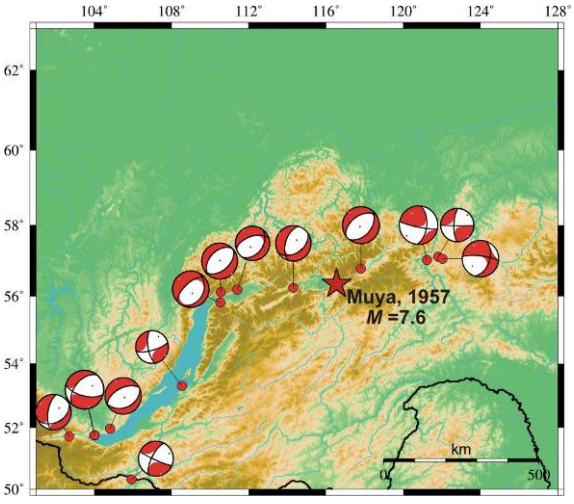

Fig. 4: Epicentre of the Muya, 1957, earthquake and source mechanisms in the Baikal region according to (Global Moment Tensor Catalog, 2009). Mechanisms for seismic events with $M_o \geq 10^{24}$ dyn·cm ($M_w \geq 5.3$) are plotted.

Materials of field studies clearly show that complex set of surface faulting can be grouped in three main segments: western, central, and eastern, with different parameters of faulting (Fig. 5a, b). The segments compose *en echelon* system WNW trending. In the western segment surface faulting outlines small graben (3 km length and 1.3 km width). The southern boundary of the graben is controlled by a normal fault with right-lateral slip component. Horizontal slip is 1.05 m and vertical offset is between 1.2 – 1.3 m (Solonenko et al., 1966). Left-lateral slip (0.3 m) accompanied with some normal faulting was observed close to the northern boundary (Kurushin, 1963). In the central part of the graben 8 meter wide through was reported (Solonenko, 1965).

A transition zone of NW trending links Western and Central segments. It is composed from two brunches. Northern brunch striking WNW is a normal fault (1.4 m offset) with left-lateral slip component (0.25 m) (Kurushin, 1963). Southern brunch is a pressure zone of NNW trending. It is most probably associated with thrusting; the amplitude of the vertical offset is either 2.4 m (Kurushin, 1963) or 4 m (Solonenko, 1965).

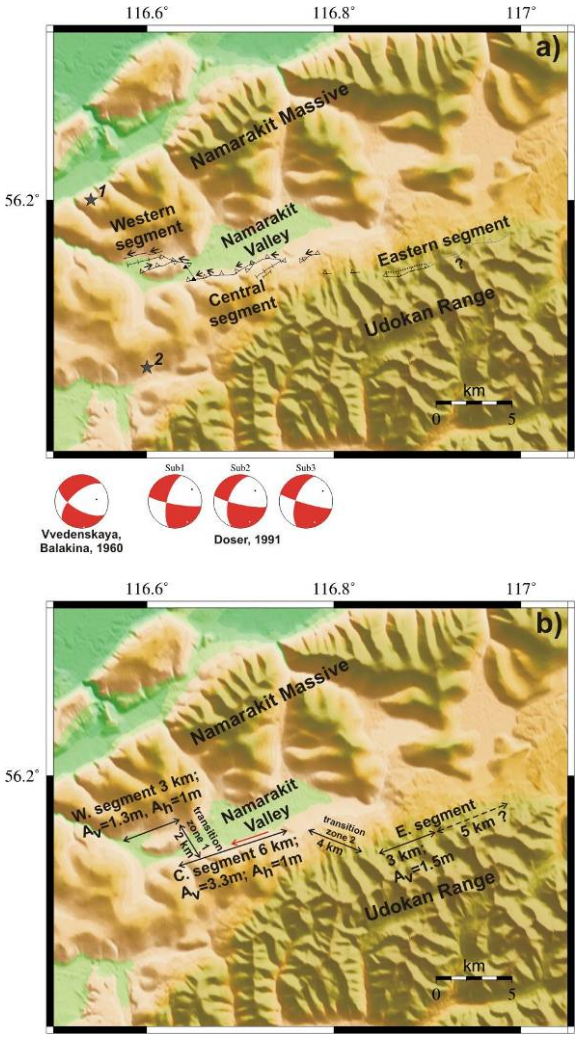

*Fig. 5: Geological manifestations, instrumental epicenter, and mechanism of the Muya earthquake. **a**) surface faulting; epicenter locations (1) by Vvedenskaya, Balakina, 1960, (2) by Balakina et al., 1972; Sub1, Sub2, Sub3 are mechanisms of sub-events. Arrows show slip direction. Question mark is for doubtful part of the surface faulting. **b**) generalized scheme of the surface faulting.*

Fault system within Central segment is presented by sequences of shear, extension, and thrust structures composing zone of left-lateral strike-slip, in which vertical offsets could be found fragmentary (Solonenko et al., 1966). There are contradictory interpretations of vertical offset character. Amplitude of vertical offset does not exceed 3.3 m, of horizontal slip – 1 m (Kurushin et al., 2007).

Eastern segment is located at the pediment of Udokan Range and is composed by extension structures (grabens). Observed steep dipping of the fault to the North is evidence of normal faulting (Kurushin et al., 2007). Amplitude of the offset varies along the fault from 0 to 1.5 m. There are no traces of horizontal slip at this fault segment (Kurushin, 1963; Solonenko et al., 1966).

Total length of definitely proved surface faulting is ca. 20 km. But in some publications pointed out that Eastern segment might be extended for another 5 km (e.g. Solonanko et al., 1985).

Macroseismic information is summarized in Fig. 6, based on questionnaires collected in the Institute of the Physics of the Earth, RAS in 1958 and data from (Solonenko et al., 1958). Though the data spatial coverage is unfavourable for compilation of a reliable isoseismal map (unpopulated epicentral area and eastern part) we can draw a very large felt area (over 700 km from surface faulting zone).

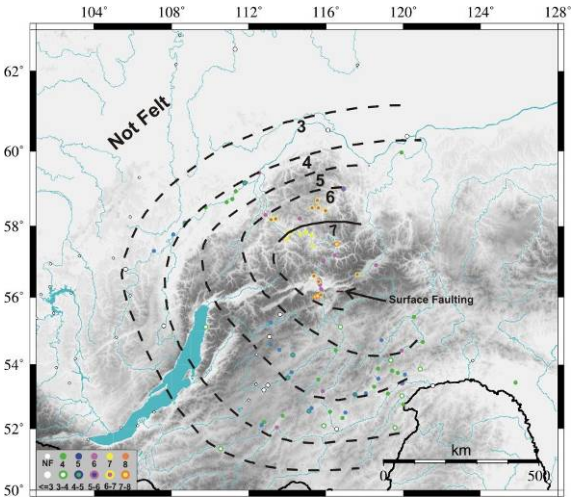

Fig. 6: Isoseismal map of the Muya earthquake.

DISCUSSION

Epicentral intensity (Io) of the Muya earthquake can be assessed based on the total length of the surface faulting. Its well-documented length is 20 km plus 5 km of doubtful piece. According to the ESI2007 scale (Michetti et al., 2007) epicentral intensity X corresponds to 20-25 km total rupture length. Maximum vertical offset is 3.3 m. For normal faulting this value is also in agreement with intensity X[1]. Therefore, both assessments give consistent result, which from one hand proves existence of correlation between SRL and offset along it, from the other hand is evidence of accurate evaluation of Io being X degrees. Nearest to the surface faulting zone localities are at 50 km distance from it. This large distance can explain why maximum observed macroseismic intensity is much lower than Io and does not exceed 8 degrees. Absence of localities in the epicentral area explains also the anomalously large size of 7 degree isoseismal compared to lower value isoseismals: certainly within the isoseismal 7 has to be higher intensities. If for epicentral intensity assessment of the Muya earthquake we considered only macroseismic effects in localities, as it is suggested by EMS98 (European Macroseismic Scale, 1998), Io would be underestimated at least by two degrees.

Epicenter instrumental location differs more than 100 km according to different seismological agencies and publications. Closest locations to the surface faulting zone are solutions by Vvedenskaya and Balakina (1960) and by Balakina et al. (1960) (Fig. 5a). But it is very possible that, deriving it they used also position of surface faulting, therefore, it is not completely instrumental. Hypocentre depth given by (Kondorskaya and Shebalin, 1977) is 15 km, by Doser (1991) – 10 km; the deepest solution (22 km) gives Balakina et al. (1972). Macroseismic data is consistent with 20 km depth. First of all, this depth together with M=7.6 is in agreement with 700 km of felt radius. Second, isometric form of isoseismals (Fig. 6) is characteristic to relatively deep source. Relatively short surface faulting zone (20-25 km) also agrees with deeper source. For comparison, we could mention two earthquakes with M=7.4: the Neftegorsk, 1995, which accompanied by 46 km of SRL and Altai, 2003, - by 70 km of SRL. According to Wells and Coppersmith (1994) 20-25 km of SRL corresponds to M=6.6, which is 1 unit less, than the magnitude of Muya earthquake. It is clear, that only small part of the rupture in the source of Muya earthquake was exposed on surface. Possibly it is characteristic to the regional seismicity. This hypothesis can explain why the reported PSS lengths are < 45 km (see Fig. 2).

First motion mechanism (Vvedenskaya, Balakina, 1960) corresponds to normal faulting with left-lateral strike-slip component along a WNW plane, and steeply dipping to the South (Fig. 5a). In general, this solution is consistent with the geometry of surface faults and kinematics of faulting. But body wave-form inversion at teleseismic distances gives different solution (Doser, 1991): three sub-events are recognized, each almost pure strike-slip with negligible normal fault component. Data quality does not permit spatial resolution of sub-events. Solution with sub-events is in much better accordance with observed segmentation of surface fault zone, but is in contradiction with the fact, that vertical offset everywhere larger than horizontal slip. A possible reason might be the following. Under extension stresses, strike-slip movement along en echelon sub-parallel faults, which are not co-axial, requires normal faulting at surface to accommodate shear deformation. According to this hypothesis, normal fault component is not representative for the source in general and its amplitude can be anomalously large, compared to the surface fault length (as it was noted in Fig. 2).

[1] To avoid confusion Roman letters are used for ESI2007 scale and Arabic numbers are for macroseismic intensities

CONCLUSIONS

1. Spatial distribution of the Muya earthquake macroseismic effects is in agreement of relatively deep source (20-25 km). Anomalously short surface faulting length (not more than 25 km) is evidence that only small portion of source rupture exposed on surface. Comparison with PSS length let us suggest this might be a regional characteristic feature.

2. Epicentral intensity of the Muya earthquake is X degrees based on surface faulting parameters. Ignoring information on environmental effects would underestimate Io by two degrees.

3. Source mechanism with three sub-events is in agreement with segmentation of surface fault zone. Faulting type in the sub-events is strike-slip with small normal component. Observed at surface significant vertical component is, probably, non-representative for the source in general. It can be related to accommodation near surface of shear deformation along system of sub-parallel en echelon faults under extension stresses.

Acknowledgements: Research is partly supported by RFBR grants 07-05-00702a and 08-05-00598a. Special thanks to A.N. Ovsyuchenko for consultations on geology.

References

Balakina, L.M., Vvedenskaya, A.V., Golubeva, N.V. et al. (1972). Pole uprugikh napryazheniy Zemli i mekhanism ochagov zemletryseniy (Earth elastic stres field and earthquake source mechanism – in Russian), Rezul'taty issledovaniy po mezhdunarodnym geofizicheskim proyektam, Seysmologiya, 8.

Doser, D.I. (1991). Faulting within the eastern Baikal rift as characterized by earthquake studies. Tectonophysics, 197, 109-139.

European Macroseismic Scale 1998 // Cahiers du Centre Europeen de Geodynamique et de Seismologie / Ed. G. Grunthal. Luxembourg, v. 15.Global Centroid Moment Tensor Catalog, 2009. http://www.globalcmt.org/CMTsearch.html. Last accessed in April, 2009.

Kondorskaya, N.V. and Shebalin N.V. (Eds.) (1977). New catalog of strong earthquakes in the U.S.S.R. from ancient times through 1975. Moscow, Nauka, 506 pp.

Kurushin, R.A. (1963). Pleystoseystovaya oblast' Muyskogo zemletryaseniya (Pleistoseist area of the Muya earthquake – in Russian), Geologiya i Geofizika, 5, 122-126.

Kurushin, R.A., Mel'nikova V.I., Gileva N.A. (2007). Muyskoye zemletryseniye 27 iyunya 1957 goda (seysmologicheskiye i seysmogeologicheskiye dannye (The Muya June 27, 1957, earthquake (seismological and geological data – in Russian). Problemy sovremennoy seysmologii i geodinamiki Tsentral'noy i Vostochnoy Azii, v.1, 193-202.

Michetti, A.M., Esposito, E., Guerrieri, L., et al. (2007) Intensity scale ESI 2007. // Memorie descriptive della carta geologica d'Italia; Vol. LXXIV. SystemCart, pp. 50.

Solonenko, V.P. (1965). Zhivaya tektonika v pleistoseistovoy oblasti Muyskogo zemletryseniya (Active tectonics in pleistoseist area of the Muya earthquake – in Russian), Izv. AN SSSR, ser. Geol., 4, 58-70.

Solonenko, V.P., Nikolaev, V.V., Semenov R.M., et al. (1985). Geologiya i seysmichnost' zony BAM. Seysmogeologiya i seysmicheskoye rayonirovaniye (Geology and seismicity of the BAM zone. Seismogeology and seismic zoning – in Russian). Novosibirsk, Nauka, pp. 192.

Solonenko, V.P., Treskov, A.A., Florensov, N.A., et al. (1958). Muyskoye zemletryaseniye 27 iyunya 1957 g. (The Muya earthquake on 27 June, 1957 – in Russian) // Voprosy Inzhenernoy Seesmologii, 1, 29- 43.

Solonenko, V.P., Treskov, A.A., Kurushin R.A., et al. (1966). Zhivaya tektonika, vulkany i seismichost' Stanovogo nagor'ya (Active tectonics, volcanoes, and seismicity of Stanovoy Highland–in Russian). Moscow, Nauka, pp. 230.

Vvedenskaya, A.V., Balakina, L.M. (1960). Metodika i rezul'taty opredeleniya napryazheniy, deystvuyushchikh v ochagakh zemletryseniy Pribaikal'ya i Mongolii (Method and results of determination of stresses acting in the earthquake sources in regions of Baikal and Mongoliya – in Russian), Bull. Soveta po seismologii, 10, 73-84.

GEOARCHAEOLOGICAL CONTEXT OF THE DESTRUCTION AND ABANDONMENT OF A FORTIFIED VILLAGE IN ASTURIAS IN THE 2ND CENTURY AD: CHAO SAMARTÍN (GRANDAS DE SALIME, ASTURIAS, SPAIN)

A. Villa Valdés (1)

(1) Dirección General de Patrimonio Cultural. Consejería de Cultura y Turismo del Principado de Asturias. C/ Eduardo Herrera "Herrerita", s.n. 33006-Oviedo. SPAIN. angel.villavaldes@asturias.org

Abstract: *Chao Samartín's origin as a human settlement goes back to the Bronze Age and was definitively abandoned at the end of the 2nd century A.D. In the proposed communication we will present the arguments of geological, orographical and archaeological kind which allow us to consider, for the first time in the geographical and cultural area of the peninsular northwestern proto-history, a disaster of seismic origin as the reason for the destruction and later abandonment of a human settlement. It is, at the same time, the most ancient evidence in this region of a seismic activity which has been reactivated in the last decades.*

Key words*: Hillfort, Iron Age, Roman settlement, Earthquake.*

INTRODUCTION

The ruins of Chao Samartín are located in Castro (Fig.1 and 2), a village about 6 km from Grandas de Salime, capital of the council (Prov. of Asturias, Spain).

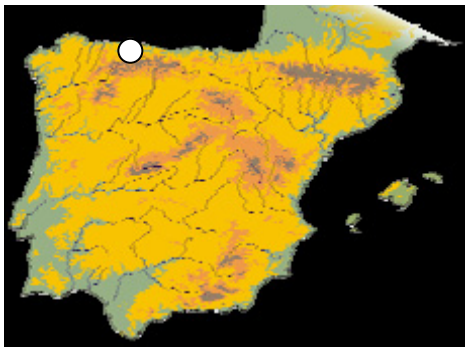

Fig. 1: Chao Samartin location

Chao Samartín's origin as a human settlement goes back to the Bronze Age when, around 800 BC., a first fortified village of ritual character was established on its top plain and then destroyed in the middle of the 7th century BC.

Fig. 2: Chao Samartín, an aerial view

During the Iron Age the defences, as a consequence of successive destructions, were renewed several times in order to give protection to a village in which, from the 6th century B.C. on, the most characteristic features of the hillfort habitat are present: ditches, module walls, huts of simple ground plan for domestic use or of bigger size for community services.

In Roman times (1st to 2nd century AD) it gets the status of administrative centre, probably the capital of the *civitas Ocela*. A luxurious *domus* is built and used as a residence for local aristocratic groups. At the end of the 2nd century A.D. it is definitively abandoned.

AN EARTHQUAKE REASON FOR THE LATER ABANDONMENT OF SETTLEMENT?

The context which characterizes this episode becomes particularly significant because of the generalized collapse of the buildings and the abundance of goods trapped under the debris (Fig.3). An exceptional richness in a cultural atmosphere – late Iron Age and early Romanization – in which household goods are scarce and not very diverse.

Fig. 3: Wall collapsed on the square

The stratigraphic sequence (Fig. 4) formed against the indigenous walls reveals that the same massive collapse took place on several occasions during the centuries previous to the Roman conquest which Augustus completed in 19 BC. Its effects can also be traced in the wide range of fossilized mural pathologies on the walls which set up the net of indigenous constructions in the settlement during the Iron Age (Fig. 5).

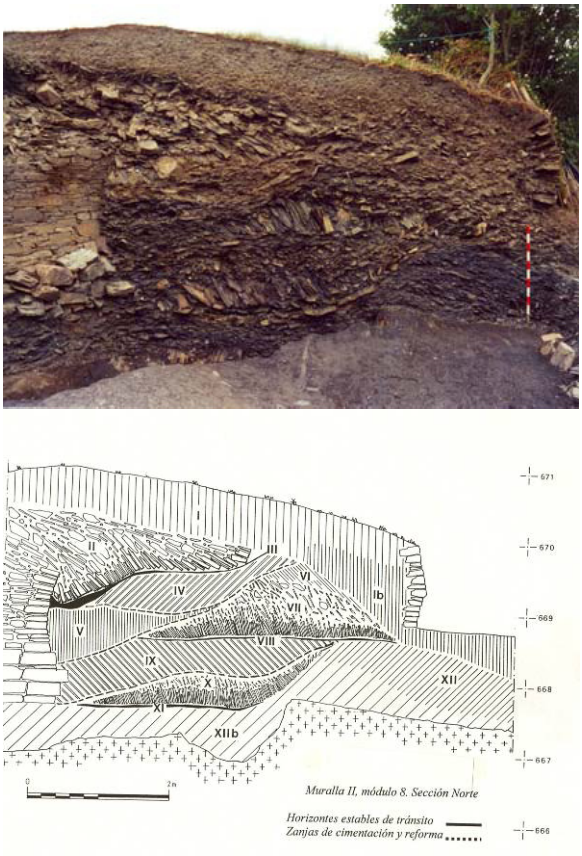

Fig. 4: Sucesive massive collapse of indigenous walls

The site lies on an area of well-known seismic activity as consequence of the reverse fault located at a depth of 15 km in the area delimited by the towns of Triacastela, Becerreá and Sarria, in the province of Lugo.

Fig. 5: The last roman wall is fall down on the ditch

In the proposed communication we will present the arguments of geological, orographical and archaeological kind which allow us to consider, for the first time in the geographical and cultural area of the peninsular northwestern proto-history, a disaster of seismic origin as the reason for the destruction and later abandonment of a human settlement. It is, at the same time, the most ancient evidence in this region of a seismic activity which has been reactivated in the last decades.

References

Fröhlig, T., Jacobelli, L. (1995). Archäologie und Seimologie. Coloquium Boscoreale, 1993. München (Germany).

Marichal, R. (1999). Archéosismicité & vulnérabilité du bâti ancien. Actes des IV^{e} Rencontres du Groupe APS, Perpignan (France).

Villa Valdés, A. (2005). El castro de Chao Samartín. Guía para su interpretación y visita. Oviedo (España).

Villa Valdés, A. (2009). Museo castro de Chao Samartín. Catálogo. Oviedo (España).

THE ORIGIN OF ROCKFALLS AND THE FORMATION OF HANGING VALLEYS ALONG THE LA LAJA RANGE FRONT (TARIFA, S SPAIN)

A. Vollmert (1), K. Reicherter (2) and C. Grützner (2)

(1) Lehrstuhl für Ingenieur- und Hydrogeologie, RWTH Aachen University, Lochnerstr. 4-20, 52056 Aachen. GERMANY. andre.vollmert@lih.rwth-aachen.de
(2) Institut für Neotektonik und Georisiken, RWTH Aachen University, Lochnerstr. 4-20, 52056 Aachen. GERMANY.

Abstract: *The La Laja Range Front is part of the Sierra de la Plata (Cádiz, south Spain). The steeply inclined sedimentary sandstone strata display a close system of discontinuities such as eastwards dipping bedding planes and E-W striking tension cracks which clearly reduce slope stability. Due to its special orientation wedge failures on two intersecting planes as well as toppling and planar failures of columns of a width of 2 m on average can be observed along the range front. The formation of three hanging valleys as a consequence of those wedge slides is one of the main topics discussed in this study. However, these landslides are also caused by water pressure from joints and bedding planes, weathering, erosion and presumably historical or even recent seismicity. Because of the steep slope below the range front falling blocks reach distances of up to 600 m and are therefore characterised as "long runout rockfalls".*

Key words*: rockfalls, hanging valleys, runout distances*

INTRODUCTION

Elonging to the western foothills of the Betic Cordilleras the Sierra de la Plata Mountain Range reaches a maximum elevation of 459 m above sea level. It is located within the region of the Strait of Gibraltar, straight north of the Bay of Bolonia (Cádiz, south Spain). Along the eastern side of this Mountain Range the La Laja Range Front follows a N-S direction for about 1 km length with a maximum height of about 80 m (Fig. 1). It shows tectonical and geomorphological anomalies, which are associated with active normal faulting processes. Triangular facets and hanging tributary valleys at about 30 m height provide evidence for this. In addition, a weakly weathered reddish ribbon at the basal knick-point, showing no lichen growth, might verify the recent tectonic uplift of the La Laja. This study describes the kinematics leading to rockfalls and provides explanations for the genesis of hanging valleys along the escarpment. Additionally, long runout rockfalls are described.

GEOLOGY OF THE STUDY AREA

The bedrock geology of the Sierra de la Plata is dominated by the Campo de Gibraltar flyschs, which were formed in lowermost Cretaceous to early Miocene times (Durand-Delga, 2006). These highly tectonized turbiditic sandstone deposits, which can also be found in northern parts of Africa, consist of Eocene to Aquitanian Aljibe, Algeciras and Bolonia sandstone units. Between the Burdigalium and the late Tortonian these strata were thrust over plastic Cretaceous to Eocene turbiditic sandy and clayey sediments of the Facinas and Almarchal units. The emplacement of the nappes took place due to the alpine orogenesis under a WNW-ESE compressive stress field (Weijermars, 1991), that led to an intensive folding. Fig. 2 shows a map section of the Campo de Gibraltar region relating to the geology of the Sierra de la Plata.

DISCONTINUITY SET OF THE LA LAJA RANGE FRONT

The steeply inclined sandstone strata offers a close discontinuity set, which mainly consists of bedding planes dipping eastwards and E-W striking tension cracks. Due to these failures in bedrock, the La Laja Range Front is affected by toppling, falling and sliding processes leading to rockfalls. The exact reasons for these kinematics are described in the following chapters.

Along the range front tension cracks have been analysed

Fig. 1: Morphology of the La Laja Escarpment

especially in the zones of hanging valleys. Fig. 3 indicates the orientation of discontinuities in terms of their strike direction. The dip angel is shown next to the joint diagram. Apart from some exceptions, the measured planes are striking nearly perpendicular to the escarpment from east to west. With an average angle of 70°-80° they dip uniformly into northern and southern directions. The distinctive topographic front shown in Fig. 1 evidence a "X-formation" of two big crossing joints, which represent the described inclination of tension cracks in a two-dimensional way.

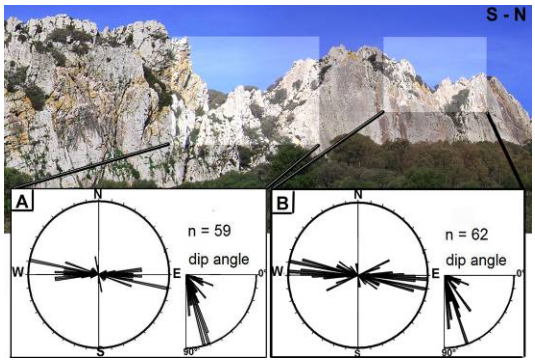

Fig. 3: Joint diagrams presenting the orientation of tension cracks in two of the hanging valleys

The La Laja slope face represents the orientation of bedding planes. Due to this fact these discontinuities also dip with approximately 70° into eastern direction. They separate abundant, plan-parallel columns with a width of 2 m on average. This is illustrated in Fig. 4, which shows the structure of the rock formation using a 3D-model developed by a light detection and ranging method (LIDAR).

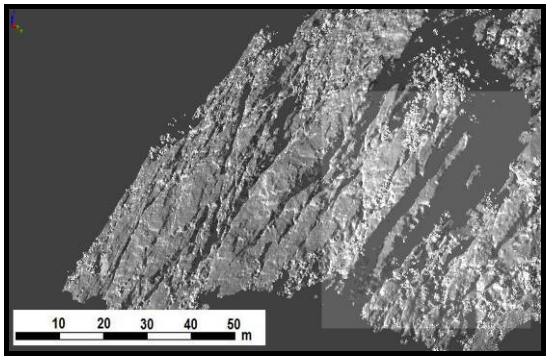

Fig. 4: 3D-LIDAR shot of the steeply inclined sandstone strata

LIDAR sends a wide-ranged laser beam and is able to detect the scattered light. The distance to an object is determined by the measured time delay between transmission of a pulse and detection of the reflected signal. In contrast to RADAR, the wavelengths of LIDAR are much. In order to reach every gap, two shoots were taken from different angles and put together with a special software. By using this method the range front was measured with millimeter precision.

KINEMATICS AND FORMATION OF HANGING VALLEYS

Due to the special orientation of bedding planes and tension cracks toppling failures of columns as well as wedge sliding failures on two intersecting planes can be observed along the range front. According to Dikau (1996), mathematical constraints shown in Table 1 depict the criteria whether a toppling or a sliding process occurs.

Table 1: Stability criteria of a cubic block

$\alpha < \varphi$	$b/h > \tan \alpha$	A block is stable
$\alpha > \varphi$	$b/h > \tan \alpha$	A block will slide but not topple
$\alpha < \varphi$	$b/h < \tan \alpha$	A block will not slide but topple
$\alpha > \varphi$	$b/h < \tan \alpha$	A block will both slide and topple

The geometrical data is based on a single block model, where α is the slope angle, φ is the friction angle, and b/h is the ration width versus height (Fig. 5).

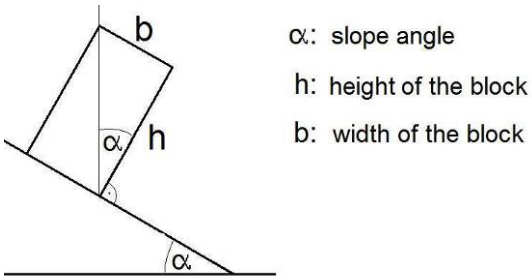

Fig. 5: Marginal case of a block between a stable position, a toppling and a sliding process

Toppling

Apart from these basics joint and bedding plane water pressures can trigger or accelerate rock movement. Such influences can be observed along the northern part of the range front, where potholes give evidences for water circulation between sandstone strata. Hence the columns lose contact to in-situ formations and topple eastwards. Fig. 6 clarifies this process and points out the sedimentation of lose masses between displaced strata. The sediments weight acts like a wedge and accelerates the toppling. The progression of weathering leads to rockfalls with its source zone at the peak of the exposed columns.

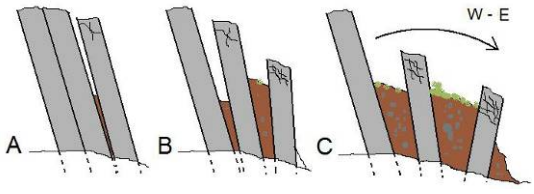

Fig. 6: E-Toppling of thick columns along the escarpment

Sliding

The sliding processes along the escarpment are closely linked to the genesis of hanging valleys. Buoyant water forces, weathering and possible seismic activity seem to be important trigger mechanisms for the examined sliding events but the principal reason for reducing slope stability lies within the intersection of tension cracks. Close to the triangular facets and hanging valleys north- and southwards dipping discontinuities often build a line of intersection that is inclined out of the slope (Fig. 7). Thereby it forms a sliding axis and causes wedge failures, a special type of movement for which Norrish and Wyllie (1996) declare the following necessary condition:

$$\alpha_{slope} > \alpha_{line\ of\ intersection} > \varphi_{friction}$$

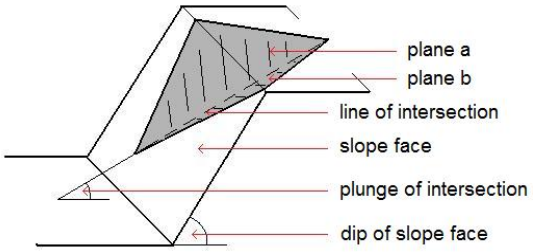

Fig. 7: Wedge failure on two intersecting discontinuities with a line of intersection which "daylights" the slope

Even if statistical evaluations indicate that most of the intersection linears dip gently, the friction angle can be exceeded because of water in cracks, that clearly reduces shear strength. A wedge failure also might be triggered by seismic energy. Recent tectonic is related to the ground failures and architectural disturbances, which are recorded at the nearby ancient Roman city of Baelo Claudia (Silva et al., 2009).

All mentioned internal and external influences cause the formation of hanging valleys which work as channels, guiding the debris and boulders down the slope.

RUNOUT DISTANCES AND ROCK DEPOSITS

According to the steep slope below the range front falling blocks reach distances of up to 600 m. In the course of this study these long runout rockfalls as well as boulders and debris up to a size of 2 m³ close to the range front have been analysed with the software ROCKFALL 6.1. Considering to selected slope and rock properties,

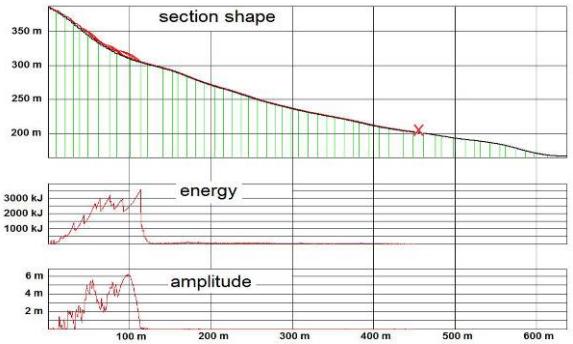

Fig. 8: Simulated rockfall along a section shape showing the steepest path from the source zone

rockfalls have been simulated along several section shapes showing the steepest pathes from the source zone on. Exemplary, one of the calculated runout distances is shown in Fig. 8 that also illustrates the energy and the amplitude of a block versus distance to the source. Most of the results concur with observed deposits being mapped along the slope during the field work. It shows that Rockfall 6.1 can offer a realistic simulation, however only approximated values are used for parameter input. This is helpful for classifying rockfalls and creating hazard maps.

References

Dikau, R., Schrott, L. & Dehn, M. (1996). Topple. In: R. Dikau, D. Brunsden, L. Schrott & M.-L. Ibsen [Hrsg.], Landslide Recognition, Identification, Movement and Courses, Wiley, Chinchester, 29-41.

Durand-Delga, M. (2006). Geological adventures and misadventures of the Gibraltar Arc. Z. dt. Ges. Geowiss., 157, 687-716.

Norrish, N.I. & Wyllie, D.C. (1996). Rock slope stability analysis. In: A.K. Turner & R.L. Schuster [Hrsg.], Spezial Report 247: Landslides, Investigation and Mitigation, TRB, National Research Council, National Academy Press, Washington, D.C., 391-425.

Silva P.G., Reicherter K., Grützner C., Bardají T., Lario J., Goy J.L., Zazo C., & Becker-Heidmann P., (2009). Surface and subsurface palaeoseismic records at the ancient Roman city of Baelo Claudia and the Bolonia Bay area, Cádiz (South Spain). Geological Society, London, Special Publications 2009; v. 316: Palaeoseismology: Historical and prehistorical records of earthquake ground effects for seismic hazard assessment.

Weijermars, R. (1991). Geology and tectonics of the Betic Zone, SE Spain. Earth-Sci. Rev., 31, 153-236.

PALAEOTSUNAMI SIGNATURES IN HOLOCENE COASTAL GEO-ARCHIVES OF THE EASTERN IONIAN SEA REGION, GREECE

A. Vött, G. Bareth (1), H. Brückner (2), I. Fountoulis (3), F. Lang (4), D. Kelletat (5), D. Sakellariou (6), A. Scheffers (7) and S. Scheffers (7)

(1) Institute for Geography, Universität zu Köln, Albertus-Magnus-Platz, 50923 Köln (Cologne), GERMANY. andreas.voett@uni-koeln.de
(2) Faculty of Geography, Philipps-Universität Marburg, 35032 Marburg, GERMANY.
(3) Department of Dynamic, Tectonic, Applied Geology, National and Kapodistrian University of Athens, 15784 Athens, GREECE.
(4) Department of Classical Archaeology, Technische Universität Darmstadt, El-Lissitzky-Str. 1, 64287 Darmstadt, GERMANY.
(5) Institute for Geography, Universität zu Köln, Albertus-Magnus-Platz, 50923 Köln (Cologne), GERMANY.
(6) Hellenic Centre for Marine Research, 19013 Anavissos, GREECE.
(7) School of Environmental Science and Management, Southern Cross University, PO Box 157, Lismore NSW 2480. AUSTRALIA.

Abstract: *This paper gives an overview of four different groups of tsunami signatures encountered in near-coast geological archives along the shores of the eastern Ionian Sea, Greece. As the study sites are exposed towards the seismically highly active Hellenic Arc, the palaeotsunami events are suggested to have been triggered by seismic events or related landslides over or underwater. The group of sedimentary tsunami signatures comprises (i) dislocated blocks and boulders, (ii) allochthonous marine sediments deposited in littoral or near-shore environments and often mixed with terrigenous material and cultural debris, (iii) allochthonous fine-grained marine deposits intersecting in-situ sediments of near-shore swamps, quiescent freshwater lakes or lagoonal environments, and (iv) beachrock-type calcarenitic tsunamites. Results from case studies are presented for each group of tsunami signatures.*

Key words*: Palaeotsunami, dislocated boulders, sandwich layers, beachrock*

INTRODUCTION

Tsunami hazard in the eastern Mediterranean belongs to the highest worldwide. This is mostly due to the high seismic activity along the Hellenic Arc where the African Plate is being subducted under the Eurasian Plate inducing numerous strong tsunamigenic earthquakes. Also, the Arabian Plate, moving northward by high rates, is a serious source of seismically related hazards. Further potential tsunami triggers in the Mediterranean are submarine slides, meteorite impacts, and explosional volcanic activity, for instance around Sicily or in the Aegean Sea. The eastern Mediterranean is characterized by comparatively short shore-to-shore distances, a highly variable underwater topography and thousands of kilometers of coastline with numerous indentations. In terms of tsunami hazard, this constellation implicates short time intervals for advance warning of local populations, strong refraction effects difficult to predict and a variety of secondary, mostly earthquake-related hazards such as rockfall, liquefaction and subaerial and underwater landslides.

Palaeotsunami research in the eastern Mediterranean has been strongly intensified during the past decades, in order to improve our understanding of the dimension and the dynamic of tsunami landfalls and to gain reliable background information for future risk assessment. Besides archival studies based on ancient accounts and historical data related to extreme wave events in the Mediterranean, an increasing number of geo-scientific field studies have been carried out to detect palaeotsunami deposits. These tsunami deposits can be classified into four main groups.

DISLOCATED BOULDERS – THE CAPE SKALA CASE STUDY

The first group comprises dislocated boulders, originating from bedrock units within the littoral zone, that were torn out, uplifted, turned over and/or transported dozens of meters inland by tsunamigenic wave action. Such deposits are reported from southern Italy (Puglia), Greece (Ionian Islands, Peloponnese, Crete), southern Turkey, Cyprus and from the Levant. In the western Mediterranean, tsunamigenically dislocated boulders were recently described from the Algerian and Tunisian coasts.

Fig. 1: Dislocated boulders near Cape Skala, southern Peloponnese with imbrications structure. Person as scale measures approx. 1.65 m.

Within the framework of our studies, tsunamigenically dislocated boulders were encountered west of Cape Skala at the Lakonian Gulf, southern Peloponnese. Large boulders were found more than 150 m inland and up to

+14 m above sea level (m a.s.l.). Some boulders show clear imbrication (Fig. 1), some are balancing on sharp rock needles which formed between rock pools in the supratidal area. Many boulders, lying fairly well above present sea level, are characterized by rock pools. In most cases, these rock pools are strongly inclined or even upside down. Such geomorphological features are usually formed by bio-erosional processes in the littoral zone and their original position is horizontal. This clearly documents that the blocks were dislocated from their original position. In case the blocks were not transported beyond the spray zone itself, fresh smaller pools with a horizontal bottom have been formed within the older inclined ones. In some cases, the blocks were re-deposited within the littoral zone so that vermetid rims could form after the dislocation. The results from dating these vermetid rims attached to dislocated boulders let us conclude that a tsunami hit the coastline around 1300 cal AD may be related to the catastrophic earthquake which affected large parts of the eastern Mediterranean in 1303 AD (Scheffers et al. 2008). Local bathymetric conditions are shallow (maximum depth < 3 m for hundreds of meters offshore) and therefore prevent larger storm waves from reaching the coast without losing energy. As a wave will break when water depth is less than 1.28 times its height, storm waves cannot have been higher than about 3 m, much too less to overturn or transport the large boulders onshore. Wave transport of the boulders is therefore suggested to be the result of tsunami landfall.

LITTORAL OR NEAR-SHORE GEOARCHAEOLOGICAL LAYERS – THE POGONIA CASE STUDY

In some cases, allochthonous marine sediments, mostly sand and/or gravel, were found in littoral or near-shore geological archives, often associated to terrigenous material and cultural debris. Examples are known from Italy, mainland Greece, the Aegean Islands, Israel and from Egypt (see e.g. Vött et al. 2008, Bruins et al. 2008).

Fig. 2: Tsunamigenic layer at the cliff near Pogonia (Akarnania) including allochthonous marine shell debris, foraminifers, sand, gravel and ceramic fragments mixed up with terrigenous deposits and covered by a palaoesol

In Akarnania (NW Greece), the cliff near Pogonia, almost 100 m long and up to 2 m high, reveals a homogeneous colluvisol including isolated ceramic fragments predominantly dating to the Byzantine epoch (Figs. 2 and 3). The colluvisol covers an up to 2 m-thick stratum with plenty of diagnostic ceramic fragments, well adjusted, partly imbricated, and mixed up with beach gravel and sand as well as with numerous remains of marine macrofossils. Due to its texture and contents, this mixed geoarchaeological layer may neither be interpreted as (i) colluvial deposit, nor as (ii) landslide deposit, nor as (iii) usual (supra-)littoral deposit. In its upper part, it shows a well developed palaeosol. Supplementary vibracoring revealed that the layer overlies, on top of an unconformity, fine-grained foreshore sand deposits. Within the mixed layer, we encountered rip-up clasts out of underlying marly bedrock. Microscopic analyses revealed that the matrix of the ceramic-rich stratum contains weathered and reworked bedrock material as indicated by mostly angularly shaped mineral grains but also marine indicators such as shell debris of marine macro- and microfauna and marine foraminifers.

Based on these distinct sedimentological and palaeontological features, we conclude that the mixed geoarchaeological layer is of tsunamigenic origin. The chaotic and wide-spread spatial distribution of archaeological remains of a nearby ancient mole, today submerged, may also be caused by destructive tsunami landfall in conjunction with co-seismic subsidence. Diagnostic ceramic fragments from the destructive layer are up to 20 cm large. We found both rounded and angular fragments. Preliminary archaeological studies show that they all date to Classical/Hellenistic to (early) Roman times. This is consistent findings of a homogeneous group of pottery wedged in the submerged mole dating to the late 4th to 2nd centuries BC. Former palaeogeographical studies in the Palairos coastal plain already suggested that the area was subject to considerable tsunami impact possibly contemporaneous to the strong tsunami which hit the nearby Lefkada coastal zone between 395 and 247 cal BC (Vött et al. 2008).

INTERSECTING MARINE DEPOSITS IN QUIESCENT NEAR-SHORE ENVIRONMENTS – THE LAKE VOULKARIA CASE STUDY

Another type of tsunami signatures is characterised by allochthonous fine-grained marine deposits intersecting homogeneous autochthonous sediments of near-shore swamps, quiescent freshwater lakes or lagoonal environments. Recent studies have shown that this constellation offers best premises for sandwich radiocarbon dating of event deposits. This is due to weaker erosional dynamics and the large availability of datable in-situ organic material not affected by marine reservoir effects.

We found evidence of multiple tsunami impact on the near-coast freshwater lake environment of the Lake Voulkaria (Akarnania, NW Greece). Sedimentological, macro- and micropalaeontological, micromorphological, geochemical and geophysical methods were used to differentiate between autochthonous quiescent water mud and intersecting layers of allochthonous material out of sand, gravel, marine shell and foraminiferal debris, organic matter and/or ceramic fragments (Fig. 3).

Analysing the Lake Voulkaria sediment trap and its environs revealed a sequence of four tsunami generations (Vött et al. 2009a). Geochronostratigraphic

interpretations are based on relative palynological age determination, radiocarbon dating and geoarchaeological findings. Tsunami generation I did probably not affect the lake itself but connected the adjacent former Lake of Cheladivaron to the open Ionian Sea; this event already took place in the 6th millennium BC or shortly afterwards. The subsequent tsunami generation II is dated to around 1000 cal BC; the following generation III hit the lake most probably during Classical-Hellenistic to maximum Roman times.

Thick deposits of tsunami generation IV from the 4th century AD were encountered all around the lake, probably representing traces of the 365 AD earthquake and tsunami catastrophe that destroyed large parts of the eastern coastal Mediterranean. We found generally good accordance between number and age of tsunami sediments found in the Lake Voulkaria and tsunami traces from adjacent coastal sites described in previous papers. Our studies revealed the Lake Voulkaria to be an outstanding tsunami sediment trap highly valuable to establish a local geochronology for large extreme events in the northwestern Ionian Sea.

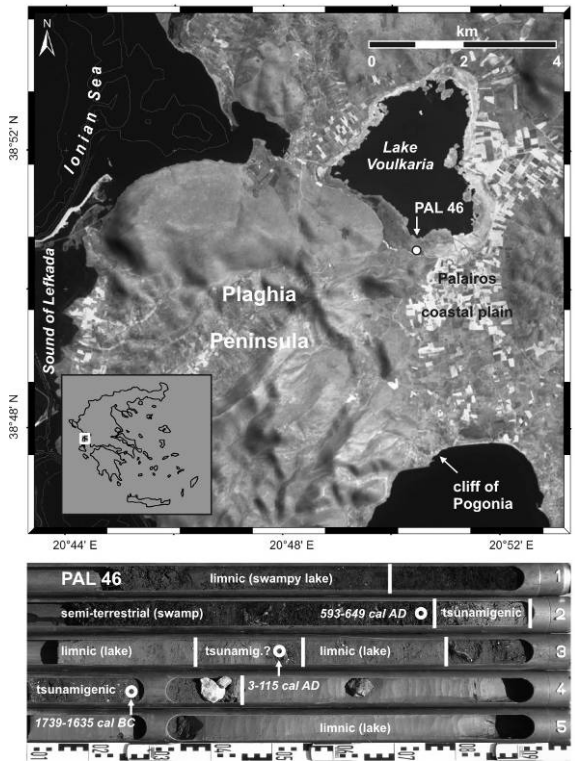

Fig. 3: The Lake Voulkaria tsunami sediment trap in northwestern Greece. The freshwater lake environment is separated from the Ionian Sea by a bedrock sill with elevations between 5-18 m a.s.l. Vibracore PAL 46 was drilled at its southwestern shore and revealed several tsunamigenic layers out of allochthonous material intersecting in-situ limnic mud or peat. Core PAL 46 thus documents multiple tsunami impact (after Vött et al. 2009a)

BEACHROCK-TYPE CALCARENITIC TSUNAMITES – THE PHEIA CASE STUDY

The fourth group of tsunami deposits – beachrock-type calcarenitic tsunamites – has been recently described, for the first time, based on three case studies from western Greece (Vött et al. 2009b). Here, we present details of the Pheia case study and describe the sedimentary characteristics of the calcarenites which help to better understand the tsunami-related sedimentation and post-event processes.

Ancient Pheia is located in the Bay of Aghios Andreas in the western Peloponnese. In antiquity, it was used as a sea harbor for Olympia which is situated some 28 km further east. The archaeological remains of Pheia are almost completely submerged and lie in water depths down to 5 m below present sea level. The harbor is said to have been destroyed by earthquakes in the 6th century AD, most probably in 521 AD and/or 551 AD. The modern beach of Aghios Andreas is characterized by thick beachrock layers. Within former studies, this beachrock was used as sea level indicator thus explaining the submergence of ancient Pheia by a complex sequence of gradual subsidence (6.5 m) and following minor uplift (1.5 m).

We carried out geomorphological, sedimentological and geoarchaeological studies and found that the beachrock, up to 3 m thick, is clearly laminated and consists of several fining upward sequences out of fine sand from the littoral zone. We also encountered coarse-grained layers including marine shell debris and ceramic fragments, partly rounded, partly angular, at the base of the fining-upward sequences. Further sedimentary structures such as convolute bedding and load casting are untypical of littoral environments (beaches) and rather indicate gravity-induced flow dynamics in a water-saturated suspension-like matrix; convolute bedding structures are thus assumed to reflect intermittent backflow shortly after high-energy deposition of thick allochthonous sand deposits onshore. The basal section of the beachrock is lying on top of an erosional discordance and consists of abundant gravel also inferring high-energy influence. In some areas, large ashlars were found incorporated into the calcarenite (Fig. 4). These man-made blocks, still angular, do not show any signs of being moved in the littoral zone; one block is even coated with original white plaster. Intra-beachrock ceramic fragments and ashlars pre-date the end of the 6th century AD; this date, marking the end of the continuous colonization of the site since the Bronze Age, is suggested a *terminus ad quem* for the event. Vibracoring revealed clear thinning land- and sideward of the beachrock, and the beachrock was discovered up to 40 m distant from the coast and up to 2.60 m a.s.l. It is, however, known from previous studies that during the Holocene the relative sea level has never been higher than at present (Kraft et al. 2005, Vött 2007, Engel et al. 2009).

Based on our results, the beachrock sequence at Aghios Andreas does not show at all sedimentary characteristics typical of a (lithified) beach but rather represents a high-energy event deposit. We therefore suggest that Olympia's ancient harbor at Pheia was hit by a strong tsunami associated to one of the strong earthquakes reported for the 6th century AD. Submergence seems to be of co-seismic nature such as observed during the southeast Asia tsunami in 2004.

Fig. 4: Beachrock-type calcarenitic tsunamite at Aghios Andreas (Peloponnese), up to 3 m thick and reaching from present sea level up to 2.60 m a.s.l. Note incorporated non-rounded ashlar with original white plaster. Likewise untypical of usual beach deposits are convolute bedding structures (inlay photo); circle symbolizes a 2 Euro coin

Associated to the beachrock, an adjacent cliff profile reveals a mixed geoarchaeological layer out of sand, gravel, ceramic fragments, and marine shell debris. The upper part of this layer subsequently weathered and formed a palaeosol. Geomorphological studies at the nearby Cape Katakolo and Tigani Island further revealed numerous dislocated blocks lying up to 40 m distant from the present shore which seem to be associated with both beachrock-type tsunamite and geoarchaeological tsunami layer.

CONCLUSIONS

By our case studies, it was possible to show that tsunami signatures in coastal sedimentary environments are highly variable. Many controlling factors have to be taken into consideration for a better understanding of the spatial distribution of tsunami deposits and the question of how, when and why tsunamigenic erosion prevails over depositional processes. Such controlling factors are, for example: (i) the availability and nature of potentially dislocatable material in foreshore, littoral and near-shore areas, (ii) the pre-existing topography and its channelling and diverging effects concerning tsunami wave dynamics, and (iii) the existence of appropriate tsunami sediment traps. Simple lists of geomorphological and sedimentological arguments currently used for identifying tsunami deposits more and more turn out to be inapt instruments for tracing tsunamis and explain major difference to storm events. Therefore, major significance has to be attributed to the geographical dimensions and variabilities of tsunamigenic processes and sedimentary signatures which will then help to better understand the overall nature of tsunami impact on coastal environments all over the world.

Acknowledgements: Sincere thanks are due to A. Bonetti (Tragata), K. Gaki-Papanastassiou, H. Maroukian, D. Papanastassiou (Athens), U. Ewelt, R. Grapmayer, (Grünberg), T. Kirkos (Vonitsa), L. Kolonas (Athens), C. Melisch (Berlin), H. Hadler, S.M. May, K. Ntageretzis, T. Willershäuser (Köln) and M. Stravropoulou (Mesolongion) for various support during field work and fruitful discussions. Work permits were kindly issued by I. Zananiri and C. Perissoratis (IGME, Athens). Funding by the German Research Foundation (Bonn, VO 938/3-1, "Quaternary tsunami events in the eastern Ionian Sea", 2009-2012) is gratefully acknowledged.

References

Bruins, H.J., MacGillivray, J.A., Synolakis, C.E., Benjamini, C., Keller, J., Kisch,. H.J., Klügel, A., van der Pflicht, J. (2008). Geoarchaeological tsunami deposits at Palaiokastro (Crete) and the Late Minoan IA eruption of Santorini. Journal of Archaeological Science, 35, 191-212.

Engel, M., Knipping, M., Brückner, H., Kiderlen, M., Kraft, J.C. (2009). Reconstructing middle to late Holocene palaeogeographies of the lower Messenian plain (southwestern Peloponnese, Greece): Coastline migration, vegetation history, and sea level change. The Holocene (accepted).

Kraft, J.C., Rapp, G. (Rip), Gifford, J.A., Aschenbrenner, S.E. (2005). Coastal change and archaeological settings in Elis. The American School of Classical Studies at Athens, Hesperia, 74 (I), 1-39.

Scheffers, A., Kelletat, D., Vött, A., May, S.M., Scheffers, S. (2008). Late Holocene tsunami traces on the western and southern coastlines of the Peloponnesus (Greece). Earth Planetary Science Letters, 269, 271-279.

Vött, A. (2007). Relative sea level changes and regional tectonic evolution of seven coastal areas in NW Greece since the mid-Holocene. Quaternary Science Reviews, 26, 894-919.

Vött, A., Brückner, H., May, M., Lang, F., Herd, R., Brockmüller, S. (2008). Strong tsunami impact on the Bay of Aghios Nikolaos and its environs (NW Greece) during Classical-Hellenistic times. Quaternary International, 181, 105-122.

Vött, A., Brückner, H., May, S.M., Sakellariou, D., Nelle, O., Lang, F., Kapsimalis, V., Jahns, S., Herd, R., Handl, M., Fountoulis, I. (2009a). The Lake Voulkaria (Akarnania, NW Greece) palaeoenvironmental archive – a sediment trap for multiple tsunami impact since the mid-Holocene. Zeitschrift für Geomorphologie N.F., Suppl. Vol., 53 (1), 1-37 (in press).

Vött, A., Bareth, G., Brückner, H., Curdt, C., Fountoulis, I., Grapmayer, R., Hadler, H., Hoffmeister, D., Klasen, N., Lang, F., Masberg, P., May, S.M., Ntageretzis, K., Sakellariou, D., Willershäuser, T. (2009b). Beachrock-type calcarenitic tsunamites along the shores of the eastern Ionian Sea (western Greece) – case studies from Akarnania, the Ionian Islands and the western Peloponnese. Zeitschrift für Geomorphologie N.F., Suppl. Vol. (accepted).

TERRESTRIAL LASER SCANNING OF AN ACTIVE FAULT IN GREECE: KAPARELLI FAULT

T. Wiatr (1), K. Reicherter (1) and I. Papanikolaou (2).

(1) Neotectonics and Natural Hazards, RWTH Aachen. Lochnerstr. 4-20. 52056 Aachen. GERMANY. t.wiatr@nug.rwth-aachen.de, k.reicherter@nug.rwth-aachen.de
(2) Lab. of Mineralogy & Geology, Department of Sciences, Agricultural University of Athens. 75 Iera Odos Str. 11855 Athens. GREECE. i.papanikolaou@ucl.ac.uk

Abstract: *The terrestrial laser scanner (TLS) has been used for the investigation of escarpments at different sites in Greece. First measurements have been conducted in spring 2009. In the future, semi-annual laser scanning will provide the possibility to monitor the fault plane and to identify the relative ages of the different earthquake events. The data acquisition with the TLS method and the high-resolution spatial surface analysis can help to improve data quality, to provide a more accurate prediction. Scientific objectives are the analysis of rock surface roughness in different scales and types which is of interest to determine relative age of the slip. Furthermore the intensity of reflexivity of the scarp surface can semi-automatically help to identify different weathering stages. Additionally, geodetic measurements with compass and GPS are carried out to cross-validate the quality of the TLS point cloud data. In this paper we want to present the preliminary results of the Kaparelli fault (central Greece) obtained the campaign 2009.*

Key words*: Greece, scarp, Kaparelli fault, LiDAR*

INTRODUCTION

During the field kamagne in Greece (April 2009) with the terrestrial laser scanning system (TLS) the focus was on the fault escarpments. These are natural exposed surfaces and give evidence of earthquakes. The concentration lies on fault scarps in neotectonics active zones in Greece. The fault plane often extends to the Earth's surface to produce ground cracks during earthquakes along the fault line or the active segment and leaves a distinctive, step-like expression in the landscape named fault scarp. Exhumation of the fault plane due to coseismic slip exposes the fault surface to differential weathering and probably to changes in surface roughness. Main aims of the investigations are to analyze the tectonic geomorphology and paleoseismology of known active faults that display post-glacial fault scarps with ground based LiDAR system to reconstruct the faulting history along surface-rupturing scarps, and to test the potential of selected locations to calibrate the roughness-index method for active faults. The hypothesis of our investigation on fault scarps shown in Fig. 1 (based on Benedetti et al. 2002). However, the first step for the analysis with TLS on this escarpment is to generate a HRDEM (High Resolution Digital Elevation Model) of the surface. For our case we need a 3-D approach to characterize the different coseismic slip events by the spatial distribution of the surface roughness from a very dense 3-D point cloud data. The spatial resolution should be in the range of a few millimeters for the following analysis. The main analytical targets are the roughness and the backscattered intensity of the escarpment surface. Primary goals are to characterize slip planes, joint orientation and spacing, the surface roughness, the dip directions and orientation and intensity distributions. Tse and Curden (1979), Kulatilake et al. (1999), Fardin et al. (2001, 2004), Rahman et al. (2006), Kokkalas er al. (2007a) or Sagy et al. (2007) discussed different approaches for calculation of the roughness of surfaces.

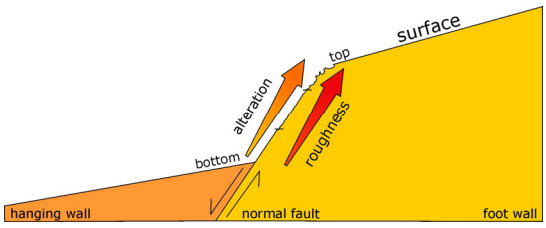

Fig. 1: Schematic diagram of the evolution of fault scarps and the related roughness (after Benedetti et al., 2002).

KAPARELLI FAULT

The Kaparelli fault is located in the eastern part of the Gulf of Corinth (Fig. 2 and 3) and is one of the most tectonically active regions in Greece (Ganas et al., 2007).

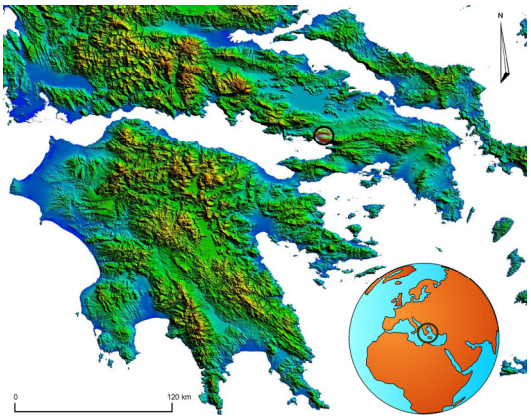

Fig. 2: Geographical overview of Greece and the location of the Kaparelli investigation area

Furthermore this region in central Greece undergoes a rapid main extension in N-S direction with approximately 6-15 mm/a (Kokkalas et al., 2007b). The Kaparelli fault is an active normal limestone fault scarp with a height of about 3 - 5 m. The last major earthquake occurred in winter 1981. Three events with magnitudes greater than 6 were measured. During the night of the 24th-25th February the fist two events had a magnitude of 6.7 and 6.4 and the third event on the 4th March reached magnitude 6.3 (Hubert et al., 1996). After those events 2-D roughness analyses (Stewart, 1996), cosmogenic dating (Benedetti et al., 2003), trenching (Kokkalas et al., 2007) and deformation monitoring by using a dense network of

Fig. 3: A) The southern segment of the Kaparelli fault. B) One scan position and the scarp layout

non-permanent GPS stations and extensometers (Ganas et al. 2007) have been carried out especially on the Kaparelli fault. Benedetti et al. (2003) assumed three events from his cosmogenic dating. The results give evidence for events at 20±3 ka, 14.5±0.5 ka and 10.5±0.5 ka. According to that the time intervals between slip events are 3000-9000 years, 4000-5000 years and 10000-11000 years. Kokkalas et al. (2007) results of the trench show again three events at around 7.5 ka, 5.8 ka and 1.4 ka. So that now seven events include the 1981 earthquake are proposed

FUNDAMENTALS OF LIDAR

The terrestrial laser scanning (TLS) was established as a good data acquisition in geoscience and geological engineering in difficult accessible areas. As the TLS has a high spatial and temporal resolution it is an effective remote sensing technology for reconstruction, monitoring and observation of mass movement phenomena and related hazards. The raw point cloud dataset includes the distance between object and TLS, the x-, y- and z-coordinates and the received intensity. With the integrated digital camera the panchromatic information is recorded. Furthermore, the working capabilities of TLS in geosciences are based in the area-measured data in safety range (> 600m). Successful investigations in geosciences with TLS were published by e.g. Kuhn & Prüfer (2007) for mass movement observation on the island Rügen, Travelletti et al. (2008) for landslide monitoring, Rabatel et. al. (2008) for mass balance of rockfall in the Alps or by Slob et. al. (2007) for fracture systems. The fundamental principle of LiDAR (*Light Detection And Ranging*) is to generate coherent laser beam with little beam divergence by stimulated emission. The electromagnetic waves are reflected by surfaces and the receiver detects portions of the backscattered signal.

Fig. 4: The terrestrial laser scanner ILRIS 3D from Optech in the field

The laser ranging system is based on measuring the time-of-flight of the short laser signal. The range or distance to the target is calculated from the time elapse of the pulse between the transmitter and receiver, and, the speed of the laser pulse. For the pulse detection the first pulse, the last pulse or the strongest pulse can be selected. In our case we used the TLS ILRIS-3D from Optech Inc., Ontario, CA (Fig.4). The technical Data of ILRIS-3D show table1.

Table 1: Technical Data

Data sampling rate	2500 points per sec.
Beam divergence	0.00974°
Minimum spot step	0.00115°
Laser wavelength	1500nm
Raw range accurancy	7mm @ 100m
Raw positional accurancy	8mm @ 100m
Digital camera	Integrated digital camera
Scanner field of view	40° x 40°

DATA ACQUISITION AND FIRST RESULTS

Major aims of the investigation were to find quantitative and qualitative data for the reconstruction of surfaces and to analyze the tectonic geomorphology and paleoseismology of active faults with TLS to reconstruct fault history and activity along surface rupturing scarps. In this context, the detailed structural analysis of rock surfaces is fundamental and can be realized by a HRDEM. The scarp surface was scanned where Benedetti et al. (2003) took samples for the cosmogenic dating method (Fig. 3B). For high quality data, the terrestrial laser scanner should detect the object from different points of view. Hence a relative complete point cloud can be produced. In this case we have four scan positions with eleven scan windows for the circa 35m long scarp. The density of points by the scans ranges between 1mm to 5.1mm.

The scan sequence is composed of approximately 94 million points.

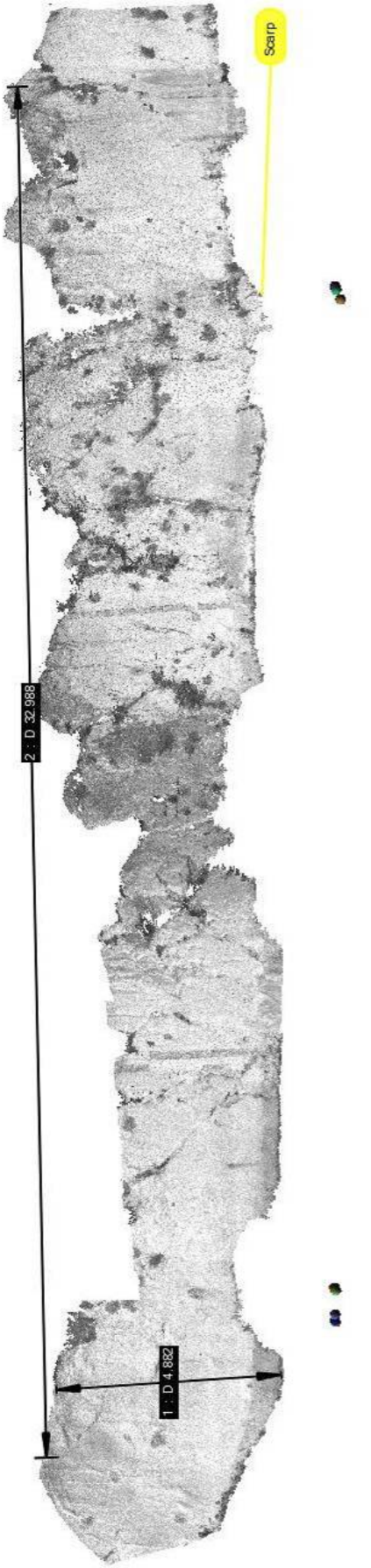

Fig. 5: Gray-scale value laser image of the whole scan sequence with circa 35m length and 3-5m altitude

The 256 gray-scale-value laser image of the Kaparelli fault scarp is in Fig. 5. In this image the heterogeneous distribution of the intensity is demonstrated. The differences of the backscattered signal between the limestone and vegetation as well as an earthquake event are clearly defined (Fig. 5).

The data pre-processing includes the alignment of the eleven scan windows, data revision, georeferencing and data management. After the data validation the point cloud has been rotated to a horizontal plane, so that for the following analysis in GIS (geographic information system) the point cloud can be processed like a normal DEM (digital elevation model). In GIS the scans have been converted in a TIN (triangulated irregular network) and subsequently in a raster format. With the grid format it is possible to calculate the basic applications for morphologic specifications. The processed data for the slope gradient is shown in Figure 6. The dark colour indicates the higher gradient values, the bright colour the lower gradient values. In this case the sampling, the vegetation and the karstification (karren) is visible (Fig.6)

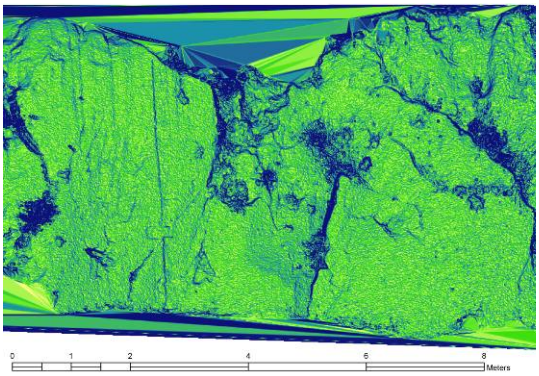

Fig. 6: Slope gradient from a detailed scan of the Kaparelli fault

Furthermore the dip direction and the dip angle is calculated virtually (Fig.7). The results confirm the measurements in the field. The Kaparelli fault has a mean dip direction of 175° and a mean dip angle of 75°.

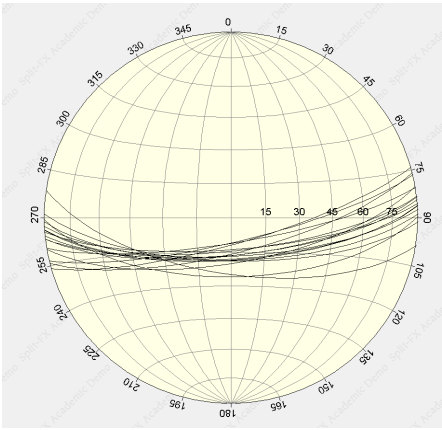

Fig. 7: Calculation of the dip orientation based on the LiDAR point cloud.

OUTLOOK

In the next step, the main focus of attention is on the intensity analysis and the calculation of the roughness in 3D-space. Different approaches have been given in the literature, within these the roughness-length method and the root mean square method are promising, which we are going to test.

Acknowledgements: We would like to thank C. Grützner and N. Hoffmann for constructive criticism, T. Fernandez-Steeger for fruitful discussions and helpful suggestions and J. Beier for various support during the field work.

References

Benedetti, L., Finkel, R., Papanastassiou, D., King, G., Armijo, R., Ryerson, F., Farber, D., Flerit, F., 2002. Postglacial slip history of the Sparta Fault (Greece) determined by ^{36}Cl cosmogenic dating: evidence for non-periodic earthquakes. Geophys. Res. Lett., 29, 87-1–87-4.

Benedetti, L., Finkel, R., King, G., Armijo, R., Papanastassiou, D., Ryerson, F., Flerit, F., Farber, D., Stavrakakis, G., 2003. Motion on the Kaparelli fault (Greece) prior to the 1981 earthquake sequence determined from ^{36}Cl cosmogenic dating. Terra Nova, 15. 118-124.

Fardin, N., Stephansson, O., Jing, J., 2001. The scale dependence of rock joint surface roughness. International Journal of Rock Mechanics & Mining Science, 38, 659-669.

Fardin, N., Feng, Q., Stephansson, O., 2004. Application of a new in situ 3D laser scanner to study the scale effect on the rock joint surface roughness. International Journal of Rock Mechanics & Mining Science, 41, 329-335.

Ganas, A., Bosy, J., Petro, L., Drakatos, G., Kontny, B., Stercz, M., Melis, N. S., Cacon, S., Kiratzi, A., 2007. Monitoring active structures in eastern Corinth Gulf (Greece): The Kaparelli fault. Acta Geodyn. Geomater., Vol.4, No.1 (145), 1-9.

Hubert, A., King, G., Armijo, R., Meyer, B., Papnastasiou, D., 1996. Fault re-activation, stress interaction and rupture propagation of 1981 Corinth earthquake sequence. Earth and Planetary Science Letters, 142, 573- 585.

Kokkalas, S., Jones, R.R., McVaffrey, K.J.W., Clegg, P., 2007a. Quantitative fault analysis at Arkitsa, central Greece, using terrestrial laser-scanning (LiDAR). Bull. Geol. Soc. Greece, vol. XXXX,1959-1972.

Kokkalas, S., Pavlides, S., Koukouvelas, I., Ganas, A., Stamatopoulos, L., 2007b. Paleoseismicity of the Kaparelli fault (eastern Corinth Gulf): evidence for earthquake recurrence and fault behavior. Boll. Soc. Geol. It. (Ital.J.Geosci.), Vol. 126, No. 2, 387-395.

Kulatilake, P.H.S.W., Um, J., 1999. Requirements for accurate quantification of self-affine roughness using the roughness-length method. Int. J. Rock Mech. Min. Sci. & Geomech. 36, 5-18.

Kuhn, D., Prüfer, S., 2007. Anwendung des Terrestrischen Laserscanners im Landslide Monitoring.- In: Otto, F. (Hrsg.): Berichte von der 16. Tagung für Ingenieurgeologie. 7.-10. März 2007, Bochum.

Rabatel, A., Deline, P., Jaillet, S., Ravanel, L., 2008. Rock falls in high-alpine rock walls quantified by terrestrial lidar measurements: A case study in the Mont Blanc area, Geophys. Res. Lett., 35, L10502, doi:10.1029/2008GL033424.

Rahman, Z., Slob, S., Hack, R., 2006. Deriving roughness characteristics of rock mass discontinuities from terrestrial laser scan data. Proceedings of the 10th IAEG Congress, Engineering geology for tomorrow's cities, Nottingham, United Kingdom, 6-10 September 2006. Engineering geology for tomorrow's cities.

Sagy, A., Brodsky, E.E., Axen, G.J., 2007. Evolution of fault-surface roughness with slip. Geology, 35: 283-286.

Slob, S., Hack, H.R.G.K., Feng, Q., Röshoff, K., Turner, A.K., 2007. Fracture mapping using 3D laser scanning techniques.- In: Sousa et. al.: 11th congress of the ISRM, 9-13 July, 2007, Lisbon, Portugal, 299-302.

Stewart, I., 1996. A rough guide to limestone fault scarps. Journal of Structural Geology, Vol. 18, No. 10., 1259-1264.

Travelletti, J., Oppikofer, T., Delacourt, C., Malet, J.-P., Jaboyedoff, M., 2008. Monitoring landslide displacements during a controlled rain experiment using a long-range terrestrial laser scanning (TLS). The International Archives of the Photogrammetry, Remote Sensing and Spatial Information Sciences. Vol. XXXVII. Part B5. Beijing 2008, 485-490.

Tse, R., Cruden, D.M., 1979. Estimating joint roughness coefficients. Int. J. Rock Mech. Min. Sci. & Geomech. 16, 303-307

TESTING THE HYPOTHESIS OF EARTHQUAKE-RELATED DAMAGE IN STRUCTURES IN THE LYCIAN ANCIENT CITY OF PINARA, SW TURKEY

B. Yerli (1) ,S. Schreiber (2), K.G. Hinzen (2), J.H. ten Veen (3) and M. and M. Sintubin (4)

(1) Institute for Geology, Mineralogy and Geophysics, Ruhr University, Universitätsstrasse 150, D-44801, Bochum, GERMANY. baris.yerli@rub.de
(2) Earthquake Geology Group, Cologne University, Vinzenz-Pallotti-Str. 26, 51429 Bergisch Gladbach. GERMANY
(3) TNO Built Environment and Geosciences, P.O. Box 80015, 3508 TA, THE NETHERLANDS
(4) Geodynamics & Geofluids Research Group, K.U. Leuven, Celestijnenlaan 200E, 3001 Leuven, BELGIUM

Abstract: *Earthquake-related damage in archaeological structures can provide important clues to increase our knowledge of the timing and magnitude of historical earthquakes. However, anthropogenic and other natural influences make the investigation more complex. The quantitative methods (e.g. laser scanning) have been used in Pınara Ancient City to distinguish the manmade damage from seismic-related damage. The geological investigations and archaeoseismological observations indicate that the city of Pınara has been affected by earthquakes but the relicts have been also despoiled. The Sarcophagus of Arttumpara in Pınara is deformed and the upper two massive limestone decks have been rotated ca. 5° in clockwise direction and traces of an explosion have been observed on the second ceiling. These features make the sarcophagus a reliable and an interesting example for testing the origin of the cause of damage.*

Key words*: archaeoseismology, laser scanning, damage modelling*

INTRODUCTION

Archaeoseismological studies usually attempt to investigate a possible connection between damage to the archaeological structures and historical or instrumental earthquakes. The important challenge lies in separating earthquake-related damage from anthropogenic and other natural causes (Ambraseys et al., 2004; Guidoboni, 2002). Recent seismological engineering models can be used to test the hypothesis that observed building damage is of seismogenic nature (e.g. Hinzen, 2005) by seeking a systematic relation between building response and the seismic source or ground motion.

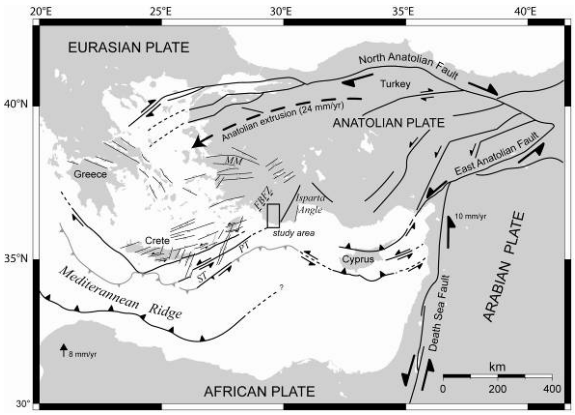

Fig. 1: Plate tectonic map of the eastern Mediterranean (modified after ten Veen, 2004). FBFZ = Fethiye Burdur Fault Zone, MM = Menderes Massive, PT = Pliny Trench, ST = Strabo Trench

In the following, the geological and seismological setting of Pınara and surroundings will be described, followed by a sketch of the archaeoseismological results. Subsequently, measurements and in-situ observations are examined with respect to being suitable traces for earthquake-related damage. We conclude that the main task will be to differentiate between earthquake-related damage and anthropogenic damage. We propose to employ methods based on laser scanning and discrete element modelling for examining causes of the damage on the structures.

THE ESEN BASIN

The tectonic evolution of southwestern Turkey (Fig. 1) is characterized by a multi-stage deformation, which is initially related to the Cretaceous – Middle Miocene Neothetys closure and subsequently to the collision of African and Eurasian plates in Late Miocene to Recent times. This tectonic process was followed by the initiation of the north and south Anatolian transform fault systems (NAF and EAF). These transform fault systems accommodate the westward extrusion of the Anatolian platelet (e.g. Barka and Kadinsky-Cade, 1988; Westaway, 1994; Armijo et al., 1999; ten Veen et al., 2008).

In southwestern Turkey the neotectonic activity is represented by the so-called Fethiye-Burdur Fault Zone (Barka and Reilinger, 1997; FBFZ); a domain with many sub-parallel NE-SW trending fault segments and basins in the area between Fethiye and Burdur. The Eşen Basin together with many similar fluvio-lacustrine extensional basins are located in the tectonically complex FBFZ and are likely foundered in response to gravitational collapse of the Lycian Orogen that formed during several thrusting phases in the Cretaceous – Middle Miocene period (e.g. Collins and Robertson, 1999; Alçiçek et al., 2006, Alçiçek, 2007).

Within the FBFZ, the Eşen Basin is formed as a ca. 15 km wide and 30 km long, NNE-trending extensional graben behind the Lycian Nappes front close to the contact with the Beydağları autochthon. The Lycian Nappes basement consists of ophiolitic rocks, limestones and turbiditic sandstones. The basin is bounded and transected by a series of N- to NE- trending faults that had exhorted important control on the character and distribution of sedimentary facies since the Late Miocene.

Historical and recent seismic reports show a density of earthquake-clustering in the FBFZ comparable to regions located along the NAF and EAF, suggesting it represents a significant seismic hazard. In spite of this the FBFZ is seismically defined by weak to moderate (M ≤ 6) earthquakes only. Important exceptions include the northeastern extremity and the off-shore southwestern extremity (Rhodes 1957, off-shore Turkey 1926, 1969, 1975, 1980, and 2001) were large earthquakes have occurred.

PINARA SITE

The ancient Lycian City of Pınara is located along the fault-controlled western border of the Eşen Basin, near the modern village of Minare. The archaeological site is spread over a 3 – 4 km^2 area that includes a variety of exposed geological units (Fig. 2A). The basement along the basin margin is characterized by a pre-Late Miocene thrust contact between two limestone nappes. This contact is demarcated by a relatively thin flysch unit with exotic limestone blocks up to 50 m width. From the Late Miocene onward, the thrust contact was down-faulted to the east along a series of sub-parallel normal faults (Fig. 2B). Just south of Pınara, strongly tilted Upper Miocene fluvial deposits with intermixed breccia levels abut against the marginal fault and are unconformably overlain by Pleistocene terrace deposits.

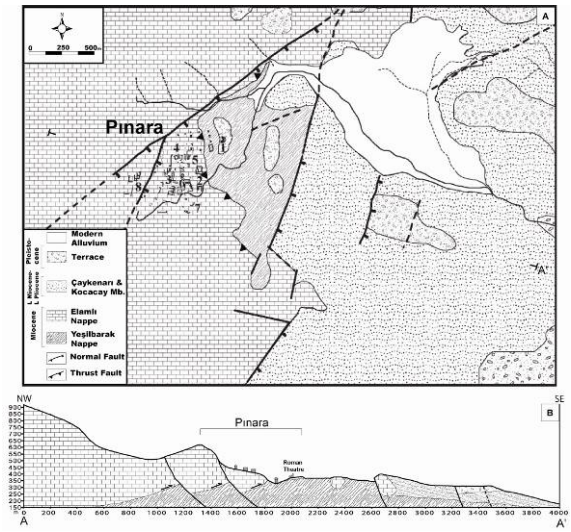

Fig. 2: Geological map (A) and cross section (B) of Pınara ancient city. 1 – Roman Theatre, 2 – Bath, 3 – Odeon, 4 – Temple, 5 – Tomb, 6 – Agora, 7 – Necropolis, 8 – Rock Tombs

The largest part of the city was built on a down-faulted limestone basement block, whereas tombs of the Acropolis were mainly carved in a ~80 m high NE-SW-trending fault face to the west *(Fig. 2B)*. No archaeological remains are present on the basement flysch, which probably was used for agricultural purposes. The Roman Theatre was built on a slightly westward-tilted Pleistocene terrace that rests on top of the flysch.

According to the ancient records, the city of Pınara was founded by colonists from Xantos between the 5th and 4th century BC. It was one of the largest cities in the powerful Lycian league and located along the main Lycian road (Akurgal, 1978). In the course of time the city was under both Roman and Byzantine control. The city was destroyed by three earthquakes in 141 AD (Guidoboni, 1994; Lang, 2003; Akşit, 2006), ~240 AD (Lang, 2003; Akşit, 2006) and 1851 (Soysal et al., 1981). Pınara received financial aid for the reconstruction of the city after the first two earthquakes (Guidoboni, 1994; Lang, 2003; Akşit, 2006). Eventually, the city lost its financial and geographic importance and at the end of the 9th century AD the city was abandoned

The observations in Pınara ancient city reveal several different kinds of damages (Fig. 3). The vertical cracks and joints of numerous beams, door and window frames and the undulated wall relict between Temple to the Odeon indicate horizontal and vertical oscillations. The reconstructed temple wall close to the tomb building shows that this structure has been destroyed and rebuild at least two times. The sliding of blocks of masonry arch close to Odeon shows a typical deformation, which has been interpreted as resulting from an earthquake (Marco, 2008; Kamai and Hatzor, 2008). Moreover, the southern collapsed edge of the Roman theatre shows a characteristic earthquake related U shape gap. The imbricate arrangements of collapsed blocks indicate rapid collapse due to seismic activity (Sintubin and Stewart, 2008). Likewise, the rotated blocks of the northern wing of the theatre are strong indication that the damage is earthquake related.

The detailed assessment of the archaeological relicts indicates that various kinds of damages are of seismogenic origin. Investigations show also that the city was destroyed several times (Yerli et al., submitted).

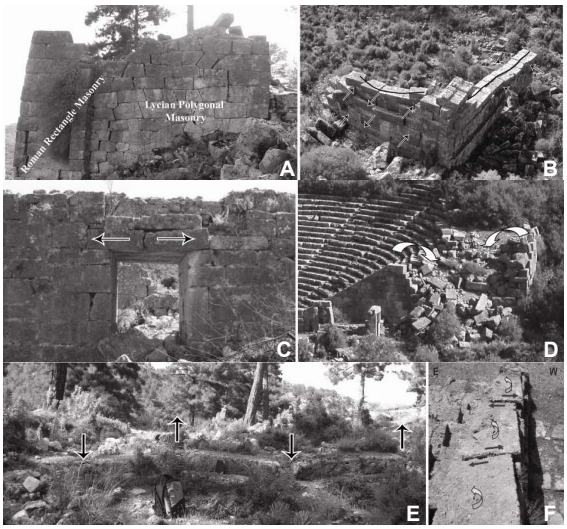

Fig. 3: Examples of probably seismic-related damage in Pınara; A- rebuild temple wall, B- sinuously deformed wall with ejected blocks, C- opened vertical joints, D- "U" shape collapse of southern wall of Roman Theatre, E- vertical undulation structure

(~40 cm), F- rotated building structures of northern wing of Roman Theatre

However, the observations in Pınara show that many structures have been destroyed by anthropogenic influence. In particular, the Lycian and Roman sarcophagi and tombs have been despoiled massively by treasure seekers. A well-preserved Lycian sarcophagus exhibits possible earthquake-related deformations as well as signs of explosion (Fig. 4B). According to the inscription on the sarcophagus from 4th century B.C., the sarcophagus was built for person called Arttumpara (Fig. 4C). The ca. 4m high sarcophagus with three ceilings in north of the Temple is deformed, and the upper two massive limestone ceilings have been rotated ca. 5° in clockwise direction with respect to the bottom block. On the rotated block a structure has been observed which likely is the result of an explosion (Wurster and Wörle, 1978). The narratives of the villagers support the sarcophagus suffered from the use of explosives in the 1970s.

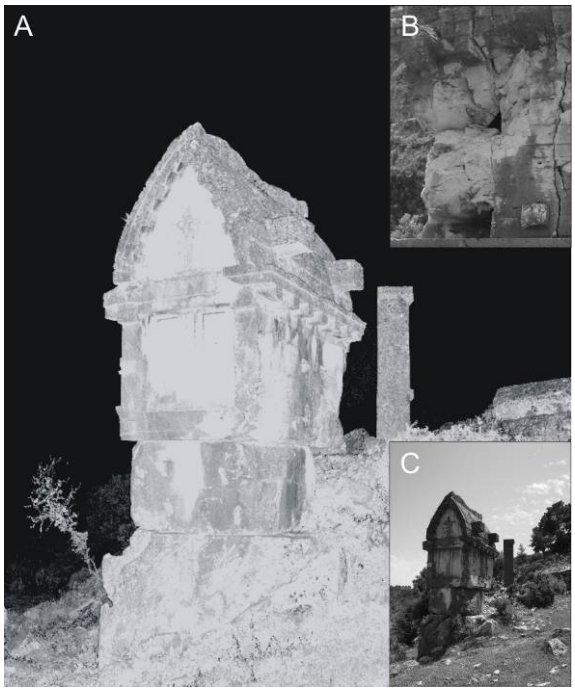

Fig. 4: A) The laser scan image of the Sarcophagus of Arttumpara. B) Explosion point on the Sarcophagus. C) Photo image of Sarcophagus

To better understand and discriminate between deformation causes, we used laser scanning technique in the field. The 3-D image of the sarcophagus (Fig. 4A) thus obtained makes it possible to construct an accurate discrete element model and test the anthropogenic and seismic damage scenarios.

The sarcophagus of Arttumpara has been scanned from ten different positions to avoid gaps in the point cloud. Subsequently, the row data-sets have been filtered and combined in to a model with 100 million points with the computer program "JRC 3D Reconstructor 2". The adjusted high resolution 3-D data enable to measure all dimensions necessary to construct a discrete element model (Fig. 5) for the dynamic analysis. After verification of correct model, behaviour with simple load tests, forces and displacements of the different damage scenarios will be used to test their plausibility.

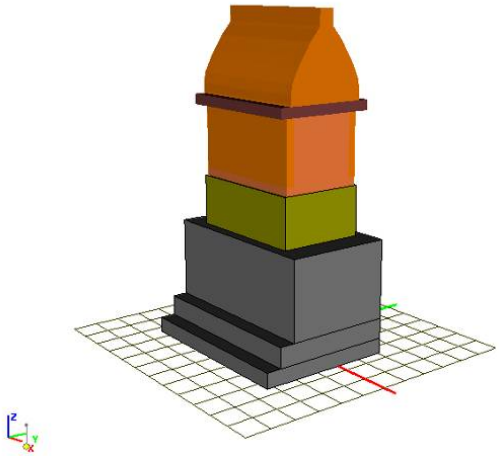

Fig. 5: Discrete element model of the Sarcophagus of Arttumpara

DISCUSSION

Due to its geological history (e.g. situation in active plate interior and closeness to basin margin faults) Pınara is a highly suitable site for conducting archaeoseismological research. Likewise the observations in Pınara indicate that most of the damages are seismic-related. However, differentiation is necessary between anthropogenic and seismic damage on a sarcophagus where traces of explosions have been found. In order to distinguish manmade from earthquake related-damage, 3D digital image resulting from an in-situ laser scan of the sarcophagus and computer modelling methods will be employed to assess the cause and the origin of deformation.

This purpose of this paper is to study and to test the archaeological hypothesis that the damage in the ancient city of Pınara, SW Turkey is earthquake-related.

Acknowledgements: We are grateful for the financial support provided by German Science Foundation (DFG VE479/1-1 and DFG HI660/2-1). We would like to thank Claus Fleischer for his support during the field work and Sharon K. Reamer for helpful suggestions and improving the manuscript.

References

Akşit, I. (2006). The land of light Lycia. Akşit Yayıncılık, İstanbul, 179 p.

Akurgal, E. (1978). Ancient civilizations and ruins of Turkey. Türk Tarih Kurumu Basim Evi, Ankara, 112 p.

Alçiçek, M.C. (2007). Tectonic development of an orogen-top rift recorded by its terrestrial sedimentation pattern: The Neogene Eşen Basin of southwestern Anatolia, Turkey. Sedimentary Geology, 200, 117-140.

Alçiçek, M.C., ten Veen, J.H., Özkul, M. (2006). Neotectonic development of the Çameli Basin, southwestern Anatolia, Turkey. In: Robertson, A.H.F., Mountrakis, D. (Eds.), Tectonic Development of the Eastern Mediterranean Region. Geological Society of London, Special Publication, 260, 591–611.

Ambraseys, N.N., Smit, P., Douglas, J., Margaris, B., Sigbjörnsson, R., Ólafsson, S., Suhadolc, P., Costa, G. (2004). Internet site for strong-motion data. Boll. Geof. Teor. Appl., 45, n. 3, 113-129.

Armijo, R., Meyer, B., Hubert, A., Barka, A. (1999). Westward propagation of the North Anatolian fault into the northern Aegean: timing and kinematics. Geology, 27 (3), 267–270.

Barka, A. and Reilinger R. (1997). Active Tectonics of Eastern Mediterranean region: deduced from GPS, neotectonic and seismicity data. Annali Di Geofisica, 40, n. 3, 587-610.

Barka, A., and Kandinsky-Cade, K. (1988). Strike-slip fault geometry in Turkey and its influence on earthquake activity. Tectonics, 7 (3), p. 663–684.

Collins, A.S., and Robertson, A.H.F. (1999). Evolution of the Lycian Allochthon, western Turkey, as a north-facing Late Palaeozoic to Mesozoic rift and passive continental margin. Geol. J., 34, 107–138.

Guidoboni, E. (1994). Catalogue of ancient earthquakes in the Mediterranean area up to the 10th century. Rome, Istituto Nazionale di Geofisica, 504 p.

Guidoboni, E. (2002). Historical seismology: the long memory of the inhabited world, in: International Handbook of Earthquake and Engineering Seismology. W. H. K. Lee, Kanamori H., Jennings P. C., and Kisslinger C., (Eds.) International Geophysics Series, 81A, Academic Press, Amsterdam, p. 775–790.

Hinzen, K.-G. (2005). The use of engineering seismological models to interpret archaeoseismological findings in Tolbiacum, Germany: a case study. Bull. Seism. Soc. Am., 95 (2), 521–539.

Kamai, R., and Hatzor, Y.H. In press. Numerical analysis of block displacements in ancient masonry structures: a new method to estimate historic ground motions. International Journal for Numerical and Analytical Methods in Geomechanics. doi:10.1002/nag.671.

Lang, G. (2003). Klassische antike Stätten Anatoliens, Band II. Lang Verlag, St. Peter am Hart, 707 p.

Marco, S. (2008). Recognition of earthquake-related damage in archaeological sites: Examples from the Dead Sea fault zone. Tectonophysics 453, 148-156.

Sintubin, M., Stewart, I. (2008). A Logical Methodology for Archaeoseismology: A Proof of Concept at the Archaeological Site of Sagalassos, Southwest Turkey. Bulletin of the Seismological Society of America, 98(5), 2209-2230; DOI: 10.1785/0120070178.

Soysal, H., Sipahioğlu, S., Kolçak, D., and Altınok, Y. (1981). Historical Earthquake Catalogue of Turkey and Surrounding Area (2100 B.C. – 1900 A.D.). Technical Report, TUBITAK, no. TBAG-341.

ten Veen, J.H. (2004). Extension of Hellenic forearc shear zones in SW Turkey: the Pliocene–Quaternary deformation of the Eşen Çay Basin. Journal of Geodynamics, 37, 181–204.

ten Veen, J.H., Boulton, S. and Alçiçek, M.C. (2008). From palaeotectonics to neotectonics in the Neotethys realm: The importance of kinematic decoupling and inherited structural grain in SW Anatolia (Turkey). Tectonophysics, doi: 10.1016/j.tecto.2008.09. 030 (in press).

Westaway, R. (1994). Present-day kinematics of the Middle and Eastern Mediterranean. J. Geophys. Res., 99, 20203–20223.

Wurster, W., Wörrle, M. (1978). Die Stadt Pinara. Deutsches Archaeologisches Intitut, Archaeologischer Anzeiger 1978 Heft 1, 74-99

Yerli, B., ten Veen, J.H., Sintubin, M., Karabacak, V., Yalciner, C., Altunel, E. Submitted. Assessment of seismically induced damage using LIDAR: the ancient city of Pınara (SW Turkey) as a case study. Geological Society of America Special Paper Ancient Earthquakes.

Index

CHART OF THE INQUA ENVIRONMENTAL SEISMIC INTENSITY SCALE 2007 - ESI 07

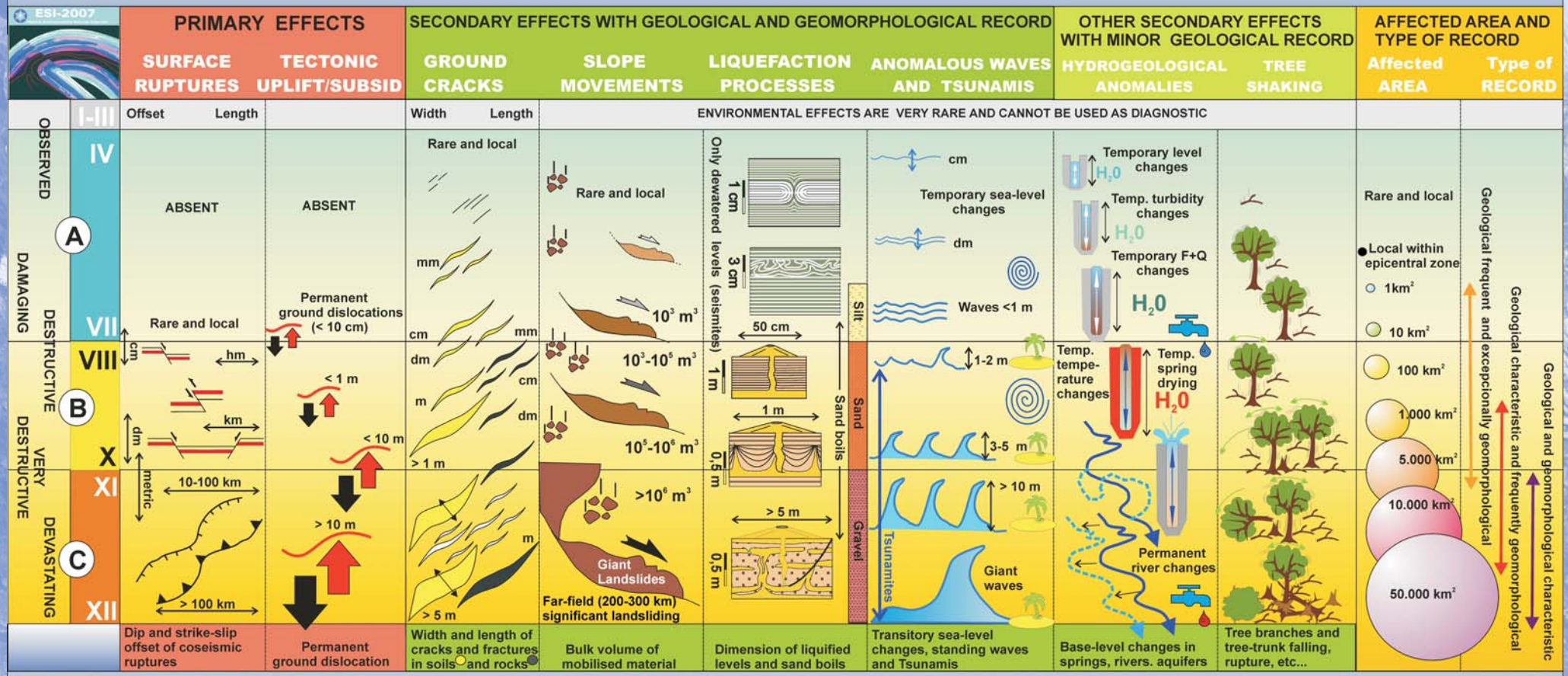

KEY REFERENCES: *Michetti, A.M., et al., 2007. Environmental Seismic Intensity scale - ESI 2007. Memorie Descrittive della Carta Geologica d'Italia, 74. Servizio Geologico d'Italia, APAT, Rome, Italy*

Silva, P.G., et al., 2008. Catalogue of the geological and environmental effects of earthquakes in Spain in the ESI-2007 Macroseismic scale. Geotemas, 10, 1063 - 1066, SGE, Spain

Reicherter, K., Michetti, A.M., Silva, P.G., 2009. Palaeoseismology: Historical and Prehistorical Records of Earthquake Ground Effects for Seismic Hazard Assessment. Geol. Soc. London, Spec. Pub., 316 1-10. London, U.K.

RWTH AACHEN UNIVERSITY

VNiVERSiDAD D SALAMANCA

UNED

Instituto Geológico y Minero de España

GOBIERNO DE ESPAÑA

MINISTERIO DE CIENCIA E INNOVACIÓN

INQUA

IUGS UNESCO

AEQUA

JUNTA DE ANDALUCIA
CONSEJERIA DE CULTURA

CSIC